SERBIAN SOCIETY OF MECHANICS

THEORETICAL
AND
APPLIED
MECHANICS

Teorijska i primenjena mehanika

Guest Editor: Katica R. (Stevanović) Hedrih

THIS JOURNAL IS EDITED BY
SERBIAN SOCIETY OF MECHANICS
(SSM)

UNDER THE AUSPICE OF
MINISTRY OF SCIENCE AND
ENVIRONMENTAL PROTECTION OF REPUBLIC OF SERBIA (MNTR)

AND IS SUPPORTED BY
SERBIAN CHAMBER OF ENGINEERS

Dear Reader,

In March 2009 research team of Project ON155002 *Theoretical and Applied Mechanics of the Rigid and Solid Bodies. Mechanics of Materials (2006-2010) and* Seminar Nonlinear Dynamics - Milutin Mialnkovic, organized a one day Scientific seminar named: **Address to Mechanics: Science, Teaching and Applications,** at Mathematical Institute of SASA. Academician RAS Valery Kozlov Opening lecture. Jubilee of the 80th birthday of Professor V.A.Vujicic was included in the Seminar program and a Booklet of each two-pages abstracts was published.

After the seminar participants and other researchers were invited to submit full papers for possible publishing in a special publication titled with the same name **Address to Mechanics: Science, Teaching and Applications.**. All submitted manuscripts for possible publishing in Special publication were evaluated by two reviewers and 19 papers were accepted for publishing.

At meeting on June 20th, 2012, Executing committee of the Serbian Society of Mechanics decided to publish a special publication titled **Address to Mechanics: Science, Teaching and Applications** in the form of **Special Issue** of the Journal **Theoretical and Applied Mechanics** with Guest editor Katica (Stevanovic) Hedrih.

This special issue contains 18 original research papers and one review paper. Research papers are grouped by area of mechanics and research results. The papers are in following areas: general mechanics and theory of stability, nonlinear dynamics, robotics, structural mechanics and damage mechanics, biomechanics, finite element method applications, control of mechanical systems, geodesic on the surface, fluid mechanics, celestial mechanics, computational mechanics, biologically inspired control in robotic systems, .fractional calculus applications in mechanics, active control in mechanical systems, estimation of life of structures, eigen sensitivity of mechanical structural systems, vector position tangent space, vector method based on the mass moment vectors applications, discrete continuum method, method of variation constants, dynamics of systems with frictions and other.

I hope, that this special issue will provoke interest and be a good addition to the quality of the Journal Theoretical and applied mechanics of our Serbian Society of Mechanics,

At Belgrade, October 2012.

Guest Editor
Katica (Stevanovic) Hedrih.

SERBIAN SCIENTIFIC SOCIETY

THEORETICAL AND APPLIED MECHANICS
TEORIJSKA I PRIMENJENA MEHANIKA

Special Issue

ADDRESS TO MECHANICS:
SCIENCE, TEACHING AND APPLICATIONS

GUEST EDITOR: KATICA R. (STEVANOVIĆ) HEDRIH

ON THE RESIDUAL MOTION IN DAMPED VIBRATING SYSTEMS

UDC 534.16

Ranislav M. Bulatović

Faculty of Mechanical Engineering, University of Montenegro,
81 000 Podgorica, Crna Gora

Abstract. *In this paper, linear vibrating systems, in which the inertia and stiffness matrices are symmetric positive definite and the damping matrix is symmetric positive semi-definite, are studied. Such a system may possess undamped modes, in which case the system is said to have residual motion. Several formulae for the number of independent undamped modes, associated with purely imaginary eigenvalues of the system, are derived. The main results formulated for symmetric systems are then generalized to asymmetric and symmetrizable systems. Several examples are used to illustrate the validity and application of the present results.*

Key words: *linear system, dissipation, residual motion*

1. INTRODUCTION

Some of the simplest and most fundamental vibrating systems can be described by a differential equation of the form

$$A\ddot{q} + B\dot{q} + Cq = 0 \, , \, q \in \Re^{n} \tag{1}$$

where A, B, and C are $n \times n$ constant real symmetric matrices, q is the n-dimensional vector of generalized coordinates and dots denote derivatives with respect to t (the time). The inertia matrix A and stiffness matrix C are positive definite (>0), and the damping matrix B may be positive definite or positive semi-definite (≥ 0). In the case $B > 0$ dissipation is complete, and the case $B \geq 0$ corresponds to incomplete dissipation. In the latter case the system is called partially dissipative (damped).

It is convenient, although not necessary, to rewrite equation (1) in the form

$$\ddot{x} + D\dot{x} + Kx = 0 \, , \tag{2}$$

using the congruent transformation $x = A^{1/2}q$, where $A^{1/2}$ denotes the unique positive definite square root of the matrix A, and $D = A^{-1/2}BA^{-1/2}$, and $K = A^{-1/2}CA^{-1/2}$.

All solutions $x(t)$ of the equation (2) (or $q(t)$ of (1)) can be characterized algebraically using properties of the quadratic matrix polynomial

$$L(\lambda) = \lambda^2 I + \lambda D + K, \tag{3}$$

where I is the identity matrix. The eigenvalues of the system are zeros of the characteristic polynomial

$$\Delta(\lambda) = \det(L(\lambda)) \tag{4}$$

Since (4) is a polynomial of degree 2n with respect to λ, there are 2n eigenvalues, counting multiplicities. If λ is an eigenvalue, the nonzero vectors X in the nullspace of $L(\lambda)$ are the eigenvectors associated with λ, i. e.,

$$L(\lambda)X = 0 \tag{5}$$

In general, eigenvalues and corresponding eigenvectors may be real or may appear in complex conjugate pairs.

If the dissipation is complete, it is well-known that the system (2) (or (1)) is asymptotically stable ($x(t) \to 0$ as $t \to \infty$ for all solutions $x(t)$), see [1]. On the other hand, the partially damped system (2) may or may not be asymptotically stable, although it is obviously stable in the Lyapunov sense (any solution of equation (2) remains bounded). Consequently, all eigenvalues of this system lie in the *closed* left-half of the complex plane ($\operatorname{Re}\lambda \le 0$). Notice that if the system is asymptotically stable, then $\operatorname{Re}\lambda < 0$.

Recently some attention has been paid to the question whether or not a damped system has pure imaginary eigenvalues, i. e., in the terminology of the mechanical vibrations, whether or not undamped modes are possible in such system (see [2] and quoted references). From the above discussion it is clear that nonexistence of undamped motions (also called "residual motions") is equivalent to the asymptotic stability of the system, and consequently, any test for asymptotic stability gives the answer of the question. A survey of the stability criteria for linear second order systems is given in [3]. Also, it should be mentioned that the paper [2] rediscovered an old criterion for asymptotic stability of the system [4], as was recently stressed in [5].

In this paper we are interested in the determination of the number of pure imaginary eigenvalues of the system without computing the zeros of the characteristic polynomial (4). The main result given in section 3 (Theorem 2) recently derived in our paper [6]. This result is based on the well-known condition of asymptotic stability [7], which coincides with the rank condition of controllability of a linear system (see [8]), and a transformation converting the system (2) into two uncoupled subsystems; one of them is r-dimensional undamped subsystem, where r is the number of conjugate pairs of purely imaginary eigenvalues of the system *including multiplicity*, the second is (n-r)-dimensional damped asymptotically stable subsystem. When the matrix K has *all distinct* eigenvalues, and r its eigenvectors lie in the nullspace of the damping matrix, the decomposability of the system in *modal* coordinates was observed in [4]. In sections 4 and 5, when one of two matrices D and K is transformed on diagonal form, two useful results are stated. Finally, in section 6 the results of section 3 are generalized to asymmetric and symmetrizable systems.

2. THE DECOMPOSABILITY OF THE SYSTEM

Theorem 1. Let $\pm i\omega_1,...,\pm i\omega_r$ be eigenvalues of $L(\lambda)$. Then there exists an orthogonal matrix Q such that

$$Q^T DQ = \hat{D} = \begin{pmatrix} 0_r & 0 \\ 0 & \hat{D}_{n-r} \end{pmatrix}, \qquad (6)$$

and

$$Q^T KQ = \hat{K} = \begin{pmatrix} \Omega_r & 0 \\ 0 & \hat{K}_{n-r} \end{pmatrix}, \qquad (7)$$

where 0_r is the zero square matrix of order r, and $\Omega_r = diag(\omega_1^2,...,\omega_r^2)$.

To prove Theorem 1 we need the following lemmas.

Lemma 1. Let $(i\omega, X), \omega \in \Re, i = \sqrt{-1}$, be an eigenpair of $L(\lambda)$. Then (ω^2, X) and $(0, X)$ are eigenpairs of the matrices K and D, respectively.

Proof. From

$$L(i\omega)X = (-\omega^2 I + i\omega D + K)X = 0, \qquad (8)$$

we obtain

$$< X, (K - \omega^2 I)X > + i\omega < X, DX >= 0, \qquad (9)$$

where $< .,. >$ denotes the inner product, and $< X, (K - \omega^2 I)X >$, and $< X, DX >$ are real quantities, since K and D are real symmetric matrices. Then $< X, DX >=0$, which implies $DX = 0$, since $D \geq 0$. This together with $L(i\omega)X = 0$ gives $KX = \omega^2 X$. $\square$

It is clear that the eigenvector X in Lemma 1 can be taken to be *unit* ($< X, X >= 1$) and *real*.

Lemma 2. a) If $(i\omega_1, X^{(1)})$ and $(i\omega_2, X^{(2)})$ are eigenpairs of $L(\lambda)$ with $\omega_1^2 \neq \omega_2^2$, then $< X^{(1)}, X^{(2)} >= 0$.

b) If the eigenvalue $i\omega$ of $L(\lambda)$ has multiplicity k, it possesses k eigenvectors which are mutually orthogonal.

Proof. a) The result follows from Lemma 1 and the additional fact that eigenvectors associated with distinct eigenvalues of a symmetric matrix are orthogonal.

b) Since the system (2) is stable, the multiple eigenvalue $i\omega$ must be semi-simple, which means that the eigenvalue has k linearly independent eigenvectors. Since a linear combination of these k vectors is also an eigenvector of $L(\lambda)$ associated with $i\omega$, the Gram-Schmidt process (see [9]) can be used to obtain k mutually orthogonal eigenvectors. $\square$

It is follows from Lemma 1 and 2 that the number of independent undamped modes is equal to the number of conjugate pairs of purely imaginary eigenvalues (natural frequencies), including multiplicity.

Proof of Theorem 1. By lemmas 1 and 2, there exists an orthonormal set of r vectors $X^{(1)},..., X^{(r)}$, such that

$$DX^{(j)} = 0 \, , \, KX^{(j)} = \omega_j^2 X^{(j)} \, , \, \text{j=1,…,r} \qquad (10)$$

Now, consider an orthogonal matrix Q having the vectors $X^{(1)}, …, X^{(r)}$ as its first r columns,

$$Q = (X^{(1)}, …, X^{(n)}) \qquad (11)$$

The matrices D and K are then orthogonally congruent to matrices $\hat{D}$ and $\hat{K}$, respectively, described by

$$\hat{D} = Q^T D Q = (< X^{(i)}, D X^{(j)} >) \qquad (12)$$

and

$$\hat{K} = Q^T K Q = (< X^{(i)}, K X^{(j)} >) \, , \qquad (13)$$

where i,j = 1,…,n. Using (10) and $< X^{(i)}, X^{(j)} >= \delta_{ij}$, where δ_{ij} is the Kronecker delta and i,j = 1,…,n, we compute

$$< X^{(i)}, D X^{(j)} >= 0 \qquad (14)$$

and

$$< X^{(i)}, K X^{(j)} >= \omega_j^2 \delta_{ij} \, , \qquad (15)$$

where i = 1,…,n and j = 1,…,r. The relations (14) and (15) show that $\hat{D}$ and $\hat{K}$ have the partitioned forms (6) and (7). $\square$

3. THE MAIN RESULTS

Introduce the $n \times n^2$ matrix

$$\Phi = \left(D \,\vdots\, KD \,\vdots\, . \,\vdots\, . \,\vdots\, . \,\vdots\, K^{n-1}D \right) \qquad (16)$$

which plays key role in a test for asymptotic stability of the system [7].

Theorem 2. The system (2) has $r = n - rank\Phi$ conjugate pairs of purely imaginary eigenvalues, including multiplicity.

Corollary 1. If $rankD = m$, then $0 \le r \le n - m$.

This follows immediately from $rankD \le rank\Phi \le n$.

Proof of Theorem 2. Suppose that $\Delta(\pm i\omega_j) = 0$, $\omega_j \in \Re$, j = 1,…,r and that remaining zeros of $\Delta(\lambda)$ take places on the open left-half of the complex plane. Then from Theorem 1 it follows that there exists an orthogonal coordinate transformation

$$x = Q \left(\frac{y}{z} \right), \, y \in \Re^r \, , \, z \in \Re^{n-r} \, , \qquad (17)$$

which transforms equation (2) to the form

$$\left(\frac{\ddot{y}}{\ddot{z}} \right) + \hat{D} \left(\frac{\dot{y}}{\dot{z}} \right) + \hat{K} \left(\frac{y}{z} \right) = \left(\frac{0}{0} \right) \qquad (18)$$

where $\hat{D}$ and $\hat{K}$ have the partitioned forms (6) and (7). Under the above assumptions it is clear that the (n-r) dimensional subsystem of (18)

$$\ddot{z} + \hat{D}_{n-r} \dot{z} + \hat{K}_{n-r} z = 0 \, , \, z \in \Re^{n-r} \qquad (19)$$

is asymptotically stable and, according to well-known result [7], we have

$$rank\left(\hat{D}_{n-r} \;\vdots\; \hat{K}_{n-r}\hat{D}_{n-r} \;\vdots\;.\;\vdots\;.\;\vdots\;.\;\vdots\; \hat{K}_{n-r}^{n-r-1}\hat{D}_{n-r}\right) = n - r \qquad (20)$$

On the other hand, the matrix Φ coincides with the matrix

$$Q\left(\hat{D} \;\vdots\; \hat{K}\hat{D} \;\vdots\;.\;\vdots\;.\;\vdots\;.\;\vdots\; \hat{K}^{n-1}\hat{D}\right)P , \qquad (21)$$

where $P = diag(Q^T,...,Q^T)$. Then

$$rank\Phi = rank\left(\hat{D}_{n-r} \;\vdots\; \hat{K}_{n-r}\hat{D}_{n-r} \;\vdots\;.\;\vdots\;.\;\vdots\;.\;\vdots\; \hat{K}_{n-r}^{n-1}\hat{D}_{n-r}\right), \qquad (22)$$

since Q and P are nonsingular, and $\hat{D} = diag(0_r, \hat{D}_{n-r})$, and $\hat{K}^j\hat{D} = diag(0_r,$ $\hat{K}_{n-r}^j\hat{D}_{n-r})$. Now, according to the Cayley-Hamilton theorem (see [9]), every matrix $\hat{K}_{n-r}^j\hat{D}_{n-r}$ with integer j ≥ n-r can be represented by a linear combination of the matrices $\hat{D}_{n-r}$, $\hat{K}_{n-r}\hat{D}_{n-r}$, ..., $\hat{K}_{n-r}^{n-r-1}\hat{D}_{n-r}$, and, consequently

$$rank\left(\hat{D}_{n-r} \;\vdots\;.\;\vdots\;.\;\vdots\;.\;\vdots\; \hat{K}_{n-r}^{n-1}\hat{D}_{n-r}\right) = rank\left(\hat{D}_{n-r} \;\vdots\;.\;\vdots\;.\;\vdots\; \hat{K}_{n-r}^{n-r-1}\hat{D}_{n-r}\right) \qquad (23)$$

The result then follows from (20), (22) and (23). □

Remark 1. The matrix (16) can be expressed in terms of the original matrices as

$$\Phi = A^{-1/2}\widetilde{\Phi}diag(A^{-1/2},...,A^{-1/2}) , \qquad (24)$$

where

$$\widetilde{\Phi} = \left(B \;\vdots\; (CA^{-1})B \;\vdots\;.\;\vdots\;.\;\vdots\; (CA^{-1})^{n-1}B\right) \qquad (25)$$

Consequently, $rank\Phi = rank\widetilde{\Phi}$, since A is nonsingular.

In the case of "classical damping" in which D and K commute the following result as a consequence of Theorem 2 can be obtained.

Theorem 3. If $DK = KD$, then the system has $r = n - rankD$ conjugate pairs of purely imaginary eigenvalues.

Proof. Since D and K commute there exists an orthogonal matrix such that both D and K are orthogonally congruent to diagonal matrices [9]. Then, evidently, $rank\Phi = rankD$, and Theorem 3 follows from Theorem 2. □

In the next, two examples are given to illustrate the application of the above results.

Example 1. Consider the two-degree-of-freedom system shown in Fig. 1, where $c_i > 0$ and $\beta > 0$ stand for the spring constants and coefficient of viscous damping, respectively, and q_1 and q_2 are the displacements from equilibrium positions of masses m_1 and m_2 .

Fig. 1 The system of example

The inertia, damping and stiffness matrices of this system are as follows

$$A = \begin{pmatrix} m_1 & 0 \\ 0 & m_2 \end{pmatrix}, B = \beta\begin{pmatrix} 1 & -1 \\ -1 & 1 \end{pmatrix}, C = \begin{pmatrix} c_1 & 0 \\ 0 & c_2 \end{pmatrix} \qquad (26)$$

It is clear that $rankB = 1$, and consequently, the system is partially damped. The matrix (25) takes the form

$$\tilde{\Phi} = \beta \begin{pmatrix} 1 & -1 & \dfrac{c_1}{m_1} & -\dfrac{c_1}{m_1} \\ -1 & 1 & -\dfrac{c_2}{m_2} & \dfrac{c_2}{m_2} \end{pmatrix} \tag{27}$$

Thus, by Theorem 2, we have

$$r = 2 - rank\tilde{\Phi} = \begin{cases} 0, c_1 m_2 \neq c_2 m_1 \\ 1, c_1 m_2 = c_2 m_1 \end{cases} \tag{28}$$

In the case $c_1 m_2 = c_2 m_1$, the system can oscillate such that relative motion between the masses is absent, so that the damper dissipates no energy. If $c_1 m_2 \neq c_2 m_1$, the system does not have pure imaginary eigenvalues, and all motions lead up to dissipation of energy.

Example 2. Consider the three-degree-of-freedom system (2) with

$$D = \begin{pmatrix} 1 & 0 & -1 \\ 0 & 0 & 0 \\ -1 & 0 & 1 \end{pmatrix}, \text{ and } K = \begin{pmatrix} 2 & -1 & 0 \\ -1 & 2 & -1 \\ 0 & -1 & 2 \end{pmatrix}, \tag{29}$$

previously studied in [10].

It can be easily verified that $rankD = 1$, and that $DK = KD$. Thus, by Theorem 3, system of this example has two conjugate pairs of purely imaginary eigenvalues.

4. THE CASE WHEN K IS DIAGONAL (PRINCIPAL COORDINATES)

It is well known that there exists an orthogonal matrix Q such that

$$Q^T KQ = \Omega = diag(\omega_1^2 I_{n_1}, ..., \omega_k^2 I_{n_k}), \tag{30}$$

where ω_j and I_{n_j} denote the distinct natural frequencies of the undamped system ($D = 0$ in (2)) with multiplicity $n_j \geq 1$ and the identity matrices of order n_j, $n_1 + ... + n_k = n$. Multiple natural frequencies are typical in vibrating systems with symmetry or as a result of optimization.

On transforming to principal (modal) coordinates defined by $p = Q^T x$ and using (30), (2) reduces to

$$\ddot{p} + R\dot{p} + \Omega p = 0, \tag{31}$$

where the matrix $R = Q^T DQ$ is known as the modal damping matrix. Form a consistent partition of R with Ω:

$$R = \begin{pmatrix} R_{11} & R_{12} & \cdot & R_{1k} \\ R_{21} & R_{22} & \cdot & R_{2k} \\ \cdot & \cdot & \cdot & \cdot \\ R_{k1} & R_{k2} & \cdot & R_{kk} \end{pmatrix} \tag{32}$$

We need the following statement.

Lemma 3. The system (31) is asymptotically stable if and only if $n_j = rankR_{jj}$, j = 1, ...,k.

Proof. See [11]. □

Theorem 4. The system (31) has $r = n - \sum_{j=1}^{k} rankR_{jj}$ conjugate pairs of purely imaginary eigenvalues, including multiplicity. If $\omega_j i$ is an eigenvalue of the system, then its multiplicity is equal to $n_j - rankR_{jj}$.

Proof. It follows from Theorem 1 and Lemma 3. □

Since $rankR_{jj} \le m = rankR$, the next result recently formulated in [5] follows directly from Theorem 4.

Corollary 2. If $\max_j(n_j) > rankR$, then system (31) has residual motion.

Next, we apply Theorem 4 to the example 1. For this example, the matrices R and Ω take the forms

$$R = \frac{\beta}{\sqrt{m_1 m_2}} \begin{pmatrix} \sqrt{m_2/m_1} & -1 \\ -1 & \sqrt{m_1/m_2} \end{pmatrix}, \Omega = \begin{pmatrix} c_1/m_1 & 0 \\ 0 & c_2/m_2 \end{pmatrix} \tag{33}$$

Thus, by Theorem 4, $r = 0$ if $c_1 m_2 \ne c_2 m_1$, i. e., the system does not have residual motion (the system is asymptotically stable), and $r = 1$ if $c_1 m_2 = c_2 m_1$.

5. THE CASE WHEN D IS DIAGONAL

Since $D = D^T \ge 0$ and $rankD = m$, there exists an orthogonal matrix Q such that

$$S = Q^T D Q = \begin{pmatrix} S_{11} & 0 \\ 0 & 0 \end{pmatrix} \tag{34}$$

where $S_{11} = diag(s_1,...,s_m,0,...,0)$, $s_j > 0$ for all j = 1,...,m. By the coordinate transformation

$$x = Q \begin{pmatrix} u \\ v \end{pmatrix}, u \in \Re^m, v \in \Re^{n-m} \tag{35}$$

the system (2) reduces to the form

$$\begin{pmatrix} \ddot{u} \\ \ddot{v} \end{pmatrix} + \begin{pmatrix} S_{11} & 0 \\ 0 & 0 \end{pmatrix} \begin{pmatrix} \dot{u} \\ \dot{v} \end{pmatrix} + \begin{pmatrix} P_{11} & P_{12} \\ P_{21} & P_{22} \end{pmatrix} \begin{pmatrix} u \\ v \end{pmatrix} = \begin{pmatrix} 0 \\ 0 \end{pmatrix} \tag{36}$$

where

$$P = Q^T K Q = \left(\begin{array}{c|c} P_{11} & P_{12} \\ \hline P_{21} & P_{22} \end{array} \right)$$ (37)

is the transformed stiffness matrix written in the consistent partitioned form with (34).

Introduce the (n-m)xm(n-m) matrix

$$F = \left(P_{21} \mid P_{22}P_{21} \mid ... \mid P_{22}^{n-m-1}P_{21} \right)$$ (38)

Lemma 4. $rank\Phi = m + rankF$.

Proof. Substituting (34) and (37) into (16), after some rank persevering manipulations, we obtain

$$rank\Phi = rank \left(\begin{array}{c|c|c|c|c|c|c} S_{11} & 0 & 0 & 0 & ... & 0 & 0 \\ \hline 0 & P_{21} & P_{22}P_{21} & P_{22}^2 P_{21} & ... & P_{22}^{n-1}P_{21} & 0 \end{array} \right)$$ (39)

Since every matrix $P_{22}^j P_{21}$ with $j \geq n - m$, according to the Cayley-Hamilton theorem, can be represented by a linear combination of the matrices P_{21}, $P_{22}P_{21}$, …, $P_{22}^{n-m-1}P_{21}$ the lemma is proved. □

Theorem 5. The system (36) has $r = n - m - rankF$ conjugate pairs of purely imaginary eigenvalues, including multiplicity.

Proof. It directly follows from Theorem 2 and Lemma 4. □

Let us give an example illustrating Theorem 5.

Example 3. (taken from [2]). Consider the tree-degree-of-freedom system (2) with

$$D = \begin{pmatrix} 0 & 0 & 0 \\ 0 & 2 & 0 \\ 0 & 0 & 0 \end{pmatrix}, \text{ and } K = \begin{pmatrix} 3 & -2 & 0 \\ -2 & 5 & -3 \\ 0 & -3 & 3 \end{pmatrix}$$ (40)

The damping matrix is positive semi-definite with m $= rankD = 1$, whereas the stiffness matrix is positive definite. By the orthogonal matrix

$$Q = \begin{pmatrix} 0 & 1 & 0 \\ 1 & 0 & 0 \\ 0 & 0 & 1 \end{pmatrix}$$ (41)

we obtain

$$S = Q^T DQ = \left(\begin{array}{c|cc} 2 & 0 & 0 \\ \hline 0 & 0 & 0 \\ 0 & 0 & 0 \end{array} \right) \text{ and } P = Q^T KQ = \left(\begin{array}{c|cc} 5 & -2 & -3 \\ \hline -2 & 3 & 0 \\ -3 & 0 & 3 \end{array} \right)$$ (42)

The matrix F takes the form

$$F = \begin{pmatrix} -2 & -6 \\ -3 & -9 \end{pmatrix}$$ (43)

Thus, by Theorem 5, we have $r = (3-1) - rankF = 1$. This fact can be corroborated by computing the eigenvalues of the system; the eigenvalues are

$$\pm 1.7321i , \quad -0.4203 \pm 0.3473i , \quad -0.5797 \pm 2.5283i .$$

6. SOME GENERALIZATIONS TO ASYMMETRIC SYSTEMS

In this section, it is shown that theorems 2 and 3 can be generalized for a class of asymmetric systems (i. e., the symmetry restriction are not met by inertia, damping and stiffness matrices) commonly known as symmetrizable systems. Asymmetric coefficient matrices appear in problems involving follower forces, gyroscopy, aero-/hydro-elasticity and control effects, etc.

Assuming that the inertia matrix A is nonsingular, the equations of motion can be written as

$$\ddot{q} + A^{-1}B\dot{q} + A^{-1}Cq = 0 \tag{44}$$

The symmetrizable systems are defined in [12] as systems that have symmetrizable matrices $A^{-1}B$ and $A^{-1}C$, i. e., such that factorizations $A^{-1}B = S_1 S_2$ and $A^{-1}C = S_1 S_3$ are permissible, where S_1 is symmetric and positive definite, while S_2 and S_3 need only be symmetric. Additionally, it is supposed that $A^{-1}B$ has nonnegative real eigenvalues and $A^{-1}C$ has positive real eigenvalues. Then, S_2 and S_3 are positive semi-definite and positive definite, respectively, and the system described by (44) is stable [12]. Consequently, all eigenvalues of this system lie in the closed left-half of the complex plane.

Using the transformation $q = S_1^{1/2}x$, Eq. (44) is reduced to

$$\ddot{x} + D\dot{x} + Kx = 0 , \tag{45}$$

where $D = D^T = S_1^{1/2}S_2 S_1^{1/2}$ and $K = K^T = S_1^{1/2}S_3 S_1^{1/2}$. Since $D = D^T \geq 0$ and $K = K^T > 0$, the results developed in the section 3 can be applied to Eq. (45). From the factorizations of $A^{-1}B$ and $A^{-1}C$, we have

$$D = S_1^{-1/2}A^{-1}BS^{1/2} \tag{46}$$

and

$$K = S_1^{-1/2}A^{-1}CS^{1/2} \tag{47}$$

Substituting (46) and (47) into (16) results in

$$\Phi = S_1^{-1/2}\overline{\Phi}diag\,(S_1^{1/2},...,S_1^{1/2}) , \tag{48}$$

where

$$\overline{\Phi} = \left(A^{-1}B \,\vdots\, A^{-1}CA^{-1}B \,\vdots\,.\,\vdots\,.\,\vdots\,.\,\vdots\, (A^{-1}C)^{n-1}A^{-1}B\right) \tag{49}$$

It is clear that $rank\Phi = rank\overline{\Phi}$. Thus, the following proposition is proved.

Theorem 6. The symmetrizable system described by Eq. (44), where $A^{-1}B$ and $A^{-1}C$ have non-negative and positive eigenvalues, respectively, has $r = n - rank\overline{\Phi}$ conjugate pairs of purely imaginary eigenvalues.

Remark 2. It is clear that $rank\overline{\Phi}$ is the same as rank of the matrix (25), because $\tilde{\Phi} = A\overline{\Phi}$.

Also, the following result can be easily established.

Theorem 7. Suppose that $A^{-1}B$ and $A^{-1}C$ have non-negative and positive eigenvalues, respectively. If $A^{-1}B$ and $A^{-1}C$ commute in multiplication, then the system (44) has $r = n - rank(A^{-1}B)$ conjugate pairs of purely imaginary eigenvalues.

Example 4. Consider the asymmetric system described by

$$\ddot{q} + \begin{pmatrix} 2 & 4 \\ 1 & 2 \end{pmatrix}\dot{q} + \begin{pmatrix} 4 & 4 \\ 1 & 4 \end{pmatrix}q = 0 \tag{50}$$

Here note that

$$A^{-1}B = \begin{pmatrix} 2 & 4 \\ 1 & 2 \end{pmatrix} = \begin{pmatrix} 1.2461 & -0.2769 \\ -0.2769 & 0.3115 \end{pmatrix}\begin{pmatrix} 2.8889 & 5.7778 \\ 5.7778 & 11.5556 \end{pmatrix}, \tag{51}$$

and

$$A^{-1}C = \begin{pmatrix} 4 & 4 \\ 1 & 4 \end{pmatrix} = \begin{pmatrix} 1.2461 & -0.2769 \\ -0.2769 & 0.3115 \end{pmatrix}\begin{pmatrix} 4.8897 & 7.5573 \\ 7.5573 & 19.5599 \end{pmatrix}, \tag{52}$$

so that the coefficient matrices have a common positive definite factor. On the other hand, the eigenvalues of $A^{-1}B$ in this example are 0 and 4, and those of $A^{-1}C$ are 2 and 6. Hence, $A^{-1}B$ and $A^{-1}C$ have nonnegative and positive real eigenvalues, respectively. Thus, the Theorem can be applied. The matrix (49) takes the form

$$\overline{\Phi} = \begin{pmatrix} 2 & 4 & 12 & 24 \\ 1 & 2 & 6 & 12 \end{pmatrix} \tag{53}$$

and, consequently, $r = 2 - rank\overline{\Phi} = 1$. This is in agreement with the eigenvalue calculation for the system, which yields $\lambda_{1,2} = \pm i\sqrt{2}$ and $\lambda_{3,4} = -2 \pm i\sqrt{2}$.

Finally, observe that $A^{-1}B$ and $A^{-1}C$ commute for this example, $rank(A^{-1}B) = 1$, and, according to the Theorem 7 , $r = 1$.

REFERENCES

1. Vujičić V. A., Theory of oscillation (in Serbian), Naučna knjiga, Belgrade, 1977.
2. Shahruz S. M. and Kessler P., Residual motion in damped linear systems, Journal of Sound and Vibration, 276, (2004), 1093-1100.
3. Pommer C. and Kliem W., Recent results on the stability and response bounds of linear systems: A Review, The Shock and Vibration Digest, 38, (2006), 489-496.
4. Moran T. J., A simple alternative to the Routh-Hurwitz criterion for symmetric systems, ASME Journal of Applied Mechanics, 37, (1970), 1168-1170.
5. Kliem W., Mailybaev A. A. and Pommer C., Conditions revisited for asymptotic stability of pervasive damped linear systems, Journal of Sound and Vibration, 298, (2006), 471-474.
6. Bulatović R. M., A note on the damped vibrating szstems, Theoretical and Applied Mechanics, 33, No 3, (2006), 213-221.
7. Wallker J. A. and Schmitendorf W. E., A simple test for asymptotic stability in partially dissipative symmetric systems, ASME Journal of Applied Mechanics, 40, (1973), 1120-1121.
8. Muller P. C. and Schiehlen W. O., Linear Vibrations, Martinus Nijhoff, Dordrecht, Netherlands, 1985.
9. Andjelić T. P., Matrices (in Serbian), Belgrade, 1977.
10. Wilms E. V. and Pinkney R. B., The finite residual motion of a damped three-degree-of-freedom vibrating system, Journal of Sound and Vibration, 224, (1999), 937-940.
11. Bulatović R. M. and Kažić M., On the dissipative systems with pervasive damping (in Serbian), Glasnik of the Section of Natural Sciences, Montenegrin Academy of Sciences and Arts, 17, (2007), 5-18.

12. Inman D. J., Dynamics of Asymmetric Nonconservative Systems, ASME Journal of Applied Mechanics, 50, (1983), 199-203.

O REZIDUALNOM KRETANJU PRIGUŠENO OSCILUJUĆIH SISTEMA

Ranislav M. Bulatović

U radu se razmatraju linearni oscilujući sistemi čije su matrice inercije i krutosti simetrične i pozitivno definitne a matrica prigušenja pozitivno semidefinitna. Izvedeno je nekoliko formula za određivanje broja nezavisnih neprigušenih modova koji odgovaraju imaginarnim sopstvenim vrijednostima razmatranih sistema. Ovi rezultati su uopšteni na klasu simetrizabilnih asimetričnih sistema. Ispravnost i pogodnost dobijenih rezultata je ilustrovana na nekoliko primjera..

Ključne riječi: *linearni system, prigušenje, rezidualno kretanje*

ON THE DETERMINATION OF SHIFTING OPERATORS ALONG GEODESICS ON A SURFACE

UDC 514.7, 517.9

Zoran Drašković

Bubnjaračka 28, Zagreb-Malešnica, Croatia (zoran.draskovic_643@yahoo.com)

Abstract: *A procedure to obtain a closed form of the shifting operators along a known geodesic line on a surface as a solution of a system of linear algebraic equations is proposed. Its correctness is numerically demonstrated in the case of a helicoid surface and a spherical one. The future use of these operators in finite element approximations of tensor fields in non-Euclidean spaces is announced.*

Key words: *surface, geodesic line, parallel transport, shifting operators*

1. INTRODUCTION

It is well known that the system of differential equations for determining the components of a vector **v** parallelly propagated along a curve $u^\alpha = u^\alpha(s)$ on a surface reads[1]

$$\frac{Dv^\alpha}{Ds} = \frac{dv^\alpha}{ds} + \Gamma^\alpha_{\beta\gamma}\, v^\beta\, \frac{du^\gamma}{ds} = 0 \quad, \tag{1}$$

where u^α are so-called surface coordinates, $\Gamma^\alpha_{\beta\gamma}$ are the Christoffel symbols of the second kind determined for this surface, and s is the arc length of this curve. The fundamental system of solutions $K^{.\alpha}_{\beta}$ of this homogeneous system of differential equations represents the operators of parallel transport (the shifting operators) with respect to the surface along this curve, establishing the relation

$$v^\alpha(P) = K^{.\alpha}_{\beta}(P_o, P)\; v^\beta(P_o) \tag{2}$$

between the components of the vector **v** before and after its parallel transport from the point P_o to the point P. However, the existence of this fundamental system, i.e. the existence of shifting operators along the given curve, does not necessarily mean it is easy

---

[1] Einstein's summation convention for diagonally repeated indices is used; Greek indices have the range {1,2}, while Latin indices will have the range {1,2,3}.

to find them. Namely, *"the explicit form of the function … [$K_\beta^{\cdot\alpha}$] is not known"* ([5], p. 260) and even in the case of the geodesic lines on a spherical surface (its great circles) the shifting operators are obtained in [6] by using a *heuristic* procedure (and not by solving the corresponding homogeneous system of differential equations).

2. ALGEBRAIC APPROACH IN THE DETERMINATION OF SHIFTING OPERATORS

Nevertheless, it turned out quite unexpectedly that one can obtain a *closed* form of these operators along a *known* geodesic line on a surface as a solution of a system of linear *algebraic* equations using the fact that the tangent vector of a geodesic is a parallel vector field along this line, i.e. the fact that

$$\frac{du^\alpha}{ds} = K_\beta^{\cdot\alpha}(P_o, P) \left. \frac{du^\beta}{ds}\right|_{P_o} \tag{3}$$

and the insufficiencies of these *two* conditions for the determination of the *four* coefficients $K_\beta^{\cdot\alpha}$ is surpassed by introducing an additional vector also *parallelly* propagated along the geodesic line

$$\mathbf{w} = \mathbf{n} \times \mathbf{t} \tag{4}$$

or in the component form

$$w_i = \varepsilon_{ijk} n^j t^k \quad . \tag{5}$$

Namely, this vector – permanently orthogonal to the tangent vector $\mathbf{t}$ of a geodesic line on this surface – is always in the tangent plane of the surface; $\mathbf{n}$ is the normal to the surface and hence (s. [1], p. 214)

$$n_i = \frac{1}{2}\varepsilon^{\alpha\beta}\varepsilon_{ijk} z_\alpha^j z_\beta^k \quad (\varepsilon_{\alpha\beta} = \sqrt{a}\, e_{\alpha\beta} \ , \ \varepsilon^{\alpha\beta} = e^{\alpha\beta}/\sqrt{a} \ , \ a \equiv \left| a_{\alpha\beta}\right|) \tag{6}$$

where z are the rectangular Cartesian coordinates, $z_\alpha^i \equiv \partial z^i/\partial u^\alpha$ and $\varepsilon_{ijk} = e_{ijk}$; for the tangent vector $\mathbf{t}$ we have

$$t^i = z_\alpha^i \, du^\alpha/ds \quad ; \tag{7}$$

the surface components of the vector $\mathbf{w}$ (lying in the surface tangent plane) are

$$w_\alpha = z_\alpha^i w_i \quad ; \tag{8}$$

in the case of the *orthogonal* coordinates u^α we have $w^\alpha = a^{\alpha\beta} w_\beta$ and finally $\qquad$ (9)

$$w^\alpha = a^{\alpha\beta} z_\beta^i w_i = a^{\alpha\beta} z_\beta^i \varepsilon_{ijk} n^j t^k = a^{\alpha\beta} z_\beta^i \varepsilon_{ijk} \delta^{j\ell} n_\ell z_\gamma^k \frac{du^\gamma}{ds} = \frac{1}{2} a^{\alpha\beta} z_\beta^i \varepsilon_{ijk} \delta^{j\ell} \varepsilon^{\mu\nu} \varepsilon_{\ell mn} z_\mu^m z_\nu^n z_\gamma^k \frac{du^\gamma}{ds}.$$

Due to the parallel transport of the vector $\mathbf{w}$ along the geodesic line we have

$$w_o^\beta K_\beta^{\cdot\alpha}(P_o, P) = w_P^\alpha \tag{10}$$

and the coefficients $K_\beta^{\cdot\alpha}$ can now be determined from (3) and (10)

$$
\left.\begin{aligned}
K_1^{\cdot 1}(P_o,P) &= \frac{1}{\det}\begin{vmatrix} \left.\dfrac{du^1}{ds}\right|_P & \left.\dfrac{du^2}{ds}\right|_{P_o} \\[2mm] w_P^1 & w_o^2 \end{vmatrix} & K_2^{\cdot 1}(P_o,P) &= \frac{1}{\det}\begin{vmatrix} \left.\dfrac{du^1}{ds}\right|_{P_o} & \left.\dfrac{du^1}{ds}\right|_P \\[2mm] w_o^1 & w_P^1 \end{vmatrix} \\[8mm]
K_1^{\cdot 2}(P_o,P) &= \frac{1}{\det}\begin{vmatrix} \left.\dfrac{du^2}{ds}\right|_P & \left.\dfrac{du^2}{ds}\right|_{P_o} \\[2mm] w_P^2 & w_o^2 \end{vmatrix} & K_2^{\cdot 2}(P_o,P) &= \frac{1}{\det}\begin{vmatrix} \left.\dfrac{du^1}{ds}\right|_{P_o} & \left.\dfrac{du^2}{ds}\right|_P \\[2mm] w_o^1 & w_P^2 \end{vmatrix}
\end{aligned}\right\} \;,\qquad (11)
$$

where

$$
\det = \begin{vmatrix} \left.\dfrac{du^1}{ds}\right|_{P_o} & \left.\dfrac{du^2}{ds}\right|_{P_o} \\[2mm] w_o^1 & w_o^2 \end{vmatrix}\;. \tag{12}
$$

These expressions are implemented in the corresponding software tool in order to compare some numerical results with the formerly checked ones for the shifting operators on the spherical surface and exceptional coincidence is obtained!

However – bearing in mind that the relations (9) are not the promising ones concerning the determination of the explicit expressions for the shifting operators and that the *surface* components of the vector **w** are present in (11) – we can proceed directly, considering **w** as a vector in the tangent plane of the surface orthogonal to the tangent vector of a geodesic line on this surface; namely

$$
w^1 = -\frac{\sqrt{a_{22}}}{\sqrt{a_{11}}}\frac{du^2}{ds} \;,\qquad w^2 = \frac{\sqrt{a_{11}}}{\sqrt{a_{22}}}\frac{du^1}{ds} \;; \tag{13}
$$

hence for the coefficients $K_\beta^{\cdot\alpha}$ we obtain the expressions

$$
\left.\begin{aligned}
K_1^{\cdot 1}(P_o,P) &= \sqrt{a_o}\left(\frac{\sqrt{a_{11}^o}}{\sqrt{a_{22}^o}}\left.\frac{du^1}{ds}\right|_P\left.\frac{du^1}{ds}\right|_{P_o} + \frac{\sqrt{a_{22}^P}}{\sqrt{a_{11}^P}}\left.\frac{du^2}{ds}\right|_P\left.\frac{du^2}{ds}\right|_{P_o}\right) \\[4mm]
K_2^{\cdot 1}(P_o,P) &= -\sqrt{a_o}\left(\frac{\sqrt{a_{22}^P}}{\sqrt{a_{11}^P}}\left.\frac{du^2}{ds}\right|_P\left.\frac{du^1}{ds}\right|_{P_o} - \frac{\sqrt{a_{22}^o}}{\sqrt{a_{11}^o}}\left.\frac{du^1}{ds}\right|_P\left.\frac{du^2}{ds}\right|_{P_o}\right) \\[4mm]
K_1^{\cdot 2}(P_o,P) &= \sqrt{a_o}\left(\frac{\sqrt{a_{11}^o}}{\sqrt{a_{22}^o}}\left.\frac{du^2}{ds}\right|_P\left.\frac{du^1}{ds}\right|_{P_o} - \frac{\sqrt{a_{11}^P}}{\sqrt{a_{22}^P}}\left.\frac{du^1}{ds}\right|_P\left.\frac{du^2}{ds}\right|_{P_o}\right) \\[4mm]
K_2^{\cdot 2}(P_o,P) &= \sqrt{a_o}\left(\frac{\sqrt{a_{11}^P}}{\sqrt{a_{22}^P}}\left.\frac{du^1}{ds}\right|_P\left.\frac{du^1}{ds}\right|_{P_o} + \frac{\sqrt{a_{22}^o}}{\sqrt{a_{11}^o}}\left.\frac{du^2}{ds}\right|_P\left.\frac{du^2}{ds}\right|_{P_o}\right)
\end{aligned}\right\} \quad \left(a_o \equiv \left\|a_{\alpha\beta}\right\|_{P_o}\right) \quad (14)
$$

and in every single case one can try to find the explicit expressions for the components of the operators of parallel transport along the known geodesic line on the surface under consideration.

3. EXAMPLES

3.1. Operators of parallel transport along geodesics on a spherical surface

In order to obtain the effective expressions for these operators, we shall use the finite equation of the geodesic line (the great circle) on a spherical surface (with the radius $r \neq 0$) in the form (s. for example [4], p. 167)

$$\operatorname{tg} \vartheta = A \cos \varphi + B \sin \varphi \quad , \tag{15}$$

where $\{\varphi, \vartheta\}$ are the geographical coordinates ($u^1 \equiv \varphi$, $u^2 \equiv \vartheta$) and the constants A and B can be obtained from the condition of passing through the points $P_o(\varphi_o, \vartheta_o)$ and $P(\varphi_P, \vartheta_P)$

$$\left. \begin{aligned} \operatorname{tg} \vartheta_o &= A \cos \varphi_o + B \sin \varphi_o \\ \operatorname{tg} \vartheta_P &= A \cos \varphi_P + B \sin \varphi_P \end{aligned} \right\} \quad ; \tag{16}$$

hence it follows

$$\left. \begin{aligned} A = A(\varphi_o, \varphi_P, \vartheta_o, \vartheta_P) &= \frac{\sin \varphi_P \tan \vartheta_o - \tan \vartheta_P \sin \varphi_o}{\sin(\varphi_P - \varphi_o)} \\ B = B(\varphi_o, \varphi_P, \vartheta_o, \vartheta_P) &= \frac{\tan \vartheta_P \cos \varphi_o - \cos \varphi_P \tan \vartheta_o}{\sin(\varphi_P - \varphi_o)} \end{aligned} \right\} \quad . \tag{17}$$

Knowing that the components of the fundamental metric tensor in the system $\{\varphi, \vartheta\}$ are

$$a_{11} = a_{\varphi\varphi} = r^2 \cos^2 \vartheta \quad , \quad a_{12} = a_{21} = a_{\varphi\vartheta} = a_{\vartheta\varphi} = 0 \quad , \quad a_{22} = a_{\vartheta\vartheta} = r^2 \tag{18}$$

we have

$$ds^2 = a_{\alpha\beta} du^\alpha du^\beta = r^2 \left(\cos^2 \vartheta d\varphi^2 + d\vartheta^2 \right) \tag{19}$$

and, bearing in mind the relation (15), we obtain

$$\left. \begin{aligned} \frac{d\varphi}{ds} &= \pm \frac{1}{r \cos \vartheta \sqrt{1 + \cos^2 \vartheta \left(A \sin \varphi - B \cos \varphi \right)^2}} \\ \frac{d\vartheta}{ds} &= \mp \frac{\cos \vartheta \left(A \sin \varphi - B \cos \varphi \right)}{r \sqrt{1 + \cos^2 \vartheta \left(A \sin \varphi - B \cos \varphi \right)^2}} \end{aligned} \right\} \quad . \tag{20}$$

Using (17), we have for example

$$\left. \begin{aligned} \frac{d\varphi}{ds} \bigg|_o &= \frac{\sin(\varphi_P - \varphi_o)}{r \cos \vartheta_o \sqrt{\sin^2(\varphi_P - \varphi_o) + \cos^2 \vartheta_o \left[\cos(\varphi_P - \varphi_o) \tan \vartheta_o - \tan \vartheta_P \right]^2}} \\ \frac{d\vartheta}{ds} \bigg|_o &= -\frac{\cos \vartheta_o \left[\cos(\varphi_P - \varphi_o) \tan \vartheta_o - \tan \vartheta_P \right]}{r \sqrt{\sin^2(\varphi_P - \varphi_o) + \cos^2 \vartheta_o \left[\cos(\varphi_P - \varphi_o) \tan \vartheta_o - \tan \vartheta_P \right]^2}} \end{aligned} \right\} \tag{21}$$

and similarly

$$\left.\frac{d\varphi}{ds}\right|_P = \frac{\sin(\varphi_P - \varphi_o)}{r\cos\vartheta_P\sqrt{\sin^2(\varphi_P - \varphi_o) + \cos^2\vartheta_P\left[\cos(\varphi_P - \varphi_o)\tan\vartheta_P - \tan\vartheta_o\right]^2}}$$

$$\left.\frac{d\vartheta}{ds}\right|_P = \frac{\cos\vartheta_P\left[\cos(\varphi_P - \varphi_o)\tan\vartheta_P - \tan\vartheta_o\right]}{r\sqrt{\sin^2(\varphi_P - \varphi_o) + \cos^2\vartheta_P\left[\cos(\varphi_P - \varphi_o)\tan\vartheta_P - \tan\vartheta_o\right]^2}} \qquad (22)$$

Finally – substituting (21) and (22) in (14) – we obtain the following explicit expressions, in the geographical coordinates $\{\varphi, \vartheta\}$, for the operators of parallel transport with respect to a spherical surface along the geodesic line connecting $P_o(\varphi_o, \vartheta_o)$ and $P(\varphi_P, \vartheta_P)$

$$K_1^{\cdot 1}(P_o, P) = \frac{1}{S}\left\{\frac{\cos\vartheta_o}{\cos\vartheta_P}\sin^2(\varphi_P - \varphi_o) - \right.$$
$$\left. - \cos^2\vartheta_o\left[\cos(\varphi_P - \varphi_o)\tan\vartheta_P - \tan\vartheta_o\right]\left[\cos(\varphi_P - \varphi_o)\tan\vartheta_o - \tan\vartheta_P\right]\right\}$$

$$K_2^{\cdot 1}(P_o, P) = -\frac{1}{S}\sin(\varphi_P - \varphi_o)\left\{\left[\cos(\varphi_P - \varphi_o)\tan\vartheta_P - \tan\vartheta_o\right] + \right.$$
$$\left. + \frac{\cos\vartheta_o}{\cos\vartheta_P}\left[\cos(\varphi_P - \varphi_o)\tan\vartheta_o - \tan\vartheta_P\right]\right\}$$

$$K_1^{\cdot 2}(P_o, P) = \frac{1}{S}\sin(\varphi_P - \varphi_o)\left\{\cos\vartheta_P\cos\vartheta_o\left[\cos(\varphi_P - \varphi_o)\tan\vartheta_P - \tan\vartheta_o\right] + \right.$$
$$\left. + \cos^2\vartheta_o\left[\cos(\varphi_P - \varphi_o)\tan\vartheta_o - \tan\vartheta_P\right]\right\}$$

$$K_2^{\cdot 2}(P_o, P) = \frac{1}{S}\left\{\sin^2(\varphi_P - \varphi_o) - \right.$$
$$\left. - \cos\vartheta_P\cos\vartheta_o\left[\cos(\varphi_P - \varphi_o)\tan\vartheta_P - \tan\vartheta_o\right]\left[\cos(\varphi_P - \varphi_o)\tan\vartheta_o - \tan\vartheta_P\right]\right\} \qquad (23)$$

where

$$S \equiv \sqrt{\sin^2(\varphi_P - \varphi_o) + \cos^2\vartheta_o\left[\cos(\varphi_P - \varphi_o)\tan\vartheta_o - \tan\vartheta_P\right]^2} \times$$
$$\times \sqrt{\sin^2(\varphi_P - \varphi_o) + \cos^2\vartheta_P\left[\cos(\varphi_P - \varphi_o)\tan\vartheta_P - \tan\vartheta_o\right]^2} \qquad (24)$$

These expressions, in comparison with the ones in **Appendix**, have considerably simpler form. Concerning the correctness of (23), as well of the expressions (11) and (14), the accordance of the four groups of results (quoted in **Table 1.**) for an arbitrarily selected pair of points on the spherical surface represents a *numerical* confirmation of the usefulness of the previously obtained expressions for shifting operators.

3.2. Operators of parallel transport along geodesics on a helicoid surface

In the case of the helicoid surface

$$\left.\begin{aligned} z^1 &= \rho\cos\varphi \\ z^2 &= \rho\sin\varphi \\ z^3 &= b\varphi \end{aligned}\right\} \quad (b = const) \qquad (25)$$

the components of the fundamental metric tensor in the system $\{\rho, \varphi\}$ ($u^1 \equiv \rho$, $u^2 \equiv \varphi$) are

$$a = a = 1 \ , \ a = a = a = a = 0 \ , \ a = a = \rho + b \tag{26}$$

and we have

$$ds^2 = a_{\alpha\beta} du^{\alpha} du^{\beta} = d\rho^2 + \left(\rho^2 + b^2\right) d\varphi^2 \quad . \tag{27}$$

On the other side, the equation of the geodesic line on this surface can be found in the form (s. for example [3], p. 45)

$$\varphi = C \pm \int \frac{D \, d\rho}{\sqrt{\left(\rho^2 + b^2\right)\left(\rho^2 + b^2 - D^2\right)}} \tag{28}$$

and, bearing in mind (27), we obtain

$$\left. \begin{aligned} \frac{d\rho}{ds} &= \pm\sqrt{\frac{\rho^2 + b^2 - D^2}{\rho^2 + b^2}} \\ \frac{d\varphi}{ds} &= \pm\frac{D}{\rho^2 + b^2} \end{aligned} \right\} \quad . \tag{29}$$

Rewriting (28) in the form

$$\varphi = C \pm \int_{\rho_o}^{\rho} \frac{D \, dr}{\sqrt{\left(r^2 + b^2\right)\left(r^2 + b^2 - D^2\right)}} \quad , \tag{30}$$

we find $C = \varphi_o$ (from the condition that $\varphi = \varphi_o$ when $\rho = \rho_o$), while the constant D should be determined from the condition that

$$\varphi_P = \varphi_o \pm \int_{\rho_o}^{\rho_P} \frac{D \, dr}{\sqrt{\left(r^2 + b^2\right)\left(r^2 + b^2 - D^2\right)}} \quad . \tag{31}$$

Due to the monotony of the subintegral function in (31), it is relatively simple to obtain a sufficiently exact value of the constant D as a numerical solution of this equation. With such approximative value for D, the evaluation of the components of the operators of parallel transport along the geodesic line connecting the points $P_o(\rho_o, \varphi_o)$ and $P(\rho_P, \varphi_P)$ on a helicoid surface can be performed according to (14), using the expressions (26) and (29).

In this case, in order to examine the correctness of the whole proposed procedure, the numerical comparison is made between two approaches: the above described one using shifting operators and the one without these operators. In the first case the contravariant components of a vector **v** shifted on this surface from P_o to P is calculated according to the formula

$$v^{\alpha}(P) = K_{\beta}^{\alpha}(P_o, P) \, v^{\beta}(P_o) \tag{32}$$

(where $v^1 \equiv v^\rho$, $v^2 \equiv v^\varphi$) and the Cartesian components of this vector at the point P are determined in the usual way

$$v^i(P) = \frac{\partial z^i}{\partial \rho}\bigg|_P v^\rho(P) \; + \; \frac{\partial z^i}{\partial \varphi}\bigg|_P v^\varphi(P) \tag{33}$$

(but now $v^1 \equiv v^x \equiv v^{z^1}$, $v^2 \equiv v^y \equiv v^{z^2}$, $v^3 \equiv v^z \equiv v^{z^3}$). In the second case, the Cartesian components of the vector **v** are obtained directly (without introducing the notion of the operator of parallel transport with respect to a surface) from the condition that a vector shifted along a geodesic line must close a constant angle with this curve at each of its points (s. p. 143 in [2]). The results for an arbitrarily selected pair of points on the helicoid surface (with $b = h/2\pi$ and $h = 5$) are quoted in **Table 2**. and the accordance is evident.

4. CONCLUDING REMARKS AND FUTURE ACTIVITIES

The relatively simple and numerically efficient way to obtain the values of components of the operators of parallel transport along a *known* geodesic line passing through two arbitrarily selected points on a surface is described. Although this procedure – based on a solution of a system of linear algebraic equations – can be used to obtain the explicit *analytical* expressions for the shifting operators in some cases, the main benefit is a possibility of its use in the future *numerical* testing of an approach in finite element approximations of tensor fields in non-Euclidean spaces proposed in [7]. Namely, instead of the usual approximation of components of tensor fields, the approximation of the whole field (as a kernel) is performed and the operators of parallel transport play the fundamental role in such approach.

REFERENCES

1. Aris R., *Vectors, Tensors and the Basic Equations of Fluid Mechanics*, Prentice-Hall, Englewood Cliffs, New Jersey, 1962.
2. Anđelić T.P., *Tensor Calculus*, Naučna knjiga, Beograd, 1967. (in Serbian)
3. Rozendorn Eh.R., *Zadachi po differentsial'noj geometrii*, Nauka, Moskva, 1971.
4. Leko M.D. and Plavšić M., *Solved Problems in Tensor Calculus*, Građevinska knjiga, Beograd, 1973. (in Serbian)
5. Vujičić V.A., (1974), General finite equations of geodesics, *Tensor*, N. S., Vol. 28, pp. 259-262.
6. Drašković Z., (2001), Contribution to the discussion on absolute integration of differential equations of geodesics in non-Euclidean spaces, *Facta Universitatis, Series Mechanics, Automatic Control and Robotics*, Vol. 3, No 11, pp. 55-70.
7. Drašković Z., (2008), On finite element approximations in non-Euclidean spaces, *Proceedings of the 2nd Meeting of Croatian Society of Mechanics*, Split (in Croatian)

Table 1. Geographical components of the shifting operators along the geodesic line connecting the points P_o and P on a spherical surface

$\begin{aligned}P_o(\varphi_o,\vartheta_o)&=P_o(7^o,77^o)\\P(\varphi_P,\vartheta_P)&=P(13^o,78^o)\end{aligned}$	$\left\{K_\beta^{.\alpha}(P_o,P)\right\}=\begin{Bmatrix}K_1^{.1}(P_o,P)&K_2^{.1}(P_o,P)\\K_1^{.2}(P_o,P)&K_2^{.2}(P_o,P)\end{Bmatrix}$
heuristic approach	$\begin{Bmatrix}1.07630424872861&0.490918399454177\\-2.296023426624826\text{E}-2&0.994777456654368\end{Bmatrix}$
algebraic approach	$\begin{Bmatrix}1.07630424872861&0.490918399454179\\-2.296023426624818\text{E}-2&0.994777456654367\end{Bmatrix}$
algebraic approach	$\begin{Bmatrix}1.07630424872861&0.490918399454177\\-2.296023426624829\text{E}-2&0.994777456654367\end{Bmatrix}$
algebraic approach	$\begin{Bmatrix}1.07630424872861&0.490918399454182\\-2.296023426624850\text{E}-2&0.994777456654367\end{Bmatrix}$

Table 2. Cartesian components of a given vector after parallel transport from the point P_o to the point P along the geodesic line on a helicoid surface

$\begin{aligned}P_o(\rho_o,\varphi_o)\\\|\\P_o(1,85^o)\end{aligned}$	$\begin{aligned}P(\rho_P,\varphi_P)\\\|\\P(4,135^o)\end{aligned}$	*approach* *without* *shifters*	*approach* *with* *shifters*
$\mathbf{v}_o=\begin{Bmatrix}v_o^{\langle\rho\rangle}\\v_o^{\langle\varphi\rangle}\end{Bmatrix}=\begin{Bmatrix}1\\0\end{Bmatrix}$	$\mathbf{v}_P=\begin{Bmatrix}v_P^{z^1}\\v_P^{z^2}\\v_P^{z^3}\end{Bmatrix}=$	$\begin{Bmatrix}-2.184434556431047\text{E}-2\\0.990432849244363\\-0.136255626322580\end{Bmatrix}$	$\begin{Bmatrix}-2.184434556431003\text{E}-2\\0.990432849244364\\-0.136255626322580\end{Bmatrix}$

O ODREĐIVANJU OPERATORA PARALELNOG POMERANJA DUŽ GEODEZIJSKIH LINIJA NA POVRŠIMA

Zoran Drašković

Apstrakt: *Predložen je postupak za dobijanje zatvorenog oblika operatora paralelnog pomeranja duž poznate geodezijske linije na nekoj površi kao rešenja sistema linearnih algebarskih jednačina. Njegova korektnost numerički je pokazana na primeru sferne i helikoidalne površi. Nagoveštena je*

buduća upotreba tih operatora u aproksimacijama konačnim elementima tenzorskih polja u neeuklidskim prostorima.

Ključne reči: *površ, geodezijska linija, paralelno pomeranje, operatori paralelnog pomeranja*

Appendix: Operators of parallel transport along geodesics on a spherical surface (heuristic approach)

The explicit expressions – obtained in [6] by using a heuristic procedure – for the operators of parallel transport with respect to a spherical surface along the geodesic line (the great circle) connecting $P_o(\varphi_o, \vartheta_o)$ and $P(\varphi_P, \vartheta_P)$ read (geographical coordinates are in question!)

$$K_1^{\cdot 1}(P_o, P) = \frac{\cos \vartheta_o}{\cos \vartheta_P} \big\{ [\sin \overline{\varphi}_P \sin(\varphi_P - \psi_{Eu}) + \cos \overline{\varphi}_P \cos(\varphi_P - \psi_{Eu}) \cos \vartheta_{Eu}] \times$$
$$\times [\sin \overline{\varphi}_o \sin(\varphi_o - \psi_{Eu}) + \cos \overline{\varphi}_o \cos(\varphi_o - \psi_{Eu}) \cos \vartheta_{Eu}] +$$
$$+ \cos(\varphi_P - \psi_{Eu}) \cos(\varphi_o - \psi_{Eu}) \sin^2 \vartheta_{Eu} \big\}$$

$$K_2^{\cdot 1}(P_o, P) = \frac{1}{\cos \vartheta_P} \big\{ [\sin \overline{\varphi}_P \sin(\varphi_P - \psi_{Eu}) + \cos \overline{\varphi}_P \cos(\varphi_P - \psi_{Eu}) \cos \vartheta_{Eu}] \times$$
$$\times \big\{ \sin \vartheta_o [\sin \overline{\varphi}_o \cos(\varphi_o - \psi_{Eu}) - \cos \overline{\varphi}_o \sin(\varphi_o - \psi_{Eu}) \cos \vartheta_{Eu}] +$$
$$+ \cos \vartheta_o \sin \vartheta_{Eu} \cos \overline{\varphi}_o \big\} -$$
$$- \cos(\varphi_P - \psi_{Eu}) \sin \vartheta_{Eu} [\sin \vartheta_o \sin(\varphi_o - \psi_{Eu}) \sin \vartheta_{Eu} + \cos \vartheta_o \cos \vartheta_{Eu}] \big\}$$

$$K_1^{\cdot 2}(P_o, P) = \cos \vartheta_o \big\{ \{ \sin \vartheta_P [\sin \overline{\varphi}_P \cos(\varphi_P - \psi_{Eu}) - \cos \overline{\varphi}_P \sin(\varphi_P - \psi_{Eu}) \cos \vartheta_{Eu}] +$$
$$+ \cos \vartheta_P \sin \vartheta_{Eu} \cos \overline{\varphi}_P \} \times$$
$$\times [\sin \overline{\varphi}_o \sin(\varphi_o - \psi_{Eu}) + \cos \overline{\varphi}_o \cos(\varphi_o - \psi_{Eu}) \cos \vartheta_{Eu}] -$$
$$- \cos(\varphi_o - \psi_{Eu}) \sin \vartheta_{Eu} [\sin \vartheta_P \sin(\varphi_P - \psi_{Eu}) \sin \vartheta_{Eu} + \cos \vartheta_P \cos \vartheta_{Eu}] \big\}$$

$$K_2^{\cdot 2}(P_o, P) = \big\{ \sin \vartheta_P [\sin \overline{\varphi}_P \cos(\varphi_P - \psi_{Eu}) - \cos \overline{\varphi}_P \sin(\varphi_P - \psi_{Eu}) \cos \vartheta_{Eu}] +$$
$$+ \cos \vartheta_P \sin \vartheta_{Eu} \cos \overline{\varphi}_P \big\} \times$$
$$\times \big\{ \sin \vartheta_o [\sin \overline{\varphi}_o \cos(\varphi_o - \psi_{Eu}) - \cos \overline{\varphi}_o \sin(\varphi_o - \psi_{Eu}) \cos \vartheta_{Eu}] +$$
$$+ \cos \vartheta_o \sin \vartheta_{Eu} \cos \overline{\varphi}_o \big\} +$$
$$+ [\sin \vartheta_P \sin(\varphi_P - \psi_{Eu}) \sin \vartheta_{Eu} + \cos \vartheta_P \cos \vartheta_{Eu}] \times$$
$$\times [\sin \vartheta_o \sin(\varphi_o - \psi_{Eu}) \sin \vartheta_{Eu} + \cos \vartheta_o \cos \vartheta_{Eu}]$$

where

$$\cos \overline{\varphi}_o = \cos \vartheta_o \cos(\varphi_o - \psi_{Eu}) \quad , \quad \cos \overline{\varphi}_P = \cos \vartheta_P \cos(\varphi_P - \psi_{Eu})$$

$$\operatorname{tg} \psi_{Eu} = \frac{\sin \varphi_o \cos \vartheta_o \sin \vartheta_P - \sin \vartheta_o \sin \varphi_P \cos \vartheta_P}{\cos \varphi_o \cos \vartheta_o \sin \vartheta_P - \sin \vartheta_o \cos \varphi_P \cos \vartheta_P}$$

$$\cos \vartheta_{Eu} = \frac{\cos \varphi_o \cos \vartheta_o \sin \varphi_P \cos \vartheta_P - \sin \varphi_o \cos \vartheta_o \cos \varphi_P \cos \vartheta_P}{\sqrt{\begin{array}{l}(\sin \varphi_o \cos \vartheta_o \sin \vartheta_P - \sin \vartheta_o \sin \varphi_P \cos \vartheta_P)^2 + \\ + (\sin \vartheta_o \cos \varphi_P \cos \vartheta_P - \cos \varphi_o \cos \vartheta_o \sin \vartheta_P)^2 + \\ + (\cos \varphi_o \cos \vartheta_o \sin \varphi_P \cos \vartheta_P - \sin \varphi_o \cos \vartheta_o \cos \varphi_P \cos \vartheta_P)^2\end{array}}}$$

and ψ_{Eu} and ϑ_{Eu} are the Euler angles: the precession ψ_{Eu} is the angle of inclination of the line which represents the intersection of the plane OP_oP and the coordinate plane Oz^1z^2, while the nutation ϑ_{Eu} is the angle between the normals to the planes Oz^1z^2 and OP_oP (the angle of proper rotation is $\varphi_{Eu} = 0$).

DIFFERENT STRUCTURES ON SUBSPACES OF $Osc^k M$

UDC 534.16

Irena Čomić* and Radu Miron**

*Faculty of Technical Sciences, University of Novi Sad,Srbia,
e-mail: comirena@uns.ac.rs, irena.comic@gmail.com
website: http://imft.ftn.uns.ac.rs/~irena/
** Faculty of Mathematics "Al. I. Cuza", RO - 6600 Iasi, Romania
e-mail: radu.miron@uaic.ro

Abstract *The geometry of $Osc^k M$ spaces was introduced by R. Miron and Gh. Atanasiu in [6] and [7]. The theory of these spaces was developed by R. Miron and his cooperators from Romania, Japan and other countries in several books and many papers. Only some of them are mentioned in references. Here we recall the construction*

of adapted bases in $T(Osc^k M)$ and $T^*(Osc^k M)$, which are comprehensive with the J structure. The theory of two complementary family of subspaces is presented as it was done in [2] and [4].

The operators J, $\overline{J}$, θ, $\overline{\theta}$, p, p^* are introduced in the ambient space and subspaces. Some new relations between them are established. The action of these operators on Liouville vector fields are examined.

Math. Subject Classification 2000: *53B40, 53C60*

Key words and phrases: *projector operators, J structure, θ structure, subspaces in $Osc^k M$.*

1. TANGENT AND COTANGENT BUNDLES ON $Osc^k M$

Let $E = Osc^k M$ be a C^∞, $(k+1)n$ dimensional space. Some point $u \in E$ in some local chart has coordinates:

$$u = \left(y^{0a}, y^{1a}, \ldots, y^{ka} \right) = \left(y^{Aa} \right), \ A = \overline{0, k}, \ a = \overline{0, n}.$$

The set of allowable coordinate transformations are given by

$$y^{0a'} = y^{0a'}\left(y^{0a} \right) \ \text{ or } \ x^{a'} = x^{a'}\left(x^a \right) \tag{1.1}$$

$$y^{1a'} = (\partial_{0a} y^{0a'}) y^{1a} , \ \ \partial_{Aa} = \frac{\partial}{\partial y^{Aa}} , \ A = \overline{0,k} ,$$

$$y^{2a'} = (\partial_{0a} y^{1a'}) y^{1a} + (\partial_{1a} y^{1a'}) y^{2a} ,...,$$

$$y^{ka'} = (\partial_{0a} y^{(k-1)a'}) y^{1a} + (\partial_{1a} y^{(k-1)a'}) y^{2a} + ... + (\partial_{(k-1)a} y^{(k-1)a'}) y^{ka}$$

Theorem 1.1. *The transformations of type (1.1) form a pseudo-group.*

The natural basis $\overline{B}^*$ of $T^*(E)$ is

$$\overline{B}^* = \{ dy^{0a}, dy^{1a},..., dy^{ka} \} .$$

As elements of this basis are not transforming as tensors, we introduce the special adapted basis

$$\overline{B}^* = \{ \delta y^{0a} , \delta y^{1a} ,..., \ \delta y^{ka} \}$$

where

$$(1.2)$$

or shorter

$$\left[\delta y^b \right] = \left[M^{(b)}_{(c)} \right] \left[dy^c \right].$$ (1.3)

Theorem 1.2. *The necessary and sufficient conditions that δy^{Aa} are transformed as d -tensors, i.e.*

$$\delta y^{Aa'} = \frac{\partial x^{a'}}{\partial x^a} \delta y^{Aa} , \ A = \overline{0,k}$$ (1.4)

are the following equations:

$$M_{0b}^{1a}\partial_{0a}y^{0b'} = \binom{1}{0}M_{0c'}^{1b'}\partial_{0b}y^{0c'} + \partial_{0b}y^{1b'}, \qquad (1.5)$$

$$M_{0b}^{2a}\partial_{0a}y^{0b'} = \binom{2}{0}M_{0c'}^{2b'}\partial_{0b}y^{0c'} + \binom{2}{1}M_{0c'}^{1b'}\partial_{0b}y^{1c'} + \binom{2}{2}\partial_{0b}y^{2b'},...,$$

$$M_{0b}^{ka}\partial_{0a}y^{0b'} = \binom{k}{0}M_{0c'}^{kb'}\partial_{0b}y^{0c'} + \binom{k}{1}M_{0c'}^{(k-1)b'}\partial_{0b}y^{1c'} + ... + \binom{k}{k}\partial_{0b}y^{kb'}.$$

The natural basis $\overline{B}$ of $T(E)$ is

$$\overline{B} = \{\partial_{0a},\partial_{1a},...,\partial_{ka}\}.$$

The elements of this basis are not tensors, so we introduce the special adapted basis

$$B = \{\delta_{0a},\delta_{1a},...,\delta_{ka}\},$$

where

$$\left[\delta_{0a},\delta_{1a},..., \delta_{ka}\right] = \left[\partial_{0a},\partial_{1a},..., \partial_{ka}\right]\left[N_{(a)}^{(b)}\right], \qquad (1.6)$$

$$\left[N_{(a)}^{(b)}\right] = \begin{bmatrix} \binom{0}{0}\delta_a^b & 0 & 0 & \cdots & 0 \\[6pt] -\binom{1}{0}N_{0a}^{1b} & \binom{1}{1}\delta_a^b & 0 & \cdots & 0 \\[6pt] -\binom{2}{0}N_{0a}^{2b} & -\binom{2}{1}N_{0a}^{1b} & \binom{2}{2}\delta_a^b & \cdots & 0 \\[6pt] \vdots & & & & \\[6pt] -\binom{k}{0}N_{0a}^{kb} & -\binom{k}{1}N_{0a}^{(k-1)b} & -\binom{k}{2}N_{0a}^{(k-2)b} & \cdots & \binom{k}{k}\delta_a^b \end{bmatrix} \begin{bmatrix} dy^{0c} \\ dy^{1c} \\ dy^{2c} \\ \vdots \\ dy^{kc} \end{bmatrix} \quad (1.7)$$

or shorter

$$[\delta_a] = [\partial_b][N_{(a)}^{(b)}]. \qquad (1.8)$$

Theorem 1.3. *The necessary and sufficient conditions that* δy_{Aa}, $A = \overline{0,k}$ *are transformed as d -tensors, i.e.*

$$\delta_{Aa'} = \frac{\partial x^a}{\partial x^{a'}}\delta_{Aa} \quad (= (\partial_{0a'}y^{0a})\delta_{Aa}) \qquad (1.9)$$

are the following equations:

$$N_{0a'}^{Bb'}(\partial_a x^{a'}) = N_{0a}^{Bc}\partial_{Bc}y^{Bb'} + N_{0a}^{(B-1)c}\partial_{(B-1)c}y^{Bb'} + ... + N_{0a}^{1c}\partial_{1c}y^{Bb'} - \partial_{0a}y^{Bb'}), \quad (1.10)$$

$$1 \le B \le k \ .$$

Theorems 1.2 and 1.3 first time was proved in [6] and [7] for the special adapted bases B and B^* which are comprehensive with the structure J . In [6] and [7] one solution of (1.5) and (1.10) using only the metric tensor in $M(x^a)$ was given. They are formally different from these theorems because in [5]-[12] instead of y^{Aa} from (1.1) it appears $\dfrac{y^{Aa}}{A!}$, $A = \overline{1,k}$.

Theorem 1.4. *If the bases* $\overline{B^*}$ *and* $\overline{B}$ *are dual to each other, then* B^* *and* B *will be dual if* $NM = I$ *i.e. the matrices* N *and* M *are inverse to each other.*

Proof. By assumption is $\left[dy^c\right]\left[\partial_b\right] = \delta_b^c I$. From (1.3) and (1.8) we have

$$[\delta y^d][\delta_a] = [M_{(c)}^{(d)}][dy^c][\partial_b][N_{(a)}^{(b)}] = [M_{(b)}^{(d)}]\delta_b^c I[N_{(a)}^{(b)}] = [M_{(b)}^{(d)}][N_{(a)}^{(b)}] = \delta_a^d I \quad (1.11)$$

In this form, Theorem 1.4 was proved in [2], [3], but in the explicit form it was given already in [6], [7].

2. THE PROJECTION OPERATORS

The projection operators are well known in linear algebra. Here they are presented in the tensor form in the special adapted bases of $Osc^k M$.

Let us denote by $H^*, V_1^*, V_2^*,...,V_k^*$ the subspaces of $T^*(E)$ generated by $\{\delta y^{0a}\}, \{\delta y^{1a}\},..., \{\delta y^{ka}\}$ respectively. The following decomposition is true:

$$T^*(E) = H^* \oplus V_1^* \oplus V_2^* \oplus ... \oplus V_k^* \ .$$

Let us denote by $H, V_1, V_2,...,V_k$ the subspaces of $T(E)$ generated by $\{\delta_{0a}\}, \{\delta_{1a}\}, \{\delta_{2a}\}..., \{\delta_{ka}\}$ respectively. Then

$$T(E) = H \oplus V_1 \oplus V_2 \oplus ... \oplus V_k \ .$$

If $X \in T(E)$, then we can write

$$X = X^{0a}\delta_{0a} + X^{1a}\delta_{1a} + X^{2a}\delta_{2a} + ... + X^{ka}\delta_{ka} = X^{Aa}\delta_{Aa} \qquad (2.1)$$

Let us define $p, p_1, p_2,..., p_k$, the projector operators of $T(E)$ on $H, V_1, V_2,...,V_k$ respectively, where:

$$p_0 = \delta_{0b} \otimes \delta y^{0b} = \left[\delta_{0b}\delta_{1b}...\delta_{kb}\right]\begin{bmatrix} 1 & 0 & \cdots & 0 \\ 0 & 0 & \cdots & 0 \\ \vdots & & & \\ 0 & 0 & \cdots & 0 \end{bmatrix} \otimes \begin{bmatrix} \delta y^{0b} \\ \delta y^{1b} \\ \vdots \\ \delta y^{kb} \end{bmatrix}, \tag{2.2}$$

$$p_1 = \delta_{1b} \otimes \delta y^{1b},$$

$$\vdots$$

$$p_0 = \delta_{0b} \otimes \delta y^{0b} = \left[\delta_{0b}\delta_{1b}...\delta_{kb}\right]\begin{bmatrix} 1 & 0 & \cdots & 0 \\ 0 & 0 & \cdots & 0 \\ \vdots & & & \\ 0 & 0 & \cdots & 0 \end{bmatrix} \otimes \begin{bmatrix} \delta y^{0b} \\ \delta y^{1b} \\ \vdots \\ \delta y^{kb} \end{bmatrix}.$$

We have:

$$p_0 + p_1 + p_2 + ... + p_k = I .$$

Theorem 2.1. *For the vector field X given by (2.1) and the projector operators defined by (2.2) the following decomposition is valid*

$$X = p_0 X + p_1 X + p_2 X + ... + p_k X = (p_0 + p_1 + p_2 + ... + p_k)X ,$$

where

$$p_0 X = X^{0b}\delta_{0b}, \ \ p_1 X = X^{1b}\delta_{1b},..., p_k X = X^{kb}\delta_{kb} .$$

The one form field $\omega \in T^*(E)$ can be written:

$$\omega = \omega_{0a}\delta y^{0a} + \omega_{1a}\delta y^{1a} + ... + \omega_{ka}\delta y^{ka} . \tag{2.3}$$

Let us define $p_0^*, p_1^*,..., p_k^*$ the projector operators of $T^*(E)$ on $H^*, V_1^*, V_2^*,..., V_k^*$ respectively, with

$$p_0^* = \delta y^{0b} \otimes \delta_{0b} \tag{2.4}$$

$$p_1^* = \delta y^{1b} \otimes \delta_{1b} ,...,$$

$$p_k^* = \delta y^{kb} \otimes \delta_{kb} .$$

If we write $p_0^*, p_1^*,..., p_k^*$ in the matrix form, it is easy to see that

$$p_0^* = \overline{p_0}, p_1^* = \overline{p_1},..., p_k^* = \overline{p_k} \tag{2.5}$$

where " $^-$ " means: transposed of.

We have

$$p_0^* + p_1^* + ... + p_k^* = I \tag{2.6}$$

Theorem 2.2. *For the one-form field* w *given by (2.3) and the projector operators* $p_0^*, p_1^*,..., p_k^*$ *defined by (2.4) the following relation is valid:*

$$w = p_0^* w + p_1^* w + ... + p_k^* w = w p_0 + w p_1 + ... + w p_k , \tag{2.7}$$

where

$$w_{0b} \delta y^{0b} = p_0^* w = w p_0 ,$$

$$w_{1b} \delta y^{1b} = p_1^* w = w p_1 ,...,$$

$$w_{kb} \delta y^{kb} = p_k^* w = w p_k .$$

3. THE J AND θ STRUCTURES

The structure J is a tensor field on space $T(E) \otimes T^*(E)$ defined by

$$J = \begin{bmatrix} \delta_{0a} \delta_{1a} \delta_{2a} ... \delta_{ka} \end{bmatrix} = \begin{bmatrix} 0 & 0 & \cdots & 0 & 0 \\ 1 & 0 & \cdots & 0 & 0 \\ 0 & 2 & \cdots & 0 & 0 \\ \vdots & \vdots & & & \\ 0 & 0 & \cdots & k & 0 \end{bmatrix} \otimes \begin{bmatrix} \delta y^{0a} \\ \delta y^{1a} \\ \delta y^{2a} \\ \vdots \\ \delta y^{ka} \end{bmatrix} =$$

$$\delta_{1a} \otimes \delta y^{0a} + 2\delta_{2a} \otimes \delta y^{1a} + 3\delta_{3a} \otimes \delta y^{2a} + ... + k\delta_{ka} \otimes \delta y^{(k-1)a} = \tag{3.1}$$

$$\partial_{1a} \otimes dy^{0a} + 2\partial_{2a} \otimes dy^{1a} + 3\partial_{3a} \otimes dy^{2a} + ... + k\partial_{ka} \otimes dy^{(k-1)a} .$$

From Definition 3.1, we get
Remark 3.1. We have

$$J\delta_{0b} = \delta_{1b}, J\delta_{1b} = 2\delta_{2b}, J\delta_{2b} = 3\delta_{3b}, ..., J\delta_{(k-1)b} = k\delta_{kb}, J\delta_{kb} = 0 \tag{3.2}$$

From the above it follows

$$J : H \rightarrow V_1 \rightarrow V_2 \rightarrow ... \rightarrow V_{k-1} \rightarrow V_k \rightarrow 0 .$$

From (3.1) it follows

Remark 3.2.

$$\delta y^{0b} J = 0 , \ \delta y^{1b} J = \delta y^{0b} , \ \delta y^{2b} J = 2\delta y^{1b} ,..., \delta y^{kb} J = k\delta y^{(k-1)b} \tag{3.3}$$

i.e.

$$0 \leftarrow H^* \leftarrow V_1^* \leftarrow V_2^* \leftarrow ... \leftarrow V_{k-1}^* \leftarrow V_k^* : J .$$

Definition 3.2. *The structure θ is a tensor field on space $T(E) \otimes T^*(E)$ defined by*

$$
\theta = \left[\delta_{0a} \delta_{1a} \delta_{2a} ... \delta_{ka} \right]
\begin{bmatrix}
0 & 1 & 0 & 0 & \cdots & 0 \\
0 & 0 & \dfrac{1}{2} & 0 & \cdots & 0 \\
0 & 0 & 0 & \dfrac{1}{3} & \cdots & 0 \\
\vdots & & & & & \vdots \\
0 & 0 & 0 & 0 & \cdots & \dfrac{1}{k} \\
0 & 0 & 0 & 0 & \cdots & 0
\end{bmatrix}
\otimes
\begin{bmatrix}
\delta y^{0a} \\
\delta y^{1a} \\
\delta y^{2a} \\
\vdots \\
\delta y^{(k-1)a} \\
\delta y^{ka}
\end{bmatrix}
=
$$

$$
\delta_{0a} \otimes \delta y^{1a} + \frac{1}{2} \delta_{1a} \otimes \delta y^{2a} + ... + \frac{1}{k} \delta_{(k-1)a} \otimes \delta y^{ka} = \tag{3.4}
$$

$$
\partial_{0a} \otimes dy^{1a} + \frac{1}{2} \partial_{1a} \otimes dy^{2a} + ... + \frac{1}{k} \partial_{(k-1)a} \otimes dy^{ka}.
$$

Remark 3.3. The structure θ satisfies the following relations:

$$
\delta y^{0b} \theta = \delta y^{1b}, \ \delta y^{1b} \theta = \frac{1}{2} \delta y^{2b}, ..., \delta y^{(k-1)b} \theta = \frac{1}{k} \delta y^{kb}, \ \delta y^{kb} \theta = 0 \tag{3.5}
$$

i.e.

$$
0 \leftarrow V_k^* \leftarrow V_{k-1}^* \leftarrow ... \leftarrow V_2^* \leftarrow V_1^* \leftarrow H : \theta .
$$

From (3.4) it follows

Remark 3.4. The following relations are valid

$$
\theta \delta_{0b} = 0, \ \theta \delta_{1b} = \delta_{0b}, \ \theta \delta_{2b} = \frac{1}{2} \delta_{1b}, ..., \theta \delta_{kb} = \frac{1}{k} \delta_{(k-1)b}, \tag{3.6}
$$

i.e.

$$
\theta : V_k \to V_{k-1} \to ... \to V_2 \to V_1 \to H \to 0 .
$$

Definition 3.3. *The transpose of the structure J denoted by $\overline{J}$ is a tensor field on $T^*(E) \otimes T(E)$ defined by*

$$
\overline{J} = \left[\delta y^{0a} \delta y^{1a} ... \delta y^{ka} \right]
\begin{bmatrix}
0 & 1 & 0 & \cdots & 0 \\
0 & 0 & 2 & \cdots & 0 \\
\vdots & & & & \\
0 & 0 & 0 & \cdots & k \\
0 & 0 & 0 & \cdots & 0
\end{bmatrix}
\otimes
\begin{bmatrix}
\delta_{0a} \\
\delta_{1a} \\
\vdots \\
\delta_{ka}
\end{bmatrix}
= \tag{3.7}
$$

$$
\delta y^{0a} \otimes \delta_{1a} + 2 \delta y^{1a} \otimes \delta_{2a} + 3 \delta y^{2a} \otimes \delta_{3a} + ... + k \delta y^{(k-1)a} \otimes \delta_{ka}
$$

Definition 3.4. *The transpose of the structure* θ *denoted by* $\overline{\theta}$ *is a tensor field on* $T^*(E) \otimes T(E)$ *defined by*

$$\overline{\theta} = \left[\delta y^{0a} \delta y^{1a} \delta y^{2a} ... \delta y^{ka}\right] \begin{bmatrix} 0 & 0 & \cdots & 0 \\ 1 & 0 & \cdots & 0 \\ 0 & \dfrac{1}{2} & \cdots & 0 \\ \vdots & & & \\ 0 & 0 & \cdots & \dfrac{1}{k} 0 \end{bmatrix} \otimes \begin{bmatrix} \delta_{0a} \\ \delta_{1a} \\ \delta_{2a} \\ \vdots \\ \delta_{ka} \end{bmatrix} = \tag{3.8}$$

$$\delta y^{1a} \otimes \delta_{0a} + \frac{1}{2} \delta y^{2a} \otimes \delta_{1a} + ... + \frac{1}{k} \delta y^{ka} \otimes \delta_{(k-1)a}$$

Remark 3.5. For the structure $\overline{J}$ the following relations are valid:

$$\overline{J}\delta y^{0b} = 0, \ \overline{J}\delta y^{1b} = \delta y^{0b}, \ \overline{J}\delta y^{2b} = 2\delta y^{1b}, ..., \overline{J}\delta y^{kb} = k\delta y^{(k-1)b}, \tag{3.9}$$

i.e.

$$\overline{J} : V_k^* \to V_{k-1}^* \to ... \to V_2^* \to V_1^* \to H^* \to 0$$

$$\delta_{0b}\overline{J} = \delta_{1b}, \ \delta_{1b}\overline{J} = 2\delta_{2b}, \ \delta_{2b}\overline{J} = 3\delta_{3b}, ..., \delta_{(k-1)b}\overline{J} = k\delta_{kb}, \ \delta_{kb}\overline{J} = 0 \tag{3.10}$$

i.e.

$$. \ 0 \leftarrow V_k \leftarrow V_{k-1} \leftarrow ... \leftarrow V_2 \leftarrow V_1 \leftarrow H : \overline{J} .$$

Remark 3.6. For the structure $\overline{\theta}$ the following relations are valid:

$$\overline{\theta}\delta y^{0b} = \delta y^{1b}, \ \overline{\theta}\delta y^{1b} = \frac{1}{2}\delta y^{2b}, ..., \overline{\theta}\delta y^{(k-1)b} = \frac{1}{k}\delta y^{kb}, \ \overline{\theta}\delta y^{kb} = 0, \tag{3.11}$$

i.e.

$$\overline{\theta} : H^* \to V_1^* \to V_2^* \to ... \to V_k^* \to 0$$

$$\delta_{0b}\overline{\theta} = 0, \ \delta_{1b}\overline{\theta} = \delta_{ob}, \ \delta_{2b}\overline{\theta} = \frac{1}{2}\delta_{1a}, ..., \delta_{kb}\overline{\theta} = \frac{1}{k}\delta_{(k-1)b}, \tag{3.12}$$

i.e.

$$0 \leftarrow H \leftarrow V_1 \leftarrow V_2 \leftarrow ... \leftarrow V_{k-1} \leftarrow V_k : \overline{\theta} .$$

.

Theorem 3.1. *The structures* J, $\overline{J}$, θ, $\overline{\theta}$, *the projectors* $p_0, p_1, ..., p_k, p_0^*, p_1^*, ..., p_k^*$
are connected by

$$J\theta = I - p_0 , \quad \overline{J}\,\overline{\theta} = I - p_k^* \qquad (3.13)$$

$$\theta J = I - p_k , \quad \overline{\theta}\,\overline{J} = I - p_0^* . \qquad (3.14)$$

Proof. It is easy to see that

$$J\theta = \delta_{1a} \otimes \delta^{1a} + \delta_{2a} \otimes \delta^{2a} + ... + \delta_{ka} \otimes \delta^{ka} ,$$

$$\theta J = \delta_{0a} \otimes \delta^{0a} + \delta_{1a} \otimes \delta^{1a} + ... + \delta_{(k-1)a} \otimes \delta^{(k-1)a} ,$$

$$\overline{J}\,\overline{\theta} = \delta y^{0a} \otimes \delta_{0a} + \delta y^{1a} \otimes \delta_{1a} + ... + \delta y^{(k-1)a} \otimes \delta_{(k-1)a} ,$$

$$\overline{\theta}\,\overline{J} = \delta y^{1a} \otimes \delta_{1a} + \delta y^{2a} \otimes \delta_{2a} + ... + \delta y^{ka} \otimes \delta_{ka} .$$

Proposition 3.1. *From the above it follows that*

$J\theta$ *is the identity operator on* $V_1 \oplus V_2 \oplus ... \oplus V_k$,

$J\theta$ *is the identity operator on* $H^* \oplus V_1^* \oplus ... \oplus V_{k-1}^*$,

$J\theta$ *is the identity operator on* $H \oplus V_1 \oplus ... \oplus V_{k-1}$,

$J\theta$ *is the identity operator on* $V_1^* \oplus V_2^* \oplus ... \oplus V_k^*$,

Theorem 3.2. *The structures* J, $\overline{J}$, θ, $\overline{\theta}$ *are* k *-tangent structures, namely:*

$$J^{k+1} = 0 , \quad \overline{J}^{k+1} = 0 , \quad \theta^{k+1} = 0 , \quad \overline{\theta}^{k+1} = 0$$

Proof. The proof is obtained by direct calculation.

Remark 3.7. In $Osc^1 M$ $\quad p_k = p_1 , p_k^* = p_1^* , p_0 + p_1 = I, p_0^* + p_1^* = I$, and from (3.13) we obtain $J\theta + \theta J = I, \overline{J}\,\overline{\theta} + \overline{\theta}\,\overline{J} = I$.

The first relation can be found in [5].

One kind of the Liouville vector fields in the natural basis of $T(Osc^k M)$ [1], have the form

$$\Gamma_{(1)} = \binom{k}{0} y^{1a} \partial_{ka} , \qquad (3.15)$$

$$\Gamma_{(2)} = \binom{k}{1} y^{2a} \partial_{ka} + \binom{k-1}{0} y^{1a} \partial_{(k-1)a} \,,$$

$$\Gamma_{(3)} = \binom{k}{3} y^{3a} \partial_{ka} + \binom{k-1}{1} y^{2a} \partial_{(k-1)a} + \binom{k-2}{0} y^{1a} \partial_{(k-2)a} \,, \dots ,$$

$$\Gamma_{(k)} = \binom{k}{k-1} y^{ka} \partial_{ka} + \binom{k-1}{k-2} y^{(k-1)a} \partial_{(k-1)a} + \dots + \binom{2}{1} y^{2a} \partial_{2a} + \binom{1}{0} y^{1a} \partial_{1a} \,.$$

It can be proved that $\left(k - (i-1)\right)! \Gamma_{(i)}$ given above are exactly the Liouville vector fields $\Gamma^{(i)}$ given by R. Miron and Gh. Atanasiu in [6], [7].

The action of J structure on Liouville vector fields was determined in [6], [7] and in some modified version in [1]-[3].

It is known that the k-structure J transform the Liouville vector fields in the following way [1]:

$$J\Gamma = 2\Gamma_{(k-1)}, J\Gamma_{(k-1)} = 3\Gamma_{(k-2)}, \dots, J\Gamma_{(3)} = (k-1)\Gamma_2, J\Gamma_{(2)} = k\Gamma_{(1)}, J\Gamma_{(1)} = 0 \qquad (3.16)$$

The connection between Liouville vector fields and the structure θ are given by

Theorem 3.3. *The action of the structure θ on the vector fields Γ are given by*

$$\Gamma_{(2)} = k\theta\Gamma_{(1)} + \binom{k}{1} y^{2a} \partial_{ka} \,, \qquad (3.17)$$

$$\Gamma_{(3)} = (k-1)\theta\Gamma_{(2)} + \binom{k}{2} y^{3a} \partial_{ka} \,,$$

$$\Gamma_{(4)} = (k-2)\theta\Gamma_{(3)} + \binom{k}{3} y^{4a} \partial_{ka} \,,$$

$$\Gamma_{(k)} = 2\theta\Gamma_{(k-1)} + \binom{k}{k-1} y^{ka} \partial_{ka} \,.$$

Proof. As $J\theta = \partial_{1a} \otimes dy^{1a} + \partial_{2a} \otimes dy^{2a} + \dots + \partial_{ka} \otimes dy^{ka}$, the action of structure J on $\Gamma_{(2)}, \Gamma_{(3)}, \dots, \Gamma_{(k)}$ gives $\left(J\partial_{ka} = 0\right)$

$$j\Gamma_{(2)} = k\Gamma_{(1)}, j\Gamma_{(3)} = (k-1)\Gamma_{(2)}, j\Gamma_{(4)} = (k-2)\Gamma_{(3)}, \dots, J\Gamma_{(k)} = 2\Gamma_{(k)} \,.$$

The above equations are (3.16).

4. THE SUBSPACES OF $Osc^k M$

The theory of subspaces of $Osc^k M$ in the form used here, is given in [4]. For the understanding the action of operators J, θ and p on subspaces, we recall the notations, definitions and theorems, which give relations between different adapted bases.

Here some special case of the general transformation (1.1) of M will be considered, namely, when

$$y^{0a} = y^{0a}(u^{01},...,u^{0m},\upsilon^{0(m+1)},...,\upsilon^{0n}) = y^{0a}(u^{0a},\upsilon^{0\hat{a}}), \tag{4.1}$$

$$a,b,c,... = 1,2,...,n\,,\ \ \alpha,\beta,\gamma,\delta,... = 1,2,...,m\,,\ \ \hat{\alpha},\hat{\beta},\hat{\gamma},\hat{\delta},... = m+1,...,n$$

and the new coordinates of the point u in the base manifold M with respect to another chart (U',φ') are $(u^{01'},...,u^{0m'},\upsilon^{0(m+1)'},...,\upsilon^{0n'})$, where

$$u^{0a'} = u^{0a'}(u^{01},...,u^{0m}),\ \ \upsilon^{0\hat{a}'} = \upsilon^{0\hat{a}'}(\upsilon^{0(m+1)},...,\upsilon^{0n}),$$

$$y^{0a'} = y^{0a'}(u^{01'},...,u^{0m'},\upsilon^{0(m+1)'},...,\upsilon^{0n'}) = y^{0a'}(u^{0a'},\upsilon^{0a'}).$$

We shall use the notations

$$\partial_\alpha = \partial_{0\alpha} = \frac{\partial}{\partial u^{0\alpha}}\,,\ \partial_{\hat{\alpha}} = \partial_{0\hat{\alpha}} = \frac{\partial}{\partial \upsilon^{0\hat{\alpha}}}\,.$$

$$B_\alpha^{\alpha'} = \partial_{0\alpha} u^{0\alpha'}\,,\ B_{\hat{\alpha}}^{\hat{\alpha}'} = \partial_{0\hat{\alpha}} \upsilon^{0\hat{\alpha}'}\,,$$

$$B_\alpha^a = \partial_{0\alpha} y^{0a} = \partial_\alpha x^a\,,\ B_{\hat{\alpha}}^a = \partial_{0\hat{\alpha}} y^{0a} = \partial_{\hat{\alpha}} x^a\,.$$

If the transformation (4.1) is regular, then there exists an inverse transformation:

$$u^{0\alpha} = u^{0\alpha}(y^{0a}),\ \ \upsilon^{0\hat{\alpha}} = \upsilon^{0\hat{\alpha}}(y^{0a}).$$

Let us denote

$$B_a^\beta = \frac{\partial u^\beta}{\partial x^a} = \frac{\partial u^{0\beta}}{\partial x^{0a}}\,,\ B_a^{\hat{\beta}} = \frac{\partial \upsilon^{\hat{\beta}}}{\partial x^a} = \frac{\partial \upsilon^{0\hat{\beta}}}{\partial y^{0a}}$$

then the following equations are valid:

$$B_a^\beta B_\alpha^a = \delta_\alpha^\beta\,,\ \ B_a^{\hat{\beta}} B_\alpha^a = 0\,,\ B_a^\beta B_{\hat{\alpha}}^a = 0\,,\ B_a^{\hat{\beta}} B_{\hat{\alpha}}^a = \delta_{\hat{\alpha}}^{\hat{\beta}}\,,\ B_\alpha^a B_b^\alpha + B_{\hat{\alpha}}^a B_b^{\hat{\alpha}} = \delta_b^a \tag{4.2}$$

We shall use the notations:

$$y^{1a} = \frac{dy^{0a}}{dt},..., y^{ka} = \frac{d^k y^{0a}}{dt^k}\,,$$

$$u^{1\alpha} = \frac{du^{0\alpha}}{dt},\ldots,u^{k\alpha} = \frac{d^k u^{0\alpha}}{dt^k},$$

$$\upsilon^{1\hat{\alpha}} = \frac{d\upsilon^{0\hat{\alpha}}}{dt},\ldots,\upsilon^{k\hat{\alpha}} = \frac{d^k \upsilon^{0\hat{\alpha}}}{dt^k}$$

In the base manifold we can construct two families of subspaces M_1 and M_2 given by equations

$$M_1 : y^{0a} = y^{0a}\left(u^{0a},C^{0\hat{\alpha}}\right),\ \ M_2 : y^{0a} = y^{0a}\left(C^{0\alpha},\upsilon^{0\hat{\alpha}}\right),$$

where we suppose, that the functions appeared in (4.1) are C^∞. The subspaces M_1 and M_2 of M induces subspaces $E_1 = Osc^k M_1$ and $E_2 = Osc^k M_2$ in $Osc^k M$. Some point $u \in E_1$ has coordinates $(u^{0\alpha},u^{1\alpha},\ldots,u^{k\alpha})$ and some point $\upsilon \in E_2$ has coordinates $(\upsilon^{0\hat{\alpha}},\upsilon^{1\hat{\alpha}},\ldots,\upsilon^{k\hat{\alpha}})$. We have

$$\dim\left(Osc^k M_1\right) = (k+1)m,\ \dim\left(Osc^k M_2\right) = (k+1)(n-m)$$

We can construct the special adapted bases B_1 and B_1^* of $T(E_1)$ and $T^*(E_1)$, further B_2 and B_2^* of $T(E_2)$ and $T^*(E_2)$ respectively.

$$B_1 = \left\{\delta_{0\alpha},\delta_{1\alpha},\ldots,\delta_{k\alpha}\right\},\ \ B_2 = \left\{\delta_{0\hat{\alpha}},\delta_{1\hat{\alpha}},\ldots,\delta_{k\hat{\alpha}}\right\},$$

$$B_1^* = \left\{\delta u^{0\alpha},\delta u^{1\alpha},\ldots,\delta u^{k\alpha}\right\},\ B_2^* = \left\{\delta\upsilon^{0\hat{\alpha}},\delta\upsilon^{1\hat{\alpha}},\ldots,\delta\upsilon^{k\hat{\alpha}}\right\}.$$

Definition 3.4. *The special adapted bases* B_1, B_1^*, B_2 , B_2^* *are defined by*

$$\left[\delta_{(\alpha)}\right] = \left[\partial_{(\beta)}\right]\left[N_{(\alpha)}^{(\beta)}\right],\ \left[\delta_{\left(\hat{\alpha}\right)}\right] = \left[\partial_{\left(\hat{\beta}\right)}\right]\left[N_{\left(\hat{\alpha}\right)}^{\left(\hat{\beta}\right)}\right],$$

$$\left[\delta u^{(\alpha)}\right] = \left[M_{(\beta)}^{(\alpha)}\right]\left[du^{(\beta)}\right],\ \left[\delta v^{\left(\hat{\alpha}\right)}\right] = \left[M_{\left(\hat{\beta}\right)}^{\left(\hat{\alpha}\right)}\right]\left[dv^{\left(\hat{\beta}\right)}\right],$$

where $\left[N_\beta^\alpha\right]$ *and* $\left[N_{\left(\hat{\beta}\right)}^{\left(\hat{\alpha}\right)}\right]$ *are matrices obtained from (1.7) by substitution* $(a,b) \to (\alpha,\beta)$

and $(a,b) \to \left(\hat{\alpha},\hat{\beta}\right)$ *respectively. The matrices* $\left[M_\beta^\alpha\right]$ *and* $\left[M_{\left(\hat{\beta}\right)}^{\left(\hat{\alpha}\right)}\right]$ *are obtained from*

(1.2) by substitution $(a,b) \to (\alpha,\beta)$ *and* $(a,b) \to \left(\overset{\wedge}{\alpha}, \overset{\beta}{\beta} \right)$ *respectively.*

Theorem 4.1. *The necessary and sufficient condition that* $\delta u^{a\alpha} (\delta v^{A\overset{\wedge}{\alpha}})$ *are transformed as* d *-tensors, i.e.*

$$\delta u^{A\alpha'} = B_\alpha^{\alpha'} \delta u^{A\alpha} \quad \left[\delta v^{a\alpha'} = B_{\overset{\wedge}{\alpha}}^{\overset{\wedge}{\alpha'}} \delta v^{A\overset{\wedge}{\alpha}} \right], A = \overline{0,k} \tag{4.3}$$

are given by (1.5) if (a,b,c,y) *is substituted by* (α,β,γ,u) *[(a,b,c,y) is substituted by* $(\overset{\wedge}{\alpha}, \overset{\wedge}{\beta}, \overset{\wedge}{\gamma}, \hat{v}]$.

Theorem 4.2. *The necessary and sufficient condition that* $\delta_{A\alpha} [\delta_{A\overset{\wedge}{\alpha}}]$ *are transformed as* d *-tensors, i.e.*

$$\delta_{A\alpha'} = B_{\alpha'}^{\alpha} \delta u_{A\alpha'} \quad \left[\delta_{A\overset{\wedge}{\alpha'}} = B_{\alpha'}^{\overset{\wedge}{\alpha}} \delta_{A\overset{\wedge}{\alpha}} \right] A = \overline{0,k} \tag{4.4}$$

are given by (1.10) if (a,b,c,y) *is substituted by* (α,β,γ,u) *[(a,b,c,y) is substituted by* $(\overset{\wedge}{\alpha}, \overset{\wedge}{\beta}, \overset{\wedge}{\gamma}, \hat{v})]$.

Theorem 4.3. *The necessary and sufficient conditions that* B_1^* *be dual* B_1 , B_2^* *be dual to* B_2 *are the following equations*

$$\left[M_{(\gamma)}^{(\beta)} \right] \left[N_{(\alpha)}^{(\gamma)} \right] = \delta_\alpha^\beta I_{m \times m}$$

$$\left[M_{\left(\overset{\wedge}{\gamma} \right)}^{\left(\overset{\wedge}{\beta} \right)} \right] \left[N_{\left(\overset{\wedge}{\alpha} \right)}^{\left(\overset{\wedge}{\gamma} \right)} \right] = \delta_{\overset{\wedge}{\alpha}}^{\overset{\wedge}{\beta}} I_{(n-m) \times (n-m)} .$$

Now we want to obtain the relations between the adapted bases B and B', where

$$B = \left\{ \delta_{0a}, \delta_{1a}, ..., \delta_{ka} \right\},$$

$$B' = B_1 \cup B_2 = \left\{ \delta_{0\alpha}, \delta_{0\overset{\wedge}{\alpha}}, \delta_{1\alpha}, \delta_{1\overset{\wedge}{\alpha}}, ..., \delta_{k\alpha}, \delta_{k\overset{\wedge}{\alpha}} \right\},$$

further between B^* and B'^*, where

$$B^* = \left\{ \delta y^{0a}, \delta y^{1a}, ..., \delta y^{ka} \right\},$$

$$B'^* = B_1^* \cup B_2^* = \left\{ \delta u^{0\alpha}, \delta v^{0\overset{\wedge}{\alpha}}, \delta u^{1\alpha}, \delta v^{1\overset{\wedge}{\alpha}}, ..., \delta u^{k\alpha}, \delta v^{k\overset{\wedge}{\alpha}} \right\}.$$

The adapted basis B, B', B^*, B'^* are functions of

$$\left[M\begin{pmatrix}(a)\\(b)\end{pmatrix}\right]\left[N\begin{pmatrix}(a)\\(b)\end{pmatrix}\right]\left[M\begin{pmatrix}(\alpha)\\(\beta)\end{pmatrix}\right]\left[N\begin{pmatrix}(\alpha)\\(\beta)\end{pmatrix}\right]\left[M\begin{pmatrix}\hat{\alpha}\\\hat{\beta}\end{pmatrix}\right],\left[N\begin{pmatrix}\hat{\alpha}\\\hat{\beta}\end{pmatrix}\right],$$

which have to satisfy the conditions given in previous text. It is clear, that the adapted bases are not uniquely determined.

For the easier calculations we want to obtain such adapted bases, for which the following relations are valid.

$$\delta_{Aa} = B_a^\alpha \delta_{A\alpha} + B_a^{\hat{\alpha}} \delta_{A\hat{\alpha}} ,\ \ A = 0,1,...,k \tag{4.5}$$

$$\delta y^{Aa} = B_\alpha^a \delta u^{A\alpha} + B_{\hat{\alpha}}^a \delta \upsilon^{A\hat{\alpha}} ,\ \ A = 0,1,...,k \tag{4.6}$$

The adapted bases B, $B^{\{*\}}$, B' and $B'^{\{*\}}$ satisfy (4.5) and (4.6)

Theorem 4.4. *The adapted bases B, B^*, B', B'^* satisfy (4.5) and (4.6) if different M and N are connected by*

$$\left[M\begin{pmatrix}(a)\\(b)\end{pmatrix}\right]\left[B\begin{pmatrix}(b)\\(\beta)\end{pmatrix}\right]=\left[B\begin{pmatrix}(a)\\(\alpha)\end{pmatrix}\right]\left[M\begin{pmatrix}(\alpha)\\(\beta)\end{pmatrix}\right],\ \left[M\begin{pmatrix}(a)\\(b)\end{pmatrix}\right]\left[B\begin{pmatrix}(b)\\(\hat{\beta})\end{pmatrix}\right]=\left[B\begin{pmatrix}(a)\\(\hat{\alpha})\end{pmatrix}\right]\left[M\begin{pmatrix}\hat{\alpha}\\\hat{\beta}\end{pmatrix}\right] \tag{4.7}$$

and

$$\left[B\begin{pmatrix}(\beta)\\(b)\end{pmatrix}\right]\left[N\begin{pmatrix}(b)\\(a)\end{pmatrix}\right]=\left[N\begin{pmatrix}(\beta)\\(\alpha)\end{pmatrix}\right]\left[B\begin{pmatrix}(\alpha)\\(a)\end{pmatrix}\right],\ \left[B\begin{pmatrix}(\hat{\beta})\\(b)\end{pmatrix}\right]\left[N\begin{pmatrix}(b)\\(a)\end{pmatrix}\right]=\left[N\begin{pmatrix}\hat{\beta}\\\hat{\alpha}\end{pmatrix}\right]\left[B\begin{pmatrix}(\hat{\alpha})\\(a)\end{pmatrix}\right]. \tag{4.8}$$

The proof of Theorems 4.1-4.4 are given in [4].

5. THE STRUCTURES P, J AND θ ON THE SUBSPACES

Let us denote by $H', V'_1, V'_2,...,V'_k$ the subspaces of $T(E_1)$ generated by $\{\delta_{0\alpha}\},\{\delta_{1\alpha}\},...,\{\delta_{k\alpha}\}$ respectively and by $H'', V''_1, V''_2,...,V''_k$ the subspaces of $T(E_2)$ generated by $\{\delta_{0\hat{\alpha}}\},\{\delta_{1\hat{\alpha}}\},...,\{\delta_{k\hat{\alpha}}\}$ respectively.

Now we have

$$T(E_1) = H' \oplus V'_1 \oplus ... \oplus V'_k ,$$

$$T(E_2) = H'' \oplus V''_1 \oplus ... \oplus V''_k$$

Let us denote by $H^{*'}, V^{*'}_1, ..., V^{*'}_k$ the subspaces of $T^*(E_1)$ generated by $\{\delta u^{0\alpha}\}, \{\delta u^{1\alpha}\}, ..., \{\delta u^{k\alpha}\}$ respectively and by $H^{*"}, V^{*"}_1, ..., V^{*"}_k$ the subspaces of $T^*(E_2)$ generated by $\left\{\delta v^{0\hat{\alpha}}\right\}, \left\{\delta v^{1\hat{\alpha}}\right\}, ..., \left\{\delta v^{k\hat{\alpha}}\right\}$.

The following relation is valid

$$T^*(E_1) = H^{*'} \oplus V^{*'}_1 \oplus ... \oplus V^{*'}_k,$$

$$T^*(E_2) = H^{*"} \oplus V^{*"}_1 \oplus ... \oplus V^{*"}_k.$$

The basis vectors of B, B^*, B_1, B_2, B^*_1 and B^*_2 are connected by (4.5) and (4.6) i.e.

$$\delta_{Aa} = B^\alpha_a \delta_{A\alpha} + B^{\hat{\alpha}}_a \delta_{A\hat{\alpha}}, \ \delta y^{Aa} = B^a_\alpha \delta u^{A\alpha} + B^a_{\hat{\alpha}} \delta v^{A\hat{\alpha}}, \ A = \overline{0,k} \quad (5.1)$$

Let us examine the operators p, J and θ on the subspaces.

Proposition 5.1. *The projector operators* $p_0, p_1, ..., p_k$ *given by (2.2) can be decomposed in the following way:*

$$p_0 = p'_0 + p''_0 \quad (5.2)$$

$$p_1 = p'_1 + p''_1, ...,$$

$$p_k = p'_k + p''_k$$

where

$$p_A' = \delta_{A\alpha} \otimes \delta u^{A\alpha}, \ p_A'' = \delta_{A\hat{\alpha}} \otimes \delta v^{A\hat{\alpha}}, \ A = \overline{0,k},$$

(no summation over A).

Proof. From (2.2) and (5.1) we get

$$p_A = \delta_{Aa} \otimes \delta y^{Aa} = \left(B^\alpha_a \delta_{A\alpha} + B^{\hat{\alpha}}_a \delta_{A\hat{\alpha}}\right) \otimes \left(B^a_\beta \delta u^{A\beta} + B^a_{\hat{\beta}} \delta v^{A\hat{\beta}}\right) =$$

$$B^\alpha_a B^a_\beta \delta_{A\alpha} \otimes \delta u^{A\beta} + B^{\hat{\alpha}}_a B^a_\beta \delta_{A\hat{\alpha}} \otimes \delta u^{A\beta} + B^\alpha_a B^a_{\hat{\beta}} \delta_{A\alpha} \otimes \delta v^{A\hat{\beta}} + B^{\hat{\alpha}}_a B^a_{\hat{\beta}} \delta_{A\hat{\alpha}} \otimes \delta v^{A\hat{\beta}}$$

From (4.2) it follows

$$B^\alpha_a B^a_\beta = \delta^\alpha_\beta, \quad B^{\hat{\alpha}}_a B^a_\beta = 0, \quad B^\alpha_a B^a_{\hat{\beta}} = 0, \quad B^{\hat{\alpha}}_a B^a_{\hat{\beta}} = \delta^{\hat{\alpha}}_{\hat{\beta}}.$$

Now we get

$$p_A = \delta_{A\alpha} \otimes \delta u^{A\alpha} + \delta_{A\hat{\alpha}} \otimes \delta v^{A\hat{\alpha}} = p'_A + p''_A, \ A = \overline{0,k}.$$

Arbitrary vector field $X \in T(E)$ given by (2.1) can be expressed in basis $B' = B_1 \cup B_2$ in the following way

$$
\begin{aligned}
X &= X^{Aa}\delta_{Aa} = X^{Aa}\left(B_a^\alpha \delta_{A\alpha} + B_a^{\hat\alpha}\delta_{\underset{A\hat\alpha}{}}\right) = \\
&= X^{A\alpha}\delta_{A\alpha} + X^{A\hat\alpha}B_{\underset{A\hat\alpha}{}} ,
\end{aligned} \tag{5.3}
$$

where

$$
X^{A\alpha} = B_a^\alpha X^{Aa} , \quad X^{A\hat\alpha} = B_a^{\hat\alpha} X^{aa}
$$

Proposition 5.2. *The vector field X can be expressed in the form*
$$
X = X' + X'' ,
$$
where
$$
X' = \left(p_0' + p_1' + \ldots + p_k'\right)X ,
$$
$$
X'' = \left(p_0'' + p_1'' + \ldots + p_k''\right)X
$$

Proof. Using (5.2) and (5.3) we get

$$
X' = \left(\delta_{0\beta} \otimes \delta u^{0\beta} + \delta_{1\beta} \otimes \delta u^{1\beta} + \ldots + \delta_{k\beta} \otimes \delta u^{k\beta}\right)\left(\begin{array}{l} X^{0\alpha}\delta_{0\alpha} + X^{1\alpha}\delta_{1\alpha} + \ldots + X^{k\alpha}\delta_{k\alpha} + \\ X^{0\hat\alpha}\delta_{\underset{0\hat\alpha}{}} + X^{1\hat\alpha}\delta_{\underset{1\hat\alpha}{}} + \ldots + X^{k\hat\alpha}\delta_{\underset{k\hat\alpha}{}} \end{array}\right)
$$

when B_1^* is dual to B_1, B_2^* is dual to B_2, i.e. the conditions of Theorem 4.3 are satisfied, i.e.

$$
\left(\delta u^{A\alpha}, \delta_{A\beta}\right) = \delta_\beta^\alpha , \quad \left(\delta v^{A\hat\alpha}, \delta_{\underset{A\hat\beta}{}}\right) = \delta_{\hat\beta}^{\hat\alpha} ,
$$

$$
\left(\delta u^{A\alpha}, \delta_{\underset{A\hat\beta}{}}\right) = 0 , \quad \left(\delta v^{A\hat\alpha}, \delta_{A\beta}\right) = 0 , \quad A = \overline{0,k}
$$

we get

$$
X' = X^{0\alpha}\delta_{0\alpha} + X^{1\alpha}\delta_{1\alpha} + \ldots + X^{k\alpha}\delta_{k\alpha} = X^{A\alpha}\delta_{A\alpha} .
$$

Similar for X''.

Proposition 5.3. *The projection operator*

$$
p'_0 + p'_1 + \ldots + p'_k = I_{m\times m} \quad on \ T(E_1)
$$

$$
p''_0 + p''_2 + \ldots + p''_k = I_{(n-m)\times(n-m)} \quad on \ T(E_2)
$$

i.e. p'_0 *is the projection operator of* $T(E)$ *on* H', $P_A'(A = \overline{1,k})$ *are the projections of* $T(E)$ *on* V_A'. *Similarly for the second part of theorem.*

Proposition 5.4. *The one-form field* $w \in T^*(E)$ *given by (2.3) can be written in the basis* $B^{*'} = B_1^* \cup B_2^*$ *in the form*

$$w = w' + w'',$$

where

$$w' = w_{0\alpha} \delta u^{0\alpha} + w_{1\alpha} \delta u^{1\alpha} + \ldots + w_{k\alpha} \delta u^{k\alpha}$$

$$w'' = w_{\underset{0\alpha}{}} \delta u^{0\hat{\alpha}} + w_{\underset{1\alpha}{}} \delta u^{1\hat{\alpha}} + \ldots + w_{\underset{k\alpha}{}} \delta u^{k\hat{\alpha}}.$$

Proposition 5.5. *The projection operators* $p_0^*, p_1^*, \ldots, p_k^*$ *defined by (2.4) can be decomposed in the form*

$$p_0^* = p_0^{*'} + p_0^{*''}, \tag{5.4}$$

$$p_1^* = p_1^{*'} + p_1^{*''}, \ldots, p_k^* = p_k^{*'} + p_k^{*''}$$

where

$$p_A^{*'} = \delta u^{A\alpha} \otimes \delta_{A\alpha}$$

$$p_A^{*''} = \delta v^{A\hat{\alpha}} \otimes \delta_{\underset{A\alpha}{}}, \ A \ fixed, \ A = \overline{0,k}.$$

Proposition 5.6. *For the* 1-*form field* w *given by (2.3) and the projector operators* $p_A^{*'}$ *and* $p_A^{*''}$ *the following relation is valid*

$$w' = (p_0^{*'} + p_1^{*'} + \ldots + p_k^{*'}) w'$$

$$w'' = (p_0^{*''} + p_1^{*''} + \ldots + p_k^{*''}) w''$$

where

$$p_A^{*'} w' = \left(\delta u^{A\alpha} \otimes \delta_{A\alpha} \right) w_{B\beta} \delta^{B\beta} =$$

$$w_{B\beta} \delta u^{A\alpha} \delta_A^B \delta_\alpha^\beta = w_{A\alpha} \delta u^{A\alpha}, \ A \ fixed.$$

From the above it is obvious that

$$p_0^{*'} + p_1^{*'} + \cdots + p_k^{*'} = I_{m \times m} \ \text{ on } \ T^*(E_1)$$

$$p_0^{*''} + p_1^{*''} + \cdots + p_k^{*''} = I_{(n-m) \times (n-m)} \ \text{ on } \ T^*(E_2)$$

and p_0^{*}'is the projection of $T^{*}(E_1)$ on H^{*}', p_A^{*}'is the projection of $T^{*}(E_1)$ on V_A^{*}'; p_0^{*}''is the projection of $T^{*}(E_2)$ on H^{*}''; p_A^{*}''is the projection of $T^{*}(E_2)$ on V_A^{*}'', $A = \overline{1,k}$.

Proposition 5.7. *The structure J which in B and B^{*} can be expressed by (3.1) in the bases $B'= B_1 \cup B_2$ and $B''^{*} = B_1^{*} \cup B_2^{*}$ can be written in the form*

$$J = J' + J'' , \tag{5.5}$$

where

$$J' = \delta_{1\alpha} \otimes \delta u^{0\alpha} + 2\delta_{2\alpha} \otimes \delta u^{1\alpha} + \cdots + k\delta_{k\alpha} \otimes \delta u^{(k-1)\alpha} , \tag{5.6}$$

$$J'' = \delta_{1\alpha} \otimes \delta v^{0\hat{\alpha}} + 2\delta_{2\hat{\alpha}} \otimes \delta v^{1\hat{\alpha}} + \cdots + k\delta_{k\hat{\alpha}} \otimes \delta v^{(k-1)\hat{\alpha}} .$$

Proof. The proof is similar to the proof of Proposition 5.1, where the relations (4.2) are used.

Remark 5.1. The structure $\overline{J}$ defined by (3.7) in the basis B' and B''^{*} can be expressed by

$$\overline{J} = \overline{J}' + \overline{J}'' , \tag{5.7}$$

where

$$\overline{J}' = \delta u^{0\alpha} \otimes \delta_{1\alpha} + 2\delta u^{1\alpha} \otimes \delta_{2\alpha} + \ldots\ldots + k\delta u^{(k-1)\alpha} \otimes \delta_{k\alpha} \tag{5.8}$$
$$\overline{J}'' = \delta u^{0\bar{\alpha}} \otimes \delta_{1\bar{\alpha}} + 2\delta u^{1\bar{\alpha}} \otimes \delta_{2\bar{\alpha}} + \ldots\ldots + k\delta u^{(k-1)\bar{\alpha}} \otimes \delta_{k\bar{\alpha}} .$$

Proposition 5.8. The structure θ defined by (3.4) in the bases B' and B''^{*} can be expressed by

$$\theta = \theta' + \theta'' , \tag{5.9}$$

where

$$\theta' = \delta_{0\alpha} \otimes \delta u^{1\alpha} + \frac{1}{2}\delta_{1\alpha} \otimes \delta u^{2\alpha} + \cdots + \frac{1}{k}\delta_{(k-1)\alpha} \otimes \delta u^{k\alpha} , \tag{5.10}$$

$$\theta'' = \delta_{0\hat{\alpha}} \otimes \delta v^{1\hat{\alpha}} + \frac{1}{2}\delta_{1\hat{\alpha}} \otimes \delta v^{2\hat{\alpha}} + \cdots + \frac{1}{k}\delta_{(k-1)\hat{\alpha}} \otimes \delta v^{k\hat{\alpha}} .$$

Remark 5.2. The structure $\overline{\theta}$ defined by (3.8) in the bases B' and B' can be expressed by

$$\overline{\theta} = \overline{\theta}' + \overline{\theta}'' , \tag{5.11}$$

where

$$\overline{\theta}' = \delta u^{1\alpha} \otimes \delta_{0\alpha} + \frac{1}{2}\delta u^{2\alpha} \otimes \delta_{1\alpha} + \ldots\ldots + \frac{1}{k}\delta u^{k\alpha} \otimes \delta_{(k-1)\alpha} \tag{5.12}$$

$$\overline{\theta''} = \delta u^{1\bar\alpha} \otimes \delta_{0\bar\alpha} + \frac{1}{2}\delta u^{2\bar\alpha} \otimes \delta_{1\bar\alpha} + \cdots\cdots + \frac{1}{k}\delta u^{k\bar\alpha} \otimes \delta_{(k-1)\bar\alpha}$$

Theorem 5.1. *The structure* J, $\overline{J}$, θ, $\overline{\theta}$, p, p^* *on the subspaces are connected by:*

$$J'\theta' = I_{m\times m} - p_0' \quad \overline{J'}\overline{\theta'} = I_{m\times m} - p^*{}'_k$$

$$J''\theta'' = I_{(n-m)\times(n-m)} - p_0'' \quad \overline{J''}\overline{\theta''} = I_{(n-m)\times(n-m)} - p^*{}''_k \qquad (5.13)$$

Proof. From (5.4)-(5.12) it follows

$$J'\theta' = \delta_{1\alpha} \otimes \delta u^{1\alpha} + \delta_{2\alpha} \otimes \delta u^{2\alpha} + \cdots + \delta_{k\alpha} \otimes \delta u^{k\alpha}, p_0' = \delta_{0\alpha} \otimes \delta u^{0\alpha} \qquad (5.14)$$

$$\overline{J'}\overline{\theta'} = \delta u^{0\alpha} \otimes \delta_{0\alpha} + \delta u^{1\alpha} \otimes \delta_{1\alpha} + \cdots + \delta u^{(k-1)\alpha} \otimes \delta_{(k-1)\alpha}, p_k^* = \delta u^{k\alpha} \otimes \delta_{k\alpha}$$

$$J''\theta'' = \delta_{1\hat\alpha} \otimes \delta v^{1\hat\alpha} + \delta_{2\hat\alpha} \otimes \delta v^{2\hat\alpha} + \cdots + \delta_{k\hat\alpha} \otimes \delta v^{k\hat\alpha}, p_0'' = \delta_{0\hat\alpha} \otimes \delta u^{0\hat\alpha}$$

$$\overline{J''}\overline{\theta''} = \delta v^{0\hat\alpha} \otimes \delta_{0\hat\alpha} + \delta v^{1\hat\alpha} \otimes \delta_{1\hat\alpha} + \cdots + \delta v^{(k-1)\hat\alpha} \otimes \delta_{(k-1)\hat\alpha}, p_k'' = \delta u^{k\hat\alpha} \otimes \delta_{k\hat\alpha}.$$

Proposition 5.9. *The following relations are valid:*

$$J'\theta \text{ is the identity operator on } V_1' \oplus V_2' \oplus \cdots \oplus V_k'$$

$$\overline{J'}\overline{\theta'} \text{ is the identity operator on } V_0^{*}{}' \oplus V_1^{*}{}' \oplus \cdots \oplus V_{k-1}^{*}{}',$$

$$J''\theta'' \text{ is the identity operator on } V_1'' \oplus V_2'' \oplus \cdots \oplus V_k''$$

$$\overline{J''}\overline{\theta''} \text{ is the identity operator on } V_1^{*}{}'' \oplus V_2^{*}{}'' \oplus \cdots \oplus V_k^{*}{}''.$$

Theorem 5.2. *The following relations are valid:*

$$\theta'J' = I_{m\times m} - p_k' \qquad\qquad \overline{\theta'}\overline{J'} = I_{m\times m} - p_0^{*}{}' \qquad (5.15)$$

$$\theta''J'' = I_{(n-m)\times(n-m)} - p_k'' \qquad\qquad \overline{\theta''}\overline{J''} = I_{(n-m)\times(n-m)} - p_0^{*}{}''.$$

Proof. It is easy to see that

$$\theta'J' = \delta_{0\alpha} \otimes \delta u^{0\alpha} + \delta_{1\alpha} \otimes \delta u^{1\alpha} + \cdots + \delta_{(k-1)\alpha} \otimes \delta u^{(k-1)\alpha}, p_k' = \delta_{k\alpha} \otimes \delta u^{k\alpha} \qquad (5.16)$$

$$\overline{\theta'}\overline{J'} = \delta u^{1\alpha} \otimes \delta_{1\alpha} + \delta u^{2\alpha} \otimes \delta_{2\alpha} + \cdots + \delta u^{k\alpha} \otimes \delta_{k\alpha}, p_0^{*}{}' = \delta u^{0\alpha} \otimes \delta_{0\alpha}$$

$$\theta''J'' = \delta_{0\hat\alpha} \otimes \delta v^{0\hat\alpha} + \delta_{1\hat\alpha} \otimes \delta v^{1\hat\alpha} + \cdots + \delta_{(k-1)\hat\alpha} \otimes \delta v^{(k-1)\hat\alpha}, p_k'' = \delta_{k\hat\alpha} \otimes \delta v^{k\hat\alpha}$$

$$\overline{\theta''}\overline{J''} = \delta v^{1\hat\alpha} \otimes \delta_{1\hat\alpha} + \delta v^{2\hat\alpha} \otimes \delta_{2\hat\alpha} + \cdots + \delta v^{k\hat\alpha} \otimes \delta_{k\hat\alpha}, p_0'' = \delta v^{0\hat\alpha} \otimes \delta_{0\hat\alpha}.$$

Proposition 5.10. *The following relations are valid:*

$\theta' J'$ is the identity operator on $H^* {}' \oplus V_1 {}' \oplus \cdots \oplus V_{k-1} {}'$

$\overline{\theta}' \overline{J}'$ is the identity operator on $V_1^* {}' \oplus V_2^* {}' \oplus \cdots \oplus V_k^* {}'$,

$\theta'' J''$ is the identity operator on $H'' \oplus V_1 {}'' \oplus \cdots \oplus V_{k-1} {}''$

$\overline{\theta}'' \overline{J}''$ is the identity operator on $V_1^* {}'' \oplus V_2^* {}'' \oplus \cdots \oplus V_k^* {}''$.

From the above we have

Theorem 5.3. *For the subspaces in $Osc^k M$ the following relations are valid:*

$$J'\theta'+\theta'J'= 2I_{m\times m} - p'_0-p'_k \tag{5.17}$$

$$J''\theta''+\theta''J''= 2I_{(n-m)\times(n-m)} - p''_0-p''_k$$

$$\overline{J}'\overline{\theta}'+\overline{\theta}'\overline{J}'= 2I_{m\times m} - p^*{}'_0-p^*{}'_k$$

$$\overline{J}''\overline{\theta}''+\overline{\theta}''\overline{J}''= 2I_{(n-m)\times(n-m)} - p^*{}''_0-p^*{}''_k .$$

Proposition 5.11. *For the subspaces in $Osc^1 M$ we have $p'_k = p'_1, p''_k = p''_1,$*

$p^*{}'_k = p^*{}'_1, p^*{}''_k = p^*{}''_1$ *and*

$$p'_0+p'_1 = I_{m\times m},   p''_0+p''_1 = I_{(n-m)\times(n-m)}$$

$$p^*{}'_0+p^*{}'_1 = I_{m\times m},   p^*{}''_0+p^*{}''_1 = I_{(n-m)\times(n-m)} .$$

From (5.16) and Proposition 5.11 we have

Theorem 5.4. *For the subspaces in $Osc^1 M$ the following relations are valid:*

$$J'\theta'+\theta'J'= I_{m\times m} \tag{5.18}$$

$$J''\theta''+\theta''J''= I_{(n-m)\times(n-m)}$$

$$\overline{J}'\overline{\theta}'+\overline{\theta}'\overline{J}'= I_{m\times m}$$

$$\overline{J}''\overline{\theta}''+\overline{\theta}''\overline{J}''= I_{(n-m)\times(n-m)} .$$

As $\dim E_1 = (k+1)m$, $\dim E_2 = (k+1)(n-m)$ the notion $I_{m\times m}$ is not precise, it means $(k+1)$ blocks on diagonal, each of which is of form $m \times m$.

The exact form of (5.16) and (5.17) can be obtained from (5.13) and (5.15).

Theorem 5.5. *The structures J' , J'' , $\overline{J}'$, $\overline{J}''$, θ', θ'', $\overline{\theta}'$, $\overline{\theta}''$, are k-tangent structures, namely*

$$\left(J'\right)^k = 0 , \left(J''\right)^k = 0, \left(\overline{J}'\right)^k = 0, \left(\overline{J}''\right)^k = 0$$
$$\left(\theta'\right)^k = 0, \left(\theta''\right)^k = 0, \left(\overline{\theta}'\right)^k = 0, \left(\overline{\theta}''\right)^k = 0$$

REFERENCES

1. Čomić, I., Liouville Vector Fields and k-Sprays Expressed in Special Adapted Basis of Miron's $Osc^k M$, Recent Advances in Geometry and Topology Clui University Press 2004.

2. Čomić, I., Stojanov, J., Grujić, G., *The Liouville vector fields in the subspaces of Miron's $Osc^k M$*, Lagrange and Hamilton Geometries and Their Applications, Radu Miron (Ed.), Handbooks, Treatises, Monographs 49(2004), Fair Partners Publishers, Bucharest, (ISBN 973-8470-29-3) 2004, pp. 67–92.

3. Čomić, I., *Sprays in k-osculator bundles*, Lagrange and Hamilton Geometries and Their Applications, Radu Miron (Ed.), Handbooks, Treatises, Monographs 49(2004), Fair Partners Publishers, Bucharest, (ISBN 973-8470-29-3) 2004, pp. 55–66.

4. Čomić, I., Grujić, G., Stojanov, J., *The theory of subspaces in Miron's $Osc^k M$*, Annales Univ. Sci. Budapest, 48(2005) pp. 39–65.

5. Bucataru, I., Miron, R., *Finsler-Lagrange Geometry*, Applications to Dynamical Systems, Editura Academiei Romane, 2007.

6. Miron, R., Atanasiu, Gh., *Differential Geometry of k-osculator Bundles*, Rev. Roumaine Math. Pures Appl., 41, (3-4), (1996) pp. 205–236.

7. Miron, R., Atanasiu, Gh., *Higher order Lagrange spaces*, Rev. Roum. Math. Pures et Appl., Tom XLI No. 3-4, (1996) pp. 251–263.

8. Miron, R., *The Geometry of Higher-Order Lagrange Spaces*, Applications to Mechanics and Physics, Kluwer Academic Publisher, FTPH, no. 82 (1997)

9. Miron, R., Anastasiei, M., *Vector Bundles and Lagrange Spaces with Applications to Relativity*, Geometry Balkan Press, Bucharest (1997)

10. Miron, R., Hrimius, D., Shimada, H., Sabau, S., *The geometry of Hamilton and Lagrange Spaces*, Kluwer Academic Publishers, FTPH (2000)

11. Munteanu, Gh., Atanasiu, Gh., *On Miron-connections in Lagrange spaces of second order*, Tensor N.S. 50(1991), pp. 241–247.

12. Munteanu, Gh., *Metric almost tangent structure of second order*, Bull. Math. Soc. Sci. Mat. Roumanie, 34(1), 1990, pp. 49–54.

13. Shen, Z., *Differential Geometry of Spray and Finsler spaces*, Kluwer Academic Publishers 2001.

RAZNE STRUKTURE U PROSTORIMA $Osc^k M$

Irena Čomić and Radu Miron

Geometrija prostora $Osc^k M$ je uveo R. Miron i Gh. Atanasiu u [6] i [7]. Teorija ovih prostora je razvijena od strane R. Mirona i njegovih saradnika iz Rumunije, Japana i drugih zemalja i prikazana je u mnogim člancima i knjigama. Samo neki od njih su spomenuti u literaturi. Ovde predstavljamo konstrukciju takvih adaptiranih baza u prostorima $T(Osc^k M)$ i $T^*(Osc^k M)$, koje su saglasne sa J strukturom. Teorija dva komplementarna podprostora je ovde data kao u [2] i [4]. Operatori J, $\overline{J}$, θ, $\overline{\theta}$, p, p^* su uvedeni u okolnom prostoru, kao i u potprostorima. Među njima su uspostavljene neke nove relacije. Ispitana je akcija ovih operatora na Liouville-ova vektorska polja.

Ključne reči i fraze: operacija projekcije, J struktura, θ struktura, potprostori u $Osc^k M$.

NINETY YEARS OF DUFFING'S EQUATION

UDC:531.36

Livija Cvetićanin

Faculty of Technical Sciences, Trg. D. Obradovica 6, 21000 Novi Sad, Serbia

4bstract. *In the paper the origin of the so named 'Duffing's equation' is shown. The author's generalization of the equation, her published papers dealing with Duffing's equation and some of the solution methods are presented. Three characteristic approximate solution procedures based on the exact solution of the strong cubic Duffing's equation are shown. Using the Jacobi elliptic functions the elliptic-Krylov-Bogolubov (EKB), the homotopy perturbation and the elliptic-Galerkin (EG) methods are described. The methods are compared. The advantages and the disadvantages of the methods are discussed.*

Key words: *Duffing's equation, elliptic-Krylov-Bogolubov method, homotopy perturbation method, elliptic-Galerkin method*

1. INTRODUCTION

In 1918, in the Edition *Vieweg*, No.41/42 the publication entitled "*Erzwungene Schwingungen bei veranderlicher Eigenfrequenz und ihre technische Bedeuting*" by Georg Duffing (Fig.1), Ingenieur, appears. The first sentence in the Preface of the book [1] is: "Die Anregung zu der vorliegenden Studie wurde mir zunachst durch Beobachtungen an Maschinen gegeben". This statement proves the appropriation of Georg Duffing to experimental-applied dynamics. He was a serious experimentalist who studied mechanical devices to discover geometric properties of dynamical systems [2]. The theory of oscillations was his explicit goal. In *Jahrbuch der Mathematik (1916-1918)*, (see [1]), a reviewer G.H. wrote that the aim of the paper [2] was to clarify the resonant oscillations which are evident in the pendulum (Fig.2) whose motion is given with a differential equation

$$\frac{d^2 y}{dt^2} + \gamma^2 (\sin y - \sin y_0) + \beta^2 (y - y_0) = k \sin \omega t \qquad (3)$$

where y is the pendulum displacement, t is time, β^2 and γ^2 are positive constants, y_0 is the initial deflection, k and ω are the amplitude and the frequency of the excitation force. Duffing simplified the equation into

$$\frac{d^2 y}{dt^2} + a^2 y - \beta y^2 - \gamma y^3 = k \sin \omega t \qquad (2)$$

and calculated the first term $H\sin\omega t$ of the periodic solution in the first approximation [3]. He obtained a cubic algebraic equation for H which has three solutions: two stable and an unstable one.

Fig.1. Georg Duffing, 1861-1944.   Fig.2. Duffing's oscillator
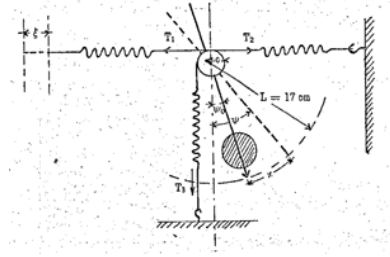
Duffing gives the problem to mathematicians to give the initial conditions for the unstable motion. Besides, Duffing considered the simplified versions of the Eq. (2) for describing the motion of the symmetrical pendulum

$$\frac{d^2 y}{dt^2} + \alpha y - \gamma y^3 = 0 \qquad (3)$$

and the unsymmetrical pendulum

$$\frac{d^2 y}{dt^2} + \alpha y - \beta y^2 = 0. \qquad (4)$$

For the case of small non-linearities ($\gamma \ll \alpha$ and $\beta \ll \alpha$), Duffing gave the approximate solutions in the form of Weierstrass $\wp(t)$ elliptic function [4]. The main disadvantage of the solutions was their complexity and unsuitability for practical use.

    During the last years the Eq. (2) is modified and some generalizations are introduced. Usually, the differential equations with polynomial type of non-linearity are called 'Duffing's equation'. The most often investigated type of the Duffing's equation is with the cubic non-linearity

$$\frac{d^2 y}{dt^2} + 2\delta \frac{dy}{dt} \pm \alpha y \pm \gamma y^3 = k \sin \omega t \qquad (5)$$

where δ is the damping coefficient.

    About 2000 papers are published dealing with qualitative and quantitative analysis of Eq. (5). Two approaches are assumed: one, based on assumption that the non-linearity is

small ($\alpha>0$, $\gamma<<\alpha$) and the other, the non-linearity is strong ($\gamma\approx\alpha$). Various analytical approximate solving procedures are developed. For the small non-linearity the most widely applied methods are: the method of multiple scales [5], the Bogolubov-Mitropolski [6], the Krylov-Bogolubov method [7], the straightforward expansion [8], Linstedt-Poincare method [9], etc. The author of this review modified the suggested methods for solving a second order differential equation with slow time variable parameters [10], a system of two coupled differential equations with constant coefficients [11]-[15] and slow time variable functions [16]-[21]. For all of these methods it is common that they represent the perturbation to the linear one and the difference between the approximate solution of the non-linear system and the linear one is of small order.

For the case of strong cubic non-linearity, the analytical approximate solution of (5) is based on the exact solution of the differential equation

$$\frac{d^2y}{dt^2} \pm \alpha y \pm \gamma y^3 = 0 \qquad (6)$$

The author of this paper developed the approximate analytical solving methods [22] for

$$\frac{d^2y}{dt^2} \pm \alpha y \pm \gamma y^3 = f(y, \frac{dy}{dt}) \qquad (7)$$

where f is an additional linear or non-linear function which need not be small, and also for the system of coupled Duffing's equations [23]-[31]. The strong non-linear differential equations with slow time variable parameters are also considered [32]. The chaotic motion in the strong coupled system with constant and changeable parameters is investigated in [33]-[36]. The special cases of differential equations are those with pure non-linear term (see [37]-[40]). In the paper [40] the general form of the pure non-linear differential equation of Duffing's type is introduced.

In spite of the fact that a numerous methods are developed for analytic solving of the strong non-linear differential equations, the asymptotic approaches still need to be considered. Namely, all of the suggested asymptotic solving procedures have beside their advantages also some disadvantages. All the methods can be grouped as: residual methods, perturbation techniques and homotopic methods. In this paper the elliptic-Galerkin method which is the conceptually simplest analytic approximate procedure, the perturbation elliptic-Krylov-Bogolubov method, and the homotopy perturbation method which is adopted for solving of the Duffing's equation, will be shown.

2. DIFFERENTIAL EQUATION WITH STRONG CUBIC NON-LINEARITY

The Eq. (6) with initial conditions

$$y(0) = y_0, \quad \dot{y}(0) = \dot{y}_0 \qquad (8)$$

has an exact analytic solution in the form

$$y = Yep(\omega t + \theta, k^2), \qquad (9)$$

where ep denotes a convenient Jacobi elliptic function [41], $\omega(Y)$ is the frequency, $k^2(Y)$ is the modulus of the elliptic function and Y and θ, i.e., the amplitude and phase angle are arbitrary constants dependent on the initial conditions (8).

Dependently on the sign of the coefficients α and γ the following type of equations are evident: 1) the hard one: $\alpha>0$ and $\gamma>0$, 2) the hard-soft one: $\alpha >0$ and $\gamma<0$, 3) soft-hard one: $\alpha<0$ and $\gamma>0$.

For the case of strong cubic non-linearity of hardening type, the differential equation

$$\ddot{y} + \alpha y + \gamma y^3 = 0 \tag{10}$$

has an exact analytical solution in the form of the Jacobi elliptic function

$$y = Ycn(\omega t + \theta, k^2) \tag{11}$$

where cn is the Jacobi elliptic function [48], ω and k are the frequency and modulus of the function

$$\omega^2 = \alpha + \gamma Y^2, \quad k^2 = \frac{\gamma Y^2}{2(\alpha + \gamma Y^2)} \tag{12}$$

and Y and θ are arbitrary constants dependent on the initial conditions (8). Substituting (11) and its time derivative into (8), we obtain the amplitude Y and the phase angle θ according to the relations

$$\frac{\gamma}{2}Y^4 + \alpha Y^2 - \left[\alpha y_0^2 + \frac{\gamma}{2} y_0^4 + \dot{y}_0^2 \right] = 0 \tag{13}$$

and

$$sc(\theta, k^2)dn(\theta, k^2) = -\frac{\dot{y}_0}{y_0 \omega} \tag{14}$$

For the special initial conditions

$$y(0) = y_0, \quad \dot{y}(0) = 0 \tag{15}$$

the amplitude and phase angle are

$$Y = y_0, \quad \theta = 0 \tag{16}$$

and for

$$y(0) = 0, \quad \dot{y}(0) = \dot{y}_0 \tag{17}$$

it yields

$$Y = \left[-\frac{\alpha}{\gamma} + \frac{\alpha}{\gamma}\sqrt{1 + \frac{2\dot{y}_0^2\gamma}{\alpha^2}} \right]^{1/2}, \quad \theta = K(k^2) \tag{18}$$

where $K(k^2)$ is the complete elliptic integral of the first kind [41]. Assuming the series expansion of the square root the approximate amplitude is $Y \approx \dot{y}_0$.

Using the aforementioned procedure Yuste and Bejarano [42] give the solutions for the hard-soft and soft-hard systems.

Table 1 Solutions for the hard-soft and soft-hard systems.

Type	Solution	Frequency	Modulus
$\alpha>0, \gamma<0$	$y^0 = Y sn(\omega t + \theta, k^2)$	$\omega^2 = \alpha - \dfrac{\gamma Y^2}{2} > 0$	$k^2 = \dfrac{\gamma Y^2}{2\omega^2}$
$\alpha<0, \gamma>0$	$y^0 = Y cn(\omega t + \theta, k^2)$	$\omega^2 = \gamma Y^2 - \alpha > 0$	$k^2 = \dfrac{\gamma Y^2}{2\omega^2}$

Remarks:

1. It is obvious that the solution for the hard oscillator exists for all values of parameters α and γ, but for other oscillators (hard-soft and soft-hard) the motion is oscillatory only for some special relations between the parameters α and γ and initial amplitude Y.

2. The arbitrary amplitude Y and phase θ are calculated according to the initial conditions (8), (15) or (17).

3. For the pure cubic equation, when $\alpha=0$, the modulus of the Jacobi elliptic function is constant ($k^2=1/2$) and the frequency is $\omega = Y\sqrt{\gamma}$. The closed form solution is

$$y = Y cn(Y t \sqrt{\gamma} + \theta, 1/2) \tag{19}$$

For the initial conditions (8), the amplitude of vibration is

$$Y = \left[y_0^4 + \frac{2}{\gamma} \dot{y}_0^2 \right] \tag{}$$

3. THE ELLIPTIC HOMOTOPY PERTURBATION METHOD

Let us rewrite the differential equation (7) in the form

$$\ddot{y} + \alpha y + \gamma y^3 = -g(y, \dot{y}) \tag{20}$$

and apply the initial conditions (15). For $g=0$ the differential equation has the exact solution (11) with (16). According to this result, we assume the initial approximate solution of (20) in the form

$$Y_0(t) \equiv Y_0 = y_0 cn(\omega_1 t, k_1^2) = y_0 cn_1 \tag{21}$$

where ω_1 and k_1^2 transform into ω and k^2 when $g=0$. Due to definition of homotopy $X: \Omega \times [0,1] \rightarrow R$, that the two continuous functions from one topological space can be "continuously deformed" into the other, and introducing the embedding artificial parameter p with the values in the interval [0,1], as it was suggested by He [43], a homotopy transformation of the differential equation (20) yields

$$(1-p)[(\ddot{X}+\alpha X+\gamma X^3)-(\ddot{Y}_0+\alpha Y_0+\gamma Y_0^3)]+p[\ddot{X}+\alpha X+\gamma X^3+g(X,\dot{X})]=0 \qquad (22)$$

with initial conditions

$$X(0,p)=y_0, \quad \dot{X}(0,p)=0 \qquad (23)$$

Namely, for $p=0$ the Eq. (22) simplifies into

$$\ddot{X}+\alpha X+\gamma X^3=0 \qquad (24)$$

with the exact solution

$$X(t,0)=y^0(t)=Ycn(\omega t+\theta,k^2) \qquad (25)$$

When $p=1$ the equation has the same form as the original equation

$$\ddot{X}+\alpha X+\gamma X^3=-g(X,\dot{X}) \qquad (26)$$

and the solution is

$$X(t,1)=y(t). \qquad (27)$$

It can be concluded that for the change of p from zero to unity the solution is continually changing from (25) to (27).

For $X(t,p)$, which is the solution of (22) in the whole domain $p\in[0,1]$ and is smooth enough to have kth order partial derivatives respect to p at $p=0$, the Maclaurin series is as follows

$$X(t,p)=Y_0(t)+\sum_{k=1}^{\infty}\left(\frac{y_k(t)}{k!}\right)p^k \qquad (28)$$

Substituting (28) into (22) and separating the terms with the same order of the parameter p a system of linear differential equations is obtained. For p^1 the first-order deformation equation is

$$\ddot{y}_1+\alpha y_1+3\gamma Y_0^2 y_1=-[\ddot{Y}_0+\alpha Y_0+\gamma Y_0^3+g(Y_0,\dot{Y}_0)] \qquad (29)$$

with initial conditions

$$y_1(0)=0, \quad \dot{y}_1(0)=0 \qquad (30)$$

Introducing (21) into (29), yields

$$\ddot{y}_1+\alpha y_1+3\gamma y_0^2 cn_1^2 y_1=-[-y_0\omega_1^2 cn_1(1-2k_1^2+2k_1^2 cn_1^2)+\alpha y_0 cn_1+\gamma y_0^3 cn_1^3$$
$$+g(y_0 cn_1,-y_0\omega_1 sn_1 dn_1)], \qquad (31)$$

where $sn_1\equiv sn(\omega_1 t,k_1)$ and $dn_1\equiv dn(\omega_1 t,k_1)$ are Jacobi elliptic functions [48].

For

$$\alpha=0, \quad g(y,\dot{y})=-\beta y^2, \quad \gamma>\beta \qquad (32)$$

the Eq. (31) is specified as

$$\ddot{y}_1 + 3\gamma y_0^2 cn_1^2 y_1 = -[-y_0 \omega_1^2 cn_1 (1 - 2k_1^2 + 2k_1^2 cn_1^2) + \gamma y_0^3 cn_1^3 + \beta y_0^2 cn_1^2)] \qquad (33)$$

Solution of (33) is assumed as a sum of a constant and a linear term of elliptic function cn_1

$$y_1 = K_1 + K_2 cn_1 \qquad (34)$$

Substituting (34) into (33) and separating the terms with the same order of elliptic function cn_1 the following system of algebraic equations is obtained

$$(K_1 + y_0)\omega_1^2(1 - 2k_1^2) = 0,$$
$$3\gamma y_0^2 K_0 + \beta K_0^2 = 0, \qquad (35)$$
$$3\beta y_0^2 K_1 + \gamma y_0^3 - 2(K_1 + y_0)k_1^2 \omega_1^2 = 0.$$

Due to initial conditions (30) the relation K_0 and K_1 is

$$K_0 + K_1 = 0 \qquad (36)$$

Solving equations (35) and (36) it follows:

$$\omega_1^2 = 3\gamma y_0^2 \frac{\gamma y_0 + \beta}{3\gamma y_0 + \beta}, \quad k_1^2 = \frac{1}{2}, \quad K_0 = -K_1 = -\frac{\beta}{3\gamma} \qquad (37)$$

Using the relations (21) and (34) with (37) and according to (27) and (28) the solution in the first approximation is

$$y(t) = -\frac{\beta}{3\gamma} + (y_0 + \frac{\beta}{3\gamma})cn(y_0 t\sqrt{3\gamma \frac{\gamma y_0 + \beta}{3\gamma y_0 + \beta}}, \frac{1}{2}) \qquad (38)$$

Analyzing (37) it is obvious that the coefficient β has no influence on modulus of Jacobi function. Frequency and argument of Jacobi function and also the accuracy of the approximate solution (38) depend on coefficient ratio β/γ. For smaller ratio $(\beta/\gamma)\ll 1$ the difference between exact solution and approximate solution is negligible. For higher values of the ratio β/γ the difference is significant and the solution in the first approximation is not acceptable.

4. ELLIPTIC-KRYLOV-BOGOLUBOV (EKB) METHOD

Let us modify the differential equation (7) by introducing the small parameter $\varepsilon \ll 1$

$$\frac{d^2 y}{dt^2} + \alpha y + \gamma y^3 = \varepsilon f(y, \frac{dy}{dt}) \qquad (39)$$

Due to idea of Krylov and Bogolubov [44], Eq. (39) can be transformed into a system of two coupled first order differential equations. Namely, the solution of (39) is assumed in the form of the solution (19) for $\varepsilon=0$, i.e.,

$$y(t) = Y(t)cn(\psi(t),k^2) \equiv Ycn \tag{40}$$

where the amplitude and the phase are time dependent

$$\psi(t) = \int_0^t \omega(s)ds + \theta(t) \tag{41}$$

and, also, the frequency and the modulus of Jacobi elliptic function (12)

$$\omega(t) = \sqrt{\alpha + \gamma[Y(t)]^2}, \quad k^2(t) = \frac{\gamma[Y(t)]^2}{2(\alpha + \gamma[Y(t)]^2)} \tag{42}$$

The first time derivative of (40) is

$$\frac{dy}{dt} = Y\omega\frac{\partial(cn)}{\partial\psi} \tag{43}$$

with the constraint

$$\frac{dY}{dt}cn + Y\frac{d\theta}{dt}\frac{\partial(cn)}{\partial\psi} + Y\frac{\partial(cn)}{\partial(k^2)}\frac{\partial(k^2)}{\partial Y}\frac{dY}{dt} = 0 \tag{44}$$

Substituting (40), (43) and the time derivative of (43) into (39), we obtain

$$\frac{dY}{dt}[(\omega + Y\frac{\partial\omega}{\partial Y})\frac{\partial(cn)}{\partial\psi} + Y\omega\frac{\partial^2(cn)}{\partial\psi\partial(k^2)}\frac{\partial(k^2)}{\partial Y}] + Y\omega\frac{d\theta}{dt}\frac{\partial^2(cn)}{\partial\psi^2} = \varepsilon f(Ycn, Y\omega\frac{\partial(cn)}{\partial\psi}) \tag{45}$$

After some transformation of (44) and (45), the two coupled first order differential equations follow

$$\frac{dY}{dt}[(\omega + Y\frac{\partial\omega}{\partial Y})(cn_\psi)^2 + Y\omega cn_{\psi k}cn_\psi\frac{\partial(k^2)}{\partial Y} - \omega cn_{\psi\psi}(cn + Ycn_k\frac{\partial(k^2)}{\partial Y})]$$
$$= \varepsilon[f(Ycn, Y\omega cn_\psi)]cn_\psi,$$
$$Y\frac{d\theta}{dt}[(\omega + Y\frac{\partial\omega}{\partial Y})(cn_\psi)^2 + Y\omega cn_{\psi k}cn_\psi\frac{\partial(k^2)}{\partial Y} - \omega cn_{\psi\psi}(cn + Ycn_k\frac{\partial(k^2)}{\partial Y})] \tag{46}$$
$$= -\varepsilon[f(Ycn, Y\omega cn_\psi)](cn + Ycn_k\frac{\partial(k^2)}{\partial Y}),$$

where $cn_\psi \equiv \frac{\partial(cn)}{\partial\psi}, cn_{\psi\psi} \equiv \frac{\partial^2(cn)}{\partial\psi^2}, cn_{\psi k} \equiv \frac{\partial^2(cn)}{\partial\psi\partial(k^2)}.$

The aim is to solve the system of differential equations.

For the pure cubic Duffing's equation, where $\alpha=0$ and the modulus of the Jacobi elliptic function is constant (see (19)), the system (46) simplifies to

$$\frac{dY}{dt}[(\omega+Y\frac{\partial\omega}{\partial Y})(cn_\psi)^2 - \omega cn_{\psi\psi}\,cn] = \varepsilon[f(Ycn,Y\omega cn_\psi)]cn_\psi,$$

$$Y\frac{d\theta}{dt}[(\omega+Y\frac{\partial\omega}{\partial Y})(cn_\psi)^2 - \omega cn_{\psi\psi}\,cn] = -\varepsilon[f(Ycn,Y\omega cn_\psi)]cn,$$

(47)

where $cn_\psi = -sndn, cn_{\psi\psi} = -cn(1-2k^2+2k^2cn^2)$. Using the value for the modulus ($k^2=1/2$) and the frequency ($\omega = Y\sqrt{\gamma}$) of the Jacobi elliptic function, and also the relations between the elliptic functions, we have

$$Y^2\sqrt{\gamma}\frac{d\theta}{dt} = -\varepsilon[f(Ycn,-Y^2\sqrt{\gamma}\,sndn]cn,$$

$$Y\sqrt{\gamma}\frac{dY}{dt} = -\varepsilon[f(Ycn,-Y^2\sqrt{\gamma}\,sndn]sndn.$$

(48)

At this point the averaging procedure is introduced. The averaging is over the period of the elliptic function $4K(k^2)$, where $K(k^2)$ is the complete elliptic integral of the first kind. The averaged first order differential equations (48) are

$$\frac{dY}{dt} = -\frac{\varepsilon}{\omega}\frac{1}{4K}\int_0^{4K} f(Ycn,-Y\omega\,sn\,dn)sn\,dn\,d\psi$$

(49)

$$\frac{d\theta}{dt} = -\frac{\varepsilon}{Y\omega}\frac{1}{4K}\int_0^{4K} f(Ycn,-Y\omega\,sn\,dn)cn\,d\psi$$

(50)

where for the modulus $k^2=1/2$ the elliptic integral is $K = K(1/2) = 1.85407$ and $cn=cn(\psi,1/2)$, $sn=sn(\psi,1/2)$, $dn=dn(\psi,1/2)$.

a) For the special case when the small non-linear function depends only on the deflection, i.e., $f \equiv f(y)$, the first order differential equations (49) and (50) simplify to

$$\frac{dY}{dt} = 0, \quad \frac{d\theta}{dt} = \frac{\varepsilon}{Y\omega}\frac{1}{4K}\int_0^{4K} f(Ycn)cn\,d\psi$$

(51)

i.e., Y=const. and $\theta=\varepsilon\theta(Y)$,
where

$$\theta = \frac{1}{4KY\omega}\int_0^{4K} f(Ycn)cn\,d\psi$$

(52)

Then, the EKB approximate solution is

$$y = Ycn[(\omega+\varepsilon\theta)t+\theta_0,1/2]$$

(53)

where from the initial conditions of the oscillations Y and θ_0 are obtained.

b) For $f \equiv f(dy/dt)$, the Eqs. (49) and (50) have the form

$$\frac{dY}{dt} = -\frac{\varepsilon}{\omega}\frac{1}{4K}\int_0^{4K} f(-Y\omega\,sn\,dn)sn\,dn\,d\psi \tag{54}$$

$$\frac{d\theta}{dt} = 0 \tag{55}$$

The EKB solution yields

$$y = Y(t)cn[(\sqrt{\gamma}\int_0^t Y(t)dt) + \theta_0, 1/2] \tag{56}$$

where $Y(t)$ is the solution of (54).

Examples

1) For the differential equation with strong non-linear cubic term and the weak linear part

$$\ddot{y} + \gamma y^3 + \varepsilon y = 0 \tag{57}$$

the phase angle is due to (52)

$$\theta = \frac{1}{4K\omega}\int_0^{4K} cn^2\,d\psi = \frac{1}{\omega}(\frac{2E}{K}-1) = \frac{0.4569}{\omega} \tag{58}$$

and the approximate solution of (57) is according to (53) and (58)

$$y = Ycn[(\omega + \frac{0.4569\varepsilon}{\omega})t + \theta_0, 1/2] \tag{59}$$

where $E=E(1/2)=1.35064$ is the complete elliptic integral of the second kind for modulus $k^2=1/2$ and $\omega = Y\sqrt{\gamma}$.

The exact solution of (57) is according to (11), (12) and (15)

$$y = Ycn[t\sqrt{\varepsilon + \gamma Y^2} + \theta_0, \gamma Y^2/2(\varepsilon + \gamma Y^2)] \tag{60}$$

For $\varepsilon \ll 1$ using the series expansion of the functions in (60) the approximate solution is obtained

$$y = Ycn[t(\omega + \frac{\varepsilon}{2\omega}) + \theta_0, 1/2] \tag{61}$$

Comparing (59) and (61) it is evident that the difference is negligible.

2) For the differential equation with small linear damping term

$$\ddot{y} + \gamma y^3 + 2\zeta\dot{y} = 0 \tag{62}$$

the amplitude of vibration is according to (54)

$$\frac{dY}{dt} = -\frac{\varepsilon(2\zeta)Y}{4K}\int_0^{4K} sn^2 \, dn^2 \, d\psi = -\frac{\varepsilon(2\zeta)Y}{4K}Q \tag{63}$$

i.e.,

$$Y = Y_0 \exp(-\frac{\varepsilon(2\zeta)}{4K}Q)t \tag{64}$$

where $Q = \int_0^{4K} sn^2 \, dn^2 \, d\psi$. Using (56) and (64) the solution of (62) follows

$$y = Y_0 \exp(-\frac{\varepsilon(2\zeta)t}{4K}Q)cn[Y_0\sqrt{\gamma} \, \frac{4K}{\varepsilon(2\zeta)Q}(1-\exp(-\frac{\varepsilon t(2\zeta)Q}{4K}))+\theta_0,1/2]$$

After some simplification the approximate solution is

$$y = Y_0 \exp(-\frac{\varepsilon(2\zeta)t}{4K}Q)cn[Y_0 t\sqrt{\gamma} + \theta_0,1/2] \tag{65}$$

The amplitude of vibration decreases exponentially. The period of vibration increases, but very slow. It allows the assumption of the constant frequency of vibration.
Remark:
The EKB method is usual known as that with time variable amplitude and phase, as it is assumed that the perturbed amplitude and phase of the solution differs for a small value to trial solution.

5. ELLIPTIC-GALERKIN (EG) METHOD

Let us consider the differential equation

$$\ddot{y} + \alpha y + \beta y^2 + \gamma Y^3 = 0 \tag{66}$$

The approximate solution will be obtained by applying the Galerkin method which represents one of the weighted residual methods. In the previous papers, usually, the trial solution of (66) is assumed as a linear combination of the circular functions and the arbitrary weight function also belongs to that group. Our intention is to extend the method by applying of the Jacobi elliptic function.
We introduce a trail solution to (66) as a linear combination of independent cn Jacobi elliptic functions

$$y = K_1 cn(\omega t,k^2) + K_2 cn^2(\omega t,k^2) = K_1 cn + K_2 cn^2 \tag{67}$$

where K_1 and K_2 are constants, ω and k are the frequency and modulus of the cn elliptic function which have to be calculated.
Substituting (67) into (66), the residual function is obtained

$$r(\psi) \equiv K_1\omega^2(cn)''+2K_2\omega^2[(cn)']^2 + 2K_2\omega^2(cn)(cn)''+\alpha[K_1cn + K_2(cn)^2]$$
$$+ \beta[K_1^2(cn)^2 + 2K_1K_2(cn)^3 + K_2^2(cn)^4] + \gamma[K_1^3(cn)^3 + 3K_1^2K_2(cn)^4 \qquad (68)$$
$$+ 3K_1K_2^2(cn)^5 + K_2^3(cn)^6],$$

where $(\cdot)'=d(\cdot)/d\psi$, $(\cdot)''=d^2(\cdot)/d\psi^2$ and $\psi=\omega t$. If (67) is the closed form solution of Eq. (66), the residual function $r(\psi)$ is zero. The goal is to construct $y(\psi)$ so that the integral of the residual will be zero for some choices of weight functions $w(\psi)$. As the weight function is arbitrary one, let us choose it as the derivatives of the constant K_1 and K_2, respectively, of the assumed solution (67), i.e., $(\partial y/\partial K_1)$ and $(\partial y/\partial K_2)$. Multiplying (68) with the weight function and integrating over the interval $[0,4K(k)]$, where K is the total elliptic integral of the first kind and $4K$ is the period of cn function, one obtains

$$\int_0^{4K(k)} r(\psi)cnd\psi = 0, \quad \int_0^{4K(k)} r(\psi)cn^2d\psi = 0 \qquad (69)$$

i.e.

$$\int_0^{4K(k)} -K_1\omega^2 cn^2(1-k^2+k^2cn^2) + \alpha K_1 cn^2 + 2\beta K_1 K_2 cn^4 + \gamma[K_1^3 cn^4 + 3K_1 K_2^2 cn^6]d\psi = 0$$

$$\int_0^{4K(k)} -2K_2 cn^4 \omega^2(1-k^2+k^2cn^2) + 2K_2\omega^2 sn^2 cn^2 dn^2 + \alpha K_2 cn^4 \qquad (70)$$
$$+ \beta[K_1^2 cn^4 + K_2^2 cn^6] + \gamma[3K_1^2 K_2 cn^6 + K_2^3 cn^8]d\psi = 0.$$

Eqs. (66) and (69), i.e. (70), are equivalent, because $w(\psi)$ is any arbitrary function. To apply the method, all we need to do is to solve the two algebraic equations for the coefficients $\omega = \omega(K_1, K_2)$ and $k^2 = k^2(K_1, K_2)$

$$\omega^2[(1-k^2)C_2 + k^2C_4] = \alpha C_2 + (2\beta K_2 + \gamma K_1^2)C_4 + 3K_2^2\gamma C_6 \qquad (71)$$

$$K_2\omega^2[2(2-3k^2)C_4 + 4k^2C_6 - 2(1-k^2)C_2]$$
$$= (\beta K_1^2 + \alpha K_2)C_4 + (\beta K_2 + 3\gamma K_1^2)K_2C_6 + \gamma K_2^3 C_8, \qquad (72)$$

where (see [48]): $k'^2=1-k^2$, $C_0=4K(k)$, $C_2 = \dfrac{4}{k^2}(E - k'^2 K)$ and

$$C_{2m+2} = \frac{2m(2k^2-1)C_{2m} + (2m-1)k'^2 C_{2m-2}}{(2m+1)k^2} \qquad \text{for} \quad m=1,2,3.$$

Eliminating ω from (71) and (72) we obtain the algebraic equation

$$\frac{K_2}{(1-k^2)C_2 + k^2 C_4}[\alpha C_2 + (2\beta K_2 + \gamma K_1^2)C_4 + 3K_2^2 \gamma C_6]$$

$$= \frac{(\beta K_1^2 + \alpha K_2)C_4 + (\beta K_2 + 3\gamma K_1^2)K_2 C_6 + \gamma K_2^3 C_8}{2(2 - 3k^2)C_4 + 4k^2 C_6 - 2(1-k^2)C_2},$$

(73)

which is not easy to be solved. Analyzing the relation (71) and (73) it is seen that the both strong non-linear terms have a significant influence on the modulus and the frequency of the Jacobi elliptic function. Only, for the case when $\alpha=\beta=0$ the modulus of the Jacobi elliptic function is independent on the initial amplitude, but the frequency depends, as it is previously stated in Eq. (19).

Remark: The accuracy of the solution depends on our ability to find the most convenient combination of functions.

6. CONCLUSION

In the paper three procedures for solving of the so called Duffing's equation are shown: the elliptic-Galerkin (EG) method, the elliptic-Krylov-Bogolubov (EKB) method and the homotopy perturbation method. For all of the methods is common that the solutions are based on the exact solution of the strong cubic differential equation given with Jacobi elliptic function. The mentioned methods have some advantages, but also disadvantages. The EG method is one of conceptually simplest analytical approximate procedure which leads to algebraic equations; however the results may be with small accuracy as it depends on the investigator to chose the most adequate weight function. The elliptic-Krylov-Bogolubov (EKB) method is of perturbation type. The perturbation method is based on the assumption that a small parameter ($\varepsilon \ll 1$) must exist in the equation. This so-called small parameter assumption greatly restricts applications of perturbation technique. Many non-linear problems described with Duffing's equation have no small parameter at all. Then, an appropriate choice of a small parameter leads to accurate results, but an unsuitable choice to a bad result. The homotopy method does not require a small parameter in the equation and eliminates the previous limitations. The main disadvantage is the question of convergence of the solution. Farther investigations are necessary.

REFERENCES

(SAMPLES FOR SERIAL, BOOK, PROCEEDING, THESIS, PATENT - *STYLE REFERENCE*)

1. Rimrott F.P.J., Georg Duffing (1861-1944), *Technische Mechanik*, Band 14, Heft 1, 77-82, 1994.
2. Duffing G., *Erzwungene Schwingungen bei veranderlicher Eigenfrequenz und ihre technische Bedeuting*, Druck und Verlag von Fridr. Vieweg & Sohn, Braunschweig.1918.
3. Abraham R.H., Shaw C.D., *Dynamics – the geometry of behavior*, Part I. Aerial Press, Santa Cruz, 2000.

4. Gradstein I. S., Rjizhik I. M., *Tablicji integralov, summ, rjadov i proizvedenij,* Nauka, Moscow, 1971.
5. Nayfeh A.H., Mook D.T., *Nonlinear Oscillations,* Wiley, New York, 1979.Goroško
6. Bogoliubov N.N., Mitropolskij Ju.A., *Asimptotichesike metodi v teorii nelinejnih kolebanij,* Nauka, Moscow, 1974.
7. Moiseev N.N., *Asimptoticheskie metodi nelinejnoj mehaniki*, Nauka, Moscow, 1981.
8. J. Kevorkian, J. D. Cole, Perturbation methods in applied mathematics, in *Applied Mathematical Sciences*, 34, Springer Verlag, New York, 1981.
9. Mickens R.E., *Nonlinear Oscillations*, Cambridge University Press, New York, 1981.
10. Cveticanin L., The influence of the reactive force on a nonlinear oscillator with variable parameter. *Trans. ASME, J. of Vibration and Acoustics*, 114, 578-580, 1992.
11. Cveticanin L., Yamakawa H., Matsushita O., An asymptotic method applied to nonlinear systems with coupled deflection. *Journal of the Franklin Institute*, 327, 71-83, 1991.
12. Cveticanin L., Approximate analytical solutions to a class of nonlinear equations with complex functions. *Journal of Sound and Vibration*, 157, 289-302, 1992.
13. Cveticanin L., An asymptotic solution to weak nonlinear vibrations of the rotor. *Mechanism and Machine Theory*, 28, 495-506, 1993.
14. L. Cveticanin, An approximate solution for a system of two coupled differential equations. *Journal of Sound and Vibration*, 153, 375-380, 1992.
15. Cveticanin L., Resonant vibrations of nonlinear rotors. *Mechanism and Machine Theory*, 30, 581-588, 1995.
16. Cveticanin L., Vibrations of a textile machine rotor. *Journal of Sound and Vibration*, 97, 181-187, 1984.
17. Cveticanin L., The vibrations of a textile machine rotor with nonlinear characteristics. *Mechanism and Machine Theory*, 21, 29-32, 1986.
18. Cveticanin L.J., The oscillations of a textile machine rotor on which the textile is wound up. *Mechanism and Machine Theory*, 26, 253-260, 1991.
19. Cveticanin L., An approximative solution of a coupled differential equation with variable parameter. *Trans. ASME, J. of Applied Mechanics*, 60, 214-217, 1993.
20. Cveticanin L., Dynamic behavior of a rotor with time-dependent parameters. *JSME, Int. J., Ser. C*, 37, 41-48, 1994.
21. Cveticanin L., The influence of the reactive force on the motion of the rotor on which the band is winding up. *Journal of Sound and Vibration*, 167, 382-384, 1993.
22. Cveticanin L., Analytical methods for solving strongly non-linear differential equations. *Journal of Sound and Vibration*, 214, 325-338, 1998.
23. Cveticanin L., Some particular solutions which describe the motion of the rotor. *Journal of Sound and Vibration*, 212, 173-178, 1998.
24. Cveticanin L., Analytic approach for the solution of the complex-valued strong non-linear differential equation of Duffing type. *Physica A*, 297, 348-360, 2001.
25. Cveticanin L., Vibrations of a coupled two-degree-of-freedom system. *Journal of Sound and Vibration*, 247, 279-292, 2001.
26. Cveticanin L., The motion of a two-mass system with non-linear connection. *Journal of Sound and Vibration*, 252, 361-369, 2002.
27. Cveticanin L., Forced non-linear vibrations of a symmetrical two-mass-system. *Journal of Sound and Vibration*, 265, 451-458, 2003.
28. Cveticanin L., Free vibration of a strong non-linear system described with complex function. *Journal of Sound and Vibration*, 277, 815-824, 2004.
29. Cveticanin L., A new approach for solving of a complex-valued differential equation. *Journal of Sound and Vibration*, 278, 1181-1195, 2004.
30. Cveticanin L., Approximate solution of a strongly non-linear complex differential equation. *Journal of Sound and Vibration*, 284, 503-512, 2005.
31. Cveticanin L., The homotopy-perturbation method applied for solving complex-valued differential equations with strong cubic non-linearity. *Journal of Sound and Vibration*, 285, 1171-1179, 2005.
32. Cveticanin L., Approximate solution of a time-dependent differential equation. *Meccanica*, 30, 665-671, 1995.
33. Cveticanin L., Extension of Melnikov criterion for the differential equation with complex function. *Nonlinear Dynamics*, 4, 139-152, 1993.
34. Cveticanin L., A necessary condition for chaos in rotor systems. *Mechanism and Machine Theory*, 32, 411-416, 1997.

35. Zukovic M., Cveticanin L., Chaotic responses in a stable Duffing system of non-ideal type. *Journal of Vibration and Control*, 13, 751-767, 2007.
36. Cveticanin L., Chaos in the rotors with slow variable mass, *Journal of Sound and Vibration*, 185, 897-901, 1995.
37. Cveticanin L., Analytical solutions of the system of two coupled pure cubic non-linear oscilators equations. *Journal of Sound and Vibration*, 245, 571-580, 2001.
38. Cveticanin L., Free vibration of a Jeffcott rotor with pure cubic non-linear elastic property of the shaft. *Mechanism and Machine Theory*, 40, 1330-1344, 2005.
39. Cveticanin L., Homotopy-perturbation method for pure non-linear differential equation. *Chaos, Solitons and Fractals*, 30, 1221-1230, 2006.
40. Cveticanin L., Oscillator with fraction order restoring force. *Journal of Sound and Vibration*, 320, 1064-1077, 2009.
41. Byrd P.F., Friedman M.D., *Handbook of Elliptic Integrals for Engineers and Physicists*, Springer-Verlag, Berlin, 1954.
42. Yuste S.B., Bejarano J.D., Extension and improvement to the Krylov-Bogoliubov methods using elliptic functions. *International Journal of Control*, 49, 1127-1141, 1989.
43. He J.H., Homotopy perturbation technique. *Comput. Methods Appl. Mech. Engrg.*, 178, 257-262, 1999.
44. Yuste S.B., Bejarano J.D., Construction of approximate analytical solutions to a new class of non-linear oscillator equations. *Journal of Sound and Vibration,* 110, 347-350, 1986.

DEVEDESET GODINA DUFINGOVE JEDNAČINE

Livija Cvetićanin

Abstrakt. U radu su dati izvorni podaci za tzv. Dufingovu jednačinu. Pirkazana je generalizacija koju je izvršio autor ovog rada, prikazani su njeni radovi koji se bave Dufingovom jednačinom kao i neke od metoda za rešavanje ove jednačine. Date su tri najznačajnije procedure nalaženja približnog rešenja na bazi tačnog rešenja Dufingove jednačine sa jakom kubnom nelinearnosti. Koristeći Jakobijeve eliptičke funkcije opisane su sledeće metode: eliptički-Krilov-Boboljubov (EKB) metod, homotopijski perturbacioni i eliptičke-Galerkinov (EG) metod. Metode su poredjene. Prikazane su prednosti i nedostaci pojedinih procedura.

Ključne reči: *Dufingova jednačina, eliptički-Krilov-Boboljubov (EKB) metod, homotopijski perturbacioni metod, eliptičke-Galerkinov (EG) metod*

ON A SHOCKLEY-READ-HALL MODEL FOR SEMICONDUCTORS

UDC:517.9;

Julka Knežević-Miljanović

Faculty of Mathematics, Belgrade, Serbia

Abstract: *The Shockley-Read-Hall model was introduced in 1952 to describe the statistics of recombination of holes and electrons in semiconductors occurring through the mechanism of trapping and we consider initial-boundary value problems with initial conditions.*
Key words*: partial differential equations, initial-boundary value problems*
AMS subject classification: Primary 35A05. Secondary 35B30

INTRODUCTION

The governing equations are given by

$$\partial_t n = \nabla\big(\mu_n(U_T\nabla n - n\nabla V)\big) + c_c n_{tr} - c_d n(N_{tr} - n_{tr}) \tag{1}$$

$$\partial_t p = \nabla\big(\mu_p(U_T\nabla p - p\nabla V)\big) + c_a n(N_{tr} - n_{tr}) - c_b n_{tr} p \tag{2}$$

$$\partial_t n_{tr} = c_a(N_{tr} - n_{tr}) + c_b n_{tr} p - c_c n_{tr} + c_d n(N_{tr} - n_{tr}) \tag{3}$$

$$\varepsilon_s \Delta V = q(n + n_{tr} - p - C) \tag{4}$$

Here n denotes the density of electrons in the conduction band, whereas p is the density of holes in the valence band, with p, n being opposite charges. The position density of occupied traps is given by n_{tr}; and by c_a, c_b, c_c, c_d we denote the rate constants. The quantity U_T is the so-called thermal voltage. In the following, we consider a semiconductor crystal with a constant (in space) number density of traps N_{tr}.

In the Poisson equation (4), V $(x; t)$ is the electrostatic potential, ε_s the permittivity of the semiconductor, q the elementary charge, and $C = C(x)$ the doping profile. By adding equations (1),(2),(3), we obtain the continuity equation

$$\partial_t(p - n - n_{tr}) + \nabla(J_n + J_p) = 0 \tag{5}$$

with current densities

$$J_n = \mu_n \left(U_T \nabla n - n \nabla V \right) \tag{6}$$

and

$$J_p = \mu_p \left(U_T \nabla p - p \nabla V \right) \tag{7}$$

Note that for the current density we use the simplest possible model, the drift diffusion ansatz, with constant mobilities μ_n, μ_p. Moreover, as there is no flux, there is no current density J_{tr}. The gap between the valence and the conduction band (which is called the bandgap) is very large for semiconductors, which means that lots of energy is needed to transfer electrons from the valence to the conduction band. This process is referred to as the generation of electron-hole pairs (or pair-generation process), i.e., an electron is created in the conduction band and a hole in the valence band. The inverse process is termed recombination of electron-hole pairs.

We now introduce a rescaling of n, p, and n_{tr} in order to render the equations (1)-(3) dimensionless: $n \to \overline{C} n$, $p \to \overline{C} p$, $n_{tr} \to N_{tr}$, $C \to \overline{C} C$, $x \to L x$, $n \to \overline{C} n$, $\mu_{n,p} \to \overline{\mu} \mu_{n,p}$, $n \to \overline{C} n$, $J_{n,p} \to \dfrac{\overline{\mu} U_T \overline{C}}{L} J_{n,p}$, and $\overline{C}$ is a typical value for C. Moreover, we rescale time $t \to \dfrac{t}{N_{tr} C}$ to make sure that all constants are of order 1, and set $c_c = c_d \overline{C} n_0$, $c_d = c_d \dfrac{\overline{C}}{\tau_n}$, $c_a = c_b \overline{C} p_0$, and $c_b = \dfrac{\overline{C}}{\tau_p}$. Given the scaling assumption $\varepsilon = \dfrac{N_{tr}}{C} \ll 1$, we finally obtain

$$\partial_t n = \nabla J_n + R_n \tag{8}$$

$$\partial_t p = -\nabla J_p + R_p \tag{9}$$

$$\varepsilon \partial_t n_{tr} = R_p - R_n \tag{10}$$

$$\nabla V = n + \varepsilon n_{tr} - p - C \tag{11}$$

where

$$J_n = \mu_n \left(\nabla n - n \nabla V \right) \tag{12}$$

and

$$J_p = -\mu_p \left(\nabla p - p \nabla V \right) . \tag{13}$$

By R_n and R_p we denote the recombination-generation rates for n and p, respectively:

$$R_n = \frac{1}{\tau_n} \left(n_0 n_{tr} - n \left(1 - n_{tr} \right) \right) \tag{14}$$

$$R_p = \frac{1}{\tau_p}\left(p_0(1-n_{tr}) - pn_{tr}\right) \tag{15}$$

Note that $0 \le n_{tr} \le 1$ should hold from physical point of view. Moreover, both n and p are nonnegative.

MAIN RESULT

We consider initial-boundary value problems with initial conditions
$$n(x,0)=n_I(x), p(x,0)= p_I(x), n_{tr}(x,0)= n_{tr,I}(x) \tag{16}$$
and with mixed Dirichlet-Neumann boundary conditions on $\partial\Omega$, i.e., let
$$n(x,t)=n_D(x), p(x,t)= p_D(x), V(x,t)=V_D(x), x \in \partial\Omega_D \subset \partial\Omega \tag{17}$$
and
$$\frac{\partial n}{\partial \nu} = \frac{\partial p}{\partial \nu} = \frac{\partial V}{\partial \nu} = 0, \partial\Omega_N := \partial\Omega \setminus \partial\Omega_D \tag{18}$$
where ν is the outward unit normal vector along $\partial\Omega_N$. It is allowed to impose only homogenous Neumann boundary conditions on all of $\partial\Omega$, i.e. we set $\partial\Omega_N = \emptyset$, and the following Theorem will hold.

Theorem Let $n_I, p_I \in L^\infty(\Omega)$ (and non-negative), $0 \le n_{tr,I} \le 1$ and let $C \in L^\infty(\Omega)$. Then, the solution of (8)-(11) satisfies $n, p \in L^\infty_{loc}\left((0,\infty), L^\infty(\Omega) \cap H^1(\Omega)\right)$ and $0 \le n_{tr} \le 1$.

Proof: We will use the result from [5], which was obtained for homogenous Neumann boundary conditions. We can show by a straightforward computation

$$\frac{d}{dt}\int\left[\frac{(n-n_D)^q}{q\mu_n} + \frac{(p-p_D)^q}{q\mu_p}\right]dx =$$

$$= \int\left[\frac{(n-n_D)^{q-1}}{\mu_n}(\nabla J_n + R_n - \partial_t n_D) + \frac{(p-p_D)^{q-1}}{\mu_p}(-\nabla J_p + R_p - \partial_t p_D)\right]dx$$

$$\le -(q-1)\int\left[(n-n_D)^{q-2}\nabla(n-n_D)\frac{J_n}{\mu_n} - (p-p_D)^{q-2}\nabla(p-p_D)\frac{J_p}{\mu_p}\right]dx$$

$$+ C_1\int\left(n^q + p^q\right)dx + C_1$$

$$= -(q-1)\int(n-n_D)^{q-2}\nabla(n-n_D)\nabla n dx +$$

$$(q-1)\int(p-p_D)^{q-2}\nabla(p-p_D)\nabla p dx$$

$$+ (q-1)\int[(n-n_D)^{q-2}n\nabla(n-n_D) - (p-p_D)^{q-2}p\nabla(p-p_D)]\nabla V dx$$

$$+ C_1 \int \left(n^q + p^q \right) dx + C_1$$

$$:= I_1 + I_2 + I_3 + I_4 \tag{19}$$

where the term I_3 from (19) can be rewritten as follows:

$$I_3 = \int [(n - n_D)^{q-1} \nabla (n - n_D) - (p - p_D)^{q-1} \nabla (p - p_D)] \nabla V dx +$$

$$+ \int [[(n - n_D)^{q-2} \nabla (n - n_D)](n_D \nabla V) - [(p - p_D)^{q-2} \nabla (p - p_D)](p_D \nabla V)] dx$$

$$= -\frac{1}{q} \int [(n - n_D)^q - (p - p_D)^q](n - p + \varepsilon n_{tr} - C) dx$$

$$- \frac{1}{q-1} \int (n - n_D)^{q-1} (\nabla n_D \nabla V + n_D (n - p + \varepsilon n_{tr} - C)) dx$$

$$+ \frac{1}{q-1} \int (p - p_D)^{q-1} (\nabla p_D \nabla V + p_D (n - p + \varepsilon n_{tr} - C)) dx .$$

We have used partial integration, and (11) to obtain the last expression. By applying Holder inequality with coefficients q', r; s and using the fact that $\frac{1}{q'} + \frac{1}{q} = 1$, we obtain the following estimate

$$I_3 \le \frac{1}{q} \int \left[(n - n_D)^q - (p - p_D)^q \right] (n - n_D - (p - p_D)) dx$$

$$+ C_2 + C_2 \int \left(n^q + p^q \right) dx + C_2 \| n + p \|_{L^q}^{q-1} \| \nabla n_D \|_{L^r} \| n + p \|_{L^q} .$$

$\Delta V = \rho, \| \nabla V \|_{L^s} \le C \| \rho \|_{L^q} \| \nabla V \|_{L^s} \le \| \nabla V \|_{W^{1,q}}$, where $\rho = n + \varepsilon n_{tr} - p - C$.

For $q \ge 2$ and even , one obtains for I_1

$$I_1 = -\int (n - n_D)^{q-2} |\nabla n|^2 dx + \int (n - n_D)^{q-2} \nabla n_D \nabla n dx \tag{20}$$

By rewriting the integrand in the second integral from (20) as

$$(n - n_D)^{q-2} \nabla n_D \nabla n = (n - n_D)^{\frac{q-2}{2}} \nabla n \nabla (n - n_D)^{\frac{q-2}{2}} \nabla n_D \tag{21}$$

and applying the Cauchy-Schwarz inequality, we have the following estimate for (20):

$$I_1 \le -\int (n - n_D)^{q-2} |\nabla n|^2 dx + \sqrt{\int (n - n_D)^{q-2} |\nabla n|^2 dx \int (n - n_D)^{q-2} |\nabla n_D|^2 dx}$$

$$\le \int (n - n_D)^{q-2} |\nabla n|^2 dx + \| \nabla n_D \|_{L^q}^2 \| n - n_D \|_{L^q}^{q-2} \tag{22}$$

For I_2 , the same reasoning (with $n.n_D$ replaced by $p.p_D$, respectively) yields an analogous estimate.

Collecting all the estimates, we finally obtain:

$$\frac{d}{dt} \int \left[\frac{(n - n_D)^q}{q \mu_n} + \frac{(p - p_D)^q}{q \mu_p} \right] dx =$$

$$\leq -\frac{1}{2}\int (n-n_D)^{q-2}|\nabla n|^2\,dx + \|n_D\|_{L^q}^2 \|n-n_D\|_{L^q}^{q-2}$$

$$-\frac{1}{2}\int (p-p_D)^{q-2}|\nabla p|^2\,dx + \|p_D\|_{L^q}^2 \|p-p_D\|_{L^q}^{q-2}$$

$$-\frac{1}{q}\int [(n-n_D)^q - (p-p_D)^q]|\nabla n|^2 (n-n_D-(p-p_D))\,dx$$

$$+C_3 + C_3\int (n^q + p^q)\,dx + C_3\|n+p\|_{L^q}^{q-1}\|\nabla n_D\|_{L^r}\|n+p\|_{L^q} \tag{23}$$

$$\frac{1}{q}\frac{d}{dt}\left[\|n-n_D\|_{L^q}^q + \|p-p_D\|_{L^q}^q\right]dx \leq \|n_D\|_{L^q}^2\int|n-n_D|^2\,dx + \|p_D\|_{L^q}^2\int|p-p_D|^q\,dx$$

$$+C_4\|n+p\|_{L^q}^q + C_4\|n\|_{L^q}^q + C_4\|p_D\|_{L^q}^q$$

$$\leq C_4 2^q\left[\|n-n_D\|_{L^q}^q + \|n_D\|_{L^q}^q + \|p-p_D\|_{L^q}^q + \|p_D\|_{L^q}^q\right] \tag{24}$$

Corollary Given the assumptions of Theorem, consider equations (8)-(11) with homogenous Neumann boundary conditions. Then $n, p \in L_{loc}^\infty\big((0,\infty), L^\infty(\Omega)\cap H^1(\Omega)\big)$.

REFERENCES

1. Arnold, A., Markowich, P., Toscani G**.**, *On Large Time Asymp for Drift-Diffusion-Poisson Systems.* 1979, New York (in English).
2. Arnold, A., Markowich, P., Toscani, G., Unterreiter, A., *On convexSobolev inequalities and the rate of convergence to equilibrium for Fokker-Planck type equations.* Arch. Rational Mech. Anal., 19, 1965, 153-362 (in English)
3. Desvillettes, L., Fellner, K., *Exponential Decay toward Equilibrium via Entropy Methods for* Reaction-Diffusion Equations, J. Math. Anal. Appl., 1978, 507-513 (in English)

4. Gajewski, H., *On Existence, Uniqueness and Asymptotic Behaviour of Solutions of the Basic Equations for Carrier Transport in Semiconductors,* ZAMM, 65(2):101-108,1985.1990.
5**.** Markowich, P.A., Ringhofer, C.A., Schmeiser,C., *Semiconductor*, Equations, Springer, New York,

O SHOCKLEY-READ-HALL MODELU ZA POLUPROVODNIKE

Julka Knežević-Miljanović

Apstrakt: *Razmatramo SHOCKLEY-READ-HALL model za poluprovodnike,i dokazuje se granični problem s datim početnim uslovima.*

VORTICITY EVOLUTION IN PERTURBED POISEUILLE FLOW

UDC 531; 534; 517.944;

Miloš M. Jovanović

University of Niš, Faculty of Mechanical Engineering, Aleksandra Medvedeva 14, 18000 Niš, Serbia, e-mail: jmilos@masfak.ni.ac.rs

Abstract. *We consider numerical simulation of temporal hydrodynamic instability with finite amplitude perturbations in plane incompressible Poiseuille flow. Two dimensional Navier Stokes equations have been used and reduced to vorticity-stream function form. Trigonometric polynomials have been used in homogeneous direction and Chebyshev polynomials in inhomogeneous direction. The problem of boundary conditions for vorticity has been solved by using the method of influence matrices. The Orr-Sommerfeld equation has been solved by Chebyshev polynomials, and linear combination of the obtained eigenfunctions has been optimized with regard to the corresponding eigenvalue. We present here the results of simulation for the perturbations optimized in regard to the least stable eigenvalue for the Reynolds number Re =1000.*

Key words: *direct numerical simulation, perturbed Poiseuille flow, subcritical instability, optimized perturbation, pseudospectral method*

.

1. INTRODUCTION

It is well known that classical Hydrodynamic stability theory is not capable of describing the initial transient growth mechanism that has been observed by experimentators for viscous channel flows. The reason for such behavior has been ascribed to the asymptotic behavior of the unstable eigenvalue, since the perturbation is formed only by the unstable eigenvalue and the corresponding eigenfunction. So, for Poiseuille flow the critical Reynolds number is 5772, and for this value of Reynolds number the eigenvalue has the positive imaginary part, and so the flow is asymptotically unstable, i.e. for large values of time, when $t \rightarrow \infty$

We have simulated the streamfunction-vorticity form of the 2D Navier-Stokes equations, and carried out the perturbation of laminar Poiseuille flow, by forming the

optimized linear combination of the all eigenfunctions normalized on the corresponding eigenvalue, in this case the least stable eigenvalue. The simulation has been carried out for the subcritical Reynolds number $Re=1000$, defined on channel half height H, middle channel maximal fluid velocity U_{max} and fluid kinematic viscosity-ν

2. PROBLEM STATEMENT AND GOVERNING EQUATIONS

We consider the problem for plane Poiseuille flow, where H is channel half height, L-is its lenght. Incompressible fluid flows through the channel from left to right, whereby the pressure at the inlet is p_i and at the outlet cross section is p_o. Momentum equation by means of which we describe this isothermal incompressible flow can be written in nondimensional form [1]

$$St \frac{\partial \vec{V}}{\partial t} + \left(\vec{V}\square\nabla\right)\vec{V} = \frac{1}{Fr}\vec{F} - Eu\nabla p + \frac{1}{Re}\Delta\vec{V}, \tag{1}$$

where is ∇-Hamilton's differential operator. In the above expression Δ-designates nondimensional Laplace's differential operator. The continuity equation reads

$$\nabla\square\vec{V} = div\vec{V} = 0. \tag{2}$$

In the above expressions $\vec{V}$ is nondimensional velocity vector of 2D flow in Cartesian coordinates, $\vec{F}$ –nondimensional force field, p–nondimensional pressure, t–nondimensional time, St–Strouhal number, Fr–Froude number, Eu–Euler number, Re–Reynolds number. Nondimensional form of the momentum equation has been obtained by using the following caracteristic scales for various independent and dependent variables: $L_0=H$ – for all lengths, $V_0 =U_{max}$ –maximal velocity at the middle of the channel, for all velocities, p_o–pressure at the outlet of the channel, for pressure, and g–gravity acceleration for body force. Four dimensionless parameters are thus occuring, namely,

$$St = \frac{L_0}{t_0 V_0}, \quad Fr = \frac{gL_0}{V_0^2}, \quad Eu = \frac{p_0}{\rho V_0^2}, \quad Re = \frac{L_0 V_0 \rho}{\mu}, \tag{3}$$

where are μ - dynamic viscosity, ρ - fluid density. We take that $St =1$, $Eu =1$ and $Fr =1$, and we introduce the ν-dimensionless kinematic viscosity, which is the inverse of Reynolds number. So we have now

$$\frac{\partial \vec{V}}{\partial t} + \left(\vec{V}\square\nabla\right) \vec{V} = \vec{F} - \nabla p + \nu\Delta\vec{V}, \tag{4}$$

If we take the curl of this equation, and having in mind the definition of vorticity

$$\vec{\omega} = \nabla \times \vec{V} = curl\vec{V}, \tag{5}$$

then we obtain the following transport expression for vorticity

$$\frac{\partial \vec{\omega}}{\partial t} + \left(\vec{V}\square\nabla\right)\ \vec{\omega} = \nabla \times \vec{F} + \nu\Delta\vec{\omega}. \tag{6}$$

We have taken into account that the curl of arbitrary scalar function gradient, in this case pressure function, is by definition equal to zero. The velocity vector can be expressed as curl of stream function

$$\vec{V} = \nabla \times \vec{\psi} = curl\vec{\psi}, \tag{7}$$

and after substitution of this expression (7) into (6), and after projection to z-axe, we obtain the following equation for transport of vorticity

$$\frac{\partial \omega}{\partial t} + \frac{\partial \psi}{\partial y}\frac{\partial \omega}{\partial x} - \frac{\partial \psi}{\partial x}\frac{\partial \omega}{\partial y} = \frac{\partial f_y}{\partial x} - \frac{\partial f_x}{\partial y} + \nu\left(\frac{\partial^2 \omega}{\partial x^2} + \frac{\partial^2 \omega}{\partial y^2}\right). \tag{8}$$

If we substitute the expression (7) in (2) the continuity equation is identically satisfied, and can not be used for closure the system of equations. For closure the system of equations we use the definition of vorticity given by the expression (5) and velocity vector given through the streamfunction vector by (7). So the second equation for closure the system of equations reads

$$\omega + \frac{\partial^2 \psi}{\partial x^2} + \frac{\partial^2 \psi}{\partial y^2} = 0. \tag{9}$$

The system of the equations (8) and (9) with appropriate initial and boundary conditions should be solved in space and time. Boundary conditions can be formulated in the following manner

$$\psi\left(x,1,t\right) = g_+\left(x,t\right), \quad \frac{\partial \psi}{\partial y}\left(x,1,t\right) = h_+\left(x,t\right) \ on \ \Gamma_u \times T, \tag{10}$$

$$\psi\left(x,-1,t\right) = g_-\left(x,t\right), \quad \frac{\partial \psi}{\partial y}\left(x,-1,t\right) = h_-\left(x,t\right) \ on \ \Gamma_l \times T, \tag{11}$$

$$\psi\left(x,y,0\right) = \psi_0\left(x,y\right) \ on \ \Omega, \tag{12}$$

here domain Ω is defined as $\Omega = \{ (x,y)\in\hat{h}^2 \mid 0\leq x{\leq}2\pi \wedge -1 < y{<}1 \}$. We have designated the upper domain boundary $\Gamma_u = \{(x,y)\in\hat{h}^2 \mid 0{\leq}x{\leq}2\pi \wedge y{=}1 \}$ and the lower domain boundary $\Gamma_l = \{ (x,y)\in\hat{h}^2 \mid 0 \leq x \leq 2\pi \wedge y = -1\}$. The time domain is defined as T$=\{ t\in\hat{h} \mid 0{\leq} t{\leq}T_e \}$, where T_e is the end of the simulation. We have anticipated the periodic boundary conditions in streamwise direction (x-axe), which are in accordance with the periodic perturbations obtained by the solution of Orr-Sommerfeld equation of hydrodynamic stability.

3. NUMERICAL PROCEDURE FOR THE SOLUTION OF PROBLEM

For the problem stated in the previous section, for the basis function in *x*-direction we have taken trigonometric polynomials, and for *y*-direction we have taken Chebyshev polynomials. The domain in *x*-direction is equally discretised $\Delta x = 2\pi/N$, and domain in *y*-direction is discretised by Gauss-Lobatto-Chebyshev points defined as $y_j = \cos(\pi j/N)$ for $0 \le j \le N$, where is *N*-number of discretization points in *x*- and *y*-direction. For streamwise direction we have used Fourier-Galerkin method, and for stream normal direction Chebyshev-collocation method. The truncated Fourier series for streamfunction and vorticity read

$$\omega_N(x,y,t) = \sum_{k=-N/2}^{k=N/2} \hat{\omega}_k(y,t)\, e^{Ikx}, \tag{13}$$

$$\psi_N(x,y,t) = \sum_{k=-N/2}^{k=N/2} \hat{\psi}_k(y,t)\, e^{Ikx}, \tag{14}$$

In the above expressions $I = \sqrt{-1}$ is imaginary unit, *k*-wave number, $\hat{\omega}_k(y_j,t)$ and $\hat{\psi}_k(y_j,t)$ are Fourier coefficients for vorticity and streamfunction respectively. In order to have 2π-periodicity in the flow domain, we have chosen that wave number must be from the set of integers, $k \in \mathbb{H}$. In order to implement Fourier-Galerkin method to the system of equation (8) and (9), we firstly approximate nonlinear convective terms on left hand side, in the following manner

$$N_1 = \left(\frac{\partial \psi}{\partial y}\frac{\partial \omega}{\partial x}\right)_N (x,y,t) = \sum_{k=-N/2}^{N/2}\left[\frac{\partial \psi}{\partial y}\frac{\partial \omega}{\partial x}\right]_k (y,t)\, e^{Ikx} \tag{15}$$

$$N_2 = \left(\frac{\partial \psi}{\partial x}\frac{\partial \omega}{\partial y}\right)_N (x,y,t) = \sum_{k=-N/2}^{N/2}\left[\frac{\partial \psi}{\partial x}\frac{\partial \omega}{\partial y}\right]_k (y,t)\, e^{Ikx} \tag{16}$$

Substituting the (13), (14), (15) and (16) in the (8) and (9), we obtain the following residual equations

$$\frac{\partial}{\partial t}\sum_{k=-N/2}^{N/2}\hat{\omega}_k(y,t)e^{Ikx} + \sum_{k=-N/2}^{N/2}\left[\frac{\partial \psi}{\partial y}\frac{\partial \omega}{\partial x}\right]_k (y,t)e^{Ikx} - \sum_{k=-N/2}^{N/2}\left[\frac{\partial \psi}{\partial x}\frac{\partial \omega}{\partial y}\right]_k (y,t)e^{Ikx} -$$
$$- \sum_{k=-N/2}^{N/2}\hat{\mathrm{F}}_k(y,t)e^{Ikx} - \nu\left(\frac{\partial^2}{\partial x^2} + \frac{\partial^2}{\partial y^2}\right)\sum_{k=-N/2}^{N/2}\hat{\omega}_k(y,t)e^{Ikx} \ne 0, \tag{17}$$

$$\sum_{k=-N/2}^{N/2}\hat{\omega}_k(y,t)e^{Ikx} + \left(\frac{\partial^2}{\partial x^2} + \frac{\partial^2}{\partial y^2}\right)\sum_{k=-N/2}^{N/2}\hat{\psi}_k(y,t)e^{Ikx} \ne 0. \tag{18}$$

We have introduced the following expression for the curl of body force,

$$F = \frac{\partial f_y}{\partial x} - \frac{\partial f_x}{\partial y} = \sum_{k=-N/2}^{N/2} \hat{F}_k(x,y,t) e^{Ikx} \tag{19}$$

If we apply Galerkin method to the equations (17) and (18), i.e. we take for the weight functions the same as basis functions , we obtain

$$\frac{\partial}{\partial t} \sum_{k=-N/2}^{N/2} \hat{\omega}_k(y,t) \left\langle e^{Ikx}, e^{Ilx} \right\rangle + \sum_{k=-N/2}^{N/2} \left[\frac{\partial \psi}{\partial y} \frac{\partial \omega}{\partial x} \right]_k (y,t) \left\langle e^{Ikx}, e^{Ilx} \right\rangle -$$

$$- \sum_{k=-N/2}^{N/2} \left[\frac{\partial \psi}{\partial x} \frac{\partial \omega}{\partial y} \right]_k (y,t) \left\langle e^{Ikx}, e^{Ilx} \right\rangle - \sum_{k=-N/2}^{N/2} \hat{F}_k(y,t) \left\langle e^{Ikx}, e^{Ilx} \right\rangle - \tag{20}$$

$$- \nu \left(\frac{\partial^2}{\partial x^2} + \frac{\partial^2}{\partial y^2} \right) \sum_{k=-N/2}^{N/2} \hat{\omega}_k(y,t) \left\langle e^{Ikx}, e^{Ilx} \right\rangle = 0, \quad l = 0,1,\ldots,N/2.$$

$$\sum_{k=-N/2}^{N/2} \hat{\omega}_k(x,y,t) \left\langle e^{Ikx}, e^{Ilx} \right\rangle + \left(-k^2 + \frac{\partial^2}{\partial y^2} \right) \sum_{k=-N/2}^{N/2} \hat{\psi}_k(x,y,t) \left\langle e^{Ikx}, e^{Ilx} \right\rangle = 0, \tag{21}$$
$$l = 0,1,\ldots,N/2.$$

where we have denoted with $\left\langle \,,\, \right\rangle$ the inner product. Recalling that $\hat{\omega}_{-k} = \hat{\omega}_k^*$, i.e. Fourier coefficient of inverse wave number is complex conjugate of the corresponding wave number, it is not necessary to take $l = -N/2,\ldots,N/2$, but $l=0,1,\ldots,N/2$. Having in mind the orthogonality relation

$$\left\langle e^{Ikx}, e^{Ilx} \right\rangle = \int_0^{2\pi} e^{Ikx} e^{-Ilx} dx = \begin{cases} 2\pi, \, l = k, \\ 0, \, l \neq k, \end{cases} \tag{22}$$

the system of equations (20) and (21) takes the following form

$$\frac{\partial \hat{\omega}_k(y,t)}{\partial t} + \left[\frac{\partial \psi}{\partial y} \frac{\partial \omega}{\partial x} \right]_k (y,t) - \left[\frac{\partial \psi}{\partial x} \frac{\partial \omega}{\partial y} \right]_k (y,t) = \hat{F}_k(y,t) + \nu \left(\frac{\partial^2}{\partial y^2} - k^2 \right) \hat{\omega}_k(y,t) \tag{23}$$
$$l = k = 0,1,\ldots,N/2.$$

$$\hat{\omega}_k(y,t) + \left(-k^2 + \frac{\partial^2}{\partial y^2} \right) \hat{\psi}_k(y,t) = 0, \quad l = k = 0,1,\ldots,N/2. \tag{24}$$

Applying now the Chebyshev-collocation method in inhomogenuous direction (y-axe) to the above system of equations, we obtain the following system

$$\frac{\partial \hat{\omega}_{kN}\left(y_j,t\right)}{\partial t} + \left[\frac{\partial \psi}{\partial y}\frac{\partial \omega}{\partial x}\right]_{kN}\left(y_j\right) - \left[\frac{\partial \psi}{\partial x}\frac{\partial \omega}{\partial y}\right]_{kN}\left(y_j\right) = \hat{\mathrm{F}}_{kN}\left(y_j,t\right) +$$

$$+\nu\left(-k^2 + \sum_{l=0}^{N} d_{j,l}^{(2)}\right)\hat{\omega}_{kN}\left(y_j,t\right), \quad k=0,1,\ldots,N/2, \quad j=1,\ldots,N-1, \tag{25}$$

$$\hat{\omega}_{kN}\left(y_j,t\right) + \left(-k^2 + \sum_{l=0}^{N} d_{j,l}^{(2)}\right)\hat{\psi}_{kN}\left(y_j,t\right) = 0,$$

$$k=0,1,\ldots,N/2, \quad j=1,\ldots,N-1. \tag{26}$$

Here the subscript index N denotes the number of discretization points in y-direction, and it is worth reminding that we have taken $N_y=N_x=N$. Differentiation with regard to y-variable has been substituted with Chebyshev differentiation expressions [2] given by

$$\frac{\partial^2 \hat{\omega}_{kN}}{\partial y^2}\left(y_j\right) = \hat{\omega}_{kN}^{(2)}\left(y_j\right) = \sum_{l=0}^{N} d_{j,l}^{(2)}\hat{\omega}_{kN}\left(y_l\right), \quad j=0,\ldots,N, \tag{27}$$

$$\frac{\partial^2 \hat{\psi}_{kN}}{\partial y^2}\left(y_j\right) = \hat{\psi}_{kN}^{(2)}\left(y_j\right) = \sum_{l=0}^{N} d_{j,l}^{(2)}\hat{\psi}_{kN}\left(y_l\right), \quad j=0,\ldots,N. \tag{28}$$

The next step to be carried out is the temporal discretization of the governig equations. For this purpose we have used the following two-step generalized method defined in the following way

$$\frac{(1+\varepsilon)\hat{\omega}_{kN}^{n+1}\left(y_j\right) - 2\varepsilon\hat{\omega}_{kN}^{n}\left(y_j\right) - (1-\varepsilon)\hat{\omega}_{kN}^{n-1}\left(y_j\right)}{2\Delta t} +$$

$$+\left[\gamma_1\left(\frac{\partial \psi}{\partial y}\frac{\partial \omega}{\partial x}\right)_{kN}^{n+1}\left(y_j\right) + \gamma_2\left(\frac{\partial \psi}{\partial y}\frac{\partial \omega}{\partial x}\right)_{kN}^{n}\left(y_j\right) + (1-\gamma_1-\gamma_2)\left(\frac{\partial \psi}{\partial y}\frac{\partial \omega}{\partial x}\right)_{kN}^{n-1}\left(y_j\right)\right] - \tag{29}$$

$$-\left[\gamma_1\left(\frac{\partial \psi}{\partial x}\frac{\partial \omega}{\partial y}\right)_{kN}^{n+1}\left(y_j\right) + \gamma_2\left(\frac{\partial \psi}{\partial x}\frac{\partial \omega}{\partial y}\right)_{kN}^{n}\left(y_j\right) + (1-\gamma_1-\gamma_2)\left(\frac{\partial \psi}{\partial x}\frac{\partial \omega}{\partial y}\right)_{kN}^{n-1}\left(y_j\right)\right] +$$

$$+\nu k^2\left[\theta_1\hat{\omega}_{kN}^{n+1}\left(y_j\right) + \theta_2\hat{\omega}_{kN}^{n}\left(y_j\right) + (1-\theta_1-\theta_2)\hat{\omega}_{kN}^{n-1}\left(y_j\right)\right] -$$

$$-\nu\sum_{l=0}^{N} d_{j,l}^{(2)}\left[\theta_1\hat{\omega}_{kN}^{n+1}\left(y_l\right) + \theta_2\hat{\omega}_{kN}^{n}\left(y_l\right) + (1-\theta_1-\theta_2)\hat{\omega}_{kN}^{n-1}\left(y_l\right)\right] =$$

$$= \theta_1\hat{\mathrm{F}}_{kN}^{n+1}\left(y_j\right) + \theta_2\hat{\mathrm{F}}_{kN}^{n}\left(y_j\right) + (1-\theta_1-\theta_2)\hat{\mathrm{F}}_{kN}^{n-1}\left(y_j\right),$$

$$k=0,\ldots,N/2, \quad j=1,\ldots N-1, \quad n=1,\ldots,M.$$

for the spatially discretised momentum equation (25) and

$$\hat{\omega}_j^{n+1} - k^2 \hat{\psi}_j^{n+1} + \sum_{l=0}^{N} d_{j,l}^{(2)} \hat{\psi}_l^{n+1} = 0,$$

$$k = 0,\ldots,N/2, \ \ j = 1,\ldots,N-1, \ \ n = 1,\ldots,M. \tag{30}$$

for the spatially discretised the definition of vorticity equation (26). Here is denoted $t=n\Delta t$, where Δt-time step, n-the number of time step.

The same procedure must be carried out to boundary and initial conditions.

$$g_{+,N/2}(x,t) = \sum_{k=-N/2}^{N/2} \hat{g}_{+,k}(t) \ e^{I\,k\,x} \approx g_{+}(x,t) \tag{31}$$

$$g_{-,N/2}(x,t) = \sum_{k=-N/2}^{N/2} \hat{g}_{-,k}(t) \ e^{I\,k\,x} \approx g_{-}(x,t) \tag{32}$$

$$h_{+,N/2}(x,t) = \sum_{k=-N/2}^{N/2} \hat{h}_{+,k}(t) \ e^{I\,k\,x} \approx h_{+}(x,t) \tag{33}$$

$$h_{+,N/2}(x,t) = \sum_{k=-N/2}^{N/2} \hat{h}_{+,k}(t) \ e^{I\,k\,x} \approx h_{+}(x,t) \tag{34}$$

$$\psi_{0,N/2}(x,y) = \sum_{k=-N/2}^{N/2} \hat{\psi}_{0,k}(y) \ e^{I\,k\,x} \approx \psi_{0}(x,y) \tag{35}$$

Having in mind the expression (14) for streamfunction, boundary conditions (10) and (11), as well as their trigonometric polynomial approximation given by (31)-(35), after implementing Galerkin method and applying the orthogonality relation (22), we obtain the following boundary conditions in space of Fourier coefficients

$$\hat{\psi}_k(1,t) = \hat{g}_{+,k}(t), \quad k = 0,\ldots,N/2. \tag{36}$$

$$\hat{\psi}_k(-1,t) = \hat{g}_{-,k}(t), \quad k = 0,\ldots,N/2, \tag{37}$$

$$\frac{\partial \hat{\psi}_k}{\partial y}(1,t) = \hat{h}_{+,k}(t), \quad k = 0,\ldots,N/2, \tag{38}$$

$$\frac{\partial \hat{\psi}_k}{\partial y}(-1,t) = \hat{h}_{-,k}(t), \quad k = 0,\ldots,N/2. \tag{39}$$

After time discretization and application of Chebyshev collocation method for boundary conditions, the above boundary conditions read as follow

$$\hat{\psi}_{k,0}^{n+1} = \hat{g}_{+,k}^{n+1}, \quad y = 1, \quad k = 0,\ldots,N/2, \tag{40}$$

$$\hat{\psi}_{k,N}^{n+1} = \hat{g}_{-,k}^{n+1}, \quad y = -1, \quad k = 0,\ldots,N/2, \tag{41}$$

$$\sum_{l=0}^{N} d_{0,l}^{(1)} \ \hat{\psi}_{k,l}^{n+1} = \hat{h}_{+,k}^{n+1}, \ y = 1, \ k = 0,\ldots,N/2, \tag{42}$$

$$\sum_{l=0}^{N} d_{N,l}^{(1)} \, \hat{\psi}_{k,l}^{n+1} = \hat{h}_{-,k}^{n+1}, \ \ y = -1, \ k = 0,\ldots,N/2. \tag{43}$$

This system of equations (29) and (30) together with boundary conditions (40) to (43) should be solved numerically. The system is represented by 2(N+1)×2(N+1) three time levels matrix equation. The nonlinear advective terms have been computed by pseudospectral technique [3], so that full Navier-Stokes equation in vorticity-stream-function formulation can be simulated for the case of 2D viscous channel flow. The problem of two boundary conditions for stream function and none for vorticity has been successfully resolved by applying the influence matrix method [4].

4. TEMPORAL HYDRODYNAMIC STABILTY

In order to simulate the process of instability of viscous fluid flow between two parallel horizontal plates, we solved Orr-Sommerfeld equation of hydrodynamic linear stability for the given velocity profile, in this case for plane Poiseuille flow, and formed the streamfunction perturbation as the linear combination of the eigenfunctions obtained as the solution of this equation. It is well known fact that there is no analytical solution of this equation. The first numerical solution of this equation is given in the paper [5], and the critical Reynolds number of this type of flow has been found to be 5772. In order to show how we perturbed the Poiseuille flow, we start from the equation (8) in which we substitute

$$\omega = \Omega + \omega', \quad \psi = \Psi + \psi', \quad F = F + f' \tag{44}$$

where we have taken in account the expression (19), so that we have

$$\frac{\partial}{\partial t}\left(\Omega + \omega'\right) + \frac{\partial}{\partial y}\left(\Psi + \psi'\right)\frac{\partial}{\partial x}\left(\Omega + \omega'\right) - \frac{\partial}{\partial x}\left(\Psi + \psi'\right)\frac{\partial}{\partial y}\left(\Omega + \omega'\right) =$$
$$= F + f' + \nu\left(\frac{\partial^2}{\partial x^2}\left(\Omega + \omega'\right) + \frac{\partial^2}{\partial y^2}\left(\Omega + \omega'\right)\right) \tag{45}$$

The capital letters designates the basic flow values, and the prime denotes perturbations of the corresponding physical values. If we subtract (8) from (45) the above equation is reduced to following form

$$\frac{\partial \omega'}{\partial t} + \frac{\partial \Psi}{\partial y}\frac{\partial \omega'}{\partial x} + \frac{\partial \psi'}{\partial y}\frac{\partial \Omega}{\partial x} + \frac{\partial \psi'}{\partial y}\frac{\partial \omega'}{\partial x} - \frac{\partial \psi'}{\partial x}\frac{\partial \Omega}{\partial y} + \frac{\partial \Psi}{\partial x}\frac{\partial \omega'}{\partial y} -$$
$$-\frac{\partial \psi'}{\partial x}\frac{\partial \omega'}{\partial y} = f' + \nu\left(\frac{\partial^2 \omega'}{\partial x^2} + \frac{\partial^2 \omega'}{\partial y^2}\right) \tag{46}$$

Neglecting the nonlinear terms of perturbed values as small values of higher order than we have

$$\frac{\partial \omega'}{\partial t} + \frac{\partial \Psi}{\partial y}\frac{\partial \omega'}{\partial x} + \frac{\partial \psi'}{\partial y}\frac{\partial \Omega}{\partial x} - \frac{\partial \psi'}{\partial x}\frac{\partial \Omega}{\partial y} - \frac{\partial \Psi}{\partial x}\frac{\partial \omega'}{\partial y} = f' + \nu\left(\frac{\partial^2 \omega'}{\partial x^2} + \frac{\partial^2 \omega'}{\partial y^2}\right) \tag{47}$$

In plane channel flow, better to say, in Poiseuille flow we have $U = \partial \Psi / \partial y = 1 - y^2$, $V = -\partial \Psi / \partial x = 0$, $\Omega = -dU/dy$, and also $\partial \Omega / \partial x = 0$, so finally we have

$$\frac{\partial \omega'}{\partial t} + \frac{\partial \Psi}{\partial y}\frac{\partial \omega'}{\partial x} - \frac{\partial \psi'}{\partial x}\frac{\partial \Omega}{\partial y} = f' + \nu\left(\frac{\partial^2 \omega'}{\partial x^2} + \frac{\partial^2 \omega'}{\partial y^2}\right) \tag{48}$$

We anticipate that $f' = 0$, and $\omega' = -\Delta \psi'$, so that we have now

$$\frac{\partial}{\partial t}\Delta \psi' + U\frac{\partial}{\partial x}\Delta \psi' - \frac{\partial \psi'}{\partial x}\frac{d^2 U}{d y^2} = \nu \Delta^2 \psi' \tag{49}$$

with boundary conditions

$$\psi'(y = \pm 1) = 0 \qquad \frac{\partial \psi'}{\partial y}(y = \pm 1) = 0 \tag{50}$$

We have used modal approach for solving this problem, anticipating the that the perturbations are 2π periodic in x-direction, and are represented in the following way

$$\psi'(x, y, t) = \frac{1}{2}\left(\psi_1 + \psi_1^*\right) = \frac{1}{2}\left(\hat{\psi}(y)e^{i\alpha(x-ct)} + \hat{\psi}(y)^* e^{-i\alpha^*(x-c^*t)}\right) \tag{51}$$

Here ψ_1 is the normal mode form of stream function perturbation, and the values denoted by $*$ designate their complex-conjugate value. Thus the sum of normal mode and its complex-conjugate gives the real valued function ψ'. Since the complex-conjugate value ψ_1^* can be easily obtained from the complex-valued function ψ_1 itself, it is only necessarily to substitute ψ_1 in the (49), so that it reads

$$\left(\frac{\partial}{\partial t} + U\frac{\partial}{\partial x}\right)\Delta \hat{\psi}(y)e^{i\alpha(x-ct)} - \frac{d^2 U}{d y^2}\frac{\partial}{\partial x}\hat{\psi}(y)e^{i\alpha(x-ct)} = \nu \Delta^2 \hat{\psi}(y)e^{i\alpha(x-ct)}, \tag{52}$$

which after some differentiation and rearrangements gives

$$(U - c)\left(\frac{d^2\hat{\psi}}{dy^2} - \alpha^2\hat{\psi}\right) - \hat{\psi}\frac{d^2 U}{dy^2} = \frac{\nu}{i\alpha}\left(\alpha^4\hat{\psi} - 2\alpha^2\frac{d^2\hat{\psi}}{dy^2} + \frac{d^4\hat{\psi}}{dy^4}\right). \tag{53}$$

This equation known as Orr-Sommerfeld equation, together with appropriate boundary conditions

$$\hat{\psi}(1) = 0, \quad \hat{\psi}(-1) = 0, \quad \frac{d\hat{\psi}}{dy}(1) = 0, \quad \frac{d\hat{\psi}}{dy}(-1) = 0, \tag{54}$$

should be solved numerically. Numerical procedures are given for examples in [5], [6], [7] and [8]. This equation can be reduced to operator form

$$\left(U-c\right)\left(\mathrm{D}^2\hat{\psi}-\alpha^2\hat{\psi}\right)-\hat{\psi}\,\frac{d^2U}{dy^2}=\frac{\nu}{i\alpha}\left(\alpha^4\hat{\psi}-2\alpha^2\mathrm{D}^2\hat{\psi}+\mathrm{D}^4\hat{\psi}\right) \qquad (55)$$

where is $\Delta = d/dy$ differential operator, which can be solved as generalized eigenvalue problem, where c's are eigenvalues and $\hat{\psi}$'s are eigenfunctions.

We can fix now two parameters α and ν, and compute the eigenvalue c, what correspods to the case of temporal hydrodynamic stability. If we choose to fix c and ν, and to compute α, that would be the case of spatial hydrodynamic stability. In the first case we have $\alpha\in\hat{h}$ and $c\in\hbar$, and in the second case $c\in\hat{h}$ and $\alpha\in\hbar$. Here c is the velocity of traveling wave, and α is its wave number. In general case $c=c_{Re}+i\ c_{Im}$ and $\alpha=\alpha_{Re}+i\ \alpha_{Im}$, but since we have only one equation and two unknowns, we have to make some assumptions concerning these unknowns. In our calculations we have anticipated $\alpha=1$.

The results obtained for Re=1000 (ν=1/1000) are presented in fig.1 and are obtained for the N=128 Gauss-Lobatto-Chebyshev point in y-directions. For creating the perturbation that can exhibit the transieth growth mechanism, we have used the optimized linear combination of all eigenvectors which is normalized with regard to the least stable eigenvalue. This optimized perturbation was superposed to the initial unperturbed velocity profile, and the flow was driven by the force term determined from the perturbed Navier Stokes equation. This transient growth is possible due to non-normality of Orr-Sommerfeld operator, but the all eigenvalues and eigenvectors have to be used for creating linear combination, not only the least stable eigenvalue and correspoding eigenvector, see [9],[10],[11]. The results of simulation Fig.1and Fig.2 are given in the next section for the dimensionless time $t=n\pi$, n=1,...,10.

5. THE RESULTS OF TRANSIENT FLOW SIMULATION

The initial condition for our simulation is the solution of the problem for laminar Poiseuille 2D-flow is

$$U\left(x,y,0\right)=1-y^2,\quad V\left(x,y,0\right)=0,\quad on \quad \Omega. \qquad (56)$$

Our goal is to simulate the transition process from laminar to perturbed state for the value of Reynolds number Re=1000 which is beneath the critical value Re_c=5772, to simulate the transient growth of kinetic energy and enstrophy. We have carried out this simulation by imposing the perturbations obtained by solution of Orr-Sommerfeld equation on laminar velocity profile. The simulations are driven by forcing term which is determined by the perturbed Navier-Stokes equation,

$$\begin{aligned}
F_{pert}&=\frac{\partial}{\partial t}\left(\Omega+\omega'\right)+\frac{\partial}{\partial y}\left(\Psi+\psi'\right)\frac{\partial}{\partial x}\left(\Omega+\omega'\right)-\\
&-\frac{\partial}{\partial x}\left(\Psi+\psi'\right)\frac{\partial}{\partial y}\left(\Omega+\omega'\right)-\nu\left[\frac{\partial^2}{\partial x^2}\left(\Omega+\omega'\right)+\frac{\partial^2}{\partial y^2}\left(\Omega+\omega'\right)\right].
\end{aligned} \qquad (57)$$

Here Ω and Ψ are the values determined from (56) at initial time, and later they are results obtained from our numerical procedure and our MATLAB code, and the ψ' and

ω' are obtained as solution of Orr-Sommerfeld equation, and as optimized linear combination of all eigenvectors,

$$\psi'(x,y,t) = \sum_{n=1}^{N'} \beta_n \hat{\psi}_n(y) e^{i\alpha(x-c_n t)} = \sum_{n=1}^{N'} \beta_n \hat{\psi}_n(y) e^{i\alpha\left(x-\left(c_{\mathcal{Re}}+ic_{\mathcal{Im}}\right)_n t\right)} \tag{58}$$

and,

$$\omega'(x,y,t) = -\Delta\psi'. \tag{59}$$

Here $\hat{\psi}_k$'s are eigenvectors and c_n's are eigenvalues of generalized eigenvalue problem of Orr-Sommerfeld equation for the case of plane Poiseuille flow, and β_n are coefficient which should be determined by appropriate optimization procedure. The procedure we used in this paper is according to [7, p.121,fig.4.7] and is based on method first developed in [11].

Here β is perturbation spectar obtained by using the matrix Ψ, whose columns are eigenvectors $\hat{\psi}_n(y)$, in the following way

$$\beta = \Psi^{-1}\psi'(y,0). \tag{60}$$

Functional to be minimized is

$$f = \psi'^{*}\square\psi' = (\Psi\beta)^{*}\square(\Psi\beta) = \beta^{*}\square\Psi^{*}\Psi\beta = \beta^{*}\square A\beta. \tag{61}$$

In other words, the functional is the dot product of perturbation vector of stream function and its complex conjugate. If we put the condition that the i-th mode is of unit magnitude, then the variational problem can be reduced to the following function

$$f = \beta^{*}\square A\beta + \lambda(\beta\square e_i - 1). \tag{62}$$

Here we have designated with e_i – the unit vector, i.e. the column vector whose the only the i-th element is different from null. Let find the derivative with respect to β, e.i. let find the first variation of the above function f and equal it with zero, so that we have

$$\frac{df}{d\beta} = \frac{d}{d\beta}\left[\beta^{*}\square A\beta + \lambda(\beta\square e_i - 1)\right] = A\beta + \lambda e_i = \mathbf{0}. \tag{63}$$

And after rearrangements

$$A\beta = -\lambda e_i, \tag{64}$$

so that after multiplication both side with inverse matrice A^{-1} from the left we have

$$\beta = -\lambda A^{-1}e_i. \tag{65}$$

The optimized spectar can be normalized by appropriate calculation of coefficient λ, so that the value $\beta_i=1$ can be obtained. Having this in mind we have

$$
\begin{bmatrix} \beta_1 \\ \beta_2 \\ \vdots \\ \beta_i \\ \vdots \\ \beta_N \end{bmatrix} = -\lambda \begin{bmatrix} a_{11}^{-1} & a_{12}^{-1} & \dots & a_{1i}^{-1} & \dots & a_{1N}^{-1} \\ a_{21}^{-1} & a_{22}^{-1} & \dots & a_{2i}^{-1} & \dots & a_{2N}^{-1} \\ \vdots & \vdots & \ddots & \vdots & & \vdots \\ a_{i1}^{-1} & a_{i2}^{-1} & \dots & a_{ii}^{-1} & \dots & a_{iN}^{-1} \\ \vdots & \vdots & & \vdots & \ddots & \vdots \\ a_{N1}^{-1} & a_{N2}^{-1} & \dots & a_{Ni}^{-1} & \dots & a_{NN}^{-1} \end{bmatrix} \begin{bmatrix} 0 \\ 0 \\ \vdots \\ 1 \\ \vdots \\ 0 \end{bmatrix},
\tag{66}
$$

and the value of λ is determined by this expression

$$
\lambda = \frac{-\beta_i}{a_{ii}^{-1}} = \frac{-1}{a_{ii}^{-1}}.
\tag{67}
$$

Fig.1 shows the vorticity fields for six different times, for dimensionless time $t=n\pi$, $n=1,...,6$. Since the least stable eigenvalue for $Re=1000$ equals c=0.3462–i0.0421, we can see that the velocity of traveling wave perturbation optimized with regard to this mode has 34.62% of the fluid velocity in the middle of the channel. In the time $t=\pi$ we can see the vorticity distribution similar to that given in reference [6, p.121, fig.4.7], and as we can see the middle of the channel is almost unperturbed. In the next time for $t=2\pi$ we can see that vorticity has advected and diffused in the direction of the middle of channel, and that the maximal amplitudes has been decreased, what is in our opinion the consequence of the relaxation from the initial perturbation to the exact solution to Navier-Stokes given by (56). This can be seen on colorbars in the first two figures, where on the first one we have maximal magnitude 6.2 and on the second one 5.5 in dimensionless vorticity units. In the next instant of time for t=3π, it can be observed the merging of perviously separated vortexes with the same sign, which are deformed due to wall normal velocity perturbation, which is not shown here due to space limitation.

In t=4π, two circled vortexes have been formed with the centers located at y=0.2 positive one and y=−0.2 the negative one. The positive one with counter-clockwise rotation (red color) and negative vortex with clockwise rotation (blue color), in the middle of the channel, where this vortex pair is being deformed by the velocity gradient of the flud flow. The vortex pairs on upper and lower wall are in the form of romboid since the velocity of perturbation is greater than the velocity of surronding fluid near the walls, because the velocity of perturbation is c_{Re}=0.3462 and velocity of the fluid is given by (56). This velocity difference decreases with going away from the walls according with this expression till the normal coordinate reaches the value where these two velocities are equal, better to say, till to the value of critical fluid layer y≈0.8, since U=1-0.64=0.36. So we can notice that the velocity of perturbation traveling wave (phase velocity) is much higher in the wall region than the streamwise fluid velocity, but opposite is valid for the middle of the channel, where fluid velocity U (−0.8<y<0.8) is greater than phase velocity.
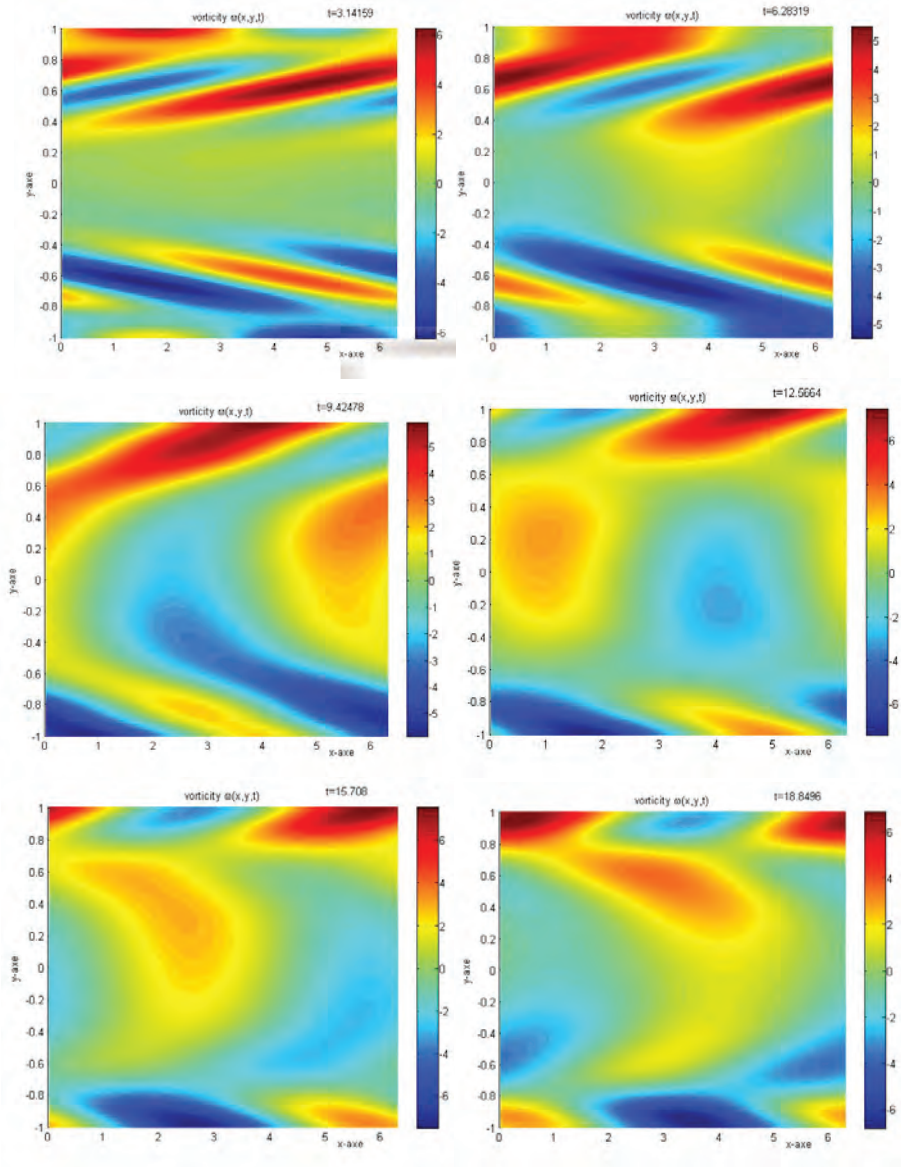
Fig.1. vorticity distribution ω(x,y,t) in 2D channel viscous fluid flow for t=π,…,6π for streamfunction perturbation optimized to least stable eigenmode.

In the next instant of time for t=5π it can be noticed that these vortex have been deformed in streamwise direction, by the mean velocity gradient., and this process is continued in the next instant of time t=6π.
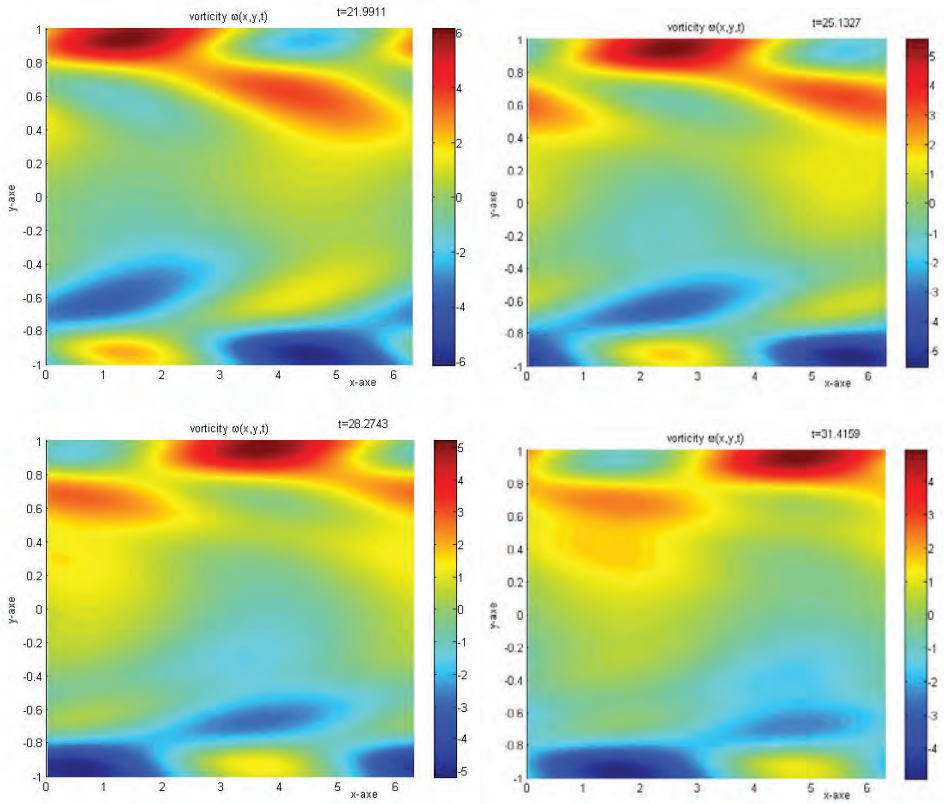
Fig.2: vorticity distribution $\omega(x,y,t)$ in 2D channel viscous fluid flow for t=7π,…,10π for streamfunction perturbation optimized to least stable eigenmode.

In the next vorticity fields for t=7,...,10π, the process of vortex distorsion is continued, and advected in downstream direction. The maximal and minimal values of vorticity are on the upper and lower wall respectively , and their values decrease with increase of time. Vortex pair on lower plate consist of two vortexes, the negative one which atains the value ω_{min}=−4.8 and positive one with the value ω_{max}=1 at instant of time t=10π. The opposite is true on the upper wall; the negative vortex attains the value ω_{min}=−1 and vortex with counter-clockwise rotation (red color) reaches the value ω_{max}=4.8. These vortex pairs moves in downstream direction with phase velocity c_{Re}=0.3462, which can be seen on the figures above, since the displacement of the center of the vortex between two instant of time can be determined in the following way: s=c_{Re} Δt=0.3462·3.1416=1.0876, and this is what we can see on this fig.2 between four different instant of time.

6. CONCLUSION

The most important results can be seen on the colorbars for ten different instant of times. It can be noticed that the maximal vorticity displayed on colorbars attains its maximal value at time t=4π (ω_{max}=6.85) and t=5π (ω_{max}=6.75), and afterwards the intensity of vorticity monotonically decreases, so that for t=10π we have the value ω_{max} =4.94. In this way we have two time periods, the first one when the maximal values of vorticity increases with time until it reaches t=4π, and second one when the extreme values of vortex intensity decline and the kinetic energy and enstrophy are monotonicaly decreasing functions of time.

REFERENCES

45. Constantinescu V.N.(1995), *Laminar Viscous Flow*, Springer Verlag,
46. Parviz M. (2001), *Fundamentals of Engineering Numerical Analysis*, CUP
47. Fornberg B (2005), *Pseudospectral methods*, Cambridge University Press
48. Kleiser L., Schumann U.,(1980):Treatment of incompressibility and boundary conditions in 3D numerical spectral simulation of plane channel flows. Hirschel E.H.(ed.): Third GAMM Conference Numerical Methods in Fluid Dynamics, Vieweg, Braunschweig, pp.165-173
49. Orszag S.A., (1971), Accurate solution of the Orr-Sommerfeld stability equation, *Journal of Fluid Mechanics*, vol.50, pp. 689-703.
50. Schmid P., Henningson D. (2002), *Stability and Transition in Shear Flows* , Springer,
51. Criminale W.O., Jackson T.L., Joslin R.D., (2003), *Theory and Computation in Hydrodynamic Stability*, Cambridge University Press,
52. Trefethen L.N., Trefethen A.E., Reddy S.C., Driscoll T.A., (1993), Hydrodynamic stability without eigenvalues, *Science*, vol.261, p.578
53. Reddy S.C.,Henningson D.S.,(1993), Energy growth in viscous channel flows , *J.Fluid Mech.*, vol 252, p.209
54. Reddy S.C., Schmid P.J., Henningson D.S., (1993), Pseudospectra of Orr-Sommerfeld operator, *SIAM J. Appl. Math.* , vol.53, p.15-47.
55. Butler K.M.,Farrell B.F.,(1992), Three-dimensional optimal perturbations in viscous shear flow, *Phys.Fluids* A 4, 1637-1650.

EVOLUCIJA VRTLOŽNOSTI U POREMEĆENOM POASEJEVOM STRUJANJU

Miloš M. Jovanović

Apstrakt: U radu se razmatra direktna numerička simulacija vrtložnosti viskoznog nestišljivog fluida za slučaj Poasejevog strujanja (strujanja između horizontalnih paralelnih ploča pod dejstvom gradienta pritiska u horizontalnom pravcu), kod koga je polju strujne funkcije fluida pridodato poremećajno polje konačne amplitude. Ovo poremećajno polje je dobijeno optimizacijom linearne kombinacije svih sopstvenih vektora dobijenih kao rešenje Orr-Sommerfeld-ove jednačine za granične uslove koji odgovaraju opisanom primeru.

Navije-Stoksova jednačina u obliku strujna funkcija–vrtložnost je numerički simulirana korišćenjem pseudospekttralnog metoda. Za aproksimaciju u pravcu x-ose korišćen je Furije-Galerkinov metod, dok u nehomogenom pravucu, u pravcu y-ose korišćen je Čebišeljev kolokacioni metod. Za diskretizaciju po vremenu korišćen je poluimplicitni metod Adams-Bašvorta koji je drugog reda tačnosti. U radu su prikazana poremećajna polja vrtložnosti za deset različitih trenutaka vremena, u periodu tzv. prelaznog rasta energije do trenutka kada ona počinje da opada, odnosno do početka procesa relaminarizacije.

Ključne reči: Direktna numerička simualacija, poremećajno Poasejevo strujanje, podkritična nesabilnost strujanja. optimizovani poremećaji, pseudospektralni metod.

A - A VIEW IN THE INVISIBLE

UDC 531; 534; 517.944;

Slavica Ristić

Institut Goša, Milana Rakića 35, Belgeade

Abstract (bold). *Flow visualization is an important topic in, experimental and computational fluid dynamics and has been the subject of research for many years. This paper presents an overview of flow visualization techniques. The physical basis and applications of different visualization methods for subsonic, transonic and supersonic flow in wind and water tunnels are described: direct injection methods, (smoke, dye, fog and different small particles), gas and hydrogen bubbles, , flow visualization by tufts, oil, liquid crystals, pressure and temperature sensitive paints, shadow, schlieren, interferometry, Laser Doppler Anemometry, Particle Image Velocimetry and other special techniques. Almost all presented photos have been recorded during tests in laboratories of MTI Belgrade.*

Key words: *flow visualization, wind tunnel, water tunnel, optical methods, LDA, PIV*

1. INTRODUCTION

Most fluids are transparent media and their motion remains invisible to the human eye during direct observations. However, the motion of such fluids can be recognized using techniques by which the flow is made visible. Such techniques are called flow visualization techniques. These techniques are valuable tools in various scientific and engineering disciplines. They allow to see the invisible: the optical inhomogeneities and motion in transparent media like air and water.

Flow visualization probably exists as long as fluid flow researches itself and dates back to the mid - 1400's, where Leonardo De Vinci sketched images of fine particles of sand and wood shavings which had been dropped into flowing liquids. Ludwig Prandtl, one of the pioneers of aerodynamics in Göttingen, performed first qualitative visualization of unsteady flows behind profiles and other models in his simple water channel by observing the movement of tracer particles on the surface of the water. Today, one hundred years later, most physical quantities of interest to mechanics,

aerodynamics and hydrodynamics can be determined quantitatively by image based experimental techniques. Modern image based measurement techniques such as Particle Image Velocimetry, following the same simple physical principles.

The progress made with optoelectronics and computer, lasers, video techniques has stimulated the development of a great number of image based measurement techniques. These techniques are now utilized for fundamental research, in industrial applications and for comparison with the results of numerical calculations. They allow a much better understanding of complex unsteady flow phenomena and providing quantitative information about the complete flow field [1-6].

Experimental flow visualization techniques are applied to get an picture of fluid flow around a real object or a scaled model of object, without any calculations and to develop or to verify new models and new theories of fluid flow.

If the flow could be made visible by some kind of flow visualization technique, then it would be possible to observe flow phenomena e.g., vortex flows, flows distant from surfaces, as well as those phenomena which are dominated by the effects of viscosity, e.g., boundary layer flows, separation) [1-41].

Flow visualization may be divided into surface flow visualization (tufts, fluorescent dye, oil or special clay mixtures) and off-the-surface visualization (tracers as smoke particles, oil droplets or helium-filled soap bubbles). Surface flow visualization gives important information on such things as the state of the boundary layer (laminar or turbulent), transition, flow separation and so on. The second type of visualization gives the information about whole flow field. Each of these methods requires appropriate lighting and some device for recording the image such as a still or video camera. Flow visualization offers integration of photographic art and engineering techniques.

Recently a new type of visualization has emerged: computer-aided visualization. In the area of fluid dynamics, computers are extensively used to calculate velocity fields and other flow quantities, using numerical techniques to solve the Navier-Stokes equations. Usually, when data sets are computed that provide a huge amount of sampled vector information spread over a two or three-dimensional domain. Without visualization it is impossible to investigate such data sets. To analyze the results computer visualization techniques are necessary and very often used. Humans are capable of comprehending much more information when it is presented visually, rather than numerically.

Three basic types of experimental techniques can be distinguished: methods with a**dding foreign material, optical methods and methods** with a**dding heat/energy. According with these principles, o**ne possible classification of the flow visualization techniques may be:

I Non optical methods:
   1.Visualization with tracers (photochemical production of tracers, elektrochemical production of tracers, injection of tracers, smoke, dye, air and hidrogen bubbles, powder, fog and so on)
   2.Surface visualization (tufts visualization (ordinary tufts, fluorescent tufts), oil emulsion, liquid cristals, termo sensitive paint, pressure sensitive paint,clay mixture)
II Optical methods:
   1.Shadow method

2.Schlieren metod (paralel or focused, gray or color)
3.Interferometry (classical, holographic)
4.Electronic speckle interferometry and shearography
5.Laser Doppler anemometry
6.Particle Image Velocimetry

III Special methods:

7.Energy adding
8.Refractometry
9.Laser light sheet

This paper reviews flow visualization techniques applied in wind and water tunnel tests. Wind tunnels are devices for experimental study of the wind effects on different structures or objects: aircraft and missiles models, vehicles, cars, bridges, buildings, machines, pipe and so on. But main task of the wind tunnels are experimental support of research and development during design phase of aircraft projects. The hydrodynamic behavior of submerged bodies in flowing water is studied in water tunnels, experimental facilities, where water is used as the working fluid [6,7].

Wind and water tunnels are equipped with modern instrumentation, making possible various measurements: force measurements on 3D models, half models or wing section (2D) models, simultaneously using external and internal wind tunnel balances, pressure distribution measurements, using Scanivalves, mechanical or electronically scanned pressure sensors, stability derivatives measurements, flow visualization, store loads measurements, hot film and hot wire anemometry, Laser Doppler anemometry, holographic interferometer, Schlieren systems, aerodynamic noise measurements and so on.

The flow visualization techniques used in aerodynamic laboratories of MTI [5,7], are: wall tracing method with pigment oil film (TiO2, color pigments, graphite powder, lampblack, fluorescent dye) and liquid crystals, surface tuft methods with thin nylon or silk monofilaments and fluorescent mini tufts, smoke visualization techniques: smoke produced in smoke generator; smoke introduced at front of the test section and by vaporization of TiCl4 for local application, water tunnel flow visualization by the use of gas bubbles, milk as tracer, aniline and methylene dye, aluminum powder and polystyrene particles, shadowgrafy, schlieren method, holographic interferometry, hot wire and hot film anemometry, Laser Doppler Anemometry.

2. TRACER METHODS

The visualization technique of streamlines, filament lines or particle paths, which injects some foreign material into a flow as a tracer is the most popular one and has been long and widely used up to the now. These three curves coincide if the flow field is stationary. But in the flow that depends on space and time as well, the tree types of curves are different from one another. Which curves will be visualized depends on the choice of: where particles are introduced, the length of the exposure time, and the reference system from which the flow is observed or photographed. There is no difference between liquid and gaseous flows [1,2,5].

2.1. Smoke Visualization of the Flow

Resent developments indicate that smoke visualization in wind tunnels, one of the oldest flow visualization technique, will continue as an important experimental tool in the study of complex flow dynamic phenomena. Improvements in generation and injection of smoke as well as in lighting (laser as a light source), in technique of acquisition and computation have continued to increase the scientific value of this method [1-5,9]. The similarly results give the flow visualizations with fog and vapor.

There exists no upper limit of speed for smoke line visualization.

a   b   c

d   e
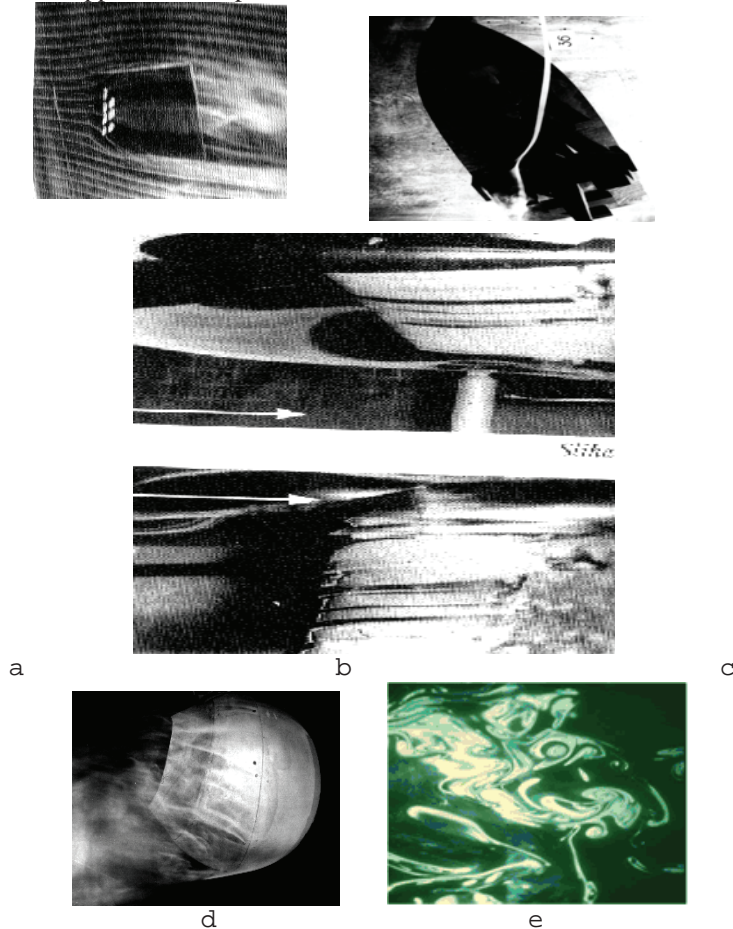
Fig. 1: Flow visualization in the MTI wind tunnels by different type of smoke.

Smoke line can be generated in a wind tunnel by introducing smoke (produced by smoke generated devices [1]) through small pipes placed in front of a test model, or through holes on the model surface. The smoke must be dense and white for visibility, no toxic, and no corrosive. The quality of the observed or photographed smoke line depends also on the choice of the illumination system. The smoke can be obtained by the vaporization of a mineral oil (paraffin, kerosene) mist resulting from the vaporization of certain

substances containing bromide or chloride, and smoke from burning or smoldering wood, paper, or tobacco. The burning or vaporization is done in a smoke generator. The flow visualization without smoke generator is possible if one deposits a drop of $TiCl_4$ (titanium tetrachloride) or $C10H_7Br$ (bromnaph-thalin) onto the surface of test model in a wind tunnel, a white stream of smoke will originate from this drop. When the liquid $TiCl_4$ contact with the moist air develops powder TiO_2 and HCl. $TiCl_4$ liquid and vapor are corrosive and toxic because of HCl [5,9].

Fig 1. shows some examples of smoke visualization (flow is left to right): the smoke line in the MTI small smoke tunnel (fig.1a), visualization obtained with smoke introduced in the flow trough the ship chimney (Fig 1b), and flow visualization with $TiCl_4$ around airplane model and sphere (figs.1c and 1d), smoke and laser sheet visualization of turbulent convection patterns (fig.1e).

One of the more significant improvements in the filed of smoke visualization in the past several years has been the introduction of laser light illumination. By using a light sheet, cross section of the wake can be illuminated and the position of the vortices can be located (fig.1e). Unsteady flow can be tested with pulsed laser. Recording of the flow visualized effects can be affected by still or movie camera. Some times that method is classified as special flow visualization method [4,5,12].

2.2. Visualization using dye

The visualization of the liquid flow patterns by ejection of a dye is an analog of the smoke visualization technique[1-6,12,13]. The dye can be injected in a tested flow either from a small ejector tube placed at a desired position or from small orifices, that are provided in the wall of a model (fig.6a), without the component perpendicular to the model surface. It can be generated in the flow too, without disturbing the flow. The dye has to be stability with respect to diffusion, to have the same specific weight as the working fluid and high contrast.

For the purpose of flow visualization can be used the food coloring dyes, aniline, methylene, potassium permanganate, ink or fluorescent dyes (fluorescent rhodamine), mixing in milk or alcohol. The fattiness of the milk retards diffusion of the dyed solution into water and give high contrast of the dye line. In a rotating flow, it is important to have dye solution with the same specific weight as working fluid (mixing dye with alcohol).

The aniline violet, red and blue dye, injected from small orifices placed in the top of the model, in the cabin region, visualizes the flow around tested models (flow is left to right): 1/48 scale model of F-18 aircraft in flow visualization facility (ONERA, fig. 2a [9]) and in MTI water tunnel, fig 2b. Fig. 2c shows flow visualization around hydro profile in MTI water tunnel with aniline dye and fig 2d. is vortex visualization Karman vortex street behind a cylinder at increasing Re number, using fluorescent dye and laser sheet.

a   b

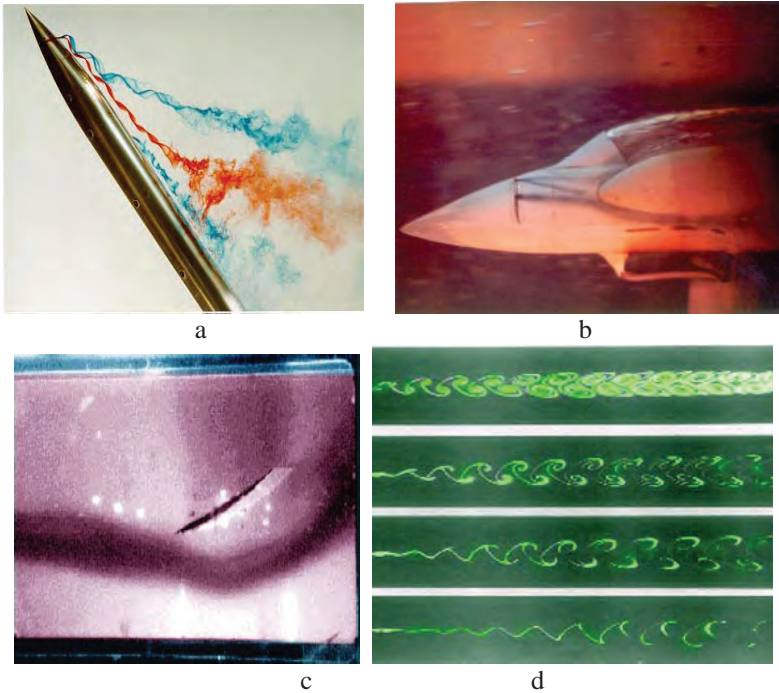c   d

Fig. 2. Flow visualization by different dyes

The dye methods used in a closed circuit water tunnel increasingly contaminate the water. The tunnel has to be emptied and refilled after each experiment. Visualization with dye is not suited for turbulent flow, since the filaments would decay and the dyes would mix with surrounding fluid immediately after being ejected [1,3,5,9-12].

Electrolytic and photochemical reactions can produce different dye in aqueous solutions, which allows flow visualization and velocity profile measurements. Focusing light from a flash tube or pulsed ruby laser onto a point in the photoactive solution fluid (pyridine dissolve in ethyl alcohol or nitrospyran in kerosene) initiates a photochemical reaction, which yields a spot of blue dye within a few microseconds [1].

2.3. Visualization by different small particles

Adding small particles in the flowing flow (water or air) supposed that the velocity of the particles and fluid are identical. The tracer particles can be either solid, liquid, or gaseous and the fluid liquid or gaseous, for example: dust, magnesium, (Mg), Al2O3, TiO2, aluminum (fig. 3) and polystyrene or cosmetic powder, licopodium, hostaflon, cigarette smoke, metaldehyde, atomized DOP, glass sphere, marble dust, oil drops, water drops, hydrogen, gas, helium bubbles, ...The diameter of the particle is between 0.1 to 20 microns [1,4,5].
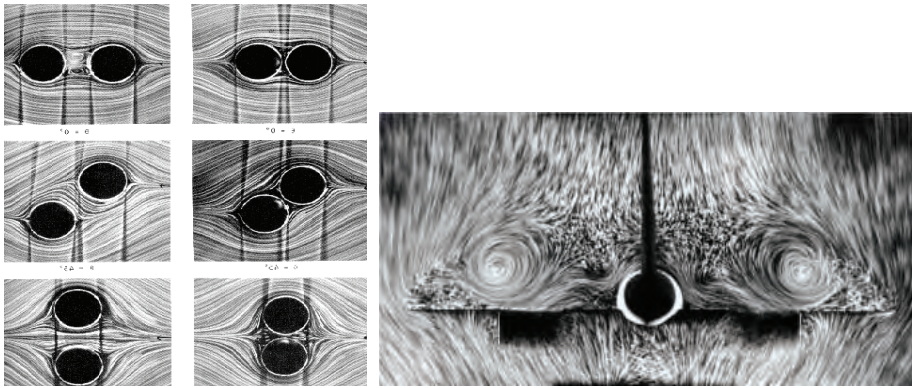
Fig. 3.Visualization the flow around two cylinders (a) and moled of Concorde with Al powder (ONERA)[1,9]

For determining the trajectory and local velocity of a spherical particle, the equation of the motion of a single particle must be solved. It is necessary to complete the equation of the motion with gravity and "lift force" acting on the particle in the flow with velocity gradient. The particle velocity approaches exponentially the constant fluid speed. The approach is the faster, the density and the size of the particle are smaller. In the compressible flow, with shock waves, particles of finite mass and size cannot follow such an abrupt change of the state of motion. The used particles should be as small as possible, neither corrosive nor toxic and to have high degree of light reflectivity. The injection into the fluid should be located far enough upstream the test regime. In principle two methods exist; to take a single or multiple photographic exposure of the flow field with controlled exposure time or to take exposure of the flow field so that each moving particle is reproduced on the photograph by a single streak of finite length. Stereoscopic photos or holograms may overcome the problem of localization of the particle. Today there are a lot of different methods for illuminating and recording. [1,2,5].

Particle Image Velocimetry (PIV) is an experimental method for indirectly flow visualization but method providing directly, instantaneous velocity vector measurement in a cross section of a flow. The method is classified as special method or as the flow visualization method by small particles. The basic principle involves photographically recording the motion of microscopic particles that follow the fluid flow [5,13]. The technique is ideal for unsteady aerodynamic flows. The software for PIV is a visual programming language combining complete control of the acquisition, redaction and analysis. The application of PIV method is illustrated with example presented in figure 4. The measured velocity distributions performed by PIV image of the flow with the Mach-4.5, on the upper part of the 20°- half angle wedge with flow is left to right (fig.4a) is shown in Figs. 4b and 4c for the horizontal and vertical velocity component, respectively.

Laser Doppler Anemometry (LDA) is optical technique for investigation of velocity and turbulence in gas, liquid, and mixing fluids, flame, rotating machinery, in combustion, channels, chemically reacting flows, wave tanks wind or water tunnels, in biomedical applications, atmospheres, oceanography and in various spectrum of scientific and industrial research. LDA is power fool method for indirect flow visualization, too[11,14,15]. The basic idea underlying LDA is to measure the velocity of

tiny particles transported by the flow. If these particles are small enough, their velocity is assumed to be that of the stream and LDA provides a measure of the local instantaneous velocity, the mean velocity as well as the turbulent quantities.
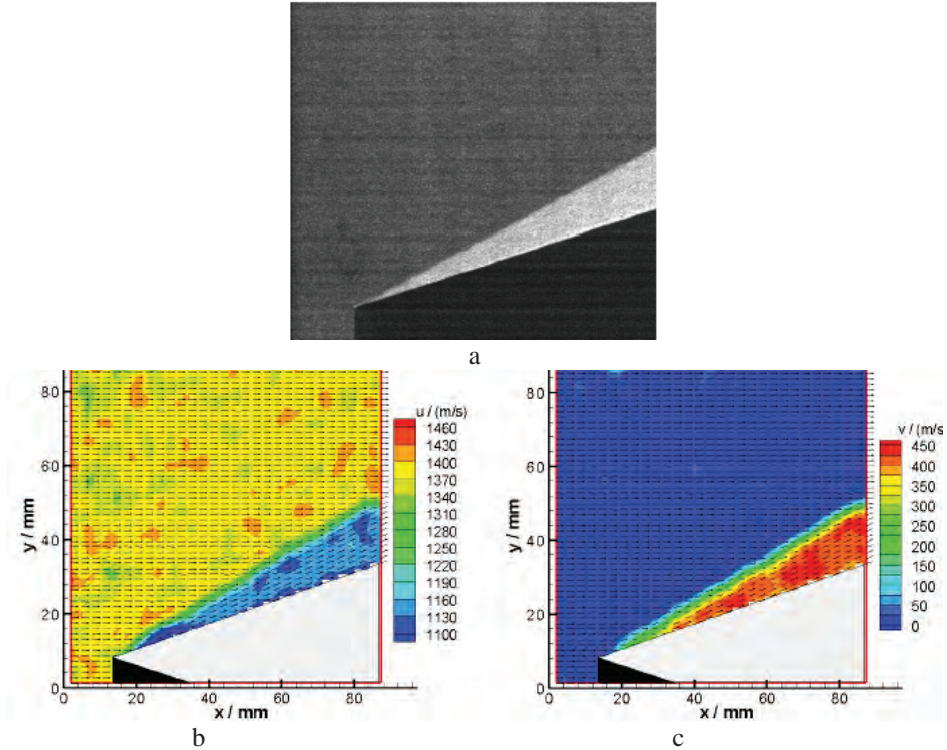

Fig. 4. (a) PIV image of wedge, (b) horizontal flow velocity, (c) vertical flow velocity [13]

Laser anemometers offer some advantages in comparison with other fluid flow instrumentation: non-contact optical measurement. LDA probe the flow with focused laser beams and can sense the velocity without disturbing the flow in the measuring volume, non calibration – no drift. The laser anemometer has a unique intrinsic response to fluid velocity–absolute linearity, well-defined directional response. The quantity measured by the LDA is the projection of the velocity vector on the measuring direction defined by the optical system, high spatial and temporal resolution, multi - component and multi - directional measurements and so on.
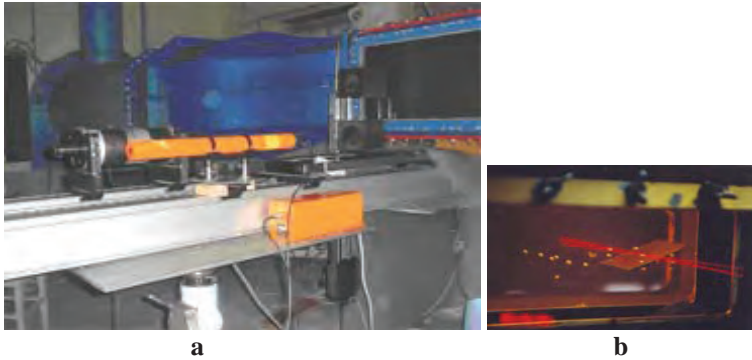
<center>**a**   **b**</center>

Fig. 5: Some details of experimental setup, a) water tunnel and 1D LDA, b) hydrofoil in WCT test section and laser beams[11]
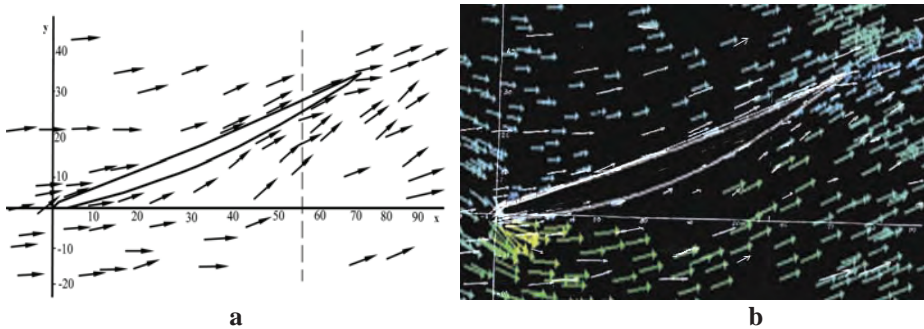

<center>**a**   **b**</center>

Fi. 6: LDA, experimental (a) and numerical (b) results of visualization by vector velocity distribution for flow around hydrofoil positioned at $\alpha = 25°$, V∞=5.32 m/s, (flow is left to right)[14]

2.4. The gas bubble visualization

Gas bubbles visualization is a tracer method where tracer particles have low (in the water), or similar density (in the air) as the flow. The observation of such gaseous tracers in a gaseous flow requires the use of optical visualization methods. The gas bubbles change its shape during the motion, and as a consequence, the drag coefficient of these gaseous tracer particles is not only a function of the velocity difference between fluid and particle, but also a function of the deforming forces acting on the particle. The gas bubbles can be injected in the flow or generated by electrolysis [1, 5].

In a conventional arrangement hydrogen bubbles are produced on the cathode. They mark a line of fluid elements whose position coincided at a given instant with the position of wire. Any later position of these rows of tracer particles is called a "time line", that is a measure of the local velocity profile (fig.7a), while fig 7b shows co-rotating vortices and saddle points upstream of a bluff protuberance mounted on a flat plate (flow from top) visualized by hydrogen bubbles and laser sheet flow visualization in a water tunnel.
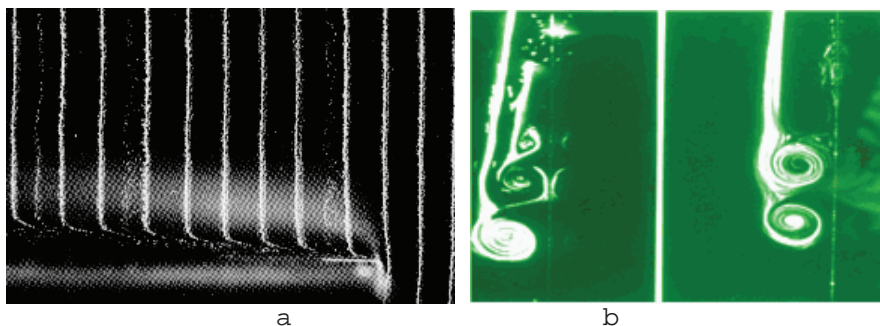
Fig. 7. Rows of the hydrogen bubbles indicete the velocity profil over the plate [1]
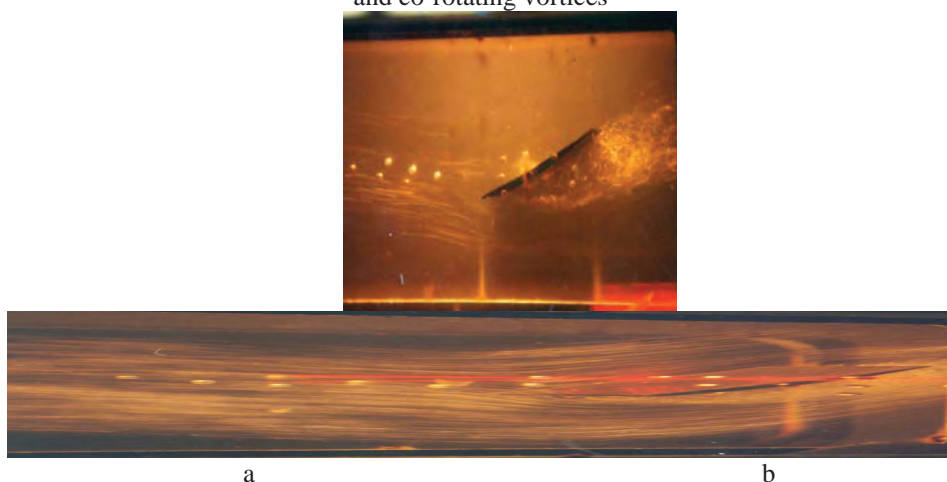and co-rotating vortices

Fig. 8: Flow visualization in MTI water tunnel with air bubbles around hydrofoil
with different quantity of injected air [11]

The bubble motion can be recorded with a still or move camera. Time of
observation bubbles in the flow is limited by the dissolution of the gas bubbles in the
fluid (in water the time is approximately 3 s). The application of this method is limited in
the laminar, low speed flow [2,3]. Fig.8 shows the flow around hydrofoil in the water
tunnel (MTI) visualized by air bubbles [11].

3. FLOW VISUALIZATION BY TUFTS

Very frequently, flow visualization in the vicinity of model, in subsonic flow, is
performed using tufts. [1-5,16-18]. However, tufts size, their distribution on the model
surface and sticking are important for turbulent flow testing and for higher quality
boundary layer visualization on complex models. A grid with attached or glued tufts as a

screen can be used to visualize the vortex shedding behind model or in the interaction regime of different field. [2].

Fluorescent tufts have numerous advantages in comparison with the ordinary silk tufts [1, 5, 16-18]. By using fluorescent dyes, the tuft diameter virtually increases as well as the illumination, thus allowing higher quality of recording and using thinner tufts (0.01-0.1 mm). They can be stuck onto the model surface using very small glue quantities, (0.04 mm), thus avoiding boundary layer disturbances. Strong centrifugal forces interfering with flow field act on tufts stuck onto the model surface and their resultant determines tuft orientation.

The problem with small size diameter is overcame by using light source with rich ultraviolet part of the spectrum, or special filters transmissible to that part of the spectrum. This increases tuft luminance making it look much thicker and brighter. Hg or Xe lamp with UV filters for $\lambda = 350$ nm are used for steady flow testing. Stroboscopic light sources are most frequently used for unsteady flow. Fluorescent tufts are also used for flow visualization in water tunnels, as well as in-flight flow testing.

Figure 7 demonstrates the results of experiment in subsonic wind tunnel; flow visualization with fluorescent silk tufts. The light combat aircraft model has surface painted in opaque black with 840 tufts stick on it. Tufts are made of silk 0.05 mm and 20 mm long (figure 9a). Fluorescent spray was used for tufts dying. The flow speeds have been between 20 and 40 m/s, and angle of attack has been altered from -8 to +24°. UV lamp with 100 W has been used as light source.
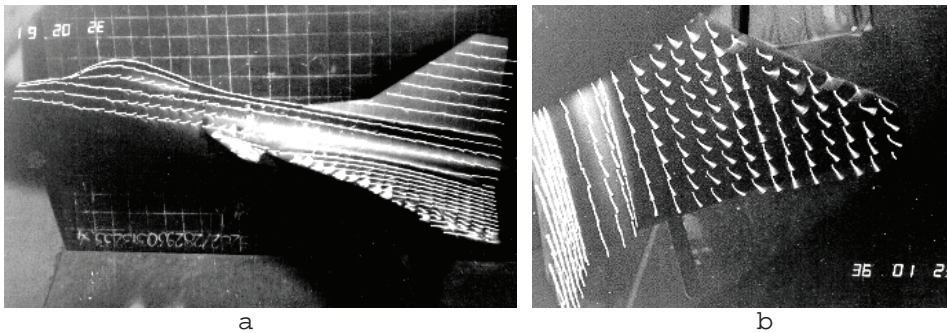

| a | b |

Fig. 9: Flow visualization with fluorescent tufts in subsonic wind tunnel (flow is left to right)[18]

4. SURFACE FLOW VISUALIZATION METHODS

For observation of flow characteristics close to the wall of a model, the body wall can be coated with a certain material which indicates the local wall temperature, surface pressure, or the streamline pattern of flow adjacent to the wall [1-5,19-22].

4.1. Surface Oil Film

Oil film or dots on the model surface enable one to quickly and easily obtain a picture of flow pattern at the surface of the model placed in wind tunnel [1-5,]. The special mixture can be prepared of appropriate oil and a fine pigment (Al_2O_3; TiO_2, powder, fluorescent dye, coloring pigments, and graffito). The technique allows observation the lines of separation and reattachment of the flow at the body.

Fig. 10a and 10b shows the visualization with TiO_2 + oil on the surface around two and three vertical cylinders fixed on the plate in subsonic wind tunnel for V=50 m/s and around sphere used for turbulence test for M=0,2 (fig. 10c)[5,22]. Figure 10d is oil flow visualization of the airflow on end wall of a turbine blade cascade. Boundary layer flow visualization on the laser guided bomb model with oil film, performed in the large trisonic wind tunnel, top of the model with fins (a) flow on the fin upper surface (b), on the wing upper surface (c) for M_∞= 0.9 is presented on fig. 11.
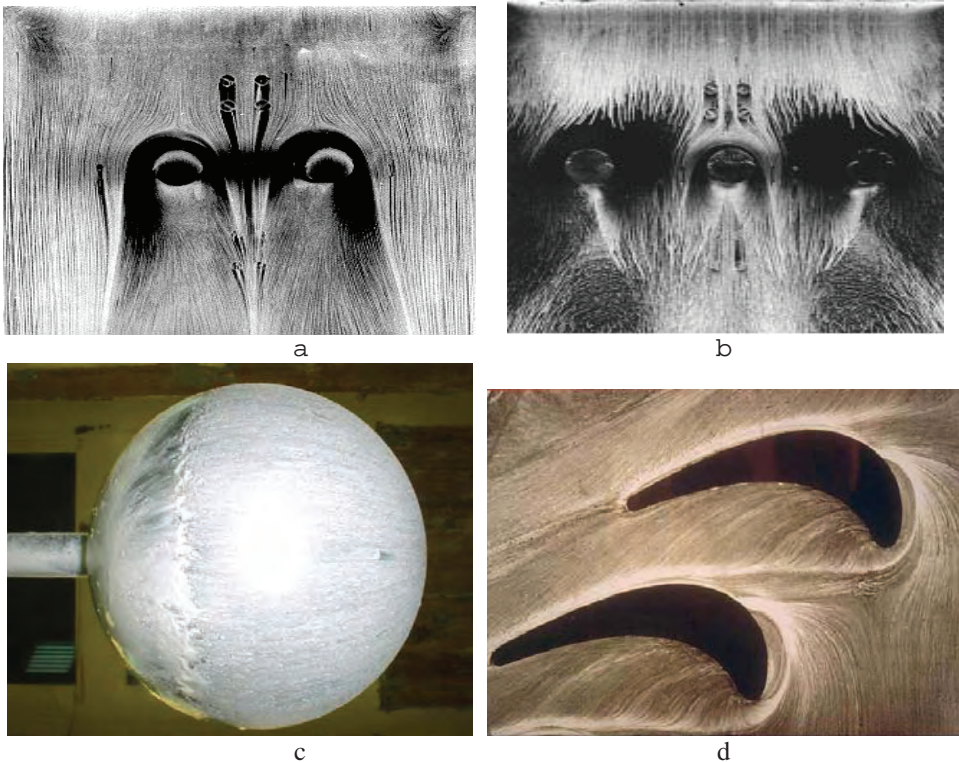

a

b

c

d

Fig. 10: Flow visualization around two (a) and three (b) cylinders fixed on plate in large wind tunnel T-35 for M= 0,5 with oil film, around sphere for M=0,2 (c) [9] and airflow on end wall of a turbine blade cascade [25].

Test of the flow field around the axysimmetrical body – model of the torpedo without fins and control surfaces, was performed in the trisonic wind tunnel T-38 of MTI, for the speed of undisturbed flow which corresponds to Mach number M_∞=0.3.

Aerodynamic forces and moments were measured by six-component internal strain gage balance. Oil emulsion film with addition of oleic acid and TiO_2 powder was used for flow visualization in the boundary layer (fig. 23)[20-23].

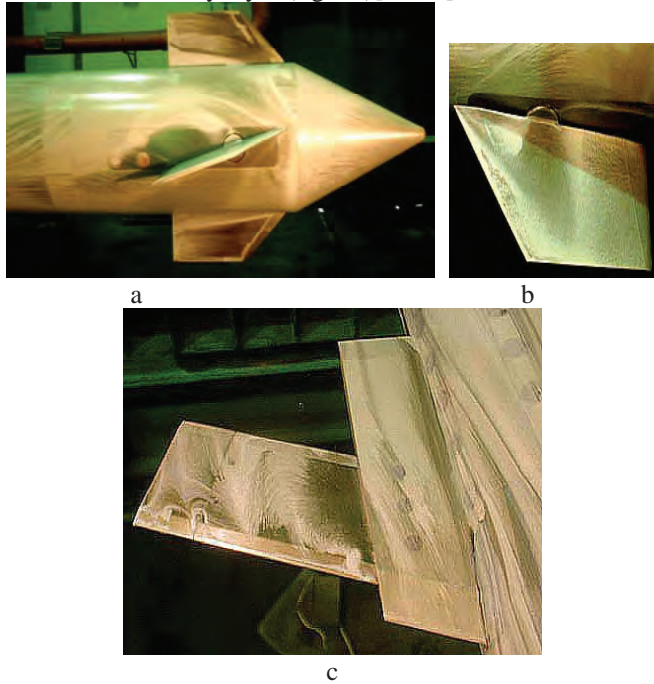a   b

c

Fig. 11. Boundary layer flow visualization on the laser guided bomb model with oil film, top of the model with fins (a), flow on the fin upper surface for $M_\infty = 0.9$(b) and flow on the wing upper surface (c)[19].

a

b

Figure 12: Flow pattern on the model obtained by the experiment (a) and by the simulation of the flow for $M\infty = 0.3$ and $\alpha = 8°$ (side view) (b) [21].

The goal of the experiment was to make possible comparison of the aerodynamic coefficients and flow pattern obtained by the experiment and by the simulations of the flow. Fluent 6 was used for simulation of the flow. Analysis of shown photographs (figure 12a and 12b) demonstrates an excellent agreement of flow patterns obtained by the experiment and the numerical simulations.

4.2. Liquid crystals and temperature sensitive paints

A surface-temperature distribution can be gained by coating a test model with cholestric liquid crystals. [1,2,5]. If they are illuminated with white light under a certain angle of incidence, then liquid crystals reflect only one light wavelength at each viewing angle, depending of small temperature changes in the crystals sheet. The colors of liquid crystals are reversal if the temperature changes in the opposite direction. Because of that, liquid crystals are very attractive for boundary-layer studies. Model to be tested should be made of a material with low heat conductivity and coated with black paint as base. Fig 13 demonstrates the application of liquid crystals for hot streams visualization in a subsonic wind tunnel.

The surface temperature, the local heat transfer rate and coefficient on a body tested in high speed flow facility can be measured by means of temperature sensitive paints. The important difference between liquid crystals and temperature sensitive paints is, that the temperature span over that liquid crystals change colors is much smaller (a few degrees only) than that of paints (several hundred degrees).
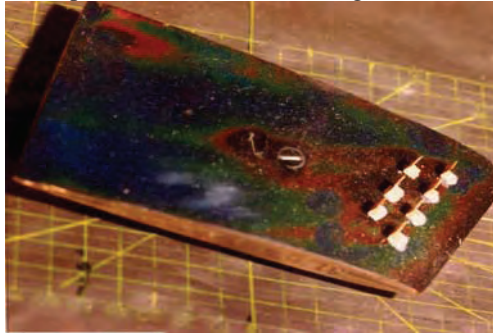

Figure 13: Flow visualization in small wind tunnel with liquid crystals [5]

4.3. Pressure sensitive paint (PSP)

The spatially continuous pressure and temperature distributions on aerodynamic test surfaces is important for understanding complex flow mechanisms and for comparison with predictions of computational-fluid-dynamics models [5,26]. Conventional pressure measurements are based on pressure taps and electronically scanned transducers. Pressure taps provide pressure information only at discrete points.

PSP technology is an alternative for determining static and transient surface-pressure fields for aerodynamic applications and for flow visualization. The pressure sensitivity is based on the oxygen (O_2) quenching of luminescent molecules dispersed in a film that is coated onto a test surface. In practice, the PSP/TSP (temperature sensitive paint) coating is illuminated with light of the appropriate energy (color) to excite the coating-entrapped probe molecules. The resulting luminescence output is inversely proportional to the surface pressure or temperature of the test model.

The output of the CCD array can be visually represented as a two-dimensional image, with the luminescence corresponding to a gray or false-color scale. Figure 14 represents the illustration for PSP applications.

5. FLOW VISUALIZATION WITH SPECIAL TECHNIQUES

Third group of visualization methods is based on two principles: introducing a foreign invisible substance into the incompressible flow, and visualizing the density variations in flow by optical methods. The foreign substance in this case is energy transferred to certain portions of the flow that increase energy level (spark, electron beam and glow discharge methods) and make artificially density variations. Such portions of the flow have an altered density and can be visualized by the optical methods.
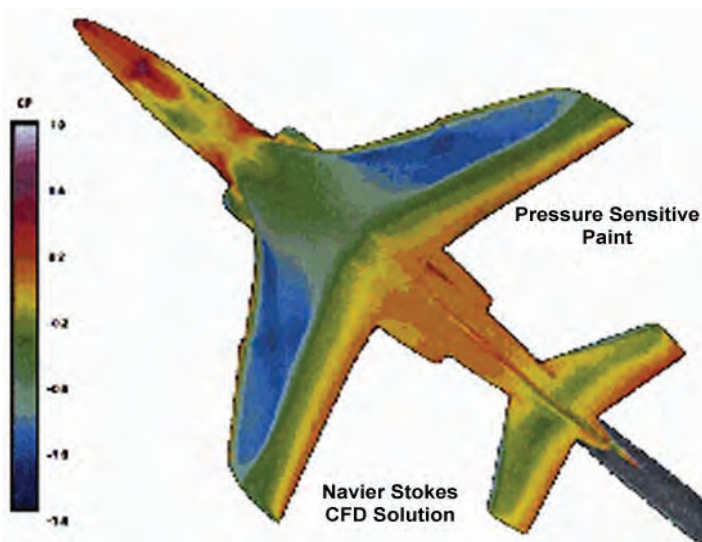

Fig. 14. A comparison of pressure results between PSP (right side of model) and Computational Fluid Dynamics (left side)[26]

They are applied to visualize the rarefied gases that are for several reasons distinguished from the ordinary compressible flows [1]. A technique which can be used even for very low density fluid flows is electron-beam flow visualization. A beam of electrons traverses the gaseous fluid. When electrons collide with gas molecules, these gas molecules will be excited and emit radiation. The intensity of the radiation is approximately proportional with the density of the fluid. By moving the electron beam, the entire flow area can be scanned (fig.15).

An intensive hot spot can be obtain by means of a spark discharge across two electrodes into a gas stream or using a giant pulse laser for producing the luminous plasma (Q-switched giant pulse ruby laser of 100 MW). Another way of artificially introducing density changes in a flow is to seed the flow with a foreign gas of different refractivity (benzene vapor, CO_2).
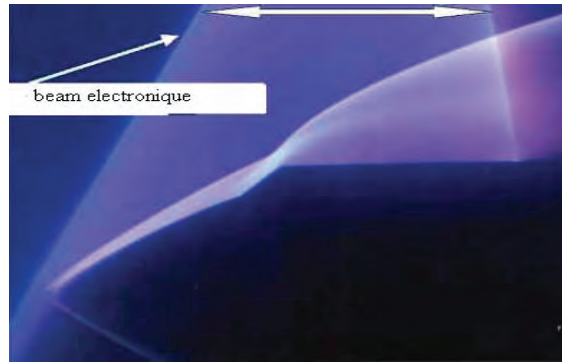
SLAVICA RISTIĆ

Fig. 15: Flow visualization by electronic beam in hypersonic wind tunnel for M= 10
[5]

Very often as special flow visualization techniques are mentioned methods where the double refracting liquids, solutions or suspension of certain macromolecules in a neutral solvent, are used. A transparent medium can be birefringent if it consists of optically anisotropic molecules.

For the purpose of flow visualization high speed photographic techniques are usually applied in connection with one of the visualizing method. High speed cameras with exposure time of 10^{-6} to 10^{-9} s in connection with associated illumination systems can record the shock wave motion.

6. COMPRESSIBLE AIR FIELD AS AN OPTICAL OBJECT

Airflow around aerodynamically models, in optical sense, is a transparent environment with complex light refraction index. Light refraction index n in each point is the function of air density, which, on the other side, is the function of speed, pressure and air temperature [1,5,27-37]. The relation between air density ρ (x,y,z) and refraction index $n(x,y,z)$ is the Gladstone-Dale: $n = 1 + K\rho$. The constant K has dimension of ρ^{-1} and it is different for each gas.

According to Snell's low [1,3,5,27], a light ray, passing through inhomogeneous refracted field, is deflected from its original direction and a light path is different from that of undisturbed ray. If recording plane is placed in front of light ray, after disturbing media, three quantities can be measure: the vertical displacement of disturbed ray, the angular deflection of disturbed ray with respect to the undisturbed, the retardation of deflected ray, i.e. the phase shift between both rays [1].

Optical visualization methods are based on the recording one of these three quantities, or a combination of them. Shadowgraph used the first phenomenon, the Schlieren the second, and interferometry the last. The shadowgraph is sensitive to changes of the second derivative of density or refractive index $\partial^2 n / \partial y^2$, Schlieren to changes of density first derivative $\partial n / \partial y$, and the interferometry is capable to measure

absolute density *n* changes. If, using the optical method, light refraction index $n(x,y,z)$ in flow is determined, another physical parameters of tested environment, significant to aerodynamic testing, can be indirectly determined as well.

6.1. Shadowgraph method

The oldest and the simplest of all optical methods for flow visualization is shadowgraph [1-5].

Figure 16a shows the bow shock wave ahead of sphere in supersonic wind tunnel T-36 at $M_\infty = 1.86$ [5,7]. The trace of the shock wave on the photo is a band of absolute darkness bounded on the downstream side by an edge of intense brightness. The exact geometrical position of the shock front is the other edge of the dark zone. The shock wave represents a jump of the refractive index. The air density increases after the shock and the incident ray deviates to inside edge.

Since the density in the disturbance is lower than in the surrounding field, (Prandtl-Meyer expansion fan at the sharp end of the nozzle) the bright band appears at the beginning of the shadow [1-5,27]. The same result is obtained when the compressible boundary layers is visualized. Figure 16b is typical shadowgraph showing flow around spherical tipped cylinder mounted on flat plate [5].

Shadowgraph methods with short duration light pulses can be used for fine visualization of turbulent compressible flow.
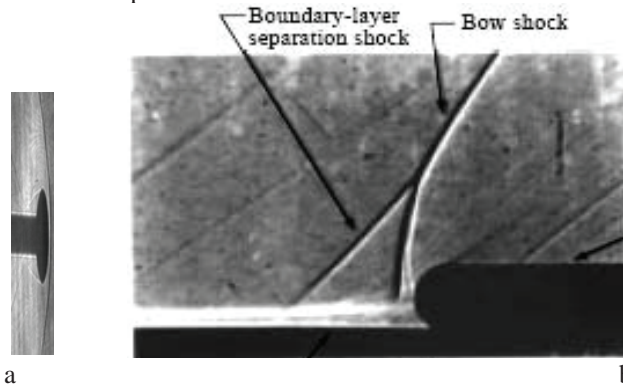

Fig. 16: Shadowgraph visualization around sphere (a), and typical shadowgraph images showing spherical tipped cylinder mounted on flat plate (b) [5]

6.2. Shlieren method

As is mention before, Schlieren method is sensitive to change of the first derivative of density $\partial n / \partial y$, (or refractive index) and it can record the angular deflection of the disturbed ray with respect to the undisturbed in a transparent medium with local in inhomogeneities [1-5,27,32,33,36,37].

The Schlieren method is the most frequently used in aerodynamic laboratories, since it is relative simple and very useful method. If a parallel beam of light passes

trough air with density gradient normal to the direction of the beam, the beam is refracted towards the region of greater density.

The most simply is the Schlieren system with parallel light through the test section of the wind tunnel. Töepler system in hypersonic wind tunnel, as the base of all other systems, is illustrated in Fig 17. Detail description of the system is presented in references [5].

The modern schlieren system uses color filter or phase optical elements instead of the knife-edge, and have several parallel, transparent, colored strips (most often three colored sheets, red-blue-yellow or blue-green- red). The color filter can be consisted of four differently colored strips arranged in a square filter for visualize the grad n in two direction. If the flow is axis symmetric, complementary colors appear for the same event (compression or expansion) above and below the flow axis.

The recorded pure colors and color combinations are a measure for the local direction of density gradient in the test section. Figure 17 shows parts of schlieren systems in T-34 hypersonic wind tunnels in MTI [5,7].
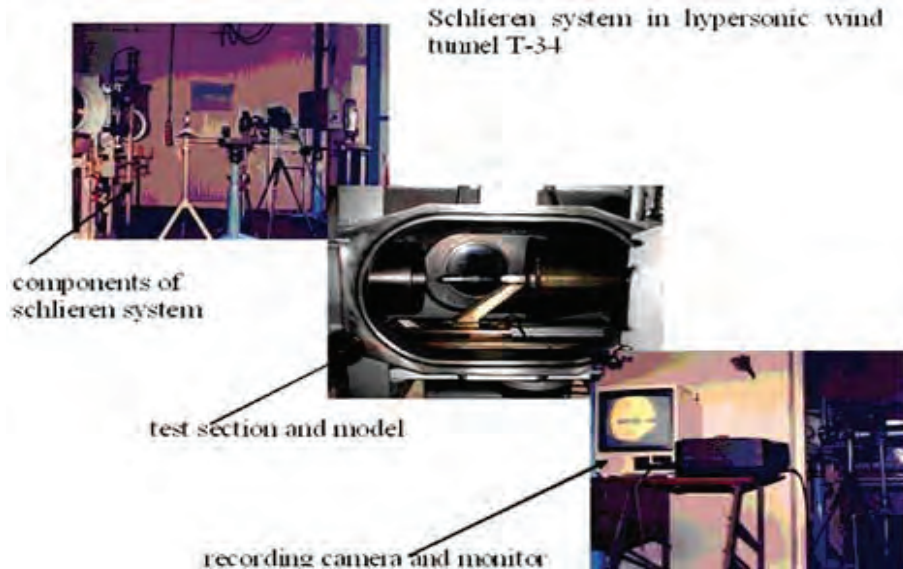

Figure 17: The photos of schlieren system components, model in the test section of hypersonic wind tunnel T-34 and TV camera with monitor

Attempts to increase the amount of information extractable from schlieren effects, the various opaque filters with different geometries, as well as transparent phase and color filters are used [1-5].
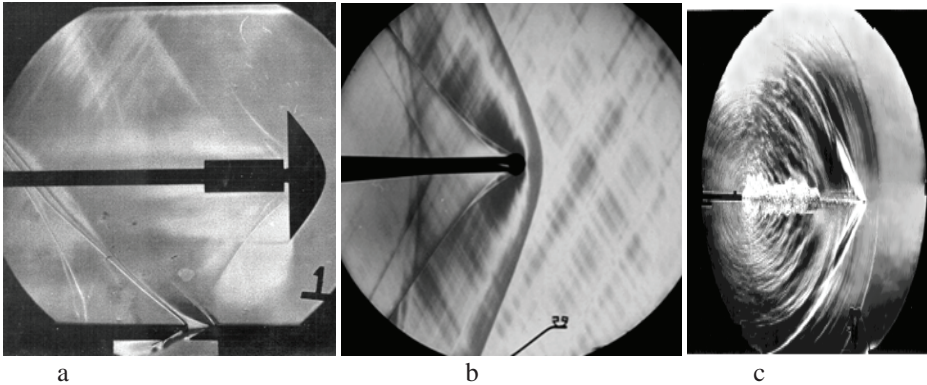
a   b   c

Fig. 18: Black and white schlieren in wind tunnel T-36 for $M_\infty = 0.86$ (a) and $M_\infty =$ 1,1 (b), and instantaneous image of Bullet and Muzzle Blast from 22-Caliber Rifle (c)

Figure 19 shows color schileren effects around blunt body and thin protruding probe mounted in front of a blunt body, used to reduce the drag and the rate of heat transfer, for $M_\infty=1.86$ [5,33]. Flow visualization in two dimensional model of the supersonic rocket nozzle without and with vertical, different height barierres is tested by schlieren method and the effects are presented in the fig 20. The nozzle is designed for Mach number in the output plane $M_\infty= 2.6$ [31,36,37].

The classical schlieren photos obtained with color schlieren system are presented in fig, 21. The flow around cone with top angle of 15° and sphere with Φ=40mm is tested in supersonic wind tunnel T-36 for different Mach number and position of color filters [5]

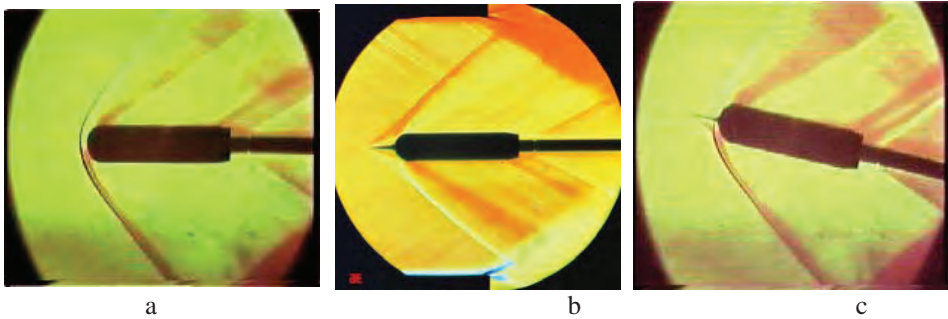a   b   c

Fig. 19: Color schileren effects around blunt body and thin protruding probe (flow is left to right)
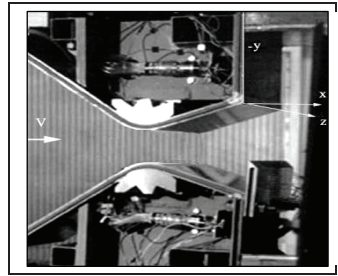
a
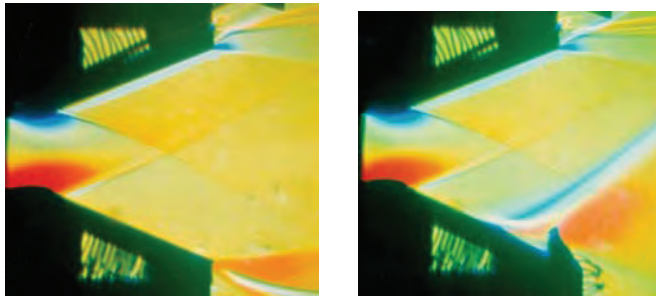
b

c
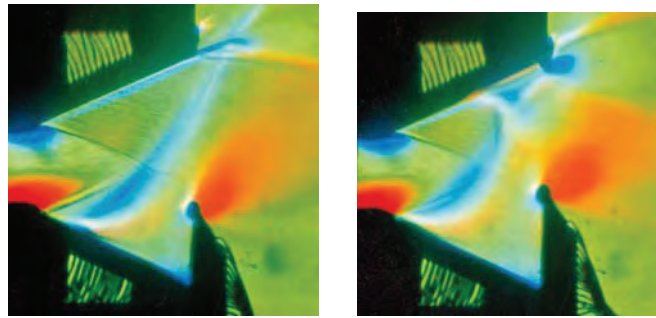
d

e

Figure 20 Schlieren visualization of the supersonic nozzle flow(flow is left to right)

The combined holographic interferometer and schlieren devices [5,35-37], have been designed, made and tested for small supersonic and large trisonic wind tunnel. The device can be included in tests either as schlieren system or interferometer.

Improvements to the basic schlieren system include the Rainbow Schlieren [1,3.5] where a colored bull's eye filter is used rather than a knife edge to quantify the strength of the refraction. The other variety of sclieren methods is obtained including laser as a light source. Figure 22 illustrates rezultats schlieren system in T-36 with He-Ne laser as a light source.

<center>a</center>

<center>b</center>

<center>c</center>

<center>d</center>
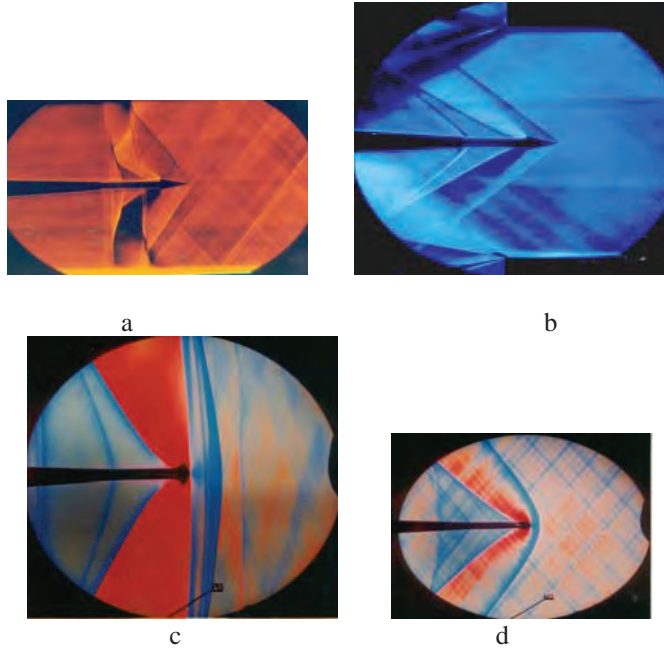
Fig. 21: Color schlieren photos obtained in T-36 wind tunnel for $M_\infty = 1.02$, and 1.56 around cone with 15 degrees top angle(a,b) and shpere with $\Phi=100mm$ (c,d) [5].
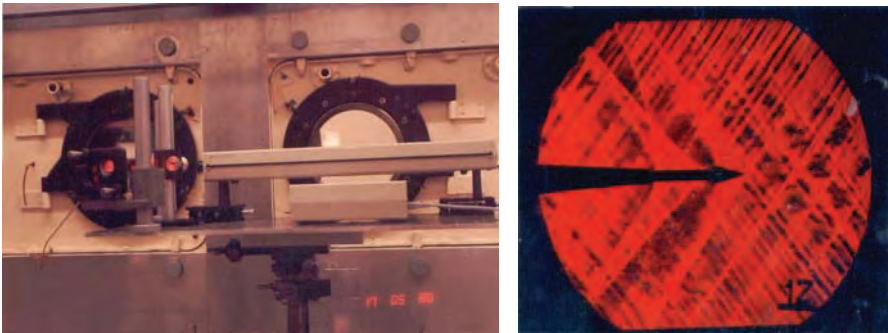
Fig. 22. Schieren system with laser as light source in T-36 and schlieren effect around cone for $M_\infty = 1.1$ [5]

6.3. Interferometry

Interferometry is based on the fact that a change in density not only results in a refraction of the light, but also in a phase shift. In an interferometer parallel light is split into two beams. One of the beams enters the flow field, the other beam does not enter the flow field. When both beams are merged and projected on the same photographic plate, interference occurs when the phase of one of the beams is shifted by a change of density in the fluid flow [1-5,27-37].

The most used classical interferometer in the wind tunnel tests is Mach-Zehnder interferometer (MZI) [1,27]. MZI can be applied to any case of gas flow investigations, where density difference becomes noticeable as: thermodynamic data, thermal conductivity of gases, dissociation, aerodynamic application, turbulence, wave or sonic booms.

6.3.1. . *Holographic Interferometry*

Holographic interferometry is an optical method that makes possible complete flow field testing. The method is non-contact and it does not disturb flow field. It is used for testing of different object and phenomenon [1-5,27]. The greatest advantage of holographic interferometry, in relation to schlieren method, is the fact that it provides complete information stored in a single plate, allowing a postponement selection of specific types of flow visualization.

The base of this method is holography, developed in last forty five years [27]. If, on the some plate, the image of one object is recorded two times in different moments, in the process of reconstruction both images appear simultaneously and on the same place in the space. Object waves interfere becouse of mutually coherence (they originate from the same light beam that illuminate the hologram) and the interference effects can be observed in the reconstructed object image. If no change occurs on object between first and second exposition, then there is no difference in images and there are no interference fringes. If certain difference appears, then the reconstructed image contains the system of interference fringes N that indicate that change.

Quantitative flow testing, using holographic interferograms is performed by determining the number of fringes $N(x,y)$ in the field image with respect to a reference point of known density. After that, the index of light refraction $n(x,y)$ and the air density $\rho(x,y)$ can be calculated. For the isentropic flow, there existed relations between N, n,,, ρ, pressure P, temperature T, velocity V, and Mach number M The physical base and mathematical interpretation of the holographic interferometry are explained in references .

The simplest case for analyzis is the 2D flow [9,21,31-35]. For the processing of interferograms of axi-symmetrical phase objects, the method of inversion, based on the Abel transformation, is used. The experiment geometry is usually selected in order to simplify the mathematical representation of flow and changes occurring at the path of the laser light beam through the test section [5,29-32].

Computer tomography is an important technique for reconstructing 3-D fields from holographic interferograms [1,27-29]. Several techniques have been developed for computer tomography as: implicit methods (series expansion, discrete element representations), explicit methods (convolution method), and Fourier transform method. The choice of the best algorithm depends on structure of the density field, the amount and format of available data.

Holographic interferometer with parallel beams is at the same time schlieren and shadow device. Fig. 1 shows the schematic diagram of the experimental setup. Detail description of interferometer components is given in previous paper. During the experiments synchronized measurements were performed. Double exposition technique was used for holographic interferograms recording: wind off (when homogeneous flow

field exists) and wind on (when there is complex flow field for testing) [1,3,5]. Stagnation pressure (P_0), atmospheric pressure (Pa), and Mach number (M_∞) were measured by the primary measurement system (*PMS*) in the wind tunnel, at the moment of recording hologram, shadow and/or schlieren results.
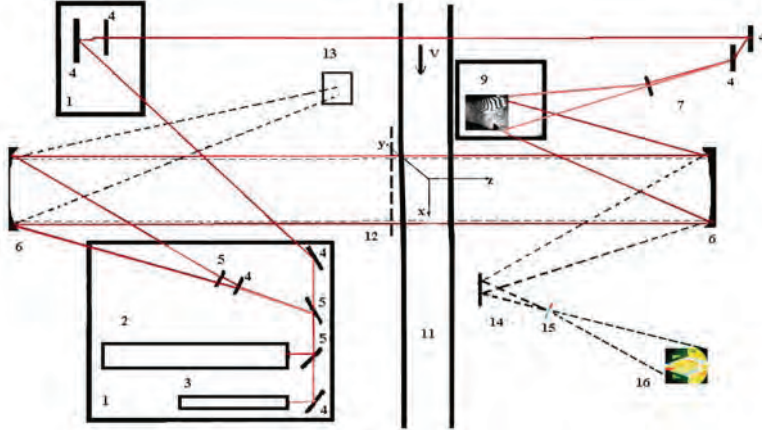
Fig. 23: The schema of the holographic interferometer/schlieren and shadow device in supersonic wind tunnel

6.3.2. Review of holographic interferograms

In order to demonstrate advantages of holographic interferometry in complex flow field testing, and compared with other classical methods, the series of experiments were performed in MTI supersonic and trisonic wind tunnel at flow velocity from $M_\infty = 0.7$ to 3.24. The photos of holographic interferograms illustrate this method. Figure 24 show some interferrograms of different flow.

a   b   c
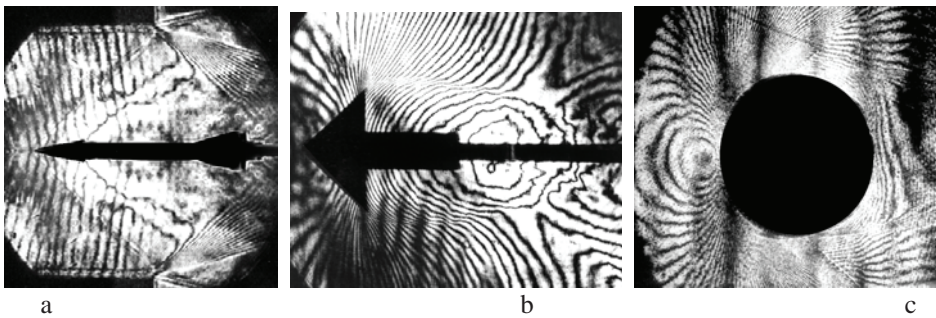
Fig. 24: Holographic interferogram of flow around missle for M_∞=1,56 (a), cone 90° and M_∞=0,86 (b) and 2D cylinder M_∞=0,76 (flow is left to right)[31]

The usage of classical methods of nozzle flow field testing comprises the introduction of probe within the expansion region and holes perforation on nozzle surface. These interventions would significantly change the flow field. Optimization of this measurement is made by the holographic interferometry.

a   b
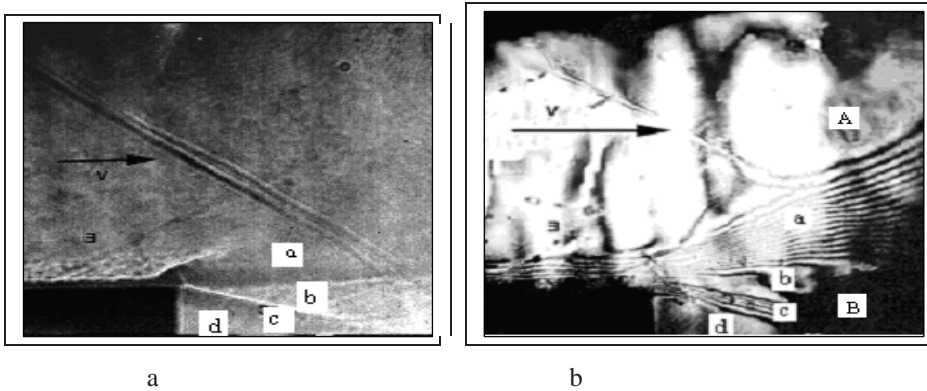
Fig. 25. Visualization of supersonic flow (left to right)around 2D 90˚ nozzle edge
(Prandelt-Mayer expansion) M_∞=1,56: a) shadow, and b) interferogram

In order to demonstrate and to compare complementary possibilities of optical
methods in quantitative flow visualization, Prandlt-Mayer expansion tested by three
optical methods is presented. Figure 25a,b and c show the flow visualization around 90°
corner end edge for supersonic nozzle M_∞ =1,56. The interferogram is recorded by
double passing, collimated, object beam trough the wind tunnel test section. The shadow
is recoded on a holographic plate, because of collimated beams. The color schlieren is
recorded in the some time with hologrphic interferogram.

The holographic interferograms were used for numerical calculation of flow field
parameters in the vicinity of nozzle edge where the expansion fen is formed (fig. 25c).
The fringe number N was read from this hologram. Points in front of expansion fen have
N=0, since the last fringe has N=17. The theoretical and experimental values of Mach
number in the expansion area are in good agreement M_{exp} = 2.15, M_{the} = 2.13 [5,29].

The photos in figure 26a and 26b present holographic interferograms of flow
around sphere for M_∞=0.8 (without shock wave) and M_∞=1,06 (bow shock wave is in
front of model). Fig. 26b is combination of holographic interferograms (upper part) and
schlieren photo for the same flow. On the interferometric part of photo easily seen are:
the stagnation point, the detached bow wave, the vortex sheet generated past sphere and
so on.

a   b
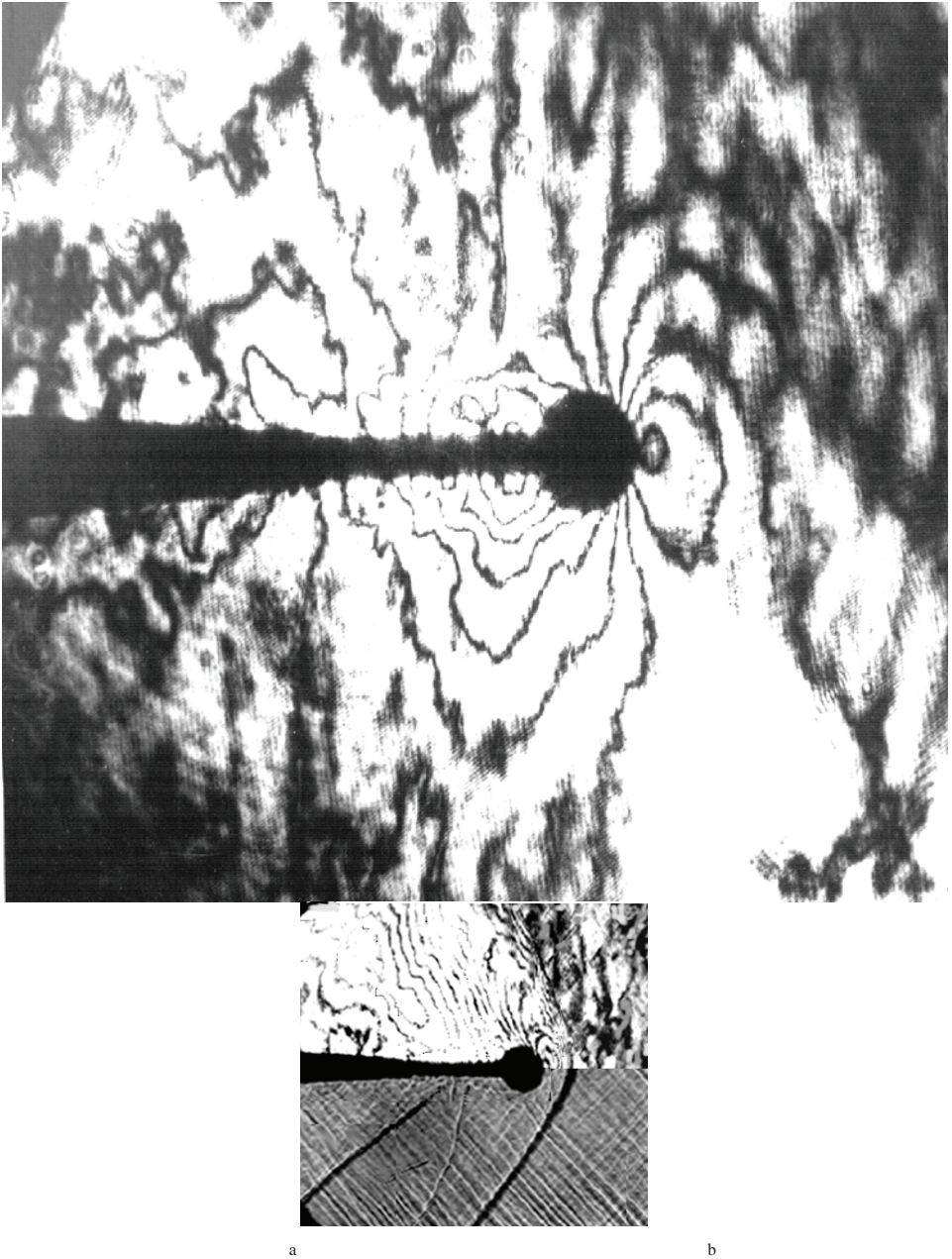
Fig. 26: Holographic interferogram of flow around sphere for $M\infty = 0.82$ (a) and mix; hologram and schlieren for $M_\infty = 1.06$ (b)

Very interesting is example of flow visualization around tunnel wall perforations [5,30,32]. Many transonic tunnels are operated with performed walls in the test section.

A number of investigations have been performed to determine how the flow in the test section is affected by the presence of the perforation. The next photos (Fig 27) reports on test performed in T-36, with a single slanted slot in the bottom plate of the test section. The disturbances originating from the slot are expressed by distortions of the parallel fringe system. A concentration of fringes indicated the formation of a pressure wave. The slanted slot was used because it had been reported that such geometry would considerably reduce the perturbation of free flow.

a   b

c
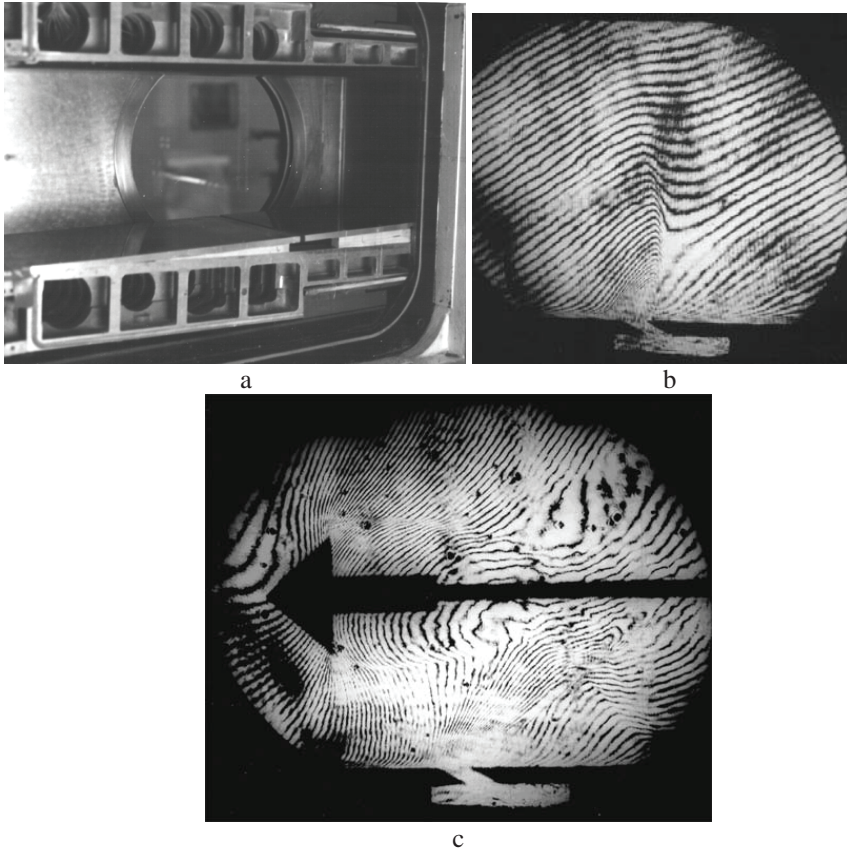
Fig. 27: Test section (a) and holographic interferograms of flow (flow is left to right)in the empty wind tunnel test section with wall perforation (slanted slot) (b) and with cone for M_∞ =0,83 (c) [30]

The interferogram however shows that the disturbance from the slot is not at all negligible and reaches even beyond the axis of the test section (to about 60 % of the test section height). The perturbation has the influence on the model sting in the central line of the test section (fig 27c).

The interferograms of several supersonic racket nozzle configurations (fig. 28a) without and with different barriers are recorded in order to provide a good insight in the physical processes (figs. 28b,c,d). [5,7,31,36,37].

The theoretical value of Mach number in the output plane of the nozzle is estimated to be M=2.6. Using the data for pressure measurements, it is obtained M=2.46 and by means of holographic calculations, Mach number is M=2.56. The placing of barriers in the supersonic flow, leads to the appearance of the stagnation zone, shock and expansion waves. Visualization of the flow field made in the experiment indicates strong interaction of the turbulent boundary layer with the oblique shock wave in the divergent part of the nozzle.

Fig. 28. Holographic interferograms for 2D supersonic nozzle without and with three barriers

Beside two-exposition method, there are used the real time method, the average or sendvich methods, the specle interferpmetry, refraction interferometry, differential interferometry and so on. Optical holography use laser light in visible spectrum, and interferencial effects are recorded on photo or thermosensitive emulsions. Electronic holography uses CCD cameras. In some specific cases acoustic and microwave holography, with electron beam, X – rays, or comput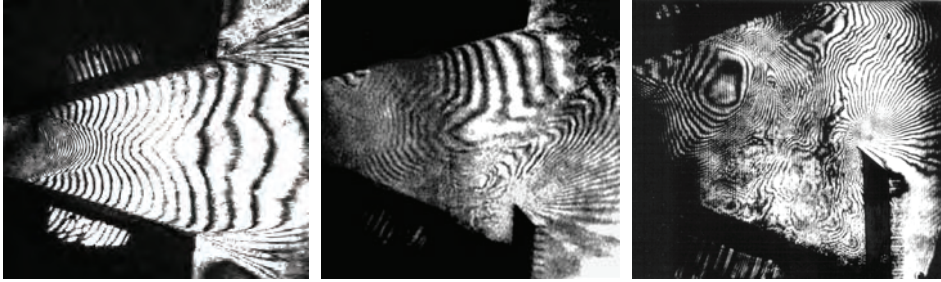er holography can be used. With similar possibilities, today are used speckle interferometry, moiré interferometry and shearography [1-5, 27,28].

6.4. Flow visualization by infrared thermography

Thermographic systems have been considered to analyse fluid-dynamic phenomena thirty years ago. Nowadays high resolution and differential infrared thermographic measurement systems open up new possibilities in it application [38,39]. Temperature field that can be measured by a thermographic system on the surface of a solid body invested by a flow is determined by a lot of combined effects. Very important effects are: conversion of kinetic energy of the flow into thermal energy, flow temperature variation in time and space, convection heat transfer phenomena between flow and body, conduction phenomena inside the body and radiation heath exchange of the body surface with surroundings. By correspondence between convective heat transfer coefficient and local turbulence it's possible to carry out information about the boundary layer. In addition to the laminar-to-turbulent transition boundary, the infrared camera was able to detect shock waves and present a time dependent view of the flow field. Figure 29 shows thermograms of tests have been performed using an high resolution thermographic system for fluid-dynamics analysis of a known test case, a wing profile, in a wind tunnel under variable and constant temperature condition at different air flow velocity[41,42].

A time dependent heat transfer code was developed to predict temperature distributions on the test subject and any necessary surface treatment. A commercially available infrared camera can be adapted for airborne use. Readily available infrared technology has the capability to provide detailed visualization of various flow phenomena in subsonic to hypersonic flight regimes.
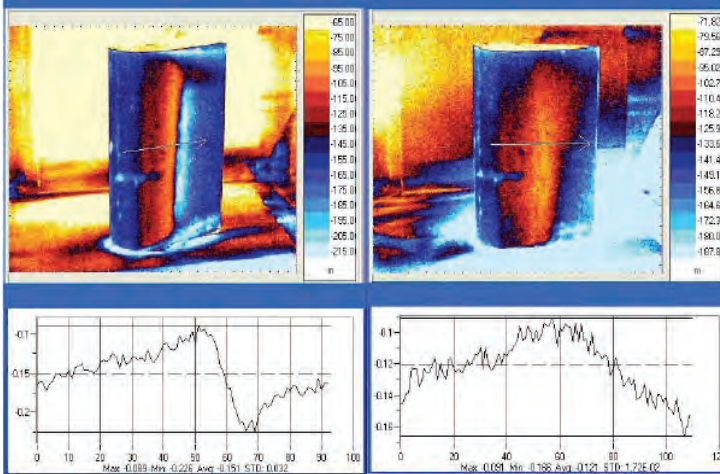
Fig. 29 Black aluminium airfoil with incidence of 7,5° clockwise (a) and airfoil with incidence of -7,5° clockwise [42]

6.5. Computer Graphics Flow Visualization

Data originates from numerical simulations, such as those of computational fluid dynamics need to be analyzed by means of visualization to understand the flow. With the rapid increase of computational power for simulations, the demand for more advanced visualization methods has grown. Computer graphics flow visualization centers around visualization mapping, or the translation of physical flow parameters to visual representations. Starting from a set of standard mappings, a number of data preparation techniques is developed, to prepare the flow data for visualization [5,36,37,41].

The current strong demand for new flow visualization techniques, especially for large scale 3D numerical flow simulations, can only be satisfied by combining the efforts of fluid dynamics specialists, numerical analysts, and computer graphics experts. Additional knowledge is required from perceptual and cognitive psychology, and artists and designers can also contribute to this effort.

Conceptually, this process centers on visualization mapping or the translation of physical flow parameters to visual representations. Starting from a set of standard mappings partly based on equivalents from experimental visualization, a number of data preparation techniques is used, to prepare the flow data for visualization. Next, a number of perceptual effects and rendering techniques are described, and some problems in visual presentation are discussed. The paper ends with some concluding remarks and suggestions for future development.

Scientific visualization with computer-generated images can be generally divided on several stages: -data generation: production of numerical data by measurement or numerical simulations

- data enrichment and enhancement: modification or selection of the data, to reduce the amount or improve the information content of the data.
- visualization mapping: translation of the physical data to suitable visual primitives and attributes.
- rendering: transformation of the mapped data into displayable images.
- display: showing the rendered images on a screen.

Test of the complex flow field (as the flow in the two dimensional supersonic nozzle with the deflector) by holographic interferometry, shows again the significant advantages of the holographic interferometry compared to shadow, schlieren and other classical ones. This method has special advantages when the complex flows are tested, e.g. flow around deflector, in the vicinity of the shock wave, etc.

Figure 30a shows   numerical flow visualization of path line colored by velocity magnitude (m/s), for different times and V∞=5.32 m/s, around 2D hydrofoil in water tunnel [15]

Recently, flow visualization methods give the broad base for comparisons with numerical methods. The considered problem is very complex because both the Reynolds number and the Mach number influence the flow in the supersonic nozzle with deflector at the exit plane. An oblique shock wave and large region of separated flow are caused by the deflector (figs 28 and figs.31).

t=0.001s   t=0.01s   t=0.1s   t=0.149s
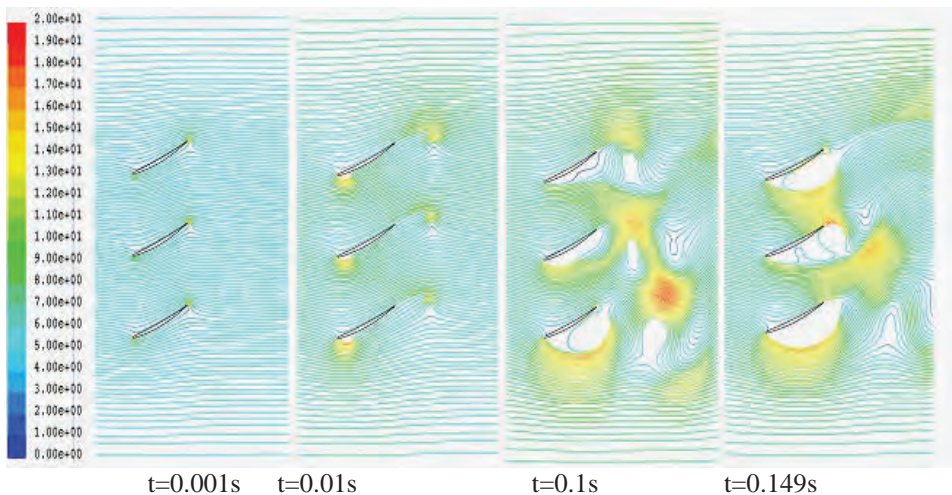
Figure 30: Numerical flow visualization of path line colored by velocity magnitude (m/s), for different times and V∞=5.32 m/s, around 2D hydrofoil in water tunnel [15].
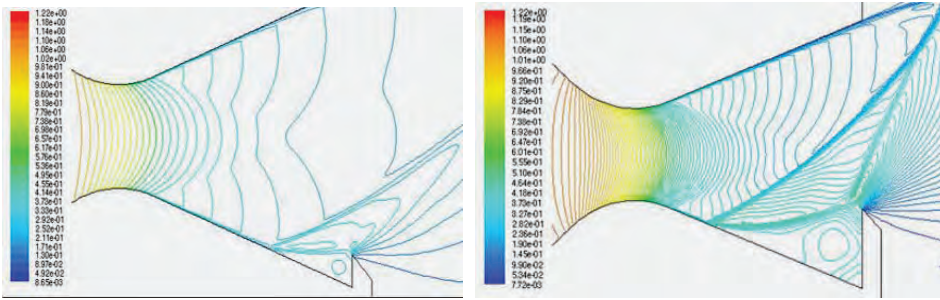
Fig.31

The complex two-dimensional supersonic flow in the nozzle with three deflectors at the exit is numerically simulated by the solution of the Reynolds-Averaged Navier-Stokes equations with a two-equation k-ω turbulent model. This model of turbulence is based on the Boussinesq approximation[36]

The used code captured main flow features and differences obtained with S-A and k-ω turbulence models are not substantial. It is shown that convergent results were obtained with all the meshes except the extra fine mesh.

7. CONCLUSION

This paper presents an overview of techniques for flow visualization. A brief introduction to experimental flow visualization methods is given. Every method is illustrated with photos of flow visualizarion effects. The advent of computer technique, new tehnology for illumination, modern and very powerfull devices for digital image recording and processing make possible automatically analyze flow visualization effects and extract qualitative and quantitative information, which may not be readily available from conventional flow measurements. Experimental flow visualization is a starting point for numerical flow visualization of simulations using computer graphics. Parallel usage of experimental and numerical methods confirms the possibilities of numerical method application for complex flow analysis.

BIBLIOGRAPHY

1. W. Marzkirich,: Flow visualization, Academic Press, New York, 1977.
2. D.H. Stedman, G.R.Carignan : Flow Visualization II, 1981
3. W.J. Yang,: Flow visualization III proc. of 3. International Symposium, An Arbor MI, 1983, Hemisphere, New York, 1985.
4. G.S. Settles: Modern Developments in Flow Visualization, AIAA Journal, 24, 8, (1986), 1313-1323.
5. S. Ristic, Flow visualization techniques in wind tunnels- Non optical methods, Part I,II, Scientific Technical Review, Belgarde, LVII, 1,2 (2007), 39-51

6. Monografija VTI, 1996, Beograd
7. Z. Anastasijevic, S. Ristic : Review of Testing Possibilities in Experimental Aerodynamics Laboratory, Tehnika, Mašinstvo 55, (2006), 15-24
8. S. Ristic: Vizualizacija strujanja u aerotunelu pomoću TiCl4, NTP, 39, 8, (1989), 8-14
9. L. Luo, & others, .Flowfield Around Ogive/Elliptic-Tip Cylinder at High Angle of Attack, AIAA J, 36, (1998), 1778-1787
10. LU F.K., G.S.Settles, Color Surface Flow Visualization of fine Generated Shock Wave Boundery Layer Interactions, Exper. in Fluids, 8, (1990), 352-356
11. S. RISTIC, P. Majstorović, Experimental investigation relative flow through model of straight profile grid., STR, 50, 6., (2000), 29-36
12. J.C. McDaniel, R.K. Hanson, Qualitative Planer Visualization in Gaseous Flow Field Using Laser Indused Fluorescent, Flow Visualization III, (1983), 113
13. M. Havermann , J. Haertig , C. Rey , and A. George : Application of Particle Image Velocimetry to High-Speed Supersonic Flows in a Shock Tunnel French-German Research Institute of Saint-Louis (ISL), 5 Rue du Général Cassagnou, F-68301 Saint-Louis, France, 1999
14. Puharić M. , S. Ristic., Kutin M., Adamović Z., Laser Doppler Anemometry in Hydrodynamic Testing, Journal of Russian Laser Research, 28, 6, (2007), 619-628
15. S. Ristic, Laser Doppler Anemometry and its Application in Wind Tunnel Tests, Scientific Technical Review, 62,3-4, (2007), 64-75
16. J.R.Growder, Fluorescent Mini Tufts For Flow Visualization On Rotating surfaces, Flow Visualization III, 3th international symposium on flow visualization, sept. 6-9, An Arbor Michigan USA, (1983), 55-64
17. G. Ocokoljića, J. Radulović, Flow visualization and aerodynamical coefficients determination for the LASTA-95 model in wind tunnel T-35., STR, n.2, (2006), 63-69
18. S. Ristic, Vizualizacija podzvučnog strujanja metodom fluorescentnih končića, Jubilarni broj NTP-a, 46, 4-5, (1996), 73-76
19. D. Damljanović, S. Ristic., Eksperimentalno ispitivanje aerodinamičkih karakteristika modela laserski vođene bombe, VTG, br. 5, (2005), 406-417
20. S. Ristić., D. Matić, A. Vitić.: Determination of aerodynamical coefficients and visualization of the flow around the axisymetrical model by experimental and numerical methods, STR, 55, 3-4, (2005), 42-49
21. S. Ristic, D. Matić, A. Vitić., Samardjić, M.: *The numerical and experimental testing of the axisymetric model flow*, Facta Universitatis Series Mechanics, Automatic Control and Robotics, 5, 1, (2006), 145-152
22. S. Ristic.: Optimizacija primene uljanih premaza u vizualizaciji strujanja u aerotunelima, 2005., Tehnika, god LX. n.5, Elektrotehnika 54, 5, (2005), 8-14
23. S. Ristic, J. Isaković, M. Srećković, D. Matić, Comparative analysis of experimental and numerical flow visualization, FME Transactions, 34, (2006), 143-149
24. S. Ristic, Optical methods in wind tunnel flow visualization, FME Transactions, 34, (2006), 7-13
25. B. Song, Experimental and Numerical Investigations of Optimized High-Turning Supercritical Compressor Blades, Dissertation, Faculty of the Virginia Polytechnic Institute and State University, November 2003, Blacksburg, Virginia

26. S. Ristic, Premazi osetljivi na pritisak, nova mogučnost vizualizacije strujanja, VTG, 1, 2006, 35-48.
27. C.M VesT, Holographic Interferometry, New York, Wiley and sons,1982.
28. D.W. Watt, C.M. Vest, Digital Interferometry for Flow Visualization, Exper. in Fluids, 5, (1987), 401-405
29. S. Ristic, Testing of the Flow Field Around the Nozzle Edge Using the Method of Holographic Interferometry, Fizika, 22, 3, (1990), 529-543
30. S. Ristic, Disturbance of Transonic wind Tunnel Flow by a Slot in the Tunnel Wall, Experiments in fluids, 11, (1990), 403-405
31. S. Ristic, Optimizacija kvantitativne obrade holografskih interferograma za 2D i osno simetrična strujanja, Jubilarni broj NTP-a, 46, 4-5, (1996) 37-45
32. S. Ristic, M.Srećković, Pressure Disturbances Testing by Schlieren Method and Holographic Interferometry, Laser '98, 7-11, Tucson, Arizona, Proceedings, (1998), 568-547
33. S. Milićev, D. Pavlović, S. Ristic, A. Vitić, On the Influence of Spike Shape at Supersonic Flow Past Blunt Bodies, 2002, Facta universitatis, series: Mechanics, Automatic, Control and Robotics, 3, 12, 371-382
34. S. Ristić, Srećković M., Testing of supersonic wind tunnel flow by holographic interferometry, Atti dela Fondazione Giorgio Ronchi, 61, (2006), 231-240
35. S. Ristic, Z. Anastasijevic, J. Isakovic, New Combined Holographic Interferometer and Schlieren Device for Wind Tunnel T-38, proceedings of ICASAT 2007, Tripoli 23-25/04/2007
36. S.Ristic, M. Kozic, Experimental and numerical investigation of flow separation in a supersonic nozzle, *Journal of Russian Laser Research*, 29, 4, (2008), .377- 389
37. S. Ristic, M. Kozic, Optical and numerical visualization in analysis of deflector angle influence on 2d supersonic nozzle flow, B06,2nd International Congress of serbian Society of Mechanics, 1-5 June 2009, Palić (Subotica), Serbia
38. *D. W. Banks, C. P. van Dam and H. J. Shiu, G. M. Miller,*Visualization of In-Flight Flow Phenomena Using Infrared Thermography, NASA/TM-2000-209027
39. dhttp://www.aivela.org/Salviuolo_paper06.pdf
40. Q. Xia Tsa and H.M. Papamoschou, Numerical Investigation of Supersonic Nozzle Flow Separation, AIIA, 29995, no. 4640 D.
41. R.L. Roe, Numerical Methods in Aeronautical Fluid Dynamics, London, Academic Press, 1982

VIZUALIZACIJA STRUJANJA – POGLED U NEVIDLJIVO

Slavica Ristić

Vizualizacija strujanja je veoma značajna oblast u eksperiemntalnoj i komjuterskoj dinamici fluida i dugi niz godina je predmet istraživanja. U ovom radu su prikazane izabrane tehnika vizualizacije strujanja. Opisani su osnovi fizički principi ovih metoda, kao i njihova pimena u vizualizaciji podzvučnih, okozvučnih i nadzvučnih strujanja u aerodinamičkim i vodenim tunelima: metode sa direktno ubacivanjem markera (dim, boje, magla, različite male čestice), gasni ihidrogenski mehurići, vizualizacija strujanja sa končićima, sa uljanim emulzijama, tečmim kristalima, bojama osetljivim na promenu temperature ipritiska, optičkim metodama kao što su metod senke, šliren, holografska interferometrija, Laser Doppler anemometrija, anemometrija za merenje vektora brzine mikroskopskih čestica u fluidu, pomoću njihovih slika i drugih specijalnih tehnika. Skoro sve prikazane slike su snimljene u labotarorijama Vojotehničkog institute u Beogradu.

MODIFICATION OF EARTH'S GRAVITY SPHERE

UDC 531.51;

Veljko A. Vujičić

Mathematical institute SANU, Belgrade, Serbia,

e-mail: vvujicic@mi.sanu.ac.rs

Abstract. *The standard radius of the Earth's gravity sphere is 917.000 km. Here we present that the radius is 1.400.000 km.*

Key words: *Celestial mechanics, gravitation, Earth, Sun.*

1. INTRODUCTION

Earth's gravity sphere is a space around the Earth (as a material point) where in the Earth's force of attraction is stronger than the gravitational forces of other bodies, including the gravitational force of Sun. The formula that determines the radius ρ of the so called sphere of influences (gravy sphere) of the Earth's gravity in this case is ([1], p. 196),

$$(1) \qquad \rho = r\sqrt[5]{(m_1/M)^2},$$

where r is the distance between the Earth and Sun, $m_1 = M_\oplus$ is the mass of the Earth, and $M_\odot \approx 333000\,m_1$ is the mass of the Sun. The size of this radius of the Earth's sphere amounts approximately to $\rho = 917\,000\,km$ or ([2], p.108) $923\,000km$.

$$(3) \qquad F = \kappa \frac{m_1 m_2}{\rho^2}.$$

Verification of the formula (1) with the use of the Newton's formula of "universal gravitational force"

$$(2) \qquad F = \kappa \frac{m_1 m_2}{\rho^2}.$$

led to a paradoxical result. According to formula (2), at the boundary of the Earth's gravity sphere, it should be $F_\oplus = F_\odot$. However, the calculation shows the opposite. And indeed, let us show this with some more details.

Let it be assumed that: $m_1 = M_\oplus$ is the mass of the Earth, $m_2 = M_\odot$ is the mass of the Sun, and m is the mass of any body at the boundary $\rho_\oplus = x = 917\,000$ km. For the above mentioned assertions of the book the mass of the Sun is $M_\odot \approx 333\,000 M_\oplus$, whereas a tabulated distance of the Earth from the Sun is $\rho_\odot = a = 149\,600\,000$ km.

First. The Sun and the Earth act at the same time on a body having the mass m in a critical boundary point at the distance $\rho_\oplus = x$ with the forces according to Newton's formula (2):

$$(3) \qquad\qquad F_\oplus = \kappa\frac{M_\oplus m}{x^2}, \qquad F_\odot = \kappa\frac{M_\odot\, m}{(r-x)^2}.$$

Therefore, in a critical point $\rho_\oplus = x = 917\,000$, it should be

$$(4) \qquad\qquad F_\odot = \kappa\frac{M_\odot\, m}{(149\,600\,000 - x)^2} = 1,5063\cdot 10^{-11}\kappa M_\odot m.$$

and

$$(5) \qquad\qquad F_\oplus = \kappa\frac{M_\oplus\, m}{x^2} = 0.11892\cdot 10^{-11}\kappa M_\oplus m.$$

This shows that, according to Newton's formula, the gravitational force of the Sun at the distance of $917\,000$ km from the center of the Earth is more than 12 times greater than the value of the Earth's gravitational force, i.e.

$$F_\odot = 12,666\,611\, F_\oplus \iff F_\oplus = 0,0789478\, F_\odot.$$

However, this is not in compliance either with the definition of gravity sphere, or with the phenomena in the nature. The Moon moves around the Earth at an average distance of $384\,400$ km, under the dominant attraction of the Earth, not the Sun.[7]

The second. Let's determine the boundary of the Earth's gravity sphere with the use of a strict procedure, by means of the universal gravity formula (2). According to the Newton's gravity theory (2) would follow, so that it should be:

$$\frac{M_\oplus m}{x^2} = \frac{M_\odot m}{(r-x)^2},$$

or for $M_\odot = 333\,000 M_\oplus$ follow $(\rho - x)/x)^2 = M_\odot/M_\oplus = 333\,000$.

Further calculation gives: $(\rho - x)^2 = (577,6152\,x)^2$, i.e. $\rho - x = 577,6152\,x$, or $\rho = 578,0652\,x$, and from there, for $\rho = 149\,600\,000$ km, it follows that

$$x = 258\,795,993\,\text{km}.$$

This is contradictory to the fundamental laws of dynamics, as well as the actual state of the motion of the Moon around the Earth at an average distance of $384\,400$ km, and particularly the formula (1), which demonstrates the radius of the sphere of the Earth's gravity. Doubt about the validity of the Newton's formula is increased by a fact from the above mentioned book. According to the Newton's formula (1) it follows that the acceleration of gravity depends not only on the distance, but it is asserted that at the first cosmic velocity of $7,91$ km/s, a body will escape from the Earth's attraction and will rotate around the planet Earth under an assumption that the resistance of the medium is ignored. At the second cosmic velocity $v_{or} = 11,19$ km/s, a missile will leave the area of the Earth's gravity sphere.

2. One modification theory of gravity

In the papers [1, 2, 3, 4] author is demonstrated that our formula of mutual action of two bodies has the form

$$(8) \qquad F_\rho = \frac{\dot\rho^2 + \rho\ddot\rho - v_{or}^2}{m_1 + m_2}\frac{m_1 m_2}{\rho} = M^* \frac{\dot\rho^2 + \rho\ddot\rho - v_{or}^2}{\rho} = F^* + F^{**}.$$

where we introduced notations:

$$M^* = \frac{m_1 m_2}{m_1 + m_2}, \quad F^* = M^* \frac{\dot\rho^2 + \rho\ddot\rho}{\rho}, \quad F^{**} = M^* \frac{v_{or}^2}{\rho}.$$

For the escaping boundary of the attraction of a body having a mass of m and the body having a mass of M, it will be

$$M^* \frac{\dot\rho^2 + \rho\ddot\rho - v_{or}^2}{\rho} = 0,$$

or in Simić's form

$$\frac{d}{dt}(\rho\dot\rho) - v_{or}^2 = 0.$$

For the purpose of clearer and more straightforward comprehension of this assertion, let us mention that formula (6), in relation to the natural coordinate system, can be reduced to a simpler form. It is sufficient to observe that it is $v^2 = \dot\rho^2 + \rho^2\dot\theta^2$ so as to reduce the formula (6) to a form

$$F_\rho = M^*(\ddot\rho - \rho\dot\theta^2).$$

In the state of motion where $F_\rho = 0$, the known formula for normal acceleration follows

$$\ddot\rho = \rho\dot\theta^2 = \frac{v^2}{\rho},$$

as well as formula for the force of mutual attraction

$$(7) \qquad F^{**} = M^*\frac{v^2}{\rho},$$

where $\rho = R = const.$

Table. It has been shown what the radial accelerations of the satellites are at different altitudes H above the Earth according to the standard formula $\gamma = gR^2/\rho^2$, as well as the formula $\gamma^* = v^2/\rho$, which follows from the formula (6).

Altitude	Velocity	Acceleration	Acceleration
H km	v km/s	γ	γ^*
0	7,91	981,0	982,3
100	7,84	948,9	950,0
1000	7,35	732,1	733,0
10000	4,93	148,4	148,4
100000	1,94	3,5	3,5
384400	1,02	0,002693	0.002706

Let's note that the last type of table refers to the average speed of the Moon's motion around the Earth and its average distance from the center of the Earth.

By the application of formula (8) to the motion of the Moon in relation to the Sun and in relation to the Earth, it has been proven that the gravitational force of the Earth, which acts on the Moon, is greater than the corresponding force of the Sun. In this way, dynamical paradox in the theory of the Moon's motion has been removed, [8]. It is logical that it is possible to determine the boundary of the Earth's gravity sphere in the same way.

Using this procedure, we obtain a significant modification of the Earth's gravitation sphere . Starting from the aforementioned definitional of the gravity sphere of two bodies, let us find the boundary x of the gravity sphere of the Earth in relation to the gravitational force of the Sun for that same body. By the very nature of things and by mathematical logics, initial relation of that task is that the gravitational force of the Earth is greater than, and at the boundary of the sphere $\rho = x$ is equal to, the Sun's gravitational force, i.e.,

$$F_\oplus = F_\odot,$$

where :

$$F_\oplus = \frac{M_\oplus m}{M_\oplus + m} \frac{v_{or\oplus}^2}{x}, \quad v_{or\oplus} < 1\mathrm{km/s}.$$

$$F_\odot = \frac{M_\odot m}{M_\odot + m} \frac{v_{or\odot}^2}{a - x}, \quad v_{or\odot} = 29,8 - (19,5 + 0,3) = 10\,\mathrm{km/s}.$$

Ratio of the gravitational forces $F_\oplus$ and $F_\odot$ at the boundary of the Earth's gravity sphere is:

$$\frac{F_\oplus}{F_\odot} \equiv \frac{v_{or\oplus}^2}{x} : \frac{v_{or\odot}^2}{a - x} = 1.$$

From here, it follows that

(8)
$$x = \frac{a}{1 + (v_{or\odot}/v_{or\oplus})^2}.$$

Value of the fraction which is derived, depends, as we can see, on the ratio of the orbital speeds of bodies in relation to the Sun and the Earth at the boundary x of the Earth's gravity sphere. Let us analyze that for our needs.

First: $v_{or\odot} \neq v_{or\oplus}$, because it is $v_{or\odot} = v_\oplus \pm v_{or\oplus} - v_\odot$: $v_{or\oplus} \neq v_\odot$.

The second: For $v_\oplus = 1$ is $x = a/(1 + v_{or\odot}^2)$.

The third: for $v_{or} > 1$ the value of the fraction is decreased, and already for $v_{or} > 1$ the fraction (10) is decreased, and for $v_{or} < 1$ it is increased. In view of the fact, let as choose $v_{or} = 1$. As it can be seen, the boundary of the Earth's gravy sphere depends on the ratio of the speeds of two bodies in relation to the Earth $v_{or\oplus}$ and in relation to the Sun $v_{or\odot}$. Usually the velocity $v_{or\oplus}$ is not known, so that we are left only with a hypothetical analysis on the basis of the average standard data. The velocity of the Sun $v_{or\odot}$ is even less known. Speeds of the Sun in relation

to various groups of stars [4]. The standard velocity of the Sun is usually taken to be $v_\odot = 20\,000$ km/s. Since the mean velocity of the Earth's motion around the Sun is $v_\oplus \approx 30\,000$ km/s. In this state of motion, it is

$$v_{or\odot} \approx v_\oplus - v_\odot = 10\,\text{km/s}.$$

For this logical choice and numerical values of the standard quantities (see for example [3]):

$$\frac{M_\oplus \, m}{M_\oplus + m} = 0,987; \quad \frac{M_\odot \, m}{M_\odot + m} = 0,999;$$
$$a = 149\,600\,000 km, \quad M_\odot = 333\,000 \, M_\oplus,$$

it is obtained that the radius of the gravitation sphere of the Earth is $x = 1\,481\,188$ km, or

$$(9) \qquad\qquad x \approx 1\,481\,000\,\text{km}.$$

Therefore, for the standard data which are taken, the radius of the gravitation sphere of the Earth is significantly greater than the radius $x = 917\,000$km, and expressly than $x = 258\,795$km.

Conclusion

In the first part of this paper it is proven that the formula of the gravitational sphere of the Earth (1) has not been derived on the basis of the Newton's formula (3). By direct calculation with the use of the formula (3) it is shown that the formula leads to the results, which are not in accordance with the nature of the motion between the Sun and the Earth. Convincing example is the motion of the Moon, for which the formula (3) leads to paradoxical dynamic result of the Newton's gravity theory.

With the use of the formula (6) for the mutual attraction of two bodies, the above mentioned paradox in the theory of the Moon's motion is removed and one solution to the problem of three bodies (Sun-Earth-Moon) is obtained. That was a reason to consider the boundary (2) of the gravity sphere of the Earth in this paper. Approximately correct result for the radius of the Earth's gravity sphere on the basis of the formula (11) amounts to **1 400 000** km, which is considerably different from the value (2).

REFERENCES

[1] T. Andjelić and R. Stojanović, Racionalna mehanika, Zavod za udžbenike, Beograd, 1966.

[2] T. Andjelić, Uvod u astrodinamiku, Matematički Institut, Beograd, 1987.

[3] A. Hannes, Evolution of the Solar System, National Aeronautics and Space Administration, Washington. 1976.

[4] K. F. Ogorodnikov, Dinamika zvezdnyh sistem, Gosudarstvennoe izdatel'stvo, Moskva, 1958. p. 627.

[5] V. A. Vujičić, *On one generalization of Newton's law of gravitation*, International Applied Mechanics, Plenum, 40(3),(2004), 351–359,

[6] V. A. Vujičić, *On a generalization of Kepler's third law*, Astronomical and Astrophysical Transactions, Taylor & Francis, 24(6),(2005), 489–495.

[7] V. A. Vujičić, *Modification of the characteristic gravitation constants*, Astronomical and Astrophysical Transactions, Taylor & Francis, 25(4), (2006), 317–325.

[8] Veljko A. Vujičić, *Dynamical Paradox in Theory of Lunar Motion*, International Journal of Nonlinear Sciences and Numerical Simulation, Freund Publishing House Ltd, 10(11-12): 1539-1543, (2009).

[9 8] V. A. Vujičić, *The inverse three-body problem*. (Sbornik Izbrannykh trudov konferentsii).Selected papers International scientific conference on mechanics "Polyakhov reading V". SPb: NIIKh SPbGU. 2009. P.165-169.

MODIFIKACIJA ZEMLJINE GRAVITACIONE SFERE

Veljko A. Vujičić

Mathematical institute SANU, Belgrade, Serbia,

e-mail: vvujicic@mi.sanu.ac.rs

Apstrakt. *Standardni radijus Zemljine gravitacione sfere je 917.000 km. Ovde se prikazuje je radijus 1.400.000 km.*

Key words: *Nebeska mehanika, gravitacija, Zemlja, Sunce.*

LOOPS IN THE SUN'S ORBIT

Milutin Marjanov
Beograd, 27 marta 39
e-mail: mimar@bvcom.net

Abstract. *Besides translation, spin around its axis and rotation around center of the Milky Way, the Sun performs relative motion in the solar system Laplacian plane, also. This motion was anticipated by Newton himself, in his Principia.*

The form of the Sun's orbit is substantially different from the other solar system bodies' orbits. Namely, the Sun moves along the path composed of the chain of large and small loops [1, 2, 6, 9]. This chain is situated within the circular outline with the diameter approximately twice as large as the Sun's is. Under supposition that the solar system is stable, the Sun is going to move along it, in the same region, for eternity, never reitereiting the same path.

It was also shown in this work that velocity and acceleration of the Sun's center of mass are completely defined by the relative velocities and accelerations of the planets with respect to the Sun.

Key words: *loops in the Sun's orbit, velocity, acceleration*

.

1. INTRODUCTION

As said, Isaac Newton was the first who pointed to the fact that the Sun moves around the center of mass of the solar system (*Philosophiae Naturalis Principia Mathematica*): „ ...since that centre of gravity (the solar system mass centre) is constantly at rest, the sun, according to the various positions of the planets, must continually move every way, but will never recede far from that centre".

If the solar system is treated as a stable, isolated system of the point mass particles moving under mutual gravitational interactions, two dynamic conservation principles may be used for the study of its motion: conservation of the momentum and of the angular momentum of the system.

The consequence of the first rule is uniform motion of the system's mass center C, while the consequence of the second is motion of the system in one, Laplacian, or invariant plane [3].

This plane is within 0, 5^0 of the Jupiter's orbital plane and may be regarded as the weighted average of all planetary orbital planes. The point mass particles solar system model, involves necessity of neglecting differences between the orbital planes mainly

originated in the transfer of the (small, but changeable) Sun's and planet's spin angular momenta to its total angular momentum.

Neglecting rotation of the solar system, as a whole, around the center of our galaxy, this plane moves translatory, together with the mass center C through the space.

2. COORDINATE SYSTEMS

Existence of the invariant plane permits introduction of an "inertial" reference frame xCy lying in it. Another Cartesian coordinate system x'0y' (0x' and 0y' parallel with Cx and Cy) was adopted as the relative, that is, the heliocentric frame of reference (Fig. 1).
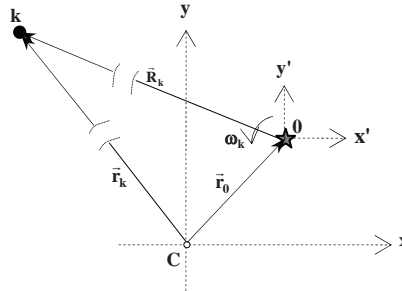
Fig. 1. Inertial and Relative Frame of Reference.

3. POSITION, VELOCITY AND ACCELERATION VECTORS OF THE SUN

It seems that, using astronometrical data positioning the outer planets from 1653. to 2060., P. D. Jose was the first one to determine the Sun's orbit, in his work [1], 1965. This paper was abundantly cited later in the works treating the sunspot activities.

In his work [2] R. Bitsch has determined the Sun's orbit integrating differential equations of motions of this celestial body exposed to the resultant of the planets' attracting gravitational forces. It was supposed that these heavenly bodies are in circular, uniform motions around the Sun. The initial planet's configuration was adopted arbitrary, because the author assumed that, in the long term, it does not affect the shape of the orbit.

One would be tempted to use term Kepler's for the model employed in the work [1] and Copernicus' for the model in [2], but it would not be correct, since the Sun moves in both models, of course.

In fact, the choice of either model in determining the trajectory, velocity or acceleration of the Sun is completely irrelevant, since the orbit, velocity and acceleration of the Sun's center of mass are very small compared with the correspondent kinematic parameters characterizing motions of the planets. Correctly defining the initial conditions is all that matters.

For that reason "Copernican" model is the adopted here: the planets move at an average distance, with average angular velocity around the Sun.

Taking the planets' configuration on 21 March 1978 [5] as initial conditions and the model in which all planets, excepting Mercury (its orbit is not stabilized in the solar system's invariant plane yet) move uniformly around the Sun, M.Marjanov [9] obtained, practically, the same form of the Sun's path as Jose had. This trajectory covers the time interval of fifty years: 21. 03. 1978. + 50.

Since, in the inertial plane of reference must be

$$\sum_{k=1}^{8} m_k \vec{r}_k = \sum_{k=1}^{8} m_k \vec{v}_k = \sum_{k=1}^{8} m_k \vec{a}_k = 0$$

and

$$m_0 \vec{r}_0 + \sum_{k=1}^{8} m_k \left(\vec{r}_0 + \vec{R}_k \right) = 0, \quad m_0 \vec{v}_0 + \sum_{k=1}^{8} m_k \left(\vec{v}_0 + \dot{\vec{R}}_k \right) = 0, \quad m_0 \vec{a}_0 + \sum_{k=1}^{8} m_k \left(\vec{a}_0 + \ddot{\vec{R}}_k \right) = 0$$

it follows out that

$$\vec{r}_0 = -\frac{\sum_{k=1}^{8} m_k \vec{R}_k}{M}, \quad \vec{v}_0 = -\frac{\sum_{k=1}^{8} m_k \dot{\vec{R}}_k}{M} \quad \text{and} \quad \vec{a}_0 = -\frac{\sum_{k=1}^{8} m_k \ddot{\vec{R}}_k}{M}, \text{ where } M = \sum_{k=1}^{8} m_k$$

Thus, position, velocity and acceleration of the Sun's center of mass are completely defined by the relative positions, velocities and accelerations of the planets with respect to the Sun.

Fig.2 shows the orbit of the Sun from 21. 03.2000. to 21. 03.2040. It, as mentioned, corresponds to the orbit that got Jose /1/, but is substantially different from the one given by Bish /2/, as the latter had wrongly assumed that initial conditions do not affect the form of a path.

The contour of the Sun is given as referential and the dot marks denote years.

Concerning the influence of the inner planets on the form of the path, Jose was right: it is quite negligible. Their influence would become visible only if a part of seemingly smooth path was magnified thousand to ten thousand times. The influence of the inner planets actions is far more evident when speed and acceleration of the Sun are considered.

The maximal distance from Sun to the center of mass of C $\sim 1,5 \cdot 10^6$ km is obtainable when all planets are lined up on the same side of the star and the minimal $\sim 21\ 000\ km$, when Jupiter is on one side and all the other planets on the other side of the Sun, in the same direction.

Of course, chances for exactly such alignments of the celestial bodies are reduced to zero /11/.

The anticipated path of the Sun over the next 2000 years is represented in the Figure 3. It is situated within the circular outline with the diameter at least twice size of the Sun's. Again, the Sun's disk is given for comparison.

Provided that the solar system is stable, Sun is going to move in this region for eternity, never reitereiting the same path.
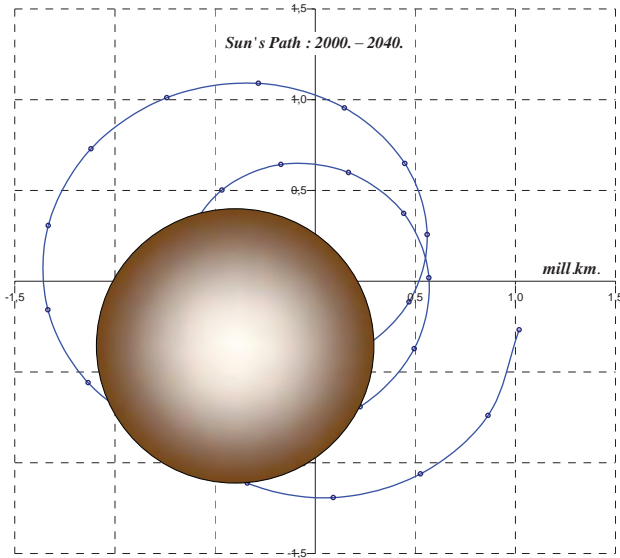
Fig.2. Sun's Path from 21.03.2000. – 21. 03.2040.
4. ORBIT

6. VELOCITY

Sun's velocity from 21 03.2000. to 21 03.2040. is represented in the Figure 4. Here we can see again that the outer, giant planets, especially Jupiter and Saturn have dominant influence on this kinematical quantity. When these two planets are in conjunction (~ every 20 years), the speed of the Sun is maximal $\sim 16\ m/s\ (15,7m/s)$, and when in opposition, the velocity is minimal, about $9\ m/s\ (8,8m/s)$.

6. ACCELERATION

The acceleration diagram from 21. 03.2000. to 21. 03.2040. is given in the Figure 5. It shows much more irregularities and roughness than the previous diagram and represents, of course, a measure of the resulting planets' gravitational attractions. No need to say that the peaks in this diagram correspond to the different conjunctional combinations of two or more planets.
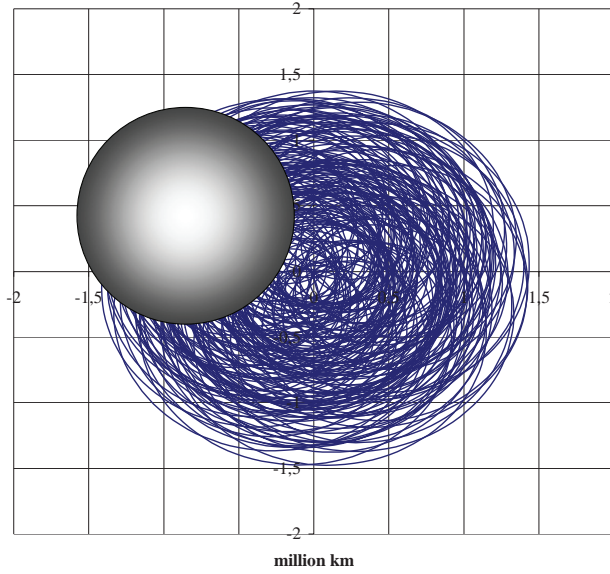
Fig. 3. Sun's Orbit Over 2000 Years.

$$\vec{v}_0 = -\frac{\sum_{k=1}^{8} m_k \vec{R}_k}{M} \Rightarrow$$

Fig. 4. Sun's Velocity from 21. 03.2000. to 21. 03.2040.

If all the planets fell in the same direction, on the same side of the Sun, therefore, when they were all in conjunction, the Sun would have a maximal acceleration $\sim 0{,}27\,\mu/s^2$.

When Jupiter is on one side and all the other planets on the other side of the Sun, in the same direction, acceleration of the Sun is minimal $\sim 0{,}14\,\mu/s^2$.

$$\vec{a}_0 = -\frac{\sum_{k=1}^{8} m_k \ddot{\vec{R}}_k}{M} \Rightarrow$$

Fig. 5. Sun's Acceleration from 21 03.2000. to 21 03.2040.

Table: Average Sun - Planets & Maximal Planet- Planets Interactions

	Sun	Me	V	E	Ma	J	S	U	N
Sun		3,13	13,20	8,52	0,39	100,00	8,90	0,34	0,16
Me	3,13		0,00	0,00	0,00	0,00	0,00	0,00	0,00
V	13,20	0,00		0,00	0,00	0,00	0,00	0,00	0,00
E	8,52	0,00	0,00		0,00	0,00	0,00	0,00	0,00
Ma	0,39	0,00	0,00	0,00		0,00	0,00	0,00	0,00
J	100,00	0,00	0,00	0,00	0,00		0,04	0,00	0,00
S	8,90	0,00	0,00	0,00	0,00	0,04		0,00	0,00
U	0,34	0,00	0,00	0,00	0,00	0,00	0,00		0,00
N	0,16	0,00	0,00	0,00	0,00	0,00	0,00	0,00	

7. SOLAR SYSTEM BODIES' GRAVITATIONAL INTERACTIONS

Previous diagram will be more understandable if one looks at the following Table of the of the mean Sun - planets and the maximal planet- planets interactions.

The exposed table contains two kinds of data. The first row and the first column represent $mean\ F_{0-k},\ k = 1,2,...,8$, that is, the *average* Sun – planets interactions. These forces are average because of the adopted "Copernicus'" and not of the "Kepler's" model.

Of course, the Sun-Jupiter interaction is the greatest one and it was taken to be the referential: its value is 100. An interesting fact is that the second one is the Sun - Venus interaction and that the Sun-Earth is of the same order of magnitude as the Sun-Saturn interaction, although the Saturn's mass is 95 times greater than the Earth's.

All the other values in the Table 1 represent $sup\ F_{k-j},\ k,j = 1,2,...,8$: *maximal*, that is, conjunctional interactions of the planets. In the range of the here adopted *five digit precision*, the only existing is the one between Jupiter and Saturn.

It is evident that motions of the inner planets, especially that of Venus and Earth are the main cause of the fluctuations around a smooth acceleration curve representing the influence of the outer planets, and above all, the influence of Jupiter Saturn.

8. CONCLUSION

The Sun and the planets in the paper were simulated by the model of stable, isolated system of the point mass particles, moving under mutual gravitational interactions in the averaged Laplacian plane.

Shape of the solar path is entirely different from the orbits of the other bodies moving around it. Namely, the Sun moves along the path in the form of chain consisting of large and small loops. This chain is situated within the circular outline with the diameter approximately twice as large as the Sun's is. Under supposition that the solar system is stable, the Sun is going to move along it, in the same region, for eternity, never reitereiting the same path.

Then the velocity and acceleration diagrams of center of mass of the Sun were given.

At last, for better understanding of the obtained results, Table of the of the mean Sun - planets and the maximal planet- planets interactions was contributed.

REFERENCES.

[1] P. D. Jose: Sun's Motion and Sunspots, The Astronomical Journal, Vol. 70, Nr. 3, 1965.
[2] R. Bitsch: The Sun Moves! attn@sunorbit.net, 2003.
[3] M. Milanković: Osnovi nebeske mehanike, Naučna knjiga, Beograd, 1988.
[4] T. Anđelić: Uvod u astrodinamiku, Matematički institut, Beograd, 1983.
[5] 1978 Yearbook of Astronomy, Ed. P. Moore, W.W.Northon&Company Inc, New York.
[6] K. Croswell: Planet Quest, Oxford University Press, Oxford, 1999.
[7] Heliocentric Ephemeris – 2000 – Achenar – UK Mirror.
[8] Marjanov M.: Gravitational Resonances, Bull. Astron., Belgrade, 156, 9 – 19, 1997.
[9] Marjanov M.: The Sun's Orbit and Centers of Gravitation of the Solar System, Lecture on the Mathematical Institute SANU, Department of Mechanics, March 2005.

[10] Marjanov M.: On the Cause of Resonant Motions of Celestial Bodies, Facta Universitatis, Series: Mechanics, Automatic Control and Robotics, vol. 4, N° 17, 2005.
[11] Marjanov M.: Pythagoras Numbers and Quasiperiodicity of the Solar System, Zbornik radova Gradjevinskog fakulteta u Subotici, 2006.
[12] Marjanov M.: One Solution of the Newton's Three Body Problem, Lecture on the Mathematical Institute SANU, Department of Mechanics, Dec. 2008.

PETLJE U SUNČEVOJ PUTANJI
Milutin Marjanov

Pored translatornog kretanja, rotacije oko centra Mlečnog Puta i oko svoje ose, Sunce obavlja i relativno kretanje u Laplasovoj ravni Sunčevog sistema. Na to kretanje je ukazao još Njutn, u svome delu Principia.

Oblik Sunčeve putanje bitno se razlikuje od orbita ostalih tela koje oko njega kruže. Sunce se, naime, kreće duž putanje u formi lanca sačinjenog od velikih i malih petlji. Taj lanac je smešten u okvir kružne konture čiji je prečnik približno dva puta veći od prečnika Sunca. Uz pretpostavku da je Sunčev sistem stabilan, Sunce će se večno kretati duž njega, u istoj oblasti, nikada ne ponavljajući isti put.

Zatim su dati dijagrami brzina i ubrzanja centra mase Sunca.

Na kraju je priložena tablica prosečnih interakcija Sunce – planete, kao i maksimalnih interakcija među planetama, s tačnošću od pet brojčanih jedinica. Ona je dobar pokazatelj zbog čega na oblik orbite, kao i na dijagram brzina najviše utiču spoljne, džinovske planete, dok na izrazito neujednačenost forme dijagrama ubrzanja utiču, pre svega, unutrašnje planete.

Ključne reči: *petlje u Sunčevoj orbiti, brzina i ubrzanje centra mase Sunca*

_____

THE LUNAR ORBIT PARADOX

UDC: 52-333;52-336;523.3;530.1:140.8;531.51;531.555;165.41

Aleksandar S. Tomić

Nano Lab, Faculty of Mechanical Engineering, University of Belgrade
Kraljice Marije 16, 11120 Belgrade
aleksandartomic@hotmail.com

Abstract: *Newton's formula for gravity force gives greather force intensity for atraction of the Moon by the Sun than atraction by the Earth. However, central body in lunar (primary) orbit is the Earth. So appeared paradox which were ignored from competent specialist, beacause the most important problem, determination of lunar orbit, was inmediately solved sufficiently by mathematical ingeniosity – introducing the Sun as dominant body in the three body system by Delaunay, 1860. On this way the lunar orbit paradox were not canceled. Vujičić made a owerview of principles of mechanics in year 1998, in critical consideration. As an example for application of corrected procedure he was obtained gravity law in some different form, which gave possibility to cancel paradox of lunar orbit. The formula of Vujičić, with our small adaptation, content two type of acceleration – related to inertial mass and related to gravity mass. So appears carried information on the origin of the Moon, and paradox cancels.*

Key words: *Lunar orbit paradox, gravity law, gravity and inertial mass, concepts in physics*

1. INTRODUCTION

The Earth's satelite Moon is the nearest celestial body, with very complex description from standpoint of celestial mechanics. The Earth / Moon mass ratio is equal 81.3, mean density ratio 1.647, enough that baricenter of this two body system lies inside of Earth and out of Earth's planetary nucleus. It produce many effects which can be important for geophysics, as termal and tidal influence, and effect which are not neglegible for celestial mechanics – Earth's baricentric motion along orbit around the Sun. Determination of lunar orbit around the Earth was additionaly complex because the solar gravity force to the Moon calculated from Newton's gravity law formula gives 2.2 times greather value than Earth's gravity force to the Moon. So appeared a paradox that the Moon's orbital motion is around the Earth, and as secondary with the Earth around the Sun [1].

2. LUNAR ORBIT SOLUTION

The lunar orbit paradox was noted in Newton's time. In the 18. century astronomers made attempts to solve this problem, but it was not satisfactory succesful. Clairaut (1742) introduced the furth order corective term:

$$F = -\kappa \cdot m_1 \left(\frac{m_2}{r^2} - \alpha \frac{m_2}{r^4} \right). \tag{1}$$

D'Alembert (1749) made the same using the third order term, [2]:

$$F = -\kappa \cdot m_1 \left(\frac{m_2}{r^2} - \beta \frac{m_2}{r^3} \right). \tag{2}$$

Both solution can be mathematically satisfactory. But what is their physical sense? This type of solution today presents only a numerical fitting if additional term is not assumed as gravitational influence of the third mass. How the most might in gravity interaction with the Moon is the Sun, and solar gravity force is bigger than the one produced by Earth's over two times, both formulas can not be adequate physically. Other words, these solutions are out of conceptual foundation of physics.

In the next century problem was pushed at margins of interest by succesful solving most important problem for astronomers – analitical determination of lunar orbit around the Earth, for needs of ephemeridal astronomy. Delaunay (1860) are simple considered the Earth – Moon system as double planet system in motion around the Sun [3], and solved orbital motion. (Fig.1)
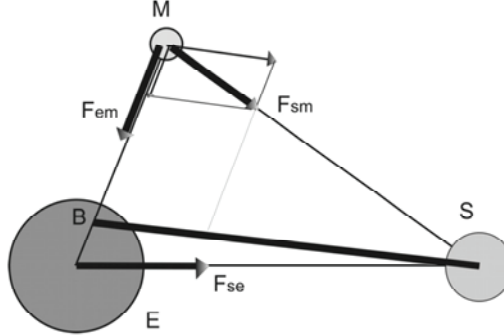
Fig.1. Earth (E) – Moon (M) system with baricenter (B) in motion along eliptic orbit around the Sun (S) governed by gravity forces F_{se}, F_{sm}, F_{em}.

Lunar motion in geocentric orthogonal coordinate system OXYZ was determined by equations [4]:

$$\frac{d^2 X}{dt^2} = -\kappa^2 (m_E + m_M) \frac{X}{r^3} + \frac{dR}{dX} \tag{3.1}$$

$$\frac{d^2 Y}{dt^2} = -\kappa^2 (m_E + m_M) \frac{Y}{r^3} + \frac{dR}{dY} \tag{3.2}$$

$$\frac{d^2 Z}{dt^2} = -\kappa^2 (m_E + m_M)\frac{Z}{r^3} + \frac{dR}{dZ}$$

(3.3)

$$R = -\kappa^2 \cdot m_S \frac{m_E + m_M}{m_E \cdot m_M}\left(\frac{m_E}{r_{SE}} + \frac{m_M}{r_{SM}}\right) .$$

(3.4)

Here are: R – perturbation function, κ − gravity constante. Solar motion is along elipse in XOY plane around baricenter (B) of the Earth – Moon system.

This solution were often quoted as argument that paradox of lunar orbit exist not. Solar force to the Moon converts into components with origin in lunar center, the first is paralel to direction of baricenter – Sun, and the second in direction to the Earth. But, this explanation is not correct as argument that lunar orbit paradox exists not. The Moon – Earth distance visible from the Sun is under angle of only ≤ 0.147 degree, and additional force which the Sun gives to the Moon in direction towards Earth is insufficient to explain rotation around the Earth. Because the force component to the Sun stay twice bigger than the sum of solar force component of Moon to the Earth and Earth's atraction of the Moon, problem stay open.

3. GRAVITY LAW DERIVED BY NEWTON

Deduction of gravity law Isaac Newton started from Kepler laws, Galilean determination of gravity acceleration at Earths surface, Piccard's determination of Earths radius, and Huygens centripetal acceleration. All other were assumptions and principles introduced by him self. The first hypothesis was that at Earth surface centripetal acceleration g, determined by Galilei, must be equivalent to centrifugal acceleration caused by lunar rotation around the Earth – biger ("central") body in the Earth – Moon system. These hypothesis must be valid in the system Sun – Earth, general in solar system, too. Newton so obtained gravity law in well known form:

$$F = -\kappa \frac{m_1 \cdot m_2}{r^2},$$

(4)

with κ − gravity constante. This form of law is usable for two masive body in relative quite too, because gravity constante value is known. Obvious in text books is not given what is contented in Newton's gravity constante. Here we quote result derived by Newton:

$$\kappa = \frac{4\pi^2 \cdot a^3}{m_1 \cdot T^2},$$

(5)

with a – big semiaxis of planetary orbit, T – period of planetary revolution. It presents the third Keplers law – in astronomy known as Kepler's constante, divided by mass of central body. It can be usefull explanation with purpose to make Newton's procedure simplest to understand, now from standpoint of mathematical logic [5].

Kepler (1609) introduced hypothesis on the mass of central body as the cause of planetary orbital motion in *Astronomia nova sive Physica coelestis.* It is conceptualy logical, because only this quantity is the same (or equal) in the interaction with each

planet. In the third Kepler's law, the constante is expresed as product of the central body mass and new constant - gravity constant:

$$v^2 r = const = \gamma \cdot m_1 . \qquad (6)$$

Here we used mean planetary distance from the Sun, physical notion of mathematical term big semiaxis, and mean planet velocity along orbit. Now we easy insert centripetal acceleration which is equal to the ratio of squared velocity and distance. From previous formula dividing by r^2 obtain acceleration to the central body:

$$v^2 / r = \gamma \cdot m_1 / r^2 = a_c , \qquad (7)$$

enough for description of planetary motion. Just connection of centripetal acceleration and planetary mass into gravity force made Newton, using his the second principle. So follows directly the gravity law:

$$F = m_2 \cdot a_c = \gamma \cdot m_1 \cdot m_2 / r^2 . \qquad (8)$$

The previous consideration gave a possibility for definition of the gravity constante in solar system as Kepler's constante on mass unit of central body, i.e. via kinetic parameters of planetary body :

$$\gamma = v^2 r / m_1 . \qquad (9)$$

Also, we see that gravity constant connect Kepler's kinetic concept with Newton's dynamical concept in description of motion. Mass stay as a cause of motion, but kinetic parameters describe motion. (The other known explanation is Einstein's space curvature, introduced 3 century later, into different mathematical concept.) In the pairs of body as Earth – Moon and other planet – satelite, the same numerical value were obtained for gravity constante, so that can be word on the universality of this constante. Validity of this constante for gravity atraction between two body in relative quite confirmed Cavendish (1798).

From inverse procedure, i.e. by application of Newton formula to binary star system (where mass ratio is not much bigger than 1, how it is in solar system) obtains more general formula for gravity constant:

$$\gamma = r^2 (v_1^2 / m_2 r_1 + v_2^2 / m_1 r_2) , \qquad (10)$$

where are v_1, v_2 – baricentric velocities, r_1, r_2 – baricentric distances both bodies, and $r = r_1 + r_2$. It is important underline, because a general trend is colloquial present in many text books on the gravity constant as only proportionality parameter for dimensional equalization.

4. NEWS INSERTED BY VUJIČIĆ

Vujičić made in *Preprinciples of Mechanics* [6] an critical consideration and overview of foundation of mechanics, where gave few important critical opinion and suggestion very important from conceptual standpoint. As a result, by application of corrected procedure to two body motion appeared gravity law formula in some different form (see also [7],[8]):

$$F_2 = \chi \frac{m_1 m_2}{\rho} \ , \quad \chi = \frac{\dot{\rho}^2 + \rho \ddot{\rho} - v_{or}^2}{m_1 + m_2} \ , \tag{11}$$

where $\rho -$ denote previously used r and $\dot{\rho}, \ddot{\rho} -$ radial velocity and acceleration. Authors opinion is that this form of gravity law is more general than Newton's. Our opinion is the same, but after small intervention. Applied in given form equivalent of gravity constant (11) appears not constant, as it is (9). Physicaly, we underline two remarks:

Fig.2. The Moon's face visible from the Earth is the same, modified in periode 19 years 11.3 day by Moon phases and lunar libration in latitude and longitude. This uniqual composite picture obtained Hubble space telescope.(Photo:NASA)

a/ it is confirmed as reality that values of gravity force depend from distance not linear than squared (for two body as considered examples it is not controversial),

b/ constante in Newton formula realy present a constant. (Into interval of time used for measurement, it is not discutable, too.)

This two fact previous formula give not. How harmonize new result with physical facta? The simplicity in natural science is often present, and here it appears as simultaneous multiplying and dividing with distance:

$$F_2 = \gamma \frac{m_1 m_2}{\rho^2}, \qquad \gamma = \frac{\dot{\rho}^2 + \rho \ddot{\rho} - v_{or}^2}{m_1 + m_2} \rho \, . \tag{12}$$

This form of Vujičić equation is fully adequate and realy present generalization of Newton's formula, and γ is equal to known gravity constant.

5. INERTIAL AND GRAVITY MASS

Before of application this corriged formula to the lunar orbit paradox we wish underline the importance of dual nature of the mass, which follow from kinetic description of motion. Galilean physics describe radial motion in gravity field, Kepler – Huygens – Newton's physics describes circular / tangential motion around field source.

Einstein (1905) derived complete (kinetic) physical theory of gravity from Galilean starting position. Oetwes (1911) confirmed in ingenios experiment impossibility of differentiate in realy messure eventualy different numerical mass values for inertial and gravity mass. Eight decade later Hayashy derived complete physical theory of gravity starting from circular motion.

Einstein's work on theory relativity presents just an example of building physical theory based on philosophycal concept. In principles of general theory of relativity Einstein introduced the assumption on equivalence between each mass, gravity, inertial, electromagnetic, etc. But the equivalence is not the same as to bee identical. Into same principle implicite is built a reserve, that in any way can exist situation in which these peculiar properties can be dominant, and can not be ignored.

6. THE PARADOX EXPLANATION

Vujičić's formula for gravity force applied with purpose to calculate acceleration obtain form:

$$a = \frac{F}{m_1 m_2 / (m_1 + m_2)} = \frac{\dot{\rho}^2 + \rho \ddot{\rho} - v_{or}^2}{\rho} \cdot \frac{\rho}{\rho} \, . \tag{13}$$

Strictly, this formula content two type of acceleration – a_g - which is related to gravity mass, a_i – related to inertial mass:

$$a = a_g + a_i = \frac{\dot{\rho}^2 + \rho \ddot{\rho}}{\rho} - \frac{v_{or}^2}{\rho} \, . \tag{14}$$

This formula we applied to explain and cancel paradox of lunar orbit. Orbital data - mean distance (ρ) , period (T), eccentricity (e) and mean tangential velocity (v) for the Earth and the Moon used in calculation are:

$$\rho_{SZ} \approx 1.496 \cdot 10^{11}(m); \qquad e = 0.01667$$

$$T_{ZS} = 365.2422 \cdot 86400(s); \ v_Z = 29700(m/s)$$

$$\rho_{ZM} \approx 3.844 \cdot 10^{8}(m); \qquad e = 0.0549$$

$$T_{MZ} = 29.53 \cdot 86400(s); \qquad v_M = 1020(m/s)$$

Both derivation of distance as mean value can be calculated via orbital eccentricity:

$$\dot{\rho} = \frac{\rho \cdot e}{T/4}; \quad \ddot{\rho} = \frac{\dot{\rho}}{T/4}. \tag{15}$$

Calculated values for the Sun – Moon / Earth system (index *SM*) and the Earth – Moon system (index *EM*) are:

$$(\dot{\rho}_{SM}^2 / \rho) = 0.068 \ (\mu \cdot g); \quad \ddot{\rho}_{SM} = 4.084 \ (\mu g); \quad (v_{or}^2 / \rho)_{SM} = 601.052 \ (\mu g)$$

$$(\dot{\rho}_{EM}^2 / \rho) = 0.290 \ (\mu \cdot g); \quad \ddot{\rho}_{EM} = 5.288 \ (\mu g); \quad (v_{or}^2 / \rho)_{EM} = 275.898 \ (\mu g)$$

.

Here acceleration is expressed in gravity acceleration $g = 9.81(m/s^2)$ at Earth's surface as unit, giving for acceleration:

$$a_{SM} = 4.152(\mu g) - 601.052(\mu g)$$

$$a_{EM} = 5.578(\mu g) - 275.595(\mu g) .$$

Evidently, summary value is practically the same which gave Newton's formula, but here we have possibility to separate acceleration connected with gravity mass (the first term) and with inertial mass.

Solar acceleration to the inertial mass of the Moon (the second term) is greather than Earth's, 2.18 times but Earth's acceleration to the gravity mass of the Moon (the first term) is 1.34 times greather than solar acceleration. The relation between inertial mass acceleration and gravity mass acceleration is equal 1.622 what is very close (99.97%) to Fibonacci golden ratio number, with meaning of stable harmonized ratio.

This can be explained as *generic origin of the Earth and the Moon*, strictly – the same primary mass from which were built both body, with the same kinetic properties according to the Sun as central body. This can be read just as *the same what implicite assumed Delaunay* solving problem of lunar orbit !

If it is correct idea, paradox of lunar orbit is canceled. We have additional argument to support this opinion – the same side of the lunar surface (Fig. 2) is permanent visible from the Earth. What is realy meaning of this fact? Answer gave P. Savić and R. Kašanin in monograph "The Behaviour of the Materials under high Pressures", I – IV, 1962 – 1965. Here we quote last paragraph No 22 in the fourth part of monograph [9]:

"**The Moon:** By studying the ionization of various elements (as we have done in part III), we reached the conclusion that the ionization due to pressure can be brought about at the earliest moment during transition from phase 2 to phase 3 (for instance, in case of aluminum). If thus, a certain celestial body has not the phase 3 in its interior, because of its small mass, then it certainly does not have a magnetic moment, no matter of which material it is made.

This is the case, for instance, with *our Moon,* since *its mass is small for such a process*; this was shown in parts II and III. *This is why the Moon has neither a magnetic moment nor a rotation of its own.»*

Finally, we can add the sense of this comment, in context of our consideration: The Moon is generic originated with the Earth. Also, the same conclusion derived N. Tesla (1919) from analisys of lunar mechanical motion [10].

7. NIELSEN'S INTERPRETATION OF GRAVITY

Previous exposed present only one from few different form of gravity conceptual interpretation. For correct presentation mathematical forms must be in the same conceptual frame, what many people did not. Analogy between electricity and gravity was subject of many authors, but mostly not in the correct way. Maxwell's equations are the crown of classical physics. It is not well known that exist analog equations form for gravity, too [11], [12], by Nielsen. For fully understand result exposed here, Nielsen's paper is crucial appendix which must be present in the consciousness.

Nielsen introduced in fully correct way rotational gravity field as analog form with electricity and magnetic field, starting from special theory of relativity and invariance of electric charge. Static and dynamic components of electric interaction (here important – with very different amplitude, much stronger static) as conceptual correct notation, following formal mathematical analogy Newton's and Coulomb's formula obtained from measurement, must posses full analog for gravity, too. Electromagnetic induction as consequence of relativistic Thomas rotation, generate the same effect for gravity, what Nielsen shown. It is bright final completing of classical physics, but in the time (year 1972) in which it is not in main stream of physics, and so in fact – ignored!

Nielsen used Lorentz equations for position, time, velocity and force, and presumption that gravity mass is Lorentz invariant, too. Newton's formula obtain form

$$\vec{F}_g = \frac{m_1 \cdot m_2}{\lambda_0 \cdot 4\pi \cdot r^2} \frac{\vec{r}}{|r|} \tag{16}$$

in which gravity constant is changed into form equivalent to electric constant

$$\lambda_0 = -\frac{1}{4\pi \cdot \gamma} \tag{17}$$

in Coulomb's formula

$$\vec{F}_e = \frac{q_1 \cdot q_2}{\varepsilon_0 \cdot 4\pi \cdot r^2} \frac{\vec{r}}{|r|}. \tag{18}$$

Electric charges of the same sign show repulsiveness, charges of the different sign attractiveness. Gravity interaction is only attractiveness. Nielsen searched full analogy, so that mathematic isomorphism must be physical content, too. Formal analogy with

electricity is possible in physical sense if introduce two different mass, too. So appeared except of positive mass in static, negative mass in motion, what follows from Newton's formula. Conceptual, this is *condition sine qua non* for analogy. And, this condition really equalized both law in the frame of classical physics.

Maxwell's, for electricity:

$$\vec{\nabla} \cdot \vec{E} = \frac{\rho_e}{\varepsilon_0}, \ \vec{\nabla} \times \vec{E} = -\frac{\partial \vec{B}}{\partial t} \ , \ \vec{\nabla} \cdot \vec{B} = 0 \ , \ \vec{\nabla} \times \vec{B} = \mu_0 \cdot \vec{j}_e + \mu_0 \cdot \varepsilon_0 \cdot \frac{\partial \vec{E}}{\partial t} \qquad (19)$$

Nielsen's, for gravity:

$$\vec{\nabla} \cdot \vec{G} = \frac{\rho_g}{\lambda_0}, \ \vec{\nabla} \times \vec{G} = -\frac{\partial \vec{N}}{\partial t}, \ \vec{\nabla} \cdot \vec{N} = 0 \ , \ \vec{\nabla} \times \vec{N} = K_0 \cdot \vec{j}_G + K_0 \cdot \lambda_0 \cdot \frac{\partial \vec{G}}{\partial t}. \qquad (20)$$

Here are ε_0, μ_0 – dielectric constant and magnetic permeability of vacuum, λ_0, K_0 - gravity constant and eddy permeability for mass in vacuum, ρ_g, ρ_e – density of mass and charge, j_e, j_g – density of charge and mass current. It is obvious that nature of acceleration given by formula presented here

$$a = a_g + a_i = \frac{\dot{\rho}^2 + \rho\ddot{\rho}}{\rho} - \frac{v_{or}^2}{\rho} \qquad (21)$$

is in congruence with Nielsen's conclusions, because tangential component of velocity (3rd term in formula) produce acceleration in direction normal to motion (for negative mass). If radial acceleration component (2nd term in formula) determines (static) radial acceleration for positive mass, radial velocity (1st term in formula) determines acceleration normal to radial acceleration, what can be responsible for baricentric motion, and evolution of circular orbit to eliptic.

8. REMARKS ON THE BARICENTRIC MOTION

Solar system are described in different paradigm, depending of accuracy in measurement. In all presentations planets motion is described as "around the Sun", Moon motion "around the Earth". Baricenter of solar system describes curve like pulsating (Arhimedes) spiral [13], and baricenter can be distant from center of the Sun up to 2.3 solar radius. (Fig.3.)

Objection of some criticist was that the Moon and the Earth motions must be described as motion around of his baricenter, and around the Sun. It is Delaunay interpretacion, mostly correct mathematicaly. Baricenter of lunar motion is always into Earth. Conceptual correct is just motion around the Earth.

Each opinion with pretension to explanation must be presented in conceptual frame so that it can exist in time longer than time in which is reported. Mathematic is fundament of physics, but it is not physics. Needs measurement, concept, experiment, modeling, etc, what leads to development by permanent expansion of physics into other scientific area, also in philosophy.
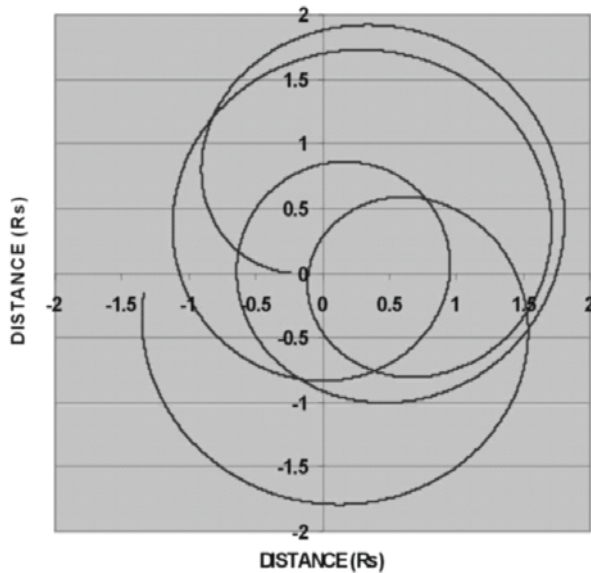
Fig. 3. Orbit of the baricenter around the solar center, in solar radius as unit,

in period 1939 -1990. year.

9. CONCLUSIONS

The law of gravity interaction between two body was derived by Newton, 1687, primary from Kepler laws for planetary motion and few axioms which established dynamics. It has been applied on the lunar motion around the Earth and Earth's motion around the Sun. Newton's formula gives greather force for atraction of the Moon by the Sun than by the Earth. However, central body in lunar (primary) orbit is the Earth, not the Sun. Theoretical foundation of physics stay at formal logic and philosophical concepts. («Physics is an attempt of conceptual construction of the real world and its legal structure.» [14])

So appeared paradox which were ignored from competent specialist, beacause the most important problem, determination of lunar orbit, was inmediately solved sufficiently by mathematical ingeniosity – introducing the Sun as dominant body in the three body system (Delaunay, 1860). On this way the lunar orbit paradox were situated in the corner, not canceled. Vujičić (1998) in critical consideration made an owerview of principles of mechanics. As an example of application corrected procedure was obtained gravity law in some different form, which gave possibility to cancel paradox of lunar orbit. With our small intervention presented as follows in text, the result of Vujičić present a generalization of classic gravity law. This formula content two type acceleration, one related to inertial mass, the second related to gravity mass. This appendix related to gravity mass carry information on generic origin of the Earth and the Moon, i.e. information that these two body present finally formation from the same initial mass condensed in process of planet birth in solar system genesis.

With small intervention by author, which we made here, litle different formula related to Newton's formula for gravity law, which derived Vujičić in strictly defined circumstances, really present more general form of gravity law in classic physics. This formula content two type acceleration, one related to inertial mass, the second related to gravity mass. This appendix related to gravity mass carry information on generic origin of the Earth and the Moon, i.e. information that these two body present finally formation from the same initial mass condensation in process of planet birth in solar system genesis. Nielsen's analogue to gravity of Maxwell equations for electricity is conceptual fully congruent with our conclusions.

REFERENCES

1. Perel'man Ya. I., (1958), *Zanimatel'naya astronomiya*, Izdanie 9-e, pod redakciej P.G. Kulikov-skogo, Gos.izd. Fiz.Mat.lit, Moskva. (p. 212.)
2. Idel'son N.I.:(1975), *Etudi po teoriy nebesnoj mehaniki*, Nauka, Moskva.
3. Deprit A.: (1971), Ch, 1 in (Ed.) Z. Kopal, *Physics and astronomy of the Moon*, Second Edition, Academic Presss, NewYork and London.
4. GrebenikovE.A., Ryabov J.A.: (1976), Čast 4 , gl. 10 u (Red.) Duboshin G.N.: *Spravočnoe rukovodstvo po nebesnoj mehanike i astrodinamike,* Nauka, Moskva.
5. Tomić A.S.: (2007), (Eds. Šumarac D, and Kuzmanović D.) *Proceedings of the 1ˢᵗ Internat. Congress of Serbian Society of Mechanics, 10-13 April, 2007, Kopaonik, p. 636 :*Deduction of the gravity law and quantum mechanical model of discretization in the macroscopic gravity system from Solar system data, p.636 in.
6. Vujičić V.A.: (1999), *Preprincipi mehanike,* ZUNS Beograd, 1998.*(Preprinciples of mechanics,* Mathematical institute SANU, Belgrade.
7. Vujičić V.A.: (2000), *Facta Universitatis, Ser. Mechanics, Automat.Control and Robotics,* Vol.2 No 10, p. 1021-1034. (Acction of force – formality or essence)
8. Vujičić V.A., He J.H.: (2004), *Int. Journal of nonlinear Sci. and numerical Simulations,* 5 (3), 283 – 286. (On two fundamental statements of mechanics)
9. Savić P., Kašanin R.: (962, 1963, 1964, 1965), *The Behaviour of the Materials under high Pressu-res*", I – IV, SANU, Belgrade.
10. Tomić A., Jovanović B.: (1993), *Publ. Astron. Obs. Belgrade*, No 44, 119-126. (Proceedings of the X national conf. Of yugoslav Astronomers, Belgrade, 22-24. sept. 1993); (Nikola Tesla - The Moon's rotation)
11. Nielsen L.: (1972), Gamma, No 9, Niels Bohr Institute, Copenhagen. (A Maxwell analog gravita-tion theory.),
12. Nielsen L.: 2000, http//www.rostra.dk/louis/(Holistic quantum cosmology with decreasing gravity)
13. Tomić A., Koruga D.: (2005), *Publ. Astron. Soc. R.Boskovic,* No 6, 289-294, (Proceedings of IV Serbian/Bulgarian astronomical conference, 21-24 April, 2004, Belgrade). (Baricebtric motion of the Sun).
14. Marić Z.: 1979, Theoria, 22, No 4, 5 -15. (Albert Einstein) ; Holton G.:1968, Spring 1968, 636. (Deadalus)

PARADOKS MESEČEVE PUTANJE

Aleksandar S.Tomić

Apstrakt: *Njutnova formula za gravitacionu silu daje veće privlačenje Mesca Suncem nego Zemljom. Ipak, centralno telo u mesečevoj (primarnoj) putanji je Zemlja. Tako se pojavio paradoks koji kompetentni specialisti ignorišu, jer je mnogo važniji problem, određivanje Mesečeve putanje, u međuvremenu zadovoljavajuće rešen matematičkom domišljenošću – uvođenjem Sunca kao dominantnog tela u sistemu tri tela (Delaunay, 1860). Ali, tako paradoks mesečeve putanje nije razrešen. Vujičić (1998) je kritičkim razmatranjem uradio pregled principa mehanike. Kao primer primene korektne procedure dobio je formulu zakona gravitacije u malo drugačijoj formi, koja pruža mogućnost da se razreši paradoks Mesečeve putanje. Vujičićeva formula, sa našim malim prilagođenjem, sadrži dva tipa ubrzanja – koja se odnose na inercionu masu i na gravitacionu masu. Tako se pojavljuje sačuvana informacija o poreklu Meseca i otklanja paradoks.*

Ključne reči: *paradoks mesečeve putanje, zakon gravitacije, gravitaciona masa, inerciona masa, koncepti u fizici*

COMPUTATIONAL MECHANICS IN SCIENCE, APPLICATIONS AND TEACHING

UDC: 519.673:531.01

M. Kojic*   N. Filipovic**

*Research and Development Center for Bioengineering, Kragujevac, Prvoslava Stojanovica 6, 34000 Kragujevac, mkojic@hsph.harvard.edu

**Faculty of Mechanical Engineering, University of Kragujevac, Sestre Janjic 6, 34000 Kragujevac, fica@kg.ac.rs

Abstract. *We express our opinion about the role of Computational Mechanics (CM) in science, applications and education. The presented thoughts rely on our experience gained by working over decades (first author in particular) in the field of CM.*

First, as a challenge of an opinion that computational mechanics is rather a tool, not the science, we give our view that computational mechanics is a complex interdisciplinary scientific field where new methods and solutions are sought, new hypotheses are tested, and events in material world are elucidated or predicted. It is quite an art to achieve the goal that general analytical formulations or experimental findings become useful and practical numbers, graphs, and even simulations of living systems response.

Second, we would like to emphasize the enormous impact of CM in applications; ranging from the support of experimental investigations, to everyday engineering in design and industry, to bioengineering and medicine. Giant steps have been undertaken by invention of the finite element method in the 6th decade of last century. From that time on, a huge number of researchers have opened new frontiers, introducing new computational methods, improving the algorithms and incorporating achievements in computer technology.

Third, we want to address the issue of the CM participation within university programs. We believe that the CM methods, software development and application should be a significant part of the overall education in engineering departments, but also (to appropriate extent) in other departments of natural and biomedical sciences, technology and medicine. All courses should be accompanied by the corresponding software. We here cite our experience where around 40 PhD and MS theses have been completed at University of Kragujevac, with the CM topics, development of engineering software (our system of programs PAK) and applications in engineering and bioengineering. This approach in education will result in preparing students to use modern CM tools and software in their work after university studies.

1. INTRODUCTION

Mechanics is the branch of applied science concerned with the study of mechanical phenomena: the behavior of solids, fluids, and complex materials under the action of forces. CM is that sub-discipline of mechanics dealing with the use of computational methods and devices to study events governed by the principles of mechanics. It is fundamentally important part of computational science and engineering based on the use of computational approaches to characterize, predict, and simulate physical events and engineering systems governed by the laws of mechanics (Oden, 1987).

It can be considered that CM has three aspects (Felippa, 1994). The first one is engineering application; this is mainly in the fields of classical and recently developing new engineering disciplines. The second one, the backbone of the field, is the theoretical mechanics which uses continuum approach. The third one is the numerical solution of the analytical equations.
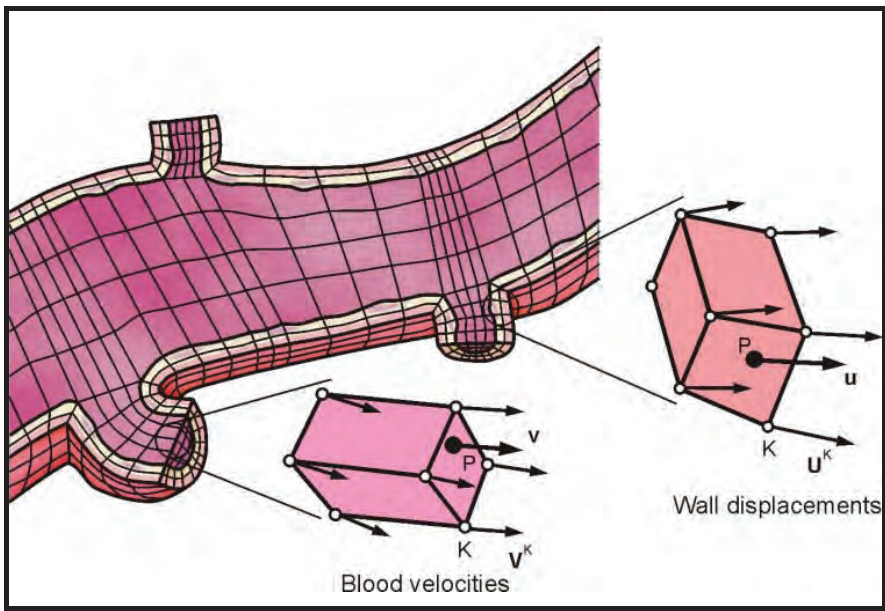

Fig. 1 Fluid and solid finite elements used in modeling blood flow with blood vessel deformation (according to Kojic et al. 2008)

The main goals of CM are directed to the development and application of computational methods based on the principles of mechanics. With the use of these

computational methods CM has had a profound impact on science and technology. It has effectively transformed much of classical Newtonian theory into practical and powerful tools for prediction and understanding of complex systems and for creating optimal designs. Active research topics include improvements of classical (Figs. 1 and 2) and development of new finite element methods (e.g. discontinuous Galerkin method), computational acoustics and fluid-¬structure interaction, algorithms for dynamical and transient transport phenomena, adaptive solution schemes using configurational forces, modeling the behavior of complex materials and biological tissue, and coupled problems (multiphysics) where multiple interacting physical fields are modeled. Methods and algorithms for high ¬performance computing including massively parallel computing (Morton, 1976) are important for complex applications are currently in development stage. A recent research in CM is focused on multiscale methods to solve problems involving mutually dependent events occurring on different time and length scales.
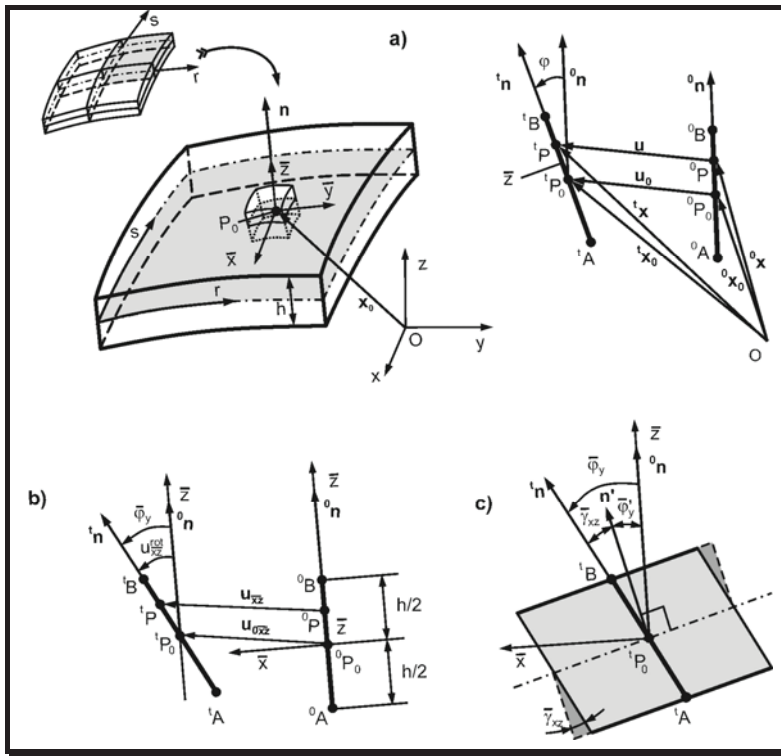

Fig. 2 Shell finite element which relies on the classical theory of shells, used in structural mechanics (according to Kojic et al. 2008)

In the next sections we present several examples to illustrate the role of CM in various fields, ranging from treating the fundamental problems in mechanics to applications to practical problems which could not be addressed without the CM

methods. Then, a brief discussion regarding the role of CM in education is given, followed by concluding remarks.

2. SELECTED EXAMPLES OF USE OF CM METHODS

Applications of CM methods in science, engineering and medicine are so broad that it is very hard to select the most representative examples. Based on our experience, we here give a few examples in which we and our collaborators have been involved, which may illustrate complexity and variety of CM methods.

2.1. Flamant problem in solid mechanics

The famous Flamant problem in solid mechanics (Flamant 1892) represent the problem of finding the solution of the stress distribution when an elastic semi-space is loaded by concentrated force normal to the free surface. It is known from experiments that tensional stresses develop in the vicinity of the force action point, but which cannot be obtained by classical continuum mechanics theory. Use of a microstructural doublet mechanics (DM) theory (Ferrari et al 1997) is illustrated graphically in Fig. 3. A challenge was to develop a computational procedure to include the DM so that it can be used for general analyses of problems involving microstructural material description.
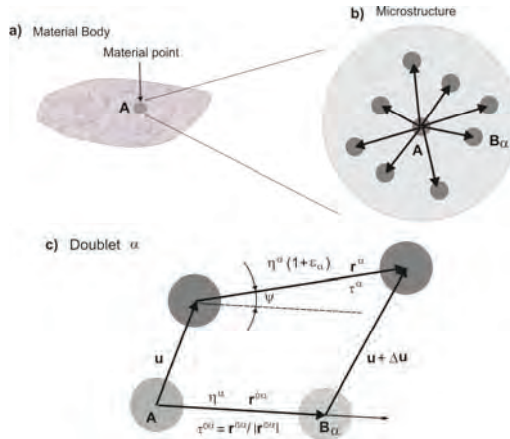
Fig. 3 Microstructural kinematics of deformation described according to doublet mechanics theory (Ferarri et al. 1997)

The basic equation expressing elongation strain of a "doublet" (a pair of neighboring particles used for microstructure representation) is given as

$$\varepsilon^{\alpha} = \sum_{\chi=1}^{M} \frac{\eta_{\alpha}^{(\chi-1)}}{\chi!} \tau_j^{\alpha} T_{k_1 k_2 \ldots k\chi}^{\alpha} \frac{\partial^{k_1 k_2 \ldots k_{\chi}} u_j}{\partial x_{k_1} \partial x_{k_2} \ldots \partial x_{k_{\chi}}} \approx T_{jk}^{\alpha} \frac{\partial u_j}{\partial x_k} + \frac{\eta_{\alpha}}{2} T_{jkm}^{\alpha} \frac{\partial^2 u_j}{\partial x_k \partial x_m} \tag{1}$$

sum on $j,k,m = 1,2,3$; no sum on α

where T_{jk}^{α} are coefficients as products of directional cosines of the doublet, u_i are displacements and η_{α} is the microstructural scaling factor. This equation has been built into the FE framework and the correctness of the methodology and software (PAK, Kojic et al. 1998, 2010) is illustrated in Fig. 4.
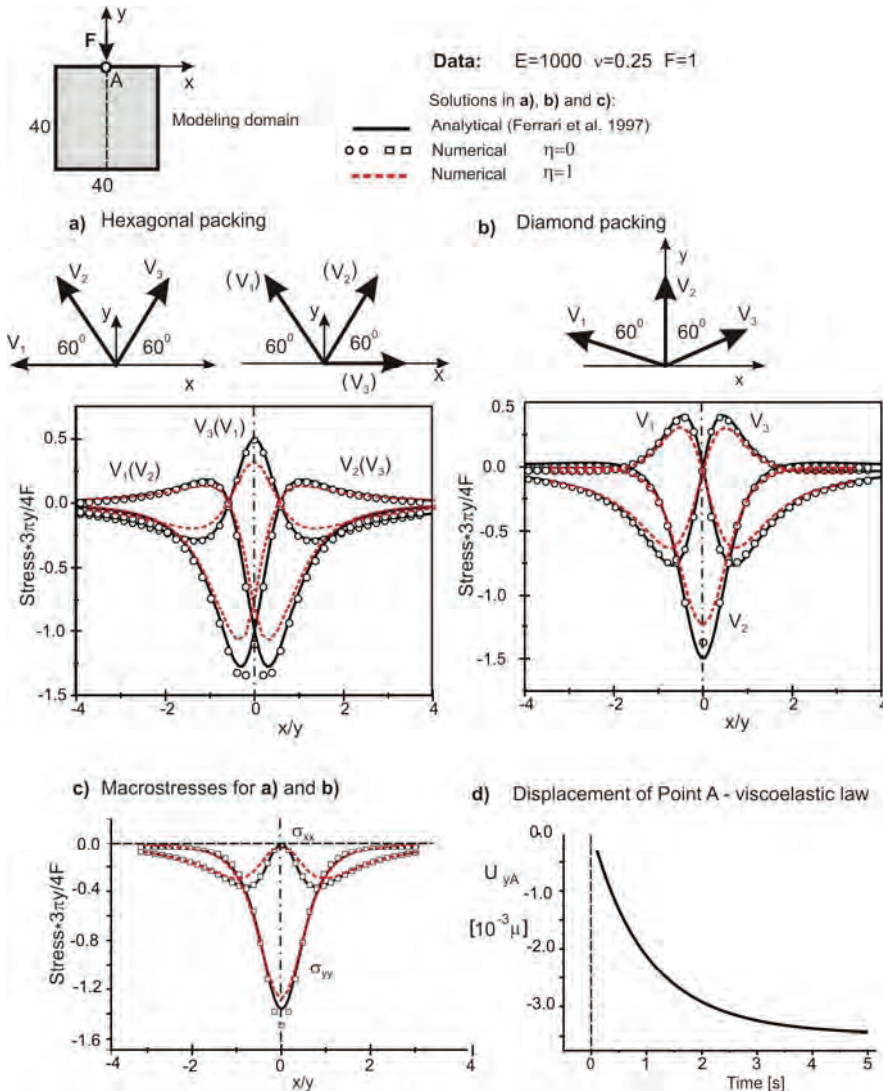
Fig. 4 Flamant problem. Microstresses for the three doublets: a) Hexagonal packing (two orientations); b) Diamond packing. c) Macrostresses for both packings a) and b). d) Displacement of the point A where the constant force is acting during time for the viscoelastic constitutive relations (according to Kojic et al. 2011).

2.2. Modeling of inelastic deformation of material

Material response to mechanical or other loadings (such as thermomechanical) is described by a constitutive law which relates the stress vs. deformation measures. The constitutive law can be simple, as linear elastic, but it can be very complex, described by complex functions and parameters, and can include the material history of deformation. Examples of these constitutive laws are those used for elastic-plastic or creep deformation of engineering materials, or for biological materials. Constitutive relationships are usually established by simple experiments (e.g. for metal plasticity, Kojic and Bathe 2005). However, it has been a challenge to find material response in real conditions of loading within structures or in biological systems, and generally represents a scientific task and art to develop adequate computational methods. We here show one concept, known as the governing parameter method (GPM), introduced in Kojic (1996) for modeling inelastic material deformation; and its application to a real engineering problem.
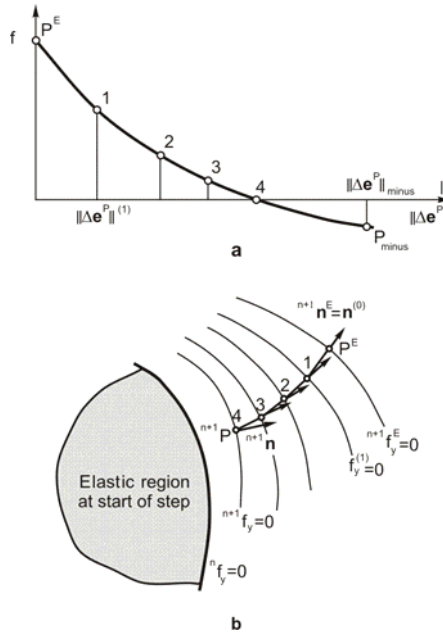
Fig. 5 Return mapping according to the GPM. a) A bisection procedure in finding zero-value of the governing function – solution is between points P^E and P_{minus}. b) Graphical interpretation of search the final point ^{n+1}P starting from P^E (according to Kojic and Bathe 2005).

Using the GPM it is possible to implicitly integrate constitutive law (providing the best solution accuracy) within a load step and to satisfy the yield condition at end of the step, see Fig. 5. In case of plasticity, the problem of calculation of stresses and plastic strains is reduced to finding the zero of a monotonic function,

$$f\left(\left\|\Delta\mathbf{e}^{P}\right\|\right) = {}^{n+1}f_{y}\left({}^{n+1}\boldsymbol{\sigma}^{E} - \left\|\Delta\mathbf{e}^{P}\right\|\mathbf{C}^{E\ n+1}\hat{\mathbf{n}}, {}^{n}\boldsymbol{\beta} - \left\|\Delta\mathbf{e}^{P}\right\|\hat{\mathbf{C}}^{P\ n+1}\mathbf{n}_{\beta}\right) \qquad (2)$$

where $\Delta\mathbf{e}^{P}$ are increments of plastic strains, $\boldsymbol{\sigma}^{E}$ are elastic stresses, $\mathbf{C}^{E}$ is elastic constitutive matrix, $\hat{\mathbf{C}}^{P}$ is the matrix related to internal parameters $\boldsymbol{\beta}$, $\hat{\mathbf{n}}$ and $\mathbf{n}_{\beta}$ are normals to corresponding to yield surface f_{y} and internal parameters; and the left upper index $n+1$ indicate that evaluation of quantities is performed at end of load step. This solution procedure is illustrated in Fig. 5, generally termed as the return mapping.

Figure 6 shows FE solution and comparison with experiment for large deformation of a car joint, based on the GPM within the program PAK.
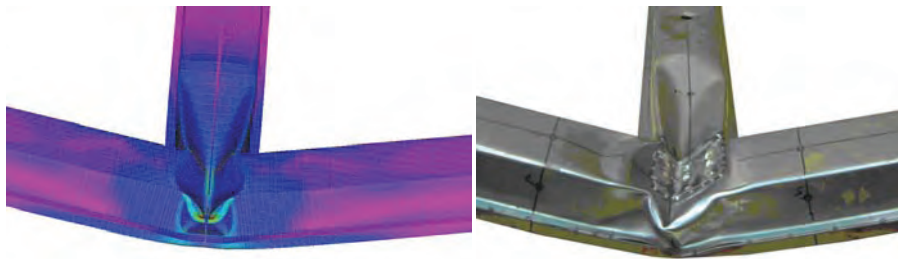
Fig. 6 Finite element solution (large strain elastic-plastic analysis) and experimentally determined deformation of a joint of car structure (Zivkovic and collaborators 2006)

2.3. Muscle model

Modeling of biological materials remains a big challenge and requires further experimental data and specific computational methods. Some solution concepts are presented in Kojic et al. (2008). Here, we show a model of tongue using a relatively simple Hill's model and imaging technique to simulate motion of tongue produced by internal excitation which is governed by the nervous system and biochemical processes within the tongue tissue.
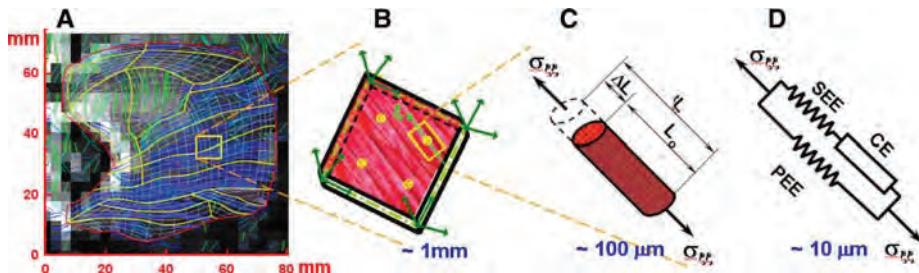
Fig. 7 Multiscale model of tongue contraction. Muscle fibers are determined using a DTI tractography images (the left panel), the domain is discretized into finite elements with fibers, and material behavior is described by Hill's model for fibers deformation (according to Mijailovic et al. 2010)

Computational procedure form muscle modeling introduced in Kojic et al. (1998) and further generalized in Stojanovic et al. (2007), is implemented to tongue model (Mijailovic et al. 2010), Fig. 7.

Field of active stresses for two specific times is shown in Fig. 8.
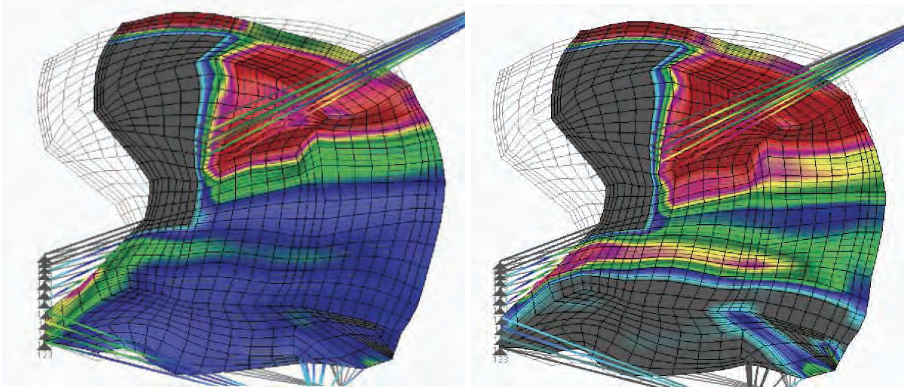
Fig. 8 Active stress distribution within the tongue for: a) t=370ms and b) t=500ms
(according to Mijailovic et al. 2010)

2.4. Mass transport of LDL through blood flow and plaque growth model

Fluid flow problems and transport phenomena have been the subject of investigations over centuries. Many problems have been solved in analytical form for simple boundary conditions. However, those analytical methods are practically of no use for complex flows and mass transport. Methods of computational mechanics enable us today to treat the real engineering, scientific and medical problems. Here we select few of those of interest in medicine. The first one is related to transport of the LDL proteins within the blood, which cause plaque initiation and growth.

The model of plaque formation include the following processes: a) transport of the LDL within blood (fluid domain); b) transport of LDL within tissue (solid domain); and plaque formation within the tissue.

The governing equations for blood flow are described by the Navier-Stokes equations and continuity equation (here for incompressible fluid), while the mass-balance diffusion equation (with diffusive and convective terms) is the governing equation for the concentration field of the LDL within the blood. Those equations can be transformed to the FE balance equations and further used for general boundary conditions, today in a routine manner.

Specifics for this problem are first related to mass transfer of LDL within the arterial wall, which coupled with the transmural flow. This mass transport is modeled by a convection-diffusion-reaction equation as follows

$$\nabla \cdot \left(-D_w \nabla c_w + k c_w u_w \right) = r_w c_w \tag{3}$$

in the wall domain, where c_w is the solute concentration in the arterial wall, D_w is the solute diffusivity in the arterial wall, K is the solute lag coefficient, and r_w is the

consumption rate constant. Second, the LDL transport in lumen of the vessel is coupled to these equations by Kedem-Katchalsky equations (details are given in (Filipovic et al 2010).

a)   b)

c)   d)
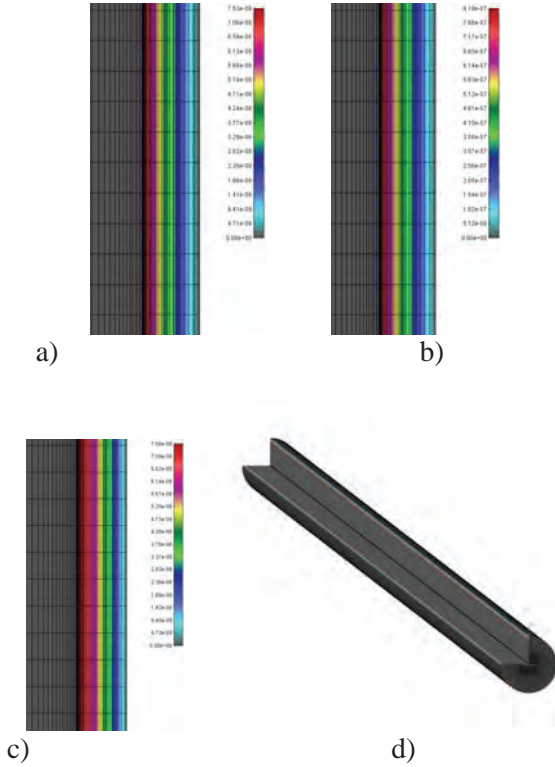
Fig. 9 a) Oxidized LDL distribution 0.37%; b) Macrophages distribution 4.2% from media; c) Cytokines distribution 0.39%; d) three-dimensional representation of the model

Finally, the model of plaque formation includes the inflammatory process. This process is described b three additional reaction-diffusion partial differential equations (Calvez et al 2008), (Boynard et al 2009):

$$\partial_t Ox = d_1 \Delta Ox - k_1 Ox \cdot M$$
$$\partial_t M + div(v_w M) = d_2 \Delta M - k_1 Ox \cdot M + S/(1-S)$$
$$\partial_t S = d_3 \Delta S - \lambda S + k_1 Ox \cdot M + \gamma(Ox - Ox^{thr})$$

(4)

where Ox is the oxidized LDL in the wall, M and S are concentrations in the intima of macrophages and cytokines, respectively; d_1, d_2, d_3 are the corresponding diffusion coefficients; λ and γ are degradation and LDL oxidized detection coefficients; and v_w is the inflammatory velocity of plaque growth, which satisfies Darcy's law and continuity equation (Filipovic et al 2010). Since geometry of the blood vessel changes during inflammation, a 3D mesh moving algorithm and ALE (Arbitrary Lagrangian Eulerian) formulation for fluid dynamics was applied (Filipovic et al 2006).

The above models are incorporated into a FE scheme and solved using massive computational procedures, as well as experimental data for material constants and imaging technique for geometry of blood vessels. The computed results are verified by experimental observations using histology analysis and image processing. Figure 9 shows the computed distributions of the three model constituents within a blood vessel wall, while in Fig. 10 are given graphs of distributions within the media of the wall.
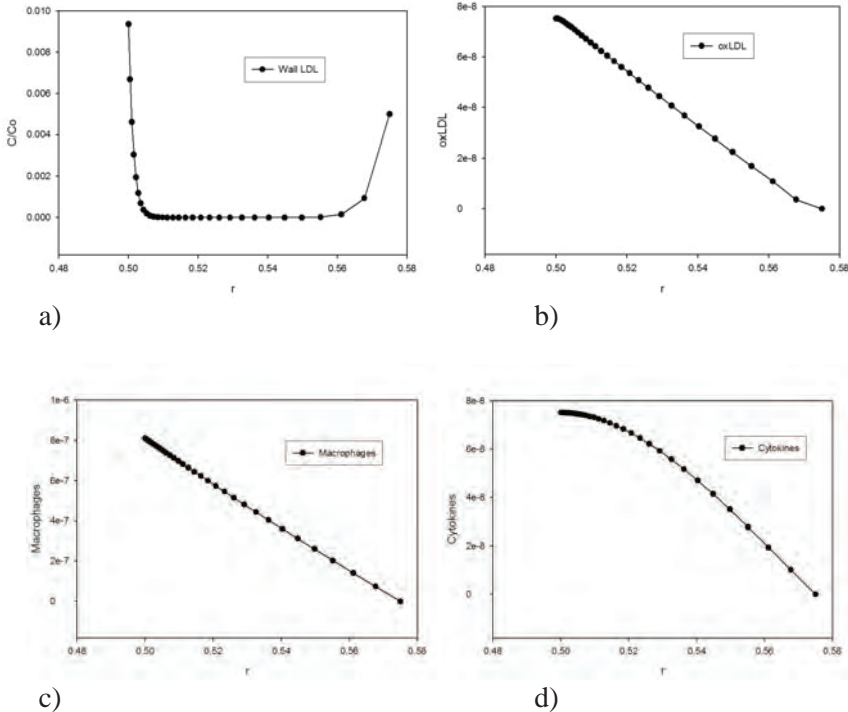
Fig. 10 a) Dimensionless wall LDL concentration profile in the media; b) Oxidized LDL concentration profile in the media c) Macrophages profile in the media d) Cytokines profile in the media

2.5. Self-healing material model using Dissipative Particle Dynamics (DPD)

A self-healing material is used to cover surfaces of vital parts of structures in order to prevent corrosion. When a nanoscopic scratch occurs, a healing material follows from nanocontainers into scratches. This process can be modeled using molecular dynamics (Tyagi et al 2004). Another approach to this problem is a mesoscoping modeling using the DPD method (Groot and Warren 1997, Filipovic et al. 2008a,b). Here we show how the DPD can be applied in modeling the self healing process.

Motion of each DPD particle (further called "particle") is described by the following Newton law equation:

$$m_i \dot{\mathbf{v}}_i = \sum_j \left(\mathbf{F}_{ij}^C + \mathbf{F}_{ij}^D + \mathbf{F}_{ij}^R \right) + \mathbf{F}_i^{ext} \tag{5}$$

where m_i is the mass of particle "i"; $\dot{\mathbf{v}}_i$ is the particle acceleration as the time derivative of velocity; $\mathbf{F}_{ij}^C$, $\mathbf{F}_{ij}^D$, and $\mathbf{F}_{ij}^R$ are the conservative (repulsive), dissipative and random (Brownian) interaction forces, that particle "j" exerts on particle "i", respectively, provided that particle "j" is within the radius of influence r_c of particle "i"; and $\mathbf{F}_i^{ext}$ is the external force exerted on particle "i", which usually represents gradient of pressure or gravity force as a driving force for the fluid domain. The total interaction force $\mathbf{F}_{ij} = \mathbf{F}_{ij}^C + \mathbf{F}_{ij}^D + \mathbf{F}_{ij}^R$ (Fig. 11). Description of these forces is given in literature (e.g. Groot and Warren 1997).
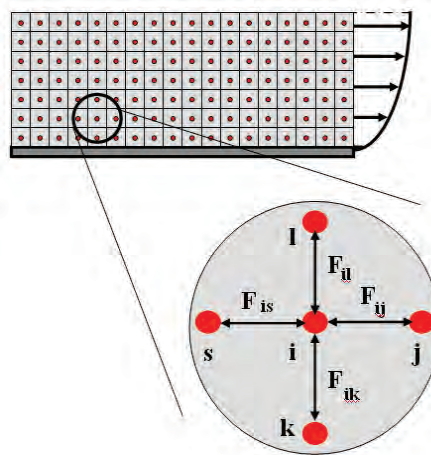
Fig. 11 Interaction forces in the DPD method.

The additional interaction forces between particles of inhibition agents, which are placed in the primer layer and metal substrate particles, are added similarly as it was done in a model of thrombosis in Filipovic et al. (2008a) (also in Jovanovic and Filipovic 2006, Filipovic et al. 2008c). These attractive forces are expressed as

$$F_a = k_{sf} \left(1 - \frac{L_{sf}}{L_{sf}^{max}} \right) \tag{6}$$

where L_{sf} is the distance of the inhibition particle from the substrate, k_{sf} is the effective spring constant, and L_{sf}^{max} is the maximum length of inhibition particle attractive domain.

Solution example is shown in Fig. 12. This DPD model, with inhibitors in the primer layer with thickness of 4 µm, consists of a 2D rectangle crack domain with depth of 0.1 mm. Total number of DPD particles was 24 000 (240x100). Diameter of nanocontainer

was 100 nm and concentration of nanocontainers inside the primer layer was 10%. The total number of time steps for simulation was 100 000.
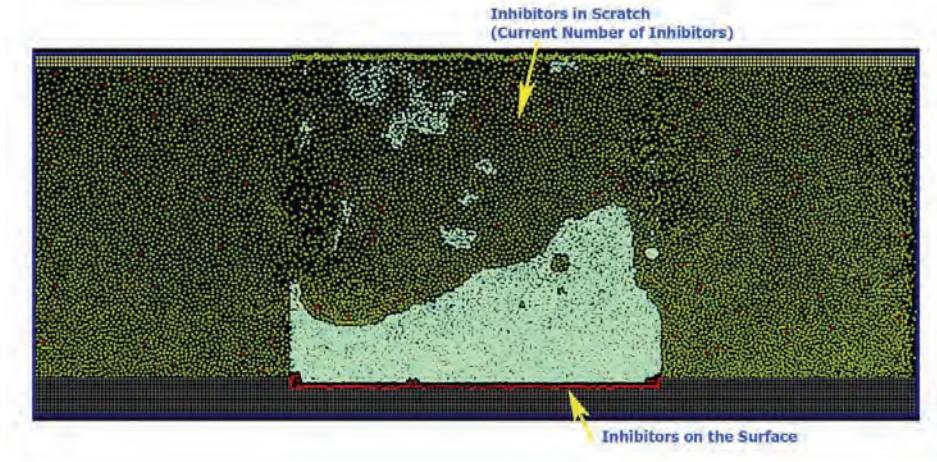
Fig. 12 The DPD model after 100 000 time steps (200s). Red particles represent the inhibition particles, green particles make primer layer, grey particles (substrate) are considered to be fixed in space domain. The surrounding particles are shown with light blue color and represent the fluid.

3. COMPUTATIONAL MECHANICS IN EDUCATION

Courses in Mechanics has a tradition in Serbia as solid, well designed and lectured, supported by exercises and literature. Those courses refer to mechanics of rigid and deformable bodies and fluid mechanics. On the other hand, due to development of computer technology new courses in informatics emerged at almost all departments in natural and technical sciences and medicine.

However, courses in computational mechanics are quite rear in any of the current level of education. Based on the current stage of CM, its use in various fields of science, technology and medicine, illustrated above through several examples, and from our experience, we offer the following ideas.

- There should be special at departments in technical sciences and mathematics devoted to computational mechanics. The courses should be accompanied by use of various software packages within exercises. Example of use of such software is shown in Fig. 13.
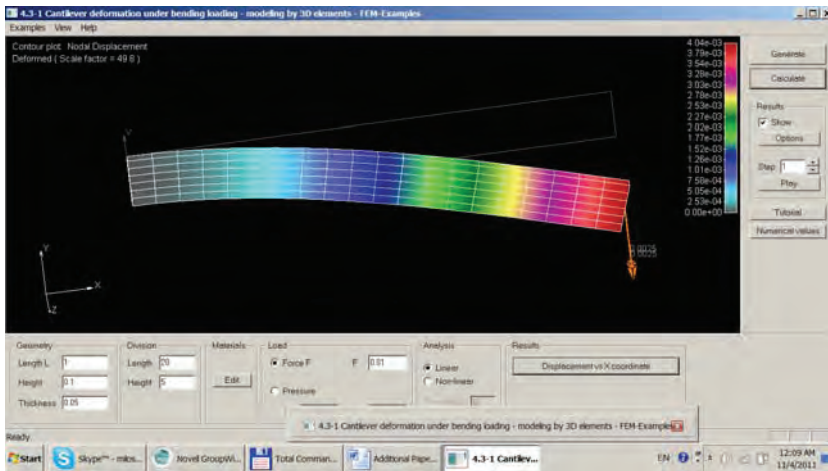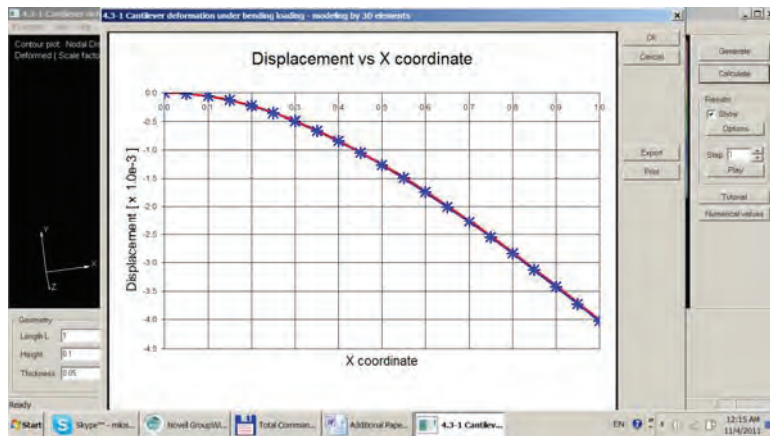
Fig. 13 Use of software in Kojic et al. (2008) to parametrically model beam bending. a)
Displacement field; b) Comparison of analytical (solid line) and FE (dots) solutions.

- Advances courses in mechanics should include parts related to CM as an
  extension of the classical analytical methods.
- Within courses in medicine there should be sections devoted to computer
  modeling. There, without going to deep into theoretical considerations, it is
  possible to connect the basic procedures in medicine with the possibilities of
  modeling using computational methods and software. Figure 14 illustrates blood
  flow through an aneurism can be modeled by using a software package.
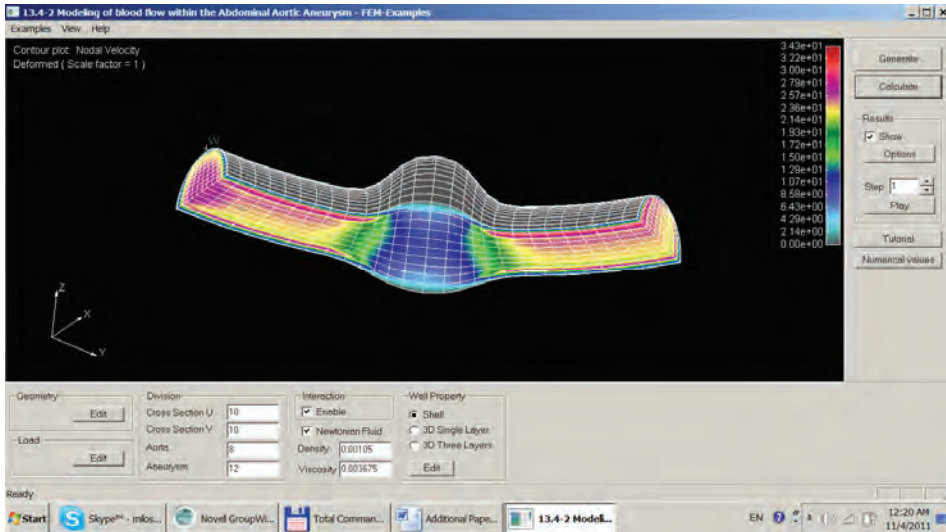
Fig. 14 Computed velocity field of blood within an aneurism (software accompanying
book Kojic et al. 2008)

The above ideas are particularly of interest in the Ph.D. programs, within courses and
research.

4. CONCLUDING REMARKS

The main goals of this discussion are to outline the role of CM in research and
education. This discussion is based on experience of the authors and their collaborators.

In modern research it is simply a necessity to use methods of CM and software to be
able to elucidate problems in various fields of science, technology and medicine.

Teaching courses in Computational Mechanics should be designed for students to
become familiar with modern methods of computational mechanics and various
applications. The courses may contain theoretical background, with details usual for any
other branch of scientific disciplines, for students of mathematically or technically
oriented studies. For students in the fields where CM and software are used as a tool for
modeling purpose, the courses should be oriented to applications, with an outline of the
theoretical background.

REFERENCES

1.   ARTreat FP7-224297 EU project 2008-2012. Multi-level patient-specific artery
      and atherogenesis model for outcome prediction, decision support treatment, and
      virtual hand-on training, www.artreat.org, www.artreat.kg.ac.rs.

2. Boynard M., Calvez V., Hamraoui A., Meunier N., Raoult A., (2009), Mathematical modelling of earliest stage of atherosclerosis, COMPDYN 2009 - SEECCM 2009, Rhodes.

3. Calvez V, Abderrhaman E., Meunier N., Raoult A., (2008), Mathematical modelling of the atherosclerotic plaque formation, *ESAIM Proceedings*, Volume 28, pages. 1-12.

4. Chavent G., (2010), Nonlinear Least Squares for Inverse Problems, Nonlinear Least Squares for Inverse Problems Theoretical Foundations and Step-by-Step Guide for Applications, Springer, second print, New York.

5. Cheng C., Tempel D., Haperen V. R., Baan A. V. D., Grosveld F., Daemen M. J. A. P., Krams R., Crom D. R., (2006), Atherosclerotic lesion size and vulnerability are determined by patterns of fluid shear stress, *Circulation*, Volume 113, Pages 2744-2753.

6. Felippa C.A., (1994), An appreciation of R. Courant's `Variational Methods for the Solution of Problems of Equilibrium and Vibrations,'1943, *International Journal for Numerical Methods in Engineering*, Volume 37, Pages 2159-2187.

7. Ferrari M., Granik V., Imam A., Nadeau J., (1997), Advances in Doublet Mechanics, Springer.

8. Filipovic N., Kojic M., Tsuda A., (2008a), Modeling thrombosis using dissipative particle dynamics method, *Phil Trans Royal*, Volume 366, Pages 3265-3279.

9. Filipovic N., Ravnic D.J., Kojic M., Mentzer S.J., Haber S., Tsuda A., (2008b), Interactions of Blood Cell Constituents: Experimental investigation and Computational Modeling by Discrete Particle Dynamics Algorithm, *Microvascular Research*, Volume 75, Pages 279-284.

10. Filipovic N., Mijailovic S., Tsuda A., Kojic M., (2006), An implicit algorithm within the Arbitrary Lagrangian-Eulerian formulation for solving incompressible fluid flow with large boundary motions, *Comp. Meth. Appl. Mech. Eng*., Volume 195, Pages 6347-6361.

11. Filipovic N., Petrovic D., Jovanovic A., Jovanovic S., Balos D., Kojic M., (2008c), DPD simulation of self-healing process of nanocoating, *J. Serb. Soc. Comp. Mech.*, Volume 2, Issue 2, Pages 42-50.

12. Flamant, (1892), Sur la repartition des pressions dans un solide rectangulaire chargé transversalment, *Comptes Rendus de l'Academie des Sciences Francaise*, Volume 114, Pages 1465-1468.

13. Groot R.D., Warren P.B., (1997), Dissipative particle dynamics: Bridging the gap between atomistic and mesoscopic simulation, *J. Chem. Phys.*, Volume 107, Issue 11, Pages 4423-4435.

14. Himburg H., Grzybowski D., Hazel A., LaMack J., Li X., Friedman M., (2004), Spatial comparison between wall shear stress measures and porcine arterial endothelial permeability, *Am J Physiol Hear Circ Pysiol*, Volume 286, Pages 1916-1922.

15. Jovanovic A, Filipovic N., (2006), Innovative modelling methods in damage assessment: application of dissipative particle dynamics to simulation of damage and self-healing of polymer coated surfaces, *J. Theoretical and Applied Mechanics*, Volume 44, Pages 637-648.

16. Kedem, O., Katchalsky, A., (1958), Thermodynamic analysis of the permeability of biological membranes to non-electrolytes, *Biochim. Biophys.*, Volume 27, Pages 229–246.

17. Kedem, O., Katchalsky, A., (1961), A physical interpretation of the phenomenological coefficients of membrane permeability, *The Journal of General Physiology*, Volume 45, Pages 143–179.

18. Kojic M., Mijailovic S., Zdravkovic N., (1998), Modelling of muscle behavior by the finite element method using Hill's three-element model, *Int. J. Num. Meth. Engng.*, Volume 43, Pages 941-953.

19. Kojic M., Slavkovic R., Zivkovic M., Grujovic N., Filipovic N., (2010), Finite Element Program for Analysis of Solids, Fluids, Field and Coupled Problems and Biomechanics, Univ. Kragujevac and R & D Center for Bioengineering Kragujevac, Serbia, 1998, 2010.

20. Kojic M., Vlastelica I., Decuzzi P., Granik V. T., Ferrari M., (2011), A finite element formulation for the doublet mechanics modeling of microstructural materials, *Comp. Meth. Appl. Mech. Engrg.*, Volume 200, Pages 1446–1454.

21. Kojic M., Bathe K.J., (2005), Inelastic Analysis of Solids and Structures, Springer, Berlin-Heildelberg.

22. Kojic M., Filipovic N., Stojanovic B., Kojic N., (2008), Computer Modeling in Bioengineering-Theoretical Background, Examples and Software, J. Wiley and Sons, Chichester, England.

23. Kojic M., (1996), The governing parameter method for implicit integration of viscoplastic constitutive relations for isotropic and orthotropic metals, *Computational Mechanics*, Volume 19, Issue 1, Pages 49-57.

24. Loscalzo J., Schafer A.I., (2003), Thrombosis and Hemorrhage, Third edition. Lippincott Williams & Wilkins, Philadelphia.

25. Meyer G., Merval R., Tedgui A., (1996), Effects of pressure-induced stretch and convection on low-Density Lipoprotein and Albumin uptake in the rabit aortic wall, *Circulation Research*, Volume 79, Pages 532-540.

26. Morton K.W., (1976), Finite Difference and Finite Element Methods, *Computer Physics Communication*, Volume 12, Pages 99-108.
27. Oden J.T., (1987), Historical Comments on Finite Elements, *Proceedings of the ACM Conference on History of Scientific and Numeric Computation*, Pages 125-130, Princeton, NJ.
28. Stojanovic B., Kojic M., Rosic M., Tsui C.P., Tang C.Y., (2007), An extension of Hill's three-component model to include different fiber types in finite element modelling of muscle, *Int. J. Num. Meth. Eng.*, Volume 71, Pages 801-817.
29. Tyagi S., Lee J.Y., Buxton G.A., Balazs A.C., (2004), Using nanocomposite coatings to heal surface defects, *Macromolecules*, Volume 37, Pages 9160-9168.
30. Zivkovic M., (2006), Nonlinear Analysis of Structures, Faculty of Mechanical Engineering, Kragujevac, ISBN 86-80581-59-3, CIP 539.3/.4, (in Serbian).

RAČUNSKA MEHANIKA U NAUCI, PRAKTIČNOJ PRIMENI I OBRAZOVANJU

M. Kojic   N. Filipovic

U radu pokazujemo ulogu računske mehanike u nauci, praktičnoj primeni i obrazovanju. Izlaganje se oslanja na naše iskustvo stečeno dugogodišnjim radom (posebno prvog autora) u oblasti proračunske mehanike.

Prvo, kao odgovor na mišljenje da je računska mehanika radije alat, a ne nauka, dajemo naš pogled da je računska mehanika kompleksna interdisciplinarna naučna oblast gde se traže nove metode i rešenja, testiraju nove hipoteze, i razjašnjavaju i predviđaju pojave u materijalnom svetu. Prava je umetnost postići da uopštene analitičke formulacije ili eksperimentalni rezultati budu pretvoreni u praktične brojeve, grafike, ili čak simulacije odziva živih sistema. Drugo, želeli bismo da naglasimo ogroman uticaj računske mehanike, počevši od podrške eksperimentalnim istraživanjima, svakodnevnih inženjerskih poslova u dizajnu i industriji, bioinženjeringu i medicini. Preduzeti su ogromni koraci otkrivanjem metode konačnih elemenata u šestoj deceniji predhodnog veka. Od tada, ogroman broj istraživača je pomerio granice, otkrivajući nove računske metode, poboljšavajući algoritme i povezujući nauča dostignuća sa kompjuterskom tehnologijom.

Treće, želimo da se pozabavimo pitanjem uključivanja računske mehanike u univerzitetske programe. Verujemo da računska mehanika, razvoj i primena softvera moraju zauzimati značajnu ulogu u ukupnom obrazovanju na inženjerskim smerovima, ali takođe (u odgovarajućoj meri) i na ostalim smerovima prirodnih i biomedicinskih nauka, tehnologiji i medicini. Sva predavanja treba da imaju softversku podršku. Naše iskustvo se ogleda u približno 40 odbranjenih doktorskih i magistaskih teza na Univerzitetu u Kragujevcu, na temu proračunske mehanike, razvoja inženjerskog softvera (naš sofver PAK) i primena u inženjerstvu i bioinženjeringu. Ovakav pristup će rezultovati osposobljavanjem studenata da rukuju modernim alatima i softverima računske mehanike u njihovom poslu posle studija.

Ključne reči: metode računske mehanike, metoda konačnih elemenata, diskretna čestična metoda, kompjuterska aplikacija, obrazovanje

BIOLOGICALLY INSPIRED CONTROL AND MODELING OF (BIO)ROBOTIC SYSTEMS AND SOME APPLICATIONS OF FRACTIONAL CALCULUS IN MECHANICS

UDC 62-52; 629.8; 681.53.

Mihailo P. Lazarević

Department of Mechanics, Faculty of Mechanical Engineering,
University of Belgrade, st. Kraljice Marije 16, Belgrade 35, Serbia,
mlazarevic@mas.bg.ac.rs

Abstract. *In this paper, the applications of biologically inspired modeling and control of (bio)mechanical (non)redundant mechanisms are presented, as well as newly obtained results of author in mechanics which are based on using fractional calculus. First, it is proposed to use biological analog–synergy due to existence of invariant features in the execution of functional motion. Second, the model of (bio)mechanical system may be obtained using another biological concept called distributed positioning (DP), which is based on the inertial properties and actuation of joints of considered mechanical system. In addition, it is proposed to use other biological principles such as: principle of minimum interaction, which takes a main role in hierarchical structure of control and self-adjusting principle (introduce local positive/negative feedback on control with great amplifying), which allows efficiently realization of control based on iterative natural learning. Also, new, recently obtained results of the author in the fields of stability, electroviscoelasticity, and control theory are presented which are based on using fractional calculus (FC).*

Key words: *biologically inspired systems, control algorithms, modeling, fractional calculus, stability*

1. INTRODUCTION

The field of biomimetics and biologically inspired principles from the application of methods and systems found in nature to engineering and technology, has spawned a number of innovations far superior to what the human mind alone could have devised, [1-3]. Also, the fast growing interest in flexible, versatile and mobile robotic manipulators demands for robots with inherent high passive safety suited for direct human-robot interaction. Traditional robotic systems and industrial manipulators

demonstrate outstanding specifications regarding, for example, precision and speed movement. Some complex industrial – and especially non-industrial tasks – recently induced a new approach to robot design and control in order to achieve very stable, fast, and accurate systems. Biologically inspired approaches have recently succeeded in design and control in robotics [2-4]. Biological systems have been evolved to optimize themselves under selective pressures for a long time. Biological organisms have evolved to perform and survive in a world characterized by rapid changes, high uncertainty, indefinite richness, and limited availability of information. General biomechanical systems including the human body as well as the bodies of mammals and insects are also redundantly actuated. For example, mobility of the human upper-extremity (arm) can be considered as 7 DOF`s, while it has 29 human actuators (i.e, muscles) and accordingly, it has 22 redundant actuators, [3]. A robotic manipulator is called kinetically redundant if it has more degrees of freedom (DOF) then required for a realization of a prescribed task in a task space. The kinematic redundancy in a manipulator structure yields increased dexterity and versality and also allows avoiding collisions with obstacles by the choice of appropriate configurations, [5]. Also, redundant actuation can be also found in many robotic applications, [6].

First, it is proposed using biological analog–synergy due to existence of invariant features in the execution of functional motion, Bernstein (1967) (i.e. rule(s) that can be developed by central nervous system (CNS) based on some principles), [1]. New, synergy approach allows resolving redundancy control problem i.e. actuator redundancy, in the framework of optimal control problem which it is solved by Pontryagin`s maximum principle. It is suggested joint actuator synergy approach which is established by optimization law at coordination level, where it is introduced a central control, [7]. In that way, one may obtain a specific constraint(s) on the control variables. Also, modeling and resolving kinematic redundancy of (bio)mechanical/robotical system in synergy like fashion, can be achieved using optimization law with suitable kinematic and dynamic criteria which are the function of generalized coordinates, velocities, accelerations and control vectors, respectively, [8, 9]. Second, model of (bio)mechanical system may be obtained using another biological concept called distributed positioning (DP) which is based on the inertial properties and actuation of joints of considered mechanical system,[3], [8-10]. At last, using other biological principles is proposed, such as: *principle of minimum interaction* which takes a main role in hierarchical structure of control, [11] and *self-adjusting principle* (introduce local positive/negative feedback on control with great amplifying), [8], which allows efficiently realization of control based on *iterative natural learning*. In that way, control problem of coordinating segments of (non)redundant (bio)mechanical system can be stated as an optimization problem which is most likely to biological   *principle of minimum interaction.* Also, the common observation that human beings can learn perfect skills trough repeated trials motivations the idea of iterative learning control for systems performing repetitive tasks where for improving the properties of tracking is proposed applying *principle of self-adaptability.*

In the second part of this paper, new, recently obtained results of author in fields of stability, electroviscoelasticity, and control theory which are based on using fractional

calculus (FC) are presented, [12-20]. FC has attracted attention of researchers from different fields in the recent years and the fractional integro-differential operators are a generalization of integration and derivation to an arbitrary order operators and they provide an excellent instrument for the description of memory and hereditary properties of various materials and processes and, also obtaining more degrees of freedom in the in the model,[3]. First of them, is an example within a new theory of electroviscoelasticity, which describes the behavior of electrified liquid-liquid interfaces in fine dispersed systems, and is based on a new constitutive model of liquids: fractional order model (generalized the Van der Pol equation) with corresponding non-integer time derivative and integral order, especially linear and nonlinear case,[4]. Also, new algorithms for fractional iterative learning control (ILC), a D^α, PD^α, $PI^\alpha D^\beta$ types are proposed for fractional time delay system and fractional process control $PI^\alpha D^\beta$ type which include ILC feedback control is also presented. At last,stability test procedure (finite time and practical stability) is shown for (non)linear (non)homogeneous time-invariant fractional order time delay systems where sufficient conditions of this kind of stability are derived. Specially, previous results can be applied for robotic system where it appears a time delay in PD^α fractional control system,[5].

2.FUNDAMENTALS OF BIOLOGICALLY INSPIRED MODELING AND CONTROL

As we know, control exists everywhere in complex biological systems. Recent rapid development of biological science and technologies will further improve the active applications of control engineering. Meanwhile, system control theory itself will also be promoted by advanced biomimetic researches, [2], [4], [12]. Several theoretical concepts have been evolved in control theory, typified by feedback control, optimal control, sequence control, and so on,[11]. The main roles of feedback control are regulation and adjustment, whereas optimal control involves planning and supervision with a higher level of control state than feedback control. Meanwhile, it becomes more and more important for the artificial systems to have high flexibility, diversity, reliability, and affinity. System control theory, which forms the core foundation for understanding, designing, and operating of systems, is still limited and insufficient to handle complex large-scale systems and to process spatial temporal information in real time as biological systems. Under this background, biomimetic and biologically inspired control research is becoming a very important subject, [2]. In the first approach, technology approximates the end result or function of an organ or organism. In the second approach, the principles extracted from bio-systems may be applied in ways very much unlike those exhibited in the originating organism. The analysis and clarification of functions of complex biological systems mathematically at the system level, and imitation of them in engineering, will lead to a deeper understanding of ourselves and will be significant for constructing the next generation of advanced artificial systems such as human friendly robots.

2.1. Biologically inspired principle-synergy

The organization and development of brain nervous system's motor control functions largely depend on the physical interaction with the external environment. Self-organization of the environmental adaptive motor function is one of the most interesting characteristics that we should learn in biomimetic control research. From a mechanical point of view, any human or animal represents a redundant mechanism,_[2],_[3]. The nervous system takes advantage of kinematic and multi-muscle redundancies to control actions in a flexible way so that, for example, the same motor goal can be reached differently depending on our intentions, external environmental (e.g. obstacles) or intrinsic (neural) constraints. Despite this flexibility, the central control of actions is unambiguous: each time the body moves, a unique action is produced despite the possibility of using other actions leading to the same goal. It is amazing how these seemingly opposite aspects – flexibility and uniqueness- are combined in the control of actions. Following Bernstein [1], we refer to these aspects of action production as the "redundancy problem". In other words, it was observed in the execution of functional motions that certain trajectories are preferred from the infinite number of options [1], [11]. Such behavior of organisms can be only explained by the existence of *inherent optimization laws* in self-organized systems governing the acquisition of motor skills. Existence of invariant features in the execution of functional motions points out that central nervous system (CNS) uses *synergy* (i.e rule(s) that can be developed by the CNS based on some principles). In fact, such behavior implies that it obeys the optimization at the coordination level where the goal is to minimize efforts in terms of synergy patterns. Speaking mathematically, the synergy imposes specific constraints on the control variables of joints which are related to the task dependent functions pertaining to classes of motor acts. For example, the control of arm movement in humans also relies very much on distributed usage of different joints, and inherent optimization of muscles which are active. Arm muscles are found grouped in pairs about simple hinge joints where even in the simplest case of two antagonist muscles about a joint there are two distinct control variables. Moreover, muscles should be regarded as functional units with more than one control and activation parameter. Also, the biological muscle is the starting point for many new approaches by the development of new actuators for robotics. Beside the direct simulation of biological systems [2], there are different approaches to mimic biological operational principles in technical systems, [11].
Here, the redundancy control problem has been discussed in the framework of optimal control problem which is solved by Pontryagin's maximum principle. Joint actuator synergy approach is suggested which is established by optimization law at coordination level, where is introduced a central control as suggested Bernstein in [1]. In that way, one may obtain a specific constraint(s) on the control variables. The dynamic model of robot can be described with application set of the $2n$ Hamiltonian equations with respect to Hamiltonian phase variables q_i, p_i [13] where conjugate (canonical) momenta p_i

$$\dot{q}_i = \frac{\partial H}{\partial p_i} \qquad \dot{p}_i = -\frac{\partial H}{\partial q_i} + Q_i\left(u\right), \quad i = 1, 2, ..., n \tag{1}$$

where is $H(q, p)$ Hamiltonian and Q_i, $i = 1, 2, .., n$ be non-conservative control forces. For a global optimization, the problem is set up as following

$$J = \int_{t_0}^{t_k} f_o(q, p, u)dt \rightarrow min \qquad (2)$$

The goal is to find $u(t)$, $t_o \le t \le t_k$ which drives system from given initial state (q_o, p_o) to a final state (q_k, p_k) under the condition that the whole trajectory minimizes the performance criterion. Performance criterion is introduced at coordination level as the energy criterion which is, in our case, functional sum of weighted controls of the robot

$$f_o(u) = \frac{1}{2} u^T Ru \qquad (3)$$

Alternatively, the control can be smoothed by minimizing an energy function, quadratic in control, in addition to time. Here, t_o, t_k are the initial and final time of an end-effector movement, which are known and fixed. The control weighting matrix $R = diag\{r_1, r_2, ..., r_m\}$ is symmetric positive definite matrix; $u(t)$ must be entry of a given subset U of admissible controls of m-dimensional Euclidean space: $u(t) \in U \subset R^m$. It is also assumed that optimal control problem has a solution. Applying biologically inspired concept of control, and introducing central control u_c as suggested Bernstein [1], one may introduce control vector $u = [u_1, u_2, u_3, u_c]^T$. Also, generalized forces can be presented as functions of components of control u as

$$Q_i = u_i + u_c, i = 1, 2, 3 \quad u = [u_1, u_2, u_3, u_c]^T \qquad (4)$$

It means that we have four motors, a "central" motor which produces u_c, and rest of motors (corresponding controls u_1, u_2, u_3) are placed at each joint separately. In that way, one of possible control strategies is established. Taking in a account condition of optimal control based on the Pontryagin's maximum principle and applying the matrix theory it implies that following condition must be fulfilled:

$$det \begin{bmatrix} 1 & 0 & 0 & u_1^* r_1 \\ 0 & 1 & 0 & u_2^* r_2 \\ 0 & 0 & 1 & u_3^* r_3 \\ 1 & 1 & 1 & u_c^* r_0 \end{bmatrix} = 0 \qquad (5)$$

After some algebraic operations it yields

$$u_c^* r_0 = u_1^* r_1 + u_2^* r_2 + u_3^* r_3 \qquad (6)$$

Equation (6) presents an *invariant on control variables* "*control synergy*"- which is established by optimization law at coordination level. In order to obtain finite solutions of the problem mentioned, it is necessary to solve two-point boundary value problem for

a system of ordinary differential equations or, even in particular cases, to solved complicate algebraic problems. The proposed biologically inspired optimal control is illustrated by simulation results of a robot with 3 DOF`s (Fig.1) and 4 control variables (Fig.2-5),see [7].
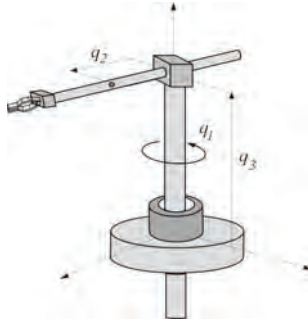
Fig 1. Autolemec ACR with three DOFs
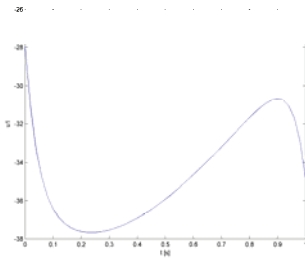
Fig.2. Optimal control *u1*
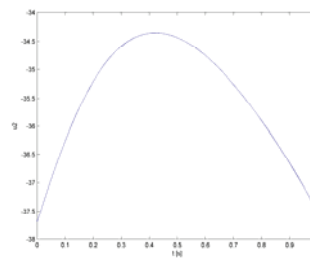
Fig.3. Optimal control *u2*
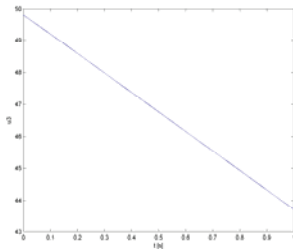
Fig.4. Optimal control *u3*
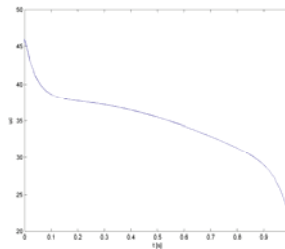
Fig.5. Optimal control *uc*

2.2 Biologically inspired principle - distributed positioning (DP)

The relatively new approach in modeling redundant mechanism is based on biological analog i.e, the modeling is based on the separation of the prescribed movement into two motions: smooth global, and fast local motion, called distributed positioning (DP). Distributed positioning is an inherent property of biological systems. It is based on the

inertial properties and actuation capabilities of joints. Humans, when writing, as shown in literature   control their proximal joints, while the movement of distal joints follow them. Writing is a good representative of task that is characteristic for humans, but at the same time interesting for robots. It is fast and accordingly very demanding from the viewpoint of dynamics (high accelerations produce high inertial loads). In humans highly inertial arm joints (shoulder and elbow) provide smooth global motion, and low inertial hand joints (fingers) perform fast and precise local motions, [3],[10]. Acceleration of massive segments leaded to drive overload and required redundancy. Let, the position of the arm <u>be</u> defined by the vector of joint (internal) coordinates of dimension $n = 8 : q = \begin{bmatrix} q_1 & q_2 & ...q_8 \end{bmatrix}^T$. The position of the terminal device (pencil) is defined by the vector of external coordinates of dimension $n_e = 5 : X = \begin{bmatrix} x & y & z & \theta & \varphi \end{bmatrix}^T$, where x,y,z define the tip position and angles θ, φ define the pencil axis. The kinematic model of the arm-hand complex i.e. the transformation of coordinates (internal to external and vice versa) is highly nonlinear

$$X = f(q) \tag{7}$$

where f is the function: $R^8 \rightarrow R^5$. The inverse kinematics (calculation of q for given X) has an infinite number of solutions since (7) represents a set of 5 equations with 8 unknowns. this is due to presence of redundancy. The dimension of redundancy is $n_r = n - n_e = 8 - 5 = 3$. The kinematic model can be written in the Jacobian form of the first or of the second order

$$\dot{X} = J(q)\dot{q}, \quad \ddot{X} = J(q)\ddot{q} + A(q,\dot{q}) \tag{8}$$

where J is $n_e \times n$ (i.e. 5x8) Jacobian matrix and A is $n_e \times 1$ (i. e. 5x1) adjoint vector containing the derivative of the Jacobian. Let X_1 be the subvector containing the accelerated motions (dimension n_a), and X_2 be the subvector containing the smooth motions ($n_e - n_a$). Now

$$X = \begin{bmatrix} X_1 \\ X_2 \end{bmatrix} \tag{9}$$

The redundant robot ($n = 8$ DOFs) is now separated into two subsystems,Fig.6. The subsystem with $n_e = 5$ DOFs with greatest inertia is called *the basic configuration.* The other subsystem is *the redundancy* having $n_r = 3$ DOFs. It holds that $n = n_e + n_r$. Analysing the plane writing task one finds that there are $n_a = 2$ accelerated external motions : *x(t)* and *y(t)*. The others (z, θ, φ) are constant or smooth. According to DP concept we introduce $X_1 = \begin{bmatrix} x & y \end{bmatrix}^T$ and $X_2 = \begin{bmatrix} z & \theta & \varphi \end{bmatrix}^T$. It can be defined the basic configuration as a mechanism $q_b = \begin{bmatrix} q_1 & q_2 & ....q_5 \end{bmatrix}^T$.The resting joints, one wrist joint q_6 and "fingers " ($q_{7,}q_8$), form the redundancy and $q_r = \begin{bmatrix} q_6 & q_7 & q_8 \end{bmatrix}^T$ defines the position of the redundancy. The DP concept solves the inverse kinematics of a redundant

robot in two steps. At the first step the motion of basic configuration is calculated (q_b) using kinematic model and properties DP concept, and at the second step the motion of redundancy (q_r) is determined, [3].
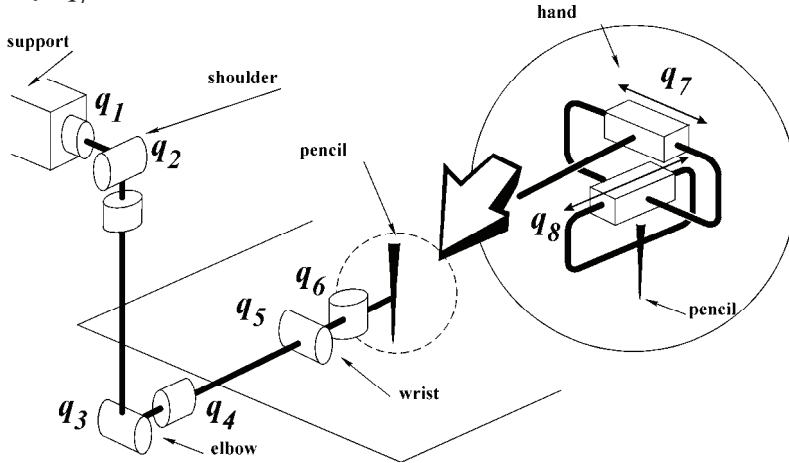
Fig. 6. Eight-DOF arm-hand complex

2.2. Principle of minimum interaction in hierarchical control

Also,motor control is organized as a multilevel structure, is generally accepted. In assistive system involves man as the decision maker, a hierarchical control structure can be proposed with three levels from the left to right: voluntary level, coordination level, actuator level. This imposes the robotic system is decomposed into several subsystems with strong coupling between subsystems. For an instance, the system dynamics of redundant robot are described by:

$$F_o = \left\{ (U, Y, Z) : F_1 = 0, F_2 = 0 \right\},$$ (10)

where $U \in R^m$ is the control input vector, $Y \in R^n$ the output vector, and $Z \in R^n$ the vector representing interactions between the two subsystems(segments),Fig.7. The cost function of a multiple-system is the sum of the cost functions of all subsystems:

$$J(U, Z, Y) = \sum_{i=1}^{N} J_i,$$ (11)
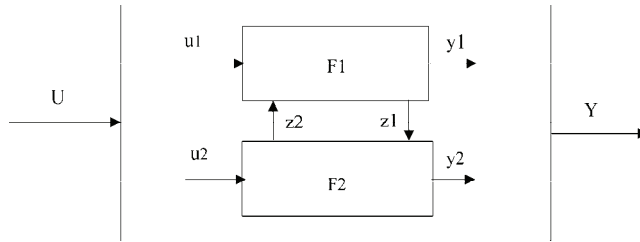
Fig.7. Coordination of two subsystems

The problem of coordinating multiple systems can be stated as an optimization problem: minimize the cost function J subject to the constraint F_o. In monograph [8], it is stated and solved the Bernstein problem which is related to kinematic redundancy of ARA. It is treated control of a anthropomorphic robot arm (ARA) with three degrees of freedom. The optimal control problem of continuous nonlinear dynamic systems - (redundant robotic manipulators), with quadratic performance index can be stated as follows. Determine $U \in L_2(t_o, t_k)$ such that under system constraints is minimized.

$$J = \frac{1}{2} \int_{t_o}^{t_f} \left[\left\| x(t) - x_d(t) \right\|_Q^2 + \left\| u(t) \right\|_R^2 + \left\| z(t) \right\|_S^2 \right] dt \rightarrow min, \tag{12}$$

$$\dot{x}(t) = \frac{dx(t)}{dt} = F(x(t), u(t)) = g(x(t)) + h(x(t))u(t), \ x(t_o) = x_o, \tag{13}$$

$$z(t) = x(t) \quad \dim x = n, \dim u = m, \dim z = n, \tag{14}$$

where x, u state and control vectors and z is interaction vector; weighting matrices Q, R, S are all block diagonal. So, problem of coordinating multiple systems can be state as an optimization problem which is most likely to biological *"principle of minimum interaction"* which is formulated by Gelfand and Tsetlin, [11]: "*For complex controlling systems, the typical structure permits the separation of individual, relatively automatic subsystems. For each subsystem of that type all the remaining subsystems belong to the outside environment and the expediency of the subsystems appears in the minimization of interaction among them so that in stable conditions these subsystems function as if independently, autonomously.*" A major consequence of this principle is that the complexity of each subsystem does not depend on the complexity of the whole system. The application of the minimum interaction principle also leads to a structural form for the "self-organizing" controller. The solution of stated problem of control is generated in a sequence of steps involving a heuristic techniques of genetic algorithm that provides reliable initial guesses. Genetic algorithms are stochastic adaptive algorithms whose search method is based on simulation of natural genetic inheritance and striving for survival. To solve local problems, the minimum principle is used where the multi-level univariate hierarchical strategies is proposed. The problem is divided into two-level optimization problem which is solved iteratively until the desired performance is achieved, [8].

2.3. Iterative learning control, self – adaptability

Recently, there have been extensive research activities in the topic of learning control for controlling dynamics non-linear systems in a iterative manner. The learning control concept differs from conventional control methodologies in that the control input can be appropriately   adjusted to improve its future performance by learning from the past experimental information as the operation is repeated. The common observation that human beings can learn perfect skills trough repeated trials motivations the idea of iterative learning control for systems performing repetitive tasks. Therefore, iterative learning control requires less *a priori* knowledge about the controlled system in the controller design phase and also less computational effort than many other kinds of control. Learning control for controlling dynamics systems, a class of tracking systems is applied where it is required to repeat a given task to desired precision.
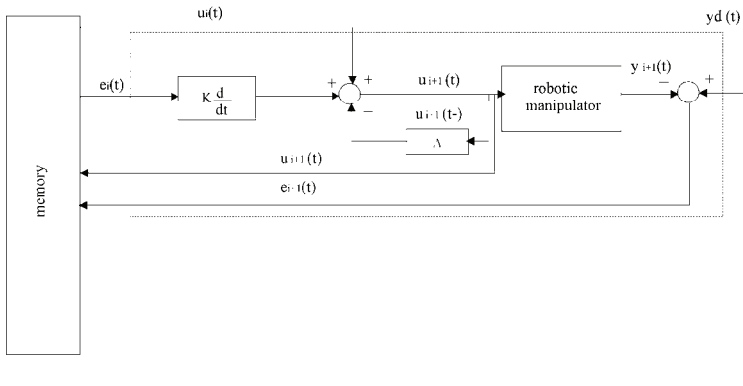
Fig.8. Block diagram of iterative learning control

In these equations t denotes time, $t \in [0, T]$, $t \in \Re$, x_i the state vector, $x_i \in \Re^n$, u_i the control vector, v_i the vector uncertainties, $u_i \in \Re^m$, y_i the output vector of the system, $y_i \in R^r$ and i denotes the i-the repetitive operation of the system. The learning controller for generating the present control input is based on the previous control history and a learning mechanism. Motivated by human learning, the basic idea of iterative learning control is to use information from previous executions of the task in order to improve performance from trial to trial in the sense that the tracking error $e_i(t)$ is sequentially reduced. It is proposed applying biological analog - *principle of self-adaptability* which introduce, here, local negative feedback on control with great amplifying. In the simplest case learning control law can be shown such as (see Fig.8):

$$u_{i+1}(t) = -\Delta u_{i+1}(t^-) + u_i(t) + K(t)\dot{e}_i(t) , \qquad (15)$$

where $u_{i+1}(t^-) = u_{i+1}(t-\tau)$, $\tau -$ the small time delay, denotes a vector of the delayed control signal. If the feedback delay   can be neglected, (for example using very fast processors) then: $u_{i+1}(t^-) = u_{i+1}(t)$.

3. SOME APPLICATIONS OF FRACTIONAL CALCULUS IN MECHANICS

In the second part of this presentation are presented, new, recently obtained results of author in fields of stability, electroviscoelasticity, and control theory which are based on using fractional calculus (FC). FC has attracted attention of researchers from different fields in the recent years and the fractional integro-differential operators is a generalization of integration and derivation to an arbitrary order operators and they provide an excellent instrument for the description of memory and hereditary properties of various materials and processes and, also obtaining more degrees of freedom in the in the model,[14-18].

3.1. Brief historical introduction

When in the 17th century the integer calculus had been developed, Leibniz and L'Hospital probed into the problems on the fractional calculus (FC) and the simplest fractional differential equations (FOEs) through letters. Leibniz asked in a letter addressed to L'Hospital:

Can the meaning of derivatives of integral order $d^n f(x)/dx^n$ *be extended to have meaning when n is not an integer but any number (irrational, fractional or even complex-valued)? L'Hospital responded: What if n be 1/2?* $d^{1/2} f(x)/dx^{1/2} = ?$ *for* $f(x) = x$ *. Leibniz, in a letter dated from Sept. 30, 1695, replied: It will lead to a paradox, from which one day useful consequences will be drawn.In these words fractional calculus was born.*

Following L'Hopital's and Liebniz's first inquisition, fractional calculus was primarily a study reserved for the best minds in mathematics. Futher, the theory of fractional-order derivative was developed mainly in the 19th century. In his 700 pages long book on Calculus, 1819 Lacroix [19] developed the formula for the n-th derivative of $y = x^m$, $m -$ is a positive integer,

$$D^n x^m = \frac{m!}{(m-n)!} x^{m-n} ,$$ (16)

where $n \ (\leq m)$ is an integer. Replacing the factorial symbol by the Gamma function, he further obtained the formula for the fractional derivative

$$D^\alpha x^\beta = \frac{\Gamma(\beta+1)}{\Gamma(\beta-\alpha+1)} x^{\beta-\alpha} , \qquad (17)$$

where α and β are fractional numbers and Gamma function $\Gamma(z)$ is defined for $z > 0$ as:

$$\Gamma(z) = \int_0^\infty e^{-x} x^{z-1} dx, \quad \Gamma(z+1) = z\Gamma(z) , \qquad (18)$$

In particular, he calculated

$$D^{1/2} x = \left[\frac{\Gamma(2)}{\Gamma(3/2)} \right] x^{1/2} = 2\sqrt{x/\pi} , \qquad (19)$$

On the other hand, Liouville (1809-1882) formally extended the formula for the derivative of integral order n

$$D^n e^{ax} = a^n e^{ax} \Rightarrow D^\alpha e^{ax} = a^\alpha e^{ax}, \ \alpha - arbitrary\, order , \qquad (20)$$

Using the series expansion of a function, he derived the formula known as *Liouville`s first formula for fractional derivative,* where α may be rational, irrational or complex.

$$D^\alpha f(x) = \sum_{n=0}^\infty c_n a_n^\alpha e^{a_n x} , \qquad (21)$$

where

$$f(x) = \sum_{n=0}^\infty c_n \exp(a_n x), \ \mathrm{Re}\, a_n > 0 , \qquad (22)$$

However, it can be only used for functions of the previous form. Also, Liouville formulated another definition of a fractional derivative based on the Gamma function (see below) such as:

$$D^\alpha x^{-\beta} = (-1)^\alpha \frac{\Gamma(\alpha+\beta)}{\Gamma(\beta)} x^{-\beta-\alpha}, \ \beta > 0 , \qquad (23)$$

which is known as *Liouville`s second definition of fractional derivative.*Also his second definition is useful only for rational functions.Neither of his definitions was found to be suitable for a wide class of definitions.The derivative of constant function $\beta = 0$ is zero because $\Gamma(0) = \infty$. On the other hand, the Lacroix definition gives:

$$D^\alpha 1 = \frac{1}{\Gamma(1-\alpha)} x^{-\alpha} \neq 0, , \qquad (24)$$

But,Lacroix's method could not be applied to many functions, so was not useful in a broad context. The modern epoch started in 1974 when a consistent formalism of the fractional calculus had grown to such extent, that in 1974 the first conference was held in New Haven. In the same year the first book on fractional calculus by Oldham and Spanier [15] was published after a joint collaboration starting in 1968. Applications of FC are very wide nowadays, in rheology, viscoelasticity, acoustics, optics, chemical physics, robotics, control theory of dynamical systems, electrical engineering, bioengineering and so on, [14-18].The main reason for the success of applications FC is that these new fractional-order models are more accurate than integer-order models, i.e. there are more degrees of freedom in the fractional order model. Furthermore, fractional derivatives provide an excellent instrument for the description of memory and hereditary properties of various materials and processes due to the existence of a "memory" term in a model. This memory term insure the history and its impact to the present and future.

3.2. Fundamentals of fractional calculus

Fracional calculus is a name for the theory of integrals and derivatives of arbitrary order, which unify and generalize the notions of integer-order differentiation and n-fold integration. At present, based on the different background and purpose there are some other definitions of FC. There exist today many different forms of fractional integral operators, ranging from divided-difference types to infinite-sum types, Riemann-Liouville fractional derivative, Grunwald–Letnikov fractional derivative, Caputo's, Weyl's and Erdely-Kober left and right fractional derivatives and so on, Kilbas *et al.*[16]. At first, one can generalize the differential and integral operators into one fundamental D_t^p operator t which is known as fractional calculus:

$$
{}_aD_t^p = \begin{cases} \dfrac{d^p}{dt^p} & \Re(p) > 0, \\ 1 & \Re(p) = 0, \\ \displaystyle\int_a^t (d\tau)^{-p} & \Re(p) < 0. \end{cases}
\tag{25}
$$

The two definitions generally used for the fractional differintegral are the Grunwald-Letnikov (GL) definition and the Riemann-Liouville (RL) definition [14-16]. The original Grunwald-Letnikov definition of fractional derivative is given by a limit, i.e

$$
{}_aD_t^p f(t) = \lim_{h \to 0} \frac{1}{h^p} \sum_{j=0}^{[(t-a)/h]} (-1)^j \binom{p}{j} f(t-jh) ,
\tag{26}
$$

where a, t are the limits of operator and [x] means the integer part of x . Integral version of GL is defined by

$$
{}_aD_t^p f(t) = \sum_{k=0}^{n-1} \frac{f^{(k)}(0) t^{-p+k}}{\Gamma(-p+k+1)} + \frac{1}{\Gamma(n-p)} \int_a^t \frac{f^{(n)}(\tau)}{(t-\tau)^{p-n+1}} d\tau,
\tag{27}
$$

The Riemann-Liouville definition of fractional derivative is given by

$$_aD_t^p f(t) = \frac{1}{\Gamma(n-p)} \frac{d^n}{dt^n} \int_a^t \frac{f(\tau)}{(t-\tau)^{p-n+1}} d\tau, \tag{28}$$

for ($n-1 < p < n$) and for the case of ($0 < p < 1$), the fractional integral is defined as

$$_0D_t^{-p} f(t) = \frac{1}{\Gamma(p)} \int_0^t \frac{f(\tau)}{(t-\tau)^{1-p}} d\tau, \tag{29}$$

where $\Gamma(.)$ is the well known Euler's gamma function. Also, the *chain rule* has the form

$$\frac{d^\beta f(g(t))}{dt^\beta} = \sum_{k=0}^\infty \binom{\beta}{k}_\Gamma \left(\frac{d^{\beta-k}}{dt^{\beta-k}} 1 \right) \frac{d^k}{dt^k} f(g(t)) \tag{30}$$

Where $k \in \square$ and $\binom{\beta}{k}_\Gamma$ are the coefficients of the generalized binomial

$$\binom{\beta}{k}_\Gamma = \frac{\Gamma(1+\beta)}{\Gamma(1+k)\Gamma(1-k+\beta)} \tag{31}$$

For convenience, Laplace domain is usually used to describe the fractional integro-differential operation for solving engineering problems. The formula for the Laplace transform of the RL fractional derivative has the form:

$$\int_0^\infty e^{-st} {}_0D_t^p f(t) dt = s^p F(s) - \sum_{k=0}^{n-1} s^k {}_0D_t^{p-k-1} f(t)_{|t=0} \tag{32}$$

In practical applications, the initial conditions ${}_0D_t^{p-k-1} f(t)_{|t=0}$ are frequently not available. Also, Caputo,[20] has proposed that one should incorporate the integer order (classical) derivative of function x, as they are commonly used in initial value problems with integer-order equations. In that way, one can use the derivatives of the Caputo type such as:

$$_0^C D_t^p [f(t)] = \frac{d^p f}{dt^p} = \frac{1}{\Gamma(1-p)} \int_0^t \frac{f^{(1)}(\tau)}{(t-\tau)^p} d\tau \ , 0 < p < 1 \ , \ f^{(1)}(\tau) = df/d\tau \tag{33}$$

From definition of Riemann-Liouville and Caputo derivatives one may observe that the relation between the two fractional derivatives is as follows:

$$_0^C D_t^p [f(t)] = {}_0D_t^p \left[(f - T_{n-1}[f])(t) \right] \ , \tag{34}$$

where $T_{n-1}[f]$ is the Taylor polynomial of order $(n-1)$ for f, centered at 0. So, one can specify the initial conditions in the classical form

$$f^{(k)}(0) = f_0^{(k)}, \quad k = 0,1,...,n-1, \tag{35}$$

The two Riemann-Liouville and Caputo formulation coincide when the initial conditions are zero. For numerical calculation of FC one can use relation which has the following form:

$$_{((t-L))}D_t^{\pm p} f(t) \approx h^{\mp p} \sum_{j=0}^{N(t)} b_j^{(\pm p)} f(t-jh), \quad b_0^{(\pm p)} = 1, \quad b_j^{(\pm p)} = \left(1 - \frac{1 \pm p}{j}\right) b_{j-1}^{(\pm p)} \tag{36}$$

where L is the *"memory length"*, h is the step size of the calculation, $N(t) = \min\left\{\left[\frac{t}{h}\right], \left[\frac{L}{h}\right]\right\}$ $[x]$ is the integer part of x and $b_j^{(\pm p)}$ is the binomial coefficient.

3.3 Electroviscoelasticity of Liquid/Liquid Interfaces: Fractional-Order Model

Also, number of theories that describe the behavior of liquid-liquid interfaces have been developed and applied to various dispersed systems e.g., Stokes, Reiner-Rivelin, Ericksen, Einstein, Smoluchowski, Kinch, etc. According to this model liquid-liquid droplet or droplet-film structure (collective of particles) is considered as a macroscopic system with internal structure determined by the way the molecules (ions) are tuned (structured) into the primary componentns of a cluster configuration. How the tuning/structuring occurs depends on the physical fields involved, both potential (elastic forces) and nonpotential (resistance forces). All these microelements of the primary structure can be considered as electromechanical oscillators assembled into groups, so that excitation by an external physical field may cause oscillations at the resonant/characteristic frequency of the system itself (coupling at the characteristic frequency),[21-24]. Up to now, there are three possible mathematical formalisms discussed related to the theory of electroviscoelasticity,where the first is tension tensor model, the second is Van der Pol derivative model,and the third model presents an effort to generalize the previous Van der Pol equation, i.e. the ordinary time derivative and integral are now replaced with corresponding fractional-order time derivative and integral of order $p < 1$. Hence, the study of the electro-mechanical oscillators is based on electromechanical and electrodynamic principles. At first, during the droplet formation it is possible that the serial analog circuits are more probable, but later, as a consequence of tuning and coupling processes the parallel circuitry become dominant. Also, since the transfer of entities by tunneling (although with low energy dissipation) is much less probable it is sensible to consider the transfer of entities by induction (medium or high energy dissipation). A nonlinear differential equation of the Van der Pol type represents the initial electromagnetic oscillation

$$C\frac{dU}{dt} + \left(\frac{U}{R} - \alpha U\right) + \gamma U^3 + \frac{1}{L}\int U dt = 0, \tag{37}$$

where U is the overall potential difference at the junction point of the spherical capacitor C and the plate, L is the inductance caused by potential difference, and R is the ohmic resistance. The α and γ are constants determining the linear and nonlinear parts of the

characteristic current and potential curves. The noise in this system, due to linear amplification of the source noise, causes the oscillations of the "continuum" particle (molecule surrounding the droplet or droplet-film structure), which can be represented by the particular integral

$$C\frac{dU}{dt}+\left(\frac{1}{R}-\alpha\right)U+\gamma U^3+\frac{1}{L}\int Udt+ = -2A_n\cos\omega t ,\qquad(38)$$

where ω is the frequency of the incident oscillations, [21]. The noise output appears as an induced anisotropic effect. In an effort to generalize the previous equation the ordinary time derivative and integral are now replaced with corresponding fractional-order time derivative and integral of order p,[22]. Here, the capacitive and inductive elements, using Riemann-Liouville definition of differintegral forms, fractional–order $p\in[0,1)$ enable formation of the fractional differintegral equation, i.e. more flexible or general model of liquid-liquid interfaces behaviour, as follows (linear case):

$$C_0D_t^p\left[U(t)\right]+\left(\frac{1}{R}-\alpha\right)U+\frac{1}{L}\,_0D_t^{-p}\left[U(t)\right]=i(t) ,\qquad(39)$$

Using Laplace transform of (39) leads to

$$G(s)=\frac{U(s)}{i(s)}=\frac{s^p}{Cs^{2p}+(1/R-\alpha)s^p+1/L}=s^pG_3(s),\ G_3(s)=\frac{1}{as^{2p}+bs^p+c},\quad(40)$$
$$a=C,\,b=(1/R-\alpha),\,c=1/L$$

The term-by-term inversion, based on the general expansion theorem for the Laplace transform, [2] produces

$$G_3(t)=\frac{1}{a}\sum_{k=0}^{\infty}\frac{(-1)^k}{k!}\left(\frac{c}{a}\right)^k t^{2p(k+1)-1}E_{p,2p+pk}^{(k)}(-\frac{b}{a}t^p) ,\qquad(41)$$

where $E_{\lambda,\mu}(z)$ is the Mittag-Leffler function in two parameters.Laplace transform of the Mittag-Leffler function in two parameters is:

$$\int_0^{\infty}e^{-t}t^{\beta-1}E_{\alpha,\beta}(zt^{\alpha})dt=\frac{1}{1-z},\ \ (|z|<1) ,\qquad(42)$$

Using inverse Laplace transform of $G(s)$ one can obtain an explicit representation of the solution (39) such as:

$$U(t)=\int_0^t G(t-\tau)i(\tau)d\tau ,\qquad(43)$$

So,the initial electromagnetic oscillation is represented by the equation (43) i.e, a (non)homogeneous solution (Fig.9) may be obtained in following manner using numerical procedure (Grunwald definition). Also, one can obtain equivalent nonlinear problem applying differentiation of (37) such as:

$$C\frac{d^2U}{dt^2}+\left(\frac{1}{R}-\alpha+3\gamma U^2\right)\frac{dU}{dt}+\frac{1}{L}U=0\,,\tag{44}$$
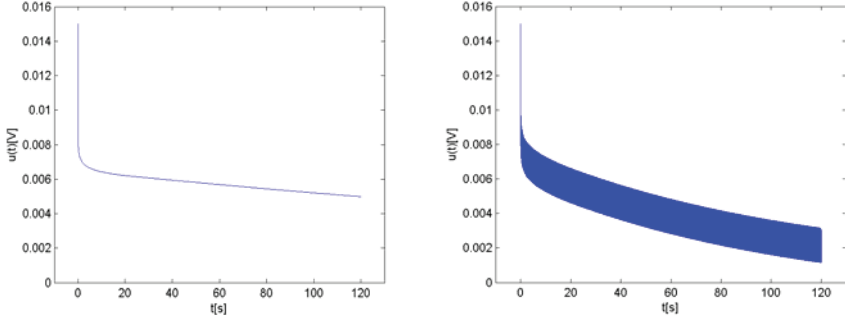
homogenous case   Fig.9   *nonhomogenous case*

$\alpha=0.9995\ Uo=15mV,$ $\alpha=0.95\ Uo=15mV,\ p=0.95,r=0.95$

$p=0.95,T=0.001s$ $T=0.01s\ An=0.05mm$

Taking into account of Caputo definition [4] and introducing vector

$$x_1(t)=U(t),\ x_2(t)={}_0D_t^C U(t),\ \ p\in\square\ \ \boldsymbol{x}(t)=\left(x_1,x_2\right)^T,\tag{45}$$

one can get:

$${}_0D_t^p\boldsymbol{x}(t)=\begin{bmatrix}0 & 1\\ -1/LC & -(1/R-\alpha)/C\end{bmatrix}\begin{Bmatrix}x_1(t)\\ x_2(t)\end{Bmatrix}+\begin{bmatrix}0 & 0\\ 0 & -3\gamma x_1^2(t)/C\end{bmatrix}\begin{Bmatrix}x_1(t)\\ x_2(t)\end{Bmatrix},\tag{46}$$

It is easily observed that previous case is a one of the general case for this nonlinear problem which can be obtained in the form:

$${}_0^C D_t^p\boldsymbol{x}(t)=f\left(t,\boldsymbol{x}(t)\right)\ \boldsymbol{x}^{(k)}(0)=\boldsymbol{x}_0^{(k)},\ \ k=0,1,...,\left[p\right],\tag{47}$$
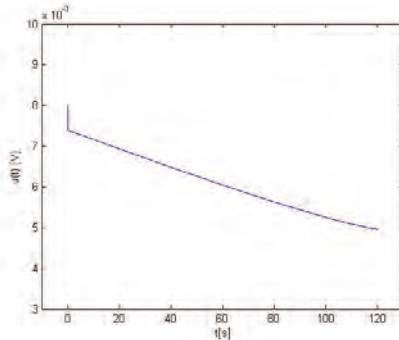
Fig. 10. Homogeneous solution of (Eq. 37)

The initial electromagnetic oscillation is represented by the non linear fractional differential equation (39), homogeneous solution may be obtained using numerical calculation of Caputo derivative and predictor-corrector algorithm as it is shown in Fig.10. The calculation has been done for the following parameters:

$$\alpha = 8 \cdot 10^{-7}, Uo = 8mV, \quad p = 1.2, T = 0.004\,s, \gamma = 3 \cdot 10^{-3}$$

3.4 Iterative learning feedback control algorithms of $PI^{\alpha}D^{\beta}$ type in process control systems

In classical control theory, state feedback and output feedback are two important techniques in system control. Also, in recent years, there has been a great deal of study to overcome limitations of conventional controllers against uncertainty due to inaccurate modelling and/or parameter variations. As one of alternatives, the iterative learning control (ILC) method has been developed [25], where the concept of ILC was originally proposed by Arimoto [26] for accurate tracking of robot trajectories. Motivated by human learning, the basic idea of iterative learning control is to use information from previous executions of the task in order to improve performance from trial to trial in the sense that the tracking error is sequentially reduced. Therefore, iterative learning control requires less *a priori* knowledge about the controlled system in the controller design phase and also less computational effort than many other kinds of control. The basic strategy is to use an iteration of the form:

$$u_{i+1}(t) = f(u_i(t), e_i(t)), \quad _i(t) = y_d(t) - y_i(t),\tag{48}$$

where $f(.,.)$ defines the learning algorithm and remains to be specified, $y_i(t)$ is the output at the ith operation resulting from the input $u_i(t)$ and $y_d(t)$ represents the desired output. The new control input $u_{i+1}(t)$ should make the system closer to the desired result in the next execution cycle. Here, it is suggested the learning control scheme comprises two types of control laws: a $PI^{\alpha}D^{\beta}$ feedback law and a feed-forward control law,[27]. In the feedback loop, the $PI^{\alpha}D^{\beta}$ controller provides stability of the system and keeps its state errors within uniform bounds. In the feed-forward path, a learning control rule/strategy is exploited to track the entire span of a reference input over a sequence of iterations i.e:

$$\boldsymbol{u}_{i+1}(t) = f(\boldsymbol{u}_i(t), \boldsymbol{e}_i(t), \boldsymbol{e}_i^{(\alpha)}(t)), 0 < \alpha \le 1\tag{49}$$

where $u_i(t)$ is the control vector at the i-the iteration, while $e_i(t) = y_d(t) - y_i(t)$, is the tracking error signal between the desired signal $y_d(t)$ and the actual output trajectory one $y_i(t)$ at the i-the iteration. Here, $t \in [0,T]$, where T presents terminal time which is known and finite. Here, it is considered the non-integer (fractional) linear system described in the form of state space and output equations.

$$x_i^{(\alpha)}(t) = Ax_i(t) + Bu_i(t), \; x_i(0) = x_d(0) = 0, \quad 0 < \alpha < 1$$
$$y_i(t) = Cx_i(t),$$

(50)

where is $f(.,.)$ fractional order derivative, A,B, and C are matrices with appropriate dimensions. Here, it is suggested the learning control scheme which comprises two types of control laws: a PD^α feedback law and a feed-forward control law (Fig.11). In the feedback loop, the $PI^\alpha D^\beta$ controller provides stability of the system and keeps its state errors within uniform bounds.
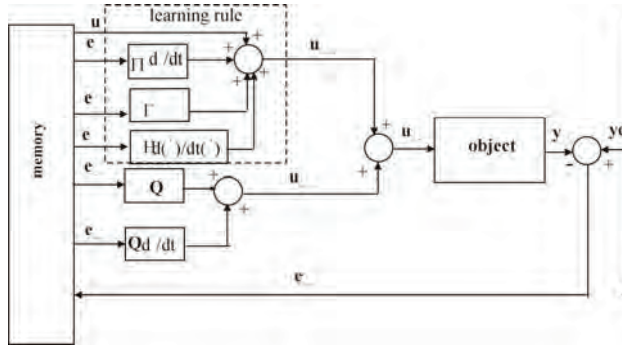
Figure11. Block diagram of $PI^\alpha D^\beta$ iterative learning feedback control for a LTI system

Here, it is introduced feedback control as follows:

$$u_{fbi+1}(t) = Q(D_t^\alpha e_{i+1}(t) + \gamma e_{i+1}(t)),$$

(51)

and in feed-forward it is proposed a new $PI^\beta D^\alpha$ -type ILC updating law for given system such as:

$$u_{fi+1}(t) = u_i(t) + \Gamma e_i(t) + \Pi_0 D_t^\alpha e_i(t) + H_0 D_t^{-\beta} e_i(t),$$

(52)

and

$$u_{i+1}(t) = u_{fi+1}(t) + u_{fbi+1}(t),$$

(53)

where Q, Γ, Π, H are gain matrices appropriate dimensions, where $\gamma > 0$ is real constant; $u_{fb}(t)$ the feedback control input, $u_f(t)$ the feed-forward input; $u(t)$ the value of the function at time t . A sufficient condition for convergence of a proposed feedback ILC is given by the main theorem and proved as follows.

Main theorem: Suppose that the update law Eqs.(51-53), is applied to the system (50) and the initial state at each iteration satisfies (50). If matrices Π, Q , exist such that

$$\left\| [I - \Pi CB][I - D] \right\| \le \rho < 1,$$

(54)

then,   when $i \to \infty$ the   bounds   of   the   tracking   errors $\|x_d(t) - x_i(t)\|, \|y_d(t) - y_i(t)\|, \|u_d(t) - u_i(t)\|,$ converge asymptotically to zero.

3.5. Finite time stability analysis of linear autonomous fractional order systems with delayed state –example PD^α fractional control of robotic time delay systems

The problem of time delay system has been discussed over many years and time delay is very often encountered in different technical systems. The existence of pure time delay, regardless of its presence in a control and/or state, may cause undesirable system transient response, or generally, even an instability. Here, another approach is presented, i.e system stability from the non-Lyapunov point of view is considered. In practice one is not only interested in system stability (e.g. in the sense of Lypunov), but also in bounds of system trajectories. A system could be stable but still completely useless because it possesses undesirable transient performances. Thus, it may be useful to consider the stability of such systems with respect to certain subsets of state-space which are defined a priori in a given problem. Besides that, it is of particular significance to concern the behavior of dynamical systems only over a finite time interval. Recently, there have been some advances in control theory of fractional differential systems for stability questions. However, for fractional order dynamic systems, it is difficult to evaluate the stability by simply examining its characteristic equation either by finding its dominant roots or by using other algebraic methods. The problem of sufficient conditions is examined that enable system trajectories to stay within the a priori given sets for the particular class of linear fractional order time-delay systems in state space form. A linear, ordinary, multivariable time-delay system can be represented by differential equation:

$$\frac{dx(t)}{dt} = A_0 x(t) + A_1 x(t - \tau), \tag{55}$$

and with associated function of initial state:

$$x(t) = \psi_x(t), \quad -\tau \le t \le 0, \tag{56}$$

or
$$\|\psi\|_C = \max_{-\tau \le \theta \le 0} \|\psi(\theta)\| \tag{57}$$

where $\tau > 0$ is a pure time delay. Dynamical behavior of an autonomous system (55) is defined over time interval $J = \{t_o, t_o + T\}$, . Time invariant sets, used as bounds of system trajectories, are assumed to be open, connected and bounded. Let index $"\varepsilon"$ stands for the set of all allowable states of system and index $"\delta"$ for the set of all initial states of the system, such that the set $S_\delta \subseteq S_\varepsilon$,and $S_\rho = \left\{x : \|x(t)\|_Q^2 < \rho\right\}$, where Q is assumed to be symmetric, positive definite, real matrix. It is assumed that the usual smoothness conditions are present so that there are no difficulties with questions of existence, uniqueness, and continuity of solutions with respect to initial data. Here, it presented a result of sufficient conditions that enable system trajectories to stay within the a priori given sets for the particular class of linear autonomous fractional order time-delay

systems.System given by (55) satisfying initial condition (56) is finite stable w.r.t $\{t_o, J, \delta, \varepsilon, \tau\}$, $\delta < \varepsilon$ if and only if:

$$\|\psi_x\|_C < \delta \tag{58}$$

implies:

$$\|x(t)\| < \varepsilon, \qquad \forall t \in J \tag{59}$$

where δ is a real positive number $\varepsilon \in R$, $\delta < \varepsilon$.

Here, it is considered a class of fractional linear autonomous system with time delay described by the state space equation:

$$\frac{d^\alpha \mathbf{x}(t)}{dt^\alpha} = A_0 \mathbf{x}(t) + A_1 \mathbf{x}(t-\tau) \tag{60}$$

with associated function of initial state (57), where it is discussed the case $0 < \alpha < 1$.

Main theorem [28]:

A) Autonomous system given by (60) satisfying initial condition (57) is finite time stable w.r.t. $\{\delta, \varepsilon, \tau, t_o, J,\}$, $\delta < \varepsilon$, if the following condition is satisfied:

$$\left[1 + \frac{\sigma_{\max}^A (t-t_0)^\alpha}{\Gamma(\alpha+1)}\right] \cdot e^{\frac{\sigma_{\max}^A (t-t_0)^\alpha}{\Gamma(\alpha+1)}} \leq \varepsilon / \delta, \quad \forall t \in J. \tag{61}$$

where $\sigma_{\max}(.)$ being the largest singular value of matrix (.), namely:

$$\sigma_{\max}^A = \sigma_{\max}(A_0) + \sigma_{\max}(A_1), \tag{62}$$

Here, particular attention is paid to the finite time stability of robotic system *Newcastle robot* where a time delay appears in PD^α fractional control system,[29].The equation of motion of Newcastle robot with one degree of freedom in case of PD^α controller is:

$$m\ddot{q}(t) + c\dot{q}(t) + kq(t) =$$
$$= Q_d(t) + K_p \left[q_d(t-\tau) - q(t-\tau)\right] + K_d \left[q_d^{(\alpha)}(t-\tau) - q^{(\alpha)}(t-\tau)\right] \tag{63}$$

For the small $y = q_d - q$ perturbation and after linearization leads to the linear time delay-differential equation as follows:

$$\ddot{y}(t) + 2\beta\dot{y}(t) + \omega^2 y(t) = k_p y(t-\tau) + k_d y^{(\alpha)}(t-\tau) \tag{64}$$

So, one may convert some linear equations with commensurate multiple fractional derivatives into linear system of fractional differential equations of low order, one can obtain:

$$D_t^{1/2}\boldsymbol{x}(t) = \begin{bmatrix} 0 & 1 & 0 & 0 \\ 0 & 0 & 1 & 0 \\ 0 & 0 & 0 & 1 \\ -\omega^2 & 0 & -2\beta & 0 \end{bmatrix}\begin{bmatrix} x_1(t) \\ x_2(t) \\ x_3(t) \\ x_4(t) \end{bmatrix} + \begin{bmatrix} 0 & 0 & 0 & 0 \\ 0 & 0 & 0 & 0 \\ 0 & 0 & 0 & 0 \\ k_P & k_D & 0 & 0 \end{bmatrix}\begin{bmatrix} x_1(t-\tau) \\ x_2(t-\tau) \\ x_3(t-\tau) \\ x_4(t-\tau) \end{bmatrix} \qquad (65)$$

In that way using results of previous theorem, one can easily check stability condition for this system. Besides, it is also established new stability result for the particular class of nonlinear perturbed autonomous fractional order time-delay systems described by the state space equation,[30],[31]:

$$\frac{d^\alpha \mathbf{x}(t)}{dt^\alpha} = \left(\mathbf{A}_0 + \Delta\mathbf{A}_0\right)\mathbf{x}(t) + \left(\mathbf{A}_1 + \Delta\mathbf{A}_1\right)\mathbf{x}(t-\tau) + \mathbf{f}_0\left(\mathbf{x}(t)\right), \qquad (66)$$

$$\left\|\mathbf{f}_0\left(\mathbf{x}(t)\right)\right\| \le c_0 \left\|\mathbf{x}(t)\right\|, \quad t \in \left[0, \infty\right) \qquad (67)$$

with the initial functions (57) of the system and vector functions f_0 satisfied (67).

Main theorem: Nonlinear autonomous system given by (66) satisfying initial condition (57) and (67) is finite time stable w.r.t. $\{\delta, \varepsilon, t_o, J,\}$, $\delta < \varepsilon$, if the following condition is satisfied:

$$\left(1 + \frac{\mu_p(t-t_0)^\alpha}{\Gamma(\alpha+1)}\right)e^{\frac{\mu_p(t-t_0)^\alpha}{\Gamma(\alpha+1)}} \le \varepsilon/\delta, \ \forall t \in J \qquad (68)$$

where
$$\mu_{Aoco} = \sigma_{Ao} + \gamma_{\Delta A_0} + c_0,$$
$$\sigma_{A1\Delta} = \sigma_{A1} + \gamma_{\Delta A_1}, \ \mu_p = \mu_{Aoco} + \sigma_{A1\Delta} \qquad (69)$$

4. CONCLUSION

Proposed synergy approach allows resolving redundancy control problem i.e. actuator redundancy, in the framework of optimal control problem which it is solved by Pontryagin`s maximum principle. Also, modeling and resolving kinematic redundancy of (bio)mechanical/robotically system in synergy like fashion, can be achieved using optimization law with suitable kinematic and dynamic criteria which are the function of generalized coordinates, velocities, accelerations and control vectors, respectively. Besides that, model of (bio)mechanical system may be obtained using another biological concept called distributed positioning (DP) which is based on the inertial properties and actuation of joints of considered mechanical system. Also, they are presented other biological principles such as: *principle of minimum interaction* which takes a main role in hierarchical structure of control and *self-adjusting principle* (introduce local positive/negative feedback on control with great amplifying), which allows efficiently

realization of control based on *iterative natural learning.* In the second part of this paper, newly, recently obtained results of author in fields of stability, electroviscoelasticity, and control theory which are based on using fractional calculus are presented. First of them, it is an example within a new theory of electroviscoelasticity, which describes the behavior of electrified liquid-liquid interfaces in fine dispersed systems, and is based on a new constitutive model of liquids: fractional order model -generalized the Van der Pol equation. Also, a new algorithms for fractional iterative learning control (ILC), a $PI^{\alpha}D^{\beta}$ types are proposed for fractional time (delay) systems are also presented. At last, new stability test procedure (finite time and practical stability) is shown for (non)linear (non)homogeneous time-invariant fractional order time delay systems where sufficient conditions of this kind of stability are derived.

REFERENCES

1. Bernstein A,The Coordination and regulation of movements,Oxford Perg,1967,pp.77-92..

2. Bar-Cohen Y, *Biomimetics-Biologically inspired techologies*, CRC Press, Taylor & Francis Group, Boca Raton,FL , 2006,pp.399-425.

3. Potkonjak V., M. Popović ,M. Lazarević and J. Sinanović, *Redundancy problem in writing: from human to anthropomorphic robot arm*, IEEE Trans. on Systems,Man and Cybernetics:part B: Cybernetics, vol.28, No.6, December,(1998), pp.790-805..

4. Northrup S., N. Sarkar, K. Kawamura, *Biologically-Inspired Control Architecture for A Humanoid Robot*,IEEE/RSJ Intern. Conf. on Intelligent Robots and Systems, October, 2001.

5. Nakamura, H. Hanafusa,*Task priority based redundancy control of robot manipulators*, In Robotics research the second int. Symposium Cambridge, MIT Press,1985.pp.155-162.

6. Harkegard O, S. T. Glad,Resolving actuator redundancy-optimal control vs. control allocation, Automatica 41,2005, pp.137-144.

7. Lazarević M., A. Obradović, Lj.Bučanović,M. Joka,Biologically inspired optimal control of robotic system:synergy approach, RoboticsII-MED'09 ,17th Mediterranean Conference on Control and Automation,Thesalloniki,Greece,2009.

8. Lazarević M., Mathematical modeling and control of redundant systems-biomechanical approach, Zadužbina Andrejević,2004,Beograd.

9. Lazarević M.,Optimal control of redundant robots in human-like fashion:general considerations,FME Trans.,Faculty of Mechanical Engineering, University of Belgrade, Vol.33,No.2, 2005, pp.53-64.

10. Potkonjak, V. *Distributed Positioning for Redundant Robotic Systems,* Robotica Cambrige Univ. Press, Vol.8, No.1, pp.61-67,1990a.

11. Tomović R., D.Popović and R. Stein,*Nonanalytical Methods for Motor Control*, World Sc.,London,1995,pp.40-45.12]A. Bilard, A. J. Ijspeert,*Biologically inspired neural controller for engine control in a quadruped robot*, IEEE-INNS-ENNS Internationally Joint Conference on Neural Networks (IJCNN'00), Volume 6, 2000.

12. LurieI.,*Analytical Mechanics*, (in Russian), G. Publishing, Moscow, 1961.

13. Podlubny I., *Fractional Differential Equations*, Academic Press,San Diego,1999.

14. Oldham K. B.,J Spanier, *The Fractional Calculus*, Academic Press, New York,1974.

15. Caputo J., Kilbas or Gorenflo, R., Mainardi, F., Fractional Calculus, Integral and Differential Equations of Fractional Order, CISM Lecture Notes, Udine, Italy, Preprint 54 pages, pp. 223-276,2000.

16. Kilbas A., H. Srivastava, J.Trujillo,Theory and applications of fractional differential equations,Elsevier, Amsterdam,2006.

17. Sabatier J., O.Agrawal, J.Atenreiro Machado, Advances in Fractional Calculus, Theoretical Developments and Applications in Physics and Engineering,Springer 2007

18. Lacroix, S. F. 1819, *Traite Du Calcul Differential et du Calcul Integral*,2nd edn.Vol .3 Paris Courcier,409-410,1819.

19. Caputo,M, Linear models of dissipation whose Q is almost frequency independent,Geophys. J. Royal Astronom .Soc., 13, pp.529-539,1967.

20. Spasić, A, Lazarević M, Chapter: Theory of electroviscoelasticity,pp.371-394 in Finely Dispersed Particles:Micro-,Nano-,and Atto-Engineering, Dekker-CRC Press-Taylor& Francis, Boca Raton,Florida, 2006,pp.950.

21. Spasić A., M. Lazarević**,** A new approach to the phenomena at the interfaces of finely dispersed systems, Journal of Colloid and Interface Science,316,(2007), pp.984-995.

22. Lazarević M., A. Spasić, Electroviscoelasticity of Liquid/Liquid Interfaces: Fractional Order Van der Pol Model – New Results**,** 1st International Congress of Serbian Society of Mechanics,10-13, April,Kopaonik, pp.109-117.

23. Lazarević M.**,**A. M. Spasić, Lj. Bučanović, D. Krstić,*Application of fractional calculus to the electroviscoelastic behaviour of liquid/liquid interfaces* ,18-th International Congress of Chemical and Process Engineering,CHISA2008,24-28, August,2008, Praha, Czech Republic,EL-14.

24. Bien Z , J. Xu 1998, *Iterative Learning Control: Analysis, Design*, Integration and Applications, Kluwer Academic Pubishers.

25. Arimoto S., KawamuraS.,Miyazaki F.,1984. *Bettering operation of robots by learning,* Journal. of Robotic Systems, vol. 1, no. 2, pp. 123-140, 1984.

26. Lazarević M.**,**A. M. Spasić, Lj. Bučanović, D. Krstić, *Iterative learning feedback control algorithms of $PI^\alpha D^\beta$ type in process control systems*,18-th International Congress of Chem.and Process Eng.,CHISA2008, 24-28, August, 2008, Praha, Czech Republic,CA-20.

27. Lazarević M.,D.Debeljković,Finite Time Stability Analysis of Linear Autonomous Fractional Order Systems with Delayed State, Asian Journal of Control,Vol.7, No.4,2005, pp.440-447.

28. Lazarević M.,Finite Time Stability Analysis of PD$^\alpha$ Fractional Control of Robotic Time Delay Systems,Journal of Mechanics Research Communications,Vol. 33,Iss.2, March-Apr.,pp.269-279,2006.
29. Lazarević M.,D. Debeljković, Robust Finite Time Stability of Perturbed Nonlinear Fractional Order Time Delay Systems,IFAC Workshop,Ismir,Turkey,17-20 May, 2007, pp.375-382.
30. Lazarević,A.Spasić,Finite-Time Stability Analysis of Fractional Order Time Delay Systems:Gronwall`s Approach, Mathematical and Computer Modelling, 49,2009,475-481.

БИОЛОШКИ ИНСПИРИСАНО УПРАВЉАЊЕ И МОДЕЛИРАЊЕ (БИ)РОБОТСКИХ СИСТЕМА И НЕКЕ ПРИМЕНЕ ФРАКЦИОНОГ РАЧУНА У МЕХАНИЦИ

Михаило П. Лазаревић

Апстракт: *У овом раду, презентоване су примене биолошки инспирисаног моделирања и управљања (био)механичким (не)редундантним механизмима, као и новодобијени резултати аутора у области примењене механике који су засновани на примени рачуна нецелобројног реда. Прво, предложено је коришћење биолошког аналогона-синергије захваљујући постојању непроменљивих одлика у извршавању функционалних покрета. Друго, модел (био)механичког система може се добити применом другог биолошког концепта познатим под називом дистрибуирано позиционирање (ДП), који је заснован на инерцијалним својства и покретању зглобова разматраног механичког система. Такође,предлаже се коришћење других биолошких принципа као што су: принцип минималне интеракције, који има главну улогу у хијерархијској структури управљања и принцип самоподешавања (уводи локалне позитивну/негативну повратну спрегу у управљачкој петљи и то са великим појачањем), који омогућава ефикасно остваривање управљања на бази итеративног природног учења. Такође, нови, недавно публиковани резултати аутора су такође представљени у области стабилности, електро-вискоеластичности и теорији управљања а који су засновани на коришћењу рачуна нецелобројног реда.*

Кључне рчи: *биолошки инспирисани системи, алгоритми управљања, фракциони рачун, стабилност.*

VIBRATIONAL PROPERTIES CHARACTERIZATION OF MOUSE EMBRYO DURING MICROINJECTION

UDC 519.673:531.01

Andjelka N. Hedrih[1], Marinko Ugrčić[2]

[1] State University in Novi Pazar
Vuka Karadžića bb, 36300 Novi Pazar, Serbia
e-mail: handjelka@hm.co.rs

[2] Economics Institute
Kralja Milana, 18, 11000 Belgrade, Serbia
e-mail: ugrcicmarinko@gmail.com

Abstract *To determine the vibration characteristics (natural frequencies and mode shapes) of a mouse embryo during microinjection the modal analysis is used. The spherical mouse embryo 60 μm in diameter is modeled as elastic finite elements biostructure consisting of 6μm thick micromembrane and 38 μm in diameter nucleus. Embryo modeling and modal analysis were based on the use of the finite elements method in the modal analysis system of ANSYS software. The modal analysis was carried out for first six modes of embryo natural frequencies. The numerical analysis of dependence of embryo own frequencies on the boundary conditions and external loads are presented. The relevant illustrations of the typical variations of the shape, deformation and particle velocities of vibrating embryo are given.*

Key words: *modal analysis, vibration properties, mouse embryo, finite elements method.*

1. INTRODUCTION

Although papers on mechanical properties of the oocyte exist (Liu et al, 2010, [1] and on structural parts of mouse embryo (Murayama et al, 2008 [2], 2006) [3], there are very few papers that regard this structure as an oscillatory system Hedrih A. (2011) [4]). Microinjection of the mouse embryo is usually used as an experimental setup for the elastic properties of the biomembrane of the embryo (Murayama et al, 2008 [2], 2006) [3], Sun et al, 2003, [5]). Embryo is placed in a liquid medium –eg HTF (human tubal fluid), in dish. Dish is placed on a heating plate of a special microscope that maintains

the body temperature of the mouse. These are typical conditions (adequate liquid medium and temperature) to keep the embryo alive. Embryo is fixed with vacuum micropipette on one side. On the opposite side is a fine glass micro-needle. See fig.1. This experimental setup could be used for developing software for training embryologists for the special procedure that is used in artificial insemination. This procedure is called intracitoplasmatic sperm injection-ICSI (one sperm cell is injected into oocyte by using a fine glass micro-needle.

Embryo vibrational characterization represents very important researching subject of modern biomechanical engineering. (See ref Ladjal*y* et al, 2011 [6]). A modal analysis is one of possible techniques used to determine the vibration properties (natural frequencies and mode shapes) of a bio structure such as the embryo. Results of modal analysis can also serve as a starting point for another, more detailed, dynamic analysis, such as a transient dynamic analysis in different scenarios, e.g. artificial insemination of human embryo. The natural frequencies and mode shapes are important parameters in the design of a micro-robotic cell manipulation system for dynamic loading conditions [6].

Due to the nature of modal analyses any nonlinearity in material behavior are ignored. Optionally, orthotropic and temperature-dependent material properties may be used. The critical requirement is to define stiffness as well as mass in some form. Stiffness may be specified using isotropic and orthotropic elastic material models (for example, Young's modulus and Poisson's ratio), using hyper-elastic material models (they are linearized to an equivalent combination of initial bulk and shear moduli), or using spring constants, for example. Mass may derive from material density or from remote masses.

The goal activities of researching presented in this paper includes:

– Create robust finite elements model of mouse embryo and basic parts of micro-robotic cell manipulation system (holding pipette, micropipette and liquid environmental medium –human tubal fluid-HTF),
– Set the contacts and boundary conditions that affect the mouse embryo vibrations,
– Run step modal analysis to simulate vibrations of embryo alone and embryo as a part assembly with other components together.
– Determine the vibrational characteristics of mouse embryo free oscillations and embryo oscillations affected by boundary conditions.

Embryo modeling and modal analysis were based on the use of the finite elements method in the modal analysis system of ANSYS WORKBENCH® products.[7]. Parameters for modal analysis were taken from the experimental data from ref [5].

2. THEORY OF MODAL ANALYSIS APPLIED IN FEM

The equations of elastic structural systems without external excitation can be written in the following form:

$$[M]\{\ddot{u}\} + [C]\{\dot{u}\} + [K]\{u\} = \{0\} \tag{1}$$

where is: [M] - structural mass matrix, [C] - structural damping matrix, [K] - structural

stiffness matrix, { ü } - nodal acceleration vector, { u̇ } - nodal velocity vector, and { u } - nodal displacement vector.

It has been recognized that performing computations in the modal subspace is more efficient than in the full eigen space. The stiffness matrix [K] can be symmetrized by rearranging the asymmetric contributions; that is, the original stiffness matrix [K] can be divided into symmetric and asymmetric parts. By dropping the damping matrix [C] and the asymmetric contributions of [K], the symmetric Block Lanczos eigen value problem is first solved to find real eigen values and the corresponding eigen vectors. In the present implementation, the asymmetric element stiffness matrix is zeroed out for Block Lanczos eigen value extraction. Following is the coordinate transformation used to transform the full eigen problem into modal subspace:

$$\{u\} = [\Phi]\{y\} \tag{2}$$

where is: [Φ] – eigen vector matrix normalized with respect to the mass matrix [M] and {y} - vector of modal coordinates
By using equation (2) in equation (1), we can write the differential equations of motion in the modal subspace as follows:

$$[I]\{\ddot{y}\} + [\Phi]^T[C][\Phi]\{\dot{y}\} + \left([\Lambda^2] + [\Phi]^T[K_{asym}][\Phi]\right)\{y\} = \{0\} \tag{3}$$

where is: [Λ^2] - a diagonal matrix containing the first n eigen frequencies ω_i.

Classically damped systems understand the oscillatory motion of an un-forced N degree of freedom elastic structure with viscous damping and given initial conditions. The modal vectors of classically damped systems depend only on [M] and [K], and are independent of [C], regardless of how heavily the system is damped. For classically damped systems, the modal damping matrix [Φ]^T[C][Φ] is a diagonal matrix with the diagonal terms being $2\xi_i\omega_i$, where ξ_i is the damping ratio of the i-th mode. In general, the damping is not classical, [Φ]^T[C][Φ] is not a diagonal matrix, and the natural frequencies, damping ratios, and modal vectors depend on the mass, stiffness, and damping matrices of the structural system. For non-classically damped systems, the modal damping matrix is either symmetric or asymmetric. Asymmetric stiffness contributions of the original stiffness are projected onto the modal subspace to compute the reduced asymmetric modal stiffness matrix [Φ]^T [K$_{asym}$] [Φ].
Introducing the 2n-dimensional state variable vector approach, equation (3) can be written in reduced form as follows:

$$[I]\{\dot{z}\} = [D]\{z\} \tag{4}$$

where is:

$$\{\dot{z}\} = \begin{Bmatrix} \{y\} \\ \{\dot{y}\} \end{Bmatrix} \tag{5}$$

and

$$[D] = \begin{bmatrix} 0 & I \\ -\left[\Lambda^2\right] - \left[\Phi\right]^T \left[K_{asym}\right]\left[\Phi\right] & -\left[\Phi\right]^T \left[C\right]\left[\Phi\right] \end{bmatrix} \qquad (6)$$

The $2n$ eigen values of Equation (4) are calculated using the QR algorithm (Press et al.,1993 [8]). The inverse iteration method (Wilkinson and Reinsch, 1971 [9]) is used to calculate the complex modal subspace eigen vectors. The full complex eigen vectors, $\{\psi\}$, of original system is recovered using the following equation:

$$\{\psi\} = \left[\Phi\right]\{z\} \qquad (7)$$

3. FEM MODELING

In modal analysis the embryo model was considered as three-dimensional axis-symmetric problem. The mouse embryo with basic parts of micro-robotic cell manipulation system described in [9] and shown in Fig. 1 (left) is simplified according the model setup shown in the same figure (right).
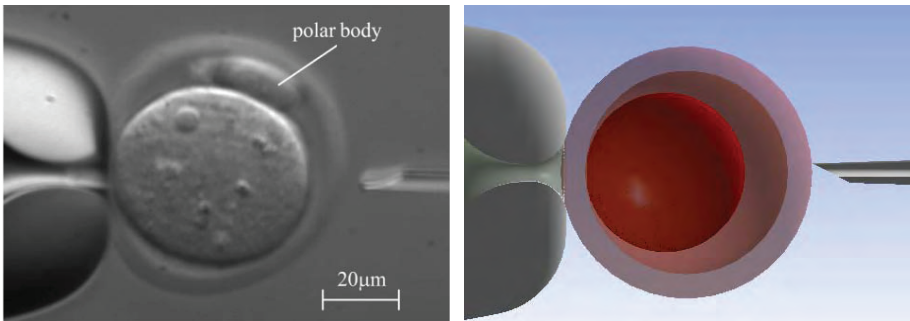
Figure 1. Photograph of cell (left) and simplified model setup of mouse embryo (right).
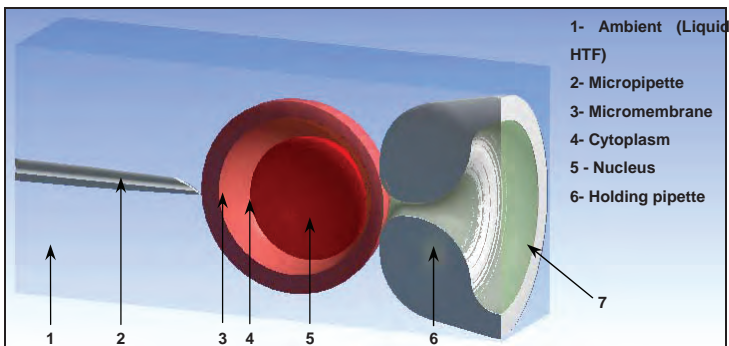
Figure 2. Axial cross-section of 3D model setup for embryo modal analysis.

3.1. Embryo model

The full model setup (Fig. 2) used in the work is consisted of embryo (micromembrane with nucleus and cytoplasm) plunged into the control volume filled with liquid medium HTF. One side of embryo is connected to the holding pipette and the second is in contact with micropipette. For all time the vacuum inside the holding pipette takes the embryo fixed independently on the way of gravity and facilitates embryo manipulation.

The review of model setup parts with used materials and basic physical characteristics is presented in Table 1. The table contains statistic data related to the number of nodes and elements for each component after medium quality meshing procedure (Fig. 3).
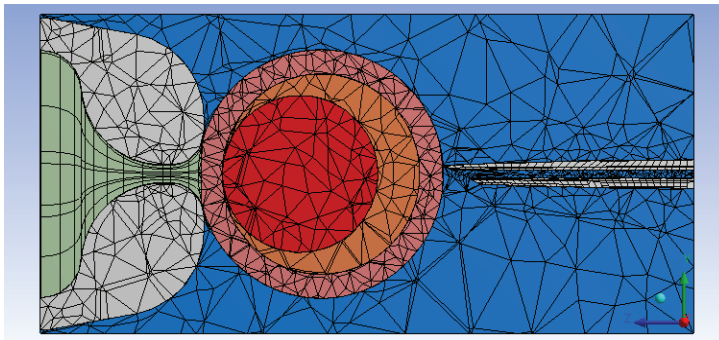
Figure 3. Details of finite elements mesh in the axial cross-section of model.

Table 1. Basic mechanical characteristics of model components with FE statistic data.

	Name	Assignment	Volume	Mass	Nodes	Elements
-	-	-	m^3	kg	-	-
1	Micromembrene	Biomembrene	5.3732E-14	5.4000E-11	7409	4288
2	Nucleus	Nucleus	2.8731E-14	2.9880E-11	685	350
3	Cytoplasm	Cytoplasm	3.0635E-14	3.1033E-11	1287	669
4	Holding pipette	Glass	1.0978E-13	2.7773E-10	3117	1776
5	Micropipette	Glass	1.4847E-15	3.7563E-12	3879	726
6	Vacuum	Air	2.8280E-14	3.4643E-14	1426	276
7	Liquid ambient	HTF	6.9430E-13	7.0333E-10	6953	3825

The initial contact regions and types of supports determine the boundary conditions of the model. All contacts regions of liquid medium HTF with micromembrane, vacuum pipette and micropipette are considered as frictional. For this kind of so-called wet friction the value 0.1 of frictional coefficient is accepted. The identical contact conditions are assumed on the contact surfaces of cytoplasm with nucleus and micromembrane.

From point of view of support boundary conditions, illustrated in Fig. 4, two types: fixed and frictionless supports, are used.
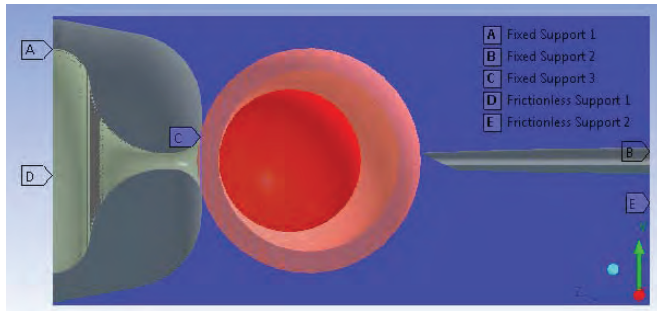
Figure 4. Details of support boundary conditions of model.

The dimensions of boundary box, represented as rectangle surface colored in dark blue in Fig. 4, filled by liquid medium HTF are 1.6E-4×7.7E-5×7.7E-5 m, and affects significantly the natural frequencies of embryo. All outer free faces of box are bonded by frictionless supports (E). Free surface of vacuum inside the holding pipette is bounded by frictionless support (D). Both the holding pipette and micropipette are constrained (fixed supports A and B) from movement in axial directions (*z*-axis).

External loads of the embryo include conservative gravity force and surface force produced by 733.1 Pa vacuum on the air-micromembrane contact region. But in the modal analysis external loads make to be equal zero, so that the embryo is connected to holding pipette along initial contact edge (C).

3.2. Material data

According to the requirements of modal analysis, all materials, including bio materials (biomembrane, nucleus and cytoplasm), then medium materials (air and liquid medium HTF) and, finally, mechanical equipments materials (special glass for medical instruments) are considered as isotropic elasticity features materials.

Table 2. Mechanical characteristics of materials

Material	Density	Reference temperature	Young's modulus	Poisson's ratio	Bulk modulus	Shear modulus
-	kg /m^3	K	Pa	-	Pa	Pa
Biomembrane	1005	310	42400	0.499	7.067E+6	14143
Nucleus	1040	310	7200	0.250	4800	2880
Cytoplasm	1013	310	17200	0.490	2.867E+5	5771,8
Liquid HTF	1013	310	1.32E+8	0.490	2.20e+9	4.430E+7
Air (vacuum)	1.225	310	3.102E+6[2]	0.490[*]	5.17E+7[*]	1.041E+6[*]
Glass	2530	310	5.448E+7	0.300	4.54E+7	2.095E+7

[2] *Given mechanical parameters of air represents the fictive values, adapted to solver requirements. It means, instead adiabatic law the linear pressure-volume dependence was assumed for small variations of air pressure up to 2E+5 Pa.*

The accepted temperature of each part of the model is same and equal to the mice body temperature of 37 °C. As was previously mention this temperature is necessary to keep the embryo alive. Although the temperature is included in the modal analysis, it doesn't take any repercussions on the final results because of the absence of thermal loads or variations of mechanical parameters that would affect the model vibrational behavior.

Mechanical characteristics of the above mentioned materials are given in Table 2.

4. RESULTS AND DISCUSSION

4.1. Natural frequences of embrio

The numerical integration of Eq. 4 facilitates the solutions for elements of diagonal matrix [Λ] containing the first n eigen frequencies ω_i. Computed natural (own) frequences of embryo are given in Table 7.

Table 3. Natural frequencies of free and bonded embryo for first six modes.

Mode n	Natural frequences of embrio ω_i, Hz				
	Free oscillations in vacuum	Free oscillations in liquid HTF	Connection with holding pipette in vacuum	Connection with holding pipette in liquid HTF	Full connection in liquid HTF
1	0	52733	2924.2	52778	52782
2	0.0282	52839	2945.7	52882	52886
3	0.0462	53321	5868.6	53486	53491
4	600.32	54242	11888	54315	54317
5	931.50	55083	19333	55113	55116
6	940.79	55112	19353	55177	55180

The modal distribution of natural frequencies of embryo vs. boundary conditions (Figs. 5 and 6) was designed based on tabular data.
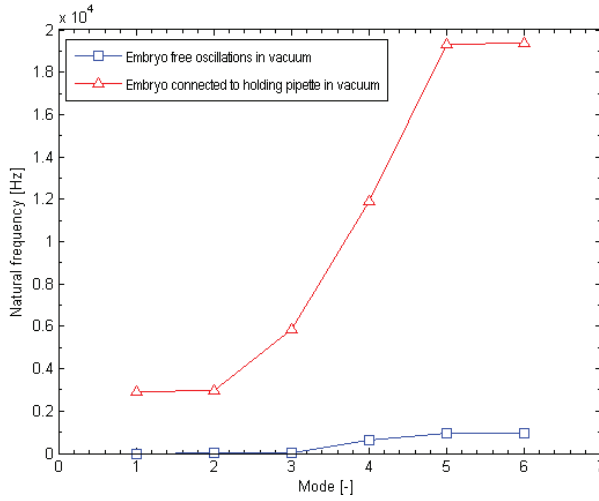
Figure 5. Modal distribution of natural frequencies of embryo vs. boundary conditions
(osillations in vacuum).
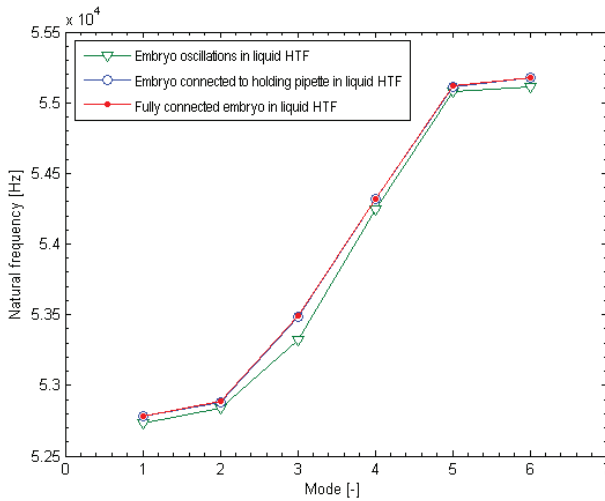
Figure 6. Modal distribution of natural frequencies of embryo vs. boundary conditions
(osillations in liquid medium HTF).

Analysis of calculated results in Table 7 and represented in Figs. 5 and 6 confirms nature
of boundary conditions influence on the natural frequency of embryo. In other words, the
natural frequency of embryo increases continually by involving each further boundary
condition. So, in the case of contact of the embryo and liquid medium HTF the highest
jump of frequency (over 52 KHz) appears and the relevant curves of frequency
distribution are very close to each other (Fig. 6). Maximum frequency of 55180 Hz was
reached for the embryo plunged into liquid medium and connected to micropipette and

vacuum, holding pipette. Besides the above mentioned, the computed results show that oscillations of free embryo in first mode are not practically possible ($\omega_i \approx 0$).

4.2. Typical variations of the vibrating embryo structural parameters

The appearance of scaled shape and fictive velocities distribution for first six modes of natural embryo oscillations are shown in Figs. 7-12.
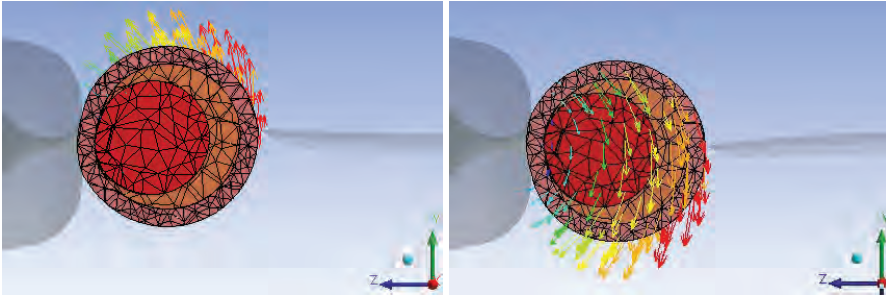
Figure 7. Shape and particle velocities distribution in extreme points of embryo vibrations in mode 1.
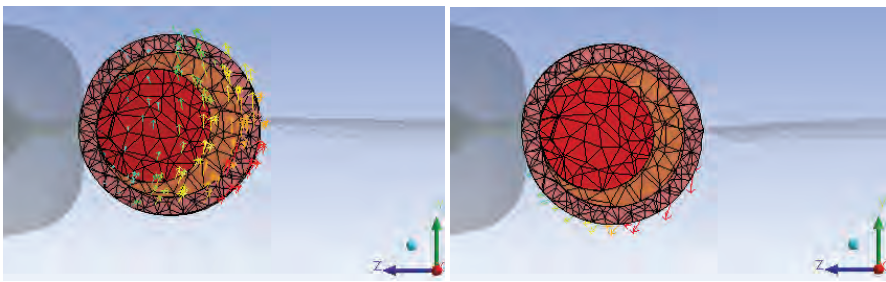
Figure 8. Shape and particle velocities distribution in extreme points of embryo vibrations in mode 2.
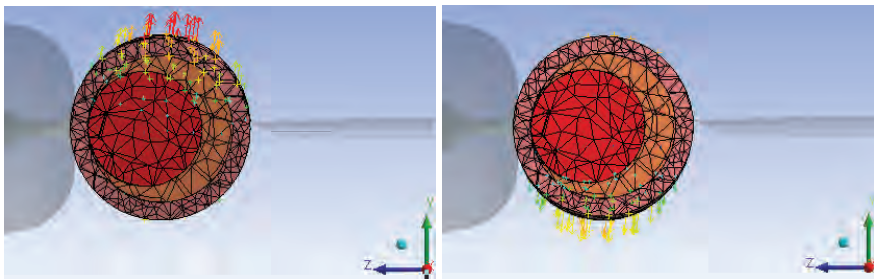
Figure 9. Shape and particle velocities distribution in extreme points of embryo vibrations in mode 3.

Based on Figs. 7 - 12 and performed 3D animations the embryo movement relative to the corresponding mode can be describes as follows:
  - Mode 1: perpendicular oscillations along *y*-axis. Due to initial connections it looks lake rolling in *yz*-plane;

- Mode 2 - perpendicular oscillations along *x*-axis. Due to initial connections it looks lake rolling in *xz*-plane;
- Mode 3 - rotation, i.e. torsion (due to initial connections) about *z*-axis;
- Mode 4 - longitudinal oscillations along *z*-axis;
- Mode 5 - rotation in *yz*-plane; and
- Mode 6 - rotation in *xz*-plane.
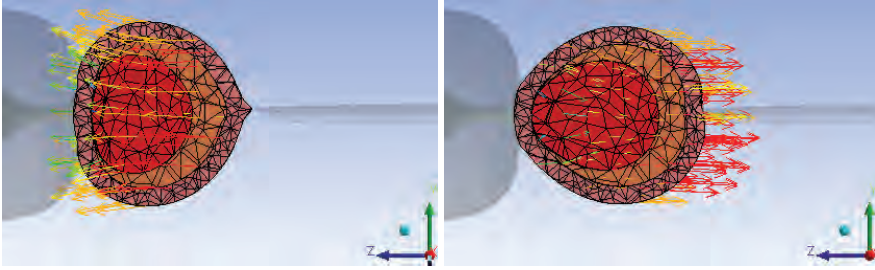
Figure 10. Shape and particle velocities distribution in extreme points of embryo vibrations in mode 4.
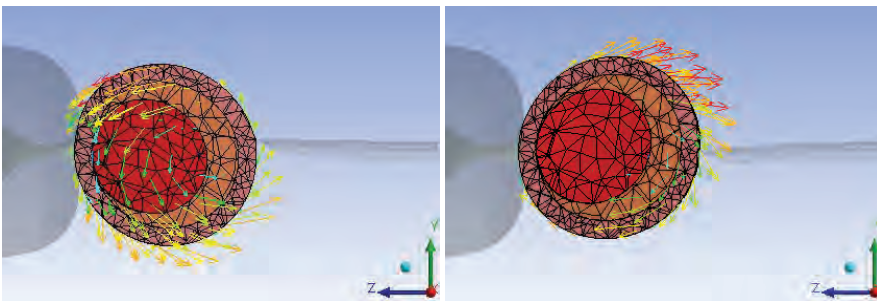
Figure 11. Shape and particle velocities distribution in extreme points of embryo vibrations in mode 5.
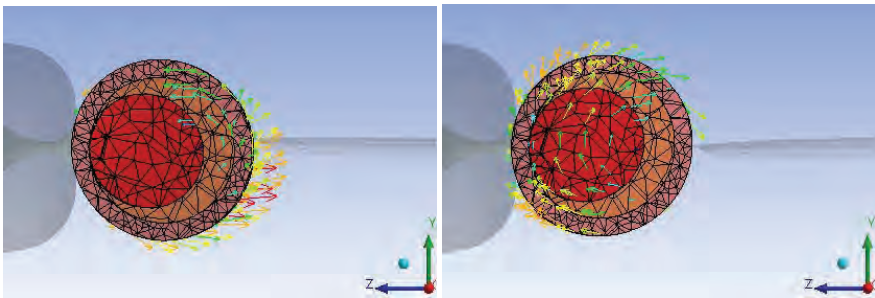
Figure 12. Shape and particle velocities distribution in extreme points of embryo vibrations in mode 6.

Finally, the appearance of scaled shape and fictive deformations for first six modes of natural embryo oscillations are illustrated in Figs. 13-18.
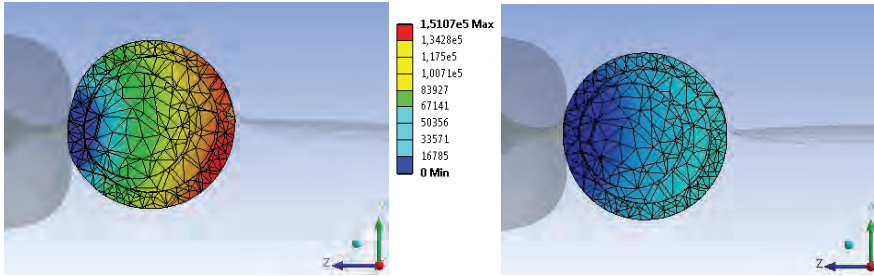
Figure 13. Total deformations in extreme points of embryo oscillations for mode 1 ($\times$ 1.65E-11 m).
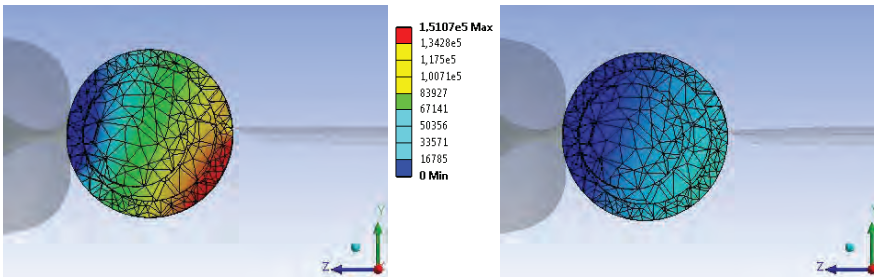
Figure 14. Total deformations in extreme points of embryo oscillations for mode 2 ($\times$ 1.60E-11 m).
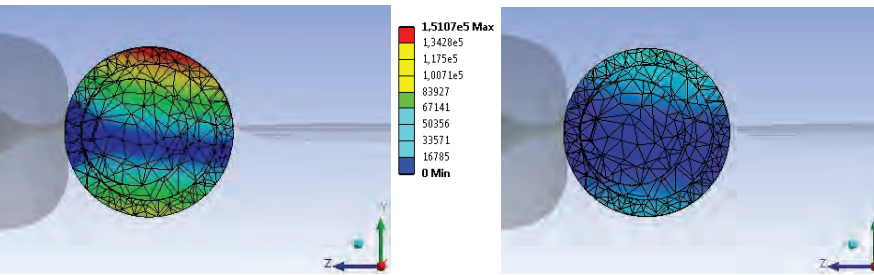
Figure 15. Total deformations in extreme points of embryo oscillations for mode 3 ($\times$ 1.40E-11 m).
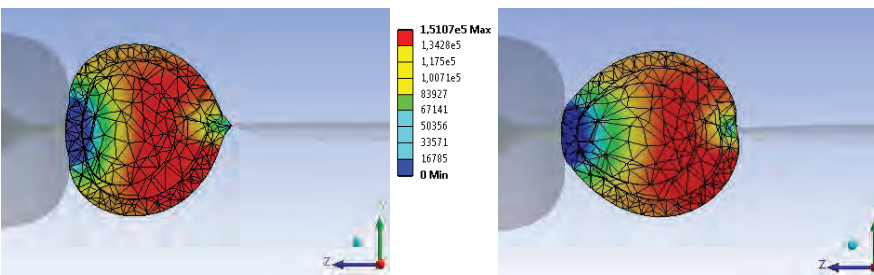
Figure 16. Total deformations in extreme points of embryo oscillations for mode 4 ($\times$ 2.15E-11 m).
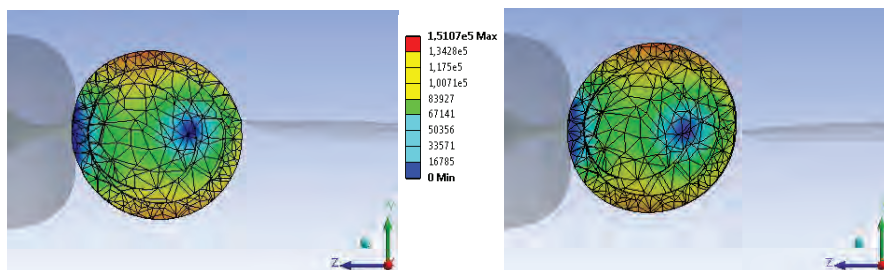
Figure 17. Total deformations in extreme points of embryo oscillations for mode 5 ($\times$ 1.55E-11 m).
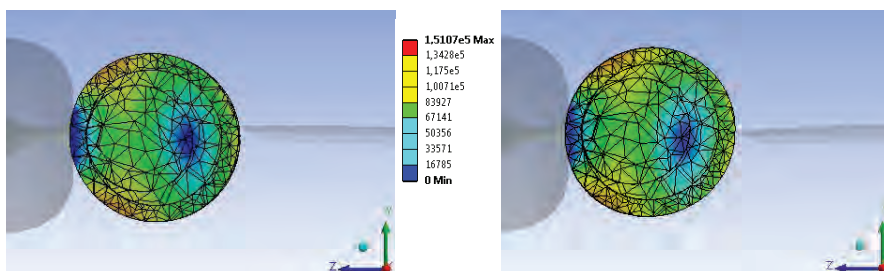
Figure 18. Total deformations in extreme points of embryo oscillations for mode 6 ($\times$ 1.60E-11 m).

Real rate of total deformations are varying from zero up to maximum 3.348 μm (Max 1.5107E+5 $\times$ 2.15E-11 m = 3.348E-6 m) in mode 4.

Ladjal*y et al, 2011[6], used the method of finite elements in modelling the* Microrobotic Simulator for Assisted Biological Cell Injection, but they regarded the cell as a unified structure*. Our model approximates the real phenomenon better as the cell is modelled as a three layer structure (biomembrane, cytoplasm, nucleus). Parameters that were used for the mouse embryo nucleus are approximative since a search of the literature yielded no adeqaute data on the subject. Data that were available to us refer to nuclei of mouse embryo fibroblasts (*Rowat et al, 2008 [10]) *or to the nucleus of amphibian egg cell (*Schaöpe et al, 2009 [11]).

5. CONCLUSION

Based on the results of numerical analysis given in the paper it is shown that the robust finite elements model of mouse embryo with basic parts of ICSI system (holding pipette and micropipette) were correctly created. All necessary contacts and boundary conditions were regularly involved facilitating the modal analysis and numerical simulation of all situations of the embryo vibrations. The determinations of the vibrational characteristics of mouse embryo free oscillations and embryo oscillations affected by boundary conditions for first six modes were successfully carried out.

To summarize, the work presented in the paper confirms possibility to use the finite elements method coupled with numerical modal analysis as powerful tool in the

vibrational characterization of bio structures such as the mouse embryo. This method can be used to analyze vibrational properties of embryos of both mice and humans, and not only in physiological conditions, but also under pathological conditions, for example when artifical insemination is unsucessful, or when the implantation of the embryo does not occur. This opens new possibilities for developing an oscillation theory of reproducation.

References

1. Liu X, Fernandes R, Jurisicova A, Casperb R.F. and Sun Y. (2010) In situ mechanical characterization of mouse oocytes using a cell holding device. *The Royal Society of Chemistry, Lab Chip*, 10, pp.2154–2161.
2. Murayama Y, Yoshida M, Mizuno J, Nakamura H, Inoue S, Watanabe Y et al. (2008) Elasticity Measurement of Zona Pellucida Using a Micro Tactile Sensor to Evaluate embrio Quality. J. Mamm. Ova Res. 25, pp.8-16.
3. Murayama Y, Mizuno J, Kamakura H, FuetaY, Nakamura H, Akaishi H et al. s (2006) Mouse zona pellucida dynamically changes its elasticity during oocyte maturation, fertilization and early embryo development. *Human Cell* **19**, pp. 119–125.
4. Hedrih A. (2011) Modeling oscillations of zona pelucida before and after fertilization. **ENOC** Young Scientist Prize Paper. *EUROMECH Newsletter* 40, Europian Mechanics Society, 40, pp. 6-14.
5. Sun Y., Wan K.T., Roberts K.P., Bischof J.C., Nelson B. J. (2003) Mechanical Property Characterization of Mouse Zona Pellucida, *IEEE Transactions On Nanobioscience*, Vol. 2, **4** pp. 279-286.
6. Ladjaly H, Hanus J-L, Ferreira A. (2011) . "IEEE International Conference on Robotics and Automation, San Francisco: United States " DOI : 10.1109/IROS.2011.6094965.
7. ANSYS AUTODYN (2010) User's Manual *Theory manual*, ANSYS Inc. Southpointe, 275 Technology Drive, Canonsburg, PA, USA.
8. Press W.H., et al., Numerical Recipes in C, (1993) *The Art of Scientific Computing*, Cambridge University Press.
9. Wilkinson J.H., Reinsch C., Linear Algebra, (1971), *Handbook for Automatic Computation*, Springer-Verlag, New York, NY, Vol. II., pp. 418–439.
10. Rowat A.C, Lammerding J, Herrmann H, and Aebi U. (2008) Towards an integrated understanding of the structure and mechanics of the cell nucleus. *BioEssays* 30.3 pp.226–236.

11. Schaöpe J, Prauße S, Radmacher M, and Stick R. (2009) Influence of Lamin A
      on the Mechanical Properties of Amphibian Oocyte Nuclei Measured by Atomic
      Force Microscopy. *Biophysical Journal* 96, pp. 4319–4325.

VIBRACIONE KARAKTERISTIKE EMBRIONA MIŠA TOKOM UBODA MIKROIGLOM

Andjelka N. Hedrih[1], Marinko Ugrčić[2]

[1] State University in Novi Pazar
Vuka Karadžića bb, 36300 Novi Pazar, Serbia
e-mail: handjelka@hm.co.rs

[2] Economics Institute
Kralja Milana, 18, 11000 Belgrade, Serbia
e-mail: ugrcicmarinko@gmail.com

Sažetak. Vibracione karakteristike embriona mogu biti od značaja za procenu njegove vitalnosti. Da bi odredili sopstvene učestalosti i oblike modova oscilovanja embriona miša tokom mikroinjekcije staklenom iglom koristili smo metod konačnih elemenata u okviru modalne analize pomoću ANSYS softvera. Embrion miša dijametra 60 μm modelovan je kao elastična biostruktura sa konačnim brojem elemenata koja se sastoji od biomembrane debljine 6μm I jedra dijametra 38 μm. U radu je prikazano prvih šest modova sopstvenih učestalosti embriona miša kao i zavisnost sopstveih učestaosti embriona od konturnih uslova i spoljašnjeg opterećenja. Tipične varijacije oblika, deformacije i raspodele brzine oscilovanja embriona date su u vidu ilustracia

Ključne reči*: modalna analiza, vibracione karakteristike, embrion miša, metod konačnih elemenata.*

ACTIVE CONTROL OF MECHANICAL STRUCTURES IN RESEARCH AND EDUCATION

UDC 531.2; 531.146; 531.8.

Tamara N. Nestorović

Ruhr-Universität Bochum, AG Mechanik adaptiver Systeme
Universitätsstraße 150, Geb. IA-01/128, D-44801 Bochum, Germany

Abstract. *Several crucial phases of the overall approach to development and design of smart structures are outlined in this paper. They are focused on control of lightweight mechanical structures with respect to active vibration and noise attenuation using piezoelectric actuators and sensors. The research experience and growing interest in development of smart structures have motivated introduction of courses on smart structures at universities, which are being studied extensively and with great interest by young researchers and students. Some of the author's experiences regarding education in this field will be addressed as well.*

Key words: *active structural control, piezoelectric actuators and sensors, system identification.*

1. INTRODUCTION

Active structural control has been intensively investigated in the recent years. It is not only a subject of the scientific and research activities, but due to its extensive application possibilities active control of mechanical structures gains more and more attention in the education and teaching processes. In that way the benefits of the further development and application can be recognized in the early stages, awaking the interest among young future experts to investigate and contribute more in this field.

In this paper a broad field of active structural control is considered within the focused frame regarding control of lightweight mechanical structures with respect to active vibration and noise attenuation using piezoelectric actuators and sensors. An overall approach to active control of piezoelectric structures involves subsequent steps of modeling, control, simulation, experimental verification and implementation. Each of these steps is regarded in more details. Numerical modeling is regarded from the finite element method (FEM) point of view [5−6, 11]. Parameter identification [13, 15, 19] is considered as a complementary approach to obtain representative models for the use in subsequent development steps, e.g. controller design. Active controller design involves optimal [16] and adaptive methods [14], whereas the simulation and verification methods

involve consideration of the real-time applications. Some application examples[3] showing the feasibility of the active structural control are presented (vibration suppression of the car roof, active noise control of the acoustic box).

Studying of active structural control is involved in education and teaching processes at the high-school level as well. This topic addresses especially teaching experiences in the field of adaptronics, mechatronics, mechanics of adaptive systems and control theory.

As an introduction an example of actively controlled vibrations of a clamped beam is explained as a benchmark example presented at the courses on active structural control and mechatronics for the students involved in higher education phases. Subsequently the overall development of smart structures is summarized and illustrated by several application examples.

2. ACTIVE VIBRATION CONTROL OF A CANTILEVER BEAM – AN EDUCATIONAL AND RESEARCH BENCHMARK EXAMPLE

Many scientific and practical, but also educational experiences can be gained by investigation of a clamped beam problem. In this section an overall approach to the vibration suppression of a clamped beam excited at the tip will be described. This example represents a valuable contribution to the educational process, since the vibration control problem formulation and its solution defined in several subsequent logical steps follow the overall approach to smart structures analysis and design procedure and therefore apply as a standard procedure in investigation and control of much more complex smart structures. On the other hand, the problem retains the scientific complexity and opens possibilities for further studies and contributions to the improvement of the problem solution.

The investigated clamped beam is considered as an active plate structure controlled by four piezoelectric patch actuators attached to the beam, two on the top and two on the bottom of the plate. Geometry of a standard beam including piezo patches as actuators and/or sensor is represented in Fig.1. The material properties of the beam and piezo electric material are listed in Table 1. In the first step the plant was represented in the form of a finite element model with a mesh of 235 passive and 80 active Semiloof shell elements [2, 5]. On the basis of this mesh the eigenfrequencies and eigenmodes are calculated using a numerical procedure supported by some standard finite element software. The eigenmodes can be determined experimentally as well, using the modal analysis approach. The eigenfrequencies of interest for bending mode case studies are considered in the subsequent investigations. Exciting forces $F(t)=A\sin(\omega_i t)$ exerted on the corner points at the tip of the beam are chosen with regard to the eigenfrequencies of interest.

An experimental rig with the clamped cantilever beam and dSPACE system, which can be used for the modal analysis and control purposes, is shown in Fig. 2.

---

235 passive Semiloof shell elements
80 active Semiloof shell elements

4 x actuators

Sensor

F(t)   F(t)
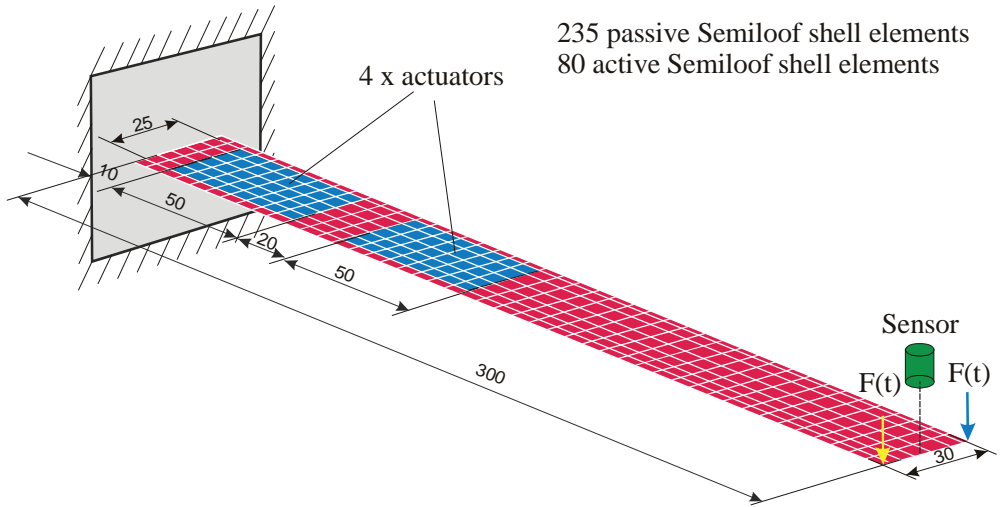
Fig. 1 Geometry and dimensions of the clamped beam with finite element mesh

Table 1. Material properties

Beam	$E = 2.00 \cdot 10^5$ N/mm^2	Piezo	$E_{11} = E_{22} = 3.77 \cdot 10^4$N/mm^2
	$\nu = 0.3$		$G_{12} = 1.3 \cdot 10^4$ N/mm^2
	$\rho = 7.86 \cdot 10^{-9}$ Ns^2/mm^4		$\nu = 0.38$
	t = 2.0 mm (thickness)		$\rho = 7.85 \cdot 10^{-9}$ Ns^2/mm^4
			$d_{31} = 2.1 \cdot 10^{-7}$ mm/V
			$\kappa_{33} = 3.36 \cdot 10^{-9}$ F/m
			$\rho = 7.85 \cdot 10^{-9}$ Ns^2/mm^4
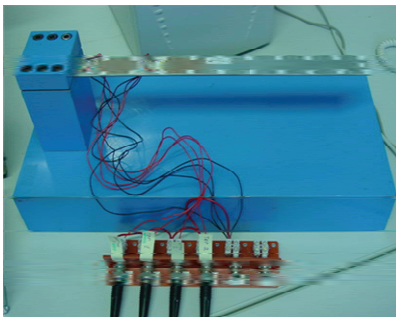
Fig. 2 Experimental rig with the clamped cantilever beam and dSPACE system

Control problem can be formulated as schematically represented in the Fig. 3. For the solution of the control task an appropriate controller is proposed (optimal LQ controller) in the way that the vibration amplitudes due to periodic excitation forces with frequencies
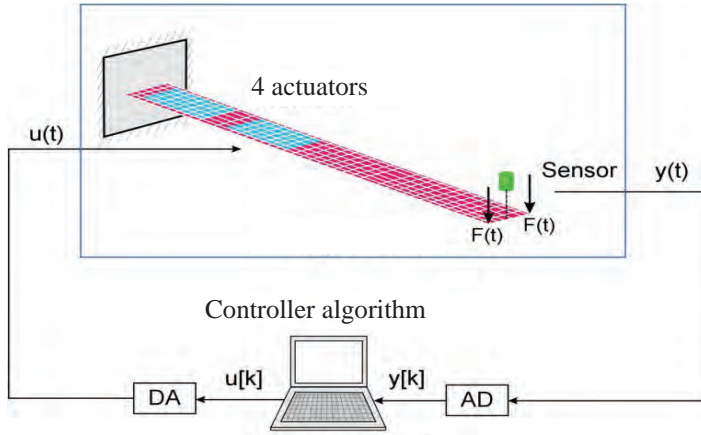
Fig. 3 Closed-loop control system for the vibration suppression of the clamped beam

corresponding to the eigenfrequencies of the clamped beam, are significantly suppressed in comparison with uncontrolled case. The study of the control problem is enabled through the simulations which are performed using the Matlab/Simulink software. As a starting point for the controller design an appropriate state space model was developed, based on the modal truncation of the finite element model of a much higher order, in such a way that the modally reduced state space model contains important information on the eigenmodes in the frequency range of interest, in this case: f_1=18.8Hz, f_2=113.1Hz, f_3=314.4Hz, f_6=619.2Hz (the eigenmodes 4 and 5 are torsion modes, and they are not relevant for the bending vibration suppression). The results of the bending modes animation preceding the state space modal truncation are represented in Fig. 4.
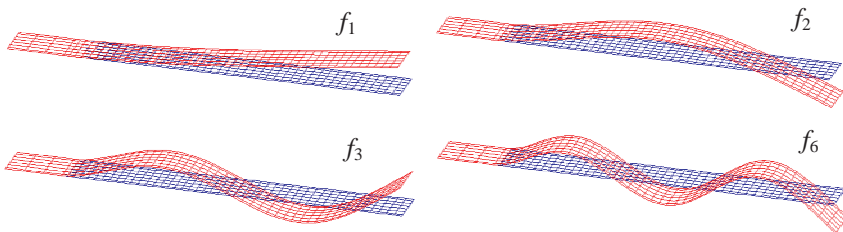
Fig. 4 Bending modes of the clamped beam

Simulation of the controller behavior is performed in Simulink using a block diagram with the optimal LQ controller and with an observer for unmeasurable state variables (Fig. 5).

Fig. 5 Simulink block diagram for the simulation of the controlled beam behavior

Controller design results and its effects are shown in the diagrams in Fig. 6 represented the uncontrolled and controlled (after 0.5 s) output – displacement at the tip of the beam, as well as the control signals (actuating voltages on the piezo patches) without and with control.

Presented example illustrates in a comprehensive way the most important phases of system modeling, analysis, controller design, simulation and verification. Analytic and detailed study of the system behavior is possible based on the developed system model. In this way an overall view of the smart structures development can be gained using a relatively simple and comprehensive benchmark example, which plays an important role in educational process. On the other hand, the knowledge gained through the investigation of such examples can be successfully used for studying of more complex structures.

In subsequent sections an overall view of the most important phases in design and control of lightweight smart structures with piezoelectric active materials will be summarized and illustrated by several application examples.

Fig. 6 Signals without control (up to 0.5 s) and with control (after 0.5s).
a) Controlled output. *b*) Actuating inputs.

3. FINITE ELEMENT APPROACH TO MODELING OF SMART STRUCTURES

The finite element (FE) based modeling of piezoelectric adaptive smart systems and structures represents a good basis for the overall simulation and design. This approach enables both a suitable controller design [14, 16] and the appropriate actuator/sensor placement [2, 8].

The FE analysis is based on the finite element semi-discrete form of the equations of motion of a piezoelectric smart system describing its electro-mechanical behavior. These equations can be derived using the established approximation method of displacements and electric potential and the standard finite element procedure [7, 9]. Here the coupled electro-mechanical behavior of smart structures will be considered. For investigations in the field of active acoustic modeling and control, appropriate consideration of the acoustic fluid is required. More on acoustic modeling can be found in [11].

Constitutive equations in the stress-charge form (1) are used for the development of the equations of motion for a smart structure:

$$\boldsymbol{\sigma} = \mathbf{C}\boldsymbol{\varepsilon} - \mathbf{e}\mathbf{E}, \qquad \mathbf{D} = \mathbf{e}^{\mathrm{T}}\boldsymbol{\varepsilon} + \boldsymbol{\kappa}\mathbf{E} \tag{1}$$

with following notations: $\boldsymbol{\sigma}^{\mathrm{T}} = \begin{bmatrix} \sigma_{11} & \sigma_{22} & \sigma_{33} & \sigma_{12} & \sigma_{23} & \sigma_{31} \end{bmatrix}$ mechanical stress vector, $\mathbf{C}_{(6\times6)}$ symmetric elasticity matrix, $\boldsymbol{\varepsilon}^{\mathrm{T}} = \begin{bmatrix} \varepsilon_{11} & \varepsilon_{22} & \varepsilon_{33} & 2\varepsilon_{12} & 2\varepsilon_{23} & 2\varepsilon_{31} \end{bmatrix}$ strain vector, $\mathbf{E}^{\mathrm{T}} = \begin{bmatrix} E_1 & E_2 & E_3 \end{bmatrix}$ electric field vector, $\mathbf{e}_{(6\times3)}$ piezoelectric matrix, $\mathbf{D}^{\mathrm{T}} = \begin{bmatrix} D_1 & D_2 & D_3 \end{bmatrix}$ vector of electrical displacement and $\boldsymbol{\kappa}_{(3\times3)}$ symmetric dielectric matrix. The system of equations which describe electromechanical behaviour consists of the constitutive equations (1) together with the mechanical equilibrium and electric equilibrium (charge equation of electrostatics resulting from the 4th Maxwell equation):

$$\mathbf{D}_u^\mathrm{T}\boldsymbol{\sigma} + \mathbf{P} - \rho\mathbf{v} = \mathbf{0}, \quad \mathbf{D}_\varphi^\mathrm{T}\mathbf{D} = \mathbf{0} \tag{2}$$

where $\mathbf{P}^\mathrm{T} = \begin{bmatrix} P_1 & P_2 & P_3 \end{bmatrix}$ represents the body force vector, $\mathbf{v}^\mathrm{T} = \begin{bmatrix} v_1 & v_2 & v_3 \end{bmatrix}$ is the vector of mechanical displacements, ρ is the mass density and $\mathbf{D}_u$ and $\mathbf{D}_\phi$ are differentiation matrices:

$$\mathbf{D}_u^\mathrm{T} = \begin{bmatrix} \dfrac{\partial}{\partial x_1} & 0 & 0 & \dfrac{\partial}{\partial x_2} & 0 & \dfrac{\partial}{\partial x_3} \\ 0 & \dfrac{\partial}{\partial x_2} & 0 & \dfrac{\partial}{\partial x_1} & \dfrac{\partial}{\partial x_3} & 0 \\ 0 & 0 & \dfrac{\partial}{\partial x_3} & 0 & \dfrac{\partial}{\partial x_2} & \dfrac{\partial}{\partial x_1} \end{bmatrix}, \quad \mathbf{D}_\varphi^\mathrm{T} = \begin{bmatrix} \dfrac{\partial}{\partial x_1} & \dfrac{\partial}{\partial x_2} & \dfrac{\partial}{\partial x_2} \end{bmatrix}. \tag{3}$$

Variational statement of the governing equations for the coupled electro-mechanical problem derived from the Hamilton's principle represents the basis for development of the finite element model [1, 17–18]. It is obtained in the form:

$$-\int_V \left(\rho\,\delta\mathbf{v}^\mathrm{T}\ddot{\mathbf{v}} - \delta\boldsymbol{\varepsilon}^\mathrm{T}\mathbf{C}\boldsymbol{\varepsilon} + \delta\boldsymbol{\varepsilon}^\mathrm{T}\mathbf{e}^\mathrm{T}\mathbf{E} \right) dV + \int_V \left(\delta\mathbf{E}^\mathrm{T}\mathbf{e}\boldsymbol{\varepsilon} + \delta\mathbf{E}^\mathrm{T}\boldsymbol{\kappa}\mathbf{E} + \delta\mathbf{v}^\mathrm{T}\mathbf{F}_\mathrm{V} \right) dV$$
$$+ \int_{\Omega_1} \delta\mathbf{v}^\mathrm{T}\mathbf{F}_\Omega\,d\Omega + \delta\mathbf{v}^\mathrm{T}\mathbf{F}_\mathrm{P} - \int_{\Omega_2} \delta\varphi\, q\, d\Omega - \delta\varphi Q = 0 \tag{4}$$

where F_Ω represents the surface applied forces (defined on surface Ω_1), F_P the point loads, ϕ the electric potential, q the surface charge brought on surface Ω_2 and Q the applied concentrated electric charges. Applying the approximation of displacements and electric potential with the shape functions over an element, representing the structure by a finite number of elements and adding up all elements contributions, the finite element semi-discrete form of the equations of motion is obtained:

$$\mathbf{M}\ddot{\mathbf{q}} + \mathbf{D}_d\dot{\mathbf{q}} + \mathbf{K}\mathbf{q} = \bar{\mathbf{E}}\mathbf{f}(t) + \bar{\mathbf{B}}\mathbf{u}(t) \tag{5}$$

where vector $\mathbf{q}$ represents the vector of generalized displacements including mechanical displacements and electric potential and contains all degrees of freedom. Matrices $\mathbf{M}$, $\mathbf{D}_d$ and $\mathbf{K}$ are the mass matrix, the damping matrix and the stiffness matrix, respectively. The total load vector is divided into the vector of the external forces $\mathbf{F}_E = \bar{\mathbf{E}}\mathbf{f}(t)$ and the vector of the control forces $\mathbf{F}_C = \bar{\mathbf{B}}\mathbf{u}(t)$, where the forces are generalized quantities including also electric charges. Vector $\mathbf{f}(t)$ represents the vector of external disturbances, and $\mathbf{u}(t)$ is the vector of the controller influence on the structure. Matrices $\bar{\mathbf{E}}$ and $\bar{\mathbf{B}}$ describe the positions of the forces and the control parameters in the finite element structure, respectively.

This approach has been used to develop a comprehensive library of multi-field finite elements: 1D, 2D, 3D elements, thick and thin layered composite shell elements, etc. which was implemented in the finite element package COSAR [3] for the simulation of the static and dynamic structural behavior of smart structures. Besides, the tools which take into account other physical effects are also available. For example, the temperature

influence can also be considered, and using the developed acoustic elements the influence of the acoustic fluid and its behavior can also be studied [10, 11].

The tools for modal reduction are also included, which enable development of appropriate models with reduced orders for the controller design. Based on the modal truncation, which was adopted as a suitable technique for the reduction of the number of equations in the FE models, a state space model of an actively controlled structure can be obtained in the form convenient for the controller design. A limited number of eigenmodes of interest is taken into account, while the remaining modes are truncated. Introducing the modal coordinates $\mathbf{z}$

$$\mathbf{q}(t) = \mathbf{\Phi}_{\mathrm{m}}\mathbf{z}(t) \tag{6}$$

into equation (5), where $\mathbf{\Phi}_{\mathrm{m}}$ represents the modal matrix, and applying the ortho-normalization with $\mathbf{\Phi}_{\mathrm{m}}^{\mathrm{T}}\mathbf{M}\mathbf{\Phi}_{\mathrm{m}} = \mathbf{I}$, $\mathbf{\Phi}_{\mathrm{m}}^{\mathrm{T}}\mathbf{K}\mathbf{\Phi}_{\mathrm{m}} = \mathbf{\Omega}$, $\mathbf{\Delta} = \mathbf{\Phi}_{\mathrm{m}}^{\mathrm{T}}\mathbf{D}_{\mathrm{d}}\mathbf{\Phi}_{\mathrm{m}}$, where $\mathbf{\Omega}$ represents the spectral matrix and $\mathbf{\Delta}$ the modal damping matrix, the state space model of the modally reduced system can be obtained in the form:

$$\dot{\mathbf{x}} = \begin{bmatrix} \mathbf{0} & \mathbf{I} \\ -\mathbf{\Omega} & -\mathbf{\Delta} \end{bmatrix}\mathbf{x} + \begin{bmatrix} \mathbf{0} \\ \mathbf{\Phi}^{\mathrm{T}}\overline{\mathbf{B}} \end{bmatrix}\mathbf{u}(t) + \begin{bmatrix} \mathbf{0} \\ \mathbf{\Phi}^{\mathrm{T}}\overline{\mathbf{E}} \end{bmatrix}\mathbf{f}(t) \tag{7}$$

where $\mathbf{x}(t) = \begin{bmatrix} \mathbf{z} & \dot{\mathbf{z}} \end{bmatrix}^{\mathrm{T}}$ represents a state-space vector. With the state and the output equations, the state space model is represented in the form:

$$\dot{\mathbf{x}}(t) = \mathbf{A}\mathbf{x}(t) + \mathbf{B}\mathbf{u}(t) + \mathbf{E}\mathbf{f}(t), \quad \mathbf{y} = \mathbf{C}\mathbf{x}(t) + \mathbf{D}\mathbf{u}(t) + \mathbf{F}\mathbf{f}(t) \tag{8}$$

which is convenient for the controller design.

4. SUBSPACE-BASED SYSTEM IDENTIFICATION

As an alternative modeling method, the subspace-based system identification can be used. It is convenient for the comparison with the results of the state space FEA-based modeling, since it results in a state space model representation as well. Based on the measured input and output signal data, the model is identified in a discrete-time state-space form, which represents a discrete-time equivalent of the state space model given by (8). In a general case a deterministic-stochastic form of a discrete-time state-space model has the following form:

$$\mathbf{x}[k+1] = \mathbf{\Phi}\mathbf{x}[k] + \mathbf{\Gamma}\mathbf{u}[k] + w[k], \quad \mathbf{y}[k] = \mathbf{C}\mathbf{x}[k] + \mathbf{D}\mathbf{u}[k] + v[k] \tag{9}$$

with discrete-time state and control matrices $\mathbf{\Phi}$ and $\mathbf{\Gamma}$, and the process and the measurement noise $w[k]$ and $v[k]$, respectively. The process noise and the measurement noise vector sequences $w[k]$ and $v[k]$ are white noise with zero mean and with covariance matrix:

$$\mathcal{E}\left\{ \begin{bmatrix} w[i] \\ v[j] \end{bmatrix} \begin{bmatrix} w[i]^{\mathrm{T}} & v[j]^{\mathrm{T}} \end{bmatrix} \right\} = \begin{bmatrix} \mathbf{Q} & \mathbf{S} \\ \mathbf{S}^{\mathrm{T}} & \mathbf{R} \end{bmatrix} \tag{10}$$

General deterministic-stochastic problem of the subspace identification is to determine the order n of the unknown system and the system matrices $\mathbf{\Phi} \in \mathrm{R}^{n \times n}$, $\mathbf{\Gamma} \in \mathrm{R}^{n \times m}$, $\mathbf{C} \in \mathrm{R}^{l \times n}$, $\mathbf{D} \in \mathrm{R}^{l \times m}$ as well as the covariance matrices $\mathbf{Q} \in \mathrm{R}^{n \times n}$, $\mathbf{S} \in \mathrm{R}^{n \times l}$, $\mathbf{R} \in \mathrm{R}^{l \times l}$ of the noise sequences $\mathbf{w}[k]$ and $\mathbf{v}[k]$. Subsequent derivations regard the pure deterministic case considered in [4].

Measured input and output data are organized into block Hankel matrices defined in the following form [13, 15, 19]:

$$
U_{0|2i-1} \overset{def}{=}
\begin{bmatrix}
\mathbf{u}_0 & \mathbf{u}_1 & \mathbf{u}_2 & \cdots & \mathbf{u}_{j-1} \\
\mathbf{u}_1 & \mathbf{u}_2 & \mathbf{u}_3 & \cdots & \mathbf{u}_j \\
\cdots & \cdots & \cdots & \cdots & \cdots \\
\mathbf{u}_{i-1} & \mathbf{u}_i & \mathbf{u}_{i+1} & \cdots & \mathbf{u}_{i+j-2} \\
\mathbf{u}_i & \mathbf{u}_{i+1} & \mathbf{u}_{i+2} & \cdots & \mathbf{u}_{i+j-1} \\
\mathbf{u}_{i+1} & \mathbf{u}_{i+2} & \mathbf{u}_{i+3} & \cdots & \mathbf{u}_{i+j} \\
\cdots & \cdots & \cdots & \cdots & \cdots \\
\mathbf{u}_{2i-1} & \mathbf{u}_{2i} & \mathbf{u}_{2i+1} & \cdots & \mathbf{u}_{2i+j-2}
\end{bmatrix}
\tag{11}
$$

The output block Hankel matrix $Y_{0|2i-1}$ is defined in a similar way. More details on definition of the Hankel matrices and the subspace-based identification method can be found in [15]. The measurement data are organized in the form of the input-output relation [19]:

$$
\mathbf{Y}[k] = \mathbf{\Gamma}_\alpha \mathbf{x}[k] + \mathbf{\Phi}_\alpha \mathbf{U}[k]
\tag{12}
$$

where $\mathbf{\Gamma}_\alpha$ represents the observability matrix for the system (1), $\mathbf{\Phi}_\alpha$ is the Toeplitz matrix [4] of impulse responses from $\mathbf{u}$ to $\mathbf{y}$:

$$
\mathbf{\Phi}_\alpha =
\begin{bmatrix}
\mathbf{D} & 0 & \cdots & \mathbf{0} \\
\mathbf{C\Gamma} & \mathbf{D} & & \mathbf{0} \\
\vdots & \ddots & \ddots & \vdots \\
\mathbf{C\Phi}^{\alpha-2}\mathbf{\Gamma} & \cdots & \mathbf{C\Gamma} & \mathbf{D}
\end{bmatrix}
\tag{13}
$$

and α is a specified number greater than the state dimension but much smaller than the data length. For a deterministic case [13] the problem is simplified to determining $\mathbf{\Gamma}_\alpha$ and $\mathbf{\Phi}_\alpha$ by computing the singular value decomposition (SVD) of $\mathbf{U}$ in the first step:

$$
\mathbf{U} = \mathbf{P\Sigma Q}^{\mathrm{T}} = [\mathbf{P}_{u1} \quad \mathbf{P}_{u2}] \, [\mathbf{\Sigma}_u \quad 0]
\begin{bmatrix}
\mathbf{Q}_{u1}^{\mathrm{T}} \\
\mathbf{Q}_{u2}^{\mathrm{T}}
\end{bmatrix}.
\tag{14}
$$

If matrix $\mathbf{U}$ has dimension $m \times n$ and rank r, then the partition in (14) is performed as follows:

$$
\mathbf{P} = \begin{bmatrix} \mathbf{p}_1 & \cdots & \mathbf{p}_r & | & \mathbf{p}_{r+1} & \cdots & \mathbf{p}_m \end{bmatrix} = \begin{bmatrix} \mathbf{P}_{u1} & \mathbf{P}_{u2} \end{bmatrix}
\tag{15}
$$

$$\mathbf{Q} = \begin{bmatrix} \mathbf{q}_1 & \cdots & \mathbf{q}_r & | & \mathbf{q}_{r+1} & \cdots & \mathbf{q}_n \end{bmatrix} = \begin{bmatrix} \mathbf{Q}_{u1} & \mathbf{Q}_{u2} \end{bmatrix} \tag{16}$$

where $\mathbf{p}_i$ are the left singular vectors of $\mathbf{U}$ [4]. It can be shown that they are eigenvectors of $\mathbf{UU}^T$. Vectors $\mathbf{q}_i$ are the right singular vectors of $\mathbf{U}$. It can be shown that they are eigenvectors of $\mathbf{U}^T\mathbf{U}$. Multiplying (12) by $\mathbf{Q}_{u2}$, matrix $\mathbf{\Gamma}_\alpha$ can be determined from a SVD of $\mathbf{YQ}_{u2}$. Then matrix $\mathbf{C}$ is obtained as the first row (in a sense of a block-row) of the observability matrix $\mathbf{\Gamma}_\alpha$, and matrix $\mathbf{\Phi}$ is calculated from: $\underline{\mathbf{\Gamma}}_\alpha = \overline{\mathbf{\Gamma}}_\alpha \mathbf{\Phi}$ applying pseudo inverse, where $\overline{\mathbf{\Gamma}}_\alpha$ is obtained by dropping the last row of $\mathbf{\Gamma}_\alpha$. Matrix $\underline{\mathbf{\Gamma}}_\alpha$ represents the matrix obtained by dropping the first row of $\mathbf{\Gamma}_\alpha$. For the calculation of $\mathbf{\Gamma}$ and $\mathbf{D}$ matrices, (12) is multiplied by the pseudo inverse of $\mathbf{U}$ on the right and by $\mathbf{P}_{u2}^T$ from (14) on the left. Thus the equation is reduced to:

$$\mathbf{P}_{u2}^T \mathbf{YU}^{-1} = \mathbf{P}_{u2}^T \mathbf{\Phi}_\alpha . \tag{17}$$

After rearranging, (17) can be solved for $\mathbf{\Gamma}$ and $\mathbf{D}$ using the least squares, see (13). In this way the system parameters in the form of state-space matrices of the model (9) are identified using the subspace-based identification method.

5. OPTIMAL LQ CONTROLLER DESIGN WITH ADDITIONAL DYNAMICS

An optimal LQ controller design with additional dynamics is suggested here as a control technique which has resulted in a successful vibration and noise reduction in several studies [12, 16].

Controller design includes available a priori knowledge about occurring disturbance type contained in the additional dynamics. Such an a priori knowledge is available in terms of the type of the disturbance function which has to be rejected or whose influence should be suppressed by the controller. Periodic disturbances with frequencies corresponding to the eigenfrequencies of the smart structure can cause resonance and their suppression is therefore important. They are taken into account via the additional dynamics.

Discrete-time state space equivalent (18) of the state space model (8) developed through the FEM procedure and modal reduction is used for the controller design.

$$\mathbf{x}[k+1] = \mathbf{\Phi x}[k] + \mathbf{\Gamma u}[k] + \mathbf{\varepsilon w}[k], \qquad \mathbf{y}[k] = \mathbf{Cx}[k] + \mathbf{Du}[k] + \mathbf{Fw}[k] \tag{18}$$

Using the a priori knowledge about the disturbance class, which has to be suppressed, the model of the disturbance is represented in an appropriate state space form, where the disturbance is assumed to be the output of the state space representation. The poles λ_i of the disturbance transfer function are used to define the additional dynamics using the coefficients of the polynomial:

$$\delta(z) = \prod_i (z - e^{\lambda_i T})^{m_i} = z^s + \delta_1 z^{s-1} + ... + \delta_s \tag{19}$$

where m_i represents the multiplicity of the pole λ_i. Additional dynamics is expressed in a state space form:

$$\mathbf{x}_a[k+1] = \mathbf{\Phi}_a\mathbf{x}_a[k] + \mathbf{\Gamma}_a\mathbf{e}[k] \; ; \tag{20}$$

where $\mathbf{x}_a$ is the vector of the state variables for the additional dynamics, $\mathbf{e}$ is the error signal and:

$$\mathbf{\Phi}_a = \begin{bmatrix} -\delta_1 & 1 & 0 & \cdots & 0 \\ -\delta_2 & 0 & 1 & \cdots & 0 \\ \vdots & \vdots & \vdots & \ddots & \vdots \\ -\delta_{s-1} & 0 & 0 & \cdots & 1 \\ -\delta_s & 0 & 0 & \cdots & 0 \end{bmatrix}, \quad \mathbf{\Gamma}_a = \begin{bmatrix} -\delta_1 \\ -\delta_2 \\ \vdots \\ -\delta_{s-1} \\ -\delta_s \end{bmatrix}. \tag{21}$$

For multiple-input multiple-output (MIMO) systems additional dynamics is replicated q times (once per each output). Replicated additional dynamics is described by:

$$\overline{\mathbf{\Phi}} \stackrel{def}{=} diag(\underbrace{\mathbf{\Phi}_a,...,\mathbf{\Phi}_a}_{q \text{ times}}), \quad \overline{\mathbf{\Gamma}} \stackrel{def}{=} diag(\underbrace{\mathbf{\Gamma}_a,...,\mathbf{\Gamma}_a}_{q \text{ times}}) \tag{22}$$

The discrete-time design model ($\mathbf{\Phi}_d$, $\mathbf{\Gamma}_d$) is formed as a cascade combination of the additional dynamics ($\mathbf{\Phi}_a$, $\mathbf{\Gamma}_a$) or $(\overline{\mathbf{\Phi}}, \overline{\mathbf{\Gamma}})$ and the discrete-time plant model ($\mathbf{\Phi}$, $\mathbf{\Gamma}$):

$$\mathbf{x}_d[k+1] = \mathbf{\Phi}_d\mathbf{x}_d[k] + \mathbf{\Gamma}_d\mathbf{u}[k] \; ; \tag{23}$$

$$\mathbf{\Phi}_d = \begin{bmatrix} \mathbf{\Phi} & 0 \\ \mathbf{\Gamma}^*\mathbf{C} & \mathbf{\Phi}^* \end{bmatrix}, \quad \mathbf{\Gamma}_d = \begin{bmatrix} \mathbf{\Gamma} \\ 0 \end{bmatrix}, \quad \mathbf{x}_d = \begin{bmatrix} \mathbf{x}[k] \\ \mathbf{x}_a[k] \end{bmatrix} \tag{24}$$

where $\mathbf{\Phi}^*$ and $\mathbf{\Gamma}^*$ denote respectively $\mathbf{\Phi}_a$ and $\mathbf{\Gamma}_a$ in the case of single-input single-output systems or $\overline{\mathbf{\Phi}}$ and $\overline{\mathbf{\Gamma}}$ for MIMO systems. For the design model (23) the feedback gain matrix $\mathbf{L}$ of the optimal LQ regulator is calculated in such a way that the feedback control law $\mathbf{u}[k] = -\mathbf{L}\mathbf{x}_d[k]$ minimizes the performance index (25) subject to the constraint (23), where $\mathbf{Q}$ and $\mathbf{R}$ are symmetric, positive-definite matrices.

$$J = \frac{1}{2}\sum_{k=0}^{\infty}(\mathbf{x}_d[k]^T\mathbf{Q}\mathbf{x}_d[k] + \mathbf{u}[k]^T\mathbf{R}\mathbf{u}[k]) \tag{25}$$

The feedback gain matrix $\mathbf{L}$ is afterwards partitioned into

$$\mathbf{L} = \begin{bmatrix} \mathbf{L}_1 & \mathbf{L}_2 \end{bmatrix} \tag{26}$$

so that $\mathbf{L}_1$ corresponds to the state space model of the structure, and $\mathbf{L}_2$ to the modelled additional dynamics.

6. DIRECT ADAPTIVE CONTROL

As an alternative approach, the model reference adaptive control (MRAC) is suggested. This control technique comprises several advantages for the large flexible structures. In the case of piezoelectric smart structures the term large can regard high

number of degrees of freedom of the finite element model used for the modeling of the structure behavior. With the model truncation, which is a necessary step to adapt the structure model to the controller design purpose, resulting state-space model does not exactly reflect the real behavior of the structure. Inaccuracies introduced in this way can be viewed as a source of the parameter variation with respect to the modeled case. The presence of disturbances in real environment also introduces variation of the parameters in comparison with the modeled case. This causes the need for the adaptive control algorithm, which can successfully face the insufficient prior knowledge or the unknown changes of the system parameters.

   The advantage of a robust adaptive controller over a fixed-gain controller can be viewed through the fact that in design of large flexible smart structures a large degree of the model uncertainty is allowable in the sense of the possible parameter variation as well as with respect to the order of the controlled structure. The robustness assumes stability in the presence of disturbances and unmodeled dynamics.

   The idea of the model reference adaptive control is based upon the existence of the reference model, specified by the designer, which reflects the desired behavior of the controlled structure. The output of the controlled structure should track the output of the reference model (Fig. 7).
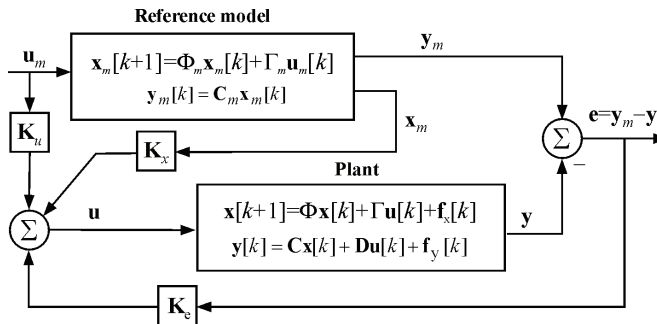
Fig. 7 General form of a discrete-time MRAC system

   A general form of a discrete-time model reference adaptive system is represented in Fig. 7. Plant representation is a discrete-time state space realization, which corresponds to the plant model (18), whereas the reference model is represented by equations in Fig. 7, where $\mathbf{f}_x$ and $\mathbf{f}_y$ represent bounded unmeasurable plant and output disturbances in a general case and $\mathbf{e}=\mathbf{e}_y$ is the output error, i.e. the difference between the desired output of the reference model and the real plant output.

Discrete-time direct model reference adaptive control law is expressed in the following form:

$$\mathbf{u}[k] = \mathbf{K}_r[k]\mathbf{r}[k] = \mathbf{K}_e[k]\mathbf{e_y}[k] + \mathbf{K}_x[k]\mathbf{x}_m[k] + \mathbf{K}_u[k]\mathbf{u}_m[k] . \qquad (27)$$

The adaptive gain $\mathbf{K}_r[k]$ in is determined as a sum of proportional and integral parts $\mathbf{K}_p$ and $\mathbf{K}_I$ respectively:

$$\mathbf{K}_r[k] = \mathbf{K}_p[k] + \mathbf{K}_I[k] \qquad (28)$$

According to the basic model reference adaptive algorithm the proportional and integral gains are adapted in the following way:

$$\mathbf{K}_p[k] = \mathbf{e_y}\mathbf{r}^{\mathrm{T}}(t)\overline{\mathbf{T}}, \quad \mathbf{K}_I[k+1] = \mathbf{e_y}\mathbf{r}^{\mathrm{T}}[k]\mathbf{T}, \quad \mathbf{K}_I(0) = \mathbf{K}_{I0} \qquad (29)$$

where $\mathbf{T}$ and $\overline{\mathbf{T}}$ are $n_r \times n_r$ time-invariant weighting matrices and $\mathbf{K}_{I0}$ is the initial integral gain, selected by the designer. In the robust model reference adaptive control approach the integral gain is determined in the form (30). This modification of the integral gain in (29) by adding a σ-term is introduced to provide the convergence of the integral gain [14] since in realistic environment due to disturbances the error **e** does not reach the zero value and the integral gain would thus never stop increasing without its limiting by the σ-term.

$$\mathbf{K}_I[k+1] = \mathbf{e_y}[k]\mathbf{r}^{\mathrm{T}}[k]\mathbf{T} - \sigma\mathbf{K}_I[k] \qquad (30)$$

The control law for a general plant in Fig. 7 including disturbances or excitations is globally stable with respect to boundness if the disturbances are bounded and the plant is is almost strictly positive real. The proof of the condition is based on the selection of the Lyapunov candidate positive definite function and on analyzing the sign of its derivative. In order to guarantee robust stability, perfect tracking is not obtained in general, but the adaptive controller maintains a small tracking error over large ranges of nonideal conditions and uncertainties.

7. APPLICATION EXAMPLES

In order to illustrate some results of the application of active control as a part of the overall design of active mechanical structures several examples are shown in this section.

7.1. Active vibration suppression of a car roof

Fig. 8   Passenger compartment and inner surface of the car roof with attached piezo-patches and exciting shakers

Vibration suppression of a car roof with attached piezoelectric patches using the optimal LQ controller with additional dynamics is demonstrated through a numerical simulation for a test structure. Piezoelectric patches attached to the surface of the car roof are used as actuators and sensors. Excitation by shakers at prescribed points is intended for the experimental investigations (Fig. 8).

FEM model including the piezoelectric effects of the actuator/sensor groups was obtained using the FEM software COSAR [3]. Based on the generated FEM mesh, an optimization

of the actuator/sensor placement was per-formed under consideration of the eigen-modes of interest and the controllability index. The actuator/sensor placement in Fig. 9 describes one of the test cases, which was calculated based on the controllability index. Comparison of the calculated an experimentally determined eigenfrequencies shows a good agreement in the considered frequency range.
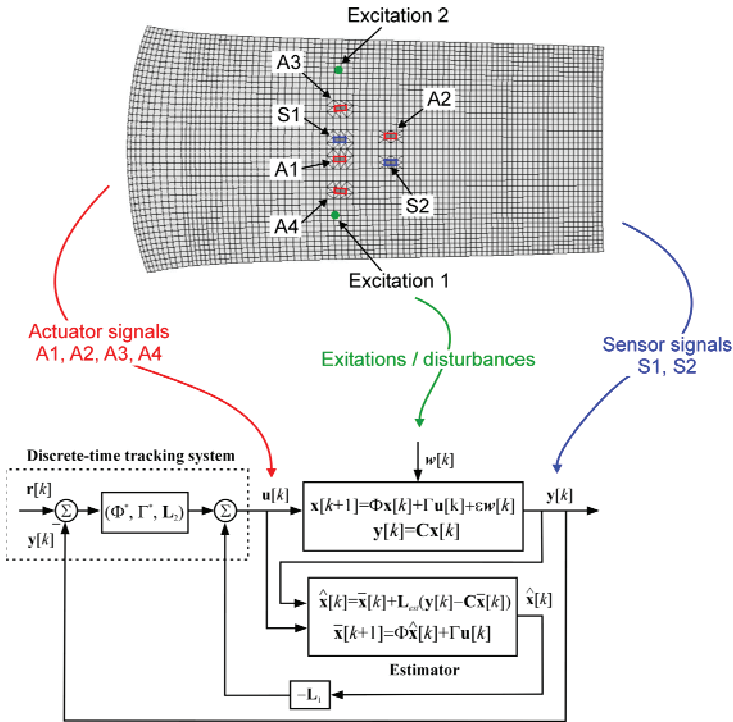
Fig. 9 FEM mesh of the car roof with actuator/sensor placement

For the controller design a modally reduced state space model was used, which takes into account five selected eigenfrequencies: f_1=48.45Hz, f_2=51.12Hz, f_3=63.23Hz, f_4=64.67Hz and f_5=68.00Hz. Using the control concept with optimal LQ controller, additional dynamics and Kalman estimator the simulation of the vibration suppression was performed in order to show the potentials of the control strategy. The results are represented in Fig. 10.

The comparison of the uncontrolled and controlled cases shows significant reduction of the vibration magnitudes in the presence of the controller. The controller was also compared with the standard optimal LQ controller without additional dynamics which compensates for the presence of the periodic sinusoidal excitations with critical frequencies. The comparison shows much better vibration suppression in the presence of the controller with additional dynamics.
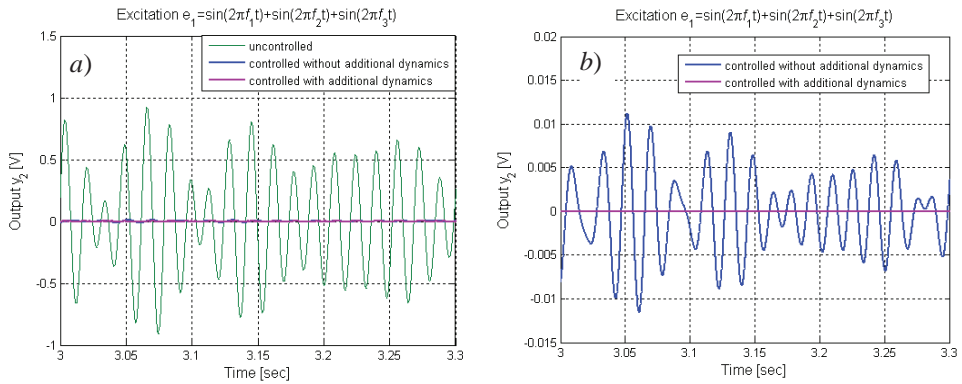
Fig. 10 *a*) Controlled and uncontrolled responses of the sensor patches.
b) Zoomed portion of the controlled responses.
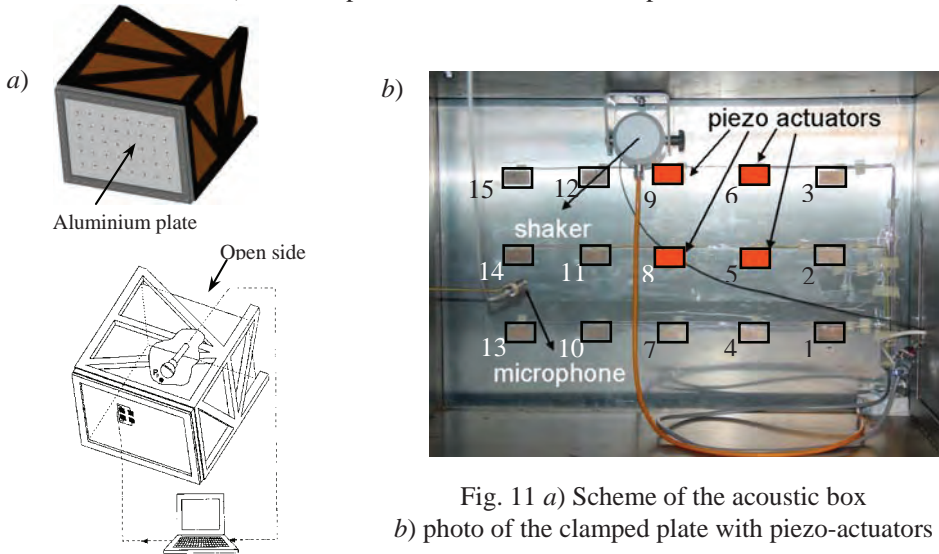
Fig. 11 *a*) Scheme of the acoustic box
b) photo of the clamped plate with piezo-actuators

7.2. Noise Control of a Smart Acoustic Box

An actively controlled smart acoustic box consisting of the clamped plate with attached piezoelectirc patches used as actuators and of the wooden box surrounding the clamped plate is designed and investigated in order to reduce the plate vibrations and the air pressure at selected points inside the box (Fig. 11).

The plate is excited by a shaker and the plate and the acoustic fluid vibrations are measured by the laser scanning vibrometer (for the velocity and displacement measurements at selected points on the plate surface) and the microphone (for the air pressure measurement) respectively. The piezopatches and the microphone are located inside the acoustic box.

   The aluminium plate of the acoustic box and the acoustic fluid inside it are modelled using the FEM approach, taking into consideration the acoustic behaviour via the appropriate acoustic finite elements. Based on the modally reduced state space model obtained through the modal truncation, the simulation and subsequently the experimental control of the plate vibration and of the fluid pressure were performed using the optimal LQ controller with additional dynamics and the model reference adaptive control.
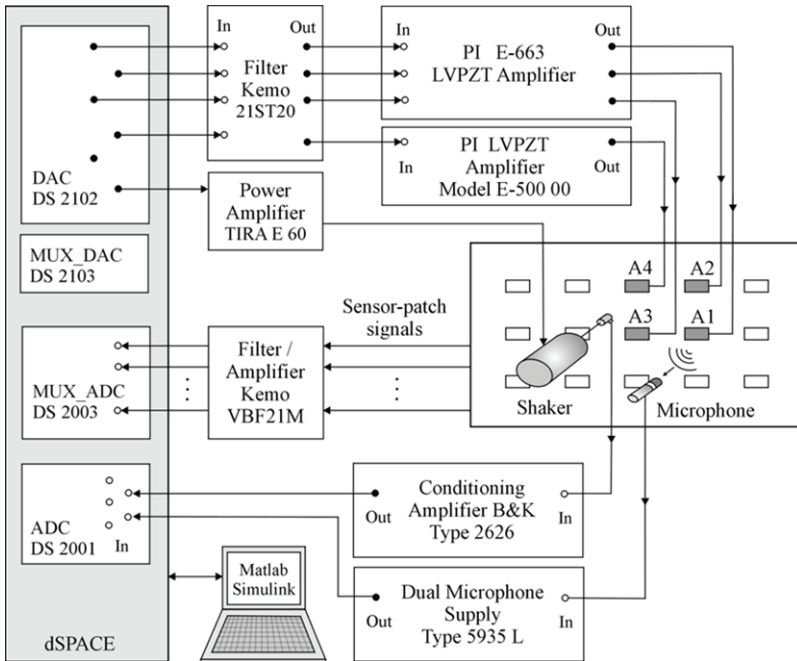
Fig. 12 Experimental setup for system identification and control implementation

The experimental setup for the control implementation as well as for the model identification using the subspace approach described in section 4 is represented in Fig. 12.

The optimal LQ controller was tested with different excitation signals. Some of the results are represented in with Fig. 13. The results for the excitation obtained as a sum of three periodic sinusoidal signals with the frequencies corresponding to the eigenfrequencies of the plate (f_{w1}=66.7Hz, f_{w2}=106.2Hz, f_{w2}=163.8Hz) are shown in Fig. 13 a). Fig. 13 b) shows the results with the random excitation signal. The pressure amplitude reduction can be observed in both cases.
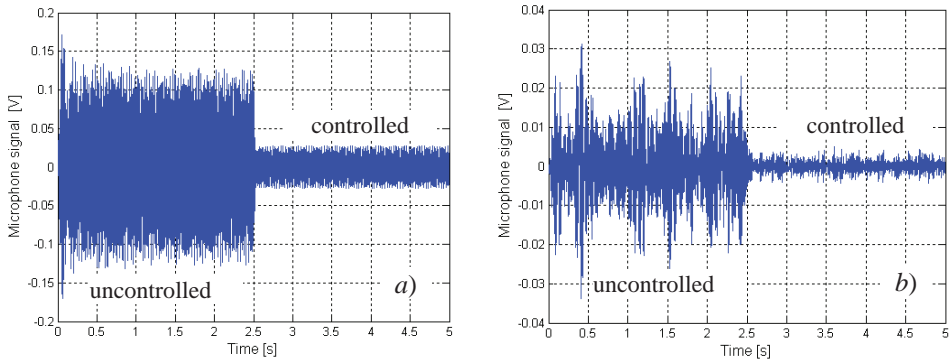
Fig. 13 Optimal LQ controller with additional dynamics: uncontrolled and controlled microphone output signal in the presence of

$$a) \text{ excitation } \sum_{i=1}^{3} \sin(f_{wi}) , \ b) \text{ random excitation.}$$
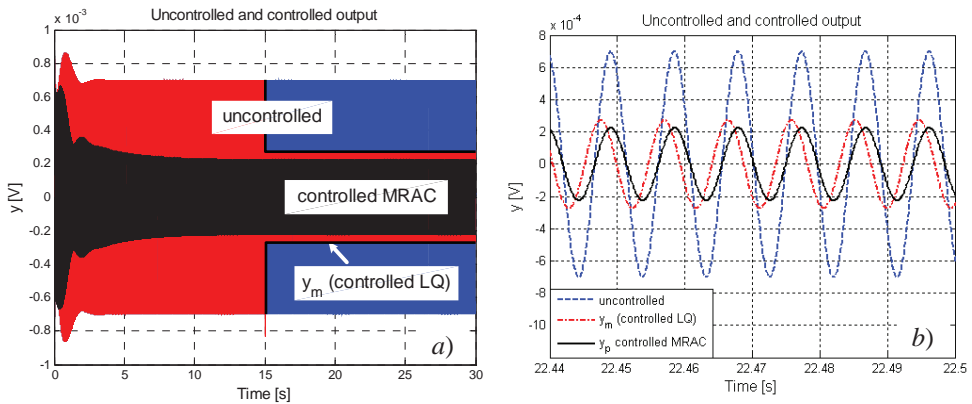
Fig. 14 *a*) Comparison of the MRAC and optimal LQ controller; *b*) zoomed portion.

The results of the adaptive MRAC controller testing are shown in Fig. 14. The adaptive controller is compared with the optimal LQ controller in the presence of the periodic excitation with the frequency f_{w2}. Uncontrolled and controlled signals are represented in Fig. 14 *a*), and a zoomed portion of the signals in Fig. 14 *b*). Both controllers perform the air pressure reduction at the microphone point. In this case the optimal controller performs a slightly higher reduction degree.

8. CONCLUSION

Active structural design is addressed in this paper considering several phases in the overall design approach, with the focus on structural control of lightweight mechanical

structures which use piezoelectric materials as active elements. The main control objective is vibration suppression and the noise attenuation. The feasibility of the approaches is demonstrated by two application examples: vibration suppression of the car roof and the noise reduction in a smart acoustic enclosure. Experience in the education is addressed as well. A benchmark example of a clamped beam controlled by piezoelectric patches used as actuators and/or sensors is explained to show the application possibilities for education purposes.

REFERENCES

1. Allik H., Hughes J. R., (1970), Finite Element Method for Piezoelectric Vibration, *International Journal for Numerical Methods in Engineering*, 2:151–157

2. Berger H., Köppe H., Gabbert U., Seeger F., (2000) On Finite Element Analysis of Piezoelectric Controlled Smart Structures, (2000) *IUTAM Symposium on Smart Structures and Structronic Systems*, Proceedings of the IUTAM Symposium held in Magdeburg, Germany, 26-29 September 2000, Edited by: U. Gabbert, H. S. Tzou, 189-196

3. COSAR General Purpose Finite Element Package: Manual, FEMCOS mbH Magdeburg, http://www.femcos.de

4. Franklin G. F., Powell J. D., Workman M. L., Digital Control of Dynamic Systems, third edition, Addison-Wesley Longman, Inc., 1998

5. Gabbert U., Berger H., Köppe H., Cao X., (2000), On Modeling and Analysis of Piezoelectric smart Structures by the Finite Element Method, *Applied Mechanics and Engineering*, 5(1), 127-142

6. Gabbert U., Köppe H., Fuchs K., Seeger F., (2000), Modeling of Smart Composites Controlled by Thin Piezoelectric Fibers, in Varadan, V.V. (Ed.): *Mathematics and Control in Smart Structures*, SPIE Proceedings Series, Vol. 3984, 2-11

7. Gabbert U., Tzou H. S. (Eds.), (2001), *Smart Structures and Structronic Systems*, Dordrecht: Kluwer Academic Publisher

8. Gabbert U., Weber C. T., (1999), Analysis and Optimal Design of Piezoelectric Smart Structures by the Finite Element Method, *ECCM'99 European Conference on Computational Mechanics*, August 31 - September 3, 1999, München, Germany

9. Janocha H. (Ed.), (2007), *Adaptronics and Smart Structures – Basics, Materials, Design, and Applications*, 2nd ed., Springer Verlag

10. Laugwitz F., Lefèvre J., Schmidt G., Nestorović T., Gabbert U., (2006), Experimental and numerical investigation of a smart acoustic box, *ISMA2006 International Conference on Noise and Vibration Engineering*, September 18-20, 2006, Katholieke Universiteit Leuven, Belgium

11. Lefèvre J., Gabbert U., (2005), Finite Element Modelling of Vibro-Acoustic Systems for Active Noise Reduction, *Technische Mechanik*, 25 (3-4), 241–247

12. Nestorović T., (2005), *Controller Design for the Vibration Suppression of Smart Structures*, Fortschritt-Berichte VDI, 8(1071), Düsseldorf

13. Nestorović T., H. Köppe, U. Gabbert, (2005), Subspace Identification for the model based controller design of a funnel-shaped structure, *Facta Universitatis, Series Mechanics, Automatic Control and Robotics*, 4(17), 257–263

14. Nestorović Trajkov T., Köppe H., Gabbert U., (2008), Direct model reference adaptive control (MRAC) design and simulation for the vibration suppression of piezoelectric smart structures, *Communications in Nonlinear Science and Numerical Simulation*, 13(9), 1896-1909

15. Nestorović-Trajkov T., Gabbert U., (2006), Active control of a piezoelectric funnel-shaped structure based on subspace identification, *Structural Control and Health Monitoring*, 13(6), 1068–1079

16. Nestorović-Trajkov T., Köppe H., Gabbert U., (2005), Active Vibration Control Using Optimal LQ Tracking System with Additional Dynamics, *International Journal of Control*, 78(15), 1182–1197

17. Tiersten H.F., (1967), Hamilton's principle for linear piezoelectric media, *Proc. IEEE*, 1523–1524

18. Tzou H. S., Tseng C. I., (1990), Distributed piezoelectric sensor/actuator design for dynamic measurement/ control of distributed parameter system: a piezoelectric finite element approach, *Journal of Sound and Vibration*, 138(1), 17–34

19. Van Overschee P., De Moor B., (1996), *Subspace Identification for Linear Systems: Theory, Implementation, Applications*, Kluwer Academic Publishers, Boston

AKTIVNO UPRAVLJANJE KONSTRUKCIJAMA U ISTRAŽIVANJU I NASTAVI

Prof. Dr.-Ing. Tamara Nestorović

U ovom radu prikazane su ključne faze u sveobuhvatnom pristupu projektovanju aktivnih konstrukcija. Težište rada je na upravljanju lakih i tankozidnih mehaničkih struktura u cilju aktivne redukcije vibracija i smanjenja nivoa emitovane buke primenom piezoelektričnih aktuatora i senzora. Rastuće interesovanje za razvoj aktivnih konstrukcija kao i iskustva u istraživanju motivisali su uvođenje predmeta o aktivnim konstrukcijama u nastavu na univerzitetima. Ove oblasti se intenzivno izučavaju u nastavi i nailaze na veliko interesovanje među studentima. U radu se takođe navode i iskustva autora na polju nastave u ovoj oblasti.

Ključne reči: *upravljanje aktivnim konstrukcijama, piezoelektrični actuatori i senzori, identifikacija sistema.*

DELAY DEPENDENT STABILITY OF LINEAR TIME-DELAY SYSTEMS

UDC 681.511.2

Sreten B. Stojanovic[1], Dragutin Lj. Debeljkovic[2]

[1]University of Nis, Faculty of Technology, Bulevar Oslobodjenja 124, 16000 Leskovac, Serbia, ssreten@ptt.rs
[2]University of Belgrade, Faculty of Mechanical Engineering, Kraljice Marije 16, 11000 Belgrade, Serbia, ddebeljkovic@mas.bg.ac.rs

Abstract. *This paper deals with the problem of delay dependent stability for both ordinary and large-scale time-delay systems. Some necessary and sufficient conditions for delay-dependent asymptotic stability of continuous and discrete linear time-delay systems are derived. These results have been extended to the large-scale time-delay systems covering the cases of two and multiple existing subsystems. The delay-dependent criteria are derived by Lyapunov's direct method and are exclusively based on the solvents of particular matrix equation and Lyapunov equation for non-delay systems. Obtained stability conditions do not possess conservatism. Numerical examples have been worked out to show the applicability of results derived.*

Key words (bold): *continuous time-delay systems, discrete time-delay systems, large-scale time-delay systems, delay-dependent stability, Lyapunov stability, necessary and sufficient conditions*

1. INTRODUCTION

The problem of investigation of time-delay systems has been exploited over many years. Time-delay is very often encountered in various technical systems, such as electric, pneumatic and hydraulic networks, chemical processes, long transmission lines, etc. The existence of pure time lag, regardless if it is present in the control or/and the state, may cause undesirable system transient response, or even instability.

During the last three decades, the problem of stability analysis of time-delay systems has received considerable attention and many papers dealing with this problem have appeared. In the literature, various stability analysis techniques have been utilized to

derive stability criteria for asymptotic stability of the time-delay systems by many researchers.

The developed stability criteria are classified often into two categories according to their dependence on the size of the delay: delay-dependent and delay-independent stability criteria. It has been shown that delay-dependent stability conditions that take into account the size of delays, are generally less conservative than delay-independent ones which do not include any information on the size of delays.

Further, the delay-dependent stability conditions can be classified into two classes: frequency-domain (which are suitable for systems with a small number of heterogeneous delays) and time-domain approaches (for systems with a many heterogeneous delays).

In the first approach, we can include the two or several variable polynomials [1], [2] or the small gain theorem based approach.

In the second approach, we have the comparison principle based techniques for functional differential equations [3], [4] and respectively the Lyapunov stability approach with the Krasovskii and Razumikhin based methods [5], [6]. The stability problem is thus reduced to one of finding solutions to Lyapunov [7] or Riccati equations [8], solving linear matrix inequalities (LMIs) [9], [10], [11] [12] or analyzing eigenvalue distribution of appropriate finite-dimensional matrices [13] or matrix pencils [14]. For further remarks on the methods see also the guided tours proposed by [15], [16], [17], [18], [19], [20].

It is well-known [21] that the choice of an appropriate Lyapunov–Krasovskii functional is crucial for deriving stability conditions. The general form of this functional leads to a complicated system of partial differential equations [22]. Special forms of Lyapunov–Krasovskii functionals lead to simpler delay-independent (Boyd et al., 1994; Verriest & Niculescu, 1998; Kolmanovskii & Richard, 1999) [9], [23], [21] and (less conservative) delay-dependent conditions [24], [25], [21], [26], [27], [28]. Note that the latter simpler conditions are appropriate in the case of unknown delay, either unbounded (delay-independent conditions) or bounded by a known upper bound (delay-dependent conditions).

In the delay-dependent stability case, special attention has been focused on the first delay interval guaranteeing the stability property, under some appropriate assumptions on the system free of delay. Thus, algorithms for computing optimal (or suboptimal) bounds on the delay size are proposed in [14] (frequency-based approach), in [29] (integral quadratic constraints interpretations), in [10], [11], [7] (Lyapunov-Razumikhin function approach) or in [12] (discretization schemes for some Lyapunov- Krasovskii functionals). For computing general delay intervals, see, for instance, the frequency based approaches proposed in [30].

In the past few years, there have been various approaches to reduce the conservatism of delay-dependent conditions by using new bounding for cross terms or choosing new Lyapunov–Krasovskii functional and model transformation. The delay-dependent stability criterion of [31], [26] is based on a so-called Park's inequality for bounding cross terms. However, major drawback in using the bounding of [31] and [26] is that some matrix variables should be limited to a certain structure to obtain controller synthesis conditions in terms of LMIs. This limitation introduces some conservatism. In [32] a new inequality, which is more general than the Park's inequality, was introduced for bounding cross terms and controller synthesis conditions were presented in terms of

nonlinear matrix inequalities in order to reduce the conservatism. It has been shown that the bounding technique in [32] is less conservative than earlier ones. An iterative algorithm was developed to solve the nonlinear matrix inequalities [32].

Further, in order to reduce the conservatism of these stability conditions, various model transformations have been proposed. However, the model transformation may introduce additional dynamics. In [33] the sources for the conservatism of the delay-dependent methods under four model transformations, which transform a system with discrete delays into one with distributed delays are analyzed. It has been demonstrated that descriptor transformation, that has been proposed in [34], leads to a system which is equivalent to the original one, does not depend on additional assumptions for stability of the transformed system and requires bounding of fewer cross-terms. In order to reduce the conservatism [35], [36] proposed some new methods to avoid using model transformation and bounding technique for cross terms.

In [37] both the descriptor system approach and the bounding technique using by [32] are utilized and the delay-dependent stability results are performed. The derived stability criteria have been demonstrated to be less conservative than existing ones in the literature.

Delay-dependent stability conditions in terms of linear matrix inequalities (LMIs) have been obtained for retarded and neutral type systems. These conditions are based on four main model transformations of the original system and application mentioned inequalities.

The majority of stability conditions in the literature available, of both continual and discrete time-delay systems, are sufficient conditions. Only a small number of works provide both necessary and sufficient conditions [38], [39], [47], [49], [50], [53] which are in their nature mainly dependent of time-delay. These conditions do not possess conservatism but often require more complex numerical computations. In our paper we represent some necessary and sufficient stability conditions.

Less attention has been drawn to the corresponding results for discrete-time delay systems [40], [41], [42], [43], [44], [45], [54]. This is mainly due to the fact that such systems can be transformed into augmented high dimensional systems (equivalent systems) without delay [22], [46]. This augmentation of the systems is, however, inappropriate for systems with unknown delays or systems with time varying delays. Moreover, for systems with large known delay amounts, this augmentation leads to large-dimensional systems. Therefore, in these cases the stability analysis of discrete time-delay systems can not be to reduce on stability of discrete systems without delay.

In our paper we present delay-dependent stability criteria for particular classes of time-delay systems: continuous and discrete time-delay systems and continuous and discrete time-delay large-scale systems. Thereat, these stability criteria are express in form necessary and sufficient conditions.

2. STABILITY OF TIME-DELAY SYSTEMS

Throughout this paper we use the following notation. R and C denote real (complex) vector space or the set of real (complex) numbers, T^+ denotes the set of all non-negative integers, λ^* means conjugate of $\lambda \in C$ and F^* conjugate transpose of matrix $F \in C^{n \times n}$.

Re(s) is the real part of $s \in C$. The superscript T denotes transposition. For real matrix F the notation $F > 0$ means that the matrix F is positive definite. $\lambda_i(F)$ is the eigenvalue of matrix F. Spectrum of matrix F is denoted with $\sigma(F)$ and spectral radius with $\rho(F)$.

2.1. Continuous time-delay systems

Considers class of continuous time-delay systems described by

$$\dot{\mathbf{x}}(t) = A_0 \mathbf{x}(t) + A_1 \mathbf{x}(t - \tau), \quad \mathbf{x}(t) = \varphi(t), \quad -\tau \le t < 0 \tag{1}$$

Theorem 1. [38] Let the system be described by (1). If for any given matrix $Q = Q^* > 0$ there exist matrix $P = P^* > 0$, such that

$$P\left(A_0 + T(0)\right) + \left(A_0 + T(0)\right)^T P = -Q \tag{2}$$

where $T(t)$ is continuous and differentiable matrix function which satisfies

$$\dot{T}(t) = \begin{cases} \left(A_0 + T(0)\right)T(t), & 0 \le t \le \tau, \quad T(\tau) = A_1 \\ 0 & , \quad t > \tau \end{cases} \tag{3}$$

then the system (1) is asymptotically stable.

In paper [38] it is emphasized that the key to the success in the construction of a Lyapunov function corresponding to the system (1) is the existence of at least one solution $T(t)$ of (3) with boundary condition $T(\tau) = A_1$. In other words, it is required that the nonlinear algebraic matrix equation

$$e^{\left(A_0 + T(0)\right)\tau} T(0) = A_1 \tag{4}$$

has at least one solution for $T(0)$. It is asserted, there, that asymptotic stability of the system (*Theorem 1*) can be determined based on the knowledge of only one or any solution of the particular nonlinear matrix equation. However, [47] gives counterexample which denies this maintenance.

2.1.1 Main results

If we introduce a new matrix,

$$R \,\square\, A_1 + T(0) \tag{5}$$

then condition (2) reads

$$PR + R^* P = -Q \tag{6}$$

which presents a well-known Lyapunov's equation for the system without time-delay. This condition will be fulfilled if and only if R is a stable matrix:

$$\mathrm{Re}\,\lambda_i(R) < 0 \tag{7}$$

Let Ω_T and Ω_R denote sets of all solutions of eq. (4) per T(0) and (6) per R, respectively.

Equation (4) can be written in a different form as follows,

$$R - A_0 - e^{-R\tau}A_1 = 0 \tag{8}$$

and there follows

$$\det\left(R - A_0 - e^{-R\tau}A_1\right) = 0 \tag{9}$$

Substituting a matrix variable R by scalar variable s in (7), the characteristic equation of the system (1) is obtained as

$$f(s) = \det\left(sI - A_0 - e^{-s\tau}A_1\right) = 0 \tag{10}$$

Let us denote

$$\Sigma \,\square\, \{s \mid f(s) = 0\} \tag{11}$$

a set of all characteristic roots of the system (1). The necessity for the correctness of desired results, forced us to propose new formulations of *Theorem 1*.

Theorem 2. [47] Suppose that there exist(s) the solution(s) $T(0) \in \Omega_T$ of (4). Then, the system (1) is asymptotically stable if and only if for any matrix $Q = Q^* > 0$ there exists matrix $P_0 = P_0^* > 0$ such that (2) holds for all solutions $T(0) \in \Omega_T$ of (4).

Conclusion 1. Statement *Theorem 2* require that condition (2) is fulfilled for all solutions $T(0) \in \Omega_T$ of (4). In other words, it is requested that condition (7) holds for all solution R of (8), especially for $R = R_{max}$, where the matrix $R_m \in \Omega_R$ is maximal solvent of (8) that contains eigenvalue with a maximal real part $\lambda_m \in \Sigma:\ \mathrm{Re}\,\lambda_m = \max_{s \in \Sigma} \mathrm{Re}\,s$. Therefore, from (7) follows condition $\mathrm{Re}\,\lambda_i(R_m) < 0$.

On the basis of *Conclusion 1,* it is possible to reformulate *Theorem 2* in the following way.

Theorem 3. [47] Suppose that there exists maximal solvent R_m of (8). Then, the system (1) is asymptotically stable if and only if for any matrix $Q = Q^* > 0$ there exists matrix $P_0 = P_0^* > 0$ such that (6) holds for the solution $R = R_m$ of (8).

2.2 Continuous large scale time-delay systems

Consider a linear continuous large scale time-delay autonomous systems composed of N interconnected subsystems. Each subsystem is described as:

$$\dot{\mathbf{x}}_i(t) = A_i \mathbf{x}_i(t) + \sum_{j=1}^{N} A_{ij} \mathbf{x}_j(t - \tau_{ij}), \ 1 \le i \le N \tag{12}$$

with an associated function of initial state $\mathbf{x}_i(\theta) = \varphi_i(\theta), \ \theta \in \left[-\tau_{m_i}, \ 0\right], \ 1 \le i \le N$. $\mathbf{x}_i(t) \in R^{n_i}$ is state vector, $A_i \in R^{n_i \times n_i}$ denote the system matrix, $A_{ij} \in \mathbf{R}^{n_i \times n_j}$ represents the interconnection matrix between the i-th and the j-th subsystems, and τ_{ij} is constant delay.

For the sake of brevity, we first observe system (12) made up of two subsystems ($N = 2$). For this system, we derive new necessary and sufficient delay-dependent conditions for stability, by Lyapunov's direct method. The derived results are then extended to the linear continuous large scale time-delay systems with multiple subsystems.

2.2.1. Main results

Theorem 4. [49] Given the following system of matrix equations (SME)

$$R_1 - A_1 - e^{-R_1 \tau_{11}} A_{11} - e^{-R_1 \tau_{21}} S_2 A_{21} = 0 \tag{13}$$

$$R_1 S_2 - S_2 A_2 - e^{-R_1 \tau_{12}} A_{12} - e^{-R_1 \tau_{22}} S_2 A_{22} = 0 \tag{14}$$

where A_1, A_2, A_{12}, A_{21} and A_{22} are matrices of system (12) for $N = 2$, n_i subsystem orders and τ_{ij} time-delays of the system. If there exists solution of SME (13)-(14) upon unknown matrices $R_1 \in R^{n_1 \times n_1}$ and $S_2 \in C^{n_1 \times n_2}$, then the eigenvalues of matrix R_1 belong to a set of roots of the characteristic equation of system (12) for $N = 2$.

Proof. By introducing the time-delay operator $e^{-\tau s}$, the system (12) can be expressed in the form

$$\dot{\mathbf{x}}(t) = \begin{bmatrix} A_1 + A_{11} e^{-\tau_{11} s} & A_{12} e^{-\tau_{12} s} \\ A_{21} e^{-\tau_{21} s} & A_2 + A_{22} e^{-\tau_{22} s} \end{bmatrix} \mathbf{x}(t) = A_e(s) \mathbf{x}(t),$$

$$\mathbf{x}(t) = \left[\mathbf{x}_1^T(t) \quad \mathbf{x}_2^T(t) \right]^T \tag{15}$$

Let us form the following matrix

$$F(s) = \left[F_{ij}(s) \right] = sI_{n_1 + n_2} - A_e(s) = \begin{bmatrix} sI_{n_1} - A_1 - A_{11} e^{-\tau_{11} s} & -A_{12} e^{-\tau_{12} s} \\ -A_{21} e^{-\tau_{21} s} & sI_{n_2} - A_2 - A_{22} s^{-\tau_{22} s} \end{bmatrix} \tag{16}$$

Its determinant is

$$\det F(s) = \det\begin{bmatrix} F_{11}(s) + S_2 F_{21}(s) & F_{12}(s) + S_2 F_{22}(s) \\ F_{21}(s) & F_{22}(s) \end{bmatrix}$$

$$= \det\begin{bmatrix} G_{11}(s, S_2) & G_{12}(s, S_2) \\ G_{21}(s) & G_{22}(s) \end{bmatrix}$$

(17)

$$G_{11}(s, S_2) = sI_{n1} - A_1 - A_{11}e^{-\tau_{11}s} - S_2 A_{21}e^{-\tau_{21}s}$$

(18)

$$G_{12}(s, S_2) = sS_2 - S_2 A_2 - A_{12}e^{-\tau_{12}s} - S_2 A_{22}e^{-\tau_{22}s}$$

(19)

The characteristic polynomial of system (12) for $N = 2$, defined by

$$f(s) \triangleq \det(sI_N - A_e(s)) = \det G(s, S_2)$$

(20)

is independent of the choice of matrix S_2, because the determinant of matrix $G(s, S_2)$ is invariant with respect to elementary row operation of type 3. Let us designate a set of roots of the characteristic equation of system (12) by $\Sigma \triangleq \{ s \mid f(s) = 0 \}$. Substituting scalar variable s by matrix X in $G(s, S_2)$ we obtain

$$G(X, S_2) = \begin{bmatrix} G_{11}(X, S_2) & G_{12}(X, S_2) \\ G_{21}(X) & G_{22}(X) \end{bmatrix}$$

(21)

If there exist transformational matrix S_2 and matrix $R_1 \in \mathbf{C}^{n_1 \times n_1}$ such that $G_{11}(R_1, S_2) = 0$ and $G_{12}(R_1, S_2) = 0$ is satisfied, i.e. if (13)-(14) hold, then

$$f(R_1) = \det G_{11}(R_1, S_2) \cdot \det G_{22}(R_1) = 0$$

(22)

So, the characteristic polynomial (20) of system (12) is annihilating polynomial [48] for the square matrix R_1, defined by (13)-(14). In other words, $\sigma(R_1) \subset \Sigma$.

Theorem 5. [49] Given the following SME

$$R_2 - A_2 - e^{-R_2\tau_{12}}S_1 A_{12} - e^{-R_2\tau_{22}}A_{22} = 0$$

(23)

$$R_2 S_1 - S_1 A_1 - e^{-R_2\tau_{11}}S_1 A_{11} - e^{-R_2\tau_{21}}A_{21} = 0$$

(24)

where A_1, A_2, A_{12}, A_{21} and A_{22} are matrices of system (12) for $N = 2$, n_i subsystem orders and τ_{ij} time-delays of the system. If there exists solution of SME (23)-(24) upon unknown matrices $R_2 \in \mathbf{C}^{n_2 \times n_2}$ and $S_1 \in \mathbf{C}^{n_2 \times n_1}$, then the eigenvalues of matrix R_2 belong to a set of roots of the characteristic equation of system (12) for $N = 2$.

Proof. Proof is similarly with the proof of *Theorem 4*.

Definition 1. The matrix R_1 (R_2) is referred to as *solvent* of SME (13)-(14) ((23)-(24)).

Definition 2. Each root λ_m of the characteristic equation (20) of the system (12) which satisfies the following condition: $\text{Re}\,\lambda_m = \max \text{Re}\,s,\ \ s \in \Sigma$ will be referred to as *maximal eigenvalue* of system (12).

Definition 3. Each solvent R_{1m} (R_{2m}) of SME (13)-(14) ((23)-(24)), whose spectrum contains maximal eigenvalue λ_m of system (12), is referred to as *maximal solvent* of SME (13)-(14) ((23)-(24)).

Theorem 6. [49] Suppose that there exists maximal solvent of SME (23)-(24) and let R_{1m} denote one of them. Then, system (12), for $N = 2$, is asymptotically stable if and only if for any matrix $Q = Q^* > 0$ there exists matrix $P = P^* > 0$ such that

$$R_{1m}^* P + P R_{1m} = -Q \tag{25}$$

Proof. *Sufficient condition.* Define the following vector continuous functions

$$\mathbf{x}_{ti} = \mathbf{x}_i(t + \theta), \quad \theta \in \left[-\tau_{m_i},\ 0\right],$$

$$\mathbf{z}(\mathbf{x}_{t1}, \mathbf{x}_{t2}) = \sum_{i=1}^{2} S_i\left(\mathbf{x}_i(t) + \sum_{j=1}^{2} \int_0^{\tau_{ji}} T_{ji}(\eta)\mathbf{x}_i(t - \eta)d\eta\right) \tag{26}$$

where $T_{ji}(t) \in \mathbf{C}^{n_i \times n_i}$, $j = 1, 2$ are varying continuous matrix functions and $S_1 = I_{n_1}$, $S_2 \in \mathbf{C}^{n_1 \times n_2}$.

The proof of the theorem follows immediately by defining Lyapunov functional for system (12) as

$$V(\mathbf{x}_{t1}, \mathbf{x}_{t2}) = \mathbf{z}^*(\mathbf{x}_{t1}, \mathbf{x}_{t2}) P \mathbf{z}(\mathbf{x}_{t1}, \mathbf{x}_{t2}), \quad P = P^* > 0 \tag{27}$$

Derivative of (27), along the solutions of system (12) is

$$\dot{V}(\mathbf{x}_{t1}, \mathbf{x}_{t2}) = \dot{\mathbf{z}}^*(\mathbf{x}_{t1}, \mathbf{x}_{t2}) P \mathbf{z}(\mathbf{x}_{t1}, \mathbf{x}_{t2}) + \mathbf{z}^*(\mathbf{x}_{t1}, \mathbf{x}_{t2}) P \dot{\mathbf{z}}(\mathbf{x}_{t1}, \mathbf{x}_{t2}) \tag{28}$$

$$\dot{\mathbf{z}}(\mathbf{x}_{t1}, \mathbf{x}_{t2}) = \sum_{i=1}^{2}\left\{ S_i\left(A_i + \sum_{j=1}^{2} T_{ji}(0)\right)\mathbf{x}_i(t)\right.$$

$$\left. + \sum_{j=1}^{2}\left(S_j A_{ji} - S_i T_{ji}(\tau_{ji})\right)\mathbf{x}_i(t - \tau_{ji}) + \sum_{j=1}^{2}\int_0^{\tau_{ji}} S_i T_{ji}^{'}(\eta)\mathbf{x}_i(t - \eta)d\eta\right\} \tag{29}$$

If we define new matrices

$$R_i = A_i + \sum_{j=1}^{2} T_{ji}(0),\ \ i = 1, 2 \tag{30}$$

and if one adopts

$$S_i T_{ji}(\tau_{ji}) = S_j A_{ji}\ ,\ \ i, j = 1, 2 \tag{31}$$

$$S_i T_{ji}^{'}(\eta) = R_1 S_i T_{ji}(\eta), \quad S_i R_i = R_1 S_i, \quad i, j = 1, 2 \tag{32}$$

then

$$\dot{\mathbf{z}}(\mathbf{x}_{t1}, \mathbf{x}_{t2}) = R_1 \mathbf{z}(\mathbf{x}_{t1}, \mathbf{x}_{t2}), \quad \dot{V}(\mathbf{x}_{t1}, \mathbf{x}_{t2}) = \mathbf{z}^*(\mathbf{x}_{t1}, \mathbf{x}_{t2})\left(R_1^* P + P R_1\right) \mathbf{z}(\mathbf{x}_{t1}, \mathbf{x}_{t2}) \tag{33}$$

It is obvious that if the following equation is satisfied

$$R_1^* P + P R_1 = -Q < 0, \tag{34}$$

then $\dot{V}(\mathbf{x}_{t1}, \mathbf{x}_{t2}) < 0$, $\forall \mathbf{x}_{ti} \neq \mathbf{0}$.

In the Lyapunov matrix equation (25), of all possible solvents R_1 only one of maximal solvents R_{1m} is of importance, because it is containing maximal eigenvalue $\lambda_m \in \Sigma$, which has dominant influence on the stability of the system.

Necessary condition. Let us assume that system (12) for $N = 2$ is asymptotically stable, i.e. $\forall s \in \Sigma$, $\mathrm{Re}\, s < 0$ hold. Since $\sigma(R_{1m}) \subset \Sigma$ follows $\mathrm{Re}\, \lambda(R_{1m}) < 0$ and the positive definite solution of Lyapunov matrix equation (25) exists.

From (31)-(32) follows

$$S_j A_{ji} = e^{R_1 \tau_{ji}} S_i T_{ji}(0), \quad S_1 = I_{n_1}, \quad i = 1, 2, \ j = 1, 2 \tag{35}$$

Using (30) and (35), for $i = 1$, we obtain (13). Multiplying (30) (for $i = 2$) from the left by matrix S_2 and using (32) and (35) we obtain (14). Taking a solvent with eigenvalue $\lambda_m \in \Sigma$ (if it exists) as a solution of the system of equations (13)-(14), we arrive at a maximal solvent R_{1m}.

Theorem 7. [49] Suppose that there exists maximal solvent of SME (23)-(24) and let R_{2m} denote one of them. Then, system (12), for $N = 2$, is asymptotically stable if and only if for any matrix $Q = Q^* > 0$ there exists matrix $P = P^* > 0$ such that

$$R_{2m}^* P + P R_{2m} = -Q \tag{36}$$

Proof. Proof is almost identical to that exposed for *Theorem 6*.

Theorem 8. [49] Given the following system of matrix equations

$$R_k S_i - S_i A_i - \sum_{j=1}^{N} e^{-R_k \tau_{ji}} S_j A_{ji} = 0, \quad S_i \in \mathbf{C}^{n_k \times n_i}, \quad S_k = I_{n_k}, \quad 1 \leq i \leq N \tag{37}$$

for a given k, $1 \leq k \leq N$, where A_i and A_{ji}, $1 \leq i \leq N$, $1 \leq j \leq N$ are matrices of system (12) and τ_{ji} is time-delay in the system. If there is a solvent of (37) upon unknown matrices $R_k \in \mathbf{C}^{n_k \times n_k}$ and S_i, $1 \leq i \leq N$, $i \neq k$, then the eigenvalues of matrix R_k belong to a set of roots of the characteristic equation of system (12).

Proof. Proof of this theorem is a generalization of proof of *Theorem* 4 or *Theorem* 5.

Theorem 9 [49] Suppose that there exists maximal solvent of (37) for given k,

$1 \leq k \leq N$ and let R_{km} denote one of them. Then, linear discrete large scale time-delay system (12) is asymptotically stable if and only if for any matrix $Q = Q^* > 0$ there exists matrix $P = P^* > 0$ such that

$$R_{km}^* \, P + P \, R_{km} = -Q \qquad (38)$$

Proof. Proof is based on generalization of proof for *Theorem* 6 or *Theorem* 7. It is sufficient to take arbitrary N instead of $N = 2$.

Example 1. Consider following continuous large scale time-delay system with delay interconnections

$$\dot{x}_1(t) = A_1 x_1(t) + A_{12} x_2(t - \tau_{12}), \quad \dot{x}_2(t) = A_2 x_2(t) + A_{21} x_1(t - \tau_{21}) + A_{23} x_3(t - \tau_{23})$$

$$\dot{x}_3(t) = A_3 x_3(t) + A_{31} x_1(t - \tau_{31}) + A_{32} x_2(t - \tau_{32}) \qquad (39)$$

$$A_1 = \begin{bmatrix} -6 & 2 & 0 \\ 0 & -7 & 0 \\ 0 & 0 & -10.9 \end{bmatrix}, \; A_{12} = \begin{bmatrix} 3 & -2 & 0 \\ 0 & 0 & 3 \\ -2 & 1 & 2 \end{bmatrix}, \; A_2 = \begin{bmatrix} -1.87 & 4.91 & 10.30 \\ -2.23 & -16.51 & -24.11 \\ 1.87 & -3.91 & -10.30 \end{bmatrix}$$

$$A_{21} = \begin{bmatrix} -1 & 0 & -2 \\ 3 & 0 & 5 \\ 1 & 0 & 2 \end{bmatrix}, \quad A_{23} = \begin{bmatrix} -1 & -1 \\ 3 & 2 \\ 1 & 1 \end{bmatrix}$$

$$A_3 = \begin{bmatrix} -18.5 & -17.5 \\ -13.5 & -18.5 \end{bmatrix}, \quad A_{31} = \begin{bmatrix} 4 & -2 & 1 \\ 2 & 0 & 1 \end{bmatrix}, \quad A_{32} = \begin{bmatrix} 1 & 2 & -1 \\ 3 & 2 & 0 \end{bmatrix},$$

Applying *Theorem* 8 to a given system, for $k = 1$, the following SME is obtained

$$R_1 - A_1 - e^{-R_1 \tau_{21}} S_2 A_{21} - e^{-R_1 \tau_{31}} S_3 A_{31} = 0, \quad R_1 S_2 - S_2 A_2 - e^{-R_1 \tau_{12}} A_{12} - e^{-R_1 \tau_{32}} S_3 A_{32} = 0$$

$$R_1 S_3 - S_3 A_3 - e^{-R_1 \tau_{23}} S_2 A_{23} = 0$$

If for pure time-delays we adopt the following values: $\tau_{12} = 5$, $\tau_{21} = 2$, $\tau_{23} = 4$, $\tau_{31} = 5$ and $\tau_{32} = 3$, by applying the nonlinear least squares algorithms, we obtain a great number of solutions upon R_1. Among those solutions is a maximal solution:

$$R_{1m} = \begin{bmatrix} -0.0484 & -0.0996 & 0.0934 \\ 0.2789 & -0.3123 & 0.2104 \\ 1.1798 & -1.1970 & -0.3798 \end{bmatrix}$$

The eigenvalues of matrix R_{1m} amount to: $\lambda_1 = -0.2517$, $\lambda_{2,3} = -0.2444 \pm j\, 0.3726$.

Therefore, for a maximal eigenvalue λ_m one of the values from the set $\{\lambda_2, \lambda_3\}$ can be adopted. Based on *Theorem* 9, it follows that the large scale time-delay system is asymptotically stable.

2.3 Discrete time-delay systems

A linear, discrete time-delay system can be represented by the difference equation

$$\mathbf{x}(k+1) = A_0 \mathbf{x}(k) + A_1 \mathbf{x}(k-h) \tag{40}$$

with an associated function of initial state

$$\mathbf{x}(\theta) = \boldsymbol{\psi}(\theta), \qquad \theta \in \{-h, -h+1, \dots, 0\} \tag{41}$$

The equation (40) is referred to as homogenous or the unforced state equation. Vector $\mathbf{x}(k) \in R^n$ is a state vector and $A_0, A_1 \in R^{n \times n}$ are constant matrices of appropriate dimensions, and pure time-delay is expressed by integers $h \in T^+$.

System (40) can be expressed with the following representation without delay [22], [46].

$$\mathbf{x}_a(k) = \left[\mathbf{x}^T(k-h) \quad \mathbf{x}^T(k-h+1) \quad \cdots \quad \mathbf{x}^T(k) \right] \in R^N, \qquad N \triangleq n(h+1)$$

$$\mathbf{x}_a(k+1) = A_a \mathbf{x}_a(k), \quad A_a = \begin{bmatrix} 0 & I_n & \cdots & 0 \\ \vdots & \vdots & \ddots & \vdots \\ 0 & 0 & \cdots & I_n \\ A_1 & 0 & \cdots & A_0 \end{bmatrix} \in R^{N \times N} \tag{42}$$

The system defined by (42) is called the augmented system, while matrix A_a, the matrix of augmented system. Characteristic polynomial of system (40) is given with:

$$f(\lambda) \triangleq \det M(\lambda) = \sum_{j=0}^{n(h+1)} a_j \lambda^j, \quad a_j \in R, \qquad M(\lambda) = I_n \lambda^{h+1} - A_0 \lambda^h - A_1 \tag{43}$$

Denote with

$$\Omega \triangleq \left\{ \lambda \mid f(\lambda) = 0 \right\} = \lambda(A_{eq}) \tag{44}$$

the set of all characteristic roots of system (40). The number of these roots amounts to $n(h+1)$. A root λ_m of Ω with maximal module:

$$\lambda_m \in \Omega : |\lambda_m| = \max |\lambda(A_a)| \tag{45}$$

let us call maximal eigenvalue.

2.3.1. Main results

If scalar variable λ in the characteristic polynomial is replaced by matrix $X \in C^{n \times n}$ the following monic matrix polynomial is obtained

$$M(X) = X^{h+1} - X^h A_0 - A_1 \tag{46}$$

For the needs stability of system (40) only the maximal solvents of (46) are usable, whose spectrums contain maximal eigenvalue λ_m. A special case of maximal solvent is

the so called dominant solvent [51], [52] which can be computed in a simple way by Bernoulii or Traub algorithm.

Definition 4. Every solvent R_m of (46) whose spectrum $\sigma(R_m)$ contains maximal eigenvalue λ_m of Ω is a *maximal solvent*.

Definition 5. [51], [52] Matrix A dominates matrix B if all the eigenvalues of A are greater, in modulus, then those of B. In particular, if the solvent R_1 of (46) dominates the solvents $R_2, \ldots, R_l$ we say it is a *dominant solvent*.

Theorem 10. [50] Suppose that there exists maximal solvent of (46) and let R_m denote one of them. Then, linear discrete time-delay system (40) is asymptotically stable if and only if for any matrix $Q = Q^* > 0$ there exists matrix $P = P^* > 0$ such that

$$R_m^* P R_m - P = -Q \tag{47}$$

Proof. S*ufficient condition.* Define the following vector discrete functions

$$\mathbf{x}_k = \mathbf{x}(k+\theta), \quad \theta \in \{-h, -h+1, \ldots, 0\}, \quad \mathbf{z}(\mathbf{x}_k) = \mathbf{x}(k) + \sum_{j=1}^{h} T(j) \mathbf{x}(k-j) \tag{48}$$

where, $T(k) \in C^{n \times n}$ is, in general, some time varying discrete matrix function. The conclusion of the theorem follows immediately by defining Lyapunov functional for the system (40) as

$$V(\mathbf{x}_k) = \mathbf{z}^*(\mathbf{x}_k) P \mathbf{z}(\mathbf{x}_k), \quad P = P^* > 0 \tag{49}$$

It is obvious that $\mathbf{z}(\mathbf{x}_k) = \mathbf{0}$ if and only if $\mathbf{x}_k = \mathbf{0}$, so it follows that $V(\mathbf{x}_k) > 0$ for $\forall \mathbf{x}_k \neq 0$.

The forward difference of (49), along the solutions of system (40) is

$$\Delta V(\mathbf{x}_k) = \Delta \mathbf{z}^*(\mathbf{x}_k) P \mathbf{z}(k) + \mathbf{z}^*(\mathbf{x}_k) P \Delta \mathbf{z}(\mathbf{x}_k) + \Delta \mathbf{z}^*(\mathbf{x}_k) P \Delta \mathbf{z}(\mathbf{x}_k) \tag{50}$$

A difference of $\Delta \mathbf{z}(\mathbf{x}_k)$ can be determined in the following manner

$$\Delta \mathbf{z}(\mathbf{x}_k) = \Delta \mathbf{x}(k) + \sum_{j=1}^{h} T(j) \Delta \mathbf{x}(k-j), \quad \Delta \mathbf{x}(k) = (A_0 - I_n) \mathbf{x}(k) + A_1 \mathbf{x}(k-h)$$

$$\sum_{j=1}^{h} T(j) \Delta \mathbf{x}(k-j) = T(1) \mathbf{x}(k) - T(h) \mathbf{x}(k-h) + (T(2) - T(1)) \mathbf{x}(k-1) + \cdots \tag{51}$$

$$+ (T(h) - T(h-1)) \mathbf{x}(k-h+1)$$

Define a new matrix R by

$$R \, \square \, A_0 + T(1) \tag{52}$$

If

$$\Delta T(h) = A_1 - T(h) \tag{53}$$

then $\Delta \mathbf{z}(\mathbf{x}_k)$ has a form

$$\Delta \mathbf{z}(\mathbf{x}_k) = (R - I_n)\mathbf{x}(k) + \sum_{j=1}^{h} \left[\Delta T(j) \cdot \mathbf{x}(k-j)\right] \tag{54}$$

If one adopts

$$\Delta T(j) = (R - I_n)T(j), \quad j = 1, 2, \ldots, h \tag{55}$$

then (50) becomes

$$\Delta V(\mathbf{x}_k) = \mathbf{z}^*(\mathbf{x}_k)\left(R^* PR - P\right)\mathbf{z}(\mathbf{x}_k) \tag{56}$$

It is obvious that if the following equation is satisfied

$$R^* PR - P = -Q, \quad Q = Q^* > 0 \tag{57}$$

then $\Delta V(\mathbf{x}_k) < 0, \ \mathbf{x}_k \neq \mathbf{0}$.

In the Lyapunov matrix equation (57), of all possible solvents R of (46), only one of maximal solvents R_m is of importance, because it is containing maximal eigenvalue $\lambda_m \in \Omega$, which has dominant influence on the stability of the system. So, (47) represent stability sufficient condition for system given by (40).

Necessary condition. If the system (40) is asymptotically stable then all roots $\lambda_i \in \Omega$ are located within unit circle. Since $\sigma(R_m) \subset \Omega$, follows $\rho(R_m) < 1$, so the positive definite solution of Lyapunov matrix equation (47) exists.

Matrix $T(1)$ can be determined in the following way. From (55), follows

$$T(h+1) = R^h T(1) \tag{58}$$

and using (52)-(53) one can get (46).

Corollary 1. [50] Suppose that there exists maximal solvent of (46) and let R_m denote one of them. Then, system (40) is asymptotically stable if and only if $\rho(R_m) < 1$.

Proof. Follows directly from *Theorem 10*.

Corollary 2. [50] Suppose that there exists dominant solvent R_1 of (46). Then, system (40) is asymptotically stable if and only if $\rho(R_1) < 1$.

Proof. Follows directly from *Corollary* 1, since dominant solution is, at the same time, maximal solvent.

Example 2. Let us consider linear discrete systems with delayed state (40) with

$$A_0 = \begin{bmatrix} 7/10 & -1/2 \\ 1/2 & 17/10 \end{bmatrix}, \quad A_1 = \begin{bmatrix} 1/75 & 1/3 \\ -1/3 & -49/75 \end{bmatrix} \tag{59}$$

A. For $h = 1$ there are two solvents of matrix polynomial equation (46) ($R^2 - RA_0 - A_1 = 0$):

$$R_1 = \begin{bmatrix} 19/30 & -1/6 \\ 1/6 & 29/30 \end{bmatrix}, \quad R_2 = \begin{bmatrix} 1/15 & -1/3 \\ 1/3 & 11/15 \end{bmatrix},$$

Since $\lambda(R_1) = \{4/5, 4/5\}$, $\lambda(R_2) = \{2/5, 2/5\}$, dominant solvent is R_1. For getting the dominant solvent Bernoulli or Traub's algorithm may be used. After $(4+3)$ iterations for Traub's algorithm [52] and 17 iterations for Bernoulli algorithm [52], dominant solvent can be found with accuracy of 10^{-4}. Since $\rho(R_1) = 4/5 < 1$, based on *Corollary* 2, it follows that the system under consideration is asymptotically stable.
B. For $h = 20$ applying Bernoulli or Traub's algorithm for computation the dominant solvent R_1 of matrix polynomial equation (46) ($R^{21} - R^{20}A_0 - A_1 = 0$), we obtain

$$R_1 = \begin{bmatrix} 0.6034 & -0.5868 \\ 0.5868 & 1.7769 \end{bmatrix}$$

Based on *Corollary* 2, the system is not asymptotically stable because $\rho(R_1) = 1.1902 > 1$.

2.4 Discrete large scale time-delay systems

Consider a large-scale linear discrete time-delay systems composed of N interconnected S_i. Each subsystem S_i, $1 \le i \le N$ is described as

$$S_i: \quad \mathbf{x}_i(k+1) = A_i\mathbf{x}_i(k) + \sum_{j=1}^{N} A_{ij}\mathbf{x}_j(k - h_{ij}) \tag{60}$$

with an associated function of initial state

$$\mathbf{x}_i(\theta) = \mathbf{\psi}_i(\theta), \quad \theta \in \left\{-h_{m_i}, -h_{m_i} + 1, \ldots, 0\right\} \tag{61}$$

where $\mathbf{x}_i(k) \in R^{n_i}$ is state vector, $A_i \in R^{n_i \times n_i}$ denotes the system matrix, $A_{ij} \in R^{n_i \times n_j}$ represents the interconnection matrix between the i-th and the j-th subsystems and the constant delay $h_{ij} \in T^+$.

Lemma 1. System (60) will be asymptotically stable if and only if

$$\left|\lambda_{\max}(A_a)\right| < 1 \tag{62}$$

holds, where matrix

$$A_a = \left[A_{aij}\right] \in R^{N_a \times N_a}, \quad N_a = \sum_{i=1}^{N} N_i, \quad N_i = n_i\left(h_{m_i} + 1\right), \quad h_{m_i} = \max_j h_{ji} \tag{63}$$

is defined in the following way

$$A_{aii} = \begin{bmatrix} \overset{\underset{\downarrow}{1}}{A_i} & 0 & \cdots & \overset{\underset{\downarrow}{h_{ii}+1}}{A_{ii}} & \cdots & 0 & 0 \\ \hline I_{n_i} & 0 & \cdots & 0 & \cdots & 0 & 0 \\ \vdots & \vdots & \cdots & \vdots & \cdots & \vdots & \vdots \\ 0 & 0 & \vdots & 0 & \vdots & I_{n_i} & 0 \end{bmatrix} \in R^{N_i \times N_i},$$

$$A_{aij} = \begin{bmatrix} \overset{\underset{\downarrow}{1}}{0} & \cdots & \overset{\underset{\downarrow}{h_{ij}+1}}{A_{ij}} & \cdots & 0 \\ \hline 0 & \cdots & 0 & \cdots & 0 \\ \vdots & \vdots & \vdots & \ddots & \vdots \\ 0 & \cdots & 0 & \cdots & 0 \end{bmatrix} \in R^{N_i \times N_i}$$

(64)

where A_i and A_{ij}, $1 \le i \le N$, $1 \le j \le N$, are matrices of system (60).

2.4.1. Main results

Theorem 11. [53] Given the following system of monic matrix polynomial equations

$$R_l^{h_{m_i}+1} S_i - R_l^{h_{m_i}} S_i A_i - \sum_{j=1}^{N} R_l^{h_{m_i}-h_{ji}} S_j A_{ji} = 0, \quad S_i \in C^{n_i \times n_i}, \quad S_l = I_{n_i}$$

(65)

for a given l, $1 \le l \le N$, where A_i and A_{ji}, $1 \le i \le N$, $1 \le j \le N$ are matrices of system (60) and h_{ji} is time-delay in the system, $h_{m_i} = \max_j h_{ji}$, $1 \le i \le N$.

If there is a solution of (65) upon unknown matrices $R_l \in C^{n_l \times n_l}$ and S_i, $1 \le i \le N$, $i \ne l$, then $\lambda(R_l) \subset \lambda(A_a)$ holds, where matrix A_a is defined by (63)-(64).

Proof. By introducing time-delay operator z^{-h}, system (60) can be expressed in the following form

$$\mathbf{x}(k+1) = A_e(z)\mathbf{x}(k), \quad \mathbf{x}(k) = \begin{bmatrix} \mathbf{x}_1^T(k) & \mathbf{x}_2^T(k) & \cdots & \mathbf{x}_N^T(k) \end{bmatrix}^T$$

$$A_e(z) = \begin{bmatrix} A_1 + A_{11}z^{-h_{11}} & \cdots & A_{1N}z^{-h_{1N}} \\ \vdots & \ddots & \vdots \\ A_{N1}z^{-h_{N1}} & \cdots & A_N + A_{NN}z^{-h_{NN}} \end{bmatrix}$$

(66)

Let us form the following matrix.

$$F(z) = zI_{N_e} - A_e(z) = \begin{bmatrix} F_{ij}(z) \end{bmatrix}$$

(67)

If we add to the arbitrarily chosen l-th block row of this matrix the rest of its block rows previously multiplied from the left by the matrices $S_j \ne 0$, $1 \le j \le N$, $j \ne l$ respectively and after multiplying i-th of the block column, $1 \le i \le N$, of the preceding matrix by $z^{h_{m_i}}$ and after integrating the matrix $S_l = I_{n_l}$, we obtain

$$z^{\sum_{i=1}^{N} n_i h_{m_i}} \cdot \det F(z) = \det \begin{bmatrix} z^{h_{m_1}} F_{11}(z) & \cdots & z^{h_{m_N}} F_{1N}(z) \\ \vdots & \vdots & \vdots \\ z^{h_{m_1}} \sum_{j=1}^{N} S_j F_{j1}(z) & \cdots & z^{h_{m_N}} \sum_{j=1}^{N} S_j F_{jN}(z) \\ \vdots & \ddots & \vdots \\ z^{h_{m_1}} F_{N1}(z) & \cdots & z^{h_{m_N}} F_{NN}(z) \end{bmatrix}$$

$$= \det \begin{bmatrix} G_{11}(z) & \cdots & G_{1N}(z) \\ \vdots & \vdots & \vdots \\ G_{l1}(z,S) & \cdots & G_{lN}(z,S) \\ \vdots & \vdots & \vdots \\ G_{N1}(z) & \cdots & G_{NN}(z) \end{bmatrix} \tag{68}$$

$$= \det G(z,S), \quad S = \{S_1, \cdots, S_N\}$$

The l-th block row of the $N \times N$ block matrix $G(z,S)$ is defined by

$$G_{li}(z,S) = z^{h_{m_i}+1} S_i - z^{h_{m_i}} S_i A_i - \sum_{j=1}^{N} z^{h_{m_i} - h_{ji}} S_j A_{ji}, \quad 1 \le i \le N, \qquad S_l = I_{n_l} \tag{69}$$

The characteristic polynomial of system (60) [46]

$$g(z) \triangleq \det G(z,S) = \sum_{j=0}^{N_e} a_j z^j, \quad N_e = \sum_{i=1}^{N} n_i (h_{m_i} + 1), \, a_j \in R, 0 \le j \le N_e \tag{70}$$

does not depend on the choice of transformation matrices $S_1, \cdots, S_N$) [48].

Let us denote

$$\Sigma \triangleq \{z \mid g(z) = 0\} \tag{71}$$

a set of all characteristic roots of system (60). This set of roots equals the set $\lambda(A_a)$. Substituting a scalar variable z by matrix $X \in C^{n_l \times n_l}$ in $G(z,S)$, a new block matrix is obtained $G(X,S)$. If there exist the transformation matrices S_i, $1 \le i \le N$, $i \ne l$ and solvent $R_l \in C^{n_l \times n_l}$ such that for the l-th block row of $G(X,S)$ holds $G_{li}(R_l, S) = 0$, $1 \le i \le N$ i.e. holds (65), then

$$g(R_l) = 0 \tag{72}$$

Therefore, the characteristic polynomial of system (60) is annihilating polynomial for the square matrix R_l and $\lambda(R_l) \subset \Sigma$ holds. The mentioned assertion holds $\forall l, \quad 1 \le l \le N$.

Definition 6. Each solvent R_{lm} of (65), for the given l, $1 \leq l \leq N$, whose spectrum contains maximal eigenvalue λ_m of system (60), is referred to as *maximal solvent* of (65).

Theorem 12 [53] Suppose that there exist at least one l, $1 \leq l \leq N$, that there exists maximal solvent of (65) and let R_{lm} denote one of them. Then, linear discrete large-scale time-delay system (60) is asymptotically stable if and only if for any matrix $Q = Q^* > 0$ there exists matrix $P = P^* > 0$ such that

$$R_{lm}^{\;*} \, P \, R_{lm} - P = -Q \, . \tag{73}$$

Proof. S*ufficient condition.* Define the following vector discrete functions

$$\mathbf{v}\left(\mathbf{x}_{k1}, \cdots, \mathbf{x}_{kN}\right) = \sum_{i=1}^{N} S_i \left[\mathbf{x}_i\left(k\right) + \sum_{j=1}^{N} \sum_{l=1}^{h_{ji}} T_{ji}\left(l\right)\mathbf{x}_i\left(k-l\right) \right], \tag{74}$$

$$\mathbf{x}_{ki} = \mathbf{x}_i\left(k+\theta\right), \quad \theta \in \left\{-h_{m_i}, \, \ldots \, , 0\right\}$$

where $T_{ji}\left(k\right) \in C^{n_i \times n_i}$, $1 \leq j \leq N$, $1 \leq i \leq N$ are, in general, some time-varying discrete matrix functions and $S_l = I_{n_l}$, $S_i \in C^{n_l \times n_i}$, $1 \leq i \leq N$, $i \neq l$. The conclusion of the theorem follows immediately by defining Lyapunov functional for system (60) as

$$V\left(\mathbf{x}_{k1}, \cdots, \mathbf{x}_{kN}\right) = \mathbf{v}^*\left(\cdot, \cdots, \cdot\right) P \, \mathbf{v}\left(\cdot, \cdots, \cdot\right), \quad P = P^* > 0 \tag{75}$$

It is obvious that $V\left(\cdot, \cdots, \cdot\right) > 0$ for $\forall \mathbf{x}_{ki} \neq \mathbf{0}$, $1 \leq i \leq N$.

The forward difference of (75), along the solutions of system (60) is

$$\mathrm{D}V\left(\cdot, \cdots, \cdot\right) = \mathrm{D}\,\mathbf{v}^*\left(\cdot, \cdots, \cdot\right) P \, \mathbf{v}\left(\cdot, \cdots, \cdot\right) + \mathbf{v}^*\left(\cdot, \cdots, \cdot\right) P \, \mathrm{D}\,\mathbf{v}\left(\cdot, \cdots, \cdot\right)$$
$$+ \mathrm{D}\,\mathbf{v}^*\left(\cdot, \cdots, \cdot\right) P \, \mathrm{D}\,\mathbf{v}\left(\cdot, \cdots, \cdot\right) \tag{76}$$

A difference of $\mathbf{v}\left(\cdot, \cdots, \cdot\right)$ can be determined in the following manner

$$\mathrm{D}\,\mathbf{v}\left(\cdot, \cdots, \cdot\right) = \sum_{i=1}^{N} S_i \left[\left(A_i - I_{n_i} + \sum_{j=1}^{N} T_{ji}\left(1\right) \right) \mathbf{x}_i\left(k\right) + \sum_{j=1}^{N} T_{ji}\left(h_{ji}\right)\mathbf{x}_i\left(k-h_{ji}\right) \right.$$
$$\left. + \sum_{j=1}^{N} \sum_{l=1}^{h_{ji}-1} \mathrm{D}\,T_{ji}\left(l\right)\mathbf{x}_i\left(k-l\right) + \sum_{j=1}^{N} A_{ij}\mathbf{x}_j\left(k-h_{ij}\right) \right] \tag{77}$$

If we define new matrices

$$R_i = A_i + \sum_{j=1}^{N} T_{ji}\left(1\right), \; 1 \leq i \leq N \tag{78}$$

then $\mathrm{D}\,\mathbf{v}\left(\cdot, \cdots, \cdot\right)$ has a form

$$\mathrm{D}\,\mathbf{v}\left(\cdot,\cdots,\cdot\right) = \sum_{i=1}^{N}\left[S_i\left(R_i - I_{n_i}\right)\mathbf{x}_i\left(k\right) + \sum_{j=1}^{N}\left(S_j A_{ji} - S_i T_{ji}\left(h_{ji}\right)\right)\mathbf{x}_i\left(k - h_{ji}\right)\right.$$
$$\left. + \sum_{j=1}^{N}\sum_{l=1}^{h_{ji}-1} S_i \Delta T_{ji}\left(l\right)\mathbf{x}_i\left(k - l\right)\right] \tag{79}$$

If

$$S_j A_{ji} - S_i T_{ji}\left(h_{ji}\right) = S_i \mathrm{D} T_{ji}\left(h_{ji}\right), \quad 1 \le i \le N, \quad 1 \le j \le N \tag{80}$$

$$S_i\left(R_i - I_{n_i}\right) = \left(R_l - I_{n_l}\right)S_i, \quad 1 \le i \le N \tag{81}$$

$$S_i \mathrm{D}\, T_{ji}\left(l\right) = \left(R_l - I_{n_l}\right)S_i\, T_{ji}\left(l\right), \quad 1 \le i \le N, \quad 1 \le j \le N \tag{82}$$

then

$$\mathrm{D}\,\mathbf{v}\left(\cdot,\cdots,\cdot\right) = \left(R_l - I_{n_l}\right)\mathbf{v}\left(\cdot,\cdots,\cdot\right),$$
$$\mathrm{D}V\left(\cdot,\cdots,\cdot\right) = \mathbf{v}^*\left(\cdot,\cdots,\cdot\right)\left(R_l^* P\, R_l - P\right)\mathbf{v}\left(\cdot,\cdots,\cdot\right) \tag{83}$$

It is obvious that if the following equation is satisfied

$$R_l^* P\, R_l - P = -Q, \qquad Q = Q^* > 0 \tag{84}$$

then $\mathrm{D}V\left(\cdot,\cdots,\cdot\right) < 0$, $\forall \mathbf{x}_{ki} \ne \mathbf{0}$, $1 \le i \le N$.

In the Lyapunov matrix equation (73), of all possible solvents R_l of (65), only one of maximal solvents R_{lm} is of importance, for it is the only one that contains maximal eigenvalue $\lambda_m \in \Sigma$, which has dominant influence on the stability of the system.

Necessary condition. If system (60) is asymptotically stable, then $\forall \lambda_i \in \Sigma$, $\left|\lambda_i\right| < 1$. Since $\lambda\left(R_{lm}\right) \subset \Sigma$, it follows that $\rho\left(R_{lm}\right) < 1$, therefore the positive definite solution of Lyapunov matrix equation (60) exists.

If it exists, maximal solvent R_{lm} can be determined in the following way. From (80) and (82) we obtain

$$S_j A_{ji} = R_l^{h_{ji}} S_i T_{ji}\left(1\right), \quad S_l = I_{n_l}, \quad 1 \le i \le N, \quad 1 \le j \le N \tag{85}$$

Multiplying i-th equation of the system of matrix equations (78) from the left by matrix $R_l^{h_{mi}} S_i$ and using (81) and (85), we obtain equation (65). Taking solvent with eigenvalue $\lambda_m \in \Sigma$ (if it exists) as a solution of the system of equations (65), we arrive at maximal solvent R_{lm}.

Corollary 3. Suppose that for the given l, $1 \le l \le N$, there exists matrix R_l being solution of (65). If system (60) is asymptotically stable, then matrix R_l is discrete stable.

Proof. If system (60) is asymptotically stable, then $\forall z \in \Sigma \;\; |z| < 1$. Since $\lambda(R_l) \subset \Sigma$, it follows that $\forall \lambda \in \lambda(R_l), \;\; |\lambda| < 1$, i.e. matrix R_l is discrete stable.

Example 3. Consider a large-scale linear discrete time-delay systems, consisting of three subsystems

$$S_1: \; x_1(k+1) = A_1 x_1(k) + B_1 u_1(k) + A_{12} x_2(k - h_{12}),$$
$$S_2: \; x_2(k+1) = A_2 x_2(k) + B_2 u_2(k) + A_{21} x_1(k - h_{21}) + A_{23} x_3(k - h_{23}), \qquad (86)$$
$$S_3: \; x_3(k+1) = A_3 x_3(k) + B_3 u_3(k) + A_{31} x_1(k - h_{31})$$

$$A_1 = \begin{bmatrix} 0.8 & 0.6 \\ 0.4 & 0.9 \end{bmatrix}, \; A_2 = \begin{bmatrix} 0.7 & 0 & -0.5 \\ -0.1 & 6 & -0.1 \\ -0.6 & 1 & 0.8 \end{bmatrix}, \; B_1 = \begin{bmatrix} 0.1 \\ 0.1 \end{bmatrix}, \; A_{12} = \begin{bmatrix} 0.1 & 0 & 0.1 \\ 0.1 & 0 & 0.1 \end{bmatrix}$$

$$B_2 = \begin{bmatrix} 0 & -0.1 \\ 0.1 & 0.2 \\ 0 & 0.1 \end{bmatrix}, \; A_{21} = \begin{bmatrix} -0.1 & -0.2 \\ 0.3 & 0.1 \\ 0.1 & 0.2 \end{bmatrix}, \; A_{23} = \begin{bmatrix} -0.1 & 0 \\ 0.2 & -0.2 \\ 0.1 & 0 \end{bmatrix},$$

$$A_3 = \begin{bmatrix} 1 & 0.1 \\ -0.1 & 0.8 \end{bmatrix}, \; B_3 = \begin{bmatrix} 0.1 & 0 \\ 0 & 0.1 \end{bmatrix}, \; A_{31} = \begin{bmatrix} 0.1 & 0.2 \\ 0.1 & 0.2 \end{bmatrix}$$

The overall system is stabilized by employing a local memory-less state feedback control for each subsystem

$$\mathbf{u}_i(k) = K_i \mathbf{x}_i(k), \; K_1 = \begin{bmatrix} -6 & -7 \end{bmatrix}, \; K_2 = \begin{bmatrix} -7 & -45 & 10 \\ 4 & -4 & -4 \end{bmatrix}, \; K_3 = \begin{bmatrix} -5 & -1 \\ 1 & -4 \end{bmatrix}$$

Substituting the inputs into this system, we obtain the equivalent closed loop system representations

$$S_i: \; \mathbf{x}_i(k+1) = \hat{A}_i \, \mathbf{x}_i(k) + \sum_{j=1}^{3} A_{ij} \mathbf{x}_j(k - h_{ij}), \;\; 1 \le i \le 3, \;\; \hat{A}_i = A_i + B_i K_i$$

For time-delay in the system, let us adopt: $h_{12} = 5$, $h_{21} = 2$, $h_{23} = 4$ and $h_{31} = 5$. Applying *Theorem 11* to a given closed loop system, for $l = 1$ we obtain

$$R_1{}^6 - R_1{}^5 \hat{A}_1 - R_1{}^3 S_2 A_{21} - S_3 A_{31} = 0 \,,$$

$$R_1{}^6 S_2 - R_1{}^5 S_2 \hat{A}_2 - A_{12} = 0 \,,$$

$$R_1{}^5 S_3 - R_1{}^4 S_3 \hat{A}_3 - S_2 A_{23} = 0$$

Solving this SMPE by minimization methods, we obtain

$$R_1 = \begin{bmatrix} 0.6001 & 0.3381 \\ 0.6106 & 0.3276 \end{bmatrix}, \; S_2 = \begin{bmatrix} 0.0922 & 1.3475 & 0.5264 \\ 0.0032 & 1.3475 & 0.4374 \end{bmatrix}, \; S_3 = \begin{bmatrix} 0.6722 & -0.3969 \\ 1.3716 & -1.0963 \end{bmatrix}.$$

Eigenvalue with maximal module of matrix R_1 equals 0.9382. Since eigenvalue λ_m of $A_a \in R^{40 \times 40}$ also has the same value, we conclude that solvent R_1 is maximal solvent. Applying *Theorem 12*, we arrive at condition $\rho(R_{1m}) = 0.9382 < 1$ wherefrom we conclude that the observed closed loop large-scale time-delay system is asymptotically stable.

3. CONCLUSION

In this paper we have presented necessary and sufficient conditions for the asymptotic stability of a particular class of linear continuous and discrete time-delay systems. These results have been extended to the large scale continuous and discrete time-delay systems covering the cases of two and multiple existing subsystems. The delay dependent criteria are derived by Lyapunov's direct method and are exclusively based on the solvents of particular matrix equation and Lyapunov equation for non delay systems. Obtained stability conditions do not possess conservatism. For discrete time-delay systems the dominant solvent of given polynomial matrix equation can be calculated using generalized Traub's or Bernoulli's algorithm which possess significantly smaller number of computation than the standard algorithm.

REFERENCES

1. Kamen E.W., (1983), Linear systems with commensurate time-delays: Stability and stabilization independent of delay, *IEEE Transactions on Automatic Control*, Vol. 27, 367-375; corrections in *IEEE Transactions on Automatic Control*, Vol. 28, 1983, pp. 248-249.
2. Hertz D., E. I. Jury, E. Zeheb, (1984), Stability independent and dependent of delay for delay differential systems, *Journal of Franklin Institute*, 318, 1984, pp. 143-150.
3. Niculescu S.I., Souza de C. E., L.Dugard, Dion J.M., (1995), Robust exponential stability of uncertain linear systems with time-varying delays, *Proceedings of 3rd European Control Conference*, Rome, Italy, 1995, pp. 1802-1807.
4. Richard J.P., A., Goubet- Bartholomeus, Tchangani P. A., M. Dambrine, (1997), Nonlinear delay systems: Tools for quantitative approach to stabilization, *Stability and Control of Time-Delay Systems*, (Eds: Dugard L. and Verriest E.I.), Springer-Verlag, 1997, pp. 218-240.
5. Hale J.K., Lunel S.M., (1993), *Introduction to Functional Differential Equations*, Applied Mathematics Sciences Series, 99, Springer-Verlag, 1993.
6. Kolmanovskii V.B., Nosov V.R., (1986), *Stability of Functional Differential Equations*, New York: Academic Press, 1986.
7. Su J.H., (1994), Further results on the robust stability of linear systems with a single delay, *Systems and Control Letters*, Vol. 23, 1994, pp. 375-379.

8. Niculescu S.I., de Souza C. E., Dion J.M., Dugard L., (1994), Robust stability and stabilization for uncertain linear systems with state delay: Single delay case (I). *Proceedings of IFAC Workshop on Robust Control Design*, Rio de Janeiro, Brazil, 1994, pp. 469-474.

9. Boyd S., El Ghaoui L., Feron E., Balakrishnan V., (1994), *Linear matrix inequalities in system and control theory*, SIAM Studies in Applied Mathematics, 15., Philadelphia, USA, 1994.

10. Li X., de Souza C., (1995), LMI approach to delay dependent robust stability and stabilization of uncertain linear delay systems, *Proceedings of 34th IEEE Conference on Decision and Control*, New Orleans, Louisiana, USA, 1995, pp. 3614-3619.

11. Niculescu S.I., Trofino-Neto A., Dion J.M., and Dugard L., (1995), Delay-dependent stability of linear systems with delayed state: An LMI approach, *Proceedings of 34th IEEE Conference on Decision and Control*, New Orleans, Louisiana, USA, 1995, pp. 1495-1497.

12. Gu K., (1997), Discretized LMI set in the stability problem of linear uncertain time-delay systems, *International Journal of Control*, Vol. 68, 1997, 923-934.

13. Su J.H., (1995), The asymptotic stability of linear autonomous systems with commensurate delays, *IEEE Transactions on Automatic Control*, Vol. 40, 1995, pp. 1114-1118.

14. Chen J., Gu G., Nett C.N., (1994), A new method for computing delay margins for stability of linear delay systems, *Proceedings of 33rd IEEE Conference on Decision and Control*, Lake Buena Vista, Florida, USA, 1994, pp. 433-437.

15. Niculescu S.I., Dion J.M., Dugard L., Li H., (1997), Stability of linear systems with delayed state: An LMI approach, *JESA*, special issue on "Analysis and control of time-delay systems", 31, 1997, pp. 955-970.

16. Niculescu S.I., Verriest E.I., Dugard L., Dion J.M., (1997), Stability and robust stability of time-delay systems: A guided tour, *Lecture notes in control and information sciences*, Vol. 228, 1997, pp. 1-71, London, Springer.

17. Kharitonov V., (1998), Robust stability analysis of time delay systems: A survey, *Proceedings of 4th IFAC System Structure and Control Conference*, Nantes, France, July, 1998.

18. Richard J.P., (1998), Some trends and tools for the study of time delay systems, *Proceedings of CESA98 IMACS/IEEE Multi conference*, Hammamet, Tunisia, 1998, pp. 27-43.

19. Niculescu S.I., Richard J.P., (2002), Analysis and design of delay and propagation systems, *IMA Journal of Mathematical Control and Information*, 19 (1-2), 2002, pp. 1-227.

20. Richard J.P., (2003), Time-delay systems: an overview of some recent advances and open problems, *Automatica*, Vol. 39, 2003, pp. 1667-1694.

21. Kolmanovskii V., Richard J.P., (1999), Stability of some linear systems with delays, *IEEE Transactions on Automatic Control*, Vil. 44, 1999, pp. 984-989.

22. Malek-Zavarei M., Jamshidi M., (1987), *Time-Delay Systems, Analysis, Optimization and Applications*, Systems and Control Series, Vol. 9, 1987.

23. Verriest E., Niculescu S.I., (1998), Delay-independent stability of linear neutral systems: a Riccati equation approach, *Stability and Control of Time-Delay Systems* (Eds: Dugard L. and Verriest E.), Vol. 227 Springer-Verlag, 1998, pp. 92-100.

24. Li X., de Souza C., (1997), Criteria for robust stability and stabilization of uncertain linear systems with state delay, *Automatica*, Vol. 33, 1997, pp. 1657-1662.

25. Kolmanovskii V., Niculescu S.I., Richard J.P., (1999), On the Lyapunov–Krasovskii functionals for stability analysis of linear delay systems, *International Journal of Control*, Vol. 72, 1999, pp. 374-384.

26. Park P., (1999), A delay-dependent stability criterion for systems with uncertain time-invariant delays, *IEEE Transactions on Automatic Control*, Vol. 44, 1999, pp. 876-877.

27. Lien C.H., Yu K.W., Hsieh J.G., (2000), Stability conditions for a class of neutral systems with multiple time delays, *Journal of Mathematical Analysis and Applications*, 245, 2000, pp. 20-27.

28. Niculescu S.I., (2001), On delay-dependent stability under model transformations of some neutral linear systems, *International Journal of Control*, Vol. 74, 2001, pp. 609-617.

29. Fu M., Li H., Niculescu S.I., (1997), Robust stability and stabilization of time-delay system via integral quadratic constraint approach, *Stability and Control of Time-Delay Systems* (Eds: Dugard L. and Verriest E.I.), Springer-Verlag, 1997, pp. 101-116.

30. Chen J., On computing the maximal delay intervals for stability of linear delay systems, *IEEE Transactions on Automatic Control*, Vol. 40, 1995, pp. 1087-1093.

31. Park P., Moon Y.S., Kwon W.H., (1998), A delay-dependent robust stability criterion for uncertain time-delay systems, *Proceedings of the American control conference*, USA, 1998, pp. 1963-1964.

32. Moon Y.S., Park P.G., Kwon W.H., Lee Y.S., (2001), Delay-dependent robust stabilization of uncertain state-delayed systems, *International Journal of Control*, Vol. 74 (14), 2001, pp. 1447-1455.

33. Fridman E., Shaked U., (2003), Delay-dependent stability and H∞ control: Constant and time-varying delays, *International Journal of Control*, Vol. 76, 2003, pp. 48-60.

34. Fridman E., Shaked U., (2002), A descriptor system approach to H∞ control of linear time-delay systems, *IEEE Transactions on Automatic Control*, Vol. 47, 2002, pp. 253-270.

35. Han Q.L., (2005), On stability of linear neutral systems with mixed time-delays: A discretized Lyapunov functional approach, *Automatica*, Vol. 41, 2005, pp. 1209-1218.

36. Han Q.L., (2005), A new delay-dependent stability criterion for linear neutral systems with norm-bounded uncertainties in all system matrices, *International Journal of Systems Science*, Vol. 36, 2005, pp. 469–475.

37. Fridman E., Shaked U., (2002), An improved stabilization method for linear time-delay systems, *IEEE Transactions on Automatic Control*, Vol. 47, 2002, pp. 1931–1937.

38. Lee T.N., Diant S., (1981), Stability of time-delay systems, *IEEE Transactions on Automatic Control*, Vol. 26, No. 4, 1981, pp. 951-953.

39. Xu S., Lam J., Yang C., H∞ and positive real control for linear neutral delay systems, *IEEE Transactions on Automatic Control*, Vol. 46, 2001, pp. 1321–1326.

40. Verriest E., Ivanov A., (1995), Robust stability of delay difference equations, *Proceedings IEEEE Conf. on Dec. and Control*, New Orleans, LA, 1995, pp. 386-391.

41. Kapila V., Haddad W., (1998), Memoryless H∞ controllers for discrete-time systems with time delay, *Automatica*, Vol. 34, 1998, pp. 1141-1144.

42. Song S., Kim J., Yim C., Kim H., (1999), H∞ control of discrete-time linear systems with time-varying delays in state, *Automatica,* Vol. 35, 1999, pp. 1587-1591.

43. Mahmoud M., (2000), Robust H∞ control of discrete systems with uncertain parameters and unknown delays, *Automatica*, Vol. 36, 2000, pp. 627-635.

44. Lee Y.S., Kwon W.H., (2002), Delay-dependent robust stabilization of uncertain discrete-time state-delayed systems, *Preprints of the 15th IFAC World Congress*, Barcelona, Spain, 2002.

45. Shi P., Agarwal R.K., Boukas E.K., Shue S.P., (2000), Robust H∞ state feedback control of discrete time delay linear systems with norm-bounded uncertainty, *International Journal of Systems Science*, Vol. 31, 2000, pp. 409- 415.

46. Gorecki H., Fuksa S., Grabovski P., Korytowski A., (1989), *Analysis and synthesis of time delay systems*, John Wiley & Sons, 1989.

47. Debeljkovic D.Lj.,., Stojanovic S.B., (2008), Asymptotic Stability Analysis of Linear Time Delay Systems: Delay Dependent Approach, *Systems, Structure and Control* (Eds: Petr Husek), I–Tech, Vienna, 2008, pp. 29-60.

48. Lancaster P., Tismenetsky M., *The theory of matrices, 2nd Edition*, Academic press, New York, 1985.

49. Stojanovic S.B., Debeljkovic D.Lj., (2005), Necessary and Sufficient Conditions for Delay-Dependent Asymptotic Stability of Linear Continuous Large Scale Time Delay Autonomous Systems, *Asian Journal of Control*, Vol. 7, No. 4, 2005, pp. 414-418.

50. Stojanovic S.B., Debeljkovic D.Lj., (2008), Necessary and Sufficient Conditions for Delay-Dependent Asymptotic Stability of Linear Discrete Time Delay Autonomous Systems, *Proceedings of 17th IFAC World Congress*, Seoul, Korea, July 06–10, 2008, pp. 2613-2618.

51. Dennis J.E., Traub J.F., Weber R.P., (1976), The algebraic theory of matrix polynomials, *SIAM J. Numer. Anal.*, Vol. 13 (6), 1976, pp. 831-845.

52. Dennis J.E., Traub J.F., Weber R.P., (1978), Algorithms for solvents of matrix polynomials, *SIAM J. Numer. Anal.*, Vol. 15 (3), 1978, pp. 523-533.

53. Stojanovic S.B., Debeljkovic D.Lj., (2008), Delay–Dependent Stability of Linear Discrete Large Scale Time Delay Systems: Necessary and Sufficient Conditions, *International Journal of Information & System Science*, Vol. 4, No. 2, 2008, pp. 241-250.

54. Stojanovic S.B., Debeljkovic D.Lj., (2008), Quadratic stability and stabilization of uncertain linear discrete-time systems with state delay: a LMI approach, *Dynamics of Continuous, Discrete and Impulsive Systems*, *Series B: Applications & Algorithms*, Vol. 15, 2008, pp. 195-206.

STABILNOST LINEARNIH SISTEMA SA KAŠNJENJEM KOJA ZAVISI OD VREMENSKOG KAŠNJENJA

Sreten B. Stojanovic, Dragutin Lj. Debeljkovic

Rad se bavi problemom stabilnosti linearnih običnih i velikih sistema koja zavisi od vremenskog kašnjenja. Izvedeni su potrebni i dovoljni uslovi asimptotske stabilnosti kontinualnih i diskretnih linearnih sistema sa kašnjenjem. Ovi rezultati su prošireni na klasu velikih sistema sa kašnjenjem pri čemu je razmatran slučaj sa dva i više podsistema. Kriterijumi stabilnosti su izvedeni koristeći Ljapunov direktni metod a zasnivaju se na rešenju posebnih klasa matričnih jednačina i Ljapunove jednačine za sisteme bez kašnjenja. Izvedeni uslovi stabilnosti ne poseduju konzervativizam. Nekoliko numeričkih primera je urađeno kako bi se pokazala primenljivost izvedenih rezultata.

Key words: *kontinualni sistemi sa kašnjenjem, diskretni sistemi sa kašnjenjem, veliki sistemi sa kašnjenjem, stsbilnost zavisna od kašnjenja, Ljapunova stabilnost, potrebni i dovoljni uslovi*

IMPROVED COMPUTATION METHOD IN RESIDUAL LIFE ESTIMATION OF STRUCTURAL COMPONENTS

UDC 539.184

Stevan M. Maksimović[*], Katarina S. Maksimović[**],

[*]Military Technical Institute
Ratka Resanovića 1, 11133 Žarkovo-Belgrade
s.maksimovic@open.telekom.rs

[**]City Administration of the City of Belgrade,
Secretariat for Utilities and Housing Services
Water Management, Belgrade, SERBIA

Abstract. *This work considers the numerical computation methods and procedures for the fatigue crack growth predicting of cracked notched structural components. Computation method is based on fatigue life prediction using the strain energy density approach. Based on the strain energy density (SED) theory, a fatigue crack growth model is developed to predict the lifetime of fatigue crack growth for single or mixed mode cracks.*

The model is based on an equation expressed in terms of low cycle fatigue parameters. Attention is focused on crack growth analysis of structural components under variable amplitude loads. Crack growth is largely influenced by the effect of the plastic zone at the front of the crack. To obtain efficient computation model plasticity-induced crack closure phenomenon is considered during fatigue crack growth. The use of the strain energy density method is efficient for fatigue crack growth prediction under cyclic loading in damaged structural components. Strain energy density method is easy for engineering applications since it does not require any additional determination of fatigue parameters (those would need to be separately determined for fatigue crack propagation phase), and low cyclic fatigue parameters are used instead.

Accurate determination of fatigue crack closure has been a complex task for years. The influence of this phenomenon can be considered by means of experimental and numerical methods. Both of these models are considered. Finite element analysis (FEA) has been shown to be a powerful and useful tool[1,6] to analyze crack growth and crack closure effects. Computation results are compared with available experimental results.

1.INTRODUCTION

Fatigue crack closure is a phenomenon that consists of the contact between fracture surfaces during a portion of the load cycle. This contact affects the local stress and plastic deformation fields near the crack tip, and thus the micro mechanisms responsible for fatigue propagation (cyclic plastic deformation, oxidation, creep, etc.). Plasticity-induced crack closure is an observed phenomenon during fatigue crack growth.

The constant search to improve aircraft safety has led, over recent years, to the increasingly widespread application of „damage tolerance" concepts. Reliable fatigue life prediction is very important for safe design and maintenance of structural components subjected to cyclic loading[1]. In general, fatigue process consists of three stages: initiation and early crack propagation, subsequent crack growth and final fracture. Due to the fact that if occurs, failure leads to catastrophe, crack growth stage must be carefully studied and analyzed. Each crack growth model for life prediction must be based on a suitable failure criterion. For crack growth analysis, as failure criteria could be used: plastic/total strain ahead of crack[3], the magnitude of crack tip opening[4,5] and the energy criteria[6,7]. Since crack closure effect is included in fatigue crack growth analysis, the concept of crack opening/closure was used in this paper.

The aim of this paper is to analyze the effect of plasticity-induced crack closure (PICC) using finite element method and determination of new corrective factors for the effective stress intensity factors. Moreover, with crack growth analysis desire was to assess how new corrective factors can to improve crack growth life prediction to failure of structural component.

Due to the fact that the formulated procedure for fatigue crack prediction includes analysis level of external loading as well as the effect of plasticity-induced crack closure we can say that it is adequate as an engineering application.

2. CRACK GROWTH PREDICTING

In this paper two numerical simulation approaches to crack propagation and, accordingly, evaluation of residual life for structural elements with initial damages are presented. First approach is based on conventional laws of crack propagation, such as Paris` law of crack propagation8. The other approach is based on the strain energy density method.

3. CONVENTIONAL CRACK PROPAGATION MODEL

When analyzing crack growth prediction, the usual starting point is relation in which the fatigue crack growth rate is expressed as a function of the stress intensity factor, i.e., a well known and widely used Paris law8 :

$$\frac{da}{dN} = C(\Delta K)^m , \tag{1}$$

where: da/dN is crack growth rate, C and m – coefficient and exponent dependent upon the materials, respectively. However, with this law, it is not possible to make allowance for the interactions found in real-life spectra.

Equation defined by Paris, even though commonly used in engineering practice, still has some deficiencies. Basic deficiency is the fact that it does not include alternating load/stress and mean load/stress. During their service life structural components could be subject to both of those loads. The mean load effect on fatigue crack growth rate is commonly introduced through the stress ratio R. Since the mean load effect is not included in Paris`s equation it was necessary to either modify Paris′ equation or develop new concepts. The crack closure concept is one of those concepts where the stress ratio is analyzed. In general, all crack closure concepts9,10 are based on the Elber′s observation10,11 which reveals the premature contact of the crack faces during the unloading portion of the loading cycle while some tensile load is still applied. Elber was the first researcher who introduced the effective stress intensity factor range instead of stress intensity factor range ΔK, i.e.:

$$\frac{da}{dN} = C\left(\Delta K_{eff}\right)^m \tag{2}$$

where the effective stress intensity factor range is the function of stress ratio as well as stress intensity factor:

$$\Delta K_{eff} = \left(0.5 + 0.4R\right)\Delta K . \tag{3}$$

After Elber, Schjive8 analyzed the same relation (2) and he found that effective stress intensity factor range could be expresed as:

$$\Delta K_{eff} = \left(0.55 + 0.33R + 0.12R^2\right)\Delta K \tag{4}$$

Previously mentioned Elber′s and Schjive′s approaches could be improved or modified by introducing the effect of plasticity-induced crack closure. As a consequence of introduction of the effect of plasticity-induced crack closure, it is necessary to correct the effective stress intensity factor.

To include the effects of the stress ratio R the conventional Forman`s crack growth model16 is used. In region III rapid and unstable crack growth occurs, so Forman at al. Proposed equation for region III as well as for region II17:

$$\frac{da}{dN} = \frac{C\left(\Delta K\right)^n}{\left(1-R\right)K_C - \Delta K} \tag{5}$$

where KC is the fracture toughness. Forman`s equation has been developed to model of unstable crack growth domain (III). To include PICC effects ΔKeff need to use in equation (5).

4. CRACK PROPAGATION MODEL BASED ON THE STRAIN ENERGY DENSITY METHOD

While predicting life of a structural element with initial damage it`s necessary to establish the functional dependency between the crack propagation gradient da/dN and the stress intensity factor K_I.

The severest damage accumulation occurs in the process zone[18,20], therefore it`s necessary to define and calculate the energy which causes damage in the process zone.

For the zone around the tip of the crack (process zone) it`s possible to define the energy generated through plastic strain ω_p in a cycle using length unit as a function of stress intensity factor range ΔK_I:

$$\omega_p = \left(\frac{1 - n'}{1 + n'}\right) \frac{\Delta K_I^2}{E \, I_{n'}} \psi \tag{6}$$

where: n' - cyclic strain hardening exponent, E – Young`s modulus of elasticity, $I_{n'}$, ψ - constants which depend on the cyclic strain hardening exponent n'. For most metals the value of n' usually varies between 0,10 and 0.25, with an average value close to 0.15. Since the dependency for energy generated due to plastic strain ω_p as a function of ΔK_I is established, it`s necessary to establish the dependency between the crack propagation gradient da/dN and ω_p. While establishing the dependency a fact that the crack propagates if energy which generates due to plastic strain during the cycle reaches the energy absorbed during the same cycle W_c must be taken into account:

$$\frac{da}{dN} = \frac{\omega_p}{W_c} \; . \tag{7}$$

In equation (7) energy absorbed during the cycle W_C can be defined if stress – strain relation, or the material behaviour equation, is known. Adequte relation for material behaviour which includes both elastic and plastic behaviour is known as Ramberg – Osgood equation[21]:

$$e_a = \frac{S_a}{E} + \left(\frac{S_a}{k'}\right)^{1/n'} \tag{8}$$

where: e_a – strain amplitude, S_a – stress amplitude and k'- cyclic strength coefficient. If the material behavior equation is presented by equation (8), energy absorbed during the cycle W_c represents the area below the curve in S-e coordinate system, or:

$$W_c = \frac{4}{1+n'} \sigma_f' \, \varepsilon_f' \tag{9}$$

where: σ_f' - fatigue strength exponent, ε_f' - fatigue ductility coefficient. Finally, if equations (6) and (8) get placed in equation (7), functional dependency between crack propagation gradient and stress intensity factor gets established. Subsequently, that dependency can be integrated from initial crack length a_i to final crack length a_c in order to obtain the relation which could be used for the prediction of life of structural elements which contain initial damage:

$$N = \frac{(1 - n')\psi}{4 \, E \, I_{n'} \sigma_f' \varepsilon_f'} \int_{a_i}^{a_c} (\Delta K_I - \Delta K_{th})^2 \tag{10}$$

where ΔK_{th} is range of threshold stress intensity factor. ΔK_{th} is a material constant but it is sensitive to stress ratio R=S_{min}/S_{max}. A relation between ΔK_{th} and R is given below based on experimental results [19]

$$\Delta K_{th} = \Delta K_{th0}(1 - R)^\gamma \tag{11}$$

where ΔK_{th0} is the range of threshold stress intensity factor for the stress ratio R=0, and γ is a material constant which varies from 0 to 1 [12,13]. For most of materials γ comes out to be 0.71 [19]. Equation (10) presents the law of crack propagation based on strain energy density method. It`s obvious that in this dependency cyclic characteristics of material from low-cycle fatigue domain are being used instead of dynamic parameters from more conventional laws for crack propagation by Paris, Forman and others. Main advantage of this Strain Energy Density (SED) approach, as shown in eq. (10), is the use of same cyclic material characteristics being used for initial and residual fatigue life predictions [19-21].

5. THE STRESS INTENSITY FACTOR

It is well known that stress intensity factors play a major role in crack growth analysis. Actually, with stress intensity factors, geometry of structural component and the type of loading are introduced. The stress intensity factor can be determined using analytical and/or numerical approaches.

In analytical approach, the stress intensity factor range could be determined as a function:

$$\Delta K = f\left(P,a,w,....\right) \tag{12}$$

where: P is load/force, a – crack length and w – width of specimen. For example, when dealing with CT specimen, relation for stress intensity factor range can be written as:

$$\Delta K = \frac{\Delta P}{B\sqrt{w}}\left(\frac{2+\dfrac{a}{w}}{\left(1-\dfrac{a}{w}\right)^{3/2}}\left(0.886+4.64\left(\frac{a}{w}\right)-13.32\left(\frac{a}{w}\right)^{2}+14.72\left(\frac{a}{w}\right)^{3}-5.6\left(\frac{a}{w}\right)^{4}\right)\right). \tag{13}$$
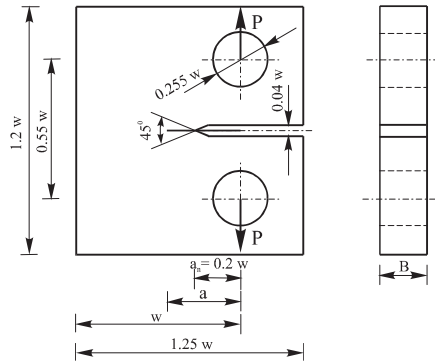
Figure 1. Geometry of Compact Tension specimen

The symbol B in equation (13) denotes the thickness of compact specimen and w is the distance between the applied force P and the left edge of the specimen (Fig.1). The

symbol a in equation (13) is the crack length measured from the line of the application of external load.

On the other hand, when using numerical approach, for determining the stress intensity factor Finite element method (FEM) is used.

A representation of the finite element analysis for CT specimen made of Al Alloy 2024 T351 (w = 0.075 m, B = 0.010 m) are shown in Figure 2. Figure 2 presents stress distribution at CT specimen for crack length a = 0.02625 m. From the same figure it can be seen that for crack length a = 0.02625 m (as a result of finite element analysis), the calculated maximum stress (for P_{max} = 3300 N and R = 0.1) is 10.39 daN/mm^2.
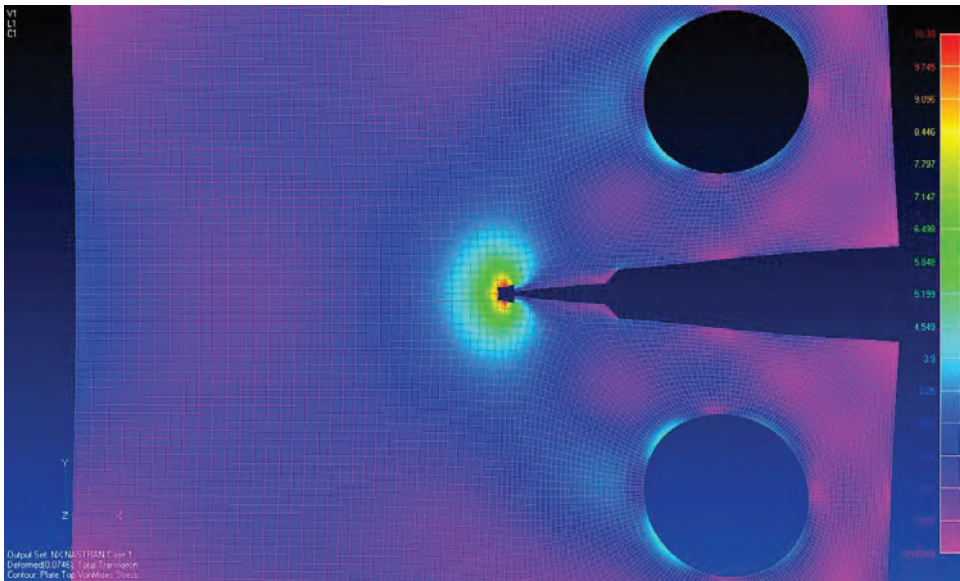
Figure 2. Stress distribution at the CT specimen (P_{max} = 3300 N and R = 0.1) using finite element analysis.

Additionally, in this paper, the finite element analysis was used to investigate the plasticity-induced crack closure effects in the calculation of stress intensity factor range. So for stress distribution shown in Figure 2, the calculated stress intensity factor was K_{Imax} = 21.93 daN mm$^{-3/2}$. Furthermore, the same calculation of stress intensity factors were made for different external forces

6. THE EFFECTIVE STRESS INTENSITY FACTOR AND CRACK CLOSURE EFFECT

For the phenomenon of crack closure is known that it has a strong influence on fatigue crack growth[11,12]. Elber called this phenomenon plasticity-induced crack closure. Namely, if the crack has reached its current length through fatigue (cyclic loading), there would be a localized plasticity region formed at the crack tip and the wake of the crack. This localized plasticity in itself will generate residual stresses and play a role in crack closure.

Due to the fact that plasticity-induced crack closure phenomenon is included in crack growth analysis, it is necessary to correct relation for the effective stress intensity factor ΔK_{eff} (Eq.(3) and Eq.(4)), i.e. to find adequate corrective factors. Since finite element analysis proved to be powerful tool[12] for determination of stress intensity factors, corrective factors were determined/introduced that include plasticity-induced crack closure effect.

When determining the stress intensity factor range, the ranging of the external force was from 3000 N to 14500 N. Namely, five different values from this range were used. For such defined range of load, as well as geometry of CT specimen (a = 0.030 m, w=0.075m, B=0.010 m) and type of material, after finite element analysis, it is possible to determine corrective factors for stress intensity factor range with including the effect of plasticity-induced crack closure. New corrective factors calculated on this way, for different approaches are listed in Table 2.

Table 1 Corrective factors

For equation	Corrective factor
$\Delta K_{eff} = (0.5 + 0.4\,R)\Delta K$	0.926
$\Delta K_{eff} = (0.55 + 0.33\,R + 0.12R^2)\Delta K$	0.928

7. NUMERICAL RESULTS

With introduced plasticity-induced crack closure effect, the validity of presented computation model for crack growth prediction could only be assessed through a comparison with experimental data which is the focus of this section. The subject of this work is improvement or modification of Elber's and Schjive's approaches and in examples that follow it is presented how important defined and introduced modification influences on the predicted fatigue crack life of structural components.

7.1. Example 1a: Crack growth rate prediction of CT specimen subjected with constant amplitude loading

This example considered crack growth rate and effective stress intensity factor calculation. The material used in this example is 2024 T351 Al Alloy, whose mechanical properties are: E = 74000 MPa; C = 1.51 10^{-10}, m = 4. The configuration of considered CT specimen is shown in Figure 1. Needed geometry parameters are: w = 0.075 m; B=0.010 m; and a=0.016 m. The external cyclic loading is with constant amplitude (Load/force P_{max}=3300 N and stress ratio R = 0.1). Before starting the crack growth rate estimation it is necessary to determine the stress intensity factor and effective intensity factor for different values of crack length. In this example, for determination of the stress intensity factor range and effective stress intensity factor range were used equations (6), (3) and (4). The effective stress intensity factor as a function of crack length a (for different models: Elber, Schijve) are illustrated in Figure 3.
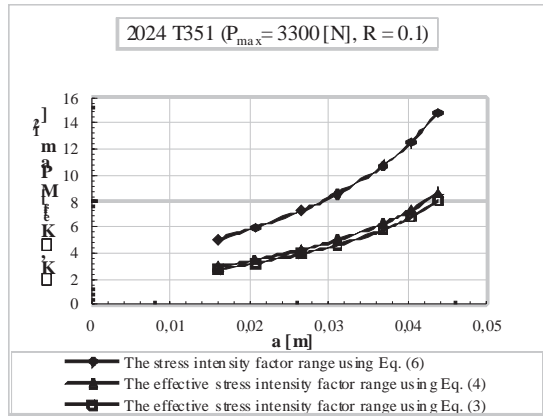
Figure 3. A crack length a versus the effective stress intensity factor range ΔK_{ee} and stress intensity factor range ΔK.
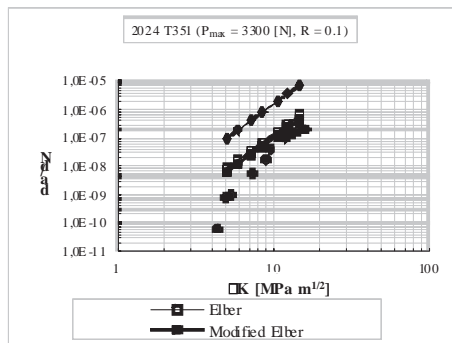
Figure 4. Fatigue crack growth rate as a function of stress intensity factor

Based on known characteristics of material, geometry and loading, calculated values of a crack growth rate using different models (Elber, Modified Elber, Schijve and Modified Schijve) are shown in Figure 4. At the same figures all predicted curves for crack growth rate are compared with experimental data[14].

As observed from Figure 4, the estimated fatigue crack growth rates are in a good agreement with the experimental observations. Additionally, Figure 4 show that Paris's model is very conservative, while Elber's and Schjive's models are less conservative when compared to experimental data. Defined improvements of Elber's and Schjive's models presented in this paper, including crack closure effect, provide better predicted values for fatigue crack growth rates. In addition, the best agreement between predicted fatigue crack growth rate and experimental data is obtained when using Modified Elber model.

7.2. Example 1b: Crack growth life estimation of CT specimen subjected with constant amplitude loading

In this example fatigue life prediction up to failure was considered. Structural element, material and the type of loading used here are the same as in example 1a. Using the fatigue parameters, according to the geometry of structural component and different fatigue growth models, enabled determination of the fatigue life to failure.
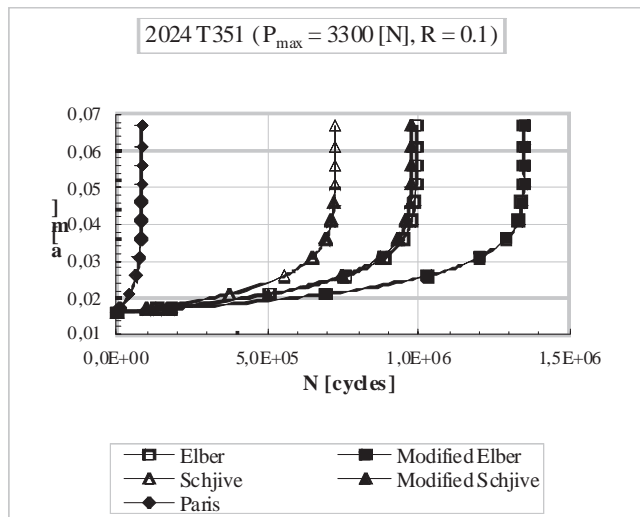
Figure 5. Crack growth analysis of CT specimen using different models.

Actually, by using equations (1) or (2) (with (6), (3) or (4)) which were first integrated, the relations between crack length a and number of cycles to failure N were formulated. Predicted results using different models (Elber, Schjive, Modified Elber and Modified

Schjive) are shown in Figure 5 for external force P_{max}= 3300 N. As it can be seen from Figure 5 improvements introduced for Elber's as well as Schjive's approaches have significant impact on predicted number of cycles to failure.

7.3. Example 2: Crack growth estimation of CT specimen subjected load spectra

Since that the structural components are usually subjected to load spectra, in this example fatigue crack growth prediction with including crack closure effect for CT specimen subjected load spectrum was carried out. From crack growth analysis in example 1 it can be concluded that Elber's and Modified Elber's approaches are more adequate for prediction of fatigue crack growth. (related to experimental data). That is the reason why they will be analyzed for crack growth prediction in this example, too.

Material used in this example is the same as previous. As a result of fatigue crack growth estimation, number of blocks to failure were obtained using equations (2), (6) and (3). For determination number of blocks to failure, equation (2) was first integrated. After integration, function between number of blocks N_{bl} and crack length a was determined.
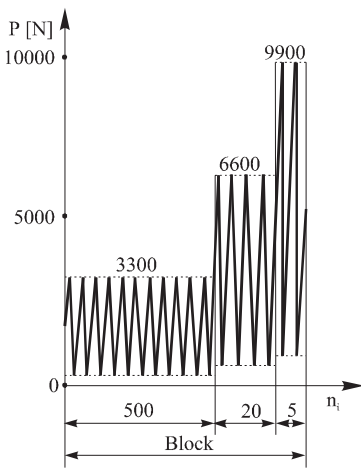
Figure 6. Load spectrum (R = 0.1)   **Fig. 7.** Crack growth analysis of CT specimen subject to load spectra
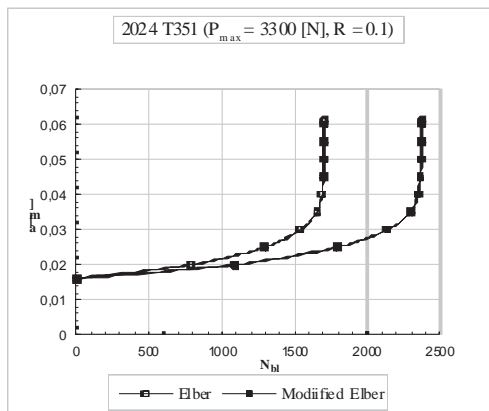
Figure 7 shows a plote of the estimated number of blocks to failure versus a crack length *a*, for Elber and Modified Elber approaches for load spectrum (Fig.6). Conclusion from Figure 7 for fatigue crack growth prediction in the case of load spectrum (Fig.6), is that the effect of plasticity-induced crack closure has significant effect on number of blocks to failure. For load spectrum presented in Figure 6 calculated number of blocks to failure are listed in Table 2.

Table 2 Comparison of number of blocks to failure for CT specimen   (P_{max} = 3300 N, R = 0.1).

	N_{bl}	Δ [%]
Elber	1704	
Modified Elber	2372	28.16

Comparison of number of blocks to failure, presented in Table 2, shows that introduced modification that include effect of plasticity-induced crack closure, has been increased the value of predicted number of blocks to failure around 30% for considered load spectrum (Fig. 6).

a.) Geometric properties   b.) FEM with initial crack
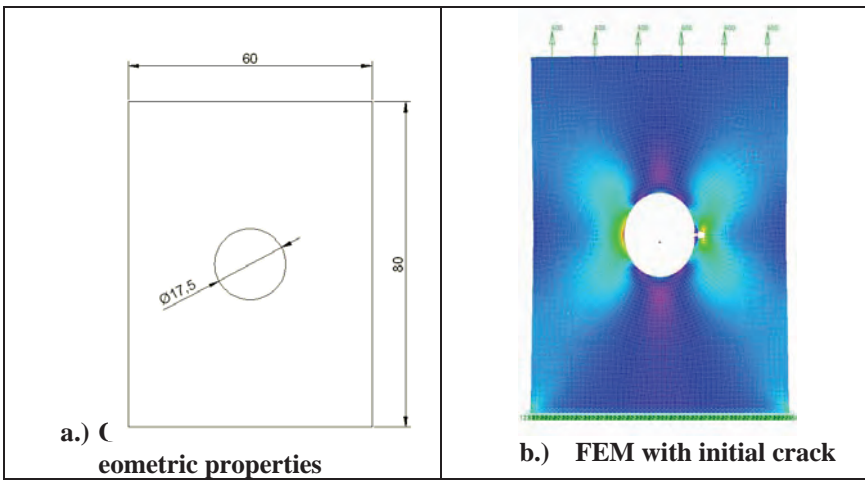
Fig. 8 Structural component with hole and initial crack under load spectrum

7.4. Example 3: Crack growth analysis of plate with a hole under load spectrum

Here is considered specimen (aluminum 2024 T4) with central hole under load spectrum, Fig 8a (w=60 mm, r=8.75 mm, t=6mm). Forman crack growth model (5) is used. Finite element model, with initial crack a_0 is used to determine stress intensity factors K_I. The complete fatigue crack growth prediction, using in-house software, are shown in Table 3 and Fig. 9.

In Table 3: C_f, n_f are Forman's constants, a_c is critical crack growth length, N1 to N13 are number of cycles at load levels within load spectrum.

Table 3: Crack growth prediction of specimen with hole under load spectrum

Ulazni podaci

nf	3,45	Cf 0,0000000000434

Korak 10 Finoca stampe 1800 Izaberite zakon širenja: Forman Brisi Izracunaj

Karakteristike materijala

a0	0,002	E	70430
ac	0,02	SigmaF	764
w	0,06	EpsilonF'	0,334
t	0,005	n'	0,098
r	0,00875	ln'	3,067
		Psi	0,95152
		Kth0	7
		KIc	37

SigmaMax1	81,6814	Min1	25,349	N1	3040
SigmaMax2	122,321	Min2	11,266	N2	200
SigmaMax3	167,789	Min3	11,266	N3	189
SigmaMax4	211,245	Min4	11,266	N4	43
SigmaMax5	245,7	Min5	-10,059	N5	15
SigmaMax6	298,559	Min6	-10,059	N6	3
SigmaMax7	316,666	Min7	-41,848	N7	1
SigmaMax8	298,559	Min8	-10,059	N8	3
SigmaMax9	254,7	Min9	-10,059	N9	15
SigmaMax10	211,245	Min10	11,266	N10	43
SigmaMax11	167,789	Min11	11,266	N11	189
SigmaMax12	122,321	Min12	11,266	N12	200
SigmaMax13	81,681	Min13	25,349	N13	3040

NUkupno	a	da/dN	KI	DeltaSigma	BrojacBlokova
0	0,002	0	10,90872305	56,3324	0
1800	0,002020447	0,0000000	10,93487646	56,3324	0
3600	0,002868501	0,0000037	32,65258141	156,523	0
5400	0,004218692	0,0000000	12,45024805	56,332	0
7200	0,004254664	0,0000000	12,46361279	56,3324	1
9000	0,004290805	0,0000000	12,47676509	56,3324	1
10800	0,007613777	0,0000004	26,21720209	111,055	1
12600	0,007718855	0,0000000	13,31957794	56,332	1
14400	0,007767462	0,0000000	13,32939311	56,3324	2
16200	0,007816230	0,0000000	13,33913555	56,3324	2
18000	0,009799163	0,0000000	13,73502042	56,332	2
19800	0,009855121	0,0000000	13,74636134	56,332	2
21600	0,009911294	0,0000000	13,75785863	56,3324	3
23400	0,009967684	0,0000000	13,76931792	56,3324	3
25200	0,011724511	0,0000000	14,13494040	56,332	3
27000	0,011788487	0,0000000	14,14859191	56,332	3
28800	0,011852756	0,0000000	14,16243002	56,3324	4
30600	0,011917320	0,0000000	14,17625463	56,3324	4
32400	0,013604021	0,0000000	14,54540134	56,332	4
34200	0,013677311	0,0000000	14,56177778	56,332	4
36000	0,013750998	0,0000000	14,57837241	56,3324	5
37800	0,013825087	0,0000000	14,59497944	56,3324	5
39600	0,015534476	0,0000000	14,98456379	56,332	5
41400	0,015619114	0,0000000	15,00415049	56,332	5
43200	0,015704296	0,0000000	15,02399450	56,3324	6
45000	0,015879858	0,0000013	29,69899725	111,055	6
46800	0,017639345	0,0000000	15,47798944	56,332	6
48600	0,017738705	0,0000000	15,50155750	56,332	6
50400	0,017838828	0,0000000	15,52543744	56,3324	7
52200	0,018531384	0,0000021	43,59665386	156,523	7

Fig. 9 Crack growth prediction of cracked plate with central hole

8. CONCLUSIONS

In this paper improvement of Elber's and Schjive's models for prediction of fatigue crack growth life are recommended. Improvement i.e. modification of Elber's as well as Schjive's model was result of plasticity-induced crack closure effect in fatigue crack growth analysis.

Based on the results of the finite element simulations and the direct comparisons with experimental results, the following conclusions are presented:

Calculated fatigue crack growth rates which were obtained using Paris law are very conservative related to experimental data. So strict conservative result are obtain due to the fact that in Paris equation stress ratio was not included. Much less conservative data were shown in predictions obtained using Elber's and Schjive's approaches;

To include the stress ratio effect Forman`s crack growth model is used here,  together with Elber`s crack closure model;

Finite element method is powerful and useful tool for analysis of plasticity-induced crack closure effect;

Comparison of closure levels between the FE model and experimental results revealed excellent agreement for all tests

By introducing the plasticity-induced crack closure effect in crack growth analysis, the predicted fatigue life can be significantly modified as well as number of blocks to failure, and with it, the high quality of crack growth estimation of cracked structural component could be improved.

Presented computation results are shown that crack growth method based on strain energy density approach is in a good agreement with conventional Forman`s approach.

REFERENCES

1. Wu J. and Ellyin, (1996), A study of fatigue crack closure by elastic-plastic finite element for constant-amplitude loading, Int. J Fracture, Vol. 82, pp 43-65.
2. Schijve, J.,(2001), Fatigue of structures and materials, Kluwer Academic Publishers.
3. Duggan, T.V. (1977), A theory of fatigue crack propagation, *Eng. Fract. Mech.*, pp.735-747.
4. Wu, S.X., Mai, Y.W., Cotterell, B. (1992), A model of fatigue crack growth based on Dugdale model and damage accumulation, *Int. J Fract*. 57, pp.253-267.
5. Glinka, G., Robin, C., Pluvinage, G., Chehimi, C.A. (1984), Cumulative model of fatigue crack growth and the crack closure effect, Int. J Fatigue, 6(1), pp.37-47.
6. Boljanovic, S., Maksimovic, S., Belic, I. (2006), Fatigue Life Prediction of Structural Components Based on Local Strain and an Energy Crack Growth Models, WSEAS TRANSACTIONS on APPLIED and THEORETICAL MECHANICS Issue 2, Volume 1, pp. 196-203.

7. Maksimović, S., Boljanović, S., Orović, V., Komnenović, M. (2008), Fatigue Life Analysis of Damaged Structural Component Using Strain Energy Density Method, 17th European Conference on Fracture – Multilevel Approach to Fracture of Materials, Components and Structures, Brno, Czech Republic, September, 2-5.
8. Paris, P.C., Gomez, P.M., Anderson, W.E. (1961), A rational analytic theory of fatigue, *Trend. Eng.* 13 (1), pp. 9-14.
9. Schijve, J. (1981), Some formulas for the crack opening stress level, *Engng. Fract. Mech. 14*, pp. 461-465.
10. Newman, J.C. (1984), A crack opening stress equation for fatigue crack growth, *Int. J Fracture 24*, R, pp. 131-135.
11. Elber, W. (1970), Fatigue crack closure under cyclic tension, *Engng. Fract. Mech.* 2, , pp. 37-45.
12. Elber, W. (1971), The significance of fatigue crack closure. Damage tolerance in aircraft structures, ASTM STP 486, pp. 230-242.
13. Newman, J.C. (1976), A finite-element analysis of fatigue crack closure, ASTM STP vol. 590, Philadelphia PA, ASTM, pp. 281-301.
14. Ranganathan, N. (2002), Certain aspects of variable amplitude fatigue, IFC-8-Fatigue 2002, Stockholm, 3–7, pp. 613 - 623.
15. Boljanović, S., Maksimović, S. (2011), Analysis of the crack growth propagation process under mixed-mode loading, Engineering Fracture Mechanics, Volume 78, Issue 8, pages 1565-1576.
16. Maksimović, S., Boljanović, S, Maksimović, K..(2002), Fatigue life prediction of Structural Components under variable amplitude loads, FATIGUE 2002, 8th International Fatigue Congress (IFC8), Stocholm, 2-6.
17. Forman, R.G., V.E. Kearney and R. M. Engle (1967) , Numerical analysis of crack propagation in cyclic loaded structures, J. Bas. Engng. Trans. ASME 89, 459.
18. Liu, Y.Y., Lin, F.S. (1984), A mathematical equation relating low cycle fatigue data to fatigue crack propagation rates, Int. J. Fatigue, Vol. 6, pp.31-36.
19. *Maksimović, S., Posavljak, S., Maksimović, K., Nikolić, V. and Djurkovic V., Total Fatigue Life Estimation of Notched Structural Components Using Low-Cycle Fatigue Properties, J. Strain (2011),* **47** *(suppl.2), pp 341-349.*
20. Boljanović, S., Maksimović, S**.,** Djurić, M. (2009), Analysis of crack propagation using Local Strain Density Method, Scientific Technical Review, Volume LVIX, No. 2, pp. 12-17.
21. Maksimović S., Vasović I., Maksimović M., Đurić M. (5-8 July 2011), RESIDUAL LIFE ESTIMATION OF DAMAGED STRUCTURAL COMPONENTS USING LOW-CYCLE FATIGUE PROPERTIES, Third Serbian Congress Theoretical and Applied Mechanics, Vlasina Lake, pp. 605-617, Organized: Serbian Society of Mechanics, ISBN 978-86-909973-3-6, COBISS:SR-ID 187662860, 531/534(082).

POBOLJŠAN PRORAČUNSKI METOD PROCENE PREOSTALOG VEKA ELEMENATA KONSTRUKCIJA

Stevan M. Maksimović[*], Katarina S. Maksimović[**],

U radu se razmatraju numeričke metode i procedure za analizu širenja prskotina kod strukturalnih elemenata sa inicijalnim oštećenjima u vidu prskotina. Proračunski metod bazira na proceni preostalog veka koristeći metod gustine energije deformacije (GED). Bazirano na teoriji gustine energije deformacije razvijen je model za za analizu širenja prskotine i procene preostalog veka strukturalnih elemenata za prskotine tipa moda I. Model je zasnovan na zakonu širenja prskotine koji bazira na korišćenju malociklusnih zamornih karakteristika materijala. Pažnja je usmerena na analize širenja prskotina pri opštem spektru opterećenja. Značajan uticaj plastifikacije oko vrha prskotine ima na širenje prskotine. Da bi se dobio efikasan i pouzdam proračunski model u radu je razmatran uticaj plasifikacije oko vrha prskotine na zatvaranje prskotine. Korišćenje gustine energije deformacije predstavlja sa svoje strane efikasan metod za analizu širenja prskotine kod strukturalnih elemenata sa inicijalnim oštećenjima u vidu prskotine. Metod gustine energije deformacije je pogodan sa aspekta inžinjerske primene jer ne zahteva dodatne dinamičke karakteristike materijala (za čije bi određivanje bila potrebna dodatna ispitivanja) već koristi samo malociklusne zamorne karakteristike materijala kakve se koriste i za problem procene veka do pojave inicijalnog oštećenja. Precizno određivanje zatvaranja prskotine zbog plastifikacije oko njenog vrha predstavljao je kompleksan problem istraživanja tokom poslednjih godina. Ovaj fenomen je istraživan preko numeričkih i eksperimentalnih metoda. Metod konačnih elemenata (FEM) se pokazao kao pouzdan alat [1,6] za analizu širenja prskotine gde su bili uključeni i efekti zatvaranja vrha prskotine. Proračunski rezultati su upoređeni sa raspoloživim eksperimentalnim rezultatima.

ABOUT EIGENSENSITIVITY ANALYSIS OF MECHANICAL STRUCTURES

UDC 531.64; 534;531.8;

Nataša R. Trišović

The University of Belgrade, Faculty of Mechanical Engineering, Department of Mechanics, Kraljice Marije 16, 11000 Belgrade, Serbia

Abstract. *Several methods for a calculation of derivatives of eigenvectors with respect to design parameters are described here. These are the finite-difference method, the modal method, a modified modal method, Nelson's method, an improved first-order approximation of eigenvalues and eigenvectors and an iterative method. By combining the other structural reanalysis techniques and one of these sensitivity methods, it is possible to enhance the efficiency and the accuracy of structural optimization techniques for determining the optimum condition of mechanical structure specified by an analyst. The sensitivity approach is based on the prior selection of updating parameters (design variables) in the initial FE model.*

Key words: *eigenvalue and eigenvector sensitivity*

1. INTRODUCTION

A good finite element (FE) or analytical model of a mechanical structure is important for structural integrity analysis. In practice, a high degree of confidence can be placed on such a FE/analytical model when the dynamic response of that model closely resembles experimental data. However, updating the FE model or inetifying the analytical model directly is usually not the main objective of structural vibration analysis because there are many situations when the dynamic response of the mechanical structure does not satisfy the requirement set by the structural analyst (designer). In such situations, the dynamic response of the mechanical structure has to be altered either (i) by controlling the forcing inputs to the structure, or (ii) by changing the dynamic characteristics of the structure. The forcing inputs often results from interaction with the structure's environment and so cannot easily be controlled at will. When this is the case, it is important to be able to alter the structural response by redesigning the dynamic characteristics of the structure. The use of structural reanalysis techniques to obtain the optimum condition of an FE model of

a mechanical structure has grown considerably in recent years. The optimal design of structures with frequency constraints is extremely useful in manipulating the dynamic characteristics in a variety of ways. For example, in most low-frequency vibration problems, the response of the structure to dynamic excitation is primarily a function of its fundamental frequency and mode shape. In such cases, the ability to manipulate the selected frequency can significantly improve the performanse of the structure. Similarly, the aeroelastic characteristics of an aircraft wing the governed primarily by its torsional and bending properties, which can best be studied by the lower torsional and bending modes. A number of techniques exist that can be applied to the dynamic reanalysis of mechanical structures. One of the most popular of these is sensitivity analysis which has been developed and applied by several workers to the general eigenvalue problem [1-7] and, more specifically, to applications of structural dynamic modification analysis in references [8-9]. Some of the areas where sensitivity analysis has been applied include (i) system identification, (ii) development of insensitive control systems, (iii) use in gradient-based mathematical programming methods, (iv) approximation of system response to a change in a system parameter, and (v) assessment of design changes on system performance [19]. In this area, both first- and higher-order eigenvalue and eigenvector sensitivities have been investigated with a view to predicting the response of a modified structure from knowledge of its spatial and modal properties in the original, or unmodified, state. The sensitivity analysis of a mechanical structure is based on a Taylor expansion of eigenvalues and eigenvectors of the unmodified structure. Traditionally, a truncated Taylor or matrix power series evaluated at a nominal design point is used to approximate the eigen parameters of modified structures [21,22]. Earlier studies [20] indicated that the compution of the higher-order terms of this series is difficult and time consuming, the effectiveness of this method is limited to small modifications. Even the use of higher-order terms in the local approximation series cannot guarantee convergence for moderate to large perturbations in the structural parameters. The implication of this observation in the context of structural optimization is that severe move limits have to be imposed in line searches to ensure convergence to a feasible design. Very few studies in the literature have addressed the structural dynamic reanalysis problem for moderate to large modifications in the structural parameters. The approach currently in use can be broadly classified into direct and iterative approaches. The objective of most direct approaches is to increase the range of validity of local approximation techniques. Inamura [25] proposed an approximation procedure in which the eigenpair perturbation equations are interpreted as differential equations in terms of the perturbation parameters. A procedure using the eigensensitivity equations was developed by Pritchard and Adelman [26] based on a similar line of approach. The sensitivity method [24] is a prime representative of the updating approach which allows selection of updating parameters but does not require full experimental mode shapes and as such this method seems to be suitable for updating of large models. Also, it is worth noting that model updating methods based on control methods, such as eigenstructure assignment method proposed by Minas and Inman [22,23] are quite promising sinse they can be defined in such a way that they do not require full experimental mode shape matrix. The general perturbation procedure followed in major papers is diagrammatically shown in Fig. 1.

Physical Structure

Creation of the
Initial FE Model

Modifying
the Initial
Model by
Hand

Analysis of
Sensitivity

Test Planning

Modal Dynamic
FE Analysis.
[K] [M], [λ], [Q]

Modal Dynamic
Measurements

Not Suitable
for Reanalysis

**Verification and
Correlation of the FE Model:**
F.E.A. Predictions and
Measurements Agree?

Suitable
for
Reanalysis

Reanalysis:
-Analysis of Sensitivity
(Updating Parameter Selection)
-Model Updating
by Perturbation - Redesign

Unsatisfactory
Results

**Assessment of the
Updated Model**

Satisfactory
Results

Updated Model: [K'], [M']
Response: {u'}, [λ'], [Q']

STOP

Fig. 1 Flowchart of General Perturbation

2. MODAL SENSITIVITY ANALYSIS. DESIGN SENSITIVITIES.
THEORETICAL BACKGROUND. SURVEY

It is becoming widely accepted that sensitivity analysis can be a valuable tool in structural reanalysis where (enough of) the modal properties are known, either through

theoretical or experimental analysis. Modal sensitivities are the derivatives of the modal properties of a dynamic system with respect to chosen structural variables. In the modal analysis literature there have been two primary applications. In the first case sensitivity data are used solely as a qualitative indicator of the location and approximate scale of design changes to achieve a desired change in structural properties. The consequences of candidate design changes would then be evaluated using exact methods. The second strategy uses the design sensitivities directly to predict the effect of proposed structural changes. The use of sensitivities in this fashion relies on the Matrix Taylor Series expansion, with the usual implications of convergence and truncation errors. Use only of first order design sensitivities assumes implicitly that the second (and higher) order derivatives are negligible. The use of these second order sensitivities as suitable criteria for the acceptability of first order sensitivities for predictive analysis can be interested in some detail. Sensitivity analysis may be applied to candidate design modifications distributed across a number of degrees of freedom of the structure but is limited in scale. Modal design sensitivities are the derivatives of the eigensystem of a dynamic system with respect to those variables which are available for modification by the designer. A typical modification would be the change in diameter of a circular section. This would affect both the mass of the section, proportional to the square of the diameter, and its stiffness, which depends on the second moment of area of the section. A change in length would have a mass effect directly proportional to length, but a stiffness change depending on the cube of length. Changing material would similarly affect mass, stiffness and damping. Shape sensitivity analysis of physical systems under dynamic loads may be important from different points of view (i) to understand and model the system's behavior better with respect to shape, (ii) to optimize the physical shapes of the desired systems responses in a prescribed time interval, or (iii) to identify shapes by utilizing the system's measured response in time.

2.1. Problem Statement. Derivation

The matrix form of the equation of undamped motion of an FE model is:

$$[M] \cdot \{\ddot{x}(t)\} + [K] \cdot \{x(t)\} = \{0\} \tag{1}$$

The free-vibration natural frequencies and mode shapes of a linear structural system can be computed by solving the above eigenvalue problem

$$[K]\{Q_i\} = \lambda_i [M]\{Q_i\} \tag{2}$$

where $[K], [M]$ are the structural stiffness and mass matrix, respectively. The system matrices are considered to be a general function of the design variables denoted by $\{V\} = \{v_1, v_2, ..., v_j, ..., v_p\}$, and λ_i and $\{Q_i\}$ are the eigenvalue and the eigenvector of mode i, respectively. Consider the case wherein the design variables are perturbed by $\{\Delta V\}$. Let $[\Delta K]$ and $[\Delta M]$ be the corresponding perturbation in the stiffness and mass matrices. The perturbed eigenvalue problem can be written as

$$([K] + [\Delta K])(\{Q_i\} + \{\Delta Q_i\}) = (\lambda_i + \Delta \lambda_i)([M] + [\Delta M])(\{Q_i\} + \{\Delta Q_i\}) \tag{3}$$

where $\Delta\lambda_i$ and $\{\Delta Q\}_i$ are the eigenvalue and eigenvector perturbations, respectively. Equation (2) can be written in a compact form as

$$[K']\{Q'_i\} = \lambda'_i[M']\{Q'_i\} \tag{4}$$

Often it is found that, even for small to moderate perturbations in the stiffness and mass matrices, significant alterations in the modal characteristics of the structure may occur. Hence, an exact reanalysis becomes necessary to compute the perturbed eigenparameters with sufficient accuracy. The objective of approximate reanalysis procedures is the computation of the perturbed eigenparameters using the results of exact analysis for the baseline system without recourse to solving Eq. (3) in its exact form. Typically, the perturbations in the eigenparameters are calculated using first-order sensitivity information as

$$\Delta\lambda_i = \sum_{j=1}^{p}\left(\frac{\partial\lambda_i}{\partial v_j}\right)\Delta v_i \quad \text{and} \quad \{\Delta Q_i\} = \sum_{j=1}^{p}\left(\frac{\partial\{Q_i\}}{\partial v_i}\right)\Delta v_i \tag{5}$$

where $\partial\lambda_i/\partial v_j$ and $\partial\{Q_i\}/\partial v_j$ are the sensitivities of the eigenvalues and eigenvectors with respect to the structural parameters, respectively. The eigenvalue and eigenvector derivatives can be calculated by performing partial differentiation of the equation (2) to an updating structural parameter v_j:

$$\left([K]-\lambda_i[M]\right)\frac{\partial\{Q_i\}}{\partial v_j} = \left(\lambda_i\frac{\partial[M]}{\partial v_j}+\frac{\partial\lambda_i}{\partial v_j}[M]-\frac{\partial[K]}{\partial v_j}\right)\{Q_i\}. \tag{6}$$

This is an equation for the eigenvector sensitivity. It can seen from Eq. (5) that the computation of the eigenvalue sensitivities involves a simple and straightforward calculation. Left-multiplying with the transpose of the eigenvector gives

$$-\frac{\partial\lambda_i}{\partial v_j}\cdot\{Q_i\}^T\cdot[M]\cdot\{Q_i\}+\{Q_i\}^T\cdot\left(\frac{\partial[K]}{\partial v_j}-\lambda_i\cdot\frac{\partial[M]}{\partial v_j}\right)\cdot\{Q_i\}+$$

$$+\left(\{Q_i\}^T\cdot[K]-\lambda_i\cdot\{Q_i\}^T\cdot[M]\right)\cdot\frac{\partial\{Q_i\}}{\partial v_j}=\{0\}$$

Because $\{Q_i\}^T\cdot[M]\cdot\{Q_i\}=1$ and $\{Q_i\}^T\cdot[K]-\lambda_i\cdot\{Q_i\}^T\cdot[M]=0$,

$$\frac{\partial\lambda_i}{\partial v_i} = \{Q_i\}^T\left(\frac{\partial[K]}{\partial v_j}-\lambda_i\frac{\partial[M]}{\partial v_j}\right)\{Q_i\} \tag{7}$$

This is the formula for the eigenvalue sensitivity of the ith mode to the jth design parameter. From this formula, it can be seen that the sensitivity of an eigenvalue to an design parameter can be calculated from the eigenvalue, the corresponding eigenvector, and the sensitivities of the stiffness and mass matrices to the design parameter (variable).

Equations (2-7) have been derived under the assumption that the baseline eigenvectors have been mass normalized.

2.2. Description of the Sensitivity Methods

There mainly exist three categories in the literature: the modal method, the direct method, and the iterative method. Several methods for calculating eigenvector derivatives, $\partial\{Q_i\}/\partial v_j$, are described. Every method, exept the finite-difference method, requires the mass matrix and stiffness matrix derivatives, $\partial[M]/\partial v_j$ and $\partial[K]/\partial v_j$, respectively.

2.2.1 Finite-Difference Method

The most straightforward approach for calculating the derivatives is the finite-difference method. In the finite-difference method, Eq. (2) is solved for $\{Q_i\} = \{Q_i\}_{old}$, the jth design variable is perturbed by Δv_j, and a new eigenvector $\{Q_i'\} = \{Q_i\}_{new}$ is obtained by solving Eq. (2) again, where $v_{j,new} = v_{j,old} + \Delta v_j$. The derivative is approximated by the expression

$$\frac{\partial\{Q_i\}}{\partial v_j} = \frac{\{Q_i\}_{new} - \{Q_i\}_{old}}{\Delta v_j} \tag{8}$$

To reduce numerical errors associated with Eq. (8), attention should be paid to the step size Δv_j. An algotithm for determining the optimum step size has been developed to further reduce numerical errors and is described in Ref. [28].

2.2.2 Modal Method

The modal method expresses the derivative of an eigenvector as a series expansion of the system eigenvectors. Because this method is based on the series expansion of the eigenvalues and eigenvectors of the modified (perturbed) system, the efficiency of this method is limited. The approximate derivative is expressed as [34]:

$$\frac{\partial\{Q_i\}}{\partial v_j} = \sum_{k=1}^{N} A_{ijk}\{Q_k\}, \tag{9}$$

where the coefficients A_{ijk} are calculated using

$$A_{ijk} = \frac{\{Q_k\}^T\left(\dfrac{\partial[K]}{\partial v_j} - \lambda_i \dfrac{\partial[M]}{\partial v_j}\right)\{Q_i\}}{\lambda_i - \lambda_k}, \quad k \neq i. \tag{10}$$

Considering the orthogonality property of the eigenvector, $\{Q_i\}$, $\{Q_i\}^T[M]\{Q_i\}=1$, and partial-differentiating this equation with respect to the updating parameter, v_j, for $k \neq i$, it can be obtained that:

$$2\{Q_i\}^T[M]\frac{\partial\{Q_i\}}{\partial v_j} + \{Q_i\}^T\frac{\partial[M]}{\partial v_j}\{Q_i\}=0 \tag{11}$$

The expression for $\partial\{Q_i\}/\partial v_j$ from Eq. (9) is substituted into Eq. (11), and using the orthogonality condition $\{Q_i\}^T[M]\{Q_i\}=1$, the coefficients A$_{ijk}$ are obtained:

$$A_{ijk} = -\frac{1}{2}\{Q_i\}^T\frac{\partial[M]}{\partial v_j}\{Q_i\}, \quad k = i. \tag{12}$$

2.2.3 Modified Modal Method

The modified modal method uses a pseudostatic solution of Eq (6) as an initial approximation to the mode shape derivative. This is similar in principle to the mode-acceleration method used in transient structural analysis [29]. Equation (6) is solved by neglecting the quantity $\lambda_i[M](\partial\{Q_i\}/\partial v_j)$ and obtaining the pseudostatic solution for $(\partial\{Q_i\}/\partial v_j)_s$, which is

$$\left(\frac{\partial\{Q_i\}}{\partial v_j}\right)_s = [K]^{-1}\cdot\left(\lambda_i\frac{\partial[M]}{\partial v_j} + \frac{\partial\lambda_i}{\partial v_j}[M] - \frac{\partial[K]}{\partial v_j}\right)\cdot\{Q_i\}. \tag{13}$$

This pseudostatic solution is added to Eq. (9) to obtain

$$\frac{\partial\{Q_i\}}{\partial v_j} = \left(\frac{\partial\{Q_i\}}{\partial v_j}\right)_s + \sum_{k=1}^{N}\overline{A}_{ijk}\{Q_k\}, \tag{14}$$

where $\overline{A}_{ijk}$ are coefficients for the modified modal method. To obtain the coefficients $\overline{A}_{ijk}$, Eq. (14) is substituted into Eq. (6), and the result is premultiplied by $\{Q_k\}^T$. When simplified, this result becomes

$$\overline{A}_{ijk} = \frac{\lambda_i\{Q_k\}^T\left(\frac{\partial[K]}{\partial v_j} - \lambda_i\frac{\partial[M]}{\partial v_j}\right)\{Q_i\}}{\lambda_k\cdot(\lambda_i - \lambda_k)}, \quad k \neq i, \tag{15}$$

$$\overline{A}_{ijk} = -\frac{1}{2}\{Q_i\}^T\frac{\partial[M]}{\partial v_j}\{Q_i\}, \quad k = i. \tag{16}$$

The relative convergence of the modified modal method vs the modal method for a given number of eigenvectors can be anticipated by dividing Eq. (15) by Eq. (10):

$$\frac{\overline{A}_{ijk}}{A_{ijk}} = \frac{\lambda_i}{\lambda_k} \tag{17}$$

Assuming that to calculate $\partial\{Q_i\}/\partial v_j$ accurately i modes or more are needed; then for k>i, $\overline{A}_{ijk}$ is smaller than A_{ijk}, and Eq. (14) will converge faster than Eq. (9).

2.2.4 Nelson's Method

Nelson's method (the direct method) obtains an exact solution to Eq. (6). This method expresses the eigenvector derivative in terms of a particular solution $\{\xi_{ij}\}$ and a complementary solution $\{Q_i\} \cdot c_{ij}$ where c_{ij} is an undetermined coefficient. In this case, any solution for equation (6) can be written in the form of [27]:

$$\frac{\partial\{Q_i\}}{\partial v_j} = \{\xi_{ij}\} + \{Q_i\} \cdot c_{ij}, \tag{18}$$

The particular solution is found by identifying the component of the eigenvector $\{Q_i\}$ with the largest absolute value and constraining the derivative of that component to zero. Combining equations (18) and (11), it is shown that

$$2\{Q_i\}^T [M](\{\xi_{ij}\} + \{Q_i\} \cdot c_{ij}) + \{Q_i\}^T \frac{\partial[M]}{\partial v_j}\{Q_i\} = 0 . \tag{19}$$

The coefficient c_{ij} can be obtained by the following formula:

$$c_{ij} = -\left(\{Q_i\}^T [M]\{\xi_{ij}\} + \frac{1}{2}\{Q_i\}^T \frac{\partial[M]}{\partial v_j}\{Q_i\} \right) \tag{20}$$

2.2.5 Improved First-Order Approximation of Eigenvalues and Eigenvectors

A method based on reduced basis approximation concepts is presented for improved first-order approximation of eigenvalues and eigenvectors of modified structural dynamic systems [33]. The approximation procedure involves the use of the baseline eigenvector and the first-order approximation term as basic vector for Ritz analysis of the perturbed eigenvalue problem. An assumption is made that the eigenvector of the perturbed system can be approximated in the subspace spanned by $\{Q_i\}$ and $\{\Delta Q_i\}$, which is computed using Eqs. (5-7), i.e., an approximation for the perturbed eigenvector can be written as

$$\{\hat{Q}_i\} = \zeta_1\{Q_i\} + \zeta_1\{\Delta Q_i\} \tag{21}$$

where ζ_1 and ζ_2 are undetermined scalar quantities in the approximate representation of the perturbed eigenvector. The assumption implicit in this proposition is that, even for moderate to large perturbations in the structural parameters, the first-order approximation yields a $\{\Delta Q_i\}$ vector, which usually gives a reasonable indication of the likely change of a baseline eigenvector, although the magnitude or even direction of change may be erroneous. Eq. (21) can be expressed in matrix form as

$$\left\{\hat{Q}_i\right\} = [T]\{Z\} \tag{22}$$

where $[T]=[Q_i, \Delta Q_i] \in \Re^{n \times 2}$ and $\{Z\}^T = \{\zeta_1, \zeta_1\} \in \Re^{1 \times 2}$.

Substituting equation (22) in to equation (4) and premultiplying by $[T]^T$, the resulting set of equations can be expressed as

$$[K_T]\{Z\} = \lambda[M_T]\{Z\} \tag{23}$$

where

$$[K_T] = [T]^T[K'][T] \in \Re^{2 \times 2} \tag{24}$$

and

$$[M_T] = [T]^T[M'][T] \in \Re^{2 \times 2}. \tag{25}$$

After matematical transformation, the mass normalized perturbed eigenvector can be written as [33]:

$$\left\{\hat{Q}_i\right\} = \frac{1}{\{Z\}^T[M_T]\{Z\}} \cdot \left[\{Q_i\} - \frac{\left(k_{11} - \hat{\lambda}_i m_{11}\right)}{\left(k_{12} - \hat{\lambda}_i m_{12}\right)} \cdot \{\Delta Q_i\}\right]. \tag{26}$$

The following inequality relationship can be estabilished as criteria for selection of the best approximation

$$\hat{\lambda}_i^{\min} \leq \lambda_i^{rqa0} \leq \hat{\lambda}_i^{\max} \tag{27}$$

where λ_i^{rqa0} is the zero order Rayleigh quotient approximation which is defined below as

$$\lambda_i^{rqa0} = \frac{\{Q_i\}^T[K]\{Q_i\}}{\{Q_i\}^T[M]\{Q_i\}}. \tag{28}$$

Hence, criteria for selection of the best approximation are (i) maximum value of $|\zeta_1/\zeta_2|$, (ii) minimum distance from the zero-order Rayleigh quotient λ_i^{rqa0}, (iii) minimum distance from λ_i, (iv) minimum magnitude, (v) minimum distance from the root selected for the previous mode. This approximation procedure could also be

interpreted as an improved Rayleigh quotient approximation procedure with one free parameter, i.e., $\left|\zeta_2 / \zeta_1\right|$.

2.2.6 Iterative Method for Calculating Eigenvectors Derivatives

The calculation of the eigenvector derivatives involves extensive computational effort. The direct method is one of the most efficient methods that produces exact solutions and does not need eigenvectors more than those whose derivatives are to be computed. But because its amount of computational effort is proportional to the number of eigenvector derivatives required, the application of the method becomes expensive when many eigenvector derivatives are demanded. On the other hand, the truncated modal method has an insuperable efficiency but suffers a serious accuracy problem. To improve the accuracy of the modal method, Wang [35] proposed a modified modal method, which was extended by Liu et al. [36] and Zhang and Zerva [37] to an iterative algorithm that can be used as an exact method as well as an approximate method and, just like the direct method, does not require additional eigenvalues and eigenvectors. The method assumes that the inverse stiffness matrix exists. Recently, Lin and Lim [38] and Zeng [39] presented an approach to deal with singular stiffness matrices. The convergence rate of the iterative method depends mainly on the ratio of the specified eigenvalue to the lowest unavailable one, and when the ratio approaches 1, the convergence rate of the corresponding eigenvector derivative will reduce quickly and the method becomes more expensive than the direct method. The iterative method used here was derived originally in Ref. [37]. The basic iterative equation after $p(p \geq 1)$ iterations is

$$\{V_{ku}\}_p = \sum_{i=q+1}^{n} \left[1 - \left(\frac{\lambda_k}{\lambda_i}\right)^p\right] \frac{\{Q_k\}^T \left(\frac{\partial[K]}{\partial v_j} - \lambda_i \frac{\partial[M]}{\partial v_j}\right)\{Q_i\}}{\lambda_i - \lambda_k} \{Q_k\} +$$

$$+ \sum_{i=q+1}^{n} \left(\frac{\lambda_k}{\lambda_i}\right)^p \{Q_k\}^T [M]\{V_{ku}\}_0 \{Q_i\},$$

$$k < q; \quad p = 1,2,... \tag{29}$$

where

$\{V_{ku}\}$ = component of $\partial\{Q_k\}/\partial v_j$ in the range of unavailable eigenvectors $\{Q_{q+1}\},...,\{Q_n\}$,

$\{V_{ku}\}_p$ = pth iterative solution for $\{V_{ku}\}$,

$\{V_{ku}\}_0$ = stands for the initial value.

The term $(\lambda_k / \lambda_i)^p$ represents the error because of the ith unknown eigenvector. When p tends to infinity, $(\lambda_k / \lambda_i)^p$ vanishes because $\lambda_k / \lambda_i < 1$, and $\{V_{ku}\}_p$ converges to the exact solution with any initial value. Equation (29) also suggests that $\{V_{ku}\}_0$ can be set equal to zero. Note that in each iteration, the roundoff error in the subspace spanned by

the lower available eigenvectors $\{Q_1\},...,\{Q_q\}$ will be automatically wiped out, which results in a very stable iterative process.

3. CONCLUDING REMARKS

This paper reviewed several methods for eigensensitivity analysis with respect to design variables. These were the finite-difference method, the modal method, a modified modal method, Nelson's method, an improved first-order approximation of eigenvalues and eigenvectors and an iterative method. Nelson's method was the least computationally intensive, and since it is an exact method, it is the method recommended. When the original mode shapes were used as initial approximations to the subspace eigensolution of the perturbed problem, the finite-difference method was competitive with Nelson's method. The modified modal method always converged faster than the modal method when at least as many modes were used in the approximation as the number of the mode shape being differentiated. The modified modal method can compete with Nelson's method for the first mode shape derivative when the number of modes needed in the summation was known before the eigensolution was performed. Detailed comparasion an improved first-order approximation [33] with other approximation techniques indicate that significant improvements are achieved with a relatively small extra computational effort. An iterative method is simple, systematic, efficient and numerically stable.

4. REFERENCES

1. Wilkinson, J.H., The Algebraic Eigenvalue Problem, Oxford University Press, London, 1963, pp. 62-109
2. Rosenbrock, H.H., Sensitivity of an Eigenvalue to Changes in the Matrix, Electronics Letters, Vol. 1, 1965, pp. 278-279
3. Reddy, D.C., Sensitivity of an Eigenvalue of a Multivariable Control System, Electronics Letters, Vol. 2, 1966, pp. 446
4. Rogers, L.C., Derivatives of Eigenvalues and Eigenvectors, AIAA Journal, Vol. 8, 1970, pp 943-944
5. Vanhonacker, P., Differential and Difference Sensitivities of Natural Frequencies and Mode Shapes of Mechanical Structure, AIAA Journal, Vol. 18, 1980, pp. 1569-1572
6. Rudisill, C.S. and Bhatia, K.G., Second Derivatives of the Flutter Velocity and the Optimization of Aircraft Structures, AIAA Journal, Vol. 10, 1972, pp 1511-1514
7. Plaut, R.H. and Huseyin, K., Derrivatives of Eigenvalues and Eigenvectors in Non-Self-Adjoint Systems, AIAA Journal, Vol. 11, 1973, pp 250-251
8. Wang, J., Heylen., W. and Sas, P., Accuracy of Structural Modification Techniques, Proc. of the 5th Int. Modal Analysis Conf., 1987., pp. 65-71
9. Noor, A.K. and Whitworth, S., Reanalysis Procedure for Large Structural Systems, Int. J. Numer. Methods Eng. Vol. 26, 1988. pp. 1729-1748
10. Ewins, D.J., Modal Analysis: Theory and Applications, Research Studies Press.,1984.
11. Flax, A.H., Comment on „Derivation and significance of second order modal design sensitivities", AIAA Journal, Vol. 23, 1985, p. 478
12. Collar, A.R. and Simpson, A., Matrices and Engineering Dynamics, Ellis Horwood, Chichester, 1987.
13. Pomazal, R.J., The Effect of Local Modifications on the Eigenvalues and Eigenvectors of Damped Linear Systems, PhD Thesis, Michigan Technological University, 1969.

14. Pomazal, R.J. and Snyder, V.W., Local Modifications of Damped Linear Systems, AIAA Journal, Vol. 9, 1970, pp. 2216-2221.
15. Lancaster, P., Free Vibrations of Lightly Damped Systems by Perturbation Methods, Quarterly Journal of Mechanics and Applied Mathematics, Vol. 13, 1960., pp. 138-155.
16. Rogers, L.C., Derivatives of eigenvalues and eigenvectors, AIAA Journal, Vol. 8, 1970, pp. 943-944.
17. Stewart, G.W., Introduction to Matrix Computation, Academic Press
18. To, W.M. and Ewins, D.J., Structural Modification Analysis using Rayleigh Quotient Iteration, in Modern Practice in Stress and Vibration Analysis, Editor, Mottershead, Pergamon, 1989, pp. 1-9.
19. Prasad, B. and Emerson, J.F., A General Capability of Design Sensitivity for Finite Element Systems, A Collection of Technical Papers, Part 2: Structural Dynamics and Design Engineering, AAIA/ASME/ASCE/AHS 23rd Structures, Structural Dynamics and Material Conf., May 1982, pp. 175-186.
20. Schmit, L.A. and Miura, H., Approximation Concepts For Efficient Structural Synthesis, NASA CR-2552, 1976.
21. Schmit, L.A. and Farshi, B., Some Approximation Concepts For Structural Synthesis, AIAA Journal, Vol. 2, No.5, 1974, pp. 692-699.
22. Minas, C. and Inman, D.J., Matching Finite Element Models to Model Data, ASME Journal of Vibration and Acoustics, Vol. 112, 1990.
23. Inman, D.J. and Minas, C., Matching Analytical Models with Experimental Modal Data in Mechanical Systems, Control and Dynamics Systems, Vol. 37, 1990.
24. Imamovic, N., Validation of Large Structural Dynamic Models Using Experimental Modal Data, PhD Thesis, 1998., IC, London
25. Inamura, T., Eigenvalue Reanalysis by Improved Perturbations, International Journal of Numerical Methods in Engineering, Vol. 26, No. 1, 1988, pp. 167-181.
26. Pritchard, J.I., and Adelman, H.M., Differential Equation Based Method for Accurate Modal Approximations, AIAA Journal, Vol. 29, No.3, 1991, pp. 484-486.
27. Nelson, R.B., Simplified Calculation of Eigenvectors Derivatives, AAIA Journal, Vol. 14, 1976, pp.1201-1225.
28. 28. Iott, J., Haftka, R.T., and Adelman, H.M., On a Procedure for Selecting Step Sizes in Sensitivity Analysis by Finite Differences, NASA TM-86382, Aug.1985. [29] Craig, R.R., Jr., Structural Dynamics – An Introduction to Computer Methods, Wiley, New York, 1981.
29. Trisovic, N., Maneski, T., Sumarac, D., Reanalysis in Structural Dynamics, SEECCM06, Kragujevac, 28-30 June 2006.
30. Maneski, T., Ph D Thesis, Faculty of Mechanical Engineering, 1992., Belgrade
31. Maneski, T., Milošević-Mitić, V., Ostrić, D., Postavke čvrstoće konstrukcija, Faculty of Mechanical Engineering, 2002, Belgrade
32. Maneski, T., Kompjutersko modeliranje i proračun struktura, Faculty of Mechanical Engineering, 1998, Belgrade
33. Nair, B.P., Keane, A.J., and Langley, R.S., Improved First-Order Approximation of Eigenvalues and Eigenvectors, AIAA Journal, Vol. 36, No. 9, September 1998, pp. 1722-1727.
34. Sutter, T.R., Camarda.,C.J., Walsh.,J.L., Adelman.,H.M., Comparison of Several Methods for Calculating Vibration Mode Shape Derivatives, AIAA Journal, Vol. 26, No. 12, Feb. 1987, pp. 1506-1511.
35. Wang, B.P., Improved Approximate Methods for Computing Eigenvector Derivatives in Structural Dinamycs,, AIAA Journal, Vol. 29, No. 6, 1991, pp. 1018-1020.
36. Liu, Z.S., Chen, S.H., Yu, M., and Zhao, Y.Q., Contribution of Truncated Modes to Eigenvector Derivatives, AIAA Journal, Vol. 32, No. 7, 1994, pp. 1551-1553.
37. Zhang, O., and Zerva, A., Iterative Method for Calculating Derivatives of Eigenvalues, AIAA Journal, Vol. 34, No. 5, 1996, pp. 1088-1090.
38. Lin, R.M., and Lim, M.K., Eigenvector Derivatives of Structures with Rigid Body Modes, AIAA Journal, Vol. 34, No. 5, 1996, pp. 1083-1085.
39. Zeng, Q.H., Highly Accurate Modal M ethod for Calculating Eigenvectors in Viscous Damping Systems, AIAA Journal, Vol. 33, No. 4, 1995, pp. 746-751.
40. Trišović, N., Modification of the Dynamics Characteristics in the Structural Dynamic Reanalysis, PhD Thesis, Belgrade, November 2007.

АНАЛИЗА ОСЕТЉИВОСТИ СОПСТВЕНИХ ВРЕДНОСТИ И СОПСТВЕНИХ ВЕКТОРА МЕХАНИЧКИХ СИСТЕМА

Наташа Тришовић,
Универзитет у Београду, Машински факултет

Резиме. *Неколико метода за израчунавање извода сопствених вектора у односу на конструкционе параметре описане су у овом раду. То су метода коначних разлика, модални метод, модификовани модални метод, Нелсонов метод, побољшана апроксимација првог реда и итеративни метод. Комбиновањем других техника реанализе и неког од ових метода, могуће је да се повећа ефикасност и тачност техника оптимизације за одређивање оптималних услова механичког система одређеног од стране аналитичара. Анализа сензитивности се заснива на селекцији конструкционих параметара у почетном коначноелементном моделу чијом модификацијом би дошло до поправљања динамичког понашања посматране конструкције.*

Кључне речи: *Анализа осетљивости сопствених вредности и сопствених вектора*

PROCESS PARAMETERS EFFECT ON MATERIAL REMOVAL MECHANISM AND CUT QUALITY OF ABRASIVE WATER JET MACHINING

UDC 621.924

P. Janković, T. Igić, D. Nikodijević

University of Niš, Faculty of Mechanical Engineering
University of Niš, Faculty of Civil Engineering and Architecture

Abstract. *The process of the abrasive water jet cutting of materials, supported by the theories of fluid mechanics, abrasive wear and damage mechanics, is a high-tech technologies that provides unique capabilities compared to conventional machining processes. This paper, along the theoretical derivations, provides original contributions in the form of mathematical models of the quantity of the cut surface damage, expressed by the values of cut surface roughness. The particular part of this paper deal with the results of the original experimental research.*
The research aim was connected with the demands of industry, i.e. the end user. Having in mind that the conventional machining processes are not only lagging behind in terms of quality of cut, or even some requests are not able to meet, but with the advent of composite materials were not able to machine them, because they occurred unacceptable damage (mechanical damage or delamination, fiber pull-out, burning, frayed edges).

Key words: *Abrasive water jet cutting, Damage mechanics, aluminium specimens test, mathematical modeling*

1. INTRODUCTION

Abrasive water jet (AWJ) cutting is a non-conventional machining process that uses high velocity water with abrasives for cutting a variety of materials. Using the damages mechanics, as the basis of the machining process, the material damage is very small and can be controlled. It is a non-contact process which produces narrow kerf on the material, without heat affected zone. Abrasive water jet cutting has become a highly developed industry technology. It is most suitable process for very thick, highly reflective or highly thermal-conductive materials, as well as hard materials. Abrasive water jets can cut a wide range of thickness. Typical thickness are 100 mm for stainless steel, 120 mm for aluminium, 140 mm for stone, 100 mm for glass, but not limited. AWJ makes it possible to cut random contours, very fine tabs and filigree structures. Abrasive water jet cutting is capable of produce parts which do not require further processing with tolerances of ± 0.1 mm. Toxic fumes, recast layers, slag and thermal stress are totally eliminated.

Abrasive water jet cutting belongs among complicated dynamical and stochastic processes with incomplete information about mechanism and side effects character. In AWJ cutting, the final cut surface roughness and the dimensional accuracy depend on the process parameters including the water pressure, the abrasive mesh number, the abrasive mass flow rate, the feed rate, and the orifice and abrasive nozzle diameters [1], [2].

2. ABRASIVE WATER JET CUTTING

Abrasive water jet is the cutting tool. The cutting process is most similar to the grinding. The difference is that the abrasive particles are moved through the material by water rather than by a solid wheel. Abrasive water jet cutting process can be divided into subsequent steps:

- Transformation of the potential energy of water under high pressure into kinetic energy of a water jet.
- Transfer of a part of the kinetic energy of the high-speed water jet to abrasive particles by accelerating them and focusing the resulting abrasive water jet.
- Use of the kinetic energy of the abrasive particles to remove small chips of the work material.

In the process of abrasive water jet cutting the high pressure pump produces the required pressure up to 400 MPa. A high pressure supply line directs the pressurized water from the pump to the cutting head (Figure 1).
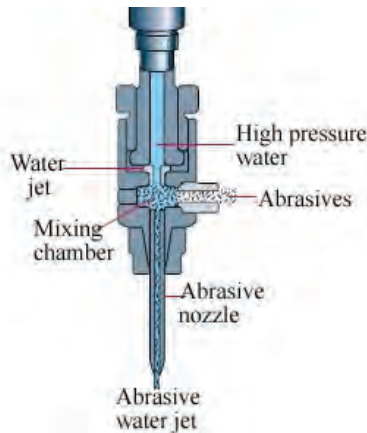
Fig. 1 Abrasive water jet cutting head

When the pressurized water comes out from the orifice, a water jet is created. The result is a very thin, extremely high velocity (approx. 900 m/s) water jet. Then, solid abrasive particles are added and mixed with the water jet. Resulting abrasive water jet is focused to the material through abrasive nozzle.

Bernoulli's equation is the law of conservation of energy applied to an ideal fluid as follows:

$$p + \frac{\rho_w v_w}{2} + \rho_w g h = const \qquad (1)$$

where: p - water pressure

v_w - velocity of water

ρ_w - density of water

g - acceleration due to gravity and

h - height of the observed points above the reference plane

By observing the leakage of high pressure water jets in the air and using equation (1), one can determine the leakage velocity of water jet from a nozzle based on water pressure.
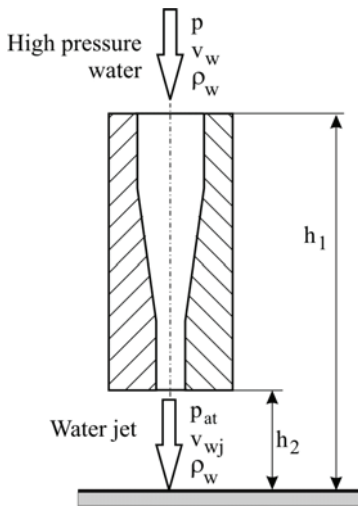
$$p + \frac{\rho_w v_w^2}{2} + \rho_w g h_1 = p_{at} + \frac{\rho_w v_{wj}^2}{2} + \rho_w g h_2 \text{ or}$$

$$p - p_{at} = \frac{1}{2}\rho_w \left(v_{wj}^2 - v_w^2\right) + \rho_w g\left(h_2 - h_1\right)$$

for $p_{at} \ll p$; $v_{wj} \gg v_w$; $h_1 \approx h_2$

$$p = \frac{1}{2}\rho_w v_{wj}^2$$

Fig. 2. Bernoulli's equation applied to the leakage of water jets in the air

If we ignore the difference in altitude (several millimeters) and assuming that the speed of the water on nozzle entrance is negligible compared to the speed of the jet at the nozzle exit (several hundred times), and the atmospheric pressure (1 bar) is much smaller than the water pressure at the entrance to the nozzle (4000 bar), we get the equation for calculating the velocity of the water jet after exiting the water nozzle:

$$v_{wj} = \sqrt{\frac{2p}{\rho_w}} \qquad (2)$$

A schematic diagram of a high-seed water jet in air is shown in Figure 3. The jet consists of three regions, namely, the initial region, the main region, and the final region.
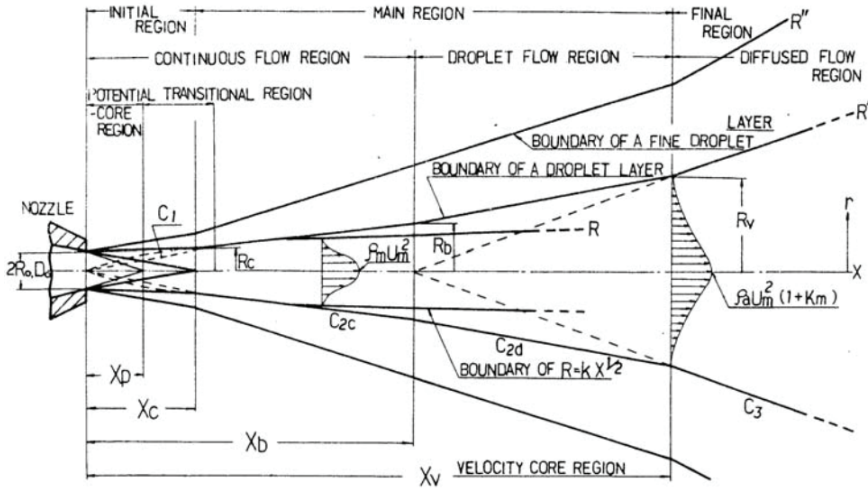
Fig. 3 Structure of a water jet in air [3]

Leakage velocity of water jet from a nozzle is crucial because its role is to accelerate the abrasive particles. Due to the extra weight, abrasive particles, however, cannot achieve velocity of water jet but only a part of that velocity.

The volume flow rate of water may be expressed as:

$$q_w = A_{orifice} v_{wj} \qquad (3)$$

$$for \quad v_{wj} = \sqrt{\frac{2p}{\rho_w}} \quad and \quad A_{orifice} = \frac{\pi}{4} d_0^2$$

where d_0 is water orifice diameter,

$$q_w = \frac{\pi}{4} d_0^2 \sqrt{\frac{2p}{\rho_w}} \qquad (4)$$

Total power of the water jet can be given as:

$$P_{wj} = p \, q_w \qquad (5)$$

$$P_{wj} = p \frac{\pi}{4} d_0^2 \sqrt{\frac{2p}{\rho_w}}$$

$$P_{wj} = \frac{\pi}{4} d_0^2 \sqrt{\frac{2p^3}{\rho_w}} \qquad (6)$$

As the high velocity water jet streams through orifice into the mixing chamber, low pressure (vacuum) is created within the mixing chamber. Metered abrasive particles are

introduced into the mixing chamber through a port (Figure 4). During mixing process, the abrasive particles are gradually accelerated due to transfer of momentum from the water phase to abrasive phase and when the jet finally leaves the abrasive nozzle, phases, water and abrasive, are assumed to be at same velocity.
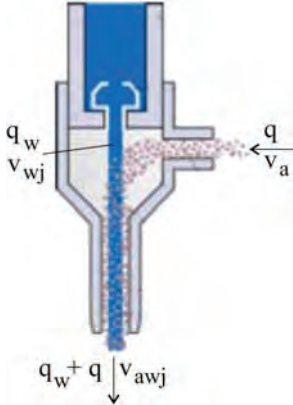
where:

q - abrasive particle flow rate

v_a - initial velocity of abrasive paritcles

Fig. 4 Mixing process

The law of conservation of momentum says that the total momentum of any closed system, i.e., the vector sum of the momentum vectors of all the things in the system, is a constant. The momentum of air before and after mixing will be neglected due to very low density. Further, it is assumed that after mixing both water and abrasive phases attain the same velocity of abrasive water jet. Moreover, when the abrasive particles are fed into the water jet through the port of the mixing chamber, their velocity is also very low and their momentum can be neglected.

$$q_w \, v_{wj} + q \, v_a = \left(q_w + q \right) v_{awj} \tag{7}$$

$$v_{awj} = \frac{q_v}{q_w + q} v_{wj}$$

$$v_{awj} = \frac{v_{wj}}{1 + \dfrac{q}{q_w}} \tag{8}$$

As during mixing process momentum loss occurs as the abrasives collide with the water jet and at the inner wall of the abrasive nozzle multiple times before being entrained, velocity of abrasive water jet is given as,

$$v_{awj} = \eta \frac{v_{wj}}{1 + \dfrac{q}{q_w}} \tag{9}$$

where η- momentum loss factor, whose values lies arond 0.65-0.85 [4].

The abrasive flow rate determines the number of impacting abrasive particles as well as their kinetic energies. The energy of the abrasives can then be expressed as:

$$E_{awj} = \frac{1}{2} q \, v_{awj} = \frac{1}{2} q \, \eta^2 \frac{v_{wj}^2}{\left(1 + \dfrac{q}{q_{wj}}\right)^2} \tag{10}$$

Combination of equations (2) and (10) gives abrasive particles kinetic energy (power) needed to overcome the fracture energy of the material in order to damage (cut) workpiece material.

$$E_{awj} = \frac{1}{2} q \, \eta^2 \frac{2p}{\rho_v} \frac{q_{wj}^2}{\left(q_{wj} + q\right)^2} \tag{11}$$

3. MATERIAL REMOVAL MECHANISM OF ABRASIVE WATER JET MACHINING

High-velocity-water jets used in water jet processes can be categorized according to the fluid medium as either pure water jets or abrasive water jets.

The most common water jets used in water jetting processes are continuous pure water jets in air issued from a nozzle having a circular cross section. This type of water jet is widely used in water jetting industries for cleaning, surface preparation, and cutting of soft materials.

The material removal capability of abrasive water jets, in which abrasive particles are added to the water stream, is much larger than the material removal capability of the pure water jets. In an abrasive water jet, the stream of the water jet accelerates abrasive particles, which erode the worpiece material.

3.1. Micro-mechanism of material removal in abrasive water jet cutting

Impact of solid particles is the main mechanism in the process of removing material by abrasive water jet [5]. Meng and Ludema [6] have defined a sub-mechanism for separating solid particles from the surface of the workpiece material, such as cutting and brittle fracture. These mechanisms do not operate separately but simultaneously. Presence of individual mechanisms of separation depends on many factors, such as stroke angle, the kinetic energy of abrasive grains, abrasive particle shape, material properties of the workpiece and ambient conditions.

Considering the mechanical properties and behavior on impact, the material of the workpiece can be classified into two groups. Some belong to the group of ductile materials, which are characterized by deformation properties, while others are brittle.

For ductile (deformable) material, the process of separating the material is divided into two mechanisms: micro-cutting and separating by material plastic deformation (Figure 5) [7].
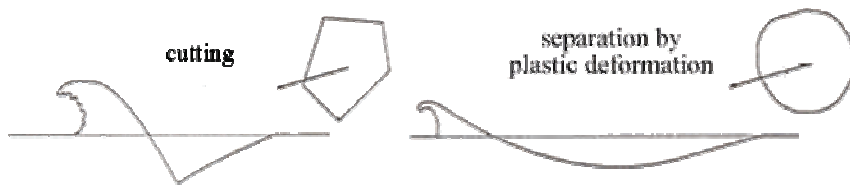
Fig. 5. The process of separating the ductile material

When observing the cutting process of brittle materials, a series of researches led to the identification of the mechanism of separation of materials, consisting of the phenomenon of brittle fracture (Figure 6) and plastic deformation. At low angles of attack are visible scratches, but it occurs to some extent and intercrystalline fracture [8], [9]. In contrast, intercrystalline fracture is the predominant method of removing material at the corner of the administrative impact. Traces of plastic deformation are present, but to a much lesser extent than at low angles of attack.
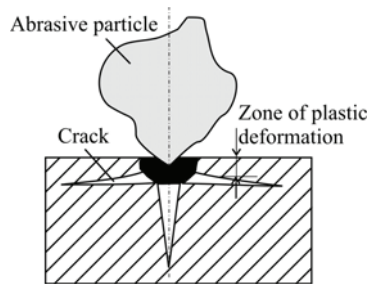
Fig. 6. Impact of abrasive particle in the surface of brittle materials

3.2. Macro-mechanism of material removal in abrasive water jet cutting

Hashish [10] proposed a general model, in which a stable cutting process takes place to a certain depth of penetration of abrasive water jet, followed by the formation of steps on the surface of the cut. Below the critical depth, the processing is unstable resulting in the creation of striated or wavy surface of the cut.

With increasing depth and creating steps, the removal mechanism is changing from cutting to the separating material by plastic deformation. The above-described mechanism, cyclic repeating, resulting in different types of material damage, which is the subject of study of damage mechanic.

The biggest problem with abrasive water jet machining, was reflected in disparity of the machined surface quality. This disparity is manifested by different parameters of cut quality as follow: surface roughness, machined surfaces deviation from the vertical plane-taper of the cut and the appearance of curved lines on machined surface-striate formation [11], as shown in Figure 7. All these phenomena significantly affect the restrictions of using abrasive water jet machining.

Fig. 7. Cut surface generated in abrasive water jet cutting of aluminium alloy

The cut surfaces produced by abrasive water jet cutting typically exhibit a smooth upper zone followed by a lower striated zone. These phenomena can be related to the jet loss of energy during the cutting process, e.g. deformation of the sharp edges of the abrasive particles as illustrated in Figure 8 [12].
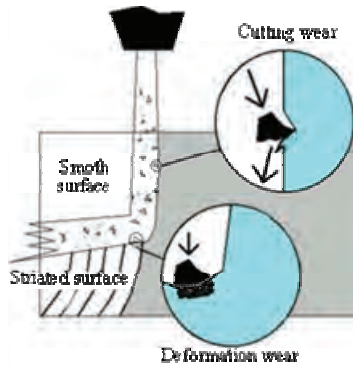
Fig. 8. Formation of different regions in abrasive water jet cutting

4. EXPERIMENTAL WORK

4.1. Cut quality

In the abrasive water jet cutting "cut quality" is a term that describes the combination of characteristics such as geometry of cut (kerf width - w, kerf taper - α) and cut surface quality (cut surface roughness - Ra). Standards for describing the cut quality, resulting in abrasive water jet cutting, are not yet established [13]. Parameters that define the cut quality (geometric characteristics of cut quality and cut surface quality) in abrasive water jet cutting are shown in Figure 9.
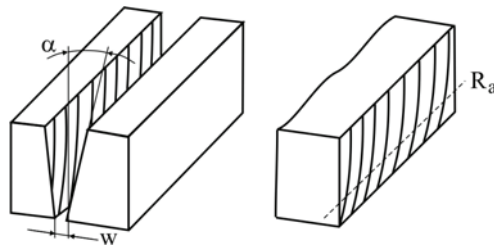
Fig. 9. Characteristics of cut quality in AWJ

The surface roughness is used to describe the cutting surface and gives an indication of whether the subsequent machining required. It is defined using the value of roughness average Ra. Cut surface can never be ideally smooth. It consists of small, finely spaced surface irregularities (micro irregularities - roughness) formed in the course of treatment. Additionally, there are surface irregularities of grater spacing (macro irregularities - waviness), which may be periodically repeatable.

4.2. Experimental set-up

A series of water jet cutting experiments were conducted using a Byjet 4022 abrasive water jet cutting machine (Bystronic AG, Switzerland). As workpiece material, aluminium alloy AA-ASTM 6060 (EN: AW-6060; ISO: Al MgSi) was used. Alloy 6060 is one of the most popular of the 6XXX series alloys. Typical uses include architectural sections, sections fit for forming processes and automotive parts. The aluminium alloy was chosen as a worpiece material because the material is very attractive, possess resistance to corrosion and can provide significant value for the end user. Also, aluminum and its alloys are characterized by high reflectivity and thermal conductivity. This makes them relatively difficult to cut with lasers. Abrasive water jet cutting, which does not create an observable heat affected zone, is much more useful for cutting aluminum for modern applications.

Although AWJ cutting involves a large number of variables and virtually all these variables affect the cutting results (kerf width, taper and surface roughness), only few major and easy-to-adjust dynamic variables were considered in the present study. Thouse are: feed rate (the speed at which the cutting head moves along workpiece during cutting operation), material thickness and abrasive flow rate. The other process parameters were kept constant using the standard machine configuration ($d_0 = 0.3$ mm; $d_A = 1.02$ mm; $p = 400$ MPa).

4.3. Results and discussion

In the present study, surface roughness as assessed by the centre-line average roughness Ra (according to standard ISO 4287:1997) was used in evaluating the cut quality. Surface roughness was measured at upper and lower region of the cut surface, and at the middle of the cut. These measurements were taken for each cut away from the ends of the slots to eliminate any effect of the cutting process at the jet entry and exit. The surface roughness was measured perpendicularly to the jet penetration axis, and parallel to the cutting head feed direction.

The cut surface has better quality at upper region (entrance area) of the jet. From the middle of the thickness downwards, the surface quality deterioration is observed. As the penetration depth of abrasive water jet increases, the jet loses its energy due to the jet–material interaction, mutual particle impacts, etc. This situation results in rougher surface characteristics at the lower region of the cut surface. Figure 10 shows dependence of roughness average (Ra) at upper, middle and lower region of the cut surface of different feed rate values for material thickness of 10 mm.
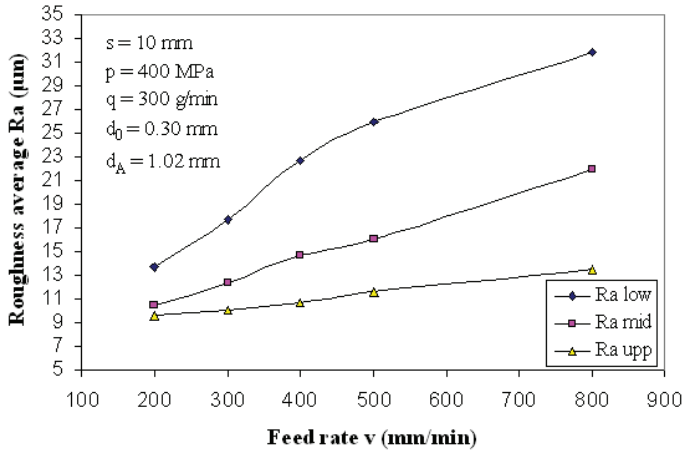
Fig. 10. Roughness average Ra in dependence of feed rate when material thickness is 10 mm at upper, middle and lower zone of the cut

The results of determining surface roughness at lower region of the cut surface with respect to the material thickness, feed rate and abrasive flow rate are graphically represented on Figure 11.
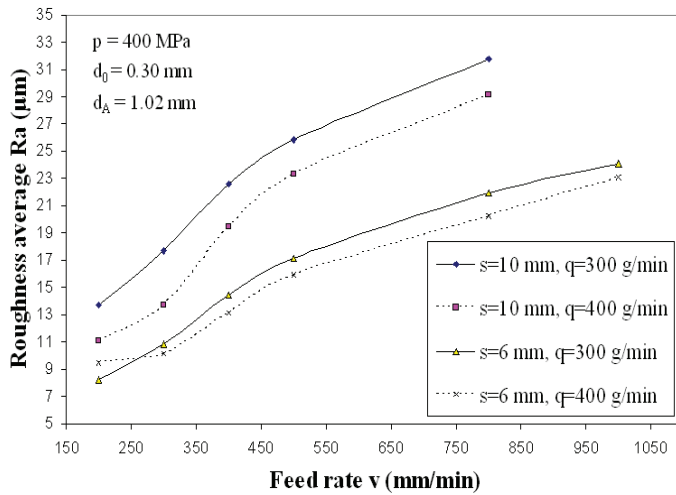
Fig. 11. Roughness average Ra in dependence of material thickness, feed rate and abrasive flow rate

It can be noticed that the surface roughness significantly increases as the feed rate increase. This may be anticipated as increasing the feed rate allows less overlap machining action and fewer abrasive particles to impinge the surface, deteriorating surface quality [14].

The influence of abrasive flow rate is found to be less significant on surface roughness. The increase in the number of impacting particles contributes to the improved surface finish. A high number of abrasive particles involved in mixing increases the probability of particle collision that decreases the average diameter of the impacting particles, so the roughness decreases with an increase of the abrasive flow rate. These results are in accordance with the literature [15].

The quantitative description of the process parameters effect on cut surface roughness was performed. Full factorial design for input factors (material thickness, feed rate and abrasive flow rate) at two levels, and output factor (roughness average Ra) with four centre point replications was adopted. Among the many process parameters that influence the cutting quality, three are selected and considered as factors in the experimental phase (Tab. 1).

Tab. 1. Process parameters and their levels

Factors	Factor level		
	-1	0	+1
Material thickness s (mm)	6	8	10
Feed rate v (mm/min)	200	400	800
Abrasive flow rate q (g/min)	300	350	400

To identify the process parameters that are statistically significant in the process, the analysis of variance is performed. The significance of independent variables is interpreted in the Pareto chart. Pareto chart (Fig. 12) shows that feed rate, material thickness and abrasive flow rate have fond to bee the most sufficient factors that affects the cut surface roughness at abrasive water jet cutting in the experiment.
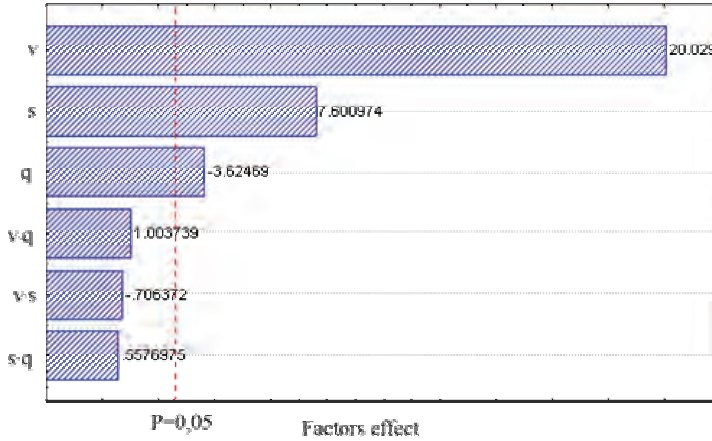
Figure 12. Pareto chart of level of significance for independent factors and their
interactions at a 95% confidence interval

For the purposes of regression analysis were selected dimensions chosen factors (variables) as: s (mm), v (mm/min), q (g/min). To get the solution that best fits the experimental results, for the mathematical model of roughness average a power function is chosen (Eq.12):

$$R_a = C s^{p_1} v^{p_2} q^{p_3} \tag{12}$$

where Ra is an output variable, s, v and q are input (independent) variables, and C, p1, p2 and p3 are regression coefficients.

A logarithmic transformation of the (Eq. 12) in form of power function into a linear function

$$\ln R_a = \ln C + p_1 \ln s + p_2 \ln v + p_3 \ln q \tag{13}$$

allows us to perform linear regression technique.

The STATISTICA software package is used to determine regression equation coefficients, which give the level of roughness average Ra as a function of independent variables. The fit of the model is expressed by the coefficient of determination $R^2 = 0.9862$.

Within the regression analysis, the empirical model for roughness average could be expressed as:

$$R_a = 0.2913 \frac{s^{0.694} v^{0.642}}{q^{0.212}} \tag{14}$$

for the chosen dimensions: Ra (μm) - roughness average, v (mm/min) – feed rate, s (mm) – material thickness, q (g/min) – abrasive flow rate

The regression analysis is applied in order to develop the response surfaces. Roughness average as a function of feed rate, and material thickness, for constant value of abrasive flow rate of 300 g/min is given in Fig. 13. These three-dimensional surface plot show predicted cut surface roughness as a function of independent variable - factors.
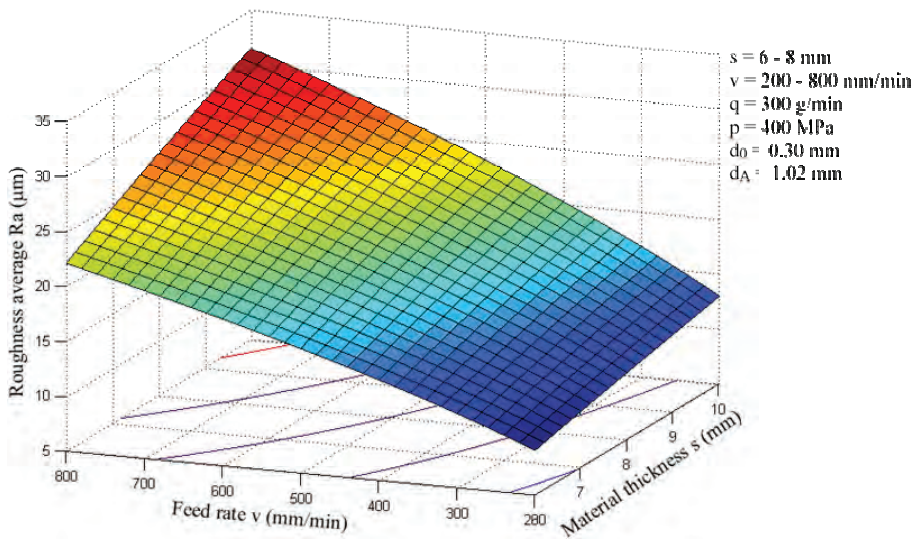
Fig, 13. Predicted average roughness as a function of feed rate v (mm/min) and material thickness s (mm) under given conditions

Proposed mathematical model allows us to choose a quantitative level of quality, which has not been the case in the theoretical and practical solution to this problem.

5. CONCLUSION

The flexibility and cool cutting characteristics of the abrasive water jet technique make it an important tool for cutting applications of new materials such as composites and sandwiched materials that are difficult to machine with traditional machining processes.

In abrasive water jet cutting the final cut surface roughness and the dimensional accuracy depend on the many process parameters. Summarizing the main features of the experimental results, the following conclusions may be drawn:

    - As the feed rate increases, the AWJ cuts narrower kerf. This is because the feed rate of abrasive water jet allows fewer abrasives to strike on the jet target and hence generates a narrower slot.

- Higher abrasive flow rate produce greater kerf width, especially lower kerf width because the larger number of abrasive particles share in machining process which has positive effect on kerf geometry.

- The surface has better characteristics in the region that starts from the upper point where abrasive water jet begins to cut to the middle of the thickness. From the middle of the thickness downwards, the surface quality deterioration is observed.

- With an increase in the abrasive flow rate, the roughness is reduced. For high abrasive mass flow rates, the roughness is less sensitive to changes in the feed rate.

Experimental study shows that, among others, the most important factors influencing the cut surface roughness of aluminium alloy are nozzle feed rate and abrasive mass flow rate.

REFERENCES

55.   Hloch S. and Fabian S., (2006), Qualitative analysis of AWJ factors affecting the surface roughness, *Wissenschaftliche Beitraege*, TFH Wildau, Germany, 113-119.

56. Lebar A. and Junkar M., (2004), Simulation of abrasive water jet cutting process, *Modeling Simul. Mater. Sci. Eng.* 12, 1159-1170.

57. Yanaida K. and Ohashi A., (1980), Flow Characteristics of Water Jets in Air, *Proceedings of 5th International Symposium on Jet Cutting Technology*, Paper A3, Hanover, 33-44.

58. Zhang S. and Nambiath P., (2005), Accurate hole drilling using an abrasive water jet in titanium, *American Watejet conference*, Houston.

59. Guo Z., Ramulu M. Jenkins M.G., (2000), Analysis of the waterjet contact/impact on target material, *Optics and Laser in Engineering*, No. 33, 121-139.

60. Meng H.C. and Ludema K.C., (1995), Wear models and prediction equations, Wear, No. 181-183, 443-457.

61. Hutchings I.M., (1979), Mechanical and etallurgical aspects of the erosion of metals*, Proc. Corrosion/Erosion of Coal Convers*, Houston, pp. 393-428.

62. Lemma E., Deam R., Chen L., (2005), Maximum depth of cut and mechanics of erosion in AWJ oscillation cutting of ductile materials, *Journal of Materials Procesing Technology*, No. 160, 188-197.

63. Zeng J. and Kim T.J., (1992), Development of an abrasive waterjet kerf cutting model for brittle materials, Jet Cutting Technology, Kluwer Academic Press, Dordrecht, 483-501.

64. Hashish M., (1987), Wear in abrasive-waterjet cutting systems, *Wear of Materials*, Vol. 2, New York, 769-776.

65. Chen F.L., Wang J., Lemma E., Siores E., (2003), Striation formation mechanisms on the jet cutting surface, *Journal of Material Processing Technology*, No. 141, 213-218.

66. Akkurt A., (2009), Cut fornt geometry characterizion in cutting applications of brass wiht abrasive water jet, *Jorunal of Materials Engineering and Performance*, Volume 19, Issue 4, 599-606.

67. Janković P. and Radovanović M., (2008), Characteristics of Part Accuracy and Errors by Abrasive Water Jet cutting, *8th International Conference "Research and Development in Mechanical Industry"* RaDMI 2008, Užice, Serbia, 215-222.
68. Jankovic P.: Modeling of abrasive water jet cutting process and forming of technological processor, Doctoral dissertation, University of Nis (in Serbian), 2009.
69. Momber A., Kovacevic R., Schüneman R, , et al, (1996), The influence of abrasive grain size distribution parameters on the abrasive water jet machining process, In:Rajukar K P (Eds) *Proc. 25 th North American Manuf. Engrs*, Dearborn, 21-26.

UTICAJ PARAMETARA PROCESA SEČENJA ABRAZIVNIM VODENIM MLAZOM NA MEHANIZAM ODNOŠENJA MATERIJALA I KVALIET REZA

P. Janković, T. Igić, D. Nikodijević

Proces sečenja materijala abrazivnim vodenim mlazom, podržan teorijom mehanike fluida, abrazivnog habanja i mehanikom oštećenja, je visoko tehnološki postupak koji nudi jedinstvene mogućnosti u poređenju sa konvencionalnim postupcima obrade. U radu se, poret teorijskih izvođenja, daje originalni doprinos u obliku matematičkog modela veličine oštećenja površine reza, izražene vrednošću hrapavosti.

Cilj istraživanja, prikazanih u radu, povezan je sa zahtevima industrije, odnosno krajnjeg korisnika. Imajući u vidu da konvencionalni postupci obrade ne samo da su u zaostatku u što se tiče kvaliteta reza, već i da izvesne zahteve nisu mogli da ispune, sa pojavom kompozitnih materijala nisu uopšte bili u stanju da ih obrađuju, jer su se javljala nedozvoljena oštećenja, kao što su reslojavanje, izvlačenje vlakana, sagorevanje krajeva).

Ključne reči: *Sečenje abrazivim vodenim mlazom, mehanika oštećenja, eksperimentalno ispitivanje uzoraka od aluminijuma, matematičko modeliranje*

ADVANCES IN CLASSICAL AND ANALYTICAL MECHANICS: A REVIEWS OF AUTHOR'S RESULTS

UDC 531; 534.2; 541.01; 531.53; 517.93; 531.3;

Katica R. (Stevanović) Hedrih

*Mathematical Institute SANU Belgrade, Department for Mechanics
and Faculty of Mechanical Engineering, University of Niš.
Priv. address: 18000-Niš, ul. Vojvode Tankosića 3/22, Serbia.
e-mail: khedrih@eunet.rs*

Abstract. *A review, in subjective choice, of author's scientific results in area of: classical mechanics, analytical mechanics of discrete hereditary systems, analytical mechanics of discrete fractional order system vibrations, elastodynamics, nonlinear dynamics and hybrid system dynamics is presented. Main original author's results were presented through the mathematical methods of mechanics with examples of applications for solving problems of mechanical real system dynamics abstracted to the theoretical models of mechanical discrete or continuum systems, as well as hybrid systems. Paper, also, presents serries of methods and scientific results authored by professors Mitropolyski, Andjelić and Rašković, as well as author's of this paper original scientific research results obtained by methods of her professors. Vector method based on mass inertia moment vectors and corresponding deviational vector components for pole and oriented axis, defined in 1991 by K. Hedrih, is presented. Results in construction of analytical dynamics of hereditary discrete system obtained in collaboration with O. A. Gorosho are presented. Also, some selections of results author's postgraduate students and doctorantes in area of nonlinear dynamics are presented. A list of scientific projects headed by author of this paper is presented with a list of doctoral dissertation and magister of sciences thesis which contain scientific research results obtained under the supervision by author of this paper or their fist doctoral candidates.*

Keywords: *Review, vector method, mass moment vectors, deviational mass moment vector, rotator, coupled rotations, no intersecting axes, basic vectors of position vector tangent space, angular velocity of the tangent space basic vectors, rheonomic constraint, rheonomic coordinate, mobility, angular velocity of basic vector rotation, velocity of basic vector extension, asymptotic approximation of solution, Krilov-Bogolyubov-Mitropolyski asymptotic averaged method, method of variation of constants, hereditary system, rheological and relaxational kernels, standard hereditary element, integro-differential equation, fractional order derivative,*

covariant coordinate, contravariant coordinate, Physical coordinate, discrete continuum method, space fractional order structure, chains, eigen main plane nets, eigen main chains, fractional order oscillator, fractional order properties characteristic number, transfer of signals, multi-frequency, material particles, rigid body, gyrorotor, deformable body, multi bdy system, transversal, longitudinal, multi-plate system, multi-belt system, stochastic stability.

1. INTRODUCTION

Main author's research results, presented in this paper, are:

* Advances in classical mechanics.

Mass moment vectors connected to pole and axis, allowed the author to give a new perspective onto rotation of bodies around stationary axis and a stationary point, and on dynamics of rotors and coupled rotors in general. By introducing definitions of mass moment vectors connected to pole and axis, and by proving their properties, and also by introducing purely kinematical rotator vectors, which he used to represent short and elegant expressions for kinetic pressures and kinetic impacts on the rotor shaft bearings, the author made a contribution to classical mechanics, as well as a contribution to the methodology of university teaching of rotor kinematics. In a monographic paper published in 1998, and a monograph published in Serbia in 2001, as well as in a series of published papers in the period 1992-2010, beginning with a paper at ICTAM in Israel (1992), and later in a series of papers published in Japan, Germany, China, Ukraine, Russia and Greece, the author shows definitions and properties, as well as applications of mass moment vectors connected to pole and axis for analyzing mass moment states and properties of kinetic parameters of rotor dynamics, dynamics of rigid body coupled rotation around no intersecting axes and dynamics of coupled rotors. (see References I [1-20]).

Angular velocity of the basic vectors rotation of a tangent space of the vector positions of material particles of mechanical system dynamics with geometrical, stationary and rheonomic constraints are obtained. Extensions of dimensions of tangent space of the vector positions of material particles of mechanical system dynamics from three dimensional real spaces to configuration space of independent generalized curvilinear coordinate systems is identified. Reductions of numbers of coordinates and extensions of tangent space of vector passions are analyzed (see References II [21-34]).

* Advances in Analytical Mechanics.
- Analytical Mechanics of Discrete Hereditary Systems.

Foundation and construction of analytical mechanics of discrete hereditary systems was the work of two authors – Oleg Aleksandrovich Goroshko and Katica R. (Stevanović) Hedrih. Their original contribution to modern analytical mechanics, the authors published in their monograph of the same name, which came into existence in the period of their cooperation between 1996-1999, and was published in 2001. The contents of this monograph represents the first, in the world published integral theory of analytical mechanics of discrete hereditary systems. Through a short review of the contents of the monograph published in Serbia, as well as a series of presented results and/or published

papers in the period 1995-2009 in Serbia, Ukraine, Russia, China and US, we shall point out the main contributions of these two authors in this area. (see References III [35-54])

- Analytical mechanics of discrete fractional order systems

Through a series of papers published or presented in the period 2005-2009 in France, Portugal, Turkey, Germany, Ukraine, China and Romania, as well as in monograph publications and international journals, the author contributed to the development of analytical mechanics of discrete systems, of fractional order with special focus of the results on oscillatory systems of fractional order. Prominent among these contributions are the results relating to homogenous chain systems of fractional order and homogenous couples chain systems of fractional order. The author introduced new terms, such as eigen main chains, main coordinates of eigen chain systems of homogenous coupled chains into hybrid systems of fractional order, as well as main partial oscillators of fractional order with corresponding main coordinates and corresponding oscillatory modes of fractional order with creep properties. (see References III [35-54])

*Advances in Elastodynamics, Nonlinear Dynamics and Hybrid System Dynamics

Among the contents of a series of papers published in international journals (2003-2010) or journals of prestigious scientific institutes in the world (1970-2009), as well as in monographs published by Kluwer and Springer, contributions of author to linear and nonlinear dynamics of deformable bodies (rods, plates, moving strips), systems of coupled deformable bodies, especially stand out and can be classifies as a single scientific area of Elastodynamics and the newly established area of hybrid system dynamics. A number of results are on the energy analysis of complex hybrid system dynamics. Five theorems on characteristic equations of complex systems, obtained by coupling deformable bodies and discrete systems with finite number of degrees of freedom, static or dynamic or combined couples have been defined and proven.

A number of original results are about nonlinear properties of systems with coupled rotation motions. A number of theorems on coupled singularities and homoclinic orbits in the form of number eight has also been defined and proven. (see References IV. [35-68], V [69-88])

2. ADVANCES IN CLASSICAL MECHANICS.

2.1* Vector method and applications

Vector method [4], based on mass moment vectors and vector rotators coupled for pole and oriented axes, is used for obtaining vector expressions for kinetic pressures on the shaft bearings of a rigid body dynamics with coupled rotations around no intersecting axes [16-19]. This method is very effective and suitable in applications. Mass inertia moment vectors and corresponding deviational vector components for pole and oriented axis are defined by K. Hedrih in 1991 [1]. A complete analysis of obtained vector expressions for derivatives of linear momentum and angular momentum give us a series of the kinematical vectors rotators around both directions determined by axes of the rigid body coupled rotations around no intersecting axes[16-19]. These kinematical vectors rotators are defined for a system with two degrees of freedom as well as for rheonomic system with two degrees of mobility and one degree of freedom and coupled

rotations around two coupled no intersecting axes as well as their angular velocities and intensity.

As an example of defined dynamics [16-19], we take into consideration a heavy gyrorotor-disk with one degree of freedom and coupled rotations when one component of rotation is programmed by constant angular velocity. For this system with nonlinear dynamics, series of graphical presentation of three parameter transformations in relations with changes of eccentricity and angle of inclination (skew position) of heavy rigid body in relation to self rotation axis are presented, as well as in relation with changing orthogonal distance between no intersecting axes of coupled rotations. Some graphical visualization of vector rotators properties are presented, too.

Using K. Hedrih's (See Refs. [1-9]) mass moment vectors and vector rotators, some characteristics members of the vector expressions of derivatives of linear momentum and angular momentum for the gyro rotor coupled rotations around two no intersecting axes obtain physical and dynamical visible properties of the complex system dynamics [16-18].

Between them there are vector terms that present deviational couple effect containing vector rotators which directions are same as kinetic pressure components on corresponding gyro rotor shaft bearings [10-15] and [18-20].

2.1.1. Mass moment vectors for the axis to the pole

The monograph [4], IUTAM extended abstract [1] and monograph paper [5] contain definitions of three mass moment vectors coupled to a axis passing through a certain point as a reference pole. Now, we start with necessary definitions of mass momentum vectors.

Definitions of selected mass moment vectors for the axis and the pole, which are used in this paper are:

1* Vector $\vec{\mathfrak{S}}_{\vec{n}}^{(O)}$ of the body mass linear moment for the axis, oriented by the unit vector $\vec{n}$, through the point – pole O, in the form:

$$\vec{\mathfrak{S}}_{\vec{n}}^{(O)} \overset{def}{=} \iiint_V [\vec{n}, \vec{\rho}] dm = [\vec{n}, \vec{\rho}_C] M \;, \qquad dm = \sigma dV \;; \tag{1}$$

where $\vec{\rho}$ is the position vector of the elementary body mass particle dm in point N, between pole O and mass particle position N.

2* Vector $\vec{\mathfrak{J}}_{\vec{n}}^{(O)}$ of the body mass inertia moment for the axis, oriented by the unit vector $\vec{n}$, through the point – pole O, in the form:

$$\vec{\mathfrak{J}}_{\vec{n}}^{(O)} \overset{def}{=} \iiint_V [\vec{\rho}, [\vec{n}, \vec{\rho}]] dm \tag{2}$$

For special cases, the details can be seen in [1-9]. In the previously cited references, the spherical and deviational parts of the mass inertia moment vector and the inertia tensor are analyzed. In monograph [4] knowledge about the change (rate) in time and, the derivatives of the mass moment vectors of the body mass linear moment, the body mass inertia moment for the pole and a corresponding axis for different properties of the body, is shown, on the basis of results from the first author's References [6-9].

The relation

$$\vec{\mathfrak{I}}_{\vec{n}}^{(O)} = \vec{\mathfrak{I}}_{\vec{n}}^{(O_1)} + \left[\vec{\rho}_O, \vec{\mathfrak{E}}_{\vec{n}}^{(O_1)}\right] + \left[\vec{\mathrm{M}}_C^{(O_1)}, \left[\vec{n}, \vec{\rho}_O\right]\right] + \left[\vec{\rho}_O, \left[\vec{n}, \vec{\rho}_O\right]\right]\mathrm{M} \qquad (3)$$

is ***the vector form of the theorem*** *for the relation of material body mass inertia moment vectors,* $\vec{\mathfrak{I}}_{\vec{n}}^{(O)}$ *and* $\vec{\mathfrak{I}}_{\vec{n}}^{(O_1)}$, *for two parallel axes through two corresponding points, pole* O *and pole* O_1 *(for details detail Refs. [   ] by K. Hedrih).* We can see that all the members in the last expression-relation (3) have the similar structure. These structures are: $\left[\vec{\rho}_o, \left[\vec{n}, \vec{r}_c\right]\right]\mathrm{M}$, $\left[\vec{r}_C, \left[\vec{n}, \vec{\rho}_o\right]\right]\mathrm{M}$ and $\left[\vec{\rho}_o, \left[\vec{n}, \vec{\rho}_o\right]\right]\mathrm{M}$.

In the case when the pole O_1 is the centre C of the body mass, the vector $\vec{r}_C$ (the position vector of the mass centre with respect to the pole O_1) is equal to zero, whereas the vector $\vec{\rho}_O$ turns into $\vec{\rho}_C$ so that the last expression (3) can be written in the following form:

$$\vec{\mathfrak{I}}_{\vec{n}}^{(O)} = \vec{\mathfrak{I}}_{\vec{n}}^{(C)} + \left[\vec{\rho}_C, \left[\vec{n}, \vec{\rho}_C\right]\right]\mathrm{M} \qquad (4)$$

This expression (4) *represents the vector form of the theorem of the rate change of the mass inertia moment vector for the axis and the pole, when the axis is translated from the pole at the mass centre* C *to the arbitrary point, pole* O .

The *Huygens-Steiner theorems* (see Refs. [4] and [5]) for the body mass axial inertia moments, as well as for the mass deviational moments, emerged *from this theorem* (4) on the change of the vector $\vec{\mathfrak{I}}_{\vec{n}}^{(O)}$ of the body mass inertia moment at point O for the axis oriented by the unit vector $\vec{n}$ passing trough the mass center C , and when the axis is moved by translate to the other point O .

Mass inertia moment vector $\vec{\mathfrak{I}}_{\vec{n}}^{(O)}$ for the axis to the pole is possible to decompose in two parts: first $\vec{n}\left(\vec{n}, \vec{\mathfrak{I}}_{\vec{n}}^{(O)}\right)$ collinear with axis and second $\vec{\mathfrak{D}}_{\vec{n}}^{(O)}$ normal to the axis. So we can write:

$$\vec{\mathfrak{I}}_{\vec{n}}^{(O)} = \vec{n}\left(\vec{n}, \vec{\mathfrak{I}}_{\vec{n}}^{(O)}\right) + \vec{\mathfrak{D}}_{\vec{n}}^{(O)} = J_{\vec{n}}^{(O)}\vec{n} + \vec{\mathfrak{D}}_{\vec{n}}^{(O)} \qquad (5)$$

Collinear component $\vec{n}\left(\vec{n}, \vec{\mathfrak{I}}_{\vec{n}}^{(O)}\right)$ to the axis corresponds to the axial mass inertia moment $J_{\vec{n}}^{(O)}$ of the body. Second component, $\vec{\mathfrak{D}}_{\vec{n}}^{(O)}$, orthogonal to the axis, we denote by the $\vec{\mathfrak{D}}_O^{(\vec{n})}$, and it is possible to obtain by both side double vector products by unit vector $\vec{n}$ with mass moment vector $\vec{\mathfrak{I}}_{\vec{n}}^{(O)}$ in the following form:

$$\vec{\mathfrak{D}}_{\vec{n}}^{(O)} = \left[\vec{n}, \left[\vec{\mathfrak{I}}_{\vec{n}}^{(O)}, n\right]\right] = \vec{\mathfrak{I}}_{\vec{n}}^{(O)}\left(\vec{n}, \vec{n}\right) - \vec{n}\left(\vec{n}, \vec{\mathfrak{I}}_{\vec{n}}^{(O)}\right) = \vec{\mathfrak{I}}_{\vec{n}}^{(O)} - J_O^{\vec{n}}\vec{n} \qquad (6)$$

In case when rigid body is balanced with respect to the axis the mass inertia moment vector $\vec{\mathfrak{I}}_{\vec{n}}^{(O)}$ is collinear to the axis and there is no deviational part. In this case axis of rotation is main axis of body inertia. When axis of rotation is not main axis then mass inertial moment vector for the axis contains deviation part $\vec{\mathfrak{D}}_{\vec{n}}^{(O)}$. That is case of rotation unbalanced rotor according to axis and bodies skew positioned to the axis of rotation.

2.1.2. Model of a rigid body coupled multi-rotation around multi-axes without intersections

Let us consider rigid body coupled multi-rotations around axes without intersections, first oriented by unit vector $\vec{n}_1$ with fixed position and second and next oriented by unit vectors $\vec{n}_j$, $j = 2,3,...,K$, which are rotating around fixed axis as well as around series of previous axes and with corresponding angular velocities $\vec{\omega}_j = \omega_j \vec{n}_j$, $j = 1,2,3,...,K$. See Figure 1. Axes of rotations are without intersections. Rigid body is positioned on the moving rotating axis oriented by unit vector $\vec{n}_K$. Rigid body rotates around rotating self rotation axis with angular velocity $\vec{\omega}_K = \omega_K \vec{n}_K$ and around series of the previous axes in order and in whole around fixed axis oriented by unit vector $\vec{n}_1$ with angular velocity $\vec{\omega}_1 = \omega_1 \vec{n}_1$. The shortest orthogonal distances between axes are defined by length $\overline{O_{(j)}\tilde{O}_{(j+1)}}$, $j = 1,2,3,...,K$ and each of these is perpendicular to both close axes that each is to the direction of component angular velocities $\vec{\omega}_j = \omega_j \vec{n}_j$ and $\vec{\omega}_{j+1} = \omega_{j+1} \vec{n}_{j+1}$. These vectors are $\vec{r}_{0(j)(j+1)} = \overrightarrow{O_{(j)1}O_{(j+1)}}$:

$$\vec{r}_{0(j)(j+1)} = \frac{r_{0(j)(j+1)}}{\sin\alpha_{(j)(j+1)}}\left[\vec{n}_{(j)},\vec{n}_{(j+1)}\right] = r_0\frac{\left[\vec{n}_{(j)},\vec{n}_{(j+1)}\right]}{\left|\left[\vec{n}_{(j)},\vec{n}_{(j+1)}\right]\right|} = r_{0(j)(j+1)}\vec{u}_{0(j)(j+1)} \tag{7}$$

and it can be seen on Fig.1.

In the considered rigid body coupled rotations around no intersecting numerous axes, an elementary mass around point N is denoted as dm, with position vector $\vec{\rho}$, and with origin in the point O_K on the movable self rotation axis, and with $\vec{r}$ vector positions of the same body elementary mass with origin in the point O_1, where point O_1 is fixed on the axis oriented by unit $\vec{n}_1$. Both points are on the ends of the corresponding shortest orthogonal distance between two in the neighborhood axes of body coupled multi-rotations. Position vector of elementary mass with origin in pole O_1 and its velocity are in the following forms:

$$\vec{r}_k = \sum_{k=1}^{K-1}\left(\vec{r}_{0(k),(k+1)} + \vec{r}_{0(k+1),(k+1)}\right) + \vec{\rho}, \quad \vec{v}_K = \sum_{k=1}^{K-1}\left[\sum_{j=1}^{k}\vec{\omega}_j, \vec{r}_{0(k),(k+1)} + \vec{r}_{0(k+1),(k+1)}\right] + \left[\sum_{j=1}^{K}\vec{\omega}_j, \vec{\rho}\right] \tag{8}$$

For the case of three coupled rotations around three axes without intersections position vector of elementary mass with origin in pole O_1 and its velocity are in the following forms (see Fig.1):

$$\vec{r} = \vec{r}_{012} + \vec{r}_{022} + \vec{r}_{023} + \vec{\rho} \quad \text{and} \quad \vec{v} = \left[\vec{\omega}_1, \vec{r}_{012} + \vec{r}_{022}\right] + \left[\vec{\omega}_1 + \vec{\omega}_2, \vec{r}_{023}\right] + \left[\vec{\omega}_1 + \vec{\omega}_2 + \vec{\omega}_3, \vec{\rho}\right]. \tag{9}$$
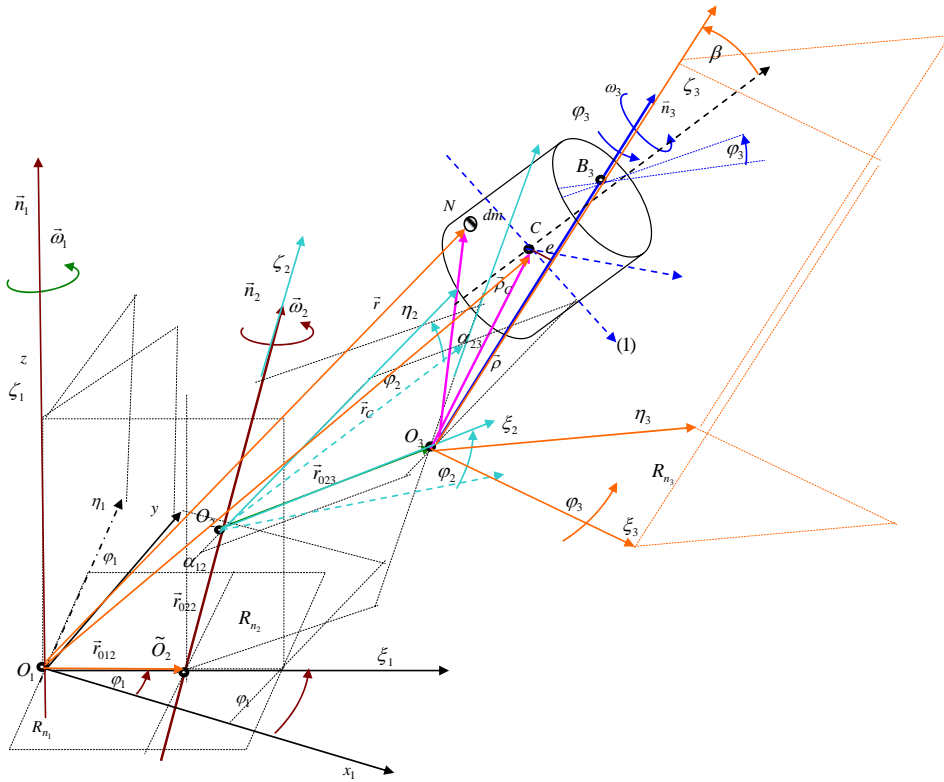
Figure 1. Arbitrary position of rigid body multi-coupled rotations around finite numbers of axes without intersections.

2.1.3. Linear momentum of a rigid body coupled multi-rotations around axes without intersections

By using basic definition of linear momentum and expression for velocity of elementary body mass (9), we can write linear momentum in the following vector form:

$$\vec{\mathfrak{K}} = \sum_{k=1}^{K-1}\sum_{j=1}^{k} \omega_j \left[\vec{n}_j, \vec{r}_{0(k),(k+1)} + \vec{r}_{0(k+1),(k+1)}\right] M + \sum_{j=1}^{K} \omega_j \vec{\tilde{\mathfrak{S}}}_{\vec{n}_j}^{(O_K)}. \tag{10}$$

where $\vec{\tilde{\mathfrak{S}}}_{\vec{n}_j}^{(O_K)} = \iiint\limits_{V} \left[\vec{n}_j, \vec{\rho}\right] dm$, $j = 1,2,3,...,K$, are corresponding body mass linear moments of

the rigid body for the axes oriented by direction of component angular velocities of coupled multi-rotations through the movable pole O_K on self rotating axis. First terms in the form of the first sum   in expression (10) presents translation part of linear momentum. This part is equal to zero in case when axes intersect in one point. Second sum in expression (10) for linear momentum present linear momentum of pure rotation,

as relative motion around all axes with intersection in the pole O_K on self rotation axis. These K terms are different from zero in all cases.

Example 1: Expression of linear momentum of a rigid body coupled rotations around two no intersecting axes, we can write in the following form:

$$\vec{\mathfrak{K}} = \vec{\mathfrak{K}}_{\vec{n}_1}^{(O_{1-2})} + \vec{\mathfrak{K}}_{\vec{n}_1}^{(O_2)} + \vec{\mathfrak{K}}_{\vec{n}_2}^{(O_2)} = [\vec{\omega}_1, \vec{r}_{012}]M + \omega_1\vec{\mathfrak{E}}_{\vec{n}_1}^{(O_2)} + \omega_2\vec{\mathfrak{E}}_{\vec{n}_2}^{(O_2)} \tag{11}$$

Example 2: Expression of linear momentum of a rigid body coupled rotations around three axes without intersections, we can write in the following form:

$$\vec{\mathfrak{K}} = \omega_1[\vec{n}_1, \vec{r}_{012} + \vec{r}_{022} + \vec{r}_{023}]M + \omega_2[\vec{n}_2, \vec{r}_{023}]M + \omega_1\vec{\mathfrak{E}}_{\vec{n}_1}^{(O_3)} + \omega_2\vec{\mathfrak{E}}_{\vec{n}_2}^{(O_3)} + \omega_3\vec{\mathfrak{E}}_{\vec{n}_3}^{(O_3)} \tag{12}$$

2.1.3. Angular momentum of a rigid body coupled multi-rotations around axes without intersections

By using basic definition of angular momentum and expression for velocity of rotation of elementary body mass and its position vector (9), we can write vector expression for angular momentum.

Example 1: Expression of angular momentum of a rigid body coupled rotations around two axes without intersection, we can write in the following form:

$$\vec{\mathfrak{L}}_{O_1} = \omega_1\vec{n}_1 r_0^2 M + \omega_1[\vec{\rho}_C, [\vec{n}_1, \vec{r}_0]]M + \omega_1[\vec{r}_0, \vec{\mathfrak{E}}_{\vec{n}_1}^{(O_2)}] + \omega_2[\vec{r}_0, \vec{\mathfrak{E}}_{\vec{n}_2}^{(O_2)}] + \omega_1\vec{\mathfrak{J}}_{\vec{n}_1}^{(O_2)} + \omega_2\vec{\mathfrak{J}}_{\vec{n}_2}^{(O_2)} \tag{13}$$

Example 2: Expresion of angular momentum of a rigid body coupled rotations around three axes without intersections, we can write in the following form:

$$\vec{\mathfrak{L}}_{O_1} = \omega_1[\vec{r}_{O_3}, \vec{\mathfrak{E}}_{\vec{n}_1}^{(O_{1-2-3})}] + \omega_1[\vec{r}_{O_3}, \vec{\mathfrak{E}}_{\vec{n}_1}^{(O_{2-3})}] + \omega_2[\vec{r}_{O_3}, \vec{\mathfrak{E}}_{\vec{n}_2}^{(O_{2-3})}] + \omega_1[\vec{\rho}_C, \vec{\mathfrak{E}}_{\vec{n}_1}^{(O_{1-2-3})}] + \omega_1\vec{\mathfrak{J}}_{\vec{n}_1}^{(O_3)} + \omega_2\vec{\mathfrak{J}}_{\vec{n}_2}^{(O_3)} + \omega_3\vec{\mathfrak{J}}_{\vec{n}_3}^{(O_3)} +$$
$$+ \omega_1[\vec{\rho}_C, \vec{\mathfrak{E}}_{\vec{n}_1}^{(O_{2-3})}] + \omega_2[\vec{\rho}_C, \vec{\mathfrak{E}}_{\vec{n}_2}^{(O_{2-3})}] + \omega_1[\vec{r}_{O_3}, \vec{\mathfrak{E}}_{\vec{n}_1}^{(O_3)}] + \omega_2[\vec{r}_{O_3}, \vec{\mathfrak{E}}_{\vec{n}_2}^{(O_3)}] + \omega_3[\vec{r}_{O_3}, \vec{\mathfrak{E}}_{\vec{n}_3}^{(O_3)}] \tag{14}$$

2.1.4. Derivative of linear momentum and angular momentum of rigid body coupled rotations around two axes without intersection

Example 1. By using expressions for linear momentum (13), the derivative of linear momentum of rigid body coupled rotations around two axes without intersection, we can write the following vector expression:

$$\frac{d\vec{\mathfrak{K}}}{dt} = \dot{\omega}_1[\vec{n}_1, \vec{r}_0]M + \omega_1^2[\vec{n}_1, [\vec{n}_1, \vec{r}_0]]M + \dot{\omega}_1\vec{\mathfrak{E}}_{\vec{n}_1}^{(O_2)} + \omega_1^2[\vec{n}_1, \vec{\mathfrak{E}}_{\vec{n}_1}^{(O_2)}] +$$
$$+ \dot{\omega}_2\vec{\mathfrak{E}}_{\vec{n}_2}^{(O_2)} + \omega_2^2[\vec{n}_2, \vec{\mathfrak{E}}_{\vec{n}_2}^{(O_2)}] + 2\omega_1\omega_2[\vec{n}_1, \vec{\mathfrak{E}}_{\vec{n}_2}^{(O_2)}] \tag{15}$$

After analysis structure of linear momentum derivative terms, we can see that there is possibility to introduce pure kinematic vectors, depending on component angular velocities and component angular accelerations of component coupled rotations, that are useful to express derivatives of linear moment in following form

$$\frac{d\vec{\mathfrak{K}}}{dt} = \vec{\mathfrak{R}}_{01}[\vec{n}_1, \vec{r}_0]M + \vec{\mathfrak{R}}_{011}|\vec{\mathfrak{E}}_{\vec{n}_1}^{(O_2)}| + \vec{\mathfrak{R}}_{022}|\vec{\mathfrak{E}}_{\vec{n}_2}^{(O_2)}| + 2\omega_1\omega_2[\vec{n}_1, \vec{\mathfrak{E}}_{\vec{n}_2}^{(O_2)}] \cdot \tag{16}$$

We can see that in previous vector expression (16), for derivative of linear momentum, are introduced the following three vector rotators:

$$\vec{\mathfrak{R}}_{01} = \dot{\omega}_1\vec{u}_{01} + \omega_1^2\vec{v}_{01} , \quad \vec{\mathfrak{R}}_{01} = \dot{\omega}_1\left[\vec{n}_1, \frac{\vec{r}_0}{r_0}\right] + \omega_1^2\left[\vec{n}_1, \left[\vec{n}_1, \frac{\vec{r}_0}{r_0}\right]\right] , \qquad \vec{\mathfrak{R}}_{011} = \dot{\omega}_1\vec{u}_{011} + \omega_1^2\vec{v}_{011} ,$$

$$\vec{\mathfrak{R}}_{011} = \dot{\omega}_1 \frac{\vec{\mathfrak{S}}_{\vec{n}_1}^{(O_2)}}{\left|\vec{\mathfrak{S}}_{\vec{n}_1}^{(O_2)}\right|} + \omega_1^2 \left[\vec{n}_1, \frac{\vec{\mathfrak{S}}_{\vec{n}_1}^{(O_2)}}{\left|\vec{\mathfrak{S}}_{\vec{n}_1}^{(O_2)}\right|}\right], \tag{17}$$

$$\vec{\mathfrak{R}}_{022} = \dot{\omega}_1 \vec{u}_{022} + \omega_1^2 \vec{v}_{022}, \qquad \vec{\mathfrak{R}}_{022} = \dot{\omega}_2 \frac{\vec{\mathfrak{S}}_{\vec{n}_2}^{(O_2)}}{\left|\vec{\mathfrak{S}}_{\vec{n}_2}^{(O_2)}\right|} + \omega_2^2 \left[\vec{n}_2, \frac{\vec{\mathfrak{S}}_{\vec{n}_2}^{(O_2)}}{\left|\vec{\mathfrak{S}}_{\vec{n}_2}^{(O_2)}\right|}\right].$$

Also, we can see that in vector expression for derivative of angular momentum appear the following vector rotators: $\vec{\mathfrak{R}}_1 = \dot{\omega}_1 \vec{u}_1 + \omega_1^2 \vec{v}_1$ and $\vec{\mathfrak{R}}_2 = \dot{\omega}_1 \vec{u}_2 + \omega_1^2 \vec{v}_2$ expressed by following expressions:

$$\vec{\mathfrak{R}}_1 = \dot{\omega}_1 \frac{\vec{\mathfrak{D}}_{\vec{n}_1}^{(O_2)}}{\left|\vec{\mathfrak{D}}_{\vec{n}_1}^{(O_2)}\right|} + \omega_1^2 \left[\vec{n}_1, \frac{\vec{\mathfrak{D}}_{\vec{n}_1}^{(O_2)}}{\left|\vec{\mathfrak{D}}_{\vec{n}_1}^{(O_2)}\right|}\right] = \dot{\omega}_1 \vec{u}_1 + \omega_1^2 \vec{v}_1, \quad \vec{\mathfrak{R}}_2 = \dot{\omega}_2 \frac{\vec{\mathfrak{D}}_{\vec{n}_2}^{(O_2)}}{\left|\vec{\mathfrak{D}}_{\vec{n}_2}^{(O_2)}\right|} + \omega_2^2 \left[\vec{n}_2, \frac{\vec{\mathfrak{D}}_{\vec{n}_2}^{(O_2)}}{\left|\vec{\mathfrak{D}}_{\vec{n}_2}^{(O_2)}\right|}\right] = \dot{\omega}_2 \vec{u}_2 + \omega_2^2 \vec{v}_2 \tag{18}$$

Example 2. By using expressions for linear momentum the derivative of linear momentum of rigid body coupled rotations around three axes without intersections, not difficult to obtain corresponding expression. Also, as in previous example, after analysis structure of linear momentum derivative terms, we can see that there is possibility to introduce pure kinematic vectors, depending on component angular velocities and component angular accelerations of component coupled three rotations. We can see that in vector expression for derivative of linear momentum series of the vector rotators appear. Some of these vector rotators are listed here:

$$\vec{\mathfrak{R}}_{011} = \dot{\omega}_1 \vec{u}_{011} + \omega_1^2 \vec{v}_{011}, \qquad \vec{\mathfrak{R}}_{011} = \dot{\omega}_1 \frac{\vec{\mathfrak{S}}_{\vec{n}_1}^{(O_3)}}{\left|\vec{\mathfrak{S}}_{\vec{n}_1}^{(O_3)}\right|} + \omega_1^2 \left[\vec{n}_1, \frac{\vec{\mathfrak{S}}_{\vec{n}_1}^{(O_3)}}{\left|\vec{\mathfrak{S}}_{\vec{n}_1}^{(O_3)}\right|}\right],$$

$$\vec{\mathfrak{R}}_{022} = \dot{\omega}_2 \vec{u}_{022} + \omega_2^2 \vec{v}_{022},$$

$$\vec{\mathfrak{R}}_{022} = \dot{\omega}_2 \frac{\vec{\mathfrak{S}}_{\vec{n}_2}^{(O_3)}}{\left|\vec{\mathfrak{S}}_{\vec{n}_2}^{(O_3)}\right|} + \omega_2^2 \left[\vec{n}_2, \frac{\vec{\mathfrak{S}}_{\vec{n}_2}^{(O_3)}}{\left|\vec{\mathfrak{S}}_{\vec{n}_2}^{(O3)}\right|}\right]. \tag{19}$$

$$\vec{\mathfrak{R}}_{033} = \dot{\omega}_3 \vec{u}_{033} + \omega_1^2 \vec{v}_{033}, \qquad \vec{\mathfrak{R}}_{033} = \dot{\omega}_3 \frac{\vec{\mathfrak{S}}_{\vec{n}_3}^{(O_3)}}{\left|\vec{\mathfrak{S}}_{\vec{n}_3}^{(O_3)}\right|} + \omega_3^2 \left[\vec{n}_2, \frac{\vec{\mathfrak{S}}_{\vec{n}_3}^{(O_3)}}{\left|\vec{\mathfrak{S}}_{\vec{n}_3}^{(O_3)}\right|}\right]$$

Also, we can see that in vector expression for derivative of angular momentum of rigid body coupled rotations around three axes without intersections appear the following vector rotators: $\vec{\mathfrak{R}}_1 = \dot{\omega}_1 \vec{u}_1 + \omega_1^2 \vec{v}_1$, $\vec{\mathfrak{R}}_2 = \dot{\omega}_2 \vec{u}_2 + \omega_2^2 \vec{v}_2$ and $\vec{\mathfrak{R}}_3 = \dot{\omega}_3 \vec{u}_3 + \omega_1^2 \vec{v}_3$ expressed by following expressions:

$$\vec{\mathfrak{R}}_1 = \dot{\omega}_1 \frac{\vec{\mathfrak{D}}_{\vec{n}_1}^{(O_3)}}{\left|\vec{\mathfrak{D}}_{\vec{n}_1}^{(O_3)}\right|} + \omega_1^2 \left[\vec{n}_1, \frac{\vec{\mathfrak{D}}_{\vec{n}_1}^{(O_3)}}{\left|\vec{\mathfrak{D}}_{\vec{n}_1}^{(O3)}\right|}\right] = \dot{\omega}_1 \vec{u}_1 + \omega_1^2 \vec{v}_1,$$

$$\vec{\mathfrak{R}}_2 = \dot{\omega}_2 \frac{\vec{\mathfrak{D}}_{\vec{n}_2}^{(O3)}}{\left|\vec{\mathfrak{D}}_{\vec{n}_2}^{(O_3)}\right|} + \omega_2^2 \left[\vec{n}_2, \frac{\vec{\mathfrak{D}}_{\vec{n}_2}^{(O_3)}}{\left|\vec{\mathfrak{D}}_{\vec{n}_2}^{(O_3)}\right|}\right] = \dot{\omega}_2 \vec{u}_2 + \omega_2^2 \vec{v}_2$$

$$\vec{\mathfrak{R}}_3 = \dot{\omega}_3 \frac{\vec{\mathfrak{D}}_{\vec{n}_3}^{(O_3)}}{\left|\vec{\mathfrak{D}}_{\vec{n}_3}^{(O_3)}\right|} + \omega_3^2 \left[\vec{n}_3, \frac{\vec{\mathfrak{D}}_{\vec{n}_3}^{(O_3)}}{\left|\vec{\mathfrak{D}}_{\vec{n}_3}^{(O_3)}\right|}\right] = \dot{\omega}_3 \vec{u}_3 + \omega_3^2 \vec{v}_3 \tag{20}$$

2.1.5. Concluding remarks

By using theorems of changes of linear momentum and angular momentum with respect to time, one may write two vector equations of dynamic equilibrium of rigid body coupled multi-rotations about axes without intersection as the follows:

$$\frac{d\vec{\mathfrak{K}}}{dt} = \vec{G} + \vec{F}_{AN} + \vec{F}_{BN} + \vec{F}_{Am} + \sum_{i=1}^{i=P} \vec{F}_i \tag{21}$$

$$\frac{d\vec{\mathfrak{L}}_{O_1}}{dt} = \left[\vec{r}_0 + \vec{\rho}_C, \vec{G}\right] + \left[\vec{r}_0 + \vec{\rho}_A, \vec{F}_{AN}\right] + \left[\vec{r}_0 + \vec{\rho}_B, \vec{F}_{BN}\right] + \left[\vec{r}_0 + \vec{\rho}_A, \vec{F}_{Am}\right] + \sum_{i=1}^{i=P} \left[\vec{r}_0 + \vec{\rho}_i, \vec{F}_i\right] \tag{22}$$

where $\vec{F}_i, i = 1,2,3,...,p$ are external active forces, $\vec{G}$ is weight of a rotor, $\vec{F}_A$ and $\vec{F}_B$ are forces of bearing reactions at fixed axis. From previous analysis, we can conclude that vector rotators appear into expressions of the kinetic reactions of the shaft bearings of the structures of the rigid body multi-coupled rotations and that is very important to analyze their intensity as well as their relative angular velocity and angular acceleration around axes of coupled multi-rotations.

Recommendation foe next research and for solving three main mathematical tasks: a* Generalization of the expressions for derivatives of linear momentum and angular momentum for rigid body coupled multi-rotations around finite numbers axes without intersections; b* expressions for kinetic pressures on bearing to series of the axes of coupled rotations and corresponding numbers of coupled nonlinear differential equations depending of number of system degree of freedom with corresponding solutions   and c* build a algorithm for using obtained results as a standard software program for analysis nonlinear dynamic phenomena in rigid body coupled rotation around finite number axes without intersections. These defined tasks need a team interdisciplinary research, and will be very useful for engineering practice in analysis and simulation numerous engineering system dynamics with coupled rotation and for vibro-diagnostic.

2.2. Tangent spaces of position vectors and angular velocities of their basic vectors in different coordinate systems

Angular velocities of the basic vectors of tangent spaces of the position vectors of mass particles of the discrete rheonomic mechanical system are obtained in different coordinate systems [22]. Starting from real three dimensional coordinate systems of Descartes orthogonal three dimensional system type with fixed coordinates axis as a reference, by different coordinate transformations for each position vector of corresponding mass particle in discrete rheonomic mechanical system, basic vectors of position vector tangent three dimensional spaces are obtained in different curvilinear coordinate systems suitable to the corresponding geometrical scleronomic or rheonomic constraints applied to the considered rheonomic system. For each basic vector of the basic triedar of position vector tangent space of each mass particle of the discrete rheonomic mechanical system, angular velocity vectors of basic vector rotations are determined.

Then, after consideration and analysis of the number and properties of the geometrical scleronomic and rheonomic constraints applied to the mass particles of the

considered discrete rheonomic mechanical system, number of system degree of mobility as well as number of system degree of freedom are determined. Corresponding number of independent coordinates are chosen and corresponding rheonomic coordinates are introduced. By use extended set of the generalized coordinates contained corresponding number of independent coordinates and corresponding number of rheonomic coordinates, position vectors of the mass particles of the discrete rheonomic mechanical system, are separated into two subsets.

First subset contain position vectors of the mass particle, keep their three dimensional tangent space each with three basic vectors.

Second subset contain position vectors of the mass particle, each depending, in general case, of the all generalized coordinates, independent and rheonomic. Then, each of the position vectors are with $n + R$ -dimensional tangent spaces and with   basic vectors.

2.2.1. Introduction

Let us consider a discrete system with N mass particles with mass m_α, and with corresponding position in real three dimensional space determined by geometrical points $N_{(\alpha)}, \alpha = 1,2,3,...,N$ (see Figure 2). For beginning we take that positions of the material points, as well as corresponding geometrical points coordinates are determined by coordinates in fixed orthogonal Descartes coordinate system with three coordinates as denoted by $N_{(\alpha)}\left(x_{(\alpha)}, y_{(\alpha)}, z_{(\alpha)}\right). \alpha = 1,2,3,...,N$, where O is fixed coordinate origin, and Ox , Oy and Oz fixed oriented coordinate strain lines-coordinate axes. Coordinates of the position vector of each material point are equal to coordinate of the geometrical point which determine mass particle position in the space. For Descartes coordinate system   for   position   of   the   each   mass   particle   we   can   write: $\vec{\rho}_{(\alpha)}\left(x_{(\alpha)}, y_{(\alpha)}, z_{(\alpha)}\right) = x_{(\alpha)}\vec{i} + y_{(\alpha)}\vec{j} + z_{(\alpha)}\vec{k}$, $\alpha = 1,2,3,...,N$.

Let us, now,   consider previous discrete system with N mass particles wirh mass m_α, and with corresponding position in real three dimensional space determined by same geometrical points $N_{(\alpha)}, \alpha = 1,2,3,...,N$ in generalized coordinate system of curvilinear coordinates $\left(q_{(\alpha)}{}^1, q_{(\alpha)}{}^2, q_{(\alpha)}{}^3\right)$ $\alpha = 1,2,3,...,N$ corresponding to mass particle positions. For same geometrical points coordinates in considered three coordinate systems   are: $N_{(\alpha)}\left(x_{(\alpha)}, y_{(\alpha)}, z_{(\alpha)}\right). \alpha = 1,2,3,...,N$ and $N_{(\alpha)}\left(q_{(\alpha)}{}^1, q_{(\alpha)}{}^2, q_{(\alpha)}{}^3\right)$, $\alpha = 1,2,3,...,N$ .. Formulae of coordinate transformation from previous coordinate system with fixed axes and new curvilinear coordinate system are:

$$x_{(\alpha)} = x_{(\alpha)}\left(q_{(\alpha)}{}^1, q_{(\alpha)}{}^2, q_{(\alpha)}{}^3\right)$$
$$y_{(\alpha)} = y_{(\alpha)}\left(q_{(\alpha)}{}^1, q_{(\alpha)}{}^2, q_{(\alpha)}{}^3\right) \qquad (1)$$
$$z_{(\alpha)} = z_{(\alpha)}\left(q_{(\alpha)}{}^1, q_{(\alpha)}{}^2, q_{(\alpha)}{}^3\right)$$

Position vectors of each mass particle and corresponding geometrical points are invariant geometrical objects in both coordinate systems, but their coordinates in

considered coordinate systems are not equal to coordinates of the corresponding geometrical point. In generalized coordinate system geometrical points $N_{(\alpha)}, \alpha = 1,2,3,...,N$ have following coordinates: $\left(q_{(\alpha)}{}^1, q_{(\alpha)}{}^2, q_{(\alpha)}{}^3\right)$, $\alpha = 1,2,3,...,N$ and coordinate of position vectors of these geometrical points are $\left(\rho_{(\alpha)}{}^1, \rho_{(\alpha)}{}^2, \rho_{(\alpha)}{}^3\right), \alpha = 1,2,3,...,N$. For position vectors we can write:

$$\vec{\rho}_{(\alpha)}\left(x_{(\alpha)}, y_{(\alpha)}, z_{(\alpha)}\right) = x_{(\alpha)}\vec{i} + y_{(\alpha)}\vec{j} + z_{(\alpha)}\vec{k} \overset{def = inv.vektor}{=} \vec{\rho}_{(\alpha)}\left(q_{(\alpha)}{}^1, q_{(\alpha)}{}^2, q_{(\alpha)}{}^3\right) \tag{2}$$

$$\vec{\rho}_{(\alpha)}\left(q_{(\alpha)}{}^1, q_{(\alpha)}{}^2, q_{(\alpha)}{}^3\right) =$$
$$= \rho_{(\alpha)}{}^1\left(q_{(\alpha)}{}^1, q_{(\alpha)}{}^2, q_{(\alpha)}{}^3\right)\vec{g}_{(\alpha)1} + \rho_{(\alpha)}{}^2\left(q_{(\alpha)}{}^1, q_{(\alpha)}{}^2, q_{(\alpha)}{}^3\right)\vec{g}_{(\alpha)2} + \rho_{(\alpha)}{}^3\left(q_{(\alpha)}{}^1, q_{(\alpha)}{}^2, q_{(\alpha)}{}^3\right)\vec{g}_{(\alpha)3}$$
$$\alpha = 1,2,3,...,N \tag{3}$$
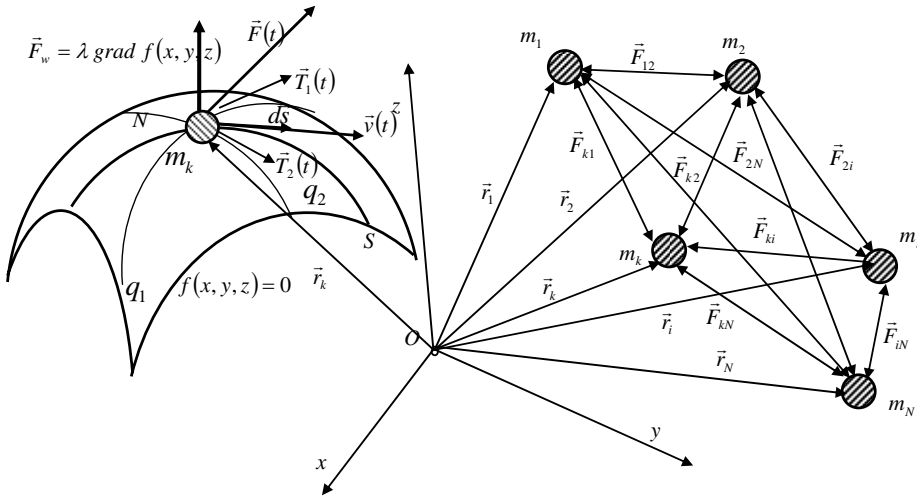
Figure 2. Discrete material system with N mass particles and geometrical rheonomic constraints

For first example in polar-cylindrical coordinate system geometrical points have the following coordinates: $N_{(\alpha)}\left(r_{(\alpha)}, \varphi_{(\alpha)}, z_{(\alpha)}\right)$ $\alpha = 1,2,3,...,N$ and position vectors $\vec{\rho}_{(\alpha)}\left(r_{(\alpha)}, \varphi_{(\alpha)}, z_{(\alpha)}\right)$ of corresponding geometrical point are: $r_{(\alpha)}, 0, z_{(\alpha)}$ and we can write:

$$\vec{\rho}_{(\alpha)}\left(r_{(\alpha)}, \varphi_{(\alpha)}, z_{(\alpha)}\right) = r_{(\alpha)}\vec{r}_{o(\alpha)} + 0 \cdot \vec{c}_{0(\alpha)} + z_{(\alpha)}\vec{k} \equiv r_{(\alpha)}\vec{r}_{o(\alpha)} + z_{(\alpha)}\vec{k} \tag{4}$$
$$\alpha = 1,2,3,...,N$$

where $\vec{r}_{o(\alpha)}, \vec{c}_{0(\alpha)}$ and $\vec{k}$, $\alpha = 1,2,3,...,N$ are basic unit vectors of tangent space of corresponding position vector in polar-cylindrical coordinate system.

For second example in spherical coordinate system geometrical points have the following coordinates: $N_{(\alpha)}\left(\rho_{(\alpha)}, \varphi_{(\alpha)}, \vartheta_{(\alpha)}\right)$ $\alpha = 1,2,3,..., N$ and position vectors $\vec{\rho}_{(\alpha)}\left(\rho_{(\alpha)}, \varphi_{(\alpha)}, \vartheta_{(\alpha)}\right)$ of corresponding geometrical point are: $\rho_{(\alpha)}, 0, 0$ and we can write:

$$\vec{\rho}_{(\alpha)}\left(\rho_{(\alpha)}, \varphi_{(\alpha)}, \vartheta_{(\alpha)}\right) = \rho_{(\alpha)}\vec{\rho}_{0(\alpha)} + 0 \cdot \vec{c}_{0(\alpha)} + 0 \cdot \vec{v}_{0(\alpha)} \equiv \rho_{(\alpha)}\vec{\rho}_{0(\alpha)} \qquad (5)$$
$$\alpha = 1,2,3,..., N$$

where $\vec{\rho}_{0(\alpha)}, \vec{c}_{0(\alpha)}$ and $\vec{v}_{0(\alpha)}, \alpha = 1,2,3,..., N$ are basic unit vectors of tangent space of corresponding position vector in polar-cylindrical coordinate system.

2.2.2. Basic vectors of the position vector three-dimensional tangent space in generalized curvilinear coordinate systems

In real two-dimensional coordinate systems, position vector tangent spaces are three-dimensional and the basic vectors of the tangent spaces of each position vector of each mass particle we denote with $\vec{g}_{(\alpha)i}$, $\alpha = 1,2,3,..., N$, $i = 1,2,3$ (see Figure 3). These vectors are in tangent directions to the corresponding curvilinear coordinate line and in general are not unit vectors. Basic vectors it is possible to obtain by following way (for detail see Refs. [22], [23], [24], [25], [26], [27], [28], [33] and [34]):

$$\vec{g}_{(\alpha)i} = \frac{\partial \vec{\rho}_{(\alpha)}}{\partial q_{(\alpha)}^{\ i}}, \ \alpha = 1,2,3,..., N, \ \ i = 1,2,3 \qquad (6)$$

or by formula coordinate transformation and by following expressions:

$$\vec{g}_{(\alpha)1} = \frac{\partial \vec{\rho}_{(\alpha)}}{\partial q_{(\alpha)}^{\ 1}} = \frac{\partial x_{(\alpha)}\left(q_{(\alpha)}^{\ 1}, q_{(\alpha)}^{\ 2}, q_{(\alpha)}^{\ 3}\right)}{\partial q_{(\alpha)}^{\ 1}}\vec{i} + \frac{\partial y_{(\alpha)}\left(q_{(\alpha)}^{\ 1}, q_{(\alpha)}^{\ 2}, q_{(\alpha)}^{\ 3}\right)}{\partial q_{(\alpha)}^{\ 1}}\vec{j} + \frac{\partial z_{(\alpha)}\left(q_{(\alpha)}^{\ 1}, q_{(\alpha)}^{\ 2}, q_{(\alpha)}^{\ 3}\right)}{\partial q_{(\alpha)}^{\ 1}}\vec{k}$$

$$\vec{g}_{(\alpha)2} = \frac{\partial \vec{\rho}_{(\alpha)}}{\partial q_{(\alpha)}^{\ 2}} = \frac{\partial x_{(\alpha)}\left(q_{(\alpha)}^{\ 1}, q_{(\alpha)}^{\ 2}, q_{(\alpha)}^{\ 3}\right)}{\partial q_{(\alpha)}^{\ 2}}\vec{i} + \frac{\partial y_{(\alpha)}\left(q_{(\alpha)}^{\ 1}, q_{(\alpha)}^{\ 2}, q_{(\alpha)}^{\ 3}\right)}{\partial q_{(\alpha)}^{\ 2}}\vec{j} + \frac{\partial z_{(\alpha)}\left(q_{(\alpha)}^{\ 1}, q_{(\alpha)}^{\ 2}, q_{(\alpha)}^{\ 3}\right)}{\partial q_{(\alpha)}^{\ 2}}\vec{k} \ \ (7)$$

$$\vec{g}_{(\alpha)3} = \frac{\partial \vec{\rho}_{(\alpha)}}{\partial q_{(\alpha)}^{\ 3}} = \frac{\partial x_{(\alpha)}\left(q_{(\alpha)}^{\ 1}, q_{(\alpha)}^{\ 2}, q_{(\alpha)}^{\ 3}\right)}{\partial q_{(\alpha)}^{\ 3}}\vec{i} + \frac{\partial y_{(\alpha)}\left(q_{(\alpha)}^{\ 1}, q_{(\alpha)}^{\ 2}, q_{(\alpha)}^{\ 3}\right)}{\partial q_{(\alpha)}^{\ 3}}\vec{j} + \frac{\partial z_{(\alpha)}\left(q_{(\alpha)}^{\ 1}, q_{(\alpha)}^{\ 2}, q_{(\alpha)}^{\ 3}\right)}{\partial q_{(\alpha)}^{\ 3}}\vec{k}$$

Contravariant coordinates of the position vectors it is possible to obtain by following formulas:

$$\rho_{(\alpha)}^{\ 1}\left(q_{(\alpha)}^{\ 1}, q_{(\alpha)}^{\ 2}, q_{(\alpha)}^{\ 3}\right) = \frac{1}{\Delta}\left[\frac{\partial y_{(\alpha)}\left(q_{(\alpha)}^{\ 1}, q_{(\alpha)}^{\ 2}, q_{(\alpha)}^{\ 3}\right)}{\partial q_{(\alpha)}^{\ 2}}\frac{\partial z_{(\alpha)}\left(q_{(\alpha)}^{\ 1}, q_{(\alpha)}^{\ 2}, q_{(\alpha)}^{\ 3}\right)}{\partial q_{(\alpha)}^{\ 3}} - \frac{\partial y_{(\alpha)}\left(q_{(\alpha)}^{\ 1}, q_{(\alpha)}^{\ 2}, q_{(\alpha)}^{\ 3}\right)}{\partial q_{(\alpha)}^{\ 3}}\frac{\partial z_{(\alpha)}\left(q_{(\alpha)}^{\ 1}, q_{(\alpha)}^{\ 2}, q_{(\alpha)}^{\ 3}\right)}{\partial q_{(\alpha)}^{\ 2}}\right]x_{(\alpha)}\left(q_{(\alpha)}^{\ 1}, q_{(\alpha)}^{\ 2}, q_{(\alpha)}^{\ 3}\right) -$$

$$- \frac{1}{\Delta}\left[\frac{\partial x_{(\alpha)}\left(q_{(\alpha)}^{\ 1}, q_{(\alpha)}^{\ 2}, q_{(\alpha)}^{\ 3}\right)}{\partial q_{(\alpha)}^{\ 2}}\frac{\partial z_{(\alpha)}\left(q_{(\alpha)}^{\ 1}, q_{(\alpha)}^{\ 2}, q_{(\alpha)}^{\ 3}\right)}{\partial q_{(\alpha)}^{\ 3}} - \frac{\partial x_{(\alpha)}\left(q_{(\alpha)}^{\ 1}, q_{(\alpha)}^{\ 2}, q_{(\alpha)}^{\ 3}\right)}{\partial q_{(\alpha)}^{\ 3}}\frac{\partial z_{(\alpha)}\left(q_{(\alpha)}^{\ 1}, q_{(\alpha)}^{\ 2}, q_{(\alpha)}^{\ 3}\right)}{\partial q_{(\alpha)}^{\ 2}}\right]y_{(\alpha)}\left(q_{(\alpha)}^{\ 1}, q_{(\alpha)}^{\ 2}, q_{(\alpha)}^{\ 3}\right) -$$

$$- \frac{1}{\Delta}\left[\frac{\partial x_{(\alpha)}\left(q_{(\alpha)}^{\ 1}, q_{(\alpha)}^{\ 2}, q_{(\alpha)}^{\ 3}\right)}{\partial q_{(\alpha)}^{\ 2}}\frac{\partial y_{(\alpha)}\left(q_{(\alpha)}^{\ 1}, q_{(\alpha)}^{\ 2}, q_{(\alpha)}^{\ 3}\right)}{\partial q_{(\alpha)}^{\ 3}} - \frac{\partial x_{(\alpha)}\left(q_{(\alpha)}^{\ 1}, q_{(\alpha)}^{\ 2}, q_{(\alpha)}^{\ 3}\right)}{\partial q_{(\alpha)}^{\ 3}}\frac{\partial y_{(\alpha)}\left(q_{(\alpha)}^{\ 1}, q_{(\alpha)}^{\ 2}, q_{(\alpha)}^{\ 3}\right)}{\partial q_{(\alpha)}^{\ 2}}\right]z_{(\alpha)}\left(q_{(\alpha)}^{\ 1}, q_{(\alpha)}^{\ 2}, q_{(\alpha)}^{\ 3}\right)$$

$$\rho_{(\alpha)}{}^2\!\left(q_{(\alpha)}{}^1,q_{(\alpha)}{}^2,q_{(\alpha)}{}^3\right)=-\frac{1}{\Delta}\!\left[\frac{\partial y_{(\alpha)}\!\left(q_{(\alpha)}{}^1,q_{(\alpha)}{}^2,q_{(\alpha)}{}^3\right)}{\partial q_{(\alpha)}{}^1}\frac{\partial z_{(\alpha)}\!\left(q_{(\alpha)}{}^1,q_{(\alpha)}{}^2,q_{(\alpha)}{}^3\right)}{\partial q_{(\alpha)}{}^3}-\frac{\partial y_{(\alpha)}\!\left(q_{(\alpha)}{}^1,q_{(\alpha)}{}^2,q_{(\alpha)}{}^3\right)}{\partial q_{(\alpha)}{}^3}\frac{\partial z_{(\alpha)}\!\left(q_{(\alpha)}{}^1,q_{(\alpha)}{}^2,q_{(\alpha)}{}^3\right)}{\partial q_{(\alpha)}{}^1}\right]x_{(\alpha)}\!\left(q_{(\alpha)}{}^1,q_{(\alpha)}{}^2,q_{(\alpha)}{}^3\right)+$$

$$+\frac{1}{\Delta}\!\left[\frac{\partial x_{(\alpha)}\!\left(q_{(\alpha)}{}^1,q_{(\alpha)}{}^2,q_{(\alpha)}{}^3\right)}{\partial q_{(\alpha)}{}^1}\frac{\partial z_{(\alpha)}\!\left(q_{(\alpha)}{}^1,q_{(\alpha)}{}^2,q_{(\alpha)}{}^3\right)}{\partial q_{(\alpha)}{}^3}-\frac{\partial x_{(\alpha)}\!\left(q_{(\alpha)}{}^1,q_{(\alpha)}{}^2,q_{(\alpha)}{}^3\right)}{\partial q_{(\alpha)}{}^3}\frac{\partial z_{(\alpha)}\!\left(q_{(\alpha)}{}^1,q_{(\alpha)}{}^2,q_{(\alpha)}{}^3\right)}{\partial q_{(\alpha)}{}^1}\right]y_{(\alpha)}\!\left(q_{(\alpha)}{}^1,q_{(\alpha)}{}^2,q_{(\alpha)}{}^3\right)-$$

$$-\frac{1}{\Delta}\!\left[\frac{\partial x_{(\alpha)}\!\left(q_{(\alpha)}{}^1,q_{(\alpha)}{}^2,q_{(\alpha)}{}^3\right)}{\partial q_{(\alpha)}{}^1}\frac{\partial y_{(\alpha)}\!\left(q_{(\alpha)}{}^1,q_{(\alpha)}{}^2,q_{(\alpha)}{}^3\right)}{\partial q_{(\alpha)}{}^3}-\frac{\partial x_{(\alpha)}\!\left(q_{(\alpha)}{}^1,q_{(\alpha)}{}^2,q_{(\alpha)}{}^3\right)}{\partial q_{(\alpha)}{}^3}\frac{\partial y_{(\alpha)}\!\left(q_{(\alpha)}{}^1,q_{(\alpha)}{}^2,q_{(\alpha)}{}^3\right)}{\partial q_{(\alpha)}{}^1}\right]z_{(\alpha)}\!\left(q_{(\alpha)}{}^1,q_{(\alpha)}{}^2,q_{(\alpha)}{}^3\right)$$

$$\rho_{(\alpha)}{}^3\!\left(q_{(\alpha)}{}^1,q_{(\alpha)}{}^2,q_{(\alpha)}{}^3\right)=\frac{1}{\Delta}\!\left[\frac{\partial y_{(\alpha)}\!\left(q_{(\alpha)}{}^1,q_{(\alpha)}{}^2,q_{(\alpha)}{}^3\right)}{\partial q_{(\alpha)}{}^1}\frac{\partial z_{(\alpha)}\!\left(q_{(\alpha)}{}^1,q_{(\alpha)}{}^2,q_{(\alpha)}{}^3\right)}{\partial q_{(\alpha)}{}^2}-\frac{\partial y_{(\alpha)}\!\left(q_{(\alpha)}{}^1,q_{(\alpha)}{}^2,q_{(\alpha)}{}^3\right)}{\partial q_{(\alpha)}{}^2}\frac{\partial z_{(\alpha)}\!\left(q_{(\alpha)}{}^1,q_{(\alpha)}{}^2,q_{(\alpha)}{}^3\right)}{\partial q_{(\alpha)}{}^1}\right]x_{(\alpha)}\!\left(q_{(\alpha)}{}^1,q_{(\alpha)}{}^2,q_{(\alpha)}{}^3\right)-$$

$$-\frac{1}{\Delta}\!\left[\frac{\partial x_{(\alpha)}\!\left(q_{(\alpha)}{}^1,q_{(\alpha)}{}^2,q_{(\alpha)}{}^3\right)}{\partial q_{(\alpha)}{}^1}\frac{\partial z_{(\alpha)}\!\left(q_{(\alpha)}{}^1,q_{(\alpha)}{}^2,q_{(\alpha)}{}^3\right)}{\partial q_{(\alpha)}{}^2}-\frac{\partial x_{(\alpha)}\!\left(q_{(\alpha)}{}^1,q_{(\alpha)}{}^2,q_{(\alpha)}{}^3\right)}{\partial q_{(\alpha)}{}^2}\frac{\partial z_{(\alpha)}\!\left(q_{(\alpha)}{}^1,q_{(\alpha)}{}^2,q_{(\alpha)}{}^3\right)}{\partial q_{(\alpha)}{}^1}\right]y_{(\alpha)}\!\left(q_{(\alpha)}{}^1,q_{(\alpha)}{}^2,q_{(\alpha)}{}^3\right)+$$

$$+\frac{1}{\Delta}\!\left[\frac{\partial x_{(\alpha)}\!\left(q_{(\alpha)}{}^1,q_{(\alpha)}{}^2,q_{(\alpha)}{}^3\right)}{\partial q_{(\alpha)}{}^1}\frac{\partial y_{(\alpha)}\!\left(q_{(\alpha)}{}^1,q_{(\alpha)}{}^2,q_{(\alpha)}{}^3\right)}{\partial q_{(\alpha)}{}^2}-\frac{\partial x_{(\alpha)}\!\left(q_{(\alpha)}{}^1,q_{(\alpha)}{}^2,q_{(\alpha)}{}^3\right)}{\partial q_{(\alpha)}{}^2}\frac{\partial y_{(\alpha)}\!\left(q_{(\alpha)}{}^1,q_{(\alpha)}{}^2,q_{(\alpha)}{}^3\right)}{\partial q_{(\alpha)}{}^1}\right]z_{(\alpha)}\!\left(q_{(\alpha)}{}^1,q_{(\alpha)}{}^2,q_{(\alpha)}{}^3\right)$$

where

$$\Delta_{(\alpha)}=\begin{vmatrix}\dfrac{\partial x_{(\alpha)}\!\left(q_{(\alpha)}{}^1,q_{(\alpha)}{}^2,q_{(\alpha)}{}^3\right)}{\partial q^1} & \dfrac{\partial y_{(\alpha)}\!\left(q_{(\alpha)}{}^1,q_{(\alpha)}{}^2,q_{(\alpha)}{}^3\right)}{\partial q^1} & \dfrac{\partial z_{(\alpha)}\!\left(q_{(\alpha)}{}^1,q_{(\alpha)}{}^2,q_{(\alpha)}{}^3\right)}{\partial q^1} \\[3mm] \dfrac{\partial x_{(\alpha)}\!\left(q_{(\alpha)}{}^1,q_{(\alpha)}{}^2,q_{(\alpha)}{}^3\right)}{\partial q^2} & \dfrac{\partial y_{(\alpha)}\!\left(q_{(\alpha)}{}^1,q_{(\alpha)}{}^2,q_{(\alpha)}{}^3\right)}{\partial q^2} & \dfrac{\partial z_{(\alpha)}\!\left(q_{(\alpha)}{}^1,q_{(\alpha)}{}^2,q_{(\alpha)}{}^3\right)}{\partial q^2} \\[3mm] \dfrac{\partial x_{(\alpha)}\!\left(q_{(\alpha)}{}^1,q_{(\alpha)}{}^2,q_{(\alpha)}{}^3\right)}{\partial q^3} & \dfrac{\partial y_{(\alpha)}\!\left(q_{(\alpha)}{}^1,q_{(\alpha)}{}^2,q_{(\alpha)}{}^3\right)}{\partial q^3} & \dfrac{\partial z_{(\alpha)}\!\left(q_{(\alpha)}{}^1,q_{(\alpha)}{}^2,q_{(\alpha)}{}^3\right)}{\partial q^3}\end{vmatrix}\neq 0$$

2.2.3. Change of the basic vectors of the position vector three-dimensional tangent space in generalized curvilinear coordinate systems

Without losing generality, we consider change of basic vectors of a position vector of one mass particle during mass particle motion through real space and described in three-dimensional space. Also, we focused our attention to the orthogonal curvilinear coordinate system. For that case change (first derivative with respect to time) with time of the basic vectors of tangent space of a position vector are (see Figure 3.):

$$\frac{d\vec{g}_1}{dt}=\overset{*}{\vec{g}}_1+$$
$$=\vec{g}_1\!\left(\Gamma_{11}^1\dot{q}^1+\Gamma_{12}^1\dot{q}^2+\Gamma_{13}^1\dot{q}^3\right)+\vec{g}_2\!\left(\Gamma_{11}^2\dot{q}^1+\Gamma_{12}^2\dot{q}^2+\Gamma_{13}^2\dot{q}^3\right)+\vec{g}_3\!\left(\Gamma_{11}^3\dot{q}^1+\Gamma_{12}^3\dot{q}^2+\Gamma_{13}^3\dot{q}^3\right)$$

$$\frac{d\vec{g}_2}{dt}=\overset{*}{\vec{g}}_2+\left[\vec{\omega}_{p2},\vec{g}_2\right]=$$

$$=\left(\Gamma_{21}^1\vec{g}_1+\Gamma_{21}^2\vec{g}_2+\Gamma_{21}^3\vec{g}_3\right)\!\dot{q}^1+\left(\Gamma_{22}^1\vec{g}_1+\Gamma_{22}^2\vec{g}_2+\Gamma_{22}^3\vec{g}_3\right)\!\dot{q}^2+\left(\Gamma_{23}^1\vec{g}_1+\Gamma_{23}^2\vec{g}_2+\Gamma_{23}^3\vec{g}_3\right)\!\dot{q}^3$$

$$\frac{d\vec{g}_3}{dt}=\overset{*}{\vec{g}}_3+\left[\vec{\omega}_{p3},\vec{g}_3\right]=$$

$$=\left(\Gamma_{31}^1\vec{g}_1+\Gamma_{31}^2\vec{g}_2+\Gamma_{31}^3\vec{g}_3\right)\!\dot{q}^1+\left(\Gamma_{32}^1\vec{g}_1+\Gamma_{32}^2\vec{g}_2+\Gamma_{32}^3\vec{g}_3\right)\!\dot{q}^2+\left(\Gamma_{33}^1\vec{g}_1+\Gamma_{33}^2\vec{g}_2+\Gamma_{33}^3\vec{g}_3\right)\!\dot{q}^3$$

(8)

$$N\left(q^1(t), q^2(t), q^3(t)\right) \qquad \vec{\rho}\left(q^1, q^2, q^3\right)$$

$$\vec{\rho}\left(q^1(t), q^2(t), q^3(t)\right) = \rho^1 \vec{g}_1 + \rho^2 \vec{g}_2 + \rho^3 \vec{g}_3$$

$$\vec{g}_1 = \frac{\partial \vec{\rho}}{\partial q^1}$$

$$\vec{g}_2 = \frac{\partial \vec{\rho}}{\partial q^2}$$

$$\vec{g}_3 = \frac{\partial \vec{\rho}}{\partial q^3}$$

$$\omega_p = \omega_p\left(q^1(t), q^2(t), q^3(t), \dot{q}^1(t), \dot{q}^2(t), \dot{q}^3(t)\right)$$
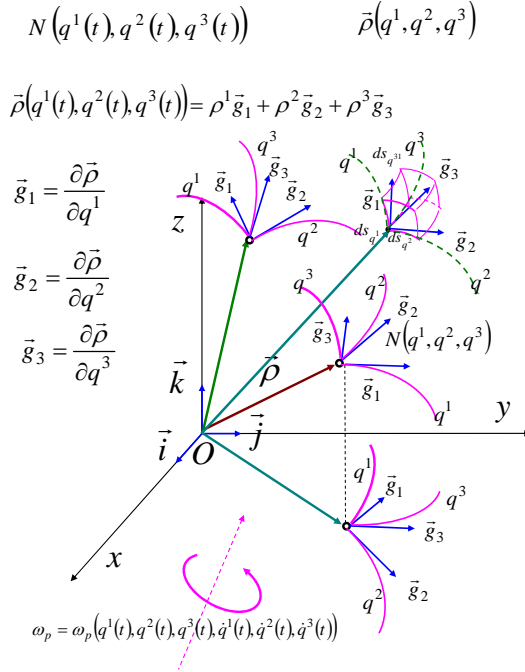
Figure 3. A position vectors and its three-dimensional space with corresponding curvilinear coordinate system and tangent space with corresponding three basic vectors of the position vector tangent spaces along mass particle motion through time

After analysis of the obtained derivatives of the basic vectors of position vector tangent spaces in three-dimensional orthogonal curvilinear coordinate systems we can separate two sets of the terms in obtained expressions (8). First set correspond to the relative derivative of the corresponding basic vectors in the following forms:

$$\overset{*}{\vec{g}}_1 = \vec{g}_1\left(\Gamma_{11}^1 \dot{q}^1 + \Gamma_{12}^1 \dot{q}^2 + \Gamma_{13}^1 \dot{q}^3\right)$$
$$\overset{*}{\vec{g}}_2 = \vec{g}_2\left(\Gamma_{21}^2 \dot{q}^1 + \Gamma_{22}^2 \dot{q}^2 + \Gamma_{23}^2 \dot{q}^3\right) \qquad (9)$$
$$\overset{*}{\vec{g}}_3 = \vec{g}_3\left(\Gamma_{31}^3 \dot{q}^1 + \Gamma_{32}^3 \dot{q}^2 + \Gamma_{33}^3 \dot{q}^3\right)$$

These vectors present vector forms of extensions of the corresponding basic vectors and in scalar form it is possible to express relative change of the intensity – dilatation of the basic vectors in direction of its previous kinetic state. In differential form is possible to write:

$$d\varepsilon_1 = \frac{d|\vec{g}_1|}{|\vec{g}_1|} = \Gamma_{11}^1 dq^1 + \Gamma_{12}^1 dq^2 + \Gamma_{13}^1 dq^3$$

$$d\varepsilon_2 = \frac{d|\vec{g}_2|}{|\vec{g}_2|} = \Gamma_{31}^2 dq^1 + \Gamma_{32}^2 dq^2 + \Gamma_{33}^2 dq^3 \qquad (10)$$

$$d\varepsilon_3 = \frac{d|\vec{g}_{31}|}{|\vec{g}_3|} = \Gamma_{31}^3 dq^1 + \Gamma_{32}^3 dq^2 + \Gamma_{33}^3 dq^3$$

From analysis of the obtained derivatives of the basic vectors of position vector tangent spaces in three-dimensional orthogonal curvilinear coordinate systems we can separate second set of the terms in obtained expressions (8). Second set correspond to the rotation change of the corresponding basic vectors in the following forms:

$$\left[\vec{\omega}_{p1}, \vec{g}_1\right] = \vec{g}_2\left(\Gamma_{11}^2 \dot{q}^1 + \Gamma_{12}^2 \dot{q}^2 + \Gamma_{13}^2 \dot{q}^3\right) + \vec{g}_3\left(\Gamma_{11}^3 \dot{q}^1 + \Gamma_{12}^3 \dot{q}^2 + \Gamma_{13}^3 \dot{q}^3\right)$$

$$\left[\vec{\omega}_{p2}, \vec{g}_2\right] = \vec{g}_1\left(\Gamma_{21}^1 \dot{q}^1 + \Gamma_{22}^1 \dot{q}^2 + \Gamma_{23}^1 \dot{q}^3\right) + \vec{g}_3\left(\Gamma_{21}^3 \dot{q}^1 + \Gamma_{22}^3 \dot{q}^2 + \Gamma_{23}^3 \dot{q}^3\right) \quad (11)$$

$$\left[\vec{\omega}_{p3}, \vec{g}_3\right] = \vec{g}_1\left(\Gamma_{31}^1 \dot{q}^1 + \Gamma_{32}^1 \dot{q}^2 + \Gamma_{33}^1 \dot{q}^3\right) + \vec{g}_2\left(\Gamma_{31}^2 \dot{q}^1 + \Gamma_{32}^2 \dot{q}^2 + \Gamma_{33}^2 \dot{q}^3\right)$$

where we introduce notation $\vec{\omega}_{p1}$, $\vec{\omega}_{p2}$ and $\vec{\omega}_{p3}$ for vectors of the angular velocities of the corresponding basic vectors of the position vector tangent space. When curvilinear coordinate system is not orthogonal and angles between three basic vectors are changeable with time these angular velocities are different for each basic vector. When basic vectors are orthogonal and without change orthogonal relation, all three angular velocity are same.

For the case of the discrete mechanical system N mass particles for each vector position of each mass particle is necessary, by analogous way as presented in previous part, is possible to determine change of the basic vectors of tangent space of position vectors.

After analysis of the obtained derivatives of the basic vectors of position vector tangent spaces for each mass particle, in three-dimensional orthogonal curvilinear coordinate systems, we can separate two sets of the terms in obtained expression and corresponding for other two sets of the basic vectors. First set correspond to the relative derivative of the corresponding basic vectors. These vectors present vector forms of extensions of the corresponding basic vectors and in scalar form it is possible to express relative changes of the intensities – dilatations of the basic vectors in direction of their previous kinetic state.

From analysis of the obtained derivatives of the basic vectors of position vector tangent spaces for each mass particle in three-dimensional orthogonal curvilinear coordinate systems, we can separate second sets of the terms in obtained expressions. Second set correspond to the rotation change of the corresponding basic vectors. We introduce notation $\vec{\omega}_{(\alpha)p1}$, $\vec{\omega}_{(\alpha)p2}$ and $\vec{\omega}_{(\alpha)p3}$ for vectors of the angular velocities of the corresponding basic vectors of the position vector tangent spaces. When basic vectors are orthogonal and without change orthogonal relation, all three angular velocity are same, for each vector position.

For example 1*: in polar-cylindrical curvilinear coordinate system by expressions (8), (9), (10) and (11) we can write (see Figure 4.a*):

$$\frac{d\vec{g}_1}{dt} = \frac{d\vec{g}_r}{dt} = \dot{\varphi}\left(-\vec{i}\sin\varphi + \vec{j}\cos\varphi\right) = \frac{d\vec{r}_0}{dt} = \dot{\varphi}\vec{c}_0 = \frac{1}{r}\dot{\varphi}\vec{g}_\varphi = \left[\vec{\omega}_{\text{Pr}}, \vec{g}_r\right]$$

$$\frac{d\vec{g}_2}{dt} = \frac{d\vec{g}_\varphi}{dt} = \dot{r}\vec{c}_0 + r\frac{d\vec{c}_0}{dt} = \dot{r}\vec{c}_0 - r\dot{\varphi}\,\vec{r}_0 = \overset{*}{\vec{g}}_\varphi + \left[\vec{\omega}_{P\varphi}, \vec{g}_\varphi\right]$$

$$\frac{d\vec{g}_3}{dt} = \frac{d\vec{g}_z}{dt} = \frac{d\vec{k}}{dt} = 0$$

$$\overset{*}{\vec{g}}_r = 0 \;, \qquad\qquad d\varepsilon_r = \frac{d\left|\vec{g}_\varphi\right|}{\left|\vec{g}_\varphi\right|} = \frac{dr}{r} \;, \qquad\qquad \vec{\omega}_{\mathrm{Pr}} = \dot{\varphi}\vec{k}$$

$$\overset{*}{\vec{g}}_\varphi = \dot{r}\vec{c}_0 = \frac{\dot{r}}{r}\vec{g}_\varphi \;, \qquad\qquad \vec{\omega}_{P\varphi} = \dot{\varphi}\vec{k} \;, \qquad \overset{*}{\vec{g}}_z = 0 \;, \qquad\qquad \vec{\omega}_{Pz} = 0$$

Angular velocities of the basic vectors of each position vector tangent space of mass particle motion in polar-cylindrical curvilinear coordinate systems are: $\vec{\omega}_{(\alpha)P} = \dot{\varphi}_{(\alpha)}\vec{k}$, $\alpha = 1,2,3,...,N$.

a*   b*
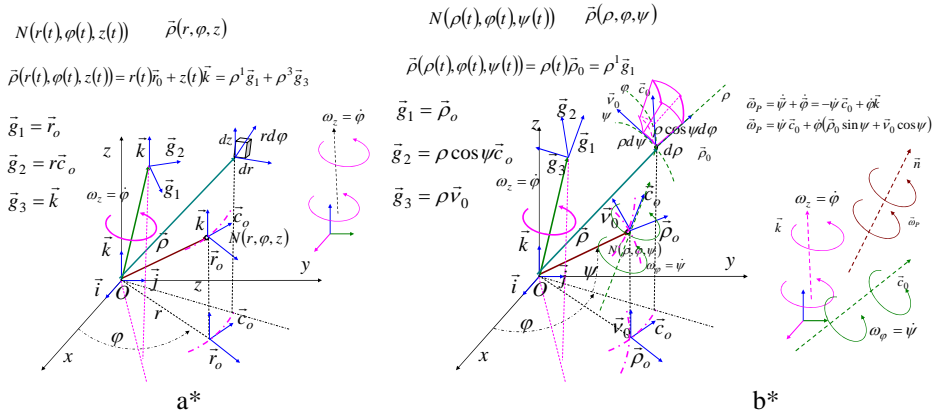
Figure 4. A position vectors and its three-dimensional spaces with corresponding curvilinear coordinate system and tangent space with corresponding three basic vectors of the position vector tangent spaces along mass particle motion through time
a* polar-cylindrical curvilinear coordinate system; b* spherical curvilinear coordinate system

For example 2*: in spherical curvilinear coordinate system by expressions (8), (9), (10) and (11), we can write (see Figure 4.b*):

$$\frac{d\vec{g}_1}{dt} = \frac{d\vec{g}_\rho}{dt} = \dot{\varphi}\vec{c}_0\cos\psi + \dot{\psi}\vec{v}_0 = \frac{1}{\rho}\dot{\varphi}\vec{g}_\varphi + \frac{1}{\rho}\dot{\psi}\vec{g}_\psi$$

$$\frac{d\vec{g}_2}{dt} = \frac{d\vec{g}_\varphi}{dt} = \vec{c}_0\left(\dot{\rho}\cos\psi - \rho\dot{\psi}\sin\psi\right) - \dot{\varphi}\left(\vec{\rho}_0\cos\psi - \vec{v}_0\sin\psi\right)\rho\cos\psi$$

$$\frac{d\vec{g}_3}{dt} = \frac{d\vec{g}_\psi}{dt} = \dot{\rho}\vec{v}_0 + \rho\left(-\dot{\varphi}\vec{c}_0\sin\psi - \dot{\psi}\vec{\rho}_0\right)$$

$$\overset{*}{\vec{\rho}}_\rho = 0 \;, \qquad \left[\vec{\omega}_{P\rho}, \vec{\rho}_\rho\right] = \dot{\psi}\vec{v}_0 + \dot{\varphi}\vec{c}_0\cos\psi$$

$$\vec{\omega}_{P\rho} = \dot{\psi}\vec{c}_0 + \dot{\varphi}\vec{k} = -\frac{\dot{\psi}}{\rho\cos\psi}\vec{g}_\varphi + \dot{\varphi}\left(\vec{g}_\rho\sin\psi + \frac{1}{\rho}\vec{g}_\psi\cos\psi\right)$$

$$\overset{*}{\vec{g}}_{\varphi} = \vec{c}_0(\dot{\rho}\cos\psi - \rho\dot{\psi}\sin\psi) = \frac{1}{\rho\cos\psi}(\dot{\rho}\cos\psi - \rho\dot{\psi}\sin\psi)\vec{g}_{\varphi}$$

$$\left[\vec{\omega}_{P\varphi}, \vec{g}_{\varphi}\right] = \left[-\dot{\psi}\,\vec{c}_0 + \dot{\varphi}(\vec{\rho}_0\sin\psi + \vec{v}_0\cos\psi), \vec{c}_0\rho\cos\psi\right] = -\dot{\varphi}(\vec{\rho}_0\cos\psi - \vec{v}_0\sin\psi)\rho\cos\psi$$

$$\vec{\omega}_{P\varphi} = -\dot{\vec{\psi}} + \dot{\vec{\varphi}} = \dot{\psi}\,\vec{c}_0 + \dot{\varphi}\vec{k} = -\frac{\dot{\psi}}{\rho\cos\psi}\vec{g}_{\varphi} + \dot{\varphi}\left(\vec{g}_{\rho}\sin\psi + \frac{1}{\rho}\vec{g}_{\psi}\cos\psi\right)$$

$$\frac{d\vec{g}_3}{dt} = \frac{d\vec{g}_{\psi}}{dt} = \dot{\rho}\,\vec{v}_0 + \rho(-\dot{\varphi}\vec{c}_0\sin\psi - \dot{\psi}\vec{\rho}_0)$$

$$\overset{*}{\vec{g}}_{\psi} = \dot{\rho}\,\vec{v}_0 = \frac{\dot{\rho}}{\rho}\vec{g}_{\psi},$$

$$\left[\vec{\omega}_{P\psi}, \vec{g}_{\psi}\right] = -\dot{\varphi}\vec{g}_{\varphi}tg\,\psi - \dot{\psi}\vec{g}_{\psi} = \left[-\dot{\psi}\,\vec{c}_0 + \dot{\varphi}(\vec{\rho}_0\sin\psi + \vec{v}_0\cos\psi), \rho\vec{v}_0\right]$$

$$\vec{\omega}_{P\psi} = -\dot{\vec{\psi}} + \dot{\vec{\varphi}} = \dot{\psi}\,\vec{c}_0 + \dot{\varphi}\vec{k} = -\frac{\dot{\psi}}{\rho\cos\psi}\vec{g}_{\varphi} + \dot{\varphi}\left(\vec{g}_{\rho}\sin\psi + \frac{1}{\rho}\vec{g}_{\psi}\cos\psi\right)$$

Angular velocities of the basic vectors of each position vector tangent space of mass particle motion in spherical curvilinear coordinate systems are:

$$\vec{\omega}_{(\alpha)P} = -\dot{\vec{\psi}}_{(\alpha)} + \dot{\vec{\varphi}}_{(\alpha)} = \dot{\psi}_{(\alpha)}\vec{c}_{0(\alpha)} + \dot{\varphi}_{(\alpha)}\vec{k}$$
$$\vec{\omega}_{(\alpha)P} = -\dot{\psi}_{(\alpha)}\vec{c}_{0(\alpha)} + \dot{\varphi}_{(\alpha)}\left(\vec{\rho}_{0(\alpha)}\sin\psi_{(\alpha)} + \vec{v}_{0(\alpha)}\cos\psi_{(\alpha)}\right)$$
$$\alpha = 1,2,3,...,N$$

2.2.4. Dimensional extension of the position vector tangent spaces of the reheonomic mechanical system in generalized curvilinear coordinate systems

Considered discrete mechanical system is constrained by G geometrical stationary constraints in the form:

$$f_{\beta}\left(q_{(1)}{}^1, q_{(1)}{}^2, q_{(1)}{}^3, q_{(2)}{}^1, q_{(2)}{}^2, q_{(2)}{}^3, ..., q_{(N)}{}^1, q_{(N)}{}^2, q_{(N)}{}^3\right) = 0, \beta = 1,2,3....G \quad (12)$$

and by R geometrical rheonomic constraints in the form (see Ref. [23]):

$$f_{\gamma}\left(q_{(1)}{}^1, q_{(1)}{}^2, q_{(1)}{}^3, q_{(2)}{}^1, q_{(2)}{}^2, q_{(2)}{}^3, ..., q_{(N)}{}^1, q_{(N)}{}^2, q_{(N)}{}^3, \phi_{\gamma}(t)\right) = 0,$$
$$\gamma = 1,2,3....R \quad\quad\quad\quad\quad\quad\quad\quad (13)$$

Considered system is rheonomic system with $p = 3N - G$ degree of the system mobility, and with $n = 3N - G - R$ degrees of the freedom. For the n generalized independent coordinates we take q^i, $i = 1,2,3,....,n$. Also, we introduce additional subsystem of the R rheonomic coordinates $q^{0\gamma} = q^{n+\gamma} = \phi_{\gamma}(t)$, $\gamma = 1,2,3....R$ which correspond to number of rheonomic constraints. Then we have extended system of the generalized curvilinear coordinates q^i, $i = 1,2,3,....,n,...,n+\gamma,......,n+R$. Then we know that subsystem of R rheonomic coordinates $q^{0\gamma} = q^{n+\gamma} = \phi_{\gamma}(t)$, $\gamma = 1,2,3....R$ contain known rheonomic coordinates as functions of the time. But, force of the rheonomic constraints change are unknown (see Ref. [21]).

Let us now take into account that first n coordinates of the position vectors of the mass particles are independent generalized coordinates. Extended system of the

generalized coordinates containing independent coordinates q^i, $i = 1,2,3,....,n$ and rheonomic coordinates $q^{0\gamma} = q^{n+\gamma} = \phi_\gamma(t)$, $\gamma = 1,2,3....R$, then it is possible to list in the form:

$$q^1 = q_{(1)}{}^1,$$
$$q^2 = q_{(1)}{}^2,$$
$$q^3 = q_{(1)}{}^3,$$
$$q^4 = q_{(2)}{}^1,$$
$$q^5 = q_{(2)}{}^2,$$
$$q^6 = q_{(2)}{}^3..$$
$$.......,$$

$$.......,$$
$$q^{n-5} = q_{(n-1)}{}^1,$$
$$q^{n-4} = q_{(n-1)}{}^2,$$
$$q^{n-3} = q_{(n-1)}{}^3$$
$$q^{n-2} = q_{(n)}{}^1,$$
$$q^{n-1} = q_{(n)}{}^2,$$
$$q^n = q_{(n)}{}^3$$

$$q^{0\gamma} = q^{n+\gamma} = \phi_\gamma(t), \gamma = 1,2,3....R \tag{14}$$

On the basic of the listed system (14), we can conclude that in considered case, we use coordinates of the positions vectors of the first $K \le \dfrac{n}{3} = \dfrac{1}{3}(3N - G - R)$ mass particle as generalized independent coordinates.

Then on the basis of previous for the coordinates of the geometrical point which correspond to the mass particle positions at arbitrary moment of the motion, we can write:

$$N_1\left(q^1 = q_{(1)}{}^1, q^2 = q_{(1)}{}^2, q^3 = q_{(1)}{}^3\right),$$
$$N_2\left(q^4 = q_{(2)}{}^1, q^5 = q_{(2)}{}^2, q^6 = q_{(2)}{}^3\right), \tag{15}$$
$$...........................,$$
$$N_K\left(q^{3K-2} = q_{(K)}{}^1, q^{3K-1} = q_{(K)}{}^2, q^{3K} = q_{(K)}{}^3\right)$$
$$N_{K+j}\left(q_{(K+j)}{}^1\left(q^1,q^2,......q^n,q_{n+1},.........q^{n+R}\right), q_{(K+j)}{}^2\left(q^1,q^2,......q^n,q_{n+1},.........q^{n+R}\right), q_{(K+j)}{}^3\left(q^1,q^2,......q^n,q_{n+1},.........q^{n+R}\right)\right)$$
$$j = 1,2,3,...,(N-K)$$
$$\bar{\rho}_1\left(q^1 = q_{(1)}{}^1, q^2 = q_{(1)}{}^2, q^3 = q_{(1)}{}^3\right),$$
$$\bar{\rho}_2\left(q^4 = q_{(2)}{}^1, q^5 = q_{(2)}{}^2, q^6 = q_{(2)}{}^3\right), \tag{16}$$
$$...........................,$$
$$\bar{\rho}_K\left(q^{3K-2} = q_{(K)}{}^1, q^{3K-1} = q_{(K)}{}^2, q^{3K} = q_{(K)}{}^3\right)$$
$$\bar{\rho}_{K+j}\left(q^1,q^2,......q^n,q_{n+1},.........q^{n+R}\right), \quad j = 1,2,3,...,(N-K)$$

2.2.5. Concluding remarks

We can see that in extended system of generalized coordinates, we can identified two sets of the position vectors of the mass particles: one set (15) contain K, $K \le \dfrac{n}{3} = \dfrac{1}{3}(3N - G - R)$ position vectors of the mass particles depending of three

generalized coordinates, and second set (16) contain the $N - K \geq \dfrac{G + R}{3}$,

$K \leq \dfrac{n}{3} = \dfrac{1}{3}(3N - G - R)$ position vectors of the mass particles depending of all

$p = 3N - G$ generalized coordinates in general case, or more then of three generalized coordinates.

       Also we can conclude that in extended system of generalized coordinates, we can identified two sets of the position vectors of the mass particles, one set (15) contain the K, $K \leq \dfrac{n}{3} = \dfrac{1}{3}(3N - G - R)$ position vectors of the mass particles with three-dimensional tangent space and each with three basic vectors of this tangent spaces, and second set (16) contain the $N - K \geq \dfrac{G + R}{3}$, $K \leq \dfrac{n}{3} = \dfrac{1}{3}(3N - G - R)$ position vectors of the mass particles with extended dimension of the tangent space and to each tangent space correspond $p = 3N - G$ basic vectors in general case, or more than three basic vectors of the tangent space.

       Open directions for next research and applications. As a possible open directions for next research and application are: an analysis of expressions for generalized Corilis forces introduced by changing position of motion observer from fixed coordinate system to rotate curvilinear coordinate system correspond to vector position tangent space; applications of the previous results for solving problems of the numerous coordinate system properties used in astro-dynamics; extension and proof of extension Lagrange differential equations to the description of the rheonomic system dynamics and necessary generalizations.

       3. ADVANCES IN ANALYTICAL MECHANICS.

3.1. Analytical mechanics of hereditary discrete system vibrations
3.1.1. Introduction

       Integro-differential equations and their applications in development of analytical mechanics of discrete hereditary systems are used by *Gorosko and Hedrih (Stevanović)* (see References III [35-54])

       Research results in area of mechanics of hereditary discrete systems, obtained by Gorosko and Hedrih (Stevanović) (see References IV [35-54]) are generalized and presented in the monograph [35] which contains first completed presentation of the analytical dynamics of hereditary discrete systems. Two classes of dynamically defined and undefined hereditary systems are defined and considered by introducing corresponding restrictions. Main results of mechanics of hereditary discrete systems are presented with new applications important to engineering.

       Approximation of expressions for the coefficients of damping and corresponding decrements as well as for circular frequency of oscillations of hereditary oscillatory systems are obtained with high accuracy in the first and second approximations.

Analogy between hereditary interactions and reactive forces in systems of automatic control is identified and a possibility to extend theory of analytical dynamics of hereditary systems to mechanical systems with automatic control is pointed out (see References [36] and [37] by Gorosko and Hedrih (Stevanović)).

The Lagrange's mechanics of hereditary systems are extended and generalized to thermo-rheological [35,52] and piezo-rheological [35] discrete mechanical systems as well as to discrete mechanical systems with standard light creep elements. .

Analytical dynamics as general science of mechanical system motions was founded by Lagrange (*Joseph Luis Lagrange* (1735-1813)) in the period of his work at Berlin Academy. The Lagrange's book "*Mècanique Analytique*" contains basic analytical methods of mechanics and was published in France in 1788. Introduced analytical methods in Mechanics by Lagrange are main and first base of analytical mechanics in general. Lagrange's equations of second kind and Lagrange's equations of first kind with unwoven Lagrange's multipliplicators of constraints are main fundament of Analytical Dynamics.

Analytical dynamics is largely applied and used in engineering system dynamics and in natural sciences as well as for investigation of mechanical system dynamics and in physics of the microworld.

Mechanics of hereditary continuum is presented by series of fundamental publications and monographs. In current literature term "*hereditary*" and "*rheological*" systems are equivalent. Mechanics of discrete hereditary systems up to a ten years before was presented only by separate single papers and containing only solutions of partial problems.

Research results in area of mechanics of hereditary discrete systems, obtained by authors of this paper, are generalized and presented in the monograph [35], published in 2001 by Gorosko and Hedrih (Stevanović)), which contains first presentation of analytical dynamics of hereditary discrete systems. We can conclude that this monograph contains *complete foundation of analytical dynamics theory of discrete hereditary systems* and by using these results, numerous examples are obtained and solved (see Refs. [35-54]). In this analytical mechanics of hereditary discrete systems, modified Lagrange's differential equations second kind in the form differential and integro-differential forms with kernels of relaxation or rhelogy are derived.

3.1.2. Models of hereditary elements in analytical dynamics of hereditary discrete systems.

Hereditary system is each system which contains mutual hereditary interaction between material particles in the form of one or more coupling constraints with hereditary properties.

Simple visco-elastic element is Voight's type element (Woldemar Voigt, 1859-1919). In the state of extension resultant force appears by two components, one by visco and one by elastic properties in the deformation of visco-elastic element and constitutive stress-strain relation given as relation between force and extension of element in the following form:

$$P(t) = cy(t) + \mu \dot{y}(t) \tag{1}$$

In Mechanics of hereditary continuum in the case of axial (in one direction) stressed and deformed Voight's type body stress strain constitutive relation is expressed by following relation: $\sigma(t) = E\varepsilon(t) + \mu\dot{\varepsilon}(t)$. More acceptable and precise and better compatible with experimental data with real hereditary body properties is model of the standard visco-elastic body (Kelvin and Poyting-Thompson's body). Constitutive stress strain relation given as relation between force and extension of element in the following form:

$$n\dot{P}(t) + P(t) = nc\dot{y}(t) + \tilde{c}y(t) \tag{2}$$

In mechanics of hereditary system constants n , c and $\tilde{c}$ obtain special names: time of relaxation, rigidity coefficients, one momenteneous and prologues one.

For generalized hereditary element model relation between force and deformation is possible to describe by differential equation high order derivative in the following form:

$$\sum_{r=1}^{m} a_k \frac{d^k P}{dt_k} + P(t) = b_0 x + \sum_{k=1}^{m} b_k \frac{d^k x}{dt^k} \tag{3}$$

For more complex viscose elements (represented by the Jeffreys' bidy (J-body) and Lethersich's body) stress-strain state is described by differential equation in the form:

$$n\dot{P}(t) + P(t) = b_1 \dot{y}(t) + nb_2 \ddot{y}(t) \tag{4}$$

Equivalency and analogy of hereditary interactions and reactive forces in systems of automatic control gives possibility to extend theory of analytical dynamics of hereditary systems to mechanical systems with automatic control. For example, automaton with transfer function presented in the following form (see References [36] and [37] by Gorosko and Hedrih (Stevanović)):

$$W(p) = \frac{b_0 + b_1 p + ... + b_n p^n}{1 + a_1 p + ... + a_n p^n} \tag{5}$$

presents a hereditary interaction (3) between material particles of the discrete mechanical system with one degree of freedom.

Parameters of the automaton of arbitrary structures are defined in an experimental way and it is possible to obtain amplitude-phase characteristic. In our opinion there are real possibilities and perspective to use method of amplitude-phase characteristic for experimental obtaining of mechanical characteristic of the hereditary discrete mechanical systems. It is possible to solve some difficulties with identification coefficient of the momenteneous rigidity which appear in the mechanical investigation of the hereditary forms and shortened longtime experiments.

3.1. 3. Integral models of the stress-strain state of the hereditary elements.

There are three mathematical forms for description of constitutive relations of hereditary properties of hereditary interaction [35], in the building of hereditary system's mechanics. These forms are(see References [36] amd [37] by Gorosko and Hedrih (Stevanović)):

1* Differential equation, expressed in the form of dependence reaction force P of the rheological coordinate x, usually presented as deformation or relative displacement of the hereditary constraint in the form (3).

2* Integral equation, expressed in the form of dependence reaction force P of the rheological coordinate y, usually presented as deformation or relative displacement of the hereditary constraint:

$$P(t) = c \left[y(t) - \int_0^t \mathfrak{R}(t-\tau)y(\tau)d\tau \right] \qquad (6)$$

where $\mathfrak{R}(t-\tau) = \dfrac{c-\tilde{c}}{nc} e^{-\frac{1}{n}(t-\tau)}$ is relaxation kernel, and $\beta = \dfrac{1}{n}$ is coefficient of the element relaxation.

This integral relation (6) can be obtained by solving equation (2) with respect to the force P. By this integral equation, the relaxation of the reaction force P depending on the rheological coordinate y, is presented and expressed.

For the case of the generalized standard hereditary element (3) integral equation is possible to obtain in the form (6) in which relaxation kernel $\mathfrak{R}(t-\tau)$ presents sum by sum of exponents.

3* Integral equation, expressed in the form of dependence rheological coordinate y, usually presented deformation or relative displacement of the hereditary constraint and reaction force P:

$$y(t) = \frac{1}{c} \left[P(t) + \int_0^t \mathfrak{K}(t-\tau)P(\tau)d\tau \right] \qquad (7)$$

where $\mathfrak{K}(t-\tau) = \dfrac{c-\tilde{c}}{nc} e^{-\frac{\tilde{c}}{nc}(t-\tau)}$ is kernel of rheology and $\beta_1 = \dfrac{\tilde{c}}{nc}$ is the coefficient of the creep or retardation or rheology.

3.1. 4. Three forms of equations of motions of a hereditary oscillator.

Simple model of a hereditary discrete system is hereditary oscillator with one degree of freedom which contains one material particle with mass m and one standard hereditary element P with material visco-elastic properties defined by following coefficients: n, c and $\tilde{c}$ constitutive stress-strain relation expressed by relation (2) between force $P(t)$ and generalized and rheological coordinate $y(t)$. Then by using principle of dynamical equilibrium of the oscillator it is possible to obtain equation of the oscillator motion in the following form:

$$m\ddot{y}(t) + P(t) = F(t) \qquad (8)$$

where $P(t)$ is resistive reaction of the rheological element, $F(t)$ external forced excitation. Using constitutive relation (2) or (10) for stressed and deformed standard hereditary (rheological) element for eliminating resistive reaction of the rheological

element $\;P(t)\;$ from last equation (8) we obtain three corresponding forms of the equation of motion of the rheological – hereditary oscillator with one degree of freedom listed as follow: one in differential form:

$$nm\dddot{y}(t)+m\ddot{y}(t)+nc\dot{y}(t)+\tilde{c}\,y(t)=n\dot{F}(t)+F(t) \qquad (9)$$

and two in integro-differential forms:

$$m\ddot{y}(t)+c\left[y(t)-\int_{-\infty}^{t}\boldsymbol{\mathfrak{R}}(t-\tau)y(\tau)d\tau\right]=F(t) \qquad (10)$$

$$m\ddot{y}(t)+c\left[y(t)+\int_{-\infty}^{t}\boldsymbol{\mathfrak{K}}(t-\tau)m\ddot{y}(\tau)d\tau\right]=F(t)+c\int_{-\infty}^{t}\boldsymbol{\mathfrak{K}}(t-\tau)F(\tau)d\tau \qquad (11)$$

For the case of the weak singular hereditary oscillator equation of the dynamic equilibrium (oscillator motion) in the differential form is not possible to obtain, but in the integro-differential forms is possible.

3.1. 5. Thermo-rheological pendulum
3.1. 5.1. Light standard thermo-rheological hereditary element

When standard hereditary element is modified by two temperatures $T_K(t)$ and $T_M(t)$, which are introduced by thermo-modification of visco-elastic properties by temperature $T_K(t)$, and by thermo-modification of elasto-viscosic   properties by temperature $T_M(t)$, than constitutive relation between stress and strain state of the thermo-rheological hereditary element (see Ref. [35]) is:

$$n\dot{P}(t)+P(t)+n\dot{F}_M(t)+F_K(t)=nc\dot{\rho}(t)+\tilde{c}\left[\rho(t)-\rho_0\right] \qquad (12)$$

in which

$$F_M(t)=c_M\alpha_M T_M(t),\;\;F_K(t)=c_K\alpha_K T_K(t) \qquad (13)$$

are thermo-elastic forces, and $\rho(t)$ is rheological coordinate, c_M,c_K are coefficients of thermo-elastic rigidity, α_M,α_K are coefficients of thermo-elastic dilatations, n is time of relaxation, and $c,\tilde{c}$ an instantaneous rigidity and a prolonged one of an element.

Constitutive relation (12) of the thermo-rhelogical hereditary element from differential form, we can rewrite in two integro-differential forms.

3.1. 5. 2. Light standard piezo-and thermo-rheological hereditary element

When standard hereditary element is modified by two polarization voltages $U_K(t)$ and $U_M(t)$, which are introduced by piezo-modification of visco-elastic properties of subelement of piezoceramics, by $U_K(t)$ and by piezo-modification of elasto-viscosic properties by $U_M(t)$, and thermo-modified by two temperatures $T_K(t)$ and $T_M(t)$, than constitutive relation between stress and strain state of the piezo-rheological hereditary hybrid element is in the form (12) in which

$$F_M(t)=c_{UM}\alpha_{UM}U_M(t)+c_{TM}\alpha_{TM}T_M(t)$$
$$F_K(t)=c_{UK}\alpha_{UK}U_K(t)+c_{TK}\alpha_{TK}T_K(t) \qquad (14)$$

are thermoelastic and piezo-elastic forces, and $\rho(t)$ is rheological coordinate, c_{TM}, c_{TK} are coefficients of thermo-elastic rigidity, α_{TM}, α_{TK} are coefficients of thermo-elastic dilatations, c_{UM}, c_{UK} are coefficients of piezo-elastic rigidity, α_{UM}, α_{UK} are coefficients of piezo-elastic dilatations n is time of relaxation, and $c, \tilde{c}$ an instantaneous rigidity and a prolonged one of an hybrid element.

3.1. 5.3. Pendulum with standard thermo-rheological hereditary element

The thermo-rheological hereditary pendulum has two degrees of freedom, one degree of motion freedom defined by angular coordinate ϑ and one degree of deformations freedom defined by changeable length of thread as a coordinate $\rho(t)$.

Let us compose the equations of the thermo-rheological pendulum dynamics with thread in which the standard thermo-rheological hereditary element with constitutive stress-strain relation (12) is incorporated. Now, by introducing force $P(t)$ of the extension of the thermorheological hereditary thread from constitutive relation (12) presented into integral form, the equations of the pendulum motion are in the forms (for detail see Reference [52] by Hedrih (Stevanović)):

$$\ddot{\rho} - (\rho_o + \rho(t))\dot{\theta}^2 + g\cos\theta + \frac{c}{m}\left[\rho(t) - \int_0^t \rho(\tau)R(t-\tau)d\tau\right] =$$

$$= \frac{1}{m}F_M(t) - \frac{c}{m(c-\tilde{c})}\int_0^t [F_M(\tau) - F_K(\tau)]R(t-\tau)d\tau P(t) \tag{15}$$

$$(\rho_0 + \rho(t))^2 \ddot{\theta} + 2(\rho_0 + \rho(t))\dot{\theta}\dot{\rho}(t) + g(\rho_0 + \rho(t))\sin\theta = \mathfrak{M}(t) \tag{16}$$

This system is a system with one integro-differential and one differential equation of the thermo-rheological hereditary pendulum with motion in vertical plane.

If the thermo-rheological pendulum is in the horizontal plane, from second differential equation of the previous system, we can obtain the relation between the length of the pendulum thread and of the angular velocity in the following form:

$$\dot{\theta}(t) = \dot{\theta}(0)\left[\frac{\rho_0 + \rho(0)}{\rho_0 + \rho(t)}\right]^2 \tag{17}$$

By introducing this previous expression (17) in the first equation of the system (16) (for the case of horizontal plane) the following integro-differential equation for the pendulum length thread is obtained:

$$\ddot{\rho}(t) - [\dot{\theta}(0)]^2 \frac{[\rho_0 + \rho(0)]^4}{[\rho_0 + \rho(t)]^3} + \frac{c}{m}\left[\rho(t) - \int_0^t \rho(\tau)R(t-\tau)d\tau\right] =$$

$$= \frac{1}{m}F_M(t) - \frac{c}{m(c-\tilde{c})}\int_0^t [F_M(\tau) - F_K(\tau)]R(t-\tau)d\tau P(t) \tag{18}$$

3.1..6. Concluding remarks

Solution of obtained integrdo-differential equation (18) is mathematical problem in analytical mechanics of hereditary discrete system dynamics.

Also, solutions of the similar integro-differential equations are tasks for mathematics in the function of applications in mechanics and engineering system dynamics with hereditary properties.

In the basis of the construction of Lagrange's mechanics of hereditary discrete systems, the classical mechanics principles are used [35]. These principles are: Principle of the work of forces along corresponding possible system displacements, as well as Principle of dynamical equilibrium.

Initial conditions of hereditary system dynamics are very important, containing the history of rheological interactions of the system. Then, it is important to take into account stress-strain history of viscoelastic elements – interactions between hereditary system material particles.

Analogy between hereditary interactions and reactive forces in the systems of automatic control gives possibility to extend theory of analytical dynamics of hereditary systems to mechanical systems with automatic control.

For description of properties of dynamics of a hereditary system by using relaxational or rheological kernel (resolvent), these kernels are expressed by exponential or fractional-exponential forms [35] . Descriptions of hereditary properties of the system by using differential forms (2) and integral form (6) and (7) with exponential kernels are equivalent. For the case of fractional-exponential forms of the kernel (6) and (7) in the integral form corresponding equivalent differential forms not exist.

The Lagrange's mechanics of hereditary systems is extended and generalized to the thermo-rheological [35, 52] and piezo-rheological [35] mechanical systems.

Open directions for next research and applications. Directions for next research in area of mechanics of hereditary discrete system must be focused to find analytical forms of solutions or approximations of solutions of integro-differential equations and to build mathematical theory of the material memory of the history of previous stress and strains in the material before starting system motion and its observation. Mathematical theory for slowing problems with determinations of the initial conditions of the hereditary system is second main task in this area. Present in science, there are numerous numerical approach and numerical experiments over the integro-differential equations and numerical procedure expressed by software tools but for advances in area of analytical dynamics of hereditary systems it is necessary analytical approach, solutions and qualitative methods for evaluations of the system solution stability.

For practical applications in mechanics and engineering system dynamics analytical forms of the approximations of solutions of intgro-differential equations are necessary for easier quantitative estimation larger class of the dynamic phenomena hereditary system behavior. All real constructions and engineering structures are with hereditary properties.

3.2. Analytical mechanics of fractional order discrete system vibrations
3. 2.1. Introduction

Differential fractional order equations and theirs applications in development of analytical dynamics of discrete and continuous fractional order systems with like single and multi-frequency modes, or fractional order modes are important results for applications in different area of science and practice (see References (see References III [39-46]).

Discrete continuum method is based on the continuum discretization and coupling by standard light hereditary, or fractional order elements (see References [49] and [50]). Main nets, main chains and mail fractional order oscillators with main fractional order modes of plane as well as space coupled mechanical chains (cases with ideal elastic, hereditary and fractional order). Fractional order standard light elements have applications in mechanics of continuum (models of longitudinal and transversal oscillations of beams), in biomechanics (mechanical models of double helix DNA chains [45]), to systems with coupled pendulums, as well is in signals transfer (see ReferencesIII.).

3.2.2. Standard light fractional order element

Standard light coupling element of negligible mass is in the form of axially stressed rod without bending, and which has the ability to resist deformation under static and dynamic conditions. **Standard light fractional order creep element** for which the constitutive stress-strain relation for the restitution force as the function of element elongation is given by fractional order derivatives in the form (see References [40] and [41] by Hedrih (Stevanović)):

$$P(t) = -\left\{c_0 x(t) + c_\alpha \mathfrak{D}_t^\alpha [x(t)]\right\} \tag{1}$$

where $\mathfrak{D}_t^\alpha[\bullet]$ is operator of the αth derivative with respect to time t in the following form:

$$\mathfrak{D}_t^\alpha[x(t)] = \frac{d^\alpha x(t)}{dt^\alpha} = x^{(\alpha)}(t) = \frac{1}{\Gamma(1-\alpha)} \frac{d}{dt} \int_0^t \frac{x(\tau)}{(t-\tau)^\alpha} d\tau \tag{2}$$

where c, c_α are rigidity coefficients – momentary and prolonged one, and α a rational number between 0 and 1, $0 < \alpha < 1$.

3.2.3. Governing equations of the fractional order multi-chain plane system model

Coupled governing fractional order differential equations of the multi chain fractional order plane system vibrations, according notation in Figures 5.a* and b*, and determined standard light fractional elements by constitutive relation (1) and (2) , used for coupling of the mass particles, are in the following form:

$$m_{k,j}\ddot{x}_{k,j} = -c_{k-1,j}\left(x_{k,j}-x_{k-1,j}\right)+c_{k,j}\left(x_{k+1,j}-x_{k,j}\right)-c_{\alpha,k-1,j}\mathfrak{D}_t^\alpha\left[x_{k,j}-x_{k-1,j}\right]+$$

$$+c_{\alpha,k,j}\mathfrak{D}_t^\alpha\left[x_{k+1,j}-x_{k,j}\right]-\tilde{c}_{k,(j-1,j)}\left(x_{k,j}-x_{k,j-1}\right)+\tilde{c}_{k,(j,j+1)}\left(x_{k,j+1}-x_{k,j}\right)- \qquad (3)$$

$$-\tilde{c}_{\alpha,k,(j-1,j)}\mathfrak{D}_t^\alpha\left[x_{k,j}-x_{k,j-1}\right]+\tilde{c}_{\alpha,k,(j,j+1)}\mathfrak{D}_t^\alpha\left[x_{k,j+1}-x_{k,j}\right]$$

$$k=1,2,3,4,....,N \ , \ \ j=1,2,3,4,....,M \ .$$
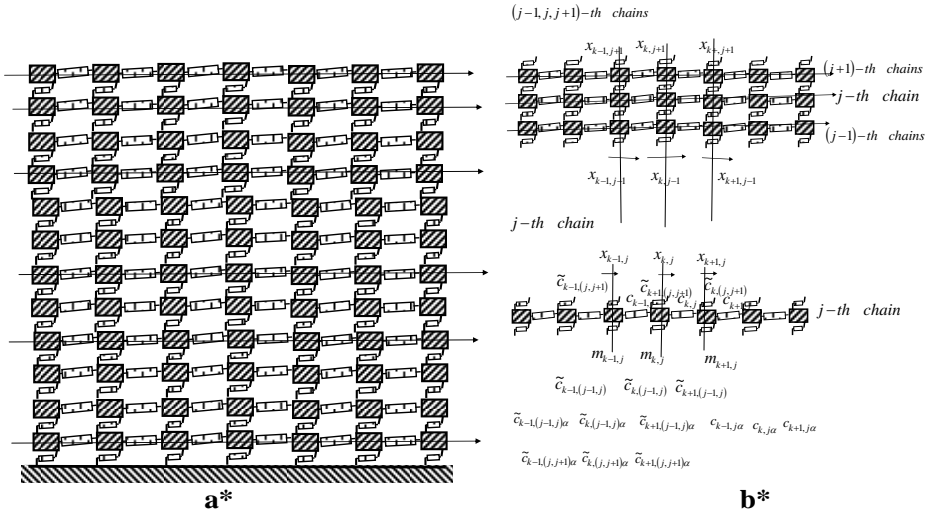
Figure 5. Discrete continuum fractional order model in a plane - Hybrid multi chain fractional order plane system. **(a*)** Hybrid multi-chain system, in one plane and in the form of coupled chains by standard light fractional order elements and in the cantilever form of boundary conditions;   **(b*)**. Three coupled chains $(j-1)$-th , j-th and $(j+1)$-th chains, $j=1,2,3,4,....,M$, as part – subsystem of the hybrid multi chain system with coupling elements and kinetic parameters: masses, stiffnesses and fractional order parameter of the fractional order element and generalized coordinates of the system. Attached a separate j-th chain of the hybrid chain system with notation of the generalized coordinates $x_{i,j}$, $k=1,2,3,4,....,N$, $j=1,2,3,4,....,M$.

For the homogeneous plane system corresponding to the system (3)   of fractional order differential equations let us introduce the coordinate transformation, in accordance with trigonometric method (see References [54] by Rašković and [43], [44] and [40] by Hedrih (Stevanović)) in the following form: :

$$x_{k,j}=\sum_{s=1}^{s=M}\xi_{k(s)}\sin j\varphi_s \ , \ k=1,2,3,4,....,N \ , \ j=1,2,3,4,....,M \cdot \qquad (4)$$

where $\xi_{k(s)}$ are normal coordinates of the main chains of the hybrid plane system as well as generalized coordinates of the s-th main chain from the sets and for the corresponding linear system are in the form: $\xi_{k(s)}=C_{k(s)}\cos\left(\tilde{\omega}_{k(s)}t+\alpha_{k(s)}\right)$ and

$\tilde{\omega}^2_{k(s)} = \tilde{u}_{k(s)}\frac{\kappa c}{m} = 4\frac{\kappa c}{m}\sin^2\frac{\varphi_s}{2}$, $\tilde{u}_{k(s)} \equiv \tilde{u}_{(s)}$ and φ_s are eigen characteristic numbers of the hybrid system obtained by using the trigonometric method (see Refs. [54] by Rašković (1965) and [40], [43], [44], [45], [46] and [48] by Hedrih (Stevanović) (2002, (2004), (2007), (2009) and (2010)) depending of boundary conditions of the transversal chains in the form of the longitudinal chain connections.

$$\frac{m}{c}\ddot{\xi}_{k(s)} - \xi_{k-1(s)} + \left(2 + \kappa\tilde{u}_{k(s)}\right)\xi_{k(s)} - \xi_{k+1(s)} + \mathfrak{D}^\alpha_t\left[-\xi_{k-1(s)} + \left(2\kappa_\alpha + \tilde{\kappa}_\alpha\tilde{u}_{k(s)}\right)\xi_{k(s)} - \xi_{k+1(s)}\right] = 0$$

$$k = 1,2,3,4,....,N \text{ , } s = 1,2,3,....,M \tag{5}$$

Let us introduce the following coordinate transformation:

$$\xi_{k(s)} = \sum_{r=1}^{r=N}\xi_{k(s)(r)} = \sum_{r=1}^{r=N}\eta_{(s)(r)}\sin k\vartheta_r \text{ , } s = 1,2,3,....,M \tag{6}$$

Taking into account that $\sin k\vartheta_r$ is different them zero in arbitrary cases from (3), we can obtain the transformed system of the governing fractional order differential equations (5) of the eigen main chains as well as the transformed basic governing system of fractional order differential equations (3), with respect to the new introduced coordinates $\eta_{(s)(r)}$ containing $M \times N$ independent subsystems for each pair of the $(s)(r)$ from the sets $s = 1,2,3,....,M$ and $r = 1,2,3,4,....,N$ in the following forms:

$$\ddot{\eta}_{(s)(r)} + \omega^2_{(s)(r)}\eta_{(s)(r)} + \omega^2_{\alpha(s)(r)}\mathfrak{D}^\alpha_t\left[\eta_{(s)(r)}\right] = 0 \text{ ,} \tag{7}$$

$$s = 1,2,3,....,M \text{ , } r = 1,2,3,4,....,N$$

where

$$\omega^2_{\alpha(s)(r)} = \frac{c}{m}\left\langle 2(\kappa_\alpha - 1) + u_{(s)(r)} + (\tilde{\kappa}_\alpha - \kappa)\tilde{u}_{k(s)}\right\rangle \text{, } s = 1,2,3,....,M \text{ , } r = 1,2,3,4,....,N \tag{8}$$

This last system of fractional order differential equations (7) represents $M \times N$ independent partial fractional order differential equations describing independent fractional order oscillators each with one degree of freedom and eigen normal coordinate $\eta_{(s)(r)}$, $s = 1,2,3,....,M$, $r = 1,2,3,4,....,N$ of the considered fractional order hybrid system and containing N sets of the M eigen main chains normal coordinates $\eta_{(s)(r)}$, $s = 1,2,3,....,M$, $r = 1,2,3,4,....,N$. Then, we can conclude that simultaneously with determination of the normal coordinates of the eigen main chains, we determine as well as normal coordinates of the considered hybrid fractional order plane system vibrations with $M \times N$ degrees of freedom. Also, we can conclude that normal coordinates for the linear system, correspond to the normal coordinates of the corresponding fractional order system and expressions for generalized coordinate transformation to the eigen normal coordinates of the basic linear system vibrations, we can use for the corresponding coordinate transformation of the corresponding fractional order hybrid system vibrations to the eigen normal coordinates.

3.2.4. Eigen factional order signals and eigen main chain signals in the fractional order multi-chain plane system model

Type of the obtained fractional order differential equations in the system (7) is same as in numerous author's papers, but with different coefficients. These coefficients

are sets of eigen circular frequencies $\omega^2_{(s)(r)}$ and fractional order material properties characteristic numbers $\omega^2_{\alpha(s)(r)}$ in the form:

$$\omega^2_{(s)(r)} = \frac{c}{m}\left[4\kappa\sin^2\frac{\varphi_s}{2} + 2(1-\cos\vartheta_r)\right] , \quad s=1,2,3,\dots,M , r=1,2,3,4,\dots,N \tag{9}$$

$$\omega^2_{\alpha(s)(r)} = \frac{c}{m}\left\langle 2(\kappa_\alpha-1) + 2(1-\cos\vartheta_r) + 4\tilde{\kappa}_\alpha\sin^2\frac{\varphi_s}{2}\right\rangle, \quad s=1,2,3,\dots,M , r=1,2,3,4,\dots,N \tag{10}$$

which depend of boundary multi-chain system conditions determining characteristic numbers: φ_s and ϑ_r (see Refs. [54] by Rašković (1965) and [40], [43], [44], [45], [46] and [48] by Hedrih (Stevanović)).

Now, taking into account solutions of the fractional order differential equation (see Reference [38] by Bačlić and Atanacković (2000)), for the system of the fractional order differential equations (7), we can write corresponding solutions of $\eta_{(s)(r)}$, $s=1,2,3,\dots,M , r=1,2,3,4,\dots,N$, in the form of fractional order like one frequency time functions which are eigen main modes and normal coordinate $\eta_{(s)(r)}$ of the fractional order plane system in the following expansion:

$$\eta_{(s)(r)}(t) = \eta_{(s)(r)}(0)\sum_{k=0}^{\infty}(-1)^k \omega^{2k}_{\alpha(s)(r)} t^{2k} \sum_{j=0}^{k}\binom{k}{j}\frac{(\mp 1)^j \omega^{2j}_{\alpha(s)(r)} t^{-\alpha j}}{\omega^{2j}_{(s)(r)}\Gamma(2k+1-\alpha j)} +$$

$$+ \dot{\eta}_{(s)(r)}(0)\sum_{k=0}^{\infty}(-1)^k \omega^{2k}_{\alpha(s)(r)} t^{2k+1} \sum_{j=0}^{k}\binom{k}{j}\frac{(\mp 1)^j \omega^{-2j}_{\alpha(s)(r)} t^{-\alpha j}}{\omega^{2j}_{(s)(r)}\Gamma(2k+2-\alpha j)} \tag{11}$$

$$s=1,2,3,\dots,M , r=1,2,3,4,\dots,N$$

This last expressions (11) determines eigen normal fraction order like one frequency modes of the hybrid fractional order system corresponding to one eigen circular frequency and corresponding eigen fractional order properties characteristic number (10) of material fractional order properties of standard light elements. Also, we can conclude that the expressions (11) are mathematical descriptions of the main normal fractional order like one frequency signals.

Now, taking into account coordinate transformation:

$$\xi_{k(s)} = \sum_{r=1}^{r=N}\xi_{k(s)(r)} = \sum_{r=1}^{r=N}\eta_{(s)(r)}\sin k\vartheta_r \tag{12}$$

$$x_{k,j} = \sum_{s=1}^{s=M}\xi_{k(s)}\sin j\varphi_s = \sum_{s=1}^{s=M}\sum_{r=1}^{r=N}\eta_{(s)(r)}\sin k\vartheta_r \sin j\varphi_s \tag{13}$$

and solutions (11), we obtain expressions for the like multi-frequency fractional order generalized coordinate in the following form:

1* eigen normal coordinates for obtaining eigen main chains and generalized coordinate of the eigen main chains,

$$\xi_{p(s)} = \sum_{r=1}^{r=N}\eta_{(s)(r)}(0)\sin p\vartheta_r \sum_{k=0}^{\infty}(-1)^k \omega^{2k}_{\alpha(s)(r)} t^{2k} \sum_{j=0}^{k}\binom{k}{j}\frac{(\mp 1)^j \omega^{2j}_{\alpha(s)(r)} t^{-\alpha j}}{\omega^{2j}_{(s)(r)}\Gamma(2k+1-\alpha j)} +$$

$$+ \sum_{r=1}^{r=N}\dot{\eta}_{(s)(r)}(0)\sin p\vartheta_r \sum_{k=0}^{\infty}(-1)^k \omega^{2k}_{\alpha(s)(r)} t^{2k+1} \sum_{j=0}^{k}\binom{k}{j}\frac{(\mp 1)^j \omega^{-2j}_{\alpha(s)(r)} t^{-\alpha j}}{\omega^{2j}_{(s)(r)}\Gamma(2k+2-\alpha j)} \tag{14}$$

$$p = 1,2,3,...,N \text{ , } s = 1,2,3,....,M$$

2* generalized coordinate of the hybrid fractional order system:

$$x_{p,q} = \sum_{s=1}^{s=M} \sum_{r=1}^{r=N} \sin p \vartheta_r \sin q \varphi_s \sum_{r=1}^{r=N} \eta_{(s)(r)}(0) \sin p \vartheta_r \sum_{k=0}^{\infty} (-1)^k \omega_{\alpha(s)(r)}^{2k} t^{2k} \sum_{j=0}^{k} \binom{k}{j} \frac{(\mp 1)^j \omega_{\alpha(s)(r)}^{2j} t^{-\alpha j}}{\omega_{(s)(r)}^{2j} \Gamma(2k+1-\alpha j)} +$$

$$+ \sum_{s=1}^{s=M} \sum_{r=1}^{r=N} \sin p \vartheta_r \sin q \varphi_s \sum_{r=1}^{r=N} \dot{\eta}_{(s)(r)}(0) \sin p \vartheta_r \sum_{k=0}^{\infty} (-1)^k \omega_{\alpha(s)(r)}^{2k} t^{2k+1} \sum_{j=0}^{k} \binom{k}{j} \frac{(\mp 1)^j \omega_{\alpha(s)(r)}^{-2j} t^{-\alpha j}}{\omega_{(s)(r)}^{2j} \Gamma(2k+2-\alpha j)}$$

$$p = 1,2,3,...,N \text{ , } Q = 1,2,3,....,M$$

$$(15)$$

3.2.5. Eigen factional order signals and eigen main chain signals in the fractional order multi-chain space system model

For the homogeneous fractional order multi-chain space system dynamics, presented in Figure 6, by the similar way as in previous chapter III.2.4. is possible to write system of covering fractional order differential equations by use coordinate notation from Figure 6, and corresponding material system coordinates.   Then let introduce the following coordinate transformation:

$$x_{(i),(j),(k)} = \sum_{s=1}^{s=K} \xi_{(i),(j)}^{(s)} \sin k\varphi_s \text{ , } i = 1,2,3,4,....,N \text{ , } j = 1,2,3,4,....,M \text{ , } k = 1,2,3,....,K .$$

$$(16)$$

where $\xi_{(i),(j)}^{(s)}$, $i = 1,2,3,4,....,N$, $j = 1,2,3,4,....,M$ for each $s = 1,2,3,....,K$, are normal coordinates of the main plane subsystems $R^{(s)}$, $s = 1,2,3,....,K$ in the form of the independent K plane nets each consisting of the coupled M chains each with N degrees of freedom.

φ_s, $s = 1,2,3,....,K$ are eigen characteristic numbers of the hybrid system and according trigonometric method (see Refs. [54] by Rašković (1965) and [40], [43], [44], [45], [46] and [48] by Hedrih (Stevanović)) depending on boundary conditions of the transversal coupled chains in the form of the normal direction of chain connections between parallel plane nets, determined by direction of increasing indices $k = 1,2,3,....,K$.   Each of these K main and independent plane nets are with $N \times M$ degree of freedom with $N \times M$ normal coordinates $\xi_{(i),(j)}^{(s)}$, $i = 1,2,3,4,....,N$, $j = 1,2,3,4,....,M$ for each $s = 1,2,3,....,K$ and are like multi frequency fractional order time functions form K independent subsets of circular frequencies $\omega_{(i),(j)}^{(s)}$ and corresponding fractional order characteristic numbers $\omega_{\alpha,(i),(j)}^{(s)}$ $i = 1,2,3,4,....,N$, $j = 1,2,3,4,....,M$ for each $s = 1,2,3,....,K$.
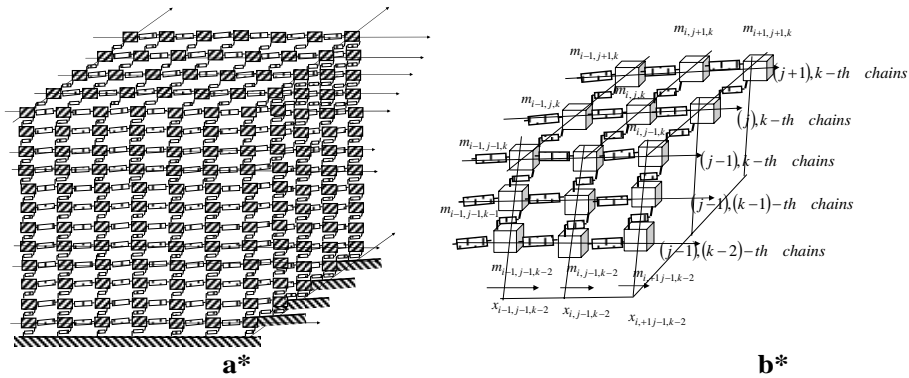
Figure 6. Discrete continuum fractional order space model - Hybrid multi chain fractional order space system. **(a*)** Hybrid multi-chain system, in space and in the form of coupled chains by standard light fractional order elements and in the cantilever form of boundary conditions; **(b*)**. The coupled chains $(j-1),k$ -th , j,k -th and $(j+1),k$ -th chains, and $(j-1),k$ -th , $(j-1),(k-1)$ -th , and $(j-1),(k-2)$ -th, $j=1,2,3,4,....,M$, $k=1,2,3,....,K$ as part – subsystem of the hybrid multi chain system with coupling elements and kinetic parameters: masses, stiffnesses and fractional order parameter of the fractional order element and generalized coordinates of the system, with notation of the generalized coordinates $x_{i,j,k}$, $k=1,2,3,4,....,N$, $j=1,2,3,4,....,M$, $k=1,2,3,....,K$.

Taking into account that $\sin k\varphi_s$ is different them zero in arbitrary cases from system of governing fractional order differential equations, we can obtain the transformed basic governing system of fractional order differential equations with respect to the coordinates $\xi^{(s)}_{(i),(j)}$, $i=1,2,3,4,....,N$, $j=1,2,3,4,....,M$ containing K independent subsystems of coupled fractional order differential equations of like multi-frequency $N \times M$ -frequency main plane nets for each s from the set of $s=1,2,3,....,K$ in the following forms:

$$\frac{m}{c}\ddot{\xi}^{(s)}_{(i),(j)} - \xi^{(s)}_{(i-1),(j)} + \left(2 + \kappa\tilde{u}^{(s)}_{(i),(j)}\right)\xi^{(s)}_{(i),(j)} - \xi^{(s)}_{(i+1),(j)} + \kappa\left[-\xi^{(s)}_{(i),(j-1)} + 2\xi^{(s)}_{(i),(j)} - \xi^{(s)}_{(i),(j+1)}\right] +$$
$$+ \kappa_\alpha\mathfrak{D}^\alpha_t\left[-\xi^{(s)}_{(i-1),(j)} + \left(2 + \kappa\tilde{u}^{(s)}_{(i),(j)}\right)\xi^{(s)}_{(i),(j)} - \xi^{(s)}_{(i+1),(j)}\right] + \kappa_\alpha\mathfrak{D}^\alpha_t\left[-\xi^{(s)}_{(i),(j-1)} + 2\xi^{(s)}_{(i),(j)} - \xi^{(s)}_{(i),(j+1)}\right] = 0$$

$$i=1,2,3,4,....,N \ , \ j=1,2,3,4,....,M \ , \ s=1,2,3,....,K \qquad\qquad (17)$$

Previous obtained K subsets of fractional order differential equations describing dynamics of the main subsystems is expressed by new coordinates $\xi^{(s)}_{(i),(j)}$, $i=1,2,3,4,....,N$, $j=1,2,3,4,....,M$ containing K independent subsystems for each s from the set of $s=1,2,3,....,K$.

These subsystems present K mathematical descriptions of dynamics of independent eigen main plane (or surface) nets containing coupled chains with corresponding subset of the eigen circular frequencies and corresponding fractional order characteristic

numbers of main plane (surface) nets. Through these eigen main plane nets is possible to transfer subset of the signals with frequencies from the corresponding subset of the eigen circular frequencies. These signals are fractional order like $N \times M$ frequency signals.

Next approach is similar as in the previous chapter III.2.4. for system containing coupled chains in one plane. Then, due to the limited length of the paper, we will not to present all derivatives and suppose writer to follow previpus chapter to obtain independent subsystems of the fractional order differential equations describing main independent fractional order oscillators each with one degree of freedom, in the form:

$$\ddot{\zeta}^{(s)(r)(p)} + \omega^2_{(s)(r)(p)}\zeta^{(s)(r)(p)} + \omega^2_{\alpha(s)(r)(p)}\mathfrak{D}^{\alpha}_t\left[\zeta^{(s)(r)(p)}\right] = 0 , \tag{18}$$

$$s = 1,2,3,....,K , \quad r = 1,2,3,....,M , \quad p = 1,2,3,....,N$$

where

$$\xi^{(s)}_{(i),(j)} = \sum_{r=1}^{r=M} \eta^{(s)(r)}_{(i)} \sin j\vartheta_r , \quad i = 1,2,3,4,....,N , \quad j = 1,2,3,4,....,M , \quad s = 1,2,3,....,K \tag{19}$$

$$\eta^{(s)(r)}_{(i)} = \sum_{p=1}^{p=N} \zeta^{(s)(r)(p)}\eta^{(s)(r)}_{(i)} \sin i\psi_p \quad , \quad i = 1,2,3,4,....,N . \quad s = 1,2,3,....,K ,$$

$$r = 1,2,3,....,M \tag{20}$$

Previous system (18) contains $N \times M \times K$ independent fractional order differential equations each only along one coordinate $\zeta^{(s)(r)(p)}$, $s = 1,2,3,....,K$, $r = 1,2,3,....,M$, $p = 1,2,3,....,N$. . These coordinates $\zeta^{(s)(r)(p)}$, $s = 1,2,3,....,K$, $r = 1,2,3,....,M$, $p = 1,2,3,....,N$, are normal coordinates of the hybrid discrete fractional order space system containing parallel coupled chains in the parallel planes and in the parallel lines in these planes.

Number of fractional order partial oscillators is equal to the product $N \times M \times K$ and equal to the number of the system degrees of freedom.

3.2.6. Concluding remarks

Then we can conclude that through eigen main plane (surface) nets $R^{(s)}$, $s = 1,2,3,....,K$, it is possible to transfer like $N \times M$ -eigen frequency fractional order signals as independent on other subsets of plane like $N \times M$ eigen frequency fractional order signals in other eigen main plane nets $R^{(s)}$, $s = 1,2,3,....,K$.

Each eigen main fractional order plane nets $R^{(s)}$, $s = 1,2,3,....,K$ is possible to decompose into M independent eigen chains, in total there are $M \times K$ main independent chains of all space system, with normal coordinates $\eta^{(s)(r)}_{(i)}$ $i = 1,2,3,4,....,N$, $s = 1,2,3,....,K$, $r = 1,2,3,....,M$ of these independent eigen chains . Then we can conclude that through each independent eigen main chain is possible to transfer like N - frequency fractional order signal, as well as that coordinate $\eta^{(s)(r)}_{(i)}$ are N - frequency fractional order time functions with corresponding main chains sub set of N - frequencies and corresponding characteristic fractional order properties numbers.

From the last obtained system (18) containing $N \times M \times K$ independent fractional order differential equations each along one normal coordinate $\zeta^{(s)(r)(p)}$, $s = 1,2,3,....,K$, $r = 1,2,3,....,M$, $p = 1,2,3,....,N$ we can conclude that each of these normal coordinates of the system is like one frequency fractional order time function with eigen circular frequency from the set $\omega^2_{(s)(r)(p)}$, $s = 1,2,3,....,K$, $r = 1,2,3,....,M$, $p = 1,2,3,....,N$ and fractional order characteristic numbers $\omega^2_{\alpha(s)(r)(p)}$, $s = 1,2,3,....,K$, $r = 1,2,3,....,M$, $p = 1,2,3,....,N$ describing fractional order properties of the system eigen vibrations. Number of fractional order partial oscillators is equal to the product $N \times M \times K$ and equal to the number of the system's degrees of freedom. Then we obtain normal coordinates for the transfer of one frequency fractional order signals through space fractional order vibration structure.

Then, we can conclude that simultaneously with determination of the normal coordinates of the eigen main nets and eigen main chains we determine as well as normal coordinates of the considered hybrid fractional order system with $N \times M \times K$ degree of freedom. Also, we can conclude that normal coordinates for the linear system, corresponding to normal coordinates of the corresponding fractional order space system and expressions for generalized coordinate transformations to the eigen normal coordinates of the basic linear system we can use for the corresponding coordinate transformation of the corresponding fractional order space hybrid system to the eigen normal coordinates for the considered hybrid system.

Open directions for next research and applications. Directions for next research in area of mechanics of fractional order discrete system must be focused to find analytical forms of solutions or approximations of solutions of fractional order differential equations different types and integrals.

Also, applications of the fractional derivatives and fractional integrals for describing constitutive relations of different types and sources of material . Research in this area nust be focused also to the experimental investigation of the material constants and parameters defined by fractional order derivatives and operators.

For practical applications in mechanics and engineering system dynamics analytical forms of the approximations of solutions of fractional order differential equations are necessary for easier quantitative estimation larger class of the dynamic phenomena fractional order system behavior. All real constructions and engineering structures are with plastic properties.

4. Advances in elastodynamics, nonlinear dynamics and hybrid system dynamics

4.1. Krilov-Bogolyubov-Mitropolyski asymptotic method of nonlinear mechanics, method of constant variation and averaging method

The different first approximations of solutions of nonlinear differential equations have very large applications in engineering practice for fast evaluations of the kinetic parameters of engineering dynamics (see Reference [55-57] by Hedrih (Stevanović) and [58-60] by by Hedrih (Stevanović) and Simonović). Some time these

first approximation are used for engineering practice with enough precisions and not necessary to use second and higher approximation. One of the main reason that in this part we take into consideration a comparison between first approximation obtained by different method, as well as used different starting known solution for obtaining first approximation.

Let compare three first approximations of the solution of a nonlinear differential equation with small nonlinearity, describing dynamics of nonlinear oscillator with one degree of freedom (see Figure 5.a*) , in the form (see Reference [55-57] by Hedrih (Stevanović)):

$$\ddot{x}_1(t) + 2\delta_1 \dot{x}_1(t) + \omega_1^2 x_1(t) = -\widetilde{\omega}_{N1}^2 x_1^3(t), \text{ for } \delta_1 \neq 0, \ \varepsilon \neq 0, \ \omega_1^2 > \delta_1^2 \tag{1}$$

in which $\delta_1 = \varepsilon_1 \widetilde{\delta}_1$ and $\widetilde{\omega}_{N1}^2 = \varepsilon \widetilde{\widetilde{\omega}}_{N1}^2$, and ε and ε_1 are small parameters.

We use three different approach and three methods for obtaining first approximation of the previous nonlinear differential equation (1). First is starting known analytical solution of a corresponding linearized differential equation which correspond to nonlinear differential equation (1).

IV.1.1* In first case, for starting known solution, we can take solution of the linear differential equation in the following form:

$$\ddot{x}_1(t) + 2\delta_1 \dot{x}_1(t) + \omega_1^2 x_1(t) = 0, \text{ for } \delta_1 \neq 0, \ \varepsilon = 0, \ \omega_1^2 > \delta_1^2 \tag{2}$$

with known analytical solution in the form:

$$x_1(t) = R_{01} e^{-\delta_1 t} \cos(p_1 t + \alpha_{01}), \text{ for } \delta_1 \neq 0, \ \varepsilon = 0, \ \omega_1^2 > \delta_1^2 \tag{3}$$

in which circular frequency of damped vibration is in the form $p_1 = \sqrt{\omega_1^2 - \delta_1^2}$ and, R_{01} and α_{01} are integral constant depending of initial conditions. Amplitude of this oscillation is in the form $R_{01} e^{-\delta_1 t}$ and decreasing with time.

4.1.2* For finding first approximation of the nonlinear differential equation (1), we take starting known analytical solution (3) of linearized differential equation in the form (2) and as a possible firs approximation of the solution we take into consideration the following

$$x_1(t) = R_1(t) e^{-\delta_1 t} \cos \Phi_1(t) , \text{ for } \delta_1 \neq 0, \ \varepsilon \neq 0, \ \omega_1^2 > \delta_1^2 \tag{4}$$

in which $a(t) = R_1(t) e^{-\delta_1 t}$ amplitude and full phase $\Phi_1(t) = p_1 t + \phi_1(t)$ contain unknown functions of time $R_1(t)$ and $\phi_1(t)$ which need to determine. For this fist approach, we applied Lagrange method of variation of constants to the known solution (3) of the linearized differential equation corresponding to nonlinear differential equation (see Reference [55-56] by Hedrih (Stevanović)). After obtaining system of differential equation along unknown functions of time $R_1(t)$ and $\phi_1(t)$ we applied average to the obtained members along one period of the $T_a = \dfrac{2\pi}{p_1} = \dfrac{2\pi}{\sqrt{\omega_1^2 - \delta_1^2}}$ damping vibrations.

Then, after differentiation along time of the proposed approximation of the solution (4) we obtain:

$$\dot{x}_1(t) = -\delta_1 R_1(t)e^{-\delta_1 t}\cos\Phi_1(t) - R_1(t)e^{-\delta_1 t}p_1\sin\Phi_1(t) +$$
$$+ \dot{R}_1(t)\,e^{-\delta_1 t}\cos\Phi_1(t) - R_1(t)e^{-\delta_1 t}\dot{\phi}_1(t)\sin\Phi_1(t) \qquad (5)$$

to which we introduce condition that this first derivative (5) of the proposed first approximation of the solution (4) have same form as solution (3) of the corresponding linearized differential equation (2), by other words, this condition express the following: that this first derivative (5) of the proposed first approximation of the solution (4) have

same form as in the case that unknown function of time $R_1(t)$ and $\phi_1(t)$ are constant.

After applying introduced previous condition we obtain first derivative of the proposed first approximation (4) of the solution in the following form:

$$\dot{x}_1(t) = -\delta_1 R_1(t)e^{-\delta_1 t}\cos\Phi_1(t) - R_1(t)e^{-\delta_1 t}p_1\sin\Phi_1(t) \qquad (6)$$

and the following condition

$$\dot{R}_1(t)\cos\Phi_1(t) - R_1(t)\dot{\phi}_1(t)\sin\Phi_1(t) = 0 \qquad (7)$$

that unknown functions of time $R_1(t)$ and $\phi_1(t)$ must to satisfy.

Second derivative of the proposed first approximation (4) of the solution is in the following form:

$$\ddot{x}_1(t) = \left(\delta_1^2 R_1(t) - R_1(t)p_1^2 - \delta_1\dot{R}_1(t) - R_1(t)p_1\dot{\phi}_1\right)e^{-\delta_1 t}\cos\Phi_1(t) +$$
$$+ \left(\delta_1 R_1(t)\dot{\phi}_1 + 2\delta_1 R_1(t)p_1 - \dot{R}_1(t)p_1\right)e^{-\delta_1 t}\sin\Phi_1(t) \qquad (8)$$

Alter introducing first (6) and second (8) derivatives of the proposed first approximation (4) of the solution into nonlinear differential equation (1) and taking into account condition (7) we obtain the system of differential equations along unknown

functions of time $R_1(t)$ and $\phi_1(t)$ in following form:

$$\dot{R}_1(t)\cos\Phi_1(t) - R_1(t)\dot{\phi}_1(t)\sin\Phi_1(t) = 0$$
$$R_1(t)p_1\dot{\phi}_1\cos\Phi_1(t) + \dot{R}_1(t)p_1\sin\Phi_1(t) = \tilde{\omega}_{N1}^2 e^{-2\delta_1 t}[R_1(t)]^3\cos^3\Phi_1(t) \quad (9)$$

Previous obtained system of differential equations along unknown functions of

time $R_1(t)$ and $\phi_1(t)$ present a non homogeneous algebra system along derivatives of

unknown function of time $\dot{R}_1(t)$ and $\dot{\phi}_1(t)$ with determinate in the form:

$$\Delta = \begin{vmatrix} \cos\Phi_1(t) & -R_1(t)\sin\Phi_1(t) \\ p_1\sin\Phi_1(t) & R_1(t)p_1\cos\Phi_1(t) \end{vmatrix} = R_1(t)p_1\left[\cos^2\Phi_1(t) + \sin^2\Phi_1(t)\right] = R_1(t)p_1 \quad (10)$$

with following solutions:

$$\dot{R}_1(t) = \frac{\Delta_1}{\Delta} = \frac{\tilde{\omega}_{N1}^2}{p_1}e^{-2\delta_1 t}[R_1(t)]^3\cos^3\Phi_1(t)\sin\Phi_1(t)$$

$$\dot{\phi}_1(t) = \frac{\Delta_2}{\Delta} = \frac{\tilde{\omega}_{N1}^2}{p_1}e^{-2\delta_1 t}[R_1(t)]^2\cos^4\Phi_1(t), \quad \text{for } \delta_1 \neq 0, \ \varepsilon \neq 0, \ \omega_1^2 > \delta_1^2 \quad (11)$$

Then, after obtaining previous system of differential equation (11) along

unknown functions of time, $R_1(t)$ and $\phi_1(t)$, we applied average to the obtained

members along full phase $\Phi_1(t) = p_1 t + \phi_1(t)$ in interval $\Phi \in [-, 2\pi]$ correspond to one period of the $T_a = \dfrac{2\pi}{p_1} = \dfrac{2\pi}{\sqrt{\omega_1^2 - \delta_1^2}}$ damping vibrations:

$$\dot{R}_1(t) = \frac{1}{2\pi} \int_0^{2\pi} \frac{\tilde{\omega}_{N1}^2}{p_1} e^{-2\delta_1 t} [R_1(t)]^3 \cos^3 \Phi_1(t) \sin \Phi_1(t) d\Phi_1(t)$$

$$\dot{\phi}_1(t) = \frac{1}{2\pi} \int_0^{2\pi} \frac{\tilde{\omega}_{N1}^2}{p_1} e^{-2\delta_1 t} [R_1(t)]^2 \cos^4 \Phi_1(t) d\Phi_1(t), \text{ for } \delta_1 \neq 0, \tag{12}$$

$\varepsilon = 0$, $\omega_1^2 > \delta_1^2$

Then, we obtain a system of differential equations along unknown functions of time $R_1(t)$ and $\phi_1(t)$ in first averaged approximation:

$$\dot{R}_1(t) = 0$$

$$\dot{\phi}_1(t) = \frac{3}{8} \frac{\tilde{\omega}_{N1}^2}{p_1} e^{-2\delta_1 t} [R_1(t)]^2 \text{ for } \delta_1 \neq 0, \ \varepsilon \neq 0, \ \omega_1^2 > \delta_1^2 \tag{13}$$

After integration of the previous system of differential equations along unknown functions of time $R_1(t)$ and $\phi_1(t)$ in first averaged approximation for known initial values in first approximation $t = 0$, $R_1(0) = R_{01}$ и $\phi_1(0) = \phi_{01} = -\dfrac{3}{16\delta_1 p_1} \tilde{\omega}_{N1}^2 R_{01}^2 + \alpha_{01}$ we obtain:

$$R_1(t) = R_{01} = const$$

$$\phi_1(t) = -\frac{3}{16\delta_1 p_1} \tilde{\omega}_{N1}^2 R_{01}^2 \left(e^{-2\delta_1 t} - 1 \right) + \phi_{01} = -\frac{3}{16\delta_1 p_1} \tilde{\omega}_{N1}^2 R_{01}^2 e^{-2\delta_1 t} + \alpha_{01}, \tag{14}$$

for $\delta_1 \neq 0$, $\varepsilon \neq 0$, $\omega_1^2 > \delta_1^2$

where $\alpha_{01} = \phi_{01} + \dfrac{3}{16\delta_1 p_1} \tilde{\omega}_{N1}^2 R_{01}^2$, and full phase is in the form:

$$\Phi_1(t) = p_1 t + \phi_1(t) = p_1 t - \frac{3}{16\delta_1 p_1} \tilde{\omega}_{N1}^2 R_{01}^2 \left(e^{-2\delta_1 t} - 1 \right) + \phi_{01} = p_1 t - \frac{3}{16\delta_1 p_1} \tilde{\omega}_{N1}^2 R_{01}^2 e^{-2\delta_1 t} + \alpha_{01},$$

for $\delta_1 \neq 0$, $\varepsilon \neq 0$, $\omega_1^2 > \delta_1^2$ \tag{15}

Then first averaged approximation of the solution of the nonlinear differential equation with hard cubic small nonlinearity (1)

$$x_1(t) = R_{01} e^{-\delta_1 t} \cos\left(p_1 t - \frac{3}{16\delta_1 p_1} \tilde{\omega}_{N1}^2 R_{01}^2 e^{-2\delta_1 t} + \alpha_{01} \right),$$

for $\delta_1 \neq 0$, $\varepsilon = 0$, $\omega_1^2 > \delta_1^2$ \tag{16}

In the case that, we have a nonlinear differential equation with sogt cubic small nonlinearity in the following form:

$$\ddot{x}_1(t) + 2\delta_1\dot{x}_1(t) + \omega_1^2 x_1(t) = +\tilde{\omega}_{N1}^2 x_1^3(t) \text{ for } \delta_1 \neq 0, \ \varepsilon \neq 0, \ \omega_1^2 > \delta_1^2 \tag{17}$$

on the basis of the previous obtained firs averaged approximation of the solution we can write:

$$x_1(t) = R_{01}e^{-\delta_1 t}\cos\left(p_1 t + \frac{3}{16\delta_1 p_1}\tilde{\omega}_{N1}^2 R_{01}^2 e^{-2\delta_1 t} + \alpha_{01}\right),$$

for $\delta_1 \neq 0$, $\varepsilon \neq 0$, $\boldsymbol{\omega_1^2} > \delta_1^2$ \hfill (18)

where for known initial values in first approximation $t = 0$, $R_1(0) = R_{01}$ иand

$\phi_1(0) = \phi_{01} = \dfrac{3}{16\delta_1 p_1}\tilde{\omega}_{N1}^2 R_{01}^2 + \alpha_{01}$ we obtain:

$$\alpha_{01} = \phi_{01} - \frac{3}{16\delta_1 p_1}\tilde{\omega}_{N1}^2 R_{01}^2. \tag{19}$$

For the case that for $\delta_1 = 0$ we can use the system of differential equations along unknown functions of time $R_1(t)$ and $\phi_1(t)$ in first averaged approximation (13) and before integration put $\delta_1 = 0$, and after that applied integration, or find limes of the solutions (16) and 18) for $\delta_1 \to 0$, and taking into account that is $\lim\limits_{\delta_1 \to 0}\dfrac{\left(e^{-2\delta_1 t} - 1\right)}{\delta_1} = -2t$,

obtain first averaged approximation of the solution of nonlinear differential equations (1) as well as (17)

$$\ddot{x}_1(t) + 2\delta_1\dot{x}_1(t) + \omega_1^2 x_1(t) = \mp\tilde{\omega}_{N1}^2 x_1^3(t) \tag{20}$$

in the following form:

$$x_1(t) = R_{01}e^{-\delta_1 t}\cos\left(p_1 t \mp \frac{3}{16\delta_1 p_1}\tilde{\omega}_{N1}^2 R_{01}^2 e^{-2\delta_1 t} + \alpha_{01}\right)$$

for $\delta_1 \neq 0$, $\varepsilon \neq 0$, $\boldsymbol{\omega_1^2} > \delta_1^2$ \hfill (21)

where $\alpha_{01} = \phi_{01} \pm \dfrac{3}{16\delta_1 p_1}\tilde{\omega}_{N1}^2 R_{01}^2$

$$x_1(t) = R_{01}\cos\left\langle\!\!\left(\omega_1 \pm \frac{3}{8\omega_1}\tilde{\omega}_{N1}^2 R_{01}^2\right)t + \phi_{01}\right\rangle,$$

for $\delta_1 = 0$, $\varepsilon_1 = 0$ $\varepsilon \neq 0$, $\omega_1^2 > \delta_1^2$ \hfill (22)

4.1. 2.1* In second case, for taking starting known solution for obtaining approximation of solution of the nonlinear differential equation (1), we can take solution of the linear differential equation in the following form:

$$\ddot{\tilde{x}}(t) + p^2\tilde{x}(t) = 0 \tag{23}$$

with known analytical solution in the form:

$$\tilde{x}(t) = a\cos(p_1 t + \alpha_0) \tag{24}$$

in which circular frequency of harmonic vibration is in the form $p = \sqrt{\omega_1^2 - \delta_1^2}$ and, a and α_0 are integral constant depending of initial conditions. Amplitude of this oscillation is in the form a and is constant and no depending of time.

a*   b*
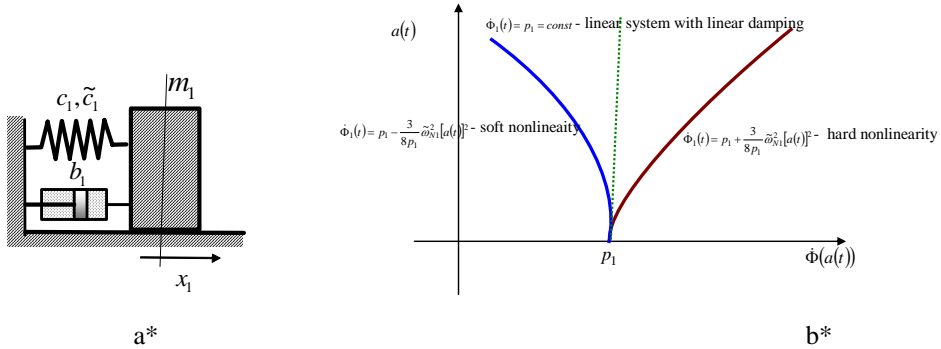
Figure 7. a* Nonlinear system with one degree of freedom. b* Amplitude-frequency characteristic for free vibrations of the system damped nonlinear dynamics with of soft and hard nonlinearity

4.1. 2.2* For that case, we must transform nonlinear differential equation (1) taking into account the following generalized coordinate transformation:

$$\tilde{x} = x e^{\delta_1 t} \text{ or } x = \tilde{x} e^{-\delta_1 t} . \tag{25}$$

After generalized coordinate transformation an transformation of differential nonlinear equation (1), we obtain:

$$\frac{d^2 \tilde{x}}{dt^2} + p^2 \tilde{x} = -\tilde{\omega}_{N1}^2 \tilde{x}^3(t) e^{-2\delta_1 t} \tag{26}$$

where

$$\varepsilon \tilde{f}\left(\tilde{x} e^{-\delta_1 t}\right) e^{\delta_1 t} = -\tilde{\omega}_{N1}^2 \tilde{x}^3(t) e^{-2\delta_1 t} . \tag{27}$$

Let start with general form of the nonlinear differential equation in the form:

$$\frac{d^2 x}{dt^2} + 2\delta \frac{dx}{dt} + \omega^2 x = \varepsilon f\left(x, \frac{dx}{dt}\right) \tag{28}$$

For small parameter $\varepsilon = 0$ we obtain linear differential equation

$$\frac{d^2 x}{dt^2} + 2\delta \frac{dx}{dt} + \omega^2 x = 0 \tag{29}$$

with solution:

$$x = a e^{-\delta t} \cos\psi = e^{-\delta t} \tilde{x} \tag{30}$$

with amplitude $a e^{-\delta t}$ with phase $\psi = pt + \alpha$, where $p = \sqrt{\omega^2 - \delta^2}$ and also:

$$\frac{da}{dt} = 0 \qquad \frac{d\psi}{dt} = p = const \tag{31}$$

In which a and α are determined by their initial values. By generalized coordinate transformation (25) nonlinear differential equation (28) take the following form:

$$\left(\frac{d^2 \tilde{x}}{dt^2} + \left\langle \omega^2 - \delta^2 \right\rangle \tilde{x} \right) = \tilde{\varepsilon f}\left(\tilde{x} e^{-\delta t}, \frac{d\tilde{x}}{dt} e^{-\delta t} \right) e^{\delta t} \tag{32}$$

or

$$\frac{d^2 \tilde{x}}{dt^2} + p^2 \tilde{x} = \tilde{\varepsilon f}\left(\tilde{x} e^{-\delta t}, \frac{d\tilde{x}}{dt} e^{-\delta t} \right) e^{\delta t} = \tilde{\tilde{\varepsilon f}}\left(\tilde{x}, \frac{d\tilde{x}}{dt}, \tau \right) \tag{33}$$

In beginning, we supposed that $\delta = \varepsilon_1 \tilde{\delta}$, and that ε_1 is same order of small value as ε and that $\tau = \varepsilon t$ is slow changing time and that for one period $T_a = \dfrac{2\pi}{p}$ change of the system dynamics is small, and that function $\tilde{\varepsilon f}\left(\tilde{x} e^{-\delta t}, \dfrac{d\tilde{x}}{dt} e^{-\delta t} \right) = \tilde{\tilde{\varepsilon f}}\left(\tilde{x}, \dfrac{d\tilde{x}}{dt}, \tau \right)$ satisfy all necessary conditions for application of the asymptotic method Ktilov-Bogolyubov-Mitropolyski for application f the method with slow changing system dynamics parameters and with slow changing time (see Reference [61-68] by Yu. A. Mitropolyskiy).

Then, the n-the asymptotic approximation of the two parametric family of a one frequency solution of differential equation (33) we suppose in the form:

$$x e^{\delta t} = \tilde{x} = a \cos\psi + \varepsilon U_1(a, \psi, \tau) + \varepsilon^2 U_2(a, \psi, \tau) + \ldots \tag{34}$$

where $U_1(a, \psi, \tau), U_2(a, \psi, \tau)$, …. periodic functions of $\psi = pt + \phi(t)$, with period 2π , and no containing first harmonic of ψ , and where amplitude and phase a and ψ are unknown functions which are determined by system of differential equations corresponding order n-th asymptotic approximation along amplitude and phase in the form:

$$\frac{da}{dt} = \varepsilon A_1(a, \tau) + \varepsilon^2 A_2(a, \tau) + \ldots$$

$$\frac{d\psi}{dt} = p + \varepsilon B_1(a, \tau) + \varepsilon^2 B_2(a, v) + \ldots \tag{35}$$

where $A_1(a, \tau)$, $A_2(a, \tau)$, …., and $B_1(a, \tau), B_2(a, v)$,…. Are unknown functions of amplitude and slow changing time.

Introducing, on the basis of previous formulated condition we can write:

$$\int_0^{2\pi} U_j(a, \psi, \tau) e^{i\psi} d\psi = 0 \qquad\qquad j = 1, 2, \ldots m \tag{36}$$

Then, we calculate first and second derivatives of the n-th supposed asymptotic approximation ot the solution in the following forms:

$$\frac{d\tilde{x}}{dt} = -ap\sin\psi + \varepsilon\left\{ A_1(a,\tau)\cos\psi - aB_1(a,\tau)\sin\psi + \varepsilon\frac{\partial U_1}{\partial \tau} + p\frac{\partial U_1}{\partial \psi} \right\} + \tag{36}$$

$$+ \varepsilon^2\left\{ A_1(a,\tau)\cos\psi - aB_2(a,\tau)\sin\psi + A_1(a,\tau)\frac{\partial U_1}{\partial a} + B_1(a,\tau)\frac{\partial U_1}{\partial \psi} + p\frac{\partial U_2}{\partial \psi} + \varepsilon\frac{\partial U_2}{\partial \tau} \right\} + \varepsilon^3 \ldots$$

$$\frac{d^2\tilde{x}}{dt^2} = -ap^2\cos\psi +$$

$$+ \varepsilon\left\{-2pA_1\sin\psi - 2paB_1\cos\psi + \frac{dA_1(a,\tau)}{d\tau}\frac{d\tau}{dt}\cos\psi - a\frac{dB_1(a,\tau)}{d\tau}\frac{d\tau}{dt}\sin\psi + p^2\frac{\partial^2 U_1}{\partial\psi^2} + \frac{\partial^2 U_1}{\partial t^2} + p\frac{\partial^2 U_1}{\partial t\partial\psi}\right\} + \quad (37)$$

$$+ \varepsilon^2\left\{\left(A_1\frac{dA_1}{da} - aB_1^2 - 2paB_2\right)\cos\psi - \left(2pA_2 + 2A_1B_1 + A_1a\frac{dB_1}{da}\right)\sin\psi\right\} +$$

$$+ \varepsilon^2\left\{2pA_1\frac{\partial^2 U_1}{\partial a\partial\psi} + 2pB_1\frac{\partial^2 U_1}{\partial\psi^2} + p^2\frac{\partial^2 U_2}{\partial\psi^2} + \frac{\partial^2 U_2}{\partial t^2} + \varepsilon p\frac{\partial^2 U_2}{\partial\varpi\psi} + \varepsilon A_1\frac{\partial^2 U_1}{\partial\varpi a} + ...\right\} +$$

$$+ \varepsilon^3 ...$$

After introducing previous asysmptotic aproximation of the solution (34) and their first and second derivatives into nonlinear differential equation (33) and applying method of equal coefficient of the small parameters un left and right side of transformation of nonlinear differential equation, we obtain series of the relation between unknown functions $U_1(a,\psi,\tau), U_2(a,\psi,\tau)$, ..., . $A_1(a,\tau)$, $A_2(a,\tau)$, ..., and $B_1(a,\tau), B_2(a,v)$,..... For the reason that we need only first asymptotic approximation of the solution, we take into account the following relation obtained from coefficients with first step of the small parameter ε

$$-2pA_1(a.\tau)\sin^2\psi = \tilde{f}\left(e^{-\delta t}\{a\cos\psi\}, e^{-\delta t}\{-ap\sin\psi\}\right)e^{\delta t}\sin\psi$$

$$-2paB_1(a.\tau)\cos^2\psi = \tilde{f}\left(e^{-\delta t}\{a\cos\psi\}, e^{-\delta t}\{-ap\sin\psi\}\right)e^{\delta t}\cos\psi \qquad (38)$$

Taking into account development of the previous expressions along full phase $\psi = pt + \phi(t)$ we obtain relations – equations for obtaining unknown functions $A_1(a,\tau)$ and $B_1(a,\tau)$ in the following form (see Reference [61-68] by Yu. A. Mitropolyskiy).:

$$A_1(a.\tau) = -\frac{1}{2\pi p}\int_0^{2\pi}\tilde{\tilde{f}}\left(e^{-\tilde{\delta}\tau}\{a\cos\psi\}, e^{-\tilde{\delta}\tau}\{-ap\sin\psi\}\right)e^{\tilde{\delta}\tau}\sin\psi d\psi$$

$$B_1(a.\tau) = -\frac{1}{2\pi pa}\int_0^{2\pi}\tilde{\tilde{f}}\left(e^{-\tilde{\delta}\tau}\{a\cos\psi\}, e^{-\tilde{\delta}\tau}\{-ap\sin\psi\}\right)e^{\tilde{\delta}\tau}\cos\psi d\psi \qquad (39)$$

Then taking into account that $\varepsilon f\left(\tilde{x}e^{-\delta t}, \frac{d\tilde{x}}{dt}e^{-\delta t}\right) = \varepsilon\tilde{\tilde{f}}\left(\tilde{x}, \frac{d\tilde{x}}{dt}, \tau\right)$ and differential

equation in the form (33) and introducing (27) in previous obtained expression (33) for obtaining functions $A_1(a,\tau)$ and $B_1(a,\tau)$ we can write:

$$\varepsilon A_1(a.t) = 0$$

$$\varepsilon B_1(a.\tau) = \frac{1}{2\pi p}\tilde{\omega}_{N1}^2 a^2 e^{-2\tilde{\delta}\tau}\frac{3}{4} = \frac{3}{8\pi p}\tilde{\omega}_{N1}^2 a^2 e^{-2\delta t} \qquad (40)$$

where δ_1 ($\delta_1 = \varepsilon_1\tilde{\delta}_1$ and $\tilde{\omega}_{N1}^2 = \varepsilon\tilde{\tilde{\omega}}_{N1}^2$, for ε and ε_1 same order small values.

Then, system of differential equation (35) along a and ψ in the first asymptotic approximation is possible to write in the following form:

$$\frac{da}{dt} = 0$$

$$\frac{d\psi}{dt} = p + \frac{3}{8\pi p}\tilde{\omega}_{N1}^2 a^2 e^{-2\delta t} \qquad (41)$$

and first asymptotic approximation of the solution in the form

$$xe^{\delta t} = \tilde{x} = a\cos\psi \text{ or in the form: } x = \tilde{x}e^{-\delta t} = ae^{-\delta t}\cos\psi \tag{42}$$

In the previous first asymptotic approximation full phase is in the form:

$$\psi(t) = pt - \frac{3}{16\delta_1 p}\tilde{\omega}_{N1}^2 R_{01}^2\left(e^{-2\delta_1 t} - 1\right) + \psi_{01} = p_1 t - \frac{3}{16\delta_1 p}\tilde{\omega}_{N1}^2 R_{01}^2 e^{-2\delta_1 t} + \alpha_{01}, \tag{43}$$

for $\delta_1 \neq 0$, $\varepsilon \neq 0$, $\omega_1^2 > \delta_1^2$, $p = \sqrt{\omega_1^2 - \delta_1^2}$.

We can see and conclude that first approximation of the solution of considered nonlinear differential equation (1) obtained by application different methods, first method of variation constant with average along full phase, and asymptotic method by Krilov – Bogolyubov-Mitropolyski (see Reference [61-68] by Yu. A. Mitropolyskiy) give us same results, but with different methods and proof.

4.1.3.1* In third case, for taking starting known solution for obtaining approximation of solution of the nonlinear differential equation (1), we can take solution of the linear differential equation in the following form:

$$\ddot{x} + \omega_1^2 x = 0 \tag{44}$$

with known analytical solution in the form:

$$x(t) = a\cos(\omega_1 t + \alpha_9). \tag{45}$$

in which circular frequency of harmonic vibration is in the form ω_1 and, a and α_0 are integral constant depending of initial conditions. Amplitude of this oscillation is in the form a and is constant and no depending of time.

4.1.3.2* For that case, for finding first approximation of the nonlinear differential equation (1), we take starting known analytical solution (45) of linearized differential equation in the form (44) and as a possible firs approximation of the solution we take into consideration the following

$$x(t) = a(t)\cos\Phi(t)., \text{ for } \delta_1 \neq 0, \ \varepsilon \neq 0, \ \omega_1^2 > \delta_1^2 \tag{46}$$

in which $a(t)$ amplitude and full phase $\Phi_1(t) = \omega_1 t + \phi_1(t)$ contain unknown functions of time $a(t)$ and $\phi_1(t)$ which must to determine. For this third approach, we applied known Krilov-Bogolyubov-Mitropolyski asymptotic method of average to find first asymptotic approximation of the solution of nonlinear differential equation (1).

Then we start with nonlinear differential equation

$$\ddot{x} + \omega_1^2 x = \varepsilon f(x, \dot{x}), \tag{47}$$

and suppose first asymptotic approximation in the form:

$$x(t) = a(t)\cos\Phi(t). \tag{48}$$

where unknown functions $a(t)$ and $\Phi(t)$ are determined from the system of differential equations of first asymptotic approximation (see Reference [61-68] by Yu. A. Mitropolyskiy) in the following form:

$$\frac{da(t)}{dt} = \varepsilon A(a),$$

$$\frac{d\Phi(t)}{dt} = \omega_1 + \varepsilon B(a),$$ (48)

where

$$A(a) = -\frac{1}{2\pi\omega_1} \int_0^{2\pi} f(a\cos\Phi, -a\omega_1\sin\Phi)\sin\Phi \, d\Phi,$$

$$B(a) = -\frac{1}{2\pi a\omega_1} \int_0^{2\pi} f(a\cos\Phi, -a\omega_1\sin\Phi)\cos\Phi \, d\Phi.$$ (49)

For our nonlinear differential equation (1)

$$f(x, \dot{x}) = -\left(2\delta\,\dot{x} + \omega_N^2 x^3\right),$$ (50)

where je $\delta_1 = \varepsilon_1\delta$, $\tilde{\omega}_{N1}^2 = \varepsilon\omega_N^2$.

Taking into account initial values in first approximation $t = 0 : a(0) = a_o$, $\Phi(0) = \Phi_o$ we obtain that

$$a(t) = a_o e^{-\varepsilon\delta t} = a_o e^{-\delta_1 t},$$

$$\Phi(t) = \omega_1 t - \frac{3}{16\delta\omega_1}\omega_N^2 a_o^2\left(e^{-2\varepsilon\delta t} - 1\right) + \Phi_o = \omega_1 t - \frac{3}{16\delta_1\omega_1}\omega_{N1}^2 a_o^2\left(e^{-2\delta_1 t} - 1\right) + \Phi_o.$$ (51)

and first asymptotic approximation of the solution of a nonlinear differential equation (1) around harmonic starting known analytical solution, we can write in the following form:

$$x(t) = a_o e^{-\delta_1 t} \cos\left[\omega_1 t - \frac{3}{16\delta_1\omega_1}\omega_{N1}^2 a_o^2\left(e^{-2\delta_1 t} - 1\right) + \Phi_o\right].$$ (52)

From this obtained first asymptotic approximation (52) of the solutions of nonlinear differential equation (1) with starting known analytical harmonic solution (45) in the case for damping coefficient tends to zero $\delta_1 \to 0$, and taking into account that is

$\lim_{\delta_1 \to 0} \dfrac{\left(e^{-2\delta_1 t} - 1\right)}{\delta_1} = -2t$, we obtain first asymptotic approximation of the solution for

conservative nonlinear system vibrations in the form as in the previous two case obtained first approximation of solution of same nonlinear differential equation (1) by use different method and different starting known analytical solution.

4.1.4. Concluding remarks

Let we made a general review of the obtained results for approximately solving of the nonlinear differential equation with small cubic nonlinearity in the form: :

$$\ddot{x}_1(t) + 2\delta_1\dot{x}_1(t) + \omega_1^2 x_1(t) = \mp\tilde{\omega}_{N1}^2 x_1^3(t)$$ (53)

in which hard or soft, refers to $\mp$ sign approximately, $\delta_1 = \varepsilon_1\tilde{\delta}_1$ and $\tilde{\omega}_{N1}^2 = \varepsilon\tilde{\tilde{\omega}}_{N1}^2$, and ε and ε_1 are small parameters (see Figure 7)..

By use first two methods, starting known analytical solutions in the form (3) and we obtained same first approximation of the solution in the following form:

$$x_1(t) = R_{01} e^{-\delta_1 t} \cos\left(p_1 t \mp \frac{3}{16 \delta_1 p_1} \tilde{\omega}_{N1}^2 R_{01}^2 e^{-2\delta_1 t} + \alpha_{01}\right),$$

for $\delta_1 \neq 0$, $\varepsilon \neq 0$, $\omega_1^2 > \delta_1^2$ (54)

where $\alpha_{01} = \phi_{01} \pm \frac{3}{16 \delta_1 p_1} \tilde{\omega}_{N1}^2 R_{01}^2$. For the case that damping coefficient tends to zero, from this first approximation (54), we obtain first approximation of the solution for conservative nonlinear system dynamics in the following form:

$$x_1(t) = R_{01} \cos\left\langle\left(\omega_1 \pm \frac{3}{8\omega_1} \tilde{\omega}_{N1}^2 R_{01}^2\right) t + \phi_{01}\right\rangle,$$

for $\delta_1 = 0$, $\varepsilon_1 = 0$ $\varepsilon \neq 0$, $\omega_1^2 > \delta_1^2$ (55)

We can see that circular frequency of nonlinear dynamic of conservative system is not isochroous and depends of initial conditions – initial amplitude.

For the case that coefficient of the cubic nonlinearity tends to zero, from this first approximation (54), we obtain known analytical solution of the linear no conservative system dynamics in the following form:

$$x_1(t) = R_{01} e^{-\delta_1 t} \cos(p_1 t + \alpha_{01}),$$

for $\delta_1 \neq 0$, $\varepsilon = 0$, $\omega_1^2 > \delta_1^2$ $\tilde{\omega}_{N1}^2 = o$ (56)

From the third case we start by harmonic known analytical solution in the form (45), we obtain the following first asymptotic approximation of the solution of same nonlinear differential equation:

$$x(t) = a_o e^{-\delta_1 t} \cos\left[\omega_1 t \mp \frac{3}{16 \delta_1 \omega_1} \omega_{N1}^2 a_o^2 \left(e^{-2\delta_1 t} - 1\right) + \Phi_o\right].$$

for $\delta_1 \neq 0$, $\varepsilon \neq 0$, $\omega_1^2 > \delta_1^2$ (57)

This asymptotical approximation is different them in previous case (54) and this is normally because we take different starting analytical known solution if different basic linear differential equations as a two different linearizations of the considered same nonlinear differential equation.

For the case that damping coefficient tends to zero, from this first approximation (57), we obtain first approximation of the solution for conservative nonlinear system dynamics in the following form:

$$x(t) = a_o e^{-\delta_1 t} \cos\left[\left(\omega_1 \pm \frac{3}{16 \delta_1 \omega_1} \omega_{N1}^2 a_o^2\right) t + \Phi_o\right],$$

for $\delta_1 = 0$, $\varepsilon_1 = 0$ $\varepsilon \neq 0$, $\omega_1^2 > \delta_1^2$ (58)

same as in the previous cases (55).

For the case that coefficient of the cubic nonlinearity tends to zero, from this first approximation (57), we cannot obtain known analytical solution of the linear no conservative system dynamics in the form (56) but we obtain:

$$x_1(t) = R_{01} e^{-\delta_1 t} \cos(\omega_1 t + \alpha_{01}),$$

for $\delta_1 \neq 0$, $\varepsilon = 0$, $\omega_1^2 > \delta_1^2$ $\tilde{\omega}_{N1}^2 = o$ (59)

not acceptable, because in this case starting solution was harmonic. In this case if we need harmonic solution we must annulled parameters of cubic nonlinearity and of dumping in the same time.

Then we can conclude that first two approach (54) for obtaining first approximation are more general and more suitable for use in the considered approximation of the solution them (59).

Open directions for next research and applications. Directions for next research in area of approximation must be focused to find analytical forms of approximations of solutions of nonlinear differential equations. Present in science, there are numerous numerical approach and numerical experiments over the nonlinear differential equations for numerical slowing nonlinear one, or coupled system of nonlinear differential equations, but these are only particular solutions without proof that these solutions are right, and general.

For practical applications in mechanics and engineering system dynamics analytical forms of the approximations of solutions are necessary for easier quantitative estimation larger class of the nonlinear dynamic phenomena and nonlinear dynamics of the stem behavior.

4.2. Hybrid system dynamics with complex structures and transfer energy

4.2. 1. Governing coupled partial differential equations of transversal vibrations of coupled axially moving double belt system

The sandwich belt system contain two belts coupled by distributed discrete light, neglected mass, ideally elastic belts with stiffness c m as a elastic layer. The both belts are represented by area of the constant cross sections A along length ℓ between rolling and fixed bearings A and B, and by ρ the density of the belt material. Let suppose that sandwich double belt system is moving in the axial directions x with an axial velocity $v(t)$. The transversal vibrations of the sandwich double belts are represented by the transverse displacements $w_1(x,t)$ of upper belt and $w_2(x,t)$ of lower belt. b is damping coefficient of the damping force distributed along belts. Also, let suppose that displacements are small, and that cross sections during the transverse vibration haven't deplanations. Also, it is supposed that both belts are loaded by active axial force, due to the belts' tension, and external distributed excitations $q_{(i)}(x,t)$, $i = 1,2$ perpendicular to the x-axis, than in stressed state in the belt's cross section appear normal stresses with intensity σ, almost sure constant intensity during the time vibrations and along the length of belt between bearings. Than we can conclude that normal stress σ in belts of sandwich double belt system for a cross section during

vibrations change only direction. For both belts in this double belt system, let's accept a string (wave)-like type model between two rolling bearings.

In Figure 8. a* the kinetic parameters of the transversal forced vibrations of the axially moving sandwich belts are presented, and in 8.b* the elementary segment, with length dx, of the axially moving sandwich belt system excited by external transversal distributed forces and notations of the kinetics parameters are pointed out. $q_1(x,t)$ and $q_2(x,t)$ are external transversal excitations distributed along upper and lower belts between rolling bearings and are function of the coordinate x directed in the direction of the axially moving belt system.

Using d'Alambert principle of dynamical equilibrium and applying to the transversal forced dynamics of the elementary segment of the axially moving sandwich belt with length dx and notations of the kinetics parameters pointed out in Figure 8.b* for both component belts in double belt system, similar as in the paper [75], we can write the following system of the transversal forced vibrations of the component belts in the axially moving double belt system:

$$\rho A dx \frac{D^2 w_1(x,t)}{Dt^2} = -\sigma A \sin \alpha_1 + \sigma A \sin(\alpha_1 + d\alpha_1) -$$

$$-b \frac{D w_1(x,t)}{Dt} dx + c[w_2(x,t) - w_1(x,t)] dx - q_1(x,t) dx$$

$$\rho A dx \frac{D^2 w_2(x,t)}{Dt^2} = -\sigma A \sin \alpha_2 + \sigma A \sin(\alpha_2 + d\alpha_2) -$$

$$\qquad (1)$$

$$-b \frac{D w_2(x,t)}{Dt} dx - c[w_2(x,t) - w_1(x,t)] dx + q_2(x,t) dx$$
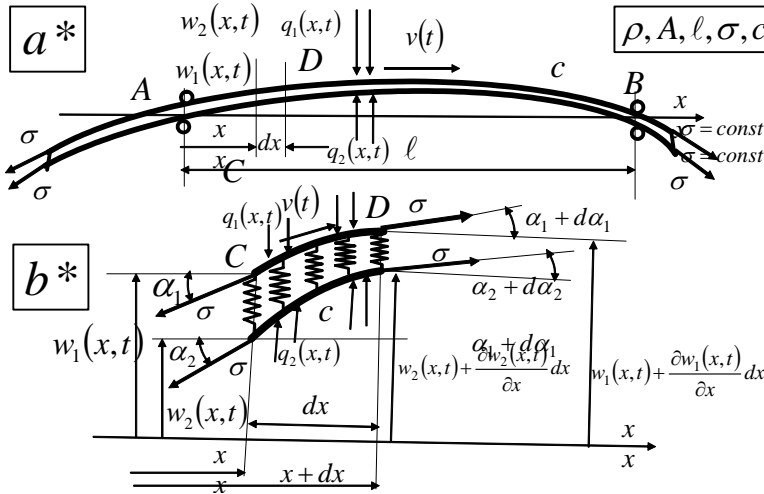

Figure 8. Transversal forced vibrations of the axially moving sandwich belts
a* Kinetics parameters of the transversal forced vibrations of the axially moving sandwich belts

b* Elementary segment of the axially moving sandwich belts with length dx and notations of the kinetics parameters for the case of the forced regime

Having in mind that the transversal belts' displacements are small it is right to take into account the approximations as in Refs. [72] and [75], and also, introducing the following denotation

$$c_0 = \sqrt{\frac{\sigma}{\rho}} \ , \quad \kappa = \sqrt{\frac{c}{\rho A}} \ , \quad 2\delta = \frac{b}{\rho A} \ , \qquad \tilde{q}_i(x,t) = \frac{q_i(x,t)}{\rho A} \tag{2}$$

and the following partial differential operator: $\mathbf{L}_{x,t}[\bullet]$

$$\mathbf{L}_{x,t}[\bullet] = \frac{\partial^2}{\partial t^2} - \left(c_0^2 - v_0^2\right)\frac{\partial^2}{\partial x^2} + 2v_0\frac{\partial^2}{\partial x \partial t} + 2\delta v_0 \frac{\partial}{\partial x} + 2\delta \frac{\partial}{\partial t} + \kappa^2 \tag{3}$$

and for the case $v = v_0 = const$, previous partial differential equations (1) it is easy to rewrite in the following forms:

$$\mathbf{L}_{x,t}[w_1(x,t)] - \kappa^2 w_2(x,t) + \tilde{q}_1(x,t) = 0$$
$$\mathbf{L}_{x,t}[w_2(x,t)] - \kappa^2 w_1(x,t) - \tilde{q}_2(x,t) = 0 \tag{4}$$

These partial differential equations are coupled by last terms.

4.2. 2. Solution of the basic decoupled partial differential equations

By using new independent coordinates in the following form:

$$\xi = x$$
$$\eta = \frac{v_0}{c_0^2 - v_0^2} x + t \tag{5}$$

the partial differential operator (3) obtain the following

$$\tilde{\mathbf{L}}_{\xi,\eta}[\bullet] = \frac{c_0^2}{c_0^2 - v_0^2}\tilde{\mathbf{L}}_{\eta}[\bullet] - \left(c_0^2 - v_0^2\right)\tilde{\mathbf{L}}_{\xi}[\bullet] \tag{6}$$

and corresponding decomposition into two independent operators in the following forms:

$$\tilde{\mathbf{L}}_{\eta}[\bullet] = \left[\frac{\partial^2}{\partial \eta^2} + 2\delta \frac{\partial}{\partial \eta}\right] \tag{7}$$

$$\tilde{\mathbf{L}}_{\xi}[\bullet] = \left[\frac{\partial^2}{\partial \xi^2} - \frac{2\delta v_0}{\left(c_0^2 - v_0^2\right)}\frac{\partial}{\partial \xi} - \frac{\kappa^2}{\left(c_0^2 - v_0^2\right)}\right] \tag{8}$$

then coupled partial differential equations (4) of the moving sandwich belts obtain the following form:

$$\frac{c_0^2}{c_0^2 - v_0^2}\tilde{\mathbf{L}}_{\eta}[w_1(\xi,\eta)] - \left(c_0^2 - v_0^2\right)\tilde{\mathbf{L}}_{\xi}[w_1(\xi,\eta)] - \kappa^2 w_2(\xi,\eta) + \tilde{q}(\xi,\eta)_1 = 0$$

$$\frac{c_0^2}{c_0^2 - v_0^2}\tilde{\mathbf{L}}_{\eta}[w_2(\xi,\eta)] - \left(c_0^2 - v_0^2\right)\tilde{\mathbf{L}}_{\xi}[w_2(\xi,\eta)] - \kappa^2 w_1(\xi,\eta) - \tilde{q}_2(\xi,\eta) = 0 \tag{9}$$

Basic decoupled partial differential equations are:

$$\tilde{\mathbf{L}}_{\xi,\eta}[w_i(\xi,\eta)] = \frac{c_0^2}{c_0^2 - v_0^2}\tilde{\mathbf{L}}_\eta[w_i(\xi,\eta)] - (c_0^2 - v_0^2)\tilde{\mathbf{L}}_\xi[w_i(\xi,\eta)] = 0 \ , i = 1,2 \tag{10}$$

Solution of the partial differential equation type from previous system (10) can be looked for Bernoulli's method of particular integrals in the form of multiplication of two functions (see book [53] by Rašković or Refs. [72] and [75]), from which the first $\mathbf{X}_{(i)}(\xi)$, $i = 1,2$ depends only on space coordinate ξ and the second $\mathbf{Y}_{(i)}(\eta)$, $i = 1,2$ is function of η:

$$w_{(i)}(\xi,\eta) = \mathbf{X}_{(i)}(\xi)\mathbf{Y}_{(i)}(\eta), \ \ i = 1,2 \tag{11}$$

For beginning, the assumed solution (11) is introduced in previous system equation (10) and we obtain two decoupled ordinary differential equations in the following forms:

$$\tilde{\mathbf{L}}_\eta[\mathbf{Y}_{(i)}(\eta)] + k^2 \frac{c_0^2 - v_0^2}{c_0^2}\mathbf{Y}_{(i)}(\eta) = 0 \tag{12}$$

$$\tilde{\mathbf{L}}_\xi[\mathbf{X}_{(i)}(\xi)] + \frac{k^2}{(c_0^2 - v_0^2)}\mathbf{X}_{(i)}(\xi) = 0 \tag{13}$$

and after denotations:

$$\tilde{\omega}^2 = k^2\frac{c_0^2 - v_0^2}{c_0^2} \ , \qquad \tilde{\delta} = \frac{\delta v_0}{(c_0^2 - v_0^2)}, \qquad \tilde{\lambda}^2 = \frac{k^2 - \kappa^2}{(c_0^2 - v_0^2)}, \tag{14}$$

we obtain:

$$\frac{d^2\mathbf{Y}_{(i)}(\eta)}{d\eta^2} + 2\delta\frac{d\mathbf{Y}_{(i)}(\eta)}{d\eta} + \tilde{\omega}^2\mathbf{Y}_{(i)}(\eta) = 0 \tag{15}$$

$$\frac{d^2\mathbf{X}_{(i)}(\xi)}{d\xi^2} - 2\tilde{\delta}\frac{d\mathbf{X}_{(i)}(\xi)}{d\xi} + \tilde{\lambda}^2\mathbf{X}_{(i)}(\xi) = 0 \tag{16}$$

Particular solution of the transversal displacement of the decoupled belts on the elastic Vincler type foundation, described by the partial differential equation (10) is in the form (11) must to satisfy the boundary conditions: displacements in the rolling bearings must be equal to zero:

$$w_{(i)}(x,t)\big|_{x=0} = 0, \ w_{(i)}(\xi,\eta)\big|_{\substack{\xi=0 \\ \eta=t}} = 0, \ \mathbf{X}_{(i)}(0) = 0, \ C_1 = 0, \ i = 1,2,$$

$$w_{(i)}(x,t)\big|_{x=\ell} = 0, \ w_{(i)}(\xi,\eta)\Big|_{\substack{\xi=\ell \\ \eta=\ell\frac{v_0^2}{c_0^2-v_0^2}+t}} = 0, \mathbf{X}_{(i)}(\ell) = 0, \ C_2 e^{\tilde{\delta}\ell}\sin p\ell = 0 \tag{17}$$

and then characteristic equation have the following roots: $p_s = \dfrac{s\pi}{\ell}, s = 1,2,3,4,.......$

Than, we obtain series of particular solutions for each of the characteristic eigen numbers. Eigen amplitude functions are particular solutions of the ordinary differential equation (15) in the following forms (see Refs. [72] and [75]):

$$\mathbf{X}_{(i)s}(\xi) = e^{\tilde{\delta}\xi}\sin p_s\xi = e^{\tilde{\delta}\xi}\sin\frac{s\pi}{\ell}\xi$$

for $\qquad p_{(1,2)s} = \mp\sqrt{\tilde{\lambda}_s^2 - \tilde{\delta}^2} = \frac{s\pi}{\ell} \qquad\qquad \tilde{\lambda} > \tilde{\delta}$ $\qquad\qquad$ (18)

$i = 1,2 \qquad s = 1,2,3,4,.......$

where

$$\tilde{\lambda}_s^2 = \frac{k_s^2 - \kappa^2}{\left(c_0^2 - v_0^2\right)} > \tilde{\delta} = \frac{\delta v_0}{\left(c_0^2 - v_0^2\right)} \qquad\qquad k_s^2 = \tilde{\lambda}_s^2\left(c_0^2 - v_0^2\right) + \kappa^2$$

$$k_s^2 = \frac{\delta^2 v_0^2}{\left(c_0^2 - v_0^2\right)} + \kappa^2 + \left(\frac{s\pi}{\ell}\right)^2\left(c_0^2 - v_0^2\right) \qquad\qquad s = 1,2,3,4,.......$$

$$\text{(19)}$$

$$\tilde{\omega}_s^2 = k_s^2\frac{c_0^2 - v_0^2}{c_0^2} = \frac{\delta^2 v_0^2}{c_0^2} + \kappa^2\frac{c_0^2 - v_0^2}{c_0^2} + \left(\frac{s\pi}{\ell}\right)^2\frac{\left(c_0^2 - v_0^2\right)^2}{c_0^2} > \delta^2$$

Corresponding space - time η-functions are particular solutions of the ordinary differential equation (16) in the following forms (for detail see Ref. [75]):

: $\qquad \mathbf{Y}_{(i)s}(\eta) = e^{-\delta\eta}\left(A_s Ch\,\tilde{q}_s\eta + B_s Sh\,\tilde{q}_s\eta\right)$

for $\ \tilde{q}_{(1,2)s} = \mp\sqrt{\delta^2 - \tilde{\omega}_s^2} \quad \tilde{\omega}_s < \delta$

$\qquad \mathbf{Y}_{(i)s}(\eta) = e^{-\delta\eta}\left(A_s\cos q_s\eta + B_s\sin q_s\eta\right)$

for $\quad q_{(1,2)s} = \mp\sqrt{\tilde{\omega}_s^2 - \delta^2} \qquad\qquad \tilde{\omega}_s > \delta$

$$q_{(1,2)s} = \mp\sqrt{\left(\kappa^2 - \delta^2\right)\frac{c_0^2 - v_0^2}{c_0^2} + \left(\frac{s\pi}{\ell}\right)^2\frac{\left(c_0^2 - v_0^2\right)^2}{c_0^2}} \qquad\qquad \text{(20)}$$

4.2.3. Approximation of the solution of the governing coupled partial differential equations

For solving coupled partial differential equations of transversal forced vibrations of the sandwich double belt system in the form (4) or (9) we take into calculus same eigen amplitude functions $\mathbf{X}_{(i)s}(\xi)$ for both belts in the form (18) and different unknown functions: $\mathbf{Y}_{(1)s}(\eta)$ and $\mathbf{Y}_{(2)s}(\eta)$. Than the solution suppose in the following expansions:

$$w_{(1)}(\xi,\eta) = \sum_{s=1}^{s=\infty}\mathbf{X}_{(1)s}(\xi)\mathbf{Y}_{(1)s}(\eta) = \sum_{s=1}^{s=\infty}e^{\tilde{\delta}\xi}\tilde{\mathbf{X}}_{(1)s}(\xi)\mathbf{Y}_{(1)s}(\eta)$$

$$w_{(2)}(\xi,\eta) = \sum_{s=1}^{s=\infty} \mathbf{X}_{(1)\,s}(\xi)\mathbf{Y}_{(2)\,s}(\eta) = \sum_{s=1}^{s=\infty} e^{\tilde{\delta}\,\xi}\tilde{\mathbf{X}}_{(1)\,s}(\xi)\mathbf{Y}_{(2)\,s}(\eta) \qquad (21)$$

These expansion we put into the equations of the system (9), taking into account (15) and (16) previous system of the equations obtain the simplest form, and after multiplying first differential equation by $e^{-2\tilde{\delta}\,\xi}\mathbf{X}_{(i)r}(\xi)d\xi$ and second by $e^{-2\tilde{\delta}\,\xi}\mathbf{X}_{(i)s}(\xi)d\xi$ and integrating along belt's length ℓ between double belt system bearings and taking into account modified conditions of the orthogonality of eigen amplitude functions $\mathbf{X}_{(i)s}(\xi)$ for both belts in the form (18), as well as that some terms of the sum disappeared for different: $\tilde{\lambda}_s \neq \tilde{\lambda}_r$ for $s \neq r$, and in the corresponding result, we obtain s-th family system of the two coupled ordinary differential equations with respect to the unknown functions $\mathbf{Y}_{(1)s}(\eta)$ and $\mathbf{Y}_{(2)s}(\eta)$ in the following form:

$$\left\{\tilde{\mathbf{L}}_\eta\left[\mathbf{Y}_{(1)s}(\eta)\right] + \tilde{\lambda}_s^2\frac{\left(c_0^2 - v_0^2\right)^2}{c_0^2}\mathbf{Y}_{(1)s}(\eta) - \kappa^2\frac{\left(c_0^2 - v_0^2\right)}{c_0^2}\left[\mathbf{Y}_{(2)s}(\eta) - \mathbf{Y}_{(1)s}(\eta)\right]\right\} = \tilde{Q}_{1s}(\eta)$$

$$\left\{\tilde{\mathbf{L}}_\eta\left[\mathbf{Y}_{(2)s}(\eta)\right] + \tilde{\lambda}_s^2\frac{\left(c_0^2 - v_0^2\right)^2}{c_0^2}\mathbf{Y}_{(2)s}(\eta) + \kappa^2\frac{\left(c_0^2 - v_0^2\right)}{c_0^2}\left[\mathbf{Y}_{(2)s}(\eta) - \mathbf{Y}_{(1)s}(\eta)\right]\right\} = \tilde{Q}_{2s}(\eta) \quad (22)$$

where

$$\tilde{Q}_{(1)s}(\eta) = -\frac{\left(c_0^2 - v_0^2\right)}{c_0^2}\frac{\int_0^\ell \tilde{q}_1(\xi,\eta)\mathbf{X}_{(1)s}(\xi)d\xi}{\int_0^\ell\left[\mathbf{X}_{(1)s}(\xi)\right]^2 d\xi}$$

$$\tilde{Q}_{(2)s}(\eta) = \frac{\left(c_0^2 - v_0^2\right)}{c_0^2}\frac{\int_0^\ell \tilde{q}_2(\xi,\eta)\mathbf{X}_{(1)s}(\xi)d\xi}{\int_0^\ell\left[\mathbf{X}_{(1)s}(\xi)\right]^2 d\xi} \qquad (23)$$

The solution of the system of second order no homogeneous ordinary differential equations (22) for the s-mode in the form of the expansion along eigen amplitude functions $X_{(1)s}(x) = X_{(1)s}(\xi) = X_{(2)s}(\xi)$, in the form (18), can be looked in the form: of the solutions for basic homogeneous system (see Ref. [75]) and we will apply the Lagrange's method of the variations of the constants of the eigen unknown function $\mathbf{Y}_{(1)s}(\eta)$ and $\mathbf{Y}_{(2)s}(\eta)$ in the form (20), introducing for integral constant the following unknown functions $C_{(1)s}(\eta), D_{(1)s}(\eta), M_{(1)s}(\eta), N_{(1)s}(\eta)$ of η for a s-mode, $s = 1,2,3,4,....\infty$. We propose that $C_{(1)s}(\eta), D_{(1)s}(\eta), M_{(1)s}(\eta), N_{(1)s}(\eta)$ are functions of η and we can write:

$$\mathbf{Y}_{(1)s}(\eta) = e^{-\delta\eta}\left\{\left[C_{(1)s}(\eta)\cos\tilde{p}_s\eta + D_{(1)s}(\eta)\sin\tilde{p}_s\eta\right] + \left[M_{(1)s}(\eta)\cos\tilde{\tilde{p}}_s\eta + N_{(1)s}(\eta)\sin\tilde{\tilde{p}}_s\eta\right]\right\} \quad (24)$$

$$\mathbf{Y}_{(2)s}(\eta) = e^{-\delta\eta}\left\{\left[C_{(1)s}(\eta)\cos\tilde{p}_s\eta + D_{(1)s}(\eta)\sin\tilde{p}_s\eta\right] - \left[M_{(1)s}(\eta)\cos\tilde{\tilde{p}}_s\eta + N_{(1)s}(\eta)\sin\tilde{\tilde{p}}_s\eta\right]\right\} \quad (25)$$

where (for detail see Refs. [[72] and [75])

$$\tilde{p}_s = \sqrt{\frac{c_0^2 - v_0^2}{c_0^2}\left\{\left(c_0^2 - v_0^2\right)\left(\frac{s\pi}{\ell}\right)^2 - \delta^2\right\}_s} \quad, \quad s = 1,2,3,4,....... \quad (26)$$

$$\tilde{\tilde{p}}_s = \sqrt{\frac{c_0^2 - v_0^2}{c_0^2}\left\{\left(c_0^2 - v_0^2\right)\left(\frac{s\pi}{\ell}\right)^2 - \delta^2 + 2\kappa^2\right\}}, \quad s = 1,2,3,4,....... \quad (26^*)$$

In order to obtain first and second derivative with respect to η of the proposed forms of functions $\mathbf{Y}_{(1)s}(\eta)$ and $\mathbf{Y}_{(2)s}(\eta)$, we suppose that first derivatives of the functions $Y_{(i)s}(\eta)$, $i=1,2$, $s=1,2,3,4,....\infty$ with respect to the η are equal to the corresponding when coefficients $C_{(1)s}(\eta), D_{(1)s}(\eta), M_{(1)s}(\eta), N_{(1)s}(\eta)$ are constant and then we obtain the two equations-conditions. After introducing first and second derivatives of the proposed functions $Y_{(i)s}(\eta)$, $i=1,2$, $s=1,2,3,4,....\infty$ with respect to η into the system of no homogeneous second order ordinary differential equations (22) for the s-mode in the following form (18) and together with previous conditions for first derivatives, we obtain the system of the no homogeneous algebra equations along unknown first derivative of the unknown coefficients $C_{(1)s}(\eta), D_{(1)s}(\eta), M_{(1)s}(\eta), N_{(1)s}(\eta)$ with respect to η. After solving previous obtained system of the equations we obtain the first derivative of the unknown coefficients $C_{(1)s}(\eta), D_{(1)s}(\eta), M_{(1)s}(\eta), N_{(1)s}(\eta)$ with respect to η and after integrating for unknown coefficients-functions $C_{(1)s}(\eta), D_{(1)s}(\eta), M_{(1)s}(\eta), N_{(1)s}(\eta)$ we have the following expressions:

$$C_{(1)s}(\eta) = C_{(1)0s} - \frac{1}{2\tilde{p}_s}\int_0^\eta e^{\delta\eta}\left[\tilde{Q}_{(1)s}(\eta) + \tilde{Q}_{(2)s}(\eta)\right]\sin\tilde{p}_s\eta\,d\eta$$

$$D_{(1)s}(\eta) = D_{(1)0s} + \frac{1}{2\tilde{p}_s}\int_0^\eta e^{\delta\eta}\left[\tilde{Q}_{(1)s}(\eta) + \tilde{Q}_{(2)s}(\eta)\right]\cos\tilde{p}_s\eta\,d\eta$$

$$M_{(1)s}(\eta) = M_{(1)0s} - \frac{1}{2\tilde{\tilde{p}}_s}\int_0^\eta e^{\delta\eta}\left[\tilde{Q}_{(1)s}(\eta) - \tilde{Q}_{(2)s}(\eta)\right]\sin\tilde{\tilde{p}}_s\eta\,d\eta \qquad (27)$$

$$N_{(1)s}(\eta) = N_{(1)0s} + \frac{1}{2\tilde{\tilde{p}}_s}\int_0^\eta e^{\delta\eta}\left[\tilde{Q}_{(1)s}(\eta) - \tilde{Q}_{(2)s}(\eta)\right]\cos\tilde{\tilde{p}}_s\eta\,d\eta$$

where $\eta = \dfrac{v_0}{c_0^2 - v_0^2} x + t$. Now, previous unknown eigen functions $Y_{(i)s}(\eta)$, $i = 1, 2$,

$s = 1, 2, 3, 4, \ldots \infty$ depending on η for s - forced mode and eigen amplitude functions

$\mathbf{X}_{(1)s}(\xi) = \mathbf{X}_{(2)s}(\xi) = e^{\tilde{\delta}\xi} \sin \dfrac{s\pi}{\ell} \xi$ are in the following form:

$$\mathbf{Y}_{(1)s}(\eta) = e^{-\delta\eta} \left[C_{(1)0s} \cos \tilde{p}_s \eta + D_{(1)0s} \sin \tilde{p}_s \eta \right] + \frac{1}{2\tilde{p}_s} \int_0^\eta e^{-\delta(\eta-\tau)} \left[\tilde{Q}_{(1)s}(\tau) + \tilde{Q}_{(2)s}(\tau) \right] \sin \tilde{p}_s (\eta - \tau) \tau d\tau$$

$$+ e^{-\delta\eta} \left\langle \left[M_{(1)0s} \cos \tilde{\tilde{p}}_s \eta + N_{(1)0s} \sin \tilde{\tilde{p}}_s \eta \right] + \frac{1}{2\tilde{\tilde{p}}_s} \int_0^\eta e^{-\delta(\eta-\tau)} \left[\tilde{Q}_{(1)s}(\tau) - \tilde{Q}_{(2)s}(\tau) \right] \sin \tilde{\tilde{p}}_s (\eta - \tau) d\tau \right\rangle$$

$$\tag{28}$$

$$\mathbf{Y}_{(2)s}(\eta) = e^{-\delta\eta} \left[C_{(1)0s} \cos \tilde{p}_s \eta + D_{(1)0s} \sin \tilde{p}_s \eta \right] - e^{-\delta\eta} \left[M_{(1)0s} \cos \tilde{\tilde{p}}_s \eta + N_{(1)0s} \sin \tilde{\tilde{p}}_s \eta \right] -$$

$$+ \frac{1}{2\tilde{p}_s} \int_0^\eta e^{-\delta(\eta-\tau)} \left[\tilde{Q}_{(1)s}(\tau) + \tilde{Q}_{(2)s}(\tau) \right] \sin \tilde{p}_s (\eta - \tau) d\tau - \frac{1}{2\tilde{\tilde{p}}_s} \int_0^\eta e^{-\delta(\eta-\tau)} \left[\tilde{Q}_{(1)s}(\tau) - \tilde{Q}_{(2)s}(\tau) \right] \sin \tilde{\tilde{p}}_s (\eta - \tau) d\tau$$

where constants $C_{(1)0s}$, $D_{(1)0s}$, $M_{(1)0s}$ and $N_{(1)0s}$ are unknown constant defined by four initial conditions: belts' point elongations and velocities at the initial moment.

.The s-family of the particular solutions are in the following forms:

$$w_{(i)s}(x, t) = \mathbf{X}_{(i)s}(x) \mathbf{Y}_{(i)s}(x, t) \tag{29}$$

$$w_{(1)s}(\xi, \eta) = \mathbf{X}_{(1)s}(\xi) \mathbf{Y}_{(1)s}(\eta) = e^{\tilde{\delta}\xi - \delta\eta} \sin \frac{s\pi}{\ell} \xi \left[C_{(1)0s} \cos \tilde{p}_s \eta + D_{(1)0s} \sin \tilde{p}_s \eta \right] +$$

$$+ e^{\tilde{\delta}\xi - \delta\eta} \sin \frac{s\pi}{\ell} \xi \left[M_{(1)0s} \cos \tilde{\tilde{p}}_s \eta + N_{(1)0s} \sin \tilde{\tilde{p}}_s \eta \right] +$$

$$+ \frac{1}{2\tilde{p}_s} e^{\tilde{\delta}\xi - \delta\eta} \sin \frac{s\pi}{\ell} \xi \int_0^\eta e^{\delta\tau} \left[\tilde{Q}_{(1)s}(\tau) + \tilde{Q}_{(2)s}(\tau) \right] \sin \tilde{p}_s (\eta - \tau) \tau d\tau$$

$$+ \frac{1}{2\tilde{\tilde{p}}_s} e^{\tilde{\delta}\xi - \delta\eta} \sin \frac{s\pi}{\ell} \xi \int_0^\eta e^{\delta\tau} \left[\tilde{Q}_{(1)s}(\tau) - \tilde{Q}_{(2)s}(\tau) \right] \sin \tilde{\tilde{p}}_s (\eta - \tau) d\tau$$

$$\tag{30}$$

$$w_{(2)s}(\xi,\eta) = \mathbf{X}_{(1)s}(\xi)\mathbf{Y}_{(2)s}(\eta) = e^{\tilde{\delta}\xi - \delta\eta}\sin\frac{s\pi}{\ell}\xi\left[C_{(1)0s}\cos\tilde{p}_s\eta + D_{(1)0s}\sin\tilde{p}_s\eta\right] -$$

$$- e^{\tilde{\delta}\xi - \delta\eta}\sin\frac{s\pi}{\ell}\xi\left[M_{(1)0s}\cos\tilde{\tilde{p}}_s\eta + N_{(1)0s}\sin\tilde{\tilde{p}}_s\eta\right] -$$

$$+ \frac{1}{2\tilde{p}_s}e^{\tilde{\delta}\xi - \delta\eta}\sin\frac{s\pi}{\ell}\xi\int_0^\eta e^{\delta\tau}\left[\tilde{Q}_{(1)s}(\tau) + \tilde{Q}_{(2)s}(\tau)\right]\sin\tilde{p}_s(\eta - \tau)d\tau - \tag{31}$$

$$- \frac{1}{2\tilde{p}_s}e^{\tilde{\delta}\xi - \delta\eta}\sin\frac{s\pi}{\ell}\xi\int_0^\eta e^{\delta\tau}\left[\tilde{Q}_{(1)s}(\tau) - \tilde{Q}_{(2)s}(\tau)\right]\sin\tilde{\tilde{p}}_s(\eta - \tau)d\tau$$

The s-family of the particular solutions for pure forced vibrations of a double belt system excited by external excitation distributed function depending only of time, are in the following forms:

$$w_{(1)}^{Forced}(x,t) = \sum_{s=1}^{\infty}\frac{e^{-\delta t}\sin\frac{s\pi}{\ell}x}{2\sqrt{\frac{c_0^2 - v_0^2}{c_0^2}\left\{\left(c_0^2 - v_0^2\right)\left(\frac{s\pi}{\ell}\right)^2 - \delta^2\right\}}} +$$

$$\int_0^{\eta = \frac{v_0}{c_0^2 - v_0^2}x + t}e^{\delta\tau}\left[\tilde{Q}_{(1)s}(\tau) + \tilde{Q}_{(2)s}(\tau)\right]\sin\sqrt{\frac{c_0^2 - v_0^2}{c_0^2}\left\{\left(c_0^2 - v_0^2\right)\left(\frac{s\pi}{\ell}\right)^2 - \delta^2\right\}}_s(\eta - \tau)d\tau - \tag{32}$$

$$+ \sum_{s=1}^{\infty}\frac{e^{-\delta t}\sin\frac{s\pi}{\ell}x}{2\sqrt{\frac{c_0^2 - v_0^2}{c_0^2}\left\{\left(c_0^2 - v_0^2\right)\left(\frac{s\pi}{\ell}\right)^2 - \delta^2 + 2\kappa^2\right\}}}$$

$$\int_0^{\eta = \frac{v_0}{c_0^2 - v_0^2}x + t}e^{\delta\tau}\left[\tilde{Q}_{(1)s}(\tau) - \tilde{Q}_{(2)s}(\tau)\right]\sin\sqrt{\frac{c_0^2 - v_0^2}{c_0^2}\left\{\left(c_0^2 - v_0^2\right)\left(\frac{s\pi}{\ell}\right)^2 - \delta^2 + 2\kappa^2\right\}}(\eta - \tau)d\tau$$

$$w_{(2)}^{Forced}(x,t) = \sum_{s=1}^{\infty}\frac{e^{-\delta t}\sin\frac{s\pi}{\ell}x}{2\sqrt{\frac{c_0^2 - v_0^2}{c_0^2}\left\{\left(c_0^2 - v_0^2\right)\left(\frac{s\pi}{\ell}\right)^2 - \delta^2\right\}}}$$

$$\int_0^{\eta = \frac{v_0}{c_0^2 - v_0^2}x + t}e^{\delta\tau}\left[\tilde{Q}_{(1)s}(\tau) + \tilde{Q}_{(2)s}(\tau)\right]\sin\sqrt{\frac{c_0^2 - v_0^2}{c_0^2}\left\{\left(c_0^2 - v_0^2\right)\left(\frac{s\pi}{\ell}\right)^2 - \delta^2\right\}}_s(\eta - \tau)d\tau - \tag{33}$$

$$- \sum_{s=1}^{\infty}\frac{e^{-\delta t}\sin\frac{s\pi}{\ell}x}{2\sqrt{\frac{c_0^2 - v_0^2}{c_0^2}\left\{\left(c_0^2 - v_0^2\right)\left(\frac{s\pi}{\ell}\right)^2 - \delta^2 + 2\kappa^2\right\}}}$$

$$\int_0^{\eta = \frac{v_0}{c_0^2 - v_0^2}x + t}e^{\delta\tau}\left[\tilde{Q}_{(1)s}(\tau) - \tilde{Q}_{(2)s}(\tau)\right]\sin\sqrt{\frac{c_0^2 - v_0^2}{c_0^2}\left\{\left(c_0^2 - v_0^2\right)\left(\frac{s\pi}{\ell}\right)^2 - \delta^2 + 2\kappa^2\right\}}(\eta - \tau)d\tau$$

IV.2. 4. Appendix

Previous solutions are obtained on the basis previously obtained solutions of the coupled partial differential equations describing free transversal vibrations of the axially moving double belt system.

The s-family of the particular solutions for decoupled belts and for free transversal vibrations are:

$$w_{(i)s}(x,t) = \mathbf{X}_{(i)s}(x)\mathbf{Y}_{(i)s}(x,t) \tag{A.1}$$

$$w_{(i)s}(x,t) = e^{-\delta\left(\frac{v_0}{c_0^2-v_0^2}x+t\right)+\tilde{\delta}x}$$

$$\sin\frac{s\pi}{\ell}x\left[R_s\cos\left\{\sqrt{\left(\frac{s\pi}{\ell}\right)^2\frac{\left(c_0^2-v_0^2\right)^2}{c_0^2}+\left(\kappa^2-\delta^2\right)\frac{c_0^2-v_0^2}{c_0^2}}\left(\frac{v_0}{c_0^2-v_0^2}x+t\right)+\beta_s\right\}\right]$$

The generalized solution for decoupled belts transversal free vibrations is expressed by expansion

$$w_{(i)}(x,t) = \sum_{s=1}^{s=\infty}w_{(i)s}(x,t) = \sum_{s=1}^{s=\infty}\mathbf{X}_{(i)s}(x)\mathbf{Y}_{(i)s}(x,t) \tag{A.2}$$

$$w_{(i)}(x,t) = e^{-\delta\left(\frac{v_0}{c_0^2-v_0^2}x+t\right)+\tilde{\delta}x}$$

$$\sum_{s=1}^{s=\infty}\sin\frac{s\pi}{\ell}x\left[R_s\cos\left\{\sqrt{\left(\frac{s\pi}{\ell}\right)^2\frac{\left(c_0^2-v_0^2\right)^2}{c_0^2}+\left(\kappa^2-\delta^2\right)\frac{c_0^2-v_0^2}{c_0^2}}\left(\frac{v_0}{c_0^2-v_0^2}x+t\right)+\beta_s\right\}\right]$$

Solution of the coupled ordinary differential equations for free oscillations

$$\left\{\frac{d^2\mathbf{Y}_{(1)s}(\eta)}{d\eta^2}+2\delta\frac{d\mathbf{Y}_{(1)s}(\eta)}{d\eta}+\tilde{\omega}_s^2\mathbf{Y}_{(1)s}(\eta)-\tilde{\omega}_0^2\mathbf{Y}_{(2)s}(\eta)\right\}=0 \tag{A.3}$$

$$\left\{\frac{d^2\mathbf{Y}_{(2)s}(\eta)}{d\eta^2}+2\delta\frac{d\mathbf{Y}_{(2)s}(\eta)}{d\eta}+\tilde{\omega}_s^2\mathbf{Y}_{(2)s}(\eta)-\tilde{\omega}_0^2\mathbf{Y}_{(1)s}(\eta)\right\}=0$$

$$\tag{A.4}$$

suppose in the following form:

$$\mathbf{Y}_{(i)s}(\eta) = D_{(i)s}e^{\lambda_s\eta} \quad, \quad \mathbf{i} = \sqrt{-\mathbf{1}}, \qquad i = 1,2 \tag{A.4}$$

Characteristic equation of the formalized dynamical system have the following four sets of the characteristic eigen numbers:

$$\lambda_{(1,2,3,4)s} = -\delta\mp\sqrt{\delta^2-\tilde{\omega}_s^2\mp\tilde{\omega}_0^2}, \quad \mathbf{i} = \sqrt{-\mathbf{1}}$$

$$\lambda_{(1,2)s} = -\delta \mp \mathbf{i} \sqrt{\frac{c_0^2 - v_0^2}{c_0^2} \left\{ \left(c_0^2 - v_0^2 \right) \left(\frac{s\pi}{\ell} \right)^2 - \delta^2 \right\}} = -\delta \mp \mathbf{i}\, \tilde{p}_s ,$$

$$s = 1,2,3,4,....... \tag{A.5}$$

$$\lambda_{(3,4)s} = -\delta \mp \mathbf{i} \sqrt{\frac{c_0^2 - v_0^2}{c_0^2} \left\{ \left(c_0^2 - v_0^2 \right) \left(\frac{s\pi}{\ell} \right)^2 - \delta^2 + 2\kappa^2 \right\}} = -\delta \mp \mathbf{i}\, \tilde{\tilde{p}}_s ,$$

$$s = 1,2,3,4,....... \tag{A.6}$$

The ratio between amplitudes of the own space-time η - functions $\mathbf{Y}_{(1)s}(\eta)$ and $\mathbf{Y}_{(2)s}(\eta)$, $\mathbf{Y}_{(i)s}(\eta) = D_{(i)s}e^{\lambda_s \eta}$ is not difficult to obtain in the form $\dfrac{D_{(1)s(r)}}{D_{(2)s(r)}} = \mp 1$, $s = 1,2,3,4,....... \ r = 1,2,3,4..$ Then, we can conclude that considered system of the coupled ordinary differential equations have four different and complex sets of roots and eigen characteristic numbers for defining unknown own space-time η - functions $\mathbf{Y}_{(1)s}(\eta)$ and $\mathbf{Y}_{(2)s}(\eta)$: having four sets of characteristic numbers we can conclude that corresponding four sets of the particular solutions for composing the functions $\mathbf{Y}_{(1)s}(\eta)$ and $\mathbf{Y}_{(2)s}(\eta)$ exists in the following form:

$$\mathbf{Y}_{(1)s(1,2,3,4)}(\eta) = \begin{cases} e^{-\delta\eta} \cos \tilde{p}_s \eta \\ e^{-\delta\eta} \sin \tilde{p}_s \eta \\ e^{-\delta\eta} \cos \tilde{\tilde{p}}_s \eta \\ e^{-\delta\eta} \sin \tilde{\tilde{p}}_s \eta \end{cases} \tag{A.7}$$

where is $\eta = \dfrac{v_0}{c_0^2 - v_0^2} x + t$, and $s = 1,2,3,4,........$, or in developed form:

$$\mathbf{Y}_{(1)s(1,2,3,4)}(\eta) = \begin{cases} e^{-\delta\left(\frac{v_0}{c_0^2-v_0^2}x+t\right)} \cos\left(\frac{v_0}{c_0^2-v_0^2}x+t\right)\sqrt{\frac{c_0^2-v_0^2}{c_0^2}\left\{\left(c_0^2-v_0^2\right)\left(\frac{s\pi}{\ell}\right)^2-\delta^2\right\}} \\[2ex] e^{-\delta\left(\frac{v_0}{c_0^2-v_0^2}x+t\right)} \sin\left(\frac{v_0}{c_0^2-v_0^2}x+t\right)\sqrt{\frac{c_0^2-v_0^2}{c_0^2}\left\{\left(c_0^2-v_0^2\right)\left(\frac{s\pi}{\ell}\right)^2-\delta^2\right\}} \\[2ex] e^{-\delta\left(\frac{v_0}{c_0^2-v_0^2}x+t\right)} \cos\left(\frac{v_0}{c_0^2-v_0^2}x+t\right)\sqrt{\frac{c_0^2-v_0^2}{c_0^2}\left\{\left(c_0^2-v_0^2\right)\left(\frac{s\pi}{\ell}\right)^2-\delta^2+2\kappa^2\right\}} \\[2ex] e^{-\delta\left(\frac{v_0}{c_0^2-v_0^2}x+t\right)} \sin\left(\frac{v_0}{c_0^2-v_0^2}x+t\right)\sqrt{\frac{c_0^2-v_0^2}{c_0^2}\left\{\left(c_0^2-v_0^2\right)\left(\frac{s\pi}{\ell}\right)^2-\delta^2+2\kappa^2\right\}} \end{cases} \tag{A.8}$$

Finally the unknown space-time η - functions $\mathbf{Y}_{(1)s}(\eta)$ and $\mathbf{Y}_{(2)s}(\eta)$ for free double belt system transversal vibrations we obtain in the following forms:

$$\mathbf{Y}_{(1)s}(\eta) = e^{-\delta\eta}\left[C_{(1)s}\cos\tilde{p}_s\eta + D_{(1)s}\sin\tilde{p}_s\eta\right] + e^{-\delta\eta}\left[M_{(1)s}\cos\tilde{\tilde{p}}_s\eta + N_{(1)s}\sin\tilde{\tilde{p}}_s\eta\right] \quad \text{(A.9)}$$

$$\mathbf{Y}_{(2)s}(\eta) = e^{-\delta\eta}\left[C_{(1)s}\cos\tilde{p}_s\eta + D_{(1)s}\sin\tilde{p}_s\eta\right] - e^{-\delta\eta}\left[M_{(1)s}\cos\tilde{\tilde{p}}_s\eta + N_{(1)s}\sin\tilde{\tilde{p}}_s\eta\right] \text{(A.10)}$$

The s-family of the particular solutions for free vibrations are in the following forms:

$$w_{(i)s}(x,t) = \mathbf{X}_{(i)s}(x)\mathbf{Y}_{(i)s}(x,t), \quad s = 1,2,3,4,....... \quad \text{(A.11)}$$

$$w_{(1)s}(x,t) = e^{-\delta t}\sin\frac{s\pi}{\ell}x\left\{R_s\cos\left\langle\left(\frac{v_0}{c_0^2-v_0^2}x+t\right)\sqrt{\frac{c_0^2-v_0^2}{c_0^2}\left\{\left(c_0^2-v_0^2\right)\left(\frac{s\pi}{\ell}\right)^2-\delta^2\right\}}+\beta_s\right\rangle\right\}+$$

$$+e^{-\delta t}\sin\frac{s\pi}{\ell}x\left\{U_s\cos\left\langle\left(\frac{v_0}{c_0^2-v_0^2}x+t\right)\sqrt{\frac{c_0^2-v_0^2}{c_0^2}\left\{\left(c_0^2-v_0^2\right)\left(\frac{s\pi}{\ell}\right)^2-\delta^2+2\kappa^2\right\}}+\gamma_s\right\rangle\right\} \quad \text{(A.12)}$$

$$w_{(2)s}(x,t) = e^{-\delta t}\sin\frac{s\pi}{\ell}x\left\{R_s\cos\left\langle\left(\frac{v_0}{c_0^2-v_0^2}x+t\right)\sqrt{\frac{c_0^2-v_0^2}{c_0^2}\left\{\left(c_0^2-v_0^2\right)\left(\frac{s\pi}{\ell}\right)^2-\delta^2\right\}}+\beta_s\right\rangle\right\}-$$

$$-e^{-\delta t}\sin\frac{s\pi}{\ell}x\left\{U_s\cos\left\langle\left(\frac{v_0}{c_0^2-v_0^2}x+t\right)\sqrt{\frac{c_0^2-v_0^2}{c_0^2}\left\{\left(c_0^2-v_0^2\right)\left(\frac{s\pi}{\ell}\right)^2-\delta^2+2\kappa^2\right\}}+\gamma_s\right\rangle\right\} \quad \text{(A.13)}$$

where R_s, U_s, β_s and γ_s are unknown constants defined by initial conditions.

Then, finally, the generalized solutions of the based coupled partial differential equations are expressed by expansion in the following forms (free vibrations):

$$w_{(i)}(x,t) = \sum_{s=1}^{s=\infty}w_{(i)s}(x,t) = \sum_{s=1}^{s=\infty}\mathbf{X}_{(i)s}(x)\mathbf{Y}_{(i)s}(x,t) \quad \text{(A.14)}$$

for coupled

$$w_{(1)}(x,t) = e^{-\delta t}\sum_{s=1}^{\infty}\sin\frac{s\pi}{\ell}x\left\{R_s\cos\left\langle\left(\frac{v_0}{c_0^2-v_0^2}x+t\right)\sqrt{\frac{c_0^2-v_0^2}{c_0^2}\left\{\left(c_0^2-v_0^2\right)\left(\frac{s\pi}{\ell}\right)^2-\delta^2\right\}}+\beta_s\right\rangle\right\}+$$

$$+e^{-\delta t}\sum_{s=1}^{\infty}\sin\frac{s\pi}{\ell}x\left\{U_s\cos\left\langle\left(\frac{v_0}{c_0^2-v_0^2}x+t\right)\sqrt{\frac{c_0^2-v_0^2}{c_0^2}\left\{\left(c_0^2-v_0^2\right)\left(\frac{s\pi}{\ell}\right)^2-\delta^2+2\kappa^2\right\}}+\gamma_s\right\rangle\right\} \quad \text{(A.15)}$$

$$w_{(2)}(x,t) = e^{-\delta t}\sum_{s=1}^{\infty}\sin\frac{s\pi}{\ell}x\left\{R_s\cos\left\langle\left(\frac{v_0}{c_0^2-v_0^2}x+t\right)\sqrt{\frac{c_0^2-v_0^2}{c_0^2}\left\{\left(c_0^2-v_0^2\right)\left(\frac{s\pi}{\ell}\right)^2-\delta^2\right\}}+\beta_s\right\rangle\right\}-$$

$$-e^{-\delta t}\sum_{s=1}^{\infty}\sin\frac{s\pi}{\ell}x\left\{U_s\cos\left\langle\left(\frac{v_0}{c_0^2-v_0^2}x+t\right)\sqrt{\frac{c_0^2-v_0^2}{c_0^2}\left\{\left(c_0^2-v_0^2\right)\left(\frac{s\pi}{\ell}\right)^2-\delta^2+2\kappa^2\right\}}+\gamma_s\right\rangle\right\} \quad \text{(A.16)}$$

where R_s, U_s, β_s and γ_s are unknown constants defined by initial conditions, two by initial transversal displacements of component belts and by two transversal velocities of the component belts (for detail see References [72] and [75]).

IV.2.5. Concluding Remarks

Subject of mathematical description and analytical study, presented in this part of the paper, is a theoretical, pure classical model of hybrid elastodynamic model very useful for university teaching of elastodynamics as a fundamental part of the engineering science (mechanical, civil and physics), as well as, a good introduction of the students and engineers of the multifrequency wave phenomena in real mechanical systems with moving material.

If we compare the expressions for coupled and uncoupled belts, we can conclude that for uncoupled belts' transverse free vibrations contain one frequency damped vibrations in one eigen amplitude shape, and for coupled vibrations contain two frequency damped vibrations in each one amplitude shape, and that these two-frequency dumped vibrations are uncoupled with relation of the other shape own vibrations. This is visible directly from corresponding expressions (A.12), (A.13) or (A.14) and (A.16) presented in Appendix.

For analysis forced regimes, we can use terms expressed by (30), (31) and (32) from which, we can conclude that forced vibrations in each mode should be contain three frequencies which are thwo frequencies of the free own double belt system vibrations,

$$\tilde{p}_s = \sqrt{\frac{c_0^2 - v_0^2}{c_0^2}\left[\left(\frac{s\pi}{\ell}\right)^2\left(c_0^2 - v_0^2\right) - \delta^2\right]} \quad \text{and} \quad \tilde{\tilde{p}}_s = \sqrt{\frac{c_0^2 - v_0^2}{c_0^2}\left[\left(\frac{s\pi}{\ell}\right)^2\left(c_0^2 - v_0^2\right) + 2\kappa^2 - \delta^2\right]}, \quad \text{and one}$$

frequency of external forced excitation, frequencies Ω_i. Free vibrations regimes are two frequency, and forced are three, or multifrequency, depending of number of frequencies of applied external transverse excitations.

From last expressions for particular or generalized solutions (30), (31) and (32) as expressions of transverse displacements of double belt system, we can conclude that we can separate eigen amplitude functions $\mathbf{X}_{(i)s}(\xi)$ along the space ξ-length-time $\eta(x,t)$ coordinate system as well two eigen phase functions $\tilde{\beta}_s(x)$ and $\tilde{\tilde{\beta}}_s(x)$ expressed by:

$$\tilde{\beta}_s(x) = \frac{v_0^2}{c_0^2 - v_0^2} x \sqrt{\frac{c_0^2 - v_0^2}{c_0^2}\left[\left(\frac{s\pi}{\ell}\right)^2\left(c_0^2 - v_0^2\right) - \delta^2\right]}, \qquad s = 1,2,3,4,....... \qquad (33)$$

$$\tilde{\tilde{\beta}}_s(x) = \frac{v_0^2}{c_0^2 - v_0^2} x \sqrt{\frac{c_0^2 - v_0^2}{c_0^2}\left[\left(\frac{s\pi}{\ell}\right)^2\left(c_0^2 - v_0^2\right) + 2\kappa^2 - \delta^2\right]}, \quad s = 1,2,3,4,.......(34)$$

Figure 9. Sixth cases pf the possible vibrations firms of the double belt system with elastic layer for different eigen amplitude functions $\mathbf{X}_{(i)s}(\xi) = e^{\tilde{\delta}\xi}\sin\dfrac{s\pi}{\ell}\xi$ for the solution in the ξ, $\eta = \dfrac{v_0}{c_0^2 - v_0^2}x + t$ coordinates system,

If we compare the expressions for solutions with respect to the other way analysis, of the solutions for coupled and uncoupled belts, we can conclude that for uncoupled belts' transverse displacements of forced vibrations contain one frequency damped vibrations and corresponding frequency forced regime in one eigen amplitude shape, with one eigen phase functions $\tilde{\beta}_s(x)$ (see expression from Ref. [75]) and for coupled double belt system vibrations contain two frequency damped free vibrations and corresponding frequency forced regime, as well as corresponding combinations in each one amplitude shape with two eigen phase functions $\tilde{\beta}_s(x)$ and $\tilde{\tilde{\beta}}_s(x)$ expressed by (33) and (34). Also, in other way, we can compare amplitude forms of the dynamics of coupled and uncoupled belts and conclude that dynamics of the uncoupled belts containing two types of eigen amplitude functions: $\mathbf{X}_{(i)s}^{(C)}(x)$ *sin SIN* AND $\mathbf{X}_{(i)s}^{(S)}(x)$ *sin cos* corresponding to one frequency free vibration mode and that double belt system dynamics contains

also two types   eigen amplitude functions, but each of the both two frequencies: $\tilde{\mathbf{X}}_{(i)s}^{(C)}(x)$ *sin cos* and $\tilde{\mathbf{X}}_{(i)s}^{(S)}(x)$ *sin sin* for first frequency of the mode and $\tilde{\tilde{\mathbf{X}}}_{(i)s}^{(C)}(x)$ *sin*

cos and $\tilde{\tilde{\mathbf{X}}}_{(i)s}^{(S)}(x)$ *sin sin* for second of the same mode, contained in expressions (30), (31), (32) and (A.12), (A.13), (A.14) (A.15).
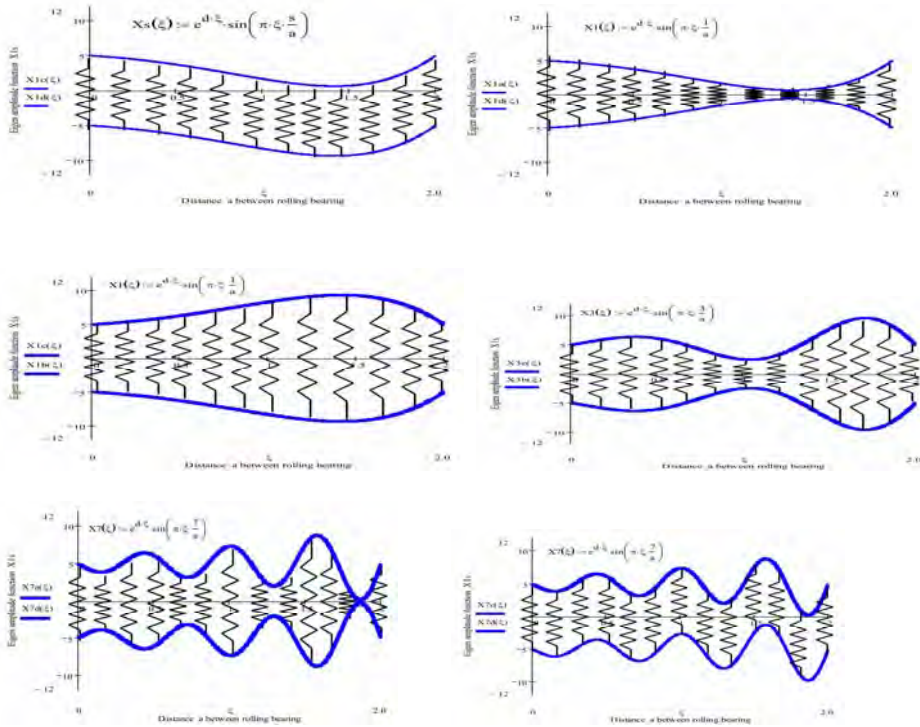
In Figure 9. sixth cases of the possible vibrations firms of the double belt system with elastic layer for different eigen amplitude functions $\mathbf{X}_{(i)s}(\xi) = e^{\tilde{\delta}\xi} \sin \dfrac{s\pi}{\ell}\xi$ for

the solution in the ξ, $\eta = \dfrac{v_0}{c_0^2 - v_0^2}x + t$ coordinates system are presented.

We haven't information if this theoretical model of a sandwich double belt system was applied in real systems, but in our opinion it is possible to use this hybrid model of sandwich belt system in the different kind of conveyer in which is necessary that upper (or lower) belt haven't vibrations under transversal periodic excitation. It is possible in the condition of the dynamic absorption, when only lower (or upper) belt is in the forced regime of vibrations. This sandwich double belt system can be project as a dynamical absorber, when upper belt in the system is excited by external periodic excitation no vibrations, and only lower belt have forced vibrations.

Series of the papers [69-92] contain results of analysis based on analytical expressions describing dynamics of hybrid systems with complex structure. These system contains coupled plates, beams or belts.

4.3. A review of the study of the transfer energy between sub-systems in the complex structure systems.

4.3.1. Transfer energy in spring pendulum system

For introducing to the problem of the energy transfer or transient in the hybrid non-linear systems, it is useful to take, for simple analysis, into consideration the change energy between parts of the energy carrying on the generalized coordinates ϕ and ρ in the very known system, known under name *spring pendulum system,* with two degree of freedom. For the analysis of the energy in the spring pendulum we can write the kinetic and potential energies in the forms (see Refs. [72], [44], [56] and [83] by Hedrih (Stevanović)):

$$E_k = \frac{1}{2}m\left[\dot{\rho}^2 + (\rho + \ell)^2\dot{\phi}^2\right]$$

and

$$E_p = \frac{1}{2}c\rho^2 + mg(\rho + \ell)(1 - \cos\phi) \tag{1}$$

where: m is mass of the pendulum, ℓ length of pendulum string-neglected mass spring in the static equilibrium state of the pendulum, and c spring axial rigidity and ϕ and ρ are respectfully, angle and extension part of length of the string-spring of the

pendulum with comparison of the sprig length in static equilibrium state of the pendulum, taken as the generalized coordinates of the system. For the linearized case for kinetic energy, after neglecting small member - part of kinetic energy on the generalized coordinate ϕ, we can taking into account following expression:

* Expression $E_{k2} = \frac{1}{2}m(\rho + \ell)^2 \dot{\phi}^2$ changes into approximation

$$E_{k2} \approx \frac{1}{2}m(\ell\dot{\phi})^2 . \tag{2}$$

Only for small oscillations – perturbations from equilibrium position it is possible to use approximation of the expression for kinetic and potential energy in the form:

$$E_k \approx \frac{1}{2}m\left[\dot{\rho}^2 + (\ell\dot{\phi})^2\right] \quad \text{and} \quad E_p \approx \frac{1}{2}c\rho^2 + \frac{1}{2}mg\ell\phi^2 \tag{3}$$

For that linerized case the generalized coordinates are normal coordinates of the small oscillations of the spring pendulum around equilibrium position $\rho = 0, \phi = 0$ and coordinates are decoupled. In this linearized case of the spring pendulum model, the energy carried on the these normal coordinates are uncoupled and transfer or transient of the total energy don't appeared between proper parts of the separate normal coordinate and on the separate processes defined by normal coordinates are conservative systems each with one degree of the freedom. In this case each of the coordinate there are conversion of the energies from kinetic to potential, but sum of the both of one normal coordinates is constant.

$$E_{k\rho} \approx \frac{1}{2}m\dot{\rho}^2 \qquad \text{and} \qquad E_{p\rho} \approx \frac{1}{2}c\rho^2 \tag{4}$$

$$E_{k\phi} \approx \frac{1}{2}m(\ell\dot{\phi})^2 \qquad \text{and} \qquad E_{p\phi} \approx \frac{1}{2}mg\ell\phi^2 \tag{5}$$

This is visible from system of the differential equations in the linearized form:

$$\ddot{\rho} + \omega_2^2\rho = 0 \text{ where } \omega_2^2 = \frac{c}{m}$$

$$\ddot{\phi} + \omega_1^2\phi = 0 \text{ where } \quad \omega_1^2 = \frac{g}{\ell} . \tag{6}$$

but for the non-linear case the interaction between coordinates is present and then energy transient appears.

$$E_k = \frac{1}{2}m\left[\dot{\rho}^2 + \ell^2\dot{\phi}^2 + \rho^2\dot{\phi}^2 + 2\rho\ell\dot{\phi}^2\right] \qquad \text{and}$$

$$E_p = \frac{1}{2}c\rho^2 + mg\ell(1 - \cos\phi) + mg\rho(1 - \cos\phi) \tag{7}$$

We can separate the following parts:

I* Kinetic and potential energies carrying on the coordinate ρ are:

$$E_{k\rho} = \frac{1}{2}m\dot{\rho}^2 \quad \text{and} \quad E_{p\rho} = \frac{1}{2}c\rho^2 + mg\rho \tag{8}$$

By analysing these previous expressions, we can see that with these expressions for decoupled oscillator with coordinate ρ, we have pure linear oscillator or harmonic oscillator with coordinate ρ and frequency $\omega_2^2 = \dfrac{c}{m}$, and separated process is isochronous.

II* Kinetic and potential energies carrying on the coordinate ϕ are

$$E_{k\phi} = \frac{1}{2}m\ell^2\dot{\phi}^2 \quad \text{and} \quad E_{p\phi} = mg\ell(1 - \cos\phi) \tag{9}$$

By analysing these previous expressions we can see that with these expression for decoupled oscillator with coordinate ϕ, we have pure non-linear oscillator with coordinate ϕ, and separated process is no isochronous. For linearized case this oscillator have eigen frequency $\omega_1^2 = \dfrac{g}{\ell}$.

III* Then formally, we can conclude that in the spring pendulum, we have coupled two oscillators, one pure linear with one degree of freedom, and second non-linear, also with one degree of freedom. In the hybrid system these oscillators are coupled and mechanical energy of the coupling contain two parts: one kinetic energy and second potential energy. Then, in the coupling, hybrid connections with static and dynamic kinetic properties are introduced.

Kinetic and potential energies of the coordinate ϕ and ρ interaction in the non-linear hybrid model are:

$$E_{k(\phi,\rho)} = \frac{1}{2}m[\rho + 2\ell]\rho\dot{\phi}^2 \quad \text{and}$$
$$E_{p(\phi,\rho)} = -mg\rho\cos\phi \tag{10}$$

For non-linear case ordinary differential equations are in the following form:

$$\ddot{\rho} + \omega_2^2\rho = -g(1 - \cos\phi) \tag{11}$$

$$\ddot{\phi} + \omega_1^2\phi = \omega_1^2(\phi - \sin\phi) - \frac{2}{\ell^2}\dot{\rho}\dot{\phi}(\rho + \ell) - \frac{1}{\ell^2}\rho(\rho + 2\ell)\ddot{\phi} \tag{12}$$

or in non-linear approximation forms for small oscillations around zero coordinates $\rho = 0, \phi = 0$ or around stable equilibrium position of the spring pendulum are

$$\ddot{\rho} + \omega_2^2\rho \approx -g\left(\frac{\phi^2}{2} - \frac{\phi^4}{24} + \frac{\phi^6}{6!} - \frac{\phi^8}{8!} + \ldots\right) \tag{13}$$

$$\ddot{\phi} + \omega_1^2\phi \approx -\omega_1^2\left(\frac{\phi^3}{3!} - \frac{\phi^5}{5!} + \frac{\phi^7}{7!} - \ldots\right) - \frac{2}{\ell^2}\dot{\rho}\dot{\phi}(\rho + \ell) - \frac{1}{\ell^2}\rho(\rho + 2\ell)\ddot{\phi} \tag{14}$$

If we introduce phase coordinate, then we can write:

$$v = \dot{\rho}$$
$$\dot{v} = -\omega_2^2\rho - g(1 - \cos\phi)$$
$$u = \dot{\phi} \tag{15}$$

$$\dot{u} = -\omega_1^2 \phi + \omega_1^2 (\phi - \sin \phi) - \frac{2}{\ell^2} \dot{\rho} \dot{\phi} (\rho + \ell) - \frac{1}{\ell^2} \rho (\rho + 2\ell) \ddot{\phi}$$

or in the approximation

$$v = \dot{\rho}$$

$$\dot{v} \approx -\omega_2^2 \rho - g \left(\frac{\phi^2}{2} - \frac{\phi^4}{24} + \frac{\phi^6}{6!} - \frac{\phi^8}{8!} + \ldots \right)$$

$$u = \dot{\phi}$$

$$\dot{u} \approx -\omega_1^2 \phi - \omega_1^2 \left(\frac{\phi^3}{3!} - \frac{\phi^5}{5!} + \frac{\phi^7}{7!} - \ldots \right) - \frac{2}{\ell^2} \dot{\rho} \dot{\phi} (\rho + \ell) - \frac{1}{\ell^2} \rho (\rho + 2\ell) \dot{u} \qquad (16)$$

From system equations (11)-(12), as well from their approximations (13)-(14), we can see that their right hand parts are non-linear and are functions of generalized coordinates, as well as of the generalized coordinates first and second derivatives. Also we can see that generalized coordinates ϕ and ρ are around their zero values, when $\rho = 0, \phi = 0$ at the stable equilibrium position of the spring pendulum, and that also are main coordinates of the linearized model. It is reason that the asymptotic averaged method is applicable for obtaining first asymptotic approximation of the particular solutions and it is possible to use for energy analysis of the transfer energy between energies carried by generalized coordinates ϕ and ρ in this non-linear system with two degree of freedom, but formally, we can take into account that we have two oscillators, one non linear and one linear each with one degree of freedom as two sub-systems coupled in the hybrid system with two degree of freedom, by hybrid connection realized by statically and dynamical connections. This interconnection have two parts of energy interaction between sub-systems expressed by kinetic and potential energies in the forms expressed by (10).
Taking into consideration some conclusion from considered system of the spring pendulum, we can conclude also that it is important to consider more simple case of the coupling between linear and non-linear systems with one degree of freedom with different types of the coupling realized by simple static or dynamic elements, for to investigate hybrid phenomena in the coupled sub-systems.

4. 3.2. Forced vibratos of spring pendulum

Let consider the energy transfer between parts of the energy carrying on the generalized coordinates ϕ and ρ in the *spring pendulum system* with two degrees of freedom excited by external excitations. For that analysis of the energy in the spring pendulum in the forced regime excited by external one frequency excitation – generalized forces $M_\phi(t) = M_0 \cos(\Omega_\phi t + \vartheta_\phi)$ and $F_\rho(t) = F_0 \cos(\Omega_\rho t + \vartheta_\rho)$, we can write the kinetic and potential energies in the forms (1). By taking into account all comments and asymptotic approximation as in the introductory part of this paper, as well as corresponding expressions (2) – (5), system of the differential equations of the linearized system is in the following form (see Refs. [72], [44], [56] and [83] by Hedrih (Stevanović)):

$$\ddot{\rho} + \omega_2^2 \rho = h_{0\rho} \cos\left(\Omega_\rho t + \vartheta_\rho\right) \tag{17}$$

where $\omega_2^2 = \dfrac{c}{m}$, $h_{0\rho} = \dfrac{F_0}{m}$

$$\ddot{\phi} + \omega_1^2 \phi = h_{0\phi} \cos\left(\Omega_\phi t + \vartheta_\phi\right) \tag{18}$$

where $\omega_1^2 = \dfrac{g}{\ell}$, $h_{0\phi} = \dfrac{M_0}{m\ell^2}$.

Solutions of the linearized equations (17) an (18) are:

$$\rho(t) = R_2 \cos\left(\omega_2 t + \alpha_{02}\right) + \frac{h_{0\rho}}{\omega_2^2 - \Omega_\rho^2} \cos\left(\Omega_\rho t + \vartheta_\rho\right) \tag{19}$$

$$\phi(t) = R_1 \cos\left(\omega_1 t + \alpha_{01}\right) + \frac{h_{0\phi}}{\omega_1^2 - \Omega_\phi^2} \cos\left(\Omega_\phi t + \vartheta_\phi\right) \tag{20}$$

For that linearized case both chosen coordinates are main coordinates of the linearized model, and from solutions (19) – (20), we can see that free and also, forced vibrations are uncoupled, and not interaction between free, and also forced modes of the vibrations. Then, we have two uncoupled oscillators with different eigen circular frequencies $\omega_1^2 = \dfrac{g}{\ell}$ and $\omega_2^2 = \dfrac{c}{m}$ and different forced external excitation frequencies Ω_ϕ and Ω_ρ and with possibilities of appearance two main uncoupled resonant regimes, when $\Omega_{\phi,resonant}^2 = \omega_1^2 = \dfrac{g}{\ell}$ and $\Omega_{\rho,resonant}^2 = \omega_2^2 = \dfrac{c}{m}$.

In this case for linearized models and in the resonant cases, expressions for solutions are in the following forms:

$$\rho(t)\big|_{\Omega_{\rho,resonant}=\omega_2} = \rho_0 \cos\omega_2 t + \frac{\dot{\rho}_0}{\omega_2}\sin\omega_2 t + \frac{h_{0\rho}}{2\omega_2}\left[\omega_2 t \sin\left(\omega_2 t + \vartheta_\rho\right) - \sin\omega_2 t \sin\vartheta_\rho\right] \tag{21}$$

$$\phi(t)\big|_{\Omega_{\phi,resonant}=\omega_1} = \phi_0 \cos\omega_1 t + \frac{\dot{\phi}_0}{\omega_1}\sin\omega_1 t + \frac{h_{0\phi}}{2\omega_1}\left[\omega_1 t \sin\left(\omega_1 t + \vartheta_\phi\right) - \sin\omega_1 t \sin\vartheta_\phi\right] \tag{22}$$

But, for the non-linear case the interaction between coordinates is present and then energy transient appears.

Expressions for kinetic and potential energies are in the same forma as presented and analyzed in first part V.1.1 for free vibrations and named by (1)-(5) and (7)-(10). Then, the expressions for coordinates are different and must be taken in the forms (19)-(20) and (21)-(22).

By analyze corresponding expressions, we can see that with these expression for decoupled oscillator with coordinate ρ , we have pure linear oscillator or harmonic oscillator with coordinate ρ and frequency $\omega_2^2 = \dfrac{c}{m}$, and separated process is isochronous. By analyzed these corresponding expressions, we can see that with these expressions for decoupled oscillators with coordinate ϕ , we have pure non-linear

oscillator with coordinate ϕ, and separated process is no isochronous. For linearyzed case this oscillator have eigen frequency $\omega_1^2 = \dfrac{g}{\ell}$.

For forced non-linear case differential equations of the system non-linear oscillation are in the following form:

$$\ddot{\rho} + \omega_2^2 \rho = -g(1 - \cos\phi) + h_{0\rho} \cos(\Omega_\rho t + \vartheta_\rho) \tag{23}$$

$$\ddot{\phi} + \omega_1^2 \phi = \omega_1^2(\phi - \sin\phi) - \frac{2}{\ell^2}\dot{\rho}\dot{\phi}(\rho + \ell) - \frac{1}{\ell^2}\rho(\rho + 2\ell)\ddot{\phi} + h_{0\phi}\cos(\Omega_\phi t + \vartheta_\phi) \tag{24}$$

or in non-linear approximation forms for small oscillations around zero coordinates $\rho = 0, \phi = 0$ or around stable equilibrium position of the spring pendulum

$$\ddot{\rho} + \omega_2^2 \rho \approx -g\left(\frac{\phi^2}{2} - \frac{\phi^4}{24} + \frac{\phi^6}{6!} - \frac{\phi^8}{8!} + \dots\right) + h_{0\rho}\cos(\Omega_\rho t + \vartheta_\rho) \tag{25}$$

$$\ddot{\phi} + \omega_1^2 \phi \approx -\omega_1^2\left(\frac{\phi^3}{3!} - \frac{\phi^5}{5!} + \frac{\phi^7}{7!} - \dots\right) - \frac{2}{\ell^2}\dot{\rho}\dot{\phi}(\rho + \ell) - \frac{1}{\ell^2}\rho(\rho + 2\ell)\ddot{\phi} + h_{0\phi}\cos(\Omega_\phi t + \vartheta_\phi)$$

$$\tag{26}$$

If we introduce phase coordinate, then we can write:

$$v = \dot{\rho}$$

$$\dot{v} = -\omega_2^2 \rho - g(1 - \cos\phi) + h_{0\rho}\cos(\Omega_\rho t + \vartheta_\rho)$$

$$u = \dot{\phi}$$

$$\dot{u} = -\omega_1^2 \phi + \omega_1^2(\phi - \sin\phi) - \frac{2}{\ell^2}\dot{\rho}\dot{\phi}(\rho + \ell) - \frac{1}{\ell^2}\rho(\rho + 2\ell)\dot{u} + h_{0\phi}\cos(\Omega_\phi t + \vartheta_\phi) \tag{25}$$

or in the approximation

$$v = \dot{\rho}$$

$$\dot{v} \approx -\omega_2^2 \rho - g\left(\frac{\phi^2}{2} - \frac{\phi^4}{24} + \frac{\phi^6}{6!} - \frac{\phi^8}{8!} + \dots\right) + h_{0\rho}\cos(\Omega_\rho t + \vartheta_\rho)$$

$$u = \dot{\phi} \tag{26}$$

$$\dot{u} \approx -\omega_1^2 \phi - \omega_1^2\left(\frac{\phi^3}{3!} - \frac{\phi^5}{5!} + \frac{\phi^7}{7!} - \dots\right) - \frac{2}{\ell^2}\dot{\rho}\dot{\phi}(\rho + \ell) - \frac{1}{\ell^2}\rho(\rho + 2\ell)\dot{u} + h_{0\phi}\cos(\Omega_\phi t + \vartheta_\phi)$$

From system of the differential equations (23)-(24), as well as from their approximations (25)-(26), we can see that their right hand parts are non-linear and are functions of generalized coordinates, as well as of the generalized coordinates first and second derivatives with respect to time and function of time. Also, we can see that generalized coordinates ϕ and ρ around their zero values, when $\rho = 0, \phi = 0$ at the stable equilibrium position of the spring pendulum are also main coordinates of the linearized model. It is reason that the asymptotic averaged method is applicable for obtaining first asymptotic approximation of the solutions

Then, it is possible that first asymptotic approximations of the solutions of the system of non-linear differential equations (23)-(24), take into account in the following asymptotic approximations for the small spring pendulum forced elongations in the form:

$$\rho = a_\rho(t)\cos(\omega_1 t + \varphi_\rho(t))$$
$$\phi = a_\phi(t)\cos(\omega_2 t + \varphi_\phi(t)) \tag{27}$$

where amplitudes $a_\rho(t)$ and $a_\varphi(t)$ and phases $\varphi_\rho(t)$ and $\varphi_\varphi(t)$ are defined by system of first order non-linear differential equations in first asymptotic approximation in the following form:

$$\dot{a}_\rho(t) = \frac{h_{0\rho}}{(\omega_2 + \Omega_\rho)}\sin(\varphi_\rho(t) - \vartheta_\rho)$$

$$\dot{\varphi}_\rho(t) = \omega_2 - \Omega_\rho - \frac{h_{0\rho}}{a_\rho(t)(\omega_2 + \Omega_\rho)}\cos(\varphi_\rho(t) - \vartheta_\rho)$$

$$\dot{a}_\phi(t) \approx -\frac{h_{0\phi}}{2(\omega_1 + \Omega_\phi)}\sin(\varphi_\phi(t) - \vartheta_\phi) + \frac{h_{0\phi}}{3(\omega_1 + \Omega_\phi)}\frac{a_\rho^2(t)}{\ell^2}\sin(\varphi_\phi(t) - \vartheta_\phi)$$

$$\dot{\varphi}_\phi(t) \approx \omega_1 - \Omega_\phi + \frac{\omega_1}{12}\left[1 - \frac{a_\rho^2(t)}{2\ell^2}\right] - \frac{h_{0\phi}}{2a_\phi(t)(\omega_1 + \Omega_\phi)}\cos(\varphi_\phi(t) - \vartheta_\phi) +$$

$$+ \frac{h_{0\phi}}{3a_\phi(t)(\omega_1 + \Omega_\phi)}\frac{a_\rho^2(t)}{\ell^2}\cos(\varphi_\phi(t) - \vartheta_\phi) \tag{28}$$

where $\Omega_\phi \approx \omega_1$ and $\Omega_\rho \approx \omega_2$ are external excitation frequencies in the resonant rages corresponding eigen frequencies of corresponding linearized system. Previous system of four non-linear and first order differential equation in the first asymptotic approximation are obtained by asymptotic Krilov-Bogoliyubov-Mitropolyskiy method and for small amplitudes of external excitations and in the resonant rages of the both frequencies.

4. 3.3. Concluding remarks

Taking into consideration some conclusion from considered system of the spring pendulum, we can conclude, also, that it is important to consider more simple case of the coupling between linear and non-linear systems each with one degree of freedom with different types of the coupling realized by simple static or dynamic elements (see Refs. [72], [44], [56] and [83] by Hedrih (Stevanović)) for to investigate hybrid phenomena in the non-linear system forced dynamics.

Also, it is possible to use for energy analysis of the transfer energy between energies carried by generalized coordinates ϕ and ρ in this non-linear system forced dynamics with two degrees of freedom, but formally, we can take into account that, we have two oscillators, one non-linear and one linear each with one degree of freedom as two sub-systems coupled in the hybrid system with two degree of freedom, by hybrid connection realized by static and dynamic coupling. This interconnection have two part

of energy interaction between sub-systems expressed by kinetic and potential energy in the form (10).

Taking into consideration some conclusion for considered system of the spring pendulum forced oscillations, we can conclude also that it is important to consider more simple case of the coupling between linear and non-linear systems each with one degree of freedom with different types of the coupling realized by simple static or dynamic elements, for to investigate hybrid phenomena in the system forced dynamics.

4.4. Analysis of the trigger of coupled singularities in nonlinear dynamic of no ideal system

4.4.1. Free vibrations of the heavy mass particle along rotate rough curvilinear line with Coulomb friction

For beginning let to consider free vibrations of the heavy mass particle along rotate rough curvilinear line with Coulomb's type friction, see Figure 8.a*. For the case that curvilinear line is in the vertical rotate plane Oxz around vertical Oz axis, we can take that equation of the curve-linear line is: $z = f(x)$, or $f_1(x, z) = z - f(x) = 0$ and with the following properties $f(-x) = f(x)$ and that coordinate pole is in the zero point $f(0) = 0$ in which line have minimum (see Figure 8.a*). Also we take that curvilinear line rotate around vertical Oz axis with constant angular velocity $\vec{\Omega} = \Omega \vec{k}$ (see Ref. [103] by Hedrih (Stevanović)).

Heavy mass particle, mass m, moving along rough curvilinear line with Coulomb's type sliding friction coefficient μ, is loaded by proper weight mg, as a active conservative force and by four no ideal constraint reactions, one F_N - normal ideal constrain reaction, second F_{BN} in binormal direction and two additional, $F_{\mu 1}$ first tangential component of the no ideal constraint reaction induced by friction and proportional to the normal component reaction F_N, $F_{\mu 1} = -\mu F_N \, sign \, \vec{v}_{rel}$, and $F_{\mu 2}$ second tangential component of the no ideal constraint reaction induced by friction caused by pressures in the binormal direction and proportional to the binormal component of the inertia force F_{BN}, $F_{\mu 2} = -\mu F_{BN} \, sign \, \vec{v}_{rel}$, caused by curvilinear line rotation around vertical Oz axis with constant angular velocity $\vec{\Omega} = \Omega \vec{k}$,
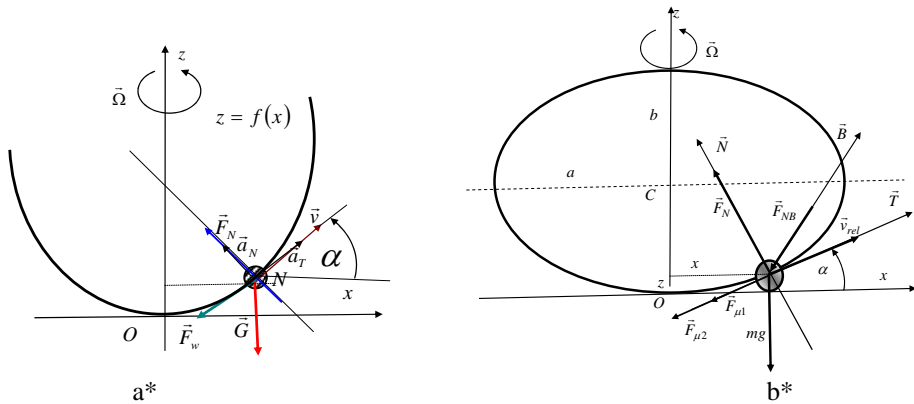
Figure 8. Heavy material particle motion along rough curvilinear line with Coulomb friction

Force of the inertia of mass particle realtive motion along the curvilinear line which rotate around vertical Oz axis with constant angular velocity $\vec{\Omega} = \Omega\vec{k}$, have two components. One component is force of the inertia of the circle rotation around vertical axis in the form $\vec{F}_{jp} = m\Omega^2 x\vec{u}$, and second is Coriolis inertia force of the system and we can write: $\vec{F}_{NB} = -\vec{F}_{jC} = 2m[\vec{\Omega}, \vec{v}_{rel}] = 2m\Omega v_{rel}\cos\alpha\vec{B}$. Corresponding force of Coulomb's type friction is in the form: $\vec{F}_{\mu2} = -\mu|\vec{F}_{NB}|\dfrac{\vec{v}_{rel}}{|\vec{v}_{rel}|} = -2\mu m\Omega v_{rel}\cos\alpha\dfrac{\vec{v}_{rel}}{|\vec{v}_{rel}|} = -2\mu m\Omega\vec{v}_{rel}\cos\alpha$.

By use principle of dynamical equilibrium we obtain expression for the intensity of normal and binormal components of curvilinear constraint reactions corresponding differential double non-linear equation of the heavy mass particle motion along rotate arbitrary curvilinear rough line, with   angular velocity of rotation $\vec{\Omega}$, and defined by function $z = f(x)$, for the case that the coefficient of the Coulomb's type sliding friction is μ, s in the following form:

$$\frac{d}{dt}\left(\dot{x}\sqrt{1+z'^2}\right) \pm \mu\dot{x}^2\,\frac{z''}{\sqrt{1+z'^2}} + \Omega^2\,\frac{x}{\sqrt{1+z'^2}}\left(1\mp\mu z'\right) +$$

$$+\frac{g}{\sqrt{1+z'^2}}\left(z'\pm\mu\right)\pm 2\mu\Omega\dot{x} = 0 \quad \begin{cases} for & v_{rel} > 0 \\ for & v_{rel} < 0 \end{cases} \tag{1}$$

For the case of heavy mass particle motion along no ideal arbitrary rough curvilinear line without rotation, differential equation is in the form:::

$$\frac{d}{dt}\left(\dot{x}\sqrt{1+z'^2}\right) + g\frac{z'}{\sqrt{1+z'^2}} \pm \mu\frac{1}{\sqrt{1+z'^2}}\left(\dot{x}^2 z'' + g\right) = 0 \quad \begin{cases} for & v_{rel} > 0 \\ for & v_{rel} < 0 \end{cases} \tag{2}$$

Let consider special case of the rough curvilinear line with friction along normal surface contact (without last term $\pm 2\mu\Omega\dot{x}$ in (1)) and let introduce new variable in the

following form: $u = \dot{x}^2$, then previous differential double equation (1) of the mass particle motion along rough line is possible to transform in the following form:

$$\frac{du}{dx} + 2u\frac{z''(z' \pm \mu)}{(1 + z'^2)} = -2\Omega^2 \frac{x}{(1 + z'^2)}(1 \mp \mu z') - \frac{2g}{(1 + z'^2)}(z' \pm \mu) \quad \begin{cases} for & v_{rel} > 0 \\ for & v_{rel} < 0 \end{cases}$$

(3)

Previous differential double equation (3) of the material particle motion along rough curvilinear line according new helping coordinate u is ordinary double differential equation first order with changeable coefficients and type in following form:

$$\frac{du}{dx} \pm P(x)u = Q(x), \text{ with following solution:}$$

$$[\dot{x}(x)]^2 =$$
$$= e^{-2\int \frac{z''(z' \pm \mu)}{(1+z'^2)}dx}\left[-2\int\left[\Omega^2 \frac{x}{(1+z'^2)}(1 \mp \mu z') + \frac{g}{(1+z'^2)}(z' \pm \mu)\right]e2^{\int \frac{z''(z' \pm \mu)}{(1+z'^2)}dx}dx + C\right]$$

(4)

From the previous first integral, the following equation of the phase trajectories in the phase plane $(x, \dot{x})$ we obtain:

$$v_{rel}^2(x) =$$
$$= (1 + z'^2)e^{-2\int \frac{z''(z' \pm \mu)}{(1+z'^2)}dx}\left[-2\int\left[\Omega^2 \frac{x}{(1+z'^2)}(1 \mp \mu z') + \frac{g}{(1+z'^2)}(z' \pm \mu)\right]e2^{\int \frac{z''(z' \pm \mu)}{(1+z'^2)}dx}dx + C\right]$$

(5)

where C integral constant depending of initial conditions, angular coordinate and angular velocity at initial moment, or starting terminate mass particle positions for next phase trajectory branch.

For reason to compare properties of kinetic parameters of main considered system dynamics and corresponding fictive (neglecting terms with acquire of velocity $\dot{x}^2$) for comparison we transform corresponding differential double equations in the form of the system of first order differential double equations and for obtaining singularities for main system and fictive systems use conditions that right hand side all equations must be equal to zero (null). Then we obtain the following conditions:

*For main system dynamics:

$$\frac{dx}{dt} = v = 0$$

$$\frac{dv}{dt} = -\dot{x}^2 \frac{z'z''}{(1 + z'^2)} \mp \mu\dot{x}^2 \frac{z''}{(1 + z'^2)} - \Omega^2 \frac{x(1 \mp \mu z')}{(1 + z'^2)} - \frac{g(z' \pm \mu)}{(1 + z'^2)} = 0 \qquad (6)$$

*For corresponding fictive systems

$$\frac{dx}{dt} = v = 0$$

$$\frac{dv}{dt} = -\Omega^2 \frac{x(1 \mp \mu z')}{(1 + z'^2)} - \frac{g(z' \pm \mu)}{(1 + z'^2)} = 0$$

(7)

and
$$\frac{dx}{dt} = v = 0$$

$$\frac{dv}{dt} = -\frac{\left(\Omega^2 x + g z'\right)}{\left(1 + z'^2\right)} = 0 \tag{8}$$

We can see that for listed main system and for fictive system, conditions for obtaining singularities are same. Depending of the curvilinear line form $z = f(x)$, we obtained two nonlinear algebra equations in the following forms:

$$-\Omega^2 \frac{x(1 \mp \mu z')}{\left(1 + z'^2\right)} - \frac{g(z' \pm \mu)}{\left(1 + z'^2\right)} = 0 \qquad \text{and} \qquad \frac{\left(\Omega^2 x + g z'\right)}{\left(1 + z'^2\right)} = 0 \tag{9}$$

from which we can obtain, one or more roots.

If corresponding algebra double equation (9) have one root for $\mu = 0$ then words are about one equilibrium position with „one side left" and „one side right" bifurcation of the equilibrium position and one fictive trigger of coupled singularities caused by Coulomb's type friction between mass particle and rough curvilinear line.

If corresponding algebra double equation (9) have odd number of roots for $\mu = 0$ then words are about trigger of coupled singularities in a dynamics of a basic non-linear system correspond to the system with friction. In this case corresponding algebra double equation (9) for $\mu \neq 0$ have corresponding odd number of roots for each of the sets of the sign $\pm$, but all these roots are selected in two subsets, first one an "one side right" singularities and other "one side left" singularities correspond to the „one side left" and „one side right" relative equilibrium positions. Then, each roots of the corresponding algebra double equation (9) for $\mu = 0$, have two corresponding roots obtained from corresponding algebra double equation (9) for $\mu \neq 0$ and then there are present new fictive triggers of coupled one side singularities. Then we have trigger of the coupled triggers of coupled one side left, one central and one side right singularities, which are present in the system with Coulomb's type friction and with a corresponding nonlinear system with ideal constraints and with minimum a trigger of coupled singularities in its nonlinear dynamics.

Example 1. For the case that line is a circle shaped by $(z - R)^2 + x^2 = R^2$, $z = R - \sqrt{R^2 - x^2}$, for $\mu = 0$ and $\mu \neq 0$, from (9) there are two corresponding algebra equations, one of which for $\mu \neq 0$ is algebra double equations:

$$\Omega^2 x + g \frac{x}{\sqrt{R^2 - x^2}} = 0 \qquad \text{and}$$

$$\Omega^2 x \left(1 \mp \frac{\mu x}{\sqrt{R^2 - x^2}}\right) + g \left(\frac{x}{\sqrt{R^2 - x^2}} \pm \mu\right) = 0 \tag{10}$$

From first algebra equation for $\mu = 0$ of previous system (10) is visible that $x = 0$ is a root correspond to the equilibrium position, but there are also pair of the roots:

$$x_{1,3} = \pm \sqrt{R^2 - \frac{g^2}{\Omega^4}} \text{ for } \left|\frac{g}{R\Omega^2}\right| \le 1.$$ In this case for $\mu = 0$ in system dynamics minimum a

trigger of coupled three singularities exists. Also, we can conclude that second algebra equation for $\mu \ne 0$ have minimum two roots. First approximation of the minimum vales

of first two roots are $x_{1,3} \approx \pm 2\mu \frac{g}{\Omega^2}$, which correspond to the "one side right" and "one

side left" equilibrium positions and with $x = 0$ build a trigger of coupled two one side singularities appeared as a result of bifurcation by introducing Coulomb's type friction. By qualitative analyzing of the second algebra double equation from system (10) in the form:

$$x^4\left(1+\mu^2\right) - x^2\left(R^2 - \left(1+4\mu^2\right)\frac{g^2}{\Omega^4}\right) - x\left(\pm 2\mu \frac{gR^2}{\Omega^2}\right) - 4\mu^2 \frac{g^2 R^2}{\Omega^4} = 0 \, ,$$

we conclude that, also, one trigger of coupled three triggers of coupled one side singularities appear.

      Example 2. For the case that line is an ellipse shaped by $\left(\frac{z-R}{a}\right)^2 + \frac{x^2}{b^2} = 1$,

$$z = R \pm a\sqrt{1 - \frac{x^2}{b^2}} \, ,$$ for $\mu = 0$ and $\mu \ne 0$, from (9) there are two corresponding algebra

equations, one of which for $\mu \ne 0$ is algebra double equations (see Figure 8.b*):

$$\Omega^2 x \pm ag \frac{\frac{x}{b^2}}{\sqrt{1 - \frac{x^2}{b^2}}} = 0 \text{ and } \Omega^2 x \left(1 - \mu a \frac{\frac{x}{b^2}}{\sqrt{1 - \frac{x^2}{b^2}}}\right) + g\left(\pm a \frac{\frac{x}{b^2}}{\sqrt{1 - \frac{x^2}{b^2}}} \pm \mu\right) = 0 \text{ (11)}$$

      From first algebra equation for $\mu = 0$ of previous system (11) is visible that $x = 0$ is a root correspond to the equilibrium position, but there are also pair of two

roots: $x_{1,3} = \pm b\sqrt{1 - \left(\frac{ag}{b^2\Omega^2}\right)^2}$ for $\frac{ag}{b^2\Omega^2} < 1$. In this case for $\mu = 0$ in system

dynamics, minimum a trigger of coupled three singularities exists. Also, we can conclude that second algebra equation for $\mu \ne 0$ have minimum two roots. First approximation of

the minimum vales of first two roots are $x_{1,3} \approx \pm 2\mu \frac{g}{\Omega^2}$, which correspond to the "one

side right" and "one side left" equilibrium positions and with $x = 0$ build a trigger of coupled two one side singularities appeared as a result of bifurcation by introducing Coulomb's type friction. By qualitative analyzing of the second algebra double equation

from system (11) in the form: $\left(x \pm \mu \frac{g}{\Omega^2}\right)^2 \left(R^2 - x^2\right) = x^2\left(\frac{g}{\Omega^2} \mp \mu x\right)^2$, we conclude that

appear also one trigger of coupled three triggers of coupled one side singularities.

4.4. 2. Theorem of trigger of coupled singularities

Previous considered differential double equations of the heavy mass particle along rough curvilinear line with Coulomb's type friction is possible to express in the following generalized form of differential double equation with double signs (see Ref. [103] by Hedrih (Stevanović)).:

$$\ddot{x} \pm b_\mu \dot{x}^2 + g\left[k, F\left(x, \mp x_\mu\right)\right] f\left(x, \pm x_\mu\right) = 0 \quad for \quad \dot{x} \begin{smallmatrix} > \\ < \end{smallmatrix} 0 \tag{12}$$

where b_μ coefficient depending of Coulombs type coefficient of friction, and x_μ parameter in coordinate dimension depending of Coulombs type coefficient of friction and with a corresponding governing differential equation for ideal system dynamics for $x_\mu = 0$ in the following form:

$$\ddot{x} + g\left[k, F(x)\right] f(x) = 0 \tag{13}$$

4.4. 3. Theorem on the existence of a trigger of the coupled singularities and the separatrix in the form of number eight in the conservative system.

By using nonlinear dynamic analysis of systems with described nonlinear phenomenon of the trigger of coupled singularities and corresponding families of phase portraits and potential energies (see References [84-103]) as well as the corresponding experimental investigations of such non-linear dynamics in mechanical engineering systems with coupled rotation motions (see Refs. [96] and [87]) it was easy to define and to prove a series of the theorem of the existence of a trigger of coupled singularities in non-linear dynamical conservative and no conservative systems with periodical structure.

Theorem: *In the system whose dynamics can be described with the use of non-linear differential equation in the form* (see Refs. [88] and [89]):

$$\ddot{x} + g\left[k, F(x)\right] f(x) = 0 \tag{14}$$

and whose potential energy is in the form:

$$\mathbf{E} = m \int_0^x g\left[k, F(x)\right] f(x) dx = \mathbf{G}\left[k, F(x)\right] \tag{15}$$

in which the functions $f(x)$ and $g(x)$ are:

$$F(x) = \int_0^x f(x) dx \qquad and \qquad G(k, x) = \int_0^x g(k, x) dx \tag{16}$$

and satisfy the following conditions:

$$f(-x) = -f(x) \qquad\qquad g(k, x + nT_0) = g(k, x)$$
$$f(x + nT_0) = f(x) \qquad\qquad g(k, -x) = g(k, x)$$
$$f(0) = 0 \qquad\qquad g\left[k, F(x_r)\right] = 0, \; for \; k \in (k_1, k_2) \cup (k_2, k_3)... \tag{17}$$

$$f(x_s) = 0 , \quad x_s = sT_0, \quad s = 1,2,3,4,... \quad x_r = \pm x_0 \pm rT_0 ,$$

$$r = 0,1,2,3,4,... \quad |x_0| < \frac{T_0}{2}$$

$$g[k, F(x)] \neq 0, \text{ for } k \notin (k_1, k_2) \cup (k_2, k_3)...$$

and both functions $f(x)$ and $g(x)$ have one maximum or minimum in the interval between two zero roots:

$a*$ for parameters values $k \notin (k_{1\neq}, k_2) \cup (k_2, k_3)...$,   outside of the intervals $(k_{1\neq}, k_2) \cup (k_2, k_3)...$, **the trigger of singularities** in the local area **does not exist.**

$b*$ for parameters values $k \in (k_{1\neq}, k_2) \cup (k_2, k_3)...$,   inside of the intervals $(k_{1\neq}, k_2) \cup (k_2, k_3)...$, **the series of triggers of coupled singularities in the local domains exist.**

We can see that for the case a* the second derivative of the potential energy can be positive or negative: :

$$\left. \frac{d^2 \mathbf{E_p}}{dx^2} \right|_{x=x_s} = \begin{cases} \text{for} \quad \dfrac{df(0)}{dx} > 0 \quad \mathbf{E_{pmin}} \quad x_0 \\[2mm] \text{stable equilibrium p.} \\[4mm] \text{for} \quad \dfrac{df(x_s)}{dx} > 0 \quad \mathbf{E_{pmin}} \quad x_s \\ s = 2p, \ p = 1,2,3,4,... \qquad \text{stable equilibrium p.} \\[4mm] \text{for} \quad \dfrac{df(x_s)}{dx} < 0 \quad \mathbf{E_{p\,max}} \quad x_s \quad s = 2p-1, \\ p = 1,2,3,4,... \\ \text{unstable equilibrium p.} \end{cases} \qquad (18)$$

and equilibrium positions can be stable and unstable with corresponding singular points alternatively change, periodically, with period T_0 .from stable center to unstable saddle point, and corresponding phase portrait is without trigger of coupled singularities and without separatrix in the form of number eight.

Also we can see that for the case b* the second derivative of the potential energy can be positive or negative

$$\left. \frac{d^2 \mathbf{E_p}}{dx^2} \right|_{x=x_s} = m \left\{ g[k, F(x)] \frac{df(x)}{dx} \right\} \Bigg|_{x=x_s} < 0 \quad \mathbf{E_{p\,max}}$$

x_s .unstable equilibrium position

$$\left. \frac{d^2 \mathbf{E_p}}{dx^2} \right|_{x=x_r} = m \left\{ \frac{dg[k, F(x)]}{dF(x)} [f(x)]^2 \right\} \Bigg|_{x=x_r} > 0 \quad \mathbf{E_{p\,min}} \qquad (19)$$

x_r .stable equilibrium positions

and equilibrium positions can be stable and unstable with corresponding singular points alternatively change, periodically, with period T_0 .from stable center to unstable saddle points, and corresponding phase portrait is with triggers of coupled singularities and with series of the separatrix in the form of numbers eights. Then, the triggers of coupled singularities exist in the phase portrait in the intervals defined by: $x \in \left(-\dfrac{T_0}{2} + sT, \dfrac{T_0}{2} + sT \right)$ $s = 0,1,2,3,4,\dots$.

Integral energy of the system is in the form:

$$\dot{x}^2 + 2G[k, F(x)] = \dot{x}_0^2 + 2G[k, F(x(t_0))] = const \tag{20}$$

Equation of homoclinic orbit in the form number "eight" trough homoclinic point (0,0) is:

$$\dot{x}^2 + 2G[k, F(x)] = 2G[k, F(0)] = h_{0hc} = const \tag{21}$$

for $g[k, F(x_r)] = 0$, for $k \in (k_1, k_2) \cup (k_2, k_3)\dots$ in which the functions $F(x)$ and $G(k, x)$ are in the form (16) and satisfy the conditions (17).

In Figure 9 B* and B* equivalent of potential energy $\mathbf{E}_p(\varphi)$ graph of basic ideal mechanical system, which corresponds to no ideal Coulomb's type friction, is presented. In Figures 9 B*b*, B*c* and B*d* the sets of the homoclinic phase trajectory layering, for $\alpha_0 = 0$ and different values of the $k = \dfrac{1}{\lambda} = \left| \dfrac{g}{\ell \Omega^2} \right| \leq 1$ and axis eccentricity are presented. Homoclinic orbits in the form of number eight appear and disappear with changing parameter $k = \dfrac{1}{\lambda} = \left| \dfrac{g}{\ell \Omega^2} \right| \begin{smallmatrix} \leq \\ \geq \end{smallmatrix} 1$. Two sets of the of the singular points:

$\varphi_s = s\pi$, $s = 1,2,3,4,\dots$ and $\varphi_s = \arccos \dfrac{g}{\ell \Omega^2} \pm 2s\pi$, $s = 1,2,3,4,\dots$ fort $k = \dfrac{1}{\lambda} = \left| \dfrac{g}{\ell \Omega^2} \right| \leq 1$ exists

together with homoclinic orbits – separatrix in the form of number eight.

In Figure 9. A*a* equivalent of potential energy $\mathbf{E}_p(\varphi)$ graph of basic ideal mechanical system, which corresponds to no ideal Coulomb's type friction, is presented as a function of coordinate the φ . In Figures 9. (A*b*), (A*c*) and (A*d*) series of the phase trajectory portraits, for $\alpha_0 = 0$, and different values of the $k = \dfrac{1}{\lambda} = \left| \dfrac{g}{\ell \Omega^2} \right| \begin{smallmatrix} \leq \\ \geq \end{smallmatrix} 1$ and eccentricity of axis of circle rotation are presented. Two sets (A*b*) and (A*c*) of the of the singular points in phase portraits are visible: $\varphi_s = s\pi$, $s = 1,2,3,4,\dots$ and $\varphi_s = \arccos \dfrac{g}{\ell \Omega^2} \pm 2s\pi$, $s = 1,2,3,4,\dots$ for $k = \dfrac{1}{\lambda} = \left| \dfrac{g}{\ell \Omega^2} \right| \leq 1$ .One set (A*d*) of singular points in phase trajectory portrait is visible: $\varphi_s = s\pi$, $s = 1,2,3,4,\dots$ for $k = \dfrac{1}{\lambda} = \left| \dfrac{g}{\ell \Omega^2} \right| \geq 1$.
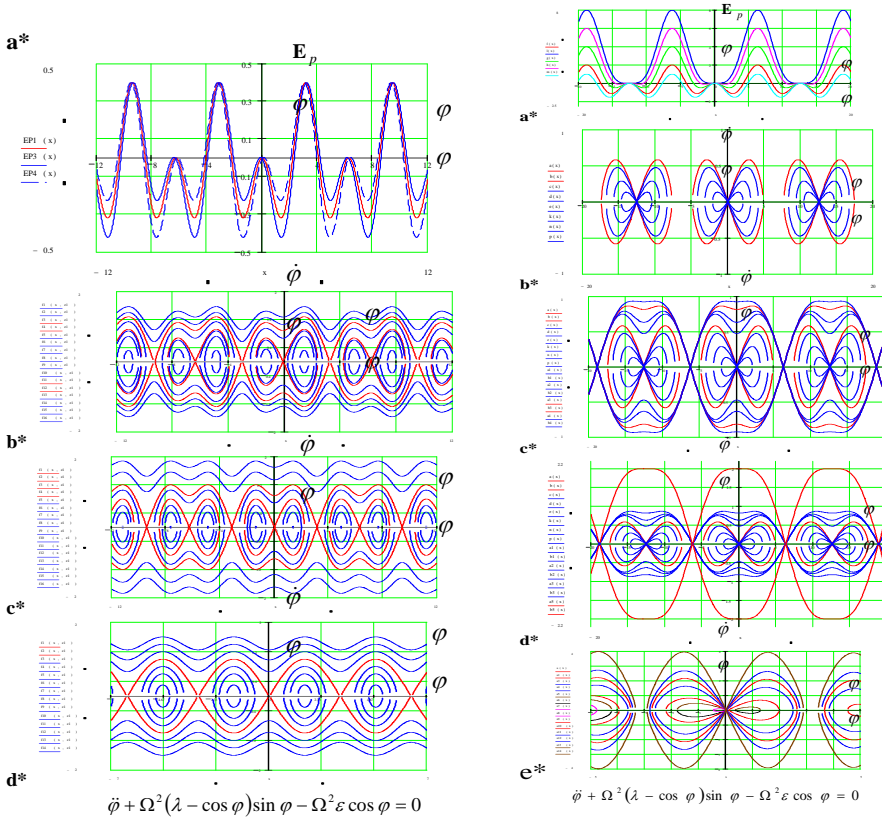
A*   B*

Figure 9. A* Equivalent of potential energy $\mathbf{E}_p(\varphi)$ graph of basic ideal mechanical system **(A*a*)** corresponding to no ideal Coulomb's type friction and phase trajectory portrait (**A*b***), (A*c*) and (A*d*) for $\alpha_0 = 0$ and different values of the $k = \frac{1}{\lambda} = \left| \frac{g}{\ell \Omega^2} \right| \begin{smallmatrix} \leq \\ \geq \end{smallmatrix} 1$ and axis eccentricity. Two sets (**A*b***) and (**A*c***) of the of the singular points: $\varphi_s = s\pi$, $s = 1,2,3,4,...$ and $\varphi_s = \arccos \frac{g}{\ell \Omega^2} \pm 2s\pi$, $s = 1,2,3,4,...$ fort $k = \frac{1}{\lambda} = \left| \frac{g}{\ell \Omega^2} \right| \leq 1$.

One set (A*d*) of singular points $\varphi_s = s\pi$, $s = 1,2,3,4,...$ for $k = \frac{1}{\lambda} = \left| \frac{g}{\ell \Omega^2} \right| \geq 1$.

Figure 9. B* Equivalent of potential energy $\mathbf{E}_p(\varphi)$ graph of basic ideal mechanical system (B* a*) correspond to no ideal wich Coulomb's type friction and homoclinic phase trajectory layering (B* b*), (B* c*) and (B* d*) for $\alpha_0 = 0$ and different values of the $k = \frac{1}{\lambda} = \left| \frac{g}{\ell \Omega^2} \right| \leq 1$ and axis eccentricity.

4.4. 4. Triggers of coupled singularities in non-linear dynamics of coupled double rotor systems with Coulomb's type friction

In this part, we start with a new model of the non-linear dynamics of two coupled rigid rotors with mass particle debalances and no ideal surfaces between rotor shafts and cylindrical bearing where appear Coulomb's type friction (for detail see Reference [87]).

In Figure 10. a* the structure of the coupled double rotor system with Coulomb's type friction into contact surfaces between rotor shafts and cylindrical bearings is presented. In Figure 10. b* decomposition of this system with plan of the Coulomb's type friction forces is presented.
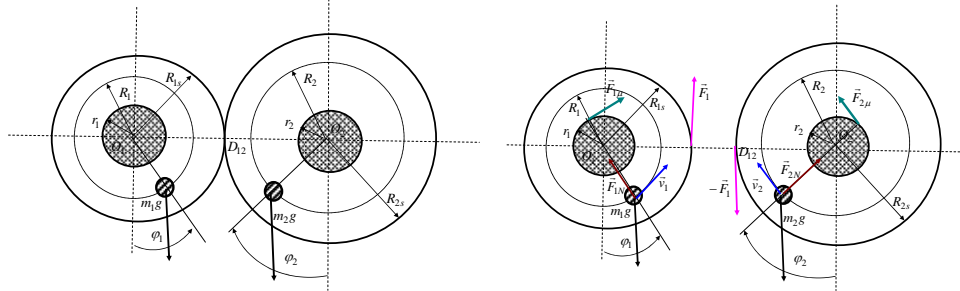

Figure 10. Coupled double rotor system (a*)with Coulomb's type friction into contact surfaces between discs and shafts; Decomposition (b*) of the system with plan of the Coulombs type friction forces

Governing nonlinear differential double equation of the coupled double rotor system dynamics with Coulomb's type friction into contact surfaces between rotor shafts and cylindrical bearings take the following form:

$$mR^3\left[\frac{1}{k}+\lambda p^2\right]\ddot{\varphi}\pm\mu mrR^2\left[\cos k\varphi-k\lambda p^2\cos\varphi\right]\ddot{\varphi}+mgR\sin\varphi\left(\frac{R}{k}\pm\mu r\cos k\varphi\right)-$$
$$-\lambda pmgR_2\sin k\varphi(R\mp\mu r\cos\varphi)\mp \quad (22)$$
$$\mp\mu rmg\left[\cos\varphi+\frac{R}{g}\dot{\varphi}^2\right]\left(\frac{R}{k}\pm\mu r\cos k\varphi\right)\mp\mu\lambda rmg\left[\cos k\varphi+\frac{pR}{g}k^2\dot{\varphi}^2\right](R\mp\mu r\cos\varphi)=0$$

For $k=2$ and for ideal constraints (by neglecting friction) previous differential equation obtain the following form:

$$\ddot{\varphi}+\frac{g}{R(1+2\lambda p^2)}(1-4\lambda p\cos\varphi)\sin\varphi=0 \quad (23)$$

Obtained differential equations (23) is in the class (13) and then on the basis of the listed theorem of trigger of coupled singularities in chapter VII.2.1.. we can conclude that non-linear dynamics in basic system when condition $\dfrac{1}{4\lambda p}\leq 1$ is satisfied appear a trigged of coupled singularities and in the phase trajectory portrait appear a homoclinic

orbit in the form of number eight. Sets of singularities are: first $\varphi_s = s\pi$ and second $\varphi_s = \arccos\dfrac{1}{4\lambda p}$ for $4\lambda p \geq 1$, presented in Figure 9..

4.4. 5. Concluding remarks

Systems with coupled multi-step rotors are important for engineering applications, then it is important to investigate ideal as well as no ideal system nonlinear dynamics. Also, no stability in the working processes of like that system dynamics caused higher level of noise and vibrations. Present Coulomb's type frictions in these kind of system dynamics caused new instability and more higher level of noise and vibrations. This is reason that is important to investigate non-linear phenomena in dynamics of other corresponding ideal as well as no ideal system dynamics. Also, system with vibro-impacts are important for engineering practice. Vibro-impacts are strong non-linearity with discontinuities in the system kinetic parameters and alternations of the forced and velocities directions in comparison before and after impacts (see Reference [102] an [104] by Hedrih (Stevanović), Raičević and Jović).

4.5. A review of the study of non-linear and stochastic vibrations through scientific research projects and doctoral dissertation and magistar thesis defended at Mechanical engineering faculty University of Niš in period 1972-2011 in area of Mechanics

IV.5.1. The study of the transfer of energy between sub-systems coupled in hybrid system (see Refs. [106-109], [55-56] by Heedrih (Stevanović) (1975, 1995a,b, 1887a,b, 2007a,b, 2008a,b), [57-60] by Hedrih (Stevanović) and Simonović (2009a,b,c) and [45] and [69]Hedrih (Stevanović) and Hedrih A. (2009a,b)) is very important for different applications. Two papers by author (see Refs. [72] and [76] by Heedrih (Stevanović) (2005, 2006 and 2008) presents analytical analysis of the transfer of energy between plates for free and forced transversal vibrations of an elastically connected double-plate system. Energy analysis of vibro-impact system dynamics with curvilinear trajectories and no ideal constraints was done by Jović in 2009 and in 2011 in his two theses (see References [128] and [12]), for Magister of science as well for   doctor's of sciences degrees. Potential energy and stress state in material with crack was study by Jovanović and presented in his Doctor's Degree Thesis in 2009 (see Ref. [126]). Energy analysis of the non-linear oscillatory motions of elastic and deformable bodies was done by Hedrih (Stevanović) her doctor's degree thesis in 1975 (see Ref. [109]). Energy analysis longitudinal oscillations of rods with changeable cross sections was original research results in 1995 presented by Filipovski in his magister of sciences degree thesis (see Ref. [119]). For all previous results see References from list in Appendix I – References VII – [105-130] and Appendix II – References VIII – [131-140] .

4.5.2. When, at an international conference ICNO in Kiev in 1969, my professor of mechanics and mathematics, D. P. Rašković (1910-1985) (see Refs. [32], [33], [34], [53]   and [54] Rašković (1965,1985) presented me to academician Yuri Alekseevich

Mitropolskiy (1917-2008) (see Refs. [61-68] by Mitropolskiy (1955, 1964, 1968, 1976 and 2003) and when I started really to understand the differences between linear and non-linear phenomena in dynamics of mechanical real systems, I knew I was on the right path of research which enchanted me ever more by understanding new phenomena and their variety in non-linear dynamics of realistic engineering and other dynamical systems. (First my knowledge about properties of non-linearity and the non-linear function I obtained in gymnasium from my excellent professor of mathematics Draginja Nikolić and during my research Matura work on the subject of Non-linear elementary functions and their graphics as a final high school examination.)

For beginning of this chapter, a review survey of original results of the author and of researchers from Faculty of Mechanical Engineering University of Niš (see References from lists in Appendix I – References VII – [105-130] and Appendix II – References VIII – [131-140]), inspired and/or obtained by the asymptotic method of Krilov-Bogolyubov-Mitropolyskiy, and as a direct influence of professor Rašković scientific instruction and also by published Mitropolskiy's papers and monographs, as well as publications by Kiev Mathematical institute scientists in area of non-linear and stochastic dynamics . These results have been published in scientific journals, and were presented on the scientific conferences and in the bachelor degree works (see [107] by Stevanović, (1967)), Magister of sciences theses (see [108] by Stevanović (1972), [110] by Kozić (1982), [112] by Pavlović (1982), [114] by Mitić (1985), [118] by Pavlov (993), [119] by Filipovski (1995), [121] by Janevski* (2004), [122] by Simonović (2008)) and doctoral dissertations (see [109] by (Stevanović) Hedrih (1975), [111] by Kozić (1990), [113] by Pavloić (1990), [115] by Mitić (1994), [127] by Knežević (2000), [124] by Perić (2005), [126] by Jovanović (2009), [127] by Janevski* (2010), [128] by Jović** (2011), [129] by Simonović (2011) and [130] by Veljović (2011)) supervised by Mitropolskiy (in period from 1972 to 1975) or by Rašković (in period from 1964 to 1974) and by Hedrih in period from 1976 to 2011 year as well. For all previous results see References from list in Appendix I – References VII – [105-130] and Appendix II – References VIII – [131-140].

In area of stochastic stability a scientific supports by series of consultation to researchers was given by Kiev stochastic research group at Institute of Matmematics NANU , S.T. Ariaratnam (Canada) and A. Tylikowski (Polad) and also by their papers.

The original results contain asymptotic analysis of the non-linear oscillatory motions of elastic bodies: beams, plates, shells and shafts (see References by (Stevanović) Hedrih (1972, 1981, 1978, 1983, 1984, 1985, 1995); Hedrih and Rašković (1974); Hedrih, Kozić, Pavlović, Mitić and Filipovski (1983, 1984, 1985, 1986, 1993, 1996, 1995)). Also, late a series of new research results are obtained by Janevski in 2003 [121] and by Simonovic in 2008 [122, 129] an in 2011 and also by Veljovic in 2011 [130] . The multi-frequency oscillatory motion of elastic bodies was studied. Corresponding system of partial differential equations of system dynamics, as well as system of first approximation of ordinary differential equations for corresponding numbers of amplitudes and phases of multi-frequency regimes of elastic bodies non-linear oscillations were composed. The characteristic properties of non-linear systems passing through coupled multi-frequency resonant state and mutual influences between excited modes were discovered.

In the same cited papers amplitude-frequency and phase frequency curves for stationary and no stationary coupled multi-frequency resonant kinetic states, based on the numerical experiment on the system of ordinary differential equations in first approximation are presented. Resonant jumps are pointed out in the both series of graphical presentation: amplitude-frequency and phase frequency curves for the case of the resonant interactions between modes in the same frequency resonant intervals.

Using ideas of averaging and asymptotic methods Krilov-Bogoliyubov-Mitropolyskiy in the Doctoral dissertation [109] and in References (see Refs. Hedrih (Stevanović) (1975, 1972, 1981, 1978, 1983, 1984, 1985, 1995)) author gives the first asymptotic approximations of the solutions for one-, two- , three- and four-frequency vibrations of non-linear elastic beams, shaft and thin elastic plates, as well as of the thin elastic shells with positive constant Gauss's curvatures and finite deformations, and system of the ordinary differential equations in first asymptotic approximation for corresponding numbers of amplitudes and phases for stationary and no stationary vibration regimes.

Some results of an investigation of multi-frequency vibrations in single-frequency regime in non-linear systems with many degrees of freedom and with slow-changing parameters are presented by Stevanović and Rašković article (1974). Application of the Krilov-Bogolyubov-Mitropolskiy asymptotic method for study of elastic bodies non-linear oscillations and energetic analysis of the elastic bodies oscillatory motions give new results in theses [108] by Stevanović in 1975. One-frequency transversal oscillations of thin rectangular plate with non-linear constitutive material stress-strain relations and non-linear transversal vibrations of a plate with special analysis of influence of weak non-linear boundary conditions are contents of the articles by Hedrih (1979, 1981).

First approximation of an asymptotic particular solution of the non-linear equations of a thin elastic shell with positive Gauss' curvature in two-frequency regime is pointed out in the article by Hedrih (1983). Two-frequency oscillations of the thin elastic shells with finite deformations and interactions between harmonics have been studied by Hedrih and Mitić (1983) and multi frequency forced vibrations of thin elastic shells with a positive Gauss's curvature and finite displacements by Hedrih (1984). Also, on the mutual influence between modes in non-linear systems with small parameter applied to the multi-frequencies plate oscillations are studied by Hedrih, Kozić, Pavlović and Mitić (1984).

Multi-frequency forced vibrations of thin elastic shells with a positive Gauss' curvature and finite deformations and initial deformations influence of the shell middle surface to the phase-frequency characteristics of the non-linear stationary forced shell's vibrations and numerical analysis of the four-frequency vibrations of thin elastic shells with Gauss' positive curvature and finite deformations are content of reference by Hedrih and Mitić (1985). Also, initial displacement deformation influence of the thin elastic shell middle surface to the resonant jumps appearance was investigated by same authors Hedrih and Mitić (1987). By means of the graphical presentations from the cited References, analysis was made and some conclusions about non-linear phenomenon in multi-frequency vibrations regimes were pointed out. Some of these conclusions we quote here: Non-linearities are the reason for the appearance of interaction between modes in multi-frequency regimes; In the coupled resonant state one or several resonant

jumps appear on the amplitude-frequency and phase frequency curves; these resonant jumps are from smaller to greater amplitudes and vice versa.

Unique trigger of coupled singularities (Hedrih (2003)) with one unstable homoclinic saddle type point, and with two singular stable center type points appear in one frequency stationary resonant kinetic state. It is visible on the phase-frequency as well as on the amplitude-frequency graphs for stationary resonant state.

In the case of the multi-frequency coupled resonant state and in the appearance of the more resonant coupled modes in resonant range of corresponding frequencies, unique trigger of coupled singularities, and multiplied triggers of coupled singularities (see Refs. by Hedrih, 2004, 2005) appear. Maximum number of triggers of coupled singularities is adequate to number of coupled modes and resonant frequencies of external excitations. Multiplied triggers contain multiple unstable saddle homoclinic points in the mapped phase plane as the number of resonant frequencies of external excitations. For example, if a four-frequency coupled resonant process in u-v plane is in question, four homoclinic saddle type points appear. The appearance of these unstable homoclinic saddle points requires further study, since it induces instability in a stationary non-linear multi-frequency kinetic process.

By use a double circular plate system, presented in the References by Hedrih (Stevanović) and Simonović (2005,2006 and 2007), the multi-frequency analysis of the non-linear dynamics with different approaches and by use different kinetic parameters of multi-frequency regimes is pointed out. Series of the amplitude-frequency and phase-frequency graphs as well as eigen-time functions–frequency graphs are obtained for stationary resonant states and analysed according present singularities and triggers of coupled singularities, as well as resonant jumps.

An analogy between non-linear phenomena in particular multi-frequency stationary resonant regimes of multi circular plate system non-linear dynamics, multi-beam system non-linear dynamics and corresponding regimes in chain system non-linear dynamics is identified (see References by Hedrih (Stevanović) listed in the reference list from period 1972-2010).

Using differential equations systems of the first approximation of multi-frequency regime of stationary and no stationary resonant kinetic states, we analysed the energy of excited modes and transfer of energy from one to other modes. On the basis of this analysis, the question of excitation of lower frequency modes by higher frequency mode in the non-linear multi-frequency vibration regimes was opened.

4.5.3. In the Reference by Hedrih (Stevanović) and Hedrih (2009), the expressions for the kinetic and potential energy as well as energy interaction between chains in the double DNA chain helix are obtained and analyzed for a linearized model. Corresponding expressions of the kinetic and potential energies of these uncoupled main chains are also defined for the eigen main chains of the double DNA chain helix. By obtained expressions, we concluded that there is no energy interaction between eigen main chains of the double DNA chain helix system. Time expressions of the main coordinates of the two eigen main chains are expressed by time, and eigen circular frequencies are obtained. Also, generalized coordinates of the double DNA chain helix are expressed by time correspond to the sets of the eigen circular frequencies. These data contribute to better understanding of biomechanical events of DNA transcription that occur parallel with biochemical processes. Considered as a linear mechanical

system, DNA molecule as a double chain helix has its eigen circular frequencies and that is its characteristic. Mathematically it is possible to decouple it into two chains with their set with corresponding eigen circular frequencies which are different. This may correspond to different chemical structure (the order of base pairs) of the complementary chains of DNA. We are free to propose that every specific set of base pair order has its eigen circular frequencies and its corresponding oscillatory energy and it changes when DNA chains are coupled in the system of double chain helix. Oscillations of base pairs and corresponding oscillatory energy for specific set of base pairs may contribute to conformational chances of DNA double helix, and its unzipping and folding.

4. 5.4. General concluding remarks

For limited length of paper, now we made only some comments concerning the following

* Lissajous' curves, orthogonal asynchronous and synchronous oscillations, asynchronization and synchronization of subsystem in hybrid system dynamics.

Series of **Lissajous curves as well as new series of the generalized Lissajous curves** obtained by software MathCad as a results of the coupled orthogonal multi-frequency oscillations are suitable for to build a method of asynchronization/synchronization for applications to the discrete continuum for synchronization some parts of discrete continuum. By this method based on attractors of asynchronization/synchronization of the component oscillations of the subsystems of hybrid system is possible and suitable for to obtain conditions of the integrity of the dynamical system. Generalized **Lissajous curves** can be used as attractors of asynchronization/synchronization of the component subsystem oscillations which are coupled as that these oscillations are orthogonal. By changing some parameters of the coupled oscillators synchronization and by use current software tools as it is MathCad (or MathLab or Mathematica), the visualization of the transformation of the generalized **Lissajous curve,** up to its degeneration into part of straight line, can be obtain as results of the orthogonal coupling of oscillatory multi-frequency signals. If this degeneration is not possible, then these oscillators it is not possible to synchronized and corresponding parameter is not parameter of synchronization. If as results of the change of some parameters of the coupled oscillators synchronization is transformation of the generalized **Lissajous curve** into one unique line then it is possible to obtain system parameters of the attractor of partially synchronization or asynchronization of the coupled oscillators.

Also, there are some models of the discrete continuum in plane or in the space, which mass particles moves oscillatory as result of coupled two in plane, or three in space, orthogonal multi-frequency oscillations Trajectories of this mass particles are generalized **Lissajous curves.** Applications of the knowledge about generalized **Lissajous curves** is important for constructions of some processing machines with working processes based on the motion of the coupled orthogonal multi frequency vibrations.

Ito's stochastic differential equations and applications to stochastic oscillations of mechanical systems with hereditary properties are also actual mathematical task for open possibilities in engineering practice, as well as in other area of science.

Mathematical analogy and phenomenological mapping by use mathematical models in applications to disparate physical models dynamics open very large interactions between different area of science and easier transfer knowledge from one area of science to other.

Also, one of main education task of Serbian mathematicians and other university professor to fined minimum volume of the classical and new current mathematical knowledge necessary to be in the programs of Ph.D. study enough for mathematical background of new Ph.D. specialist for their next two decade research and possibility to accept new and future mathematical discovery and be competent to applied these new mathematical knowledge in research and practice, as well as to define new mathematical tasks appear from his research and to directed to mathematicians for future research.

References I.

1. Hedrih (Stevanović) K., (1992), On some interpretations of the rigid bodies kinetic parameters, XVIIIth ICTAM HAIFA, Apstracts, pp. 73-74.
2. Hedrih (Stevanović) K., (1993), Same vectorial interpretations of the kinetic parameters of solid material lines, ZAMM. Angew.Math. Mech. 73(1993) 4-5, T153-T156.
3. Hedrih (Stevanović) K., (1993), The mass moment vectors at n-dimensional coordinate system, Tensor, Japan, Vol 54 (1993), pp. 83-87.
4. Hedrih (Stevanović) K., (2001), Vector Method of the Heavy Rotor Kinetic Parameter Analysis and Nonlinear Dynamics, University of Niš 2001, Monograph, p. 252. (in English), YU ISBN 86-7181-046-1.
5. Hedrih (Stevanović) K., (1998), *Vectors of the Body Mass Moments*, Monograph paper, Topics from Mathematics and Mechanics, Mathematical institute SANU, Belgrade, Zbornik radova 8(16), 1998, pp. 45-104. Published in 1999. (in English), (Zentralblatt Review).
6. Hedrih (Stevanović) K., (2001), *Derivatives of the Mass Moment Vectors at the Dimensional Coordinate System N*, dedicated to memory of Professor D. Mitrinović, Facta Universitatis Series Mathematics and Informatics, 13 (1998), pp. 139-150. (1998, published in 2001. Edited by G. Milovanović).
7. Hedrih (Stevanović) K., (1998), *Derivatives of the Mass Moments Vectors with Applications*, Invited Lecture, Proceedings, 5th National Congress on Mechanics, Ioannina, 1998, pp. 694-705.
8. Hedrih (Stevanović) K., *Leonhard Euler (1707-1783) and Rigid Body Dynamics*, Scientific Technical Review, Vol. LVII, No. 3-4, Belgrade, 2007 . pp. 3-12. YU ISSN 1820-0206.
9. Hedrih (Stevanović) K., (1991), Analogy *between models of stress state, strain state and state of the body mass inertia moments,* Facta Universitatis, Series Mechanics, Automatic Control and Robotics, Niš, vol.1, N 1, 1991, pp. 105-120.
10. Hedrih (Stevanović) K., (1994), Interpretation of the motion of a heavy body around a stationary axis in the field with turbulent damping and kinetic pressures on bearing by means of the mass moment vector for the pole and the axis, Facta Universitatis Series Mechanics, Automatic Control and Robotics, Vol. 1, No.4, 1994, pp. 519-538.

11. Hedrih (Stevanović) K., (1998), Vector method of the kinetic parameters analysis of the rotor with many axes and nonlinear dynamics, Parallel General Lecture, Third International Conference on Nonlinear Mechanics (ICNM III), August 17-20, 1998, Shanghai, China, pp. .42-47.\

12. Hedrih (Stevanović) K., (2004), *Contribution to the coupled rotor nonlinear dynamics,* Advances in nonlinear Sciences, Monograph, Belgrade, Academy of Nonlinear Sciences, 229-259. ISBN 86-905633-0-X   UDC 530-18299(082)   51-73:53(082) UKUP. STR. 261.

13. Hedrih (Stevanović) K., Interpretation of the Motion Equations of a variable mass object rotating around a atationary axis by means of the mass moment vector for the pole and the axis, Procedings of the 4th Greek National Congress on Mechanics, vol. 1, Mechanics of Solids, Democritus University of Trace, Xanthi, 1995, pp. 690-696.

14. Hedrih (Stevanović) K., (1998), Nonlinear Dynamics of the heavy Rotor with Two Rotation Axes in the Turbulent Damping Field, Invited Lecture, Abstracts, Greek–Serbian Symposium on Mechenics - Recent Advances in Mechanics, Xanthi, July 10-12, 1998, Democritus University of Thrace, pp. 43-44.

15. Hedrih (Stevanović) K R., 2010, Kinetic Impulses - Impacts On Rotating Rigid Rotor Bearings, Scientific Technical Review, 2010, Vol.60,No.3-4, pp.54-66, UDK: 531.38:514.732.4,62-253, COSATI: 12-01, 20-11, 13-07.

16. Hedrih (Stevanović) K, Veljović Lj., (2010), *The Kinetic Pressure of the Gyrorotor Eigen Shaft Bearings and Rotators*, The Third International Conference Nonlinear Dynamics – 2010, pp. 78-83

17. Hedrih (Stevanović) K., Veljović Lj., (2008), *Nonlinear dynamics of the heavy gyro-rotor with two skew rotating axes*, Journal of Physics: Conference Series, **96** (2008) 012221 DOI:10.1088/1742-6596/96/1/012221, IOP Publishing http://www.iop.org/EJ/main/-list=current/

18. Hedrih (Stevanović) K., Veljović Lj., (2008),, Vector Rotators of a Rigid Body Dynamics with Coupled Rotations around Axes without Intersection, International Journal Mathematical Problems in Engineering, MPE/351269 Hindawi Publishing Corporation, Mathematical Problems in Engineering, Volume 2011, Article ID 351269, 26 pages, doi:10.1155/2011/351269

19. Hedrih (Stevanović) K, *and Ivancevic T. ,* RIGOROUS KINETIC ANALYSIS OF THE RACKET FLICK-MOTION IN TENNIS FOR GENERATING TOPSPIN AND BACKSPIN, In: International Journal of Mathematics, Game Theory and Algebra , Volume 20, Issue 2, pp. 1–26 © 2011 Nova Science Publishers, Inc., ISSN: 1060-9881

20. Rašković, D.,(1972), *Mehanika III – Dinamika* (*Mechanics III – Dynamics)*), Naučna knjiga, 1972, p. 424.

References II.

21. Hedrih (Stevanović), K., (1994), Snaga promene reonomnih veza, (The Power of the Rheonomic Constraints Change), Zbornik radova Jugoslovenskog društva za mehaniku, Simpozijum iz Opšte mehanike, Novi Sad, 1994, pp. 177-184.

22. Hedrih (Stevanović) R. Katica , (2010), Visibility or appearance of nonlinearity, Tensor, N.S. Vol. 72, No. 1 (2010), pp. 14-33, #3. Tensor Society, Chigasaki, Japan, ISSN 0040-3504.

23. Hedrih (Stevanović), K., (1994), Snaga promene reonomnih veza, (The Power of the Rheonomic Constraints Change), Zbornik radova Jugoslovenskog društva za mehaniku, Simpozijum iz Opšte mehanike, Novi Sad, 1994, pp. 177-184.

24. Hedrih (Stevanović) K., The Dissipation Function of a Nonconservative System of Mass Particles, Tensor, N.S.,Vol.63, No.2(2002), pp.176-186. Tensor Society , Japan .

25. Hedrih (Stevanović) K., (2004), On Rheonomic Systems with Equivalent Holonomic Conservative Systems Applied to the Nonlinear Dynamics of the Watt's Regulator, Proceedings, Volume 2, The eleventh world congress in Mechanism and machine Sciences, IFToMM, China Machine press, Tianjin, China, April 1-4, 2004, pp. 1475-1479. ISBN 7-111-14073-7/TH-1438. . http://www.iftomm2003.com, Publisher: China Machine press, Tianjin, China.

26. Hedrih (Stevanovi}), K., *Rheonomic Coordinate method Applid to Nonlinear Vibration Systems with Hereditary Elements*, (www-EUROMECH 3rd ENOC, Copenhagen 1999, http:// www.imm.dtu.dk/ documents/user /mps/ENOC/proceeedings/, Technical University of Denmark.4A, pp. 1-24.).

27. Hedrih (Stevanovi}), K., *Rheonomic Coordinate method Applid to Nonlinear Vibration Systems with Hereditary Elements*, Facta Universitatis, series, Mechanics, Automatic Contrl and Robotics, Vol.2, No. 10, 2000, pp. 1111-1135.

28. Katica (Stevanovic) Hedrih, *On Rheonomic Systems in the Field with Turbulent Damping with Equaivalent Holonomic Nonconservative System*, EUROMECH Forth European Conference on

European Nonlinear Oscillations Conference (ENOC), August 19-23, 2002, Moscow, Russia. *Topics:* Analysis of Bifurcations and Chaos.

29. Hedrih (Stevanović), K., (2007),, *Prezentacija predavanja iz predmeta Mehanika III- Dinamika,* školska 2006/07, po nedelama u on-line verziji dostupna na adresi: http://www.hm.co.yu/mehanika/

30. Camelia Frigioiu, Katica (Stevanovic) Hedrih - On the Geometrization of the Rheonomic Lagrangian Mechanical Systems Analele Universit_at_ii Oradea, Fasc. Matematica, Tom XVII (2010), Issue No. 1, 89-97,

31. Vujičić, V. and Hedrih (Stevanovi}), K., (1993), The Rheonomic Constraints Force, Facta Universitatis", Series "Mechanics, Automatic Control and Robotics", Vol. 1, N3, 1993, Ni{. pp. 313-322   .
        MethSci Disc 1993-1996, reccord 2 of 4, , MR 96m:700015, Kreuzer, Edwin, J., (Hamburg) Mathematiccal Reviews.

32. Rašković P. Danilo, *Analitička mehanika*, Mašinski fakultet Kragujevac, 1974.

33. Rašković P. Danilo, *Osnovi tenzorskog računa*, Mašinski fakultet Kragujevac, 1974.

34. Rašković P. Danilo, *Mehanika II- Kinematika,* III i dalja izdanja, Zavod za izdavanje udžbenika, 1953, 1966, str.347.

References III.

35. Goroško O. A. i Hedrih (Stevanović) K., (2001), *Analitička dinamika (mehanika) diskretnih naslednih sistema, (Analytical Dynamics (Mechanics) of Discrete Hereditary Systems*), University of Niš, 2001, Monograph, p. 426, YU ISBN 86-7181-054-2.

36. Gorosko O.A., Hedrih (Stevanović) K., The construction of the Lagrange Mechanics of the discrete hereditary systems, FACTA UNIVERSITATIS, Series: Mechanics, Automatic Control and Robotics Vol. 6, Nº 1, 2007, pp. 375 - 22.

37. Goroško O. A. i Hedrih (Stevanović) K., (2008), Advances in development of the analytical dynamics of the hereditary discrete systems, Journal of Physics: Conference Series, 96 (2008) 012143, IOP Publishing.

38. Bačlić, B. S., Atanacković, T., (2000), M., *Stability and creep of a fractional derivative order viscoelastic Rod*, Bulletin T, CXXI de L'Academie Serbe des Sciences st de Arts - 2000, Class des Sciences mathematmatques et naturelles Sciences mathematiques, No. 25, 115-131.

39. Hedrih (Stevanović) K. and Filipovski A., (2002), *Longitudinal Creep Vibrations of a Fractional Derivative Order Rheological Rod with Variable Cross Section*, Facta Universitatis, Series Mechanics, Automatics Control and Robotics, Vo. 3, No. 12, 2002**,** pp. 327-350. (in English)**.**YU ISSN 0354-2009**.**

40. Hedrih (Stevanović) K., (2006), Modes of the Homogeneous Chain Dynamics, Signal Processing, Elsevier, 86(2006), 2678-2702.. ISSN: 0165-1684 www.sciencedirect.com/science/journal/01651684

41. Hedtrih (Stevanović) K., (2008), Dynamics of coupled systems, Nonlinear Analysis: Hybrid Systems, Volume 2, Issue 2, June 2008, Pages 310-334.

42. Hedrih (Stevanović) K., (2005), Partial Fractional Order Differential Equations of Transversal Vibrations of Creep-connected Double Plate Systems, in Monograph - Fractional Differentiation and its Applications, Edited by Alain Le Mahaute, J. A. Tenreiro Machado, Jean Claude Trigeassou and Jocelyn Sabatier, p. 780, U-Book, Printed in Germany, pp. 289-302.

43. Hedrih (Stevanović K., (2008), Main chains and eigen modes of the fractional order hybrid multi-pendulum system dynamics, IOP PUBLISHING PHYSICA SCRIPTA, Phys. Scr. 78 (2008) 000000 (12pp) doi:10.1088/0031-8949/78/8/000000

44. Hedtrih (Stevanović) K., (2008), *Dynamics of multi-pendulum systems with fractional order creep elements, Special Issue Vibration and Chaos,* Journal of Theoretical and Applied Mechanics, Quaterly, (Warsaw, Poland) No.3 Vol. 46, pp. 483-509.

45. Hedrih (Stevanović) and. Hedrih, N Andjelka (2009), Eigen main chain modes of the double DNA fractional order chain helix vibrations (Part I), Proceedings 2nd International Congress Of Serbian Society Of Mechanics-IConSSM 2009,M1-03, CD, pp. 1-15.

46. Hedrih (Stevanović) Katica (2009), *Considering Transfer of Signals through Hybrid Fractional Order Homogeneous Structure, Keynote Lecture*, AAS-09, Ohird, Makedonija, posvecen profesoru Pane Vidincevu, prvom profesoru automatike i rachnarskih mashina u Makedoniji Special session, Applied Automatic Systems , Proceedings of selected AAS 2009 Papers. Edited by G. Dimirovski, Skopje – Istambul , 2009, ISBN -13-978-9989-2175-6-2, National Library of R. Makedonia, Skopje, Copright«2009Authors and ETAI Society, pp. 19-24.

47. Hedrih (Stevanović K., Tensor equations of discrete dynamically defined and undefined systems with hereditary and creep light elements, Analele Stiintieice Ale Universitatii "Alexandru Ioan Cuza" Din (ASI (S.N) Matematica -Scientific Annals of "Al.I. Cuza" University of Iasi, Matematica, Tom XCI, 2010, f. 1, pp. 131-149.

48. Hedrih (Stevanović K., (2008), The fractional order hybrid system vibrations, Monograph, Advances in Nonlinear Sciences, ANN, 2008, Vol. 2, pp. 226-326.

49. Hedrih (Stevanović), K., *Discrete Continuum Method*, Symposium, Recent Advances in Analytical Dynamics Control, Stability and Differential Geometry, Proceedings Mathematical institute SANU Edited by Vladan Djordjević, p.151, 2002, pp.30-57. ISBN 86-80593-32-X. **http://www.mi.sanu.ac.yu/publications.htm**

50. Hedrih (Stevanović) K., (2004), *Discrete Continuum Method,* COMPUTATIONAL   MECHANICS, **WCCM** VI in conjunction with **APCOM'**04, *Sept. 5-10, 2004, Beijing, China,* © 2004 Tsinghua University Press & Springer-Verlag, pp. 1-11, CD. IACAM International Association for Computational Mechanics – www. iacm.info

51. Hedrih (Stevanović), K., Filipovski, A., *Longitudinal Vibrations of Rheological Rod with Variable Cross Section*, Int. Journal Comunications in Nonlinear Sciences and Numerical Simulations, Shanghai Inst. of Applied Mathem. and Mechanics, China, 1999, vol.4, No. 3, pp. 89-95. ISSN 10007 5704 - Center for Nonlinear Science peking University, China.

52. Hedrih (Stevanovi}), K., Thermorheological Hereditary Pendulum, (Ref. No. TVP-11) Thermal Stresses 99, Edited by J.J. Skrzypek and R. B. Hetnarski, Cracow 1999, pp.199-202.

53. Rašković, D., (1965), Teorija oscilacija, Naučna knjiga, 1965, 503.

54. Rašković, D., (1985), Teorija elastičnosti, Naučna knjiga, 1985, 414

References IV.

55. Hedrih (Stevanović) R. Katica, (2010), Energy analysis in the hybrid system forced regimes, Zbornik praci Institutu Matematiki NANU Ukeaini (Proceeding of Institute of Mathematics NANU Ikraine) , 2010, Vol. 7, No. 3, pp. 90-107. Збірник праць Інституту математики НАН України   2010, т. 7, № 3, 90–107

56. Hedrih (Stevanović) K., Energy and Nonlinear Dynamics of Hybrid System, Dynamical Systems and Methods, Edited by Albert Luo. Springer (in press).

57. Hedrih (Stevanović) K., (2010), Discontinuity of kinetic parameter properties in nonlinear dynamics of mechanical systems, Keynote Invited Lecture, 9th Brazilian Conference on Dynamics, Control and Their Applications - 9º Congresso Temático de Dinâmica, Controle e Aplicaçõesm,   June 07-11, 2010. UneSP, Sao Paolo (Serra negra), Brazil, Proceedings of the 9th Brazilian Conference on Dynamics Control and their Applications, Serra Negra, 2010, pp. 8-40. SP - ISSN 2178-3667.

58. Hedrih (Stevanović) K., *Simonović J. D.* , (2010), *Non-linear dynamics of the sandwich double circular plate system*, Int. J. Non-Linear Mech, Volume 45, Issue 9, November 2010, pp. 902-918, ISSN: 0218-1274.

59. Hedrih (Stevanović) K R. and Simonović J., Multi-frequency analysis of the double circular plate system non-linear dynamics", Nonlinear Dynamics, Springer, NODY1915R2, (has been accepted for publication) DOI: 10.1007/s11071-011-0147-7 .

60. Hedrih (Stevanović) K R. and Simonović J., Energies of the dynamics in a double circular plate non-linear system, #262; INTERNATIONAL JOURNAL OF BIFURCATION AND CHAOS.(in press).

61. Mitropolyskiy, Yu. A. (1955), *Nestashionarnie proshesi v nelinyeynih sistemah*, AN USSR, Kiev. (in Russian).

62. Mitropolyskiy, Yu.A and Mosseenkov, B.I., (1968), Lekciyi po primenyeniyu metodov k recheniyu uravnyeniy v chastnih proizvodnih, Int. Math. AN USSR, Kiev. (in Russian).

63. Mitropolyskiy, Yu.A, (1964), Problemi asimptoti-cheskoy   teorii nestashionarnih kolebaniy, Nauka Moskva. (in Russian).

64. Mitropolyskiy, Yu.A and Mosseenkov, B.I., (1976), *Assimptoticheskie recheniya uravnyeniya v chastnih proizvodnih*, Vichaya chkola Kiev. (in Russian).

65. Mitropolskiy Yu.A., Nguyen Van Dao, (2003), *Lectures on Asymptotic Methods of Nonlinear Dynamics*, Vietnam National University Publishing House, Hanoi, p. 494.

66. Mitropolskiy Yu.A., Some problems in the development in nonlinear mechanics theory and applications, Facta Universitatis, Series Mechanics, Automatic Control and Robotics, Vol. 1, No. 5,1995, pp. 539-560.

67. Mitropolskiy Yu.A., On Application of asymptotic methods of nonlinear mechanics for solving some problems of oscillation theory, Facta Universitatis, Series Mechanics, Automatic Control and Robotics, Vol. 2, No. 6,1996, pp. 1-9.

68. Mitropolskiy Yu.A., Adiabatic processes in nonlinear oscillation systems (Adiabaticheskie processi v nelinyeynih kolebatelynih sistemah), Simpozijum '83 – Nelinearni problemi dinamike, Arandjelovac, 23-25,, Novembar 1983. IT-Društvp za mehaniku Srbije, pp. I-1-I-12. (in Russia).

References V

69. Hedrih (Stevanović) K., Hedrih A. N., Eigen modes of the double DNA chain helix vibrations has benn qualified for publication in Journal of Theoretical and Applied Mechanics (JTAM), no. 1, vol. 48, 2010., pp. 219-231.

70. Hedrih (Stevanović K., Tensor equations of discrete dynamically defined and undefined systems with hereditary and creep light elements, Analele Stiintieice Ale Universitatii "Alexandru Ioan Cuza" Din (ASI (S.N) Matematica -Scientific Annals of "Al.I. Cuza" University of Iasi, Matematica, Tom XCI, 2010, f. 1, pp. 131-149.

71. Camelia Frigioiu, Katica (Stevanovic) Hedrih - On the Geometrization of the Rheonomic Lagrangian Mechanical Systems Analele Universit_at_ii Oradea, Fasc. Matematica, Tom XVII (2010), Issue No. 1, 89-97.

72. Hedrih (Stevanovi´c) K., Energy transfer in the hybrid system dynamics (energy transfer in the axially moving double belt system), Special Issue, **ARCHIVE OF APPLIED MECHANICS**, DOI 10.1007/s00419-008-0285-7. Archive of Applied Mechanics, (2009) vol.79, No.6-7 pp. 529-540.

73. Hedrih (Stevanović K., Main chains and eigen modes of the fractional order hybrid multipendulum system dynamics, **IOP PUBLISHING PHYSICA SCRIPTA**, vol. T136, Phys. Scr. 78 (2008) 000000 (12pp) doi:10.1088/0031-8949/78/8/000000.

74. Hedrih (Stevanović K., Energy analysis in a nonlinear hybrid system containing linear and nonlinear subsystems coupled by hereditary element (Article), **NONLINEAR DYNAMICS** , (2008) vol.51 br.1-2 str. 127 -140. DOI 10.1007/s11071-007-9197-2.

75. Hedrih (Stevanović K., Transversal forced vibrations of an axially moving sandwich belt system, Archive of Applied Mechanics, Springer, (2008) vol.78 br.9 str. 725-735

76. Katica (Stevanović) Hedrih, (2008), Energy transfer in double plate system dynamics, Acta Mechanica Sinica, Volume 24, Number 3 / June, 2008, pp. 331-344, DOI 10.1007/s10409-007-0124-z, Springer Berlin / Heidelberg, ISSN (567-7718 (Print) 1614-3116 (Online).

77. Katica (Stevanović) Hedrih, (2008), Energy interaction between linear and nonlinear oscillators (Energy transient through the subsystems in the hybrid system), *ISSN 1027-3190. Ukr. mat. Ωurn., 2008, t. 60, # 6, pp. 796-814.*

78. Hedrih (Stevanović K., Vibration Modes of a axially moving double belt system with creep layer ,Journal of Vibration and Control, (2008), 14(10-Sep): 1333-1347.

79. Hedrih (Stevanović K., Transversal vibration of a parametrically excited hereditary beam: Influence of rotatory inertia and transverse shear on stochastic stability of deformable forms and processes , International IFNA-ANS Journal "Problems of nonlinear analysis in engineering systems", ISSN 1727-687X, is published (in two languages, in English and in Russian): (No.2(30), v.14, 2008,115-140).

80. Hedrih (Stevanovic) Katica, Double plate system with a discontinuity in the elastic bonding layer (Article), *Acta Mechanica Sinica*, (2007) vol.23 br.2 str. 221-229. DOI 10.1007/s10409-007-0061-x. (hard cower and on line).

81. Hedrih (Stevanović K., Transversal forced vibrations of an axially moving sandwich belt system, **ARCHIVE OF APPLIED MECHANICS**, Springer, 22.11.2007, vol. 78, no. 9, pp. 725-735.

82. Hedrih (Stevanovic) Katica, Transversal vibrations of the axially moving sandwich belts (Article), **ARCHIVE OF APPLIED MECHANICS**, (2007) vol.77 br.7 str. 523-539.DOI10.1007/s00419-006-0105-x

83. Katica (Stevanović) Hedrih, (2008), Energy interaction between linear and nonlinear oscillators (Energy transient through the subsystems in the hybrid system), *ISSN 1027-3190. Ukr. mat. Ωurn., 2008, t. 60, # 6, pp. 796-814.*

References VI

84. Andronov, A.A., Vitt, A.A., Haykin, S.E., (1981), *Teoriya kolebaniy,* Nauka, Moskva., pp. 568.
85. Gerard I. and Daniel J., *Elementary Stability and BIfurcation Theory*, Springer Verlag, 1980.
86. Guckenheimer, J. and Holmes, Ph. , (1983), Nonlinear Oscillations, Dynamical Systems, and Bifurcations of Fields , Springer-Verlag, pp. 461.
87. Hedrih (Stevanović) K., (2005), *Nonlinear Dynamics of a Heavy Material Particle Along Circle which Rotates and Optimal Control***,** Chaotic Dynamics and Control of Systems and Processes in Mechanics (Eds: G. Rega, and F. Vestroni), p. 37-45. IUTAM Book, **in Series *Solid Mechanics and Its Applications, Editerd by G.M.L. Gladwell, Springer,*.** 2005, XXVI, 504 p., Hardcover ISBN: 1-4020-3267-6.
88. Hedrih (Stevanović), K., *(2001),Trigger of Coupled Singularities (invited plenary lecture) ,* Dynamical Systems-Theory and Applications, Edited By J. Awrejcewicz and all, Lodz 2001, pp. 51-78.
89. Hedrih (Stevanović) K., (2004), *A Trigger of Coupled Singularities*, **MECCANICA, Vol.39, No. 3, 2004., pp. 295-314**. , DOI: 10.1023/B:MECC.0000022994.81090.5f,
90. Hedrih (Stevanović), K., (200), Nonlinear Dynamics of a Gyro-rotor, and Sensitive Dependence on initial Conditions of a Heav Gyro-rotor Forced Vibration/Rotation Motion, Semi-Plenary Invited Lecture, Proceedings: COC 2000, Edited by F.L. Chernousko and A.I. Fradkov, IEEE, CSS, IUTAM, SPICS, St. Petersburg, Inst. for Problems of Mech. Eng. of RAS, 2000., Vol. 2 of 3, pp. 259-266.
91. Hedrih (Stevanović), K., (2007), *The Control in Nonlinear Dynamical Systems with Triggers of a Coupled Singularities,* Invited Participation, The 14th International Workshop on Dynamics & Control,May 28–June 2, 2007, in Zvenigorod – Moscow, Russia, Abstracts, 2007, p. 40. *Institute for Problems in Mechanics of the Russian Academy of Sciences.and Steklov Mathematical Institute of the RAS*.
92. Hedrih (Stevanović K., (2008), *The optimal control in nonlinear mechanical systems with trigger of the coupled singularities,* in the book: Advances in Mechanics : Dynamics and Control : Proceedings of the 14th International Workshop on Dynamics and Control / [ed. by F.L. Chernousko, G.V. Kostin, V.V. Saurin] : A.Yu. Ishlinsky Institute for Problems in Mechanics RAS. – Moscow : Nauka, 2008. pp. 174-182, ISBN 978-5-02-036667-1.
93. Hedrih (Stevanović K., (2008), Dynamics of coupled systems, Nonlinear Analysis: Hybrid Systems, Volume 2, Issue 2, June 2008, Pages 310-334.
94. Hedrih (Stevanović), K., (2002), On Rheonomic Systems with Equaivalent Holonomic Conservative System, Int. Conf. ICNM-IV, 2002, Edited by W. Chien and all. Shanghai, T. Nonlinear dynamics. pp. 1046-1054.
95. Katica (Stevanović) Hedrih(2008), Optimal Control of Dissipative Nonlinear Dynamical Systems with Triggers of Coupled Singularities, Journal of Physics: Conference Series, **96** (2008) 012220doi:10.1088/1742-6596/96/1/012220, IOP Publishing http://www.iop.org/EJ/main/-list=current/
96. Hedrih (Stevanović) K., (2004), On Rheonomic Systems with Equivalent Holonomic Conservative Systems Applied to the Nonlinear Dynamics of the Watt's Regulator, Proceedings, Volume 2, The eleventh world congress in Mechanism and machine Sciences, IFToMM, China Machine press, Tianjin, China, April 1-4, 2004, pp. 1475-1479. ISBN 7-111-14073-7/TH-1438. http://www.iftomm2003.com, Publisher: China Machine press, Tianjin, China.
97. Katica R. (Stevanović) Hedrih, (2007),   PHASE PLANE METHOD APPLIED TO OPTIMAL CONTROL IN NONLINEAR DYNAMICAL SYSTEMS WITH TROGGER OF COUPLED SINGULARITIES, The Scientific Journal FACTA UNIVERSITATIS *Series:* Mechanics, Automatic Control and Robotics Vol. 6, No 1, 2007, pp. 71-98.
98. Katica (Stevanović) Hedrih, (2009), Free and forced vibration of the heavy material particle along line with friction: Direct and inverse task of the theory of vibrorheology, 7th EUROMECH Solid Mechanics Conference, J. Ambrósio et.al. (eds.), Lisbon, Portugal, September 7-11, 2009, CD –MS-24, Paper 348, pp. 1-20.
99. Hedrih (Stevanović) Katica, (2009), Phase Plane Method applied to the Optimal Control in Nonlinear Dynamical Systems; Heavy Material Particle Oscillations along Rough Curvilinear Line with Friction: Phase Portraits and Optimal Control, 10th Conference on Dynamical Systems – Theory and Applications, Proceedings, DSTA Lody 2009, Edited by J.A. Awrejcewicy, M. Kazmierczak, P. Olejnik, J. Mrozowski, Lodz, December 7-10, 2009, Poland, ISBN 978-83-929120-4-0, Department for Automatic and Biomechanics, Lodz, Vol. I, pp. 201-212.

100. Katica (Stevanović) Hedrih, Free and forced vibration of the heavy material particle along line with friction: Direct and inverse task of the theory of vibrorheology, 7th EUROMECH Solid Mechanics Conference, J. Ambrósio et.al. (eds.), Lisbon, Portugal, September 7-11, 2009, ESMC 2009 Book of Abstracts ' Mini'Szmposia, izdanje Instituto Superior Tecnico, Lisbon, APMTAC, 2009, pp. 597-598, ISBN 9789899 626423.

101. Hedrih (Stevanović) K., (2009), Vibrations of a Heavy Mass Particle Moving along a Rough Line with Friction of Coulomb Type, ©Freund Publishing House Ltd., International Journal of Nonlinear Sciences & Numerical Simulation 10(11): 1705-1712, 2009. http://www.freundpublishing.com/International_Journal_Nonlinear_Sciences_Numerical%20Simulation/MathPrev.htm.

102. Hedrih (Stevanović) K., Raičević V., Jović S., Vibro-impact of a Heavy Mass Particle Moving along a Rough Circle with Two Impact Limiters, ©Freund Publishing House Ltd., International Journal of Nonlinear Sciences & Numerical Simulation 10(11): 1713-1726, 2009..

103. Hedrih (Stevanović) K., (2010), Discontinuity of kinetic parameter properties in nonlinear dynamics of mechanical systems, Keynote Invited Lecture, 9th Brazilian Conference on Dynamics, Control and Their Applications - 9º Congresso Temático de Dinâmica, Controle e Aplicaçõesm, June 07-11, 2010. UneSP, Sao Paolo (Serra negra), Brazil, Technical Program and Booklet of Abstracts, DINCON 2010, FUNUNeSP, Chair: pp. 14, Abstrac pp. 26 (Full Paper in press) http://www.rc.unesp.br/igce/demac/dincon2010/instrucao.php.

104. Hedrih (Stevanović) K R., Raičević V. and Jović S., Phase Trajectory Portrait of the Vibro-impact Forced Dynamics of Two Heavy Mass Particles Motions along Rough Circle, Communications in Nonlinear Science and Numerical Simulations, 2011 16 (12):4745-4755, DOI 10.1016/j.cnsns.2011.05.027.

Appendix I – References VII:

105. Hedrih (Stevanović) K R., Raičević V. and Jović S., Phase Trajectory Portrait of the Vibro-impact Forced Dynamics of Two Heavy Mass Particles Motions along Rough Circle, Communications in Nonlinear Science and Numerical Simulations, 2011 16 (12):4745-4755, DOI 10.1016/j.cnsns.2011.05.027.

106. Hedrih (Stevanović), K., (1975), *Selected Chapters from Theory of Nonlinear Vibrations* (in Serbian), Faculty of Mechanical Engineering, Niš, First Edition 1975), p. 180.

107. Hedrih (Stevanović), K., (1972), *Study of Methods of Nonlinear Vibrations* Theory (in Serbian), *Poligraphy,* Faculty of Mechanical Engineering, Niš, Preprint, p.500.

108. Stevanović (Hedrih) K., Teorija nelinearnih oscilacija i primene na nelinearne sisteme automatskog upravljanja (Theory of non-linear oscillations and applications to nonlinear system automatic control), [in Serbian], Faculty of Technical Sciences in Niš, 1972. Supervisor D. Rašković.

109. Stevanović (Hedrih) K., Rešrnje jednačone transverzalnih oscilacija jednoraspone grede asimptotskim metodama nelinearne mehanike (Solution of the equation of transversal oscillation one span beam by asymptotic method of nonlinear mechanics), [in Serbian], Magistar of Sciences Degree Thesis, Faculty of Technical Sciences in Niš, 1972. Supervision: Prof. dr. Ing. Math Danilo P. Rašković (Yugoslavia) and academician Yuriy Alekseevich Mitropolskiy (Ukraine).

110. Hedrih(Stevanović) K., Application of the Asymptotic Method for the Investigation of the Nonlinear Oscillations of Elastic Bodies - Energy Analysis of the Oscillatory Motions of Elastic Bodies, [in Serbian], Doctor's Degree Thesis, Faculty of Mechanical Engineering in Niš, (1975). Supervision: Prof. dr. Ing. Math Danilo P. Rašković (Yugoslavia) and academician Yuriy Alekseevich Mitropolskiy (Ukraine).

111. Kozić P., Izučavanje nelinearnih torzijskih oscilacija vratila asimptotskom metodom (Investigation of non-linear torsion oscillations of shafts by asymptotic method), [in Serbian], Magistar of Sciences Degree Thesis, Faculty of Mechanical Engineering in Belgrade, 1982. Working Supervisor K. Hedrih (Stevanović).

112. Kozić P, Stabilnost diskretnih mehaničkih sistema pri dejstvu slučajne pobude (Stability of discrete mechanical systems subjected by random excitations), [in Serbian], Doctor's Degree Thesis, Faculty of Mechanical Engineering in Niš, 1990. Supervisor K. Hedrih (Stevanović).

113. Pavlović R., Prilog nelinearnim oscilacijama plitkih cilindričnih ljuski (Contribution to the non-linear oscillations of the shallow shells), [in Serbian], Magistar of Sciences Degree Thesis, Faculty of Mechanical Engineering in Niš, 1982. Supervisor K. Hedrih(Stevanović).

114. Pavlović R. R.,   Dinamička stabilnost kontinualnih sistema od kompozitnih materaijala pod dejstvu slučajnih pobuda (Dynamic stability of continuous systems made from composite materials subjected to random excitation), [in Serbian], Doctor's Degree Thesis, Faculty of Mechanical Engineering in Niš, 1990. Supervisor K. Hedrih (Stevanović).

115. Mitić Sl., Višefrekventna analiza oscilovanja tankih elastišnih ljuski sa konstantim krivinama i početnim nepravilnostima (Multi-frequency analysis of the vibrations of thin shells with constant curvature and initial inperfetions), [in Serbian], Magistar of Sciences Degree thesis, Faculty of Mechanical Engineering in Niš, 1985. Supervisor K. Hedrih(Stevanović).

116. Mitić Sl., Stabilnost determinističkih i stohastičkih procesa u vibroudarnim sistemima Stability of desterministic and stochastic processes in vibroimpact systems), [in Serbian], Doctor's Degree Thesis, Faculty of Mechanical Engineering in Niš, 19894. Supervisor K. Hedrih (Stevanović).

117. Jovanović D., Analiza naponskog i defprmacionog stanja ravno napregnutih ploča sa primenom na eliptično prstenastu ploču (Stress and strain analysis of plane loaded plate with applications to elliptical annular plate), [in Serbian], Magistar of Sciences Degree Thesis, Faculty of Mechanical Engineering in Niš, 1989. Supervisor K. Hedrih (Stevanović).

118. Mitić Sn., Analiza naponskog i defprmacionog stanja ravno napregnutih ploča (Stress and strain analysis of plane loaded plates), [in Serbian], Magistar of Sciences Degree Thesis, Faculty of Mechanical Engineering in Niš, 1989. Supervisor K. Hedrih (Stevanović).

119. Pavlov B., Novootkriveni fenomeni u nelunearnim dinamičkim sistemima sa analogijom na sisteme opisane Mayhieu-ovom diferencijalnom jednačinom (New phenomena in non-linear dynamical systems with analogy tio the systems described by Matheu differential equations), [in Serbian], Magistar of Sciences Degree Thesis, Faculty of Mechanical Engineering in Niš, 1985,. Supervisor K. Hedrih (Stevanović).

120. Filipovski A., Energijska analiza longitudinalnih oscilacija štapova promenljivog preseka (Energy analysis longitudinal oscillations of rods with changeable cross sections), [in Serbian], Magistar of Sciences Degree Thesis, Faculty of Mechanical Engineering in Niš, 1995. Supervisor K. Hedrih (Stevanović).

121. Perić Lj., Prostorna analiza stanja napona i stanja deformacije napregntog piezokeramičkog materijala (Space analysis of stress and straon state of stressed piezoceramiv materials), Magistar of Sciences Degree Thesis, Faculty of Mechanical Engineering in Niš, 2004. Supervisor K. Hedrih (Stevanović).

122. *Janevski G, Nelinearne oscilacije ploča od kompoyitnih materijala (Nonlinear vibrations of the composite plates), [in Serbian], Magistar of Sciences Degree Thesis, Faculty of Mechanical Engineering in Niš, 2003. Supervisor R. Pavlović.

123. Simonović J., Fenomeni dinamike mehaničkih sistema složenih struktura (Phenomen of Dynamics of Complex Structure Mecanical Systems), [in Serbian], Magistar of Sciences Degree Thesis, Faculty of Mechanical Engineering in Niš, 2008. Supervisor K. Hedrih (Stevanović).

124. Jović S., Energijska analiza dinamike vibroudarnih sistema (Energy analysis of vibroimpact system dynamics), [in Serbian], Magistar of Sciences Degree Thesis, Faculty of Technical Sciences in Kosovska Mitrovica, University of Priština, 2009. Supervisor V. Raičević, Project ON144002 Leader K. Hedrih (Stevanović).

125. Perić Lj., Spregnuti tenzori stanja piezoeletričnih materijala (Coupled tensors of the piesoelectric material states), [in Serbian], Doctor's Degree Thesis, Faculty of Mechanical Engineering in Niš, 2005, Supervisor K. Hedrih (Stevanović).

126. Knežević R., (2000), Nelinearni fenomeni u dinamici planetnih prenosnika (Nonlinear phenomena in dynamics of planetary gear transmission), [in Serbian], Doctor's Degree Thesis, Niš, Yugoslavia, Faculty of Mechanical Engineering in Niš, (200). Supervisor K. Hedrih (Stevanović).

127. Jovanović D., Potencijalna energija i stanje napona u materijalu sa prslinom (Potential energy and stress state in material with crack), [in Serbian], Doctor's Degree Thesis, Faculty of Mechanical Engineering in Niš, 2009, Supervisor K. Hedrih (Stevanović).

128. * Janevski G, Dinamička stabilnost mehaničkih sistema pri dejstvu slučajnih opterećenja (Dynamic stability of mechanical system ;oaded by random excitation), Doctor's Degree Thesis, Faculty of Mechanical Engineering in Niš, 2010, Supervisor Kozić P.

129. Jović S., Energijska analiza dinamike vibroudarnih sistema sa krivolinijskim putanjama i neidealnim vezama (Energy analysis of vibroimpact system dynamics with curvilinear paths and no ideal constraints) , [in Serbian], Doctor's Degree Thesis, Faculty of Technical Sciences in Kosovska Mitrovica, University of Priština, 2011. Supervisor V. Raičević, Projects ON144002   and OI174001 Leader K. Hedrih (Stevanović).

130. Simonović J., Dinamika i stabilnost hibridnih dinamičkih sistema (Dynamics and Stability of Dynamics Hybrid Systems), [in Serbian], Doctor's Degree Thesis, Faculty of Mechanical Engineering in Niš, 2011. Supervisor K. Hedrih (Stevanović).

131. Veljović Lj., Nelinearne oscilacije giro-rotora (Non-linear oscillations of Gyro-rotors), [in Serbian], Doctor's Degree Thesis, Faculty of Mechanical Engineering in Niš, 2011. Supervisor K. Hedrih (Stevanović).

Appendix II – References VIII -List of Projects

Project Leader and SubProject Leader **Katica R. (Stevanović) Hedrih**
Mechanical Engineering Faculty University of Niš and Mathematica Institute SANU

132. Oscillations of the System with many degrees of Freedom and Elastic Bodies with Nonlinear Properties, Basic Scientific Found of Region Niš (1979-1981). Mechanical Engineering Faculty University of Niš .

133. Oscillations of the Special Elements and Systems, B Basic Scientific Found of Region Niš (1981-1986). Some research results included in two Magistar of sciences theses of P. Kozić and R. Pavlović. Mechanical Engineering Faculty University of Niš.

134. Stochastic Processes in Dynamical Systems-Applications on the Mechanical Engineering Systems, Basic Scientific Found of Region Niš (1986-1989). Some research results included in Magistar of sciences theses of Sl. Mitić and in two doctoral dissertations of P. Kozić and R. Pavlović. Mechanical Engineering Faculty University of Niš.

135. Nonlinear Deterministic and Stochastic Processes with Applications in Mechanical Engineering Systems, Ministry of Science and Technology Republic of Serbia, (1990-1995). Some research results included in two Magistar of sciences theses of Blagoj Pavlov and Alekdsandar Filipovski and in a doctoral dissertation of Sl. Mitić. Mechanical Engineering Faculty University of Niš.

136. Sub-Projects 5.1. Thema: Stress and Strain State of the Deformable Bodies and 5.2. Theme: Vector Interpretation of Body Kinetic Parameters, as a part of Project: Actual Problems on Mechanic (1990-1995), Project Leader prof. dr Mane Šašić Ministry of Sciences, Technology and Development of Republic Serbia. Some research results included in three Magistar of sciences theses of Ljubiša Perić, Dragan Jovanović and Snežana Mitić. Mathematical Institute SANU.

137. Sub-Project: 04M03A Current Problems on Mechanics and Applications (1996-2000), as a part of Project: Methods and Models in Theoretical, Industrial and Applied Mathematics, Project Leader prof. dr Gradimir Milovanović, Ministry of Sciences, Technology and Development of Republic Serbia. Mathematica Institute SANU.

138. Project 1616 – Real Problems on Mechanics (2002-2004), Basic Science-Mathematics and Mechanics, Ministry of Sciences, Technology and Development of Republic Serbia. Some research results included in two doctoral dissertations of Ljubiša Perić and Dragan Jovanović. Mathematical Institute SANU and Mechanical Engineering Faculty University of Niš.

139. *Project ON1828 Dynamics and Control of active Structures (2001-2005),* Basic Science-Mathematics and Mechanics, Ministry of Sciences, Technology and Development of Republic Serbia. Some research results included in two doctoral dissertations of Ljubiša Perić and Dragan Jovanović. Mechanical Engineering Faculty University of Niš.

140. Project ON144002 -Theoretical and Applied Mechanics of the Rigid and Solid Bodies. Mechanics of Materials (2006-2010). Support: Ministry of Sciences and Environmental Protection of Republic of Serbia. Some research results included in two Magistar of sciences theses of Srdjan Jović, and Julijana Simonović and in four doctoral dissertations of Dragan Jovanović, Srdjan Jović, Ljiljana Veljović and Julijana Simonović. Institution Coordinator: Mathematical Institute Serbian Academy of Sciences and Arts and Mechanical Engineering Faculty University of Niš.

141. **ON174001 -** Dynamics of hybrid systems with complex structures. Mechanics of materials. (2011-2014), Ministry of Sciences and Technology of Republic of Serbia. Some research results included in thre doctoral dissertations of Srdjan Jović, Ljiljana Veljović and Julijana Simonović. Institution Coordinator: Mathematical Institute Serbian Academy of Sciences and Arts and Mechanical Engineering Faculty University of Niš.

Appendix III – References IX -List of Projects

Mechanical Engineering Faculty University of Niš

142. Project 1409 Stability and nonlinear oscillations of visco-elastic and composite continuous systems, (2002 – 2005). Support: Ministry of Sciences and Environmental Protection of Republic of Serbia. Some research results included in a Magistar of sciences these of Goran Janevski. Mechanical Engineering Faculty University of Niš. (Project Leaders R. Pavloviić and P. Kozić).

143. OI 144023 Deterministic and stochastic stability of mechanical systems (2006 – 2010.), Ministry of Sciences and Technology of Republic of Serbia. Some research results included in a doctoral dissertations of Goran Janevski (supervisor Predrag Kozić). Mechanical Engineering Faculty University of Niš. (Project Leader R. Pavloviić and P. Kozić)

DOPRINOSI KLASIČNOJ I ANALITIČKOJ MEHANICI: PREGLED AUTOROVIH REZULTATA

Katica R. (Stevanović) Hedrih
Matematički institut SANU, Beograd, Srbija
i Mašinski fakultet Univerziteta u Nišu
Tel: 381 18 2 41 663;
e-mail: katica@masfak.ni.ac.yu,khedrih@eunet.yu,khedrih@sbb.co.yu

Apstrakt. Dat je pregled, u subjektivnom izboru, autorovih naučnih rezultata u oblasti klasične mehanike, analitičke mehanike diskretnih naslednih sistema, analitičke mehanike diskretnih frakcionog reda oscilatornih sistema, elastodinamike, nelinearne dinamike, kao i dinamike hibridnih sistema. Glavni originalni autorovi rezultati su predstavljrni kroz matematičke modele mehanike sa primerima primene na rešavanje zadataka dinamike realnih mehaničkih sistema apstrahovanih do teorijskih modela mehaničkih diskretnih ili kontinualnih sistema, kao i hibridnih sistema. Rad prikazuje i metode i naučne rezultate autorovih profesora Mitropoljskog, Andjelića i Raškovića, kao i originalne naučne rezultate autora og rada dobijene primenom metoda njenih profesora. Vektorska metoda je zasnovana na vektorima momenata masa i odgovarajućim devijacionim vektorskim komponentama za pol i orjentisanu osu, koje je K. Hedrih , 1991 godine, definisala i prikazala. Ovde su, takodje prikazani i rezultati u konsrukciji analitičke dinamike diskretnih naslednih sistema dobijeni u saradnji sa O.A. Goroshkom. Takodje je ukazano i na neke izabrane rezultate autorovih poslediplomaca i doktoranata u oblasti nelinearne dinamike. Spisak naucnih projekata kojima je rukovodio autor je prikazan, kao i spisak doktorskih disertacija i magistarskih teza koje sadrže naučne rezultate uradjene pod mentorstvom autora ovog rada ili njenih prvih doktoranata.

Ključne reči: Pregledni, vektorska metoda, vector momenta mase, vector devijacionog momenta mase, rotator, spregnute rotacije, mimoilazne ose, bazni vektori

tangentnog prostora vektora položaja, ugaona brzina baznih vektora tangentnog prostora, brzina ekstenzije baznog vektora, reonomne veze, reonomne coordinate, pokretljivost, asimptotska aproksimacija rešenja, asimptotska metoda usrednjenja Krilov-Bogoljubov-Mitropolzski, metoda varijacije konstanata, nasledni sistem, reološko i relaksaciono jezgro, standardni nasledni element, integrod-diferencijalna jednačina, izvod necelog reda, kovarijantne koordinate, kontravarijantne koordinate, fizičke koordinate, metoda diskretnog kontinuuma, prostorna frakcionog reda struktura, glavne sopstvene površinske mreže, glavni sopstveni lanci, oscilator frakcionog reda, karakteristični brojevi sistema frakcionog reda, prenos signala, višefrekventni, materijalne tačke, kruto telo, reduktor, deformabilno telo, sistem više tela, transverzalni, longitudinalni, spregnute ploče, spregnute trake, spregnute grede, stohastička stabilnost.